Development of a Novel, Microemulsion System for the Simultaneous Delivery of Hydrophilic and Hydrophobic Active Pharmaceutical Ingredients (APIs)

by

Shannon Priscilla Callender

A thesis
presented to the University of Waterloo
in fulfilment of the
thesis requirement for the degree of
Doctor of Philosophy
in
Pharmacy

Waterloo, Ontario, Canada, 2020

Examination Committee Membership

The following served on the Examining Committee for this thesis. The decision of the Examining Committee is by majority vote.

External Examiner	DR. AFSANEH LAVASANIFAR Professor, Faculty of Pharmacy and Pharmaceutical Sciences, University of Alberta
Supervisor(s)	DR. SHAWN D. WETTIG Professor; Associate Dean, Graduate Studies (Science)
Internal Member	DR. ANDREA EDGINTON Professor; Associate Director, Graduate Studies and Research
Internal Member	DR. OWEN VAN CAUWENBERGHE Adjunct Assistant Professor
Internal-external Member	DR. JEAN DUHAMEL Professor; Director, Institute for Polymer Research

Author's Declaration

This thesis consists of material all of which I authored or co-authored: see Statement of Contributions included in the thesis. This is a true copy of the thesis, including any required final revisions, as accepted by my examiners.

I understand that my thesis may be made electronically available to the public

Statement of Contributions

Shannon Priscilla Callender was the sole author of Chapters 2, 3, 4, 5 and 6 which were written under the supervision of Dr. Shawn Wettig and were not written for publication.

This thesis consists in part of one manuscript written for publication. Exceptions to sole authorship of material are as follows:

Research presented in Chapter 1:

This research was conducted at the University of Waterloo by Shannon Priscilla Callender under the supervision of Dr. Shawn Wettig. Shannon Priscilla Callender designed the study with consultation from Dr. Shawn Wettig who contributed to data analysis and manuscript drafting/editing. Jessica Mathews contributed to figure preparation (Figures 1.1-1.5) and database management of articles. Katheryn Kobernyk contributed to manuscript drafting of the content presented in Section 1.2.

Citation:

Chapter 1: Callender SP, Mathews J, Kobernyk K, Wettig SD. Microemulsion utility in pharmaceuticals: implications for multi-drug delivery. *International Journal of Pharmaceutics*. 2017;**526**:425-442. 2017. DOI: 10.1016/j.ijpharm.2017.05.005.

As lead author of Chapter 1, I was responsible for conceptualizing the study, carrying out data collection and analysis, and drafting and submitting manuscripts. My coauthors provided feedback on draft manuscripts.

Abstract

Concurrent chronic disease and ensuing multi-morbidity are a debilitating reality for millions of Canadians. This adversity is compounded by increased pill burden and decreased patient adherence. Microemulsions (MEs) serve as a potential multi-drug therapy solution. MEs are thermodynamically stable, colloidal systems whose oil and water compositions and nano-sized droplets have the potential to facilitate simultaneous hydrophilic and lipophilic drug delivery, while improving bioavailability. However, the area of multi-drug delivery using ME technology is largely unexplored and unfulfilled. In order to develop a ME capable of simultaneous multi-drug delivery, emulsifying agents as the heart of these systems must be investigated.

In this work, the potential for multi-drug delivery using ME systems was explored with a particular focus on emulsifying agent properties conducive to this purpose. A prenatal supplement comprised of eleven active pharmaceutical ingredients (APIs) of varying hydro- and lipophilicity was selected as a proof of concept. Five non-ionic surfactants were subjected to extensive ternary phase diagram (TPD) mapping with a medium chain triglyceride, Miglyol 812 in order to identify regions of monophasic microemulsion formation. Optimization was performed via critical micelle concentration determination and the hydrophilic-lipophilic deviation (HLD) equation. A final microemulsion comprised of 3:1 Polysorbate 80:Cremophor RH 40 surfactant, Miglyol 812 and water in a surfactant:oil:water (S:O:W) ratio of 50:40:10, was identified as optimal for monophasic, microemulsion formation. Eleven active pharmaceutical ingredients- five lipophilic (Vitamins A, D, E, K and docosahexaenoic acid) and six hydrophilic (Vitamins B_1, B_2, B_3, B_6, B_9, B_{12}) were then successfully incorporated. The resulting microemulsion was determined to be of a bicontinuous nature and after 100x aqueous dilution, spherical droplets were identified via TEM with a diameter of 164 ± 37 nm, a charge of -14.1 ± 2.2 mV and a low viscosity of 1.04 ± 0.04 mPa/s. Twelve additional non-ionic surfactants were screened for possible use in the formulation. Polysorbate 81, with 15 less ethylene oxide head groups but equivalent carbon chain length to Polysorbate 80, was identified as most promising based on droplet diameter and zeta potential. Thus, this type of multi-drug formulation appeared to be tolerable to larger changes in non-ionic surfactant head group than hydrocarbon chain length; Hydrophilic-lipophilic balance (HLB), in contrast, appeared to have little to no effect. Two additional drug-loaded microemulsion formulations comprised of 3:1

Polysorbate 81:Cremophor RH 40 surfactant, Miglyol 812 oil and water in S:O:W ratios of 40:50:10 and 50:40:10, resulted in droplet diameters of 94 ± 15 nm and 81 ± 2.4 nm, and zeta potential values of -17 ± 4 mV and -23 ± 6 mV, respectively after 100x aqueous dilution. All final multi-drug loaded MEs demonstrated >70% dissolution improvement of folic acid and >90% dissolution improvement of riboflavin in 50 mM phosphate buffer (pH 7.4) as compared to a commercial prenatal supplement in suspension form. Overall, it was demonstrated that the process of TPD mapping, HLD optimization and careful surfactant screening was instrumental in the successful development of a multi-drug microemulsion system with the potential to treat concurrent, chronic diseases in a single dose.

Acknowledgements

A sincere thank you to my supervisor, Dr. Shawn Wettig, not only for the opportunity to pursue this interesting (read as: challenging) research project, but for your guidance and unwavering support throughout my graduate studies. Your mentorship and counsel have afforded me academic, professional and personal opportunities that would not have been possible otherwise; I am truly fortunate to have studied under your direction.

Thank you to my advisory committee members: Dr. Owen Van Cauwenberghe for your scholarship support, unparalleled insight into the formulation process and encouragement of 'out of the box' thinking, Dr. Andrea Edginton for your motivational chats, biopharmaceutical expertise and efforts to help simplify this complex project and Dr. Jean Duhamel for your constructive feedback and extensive chemistry expertise.

A special thank you to the Accucaps Industries Limited/Catalent Pharma Solutions Inc. team especially Sonia Plusa, Ziheng (Harry) Wang, Doug Durham, Janine McMillen, Laura Hao and Vince Quiquero for your considerable pharmaceutical expertise, assistance in chromatographic experiments and consistent progress check-ins via biweekly meetings.

I would also like to acknowledge my wonderful lab mates in the Wettig group for their support and friendship, especially the Undergraduate students I have had the privilege of supervising: Kathryn Kobernyk, Jessica Mathews and Philip Lu who are all exceptionally talented and have contributed to this work. Thank you to my School of Pharmacy colleagues, Nyasha Gondora and Samantha Shortall, who have become my best friends and support system throughout this process, and a special thank you to all my dear friends at the School of Pharmacy- fellow graduate students, faculty, administrative and teaching staff; we truly are a family here.

I am grateful to the University of Waterloo, the School of Pharmacy, MITACS Canada, Catalent Pharma Solutions, the CIHR Drug Safety and Effectiveness Training program, the Province of Ontario via the Ontario Graduate Scholarship, the Canadian Society of Pharmaceutical Sciences (CSPS) and Gattefossé Canada Inc. for their financial support of this work.

Last but certainly not least, thank you to my wonderful family and friends. This work is the culmination of your love, support and encouragement.

Dedication

To my incredible parents, Christopher and Patricia Callender and my sister, Katrina Callender… words will never be enough. We did it.

To my husband, Satesh Singh- for always encouraging, always motivating, always believing. Thank you for being my personal cheerleader.

Table of Contents

List of Figures

Chapter 5

List of Tables

Chapter 5

List of Abbreviations

ANOVA	analysis of variance (statistics)
API	active pharmaceutical ingredient
BCS	biopharmaceutics classification system
CC	characteristic curvature
CMC	critical micelle concentration
CPP	critical packing parameter
DHA	docosahexaenoic acid
DI	deionized water
DLS	dynamic light scattering
DSC	Differential Scanning Calorimetry
EACN	effective alkane carbon number
EPA	eicosapentaenoic acid
F1A/	Formulation 1 (S:O:W 50:40:10)
F1	3:1 Polysorbate 80:Cremophor RH 40, Miglyol 812, water and Vitamins A (beta carotene), B_1, B_2, B_3, B_6, B_9, B_{12}, D, E, K and DHA/EPA
F2	Formulation 2 (S:O:W 40:50:10) 3:1 Polysorbate 81:Cremophor RH 40, Miglyol 812, water and Vitamins A (beta carotene), B_1, B_2, B_3, B_6, B_9, B_{12}, D, E, K and DHA/EPA
F3	Formulation 3 (S:O:W 50:40:10) 3:1 Polysorbate 81:Cremophor RH 40, Miglyol 812, water and Vitamins A (beta carotene), B_1, B_2, B_3, B_6, B_9, B_{12}, D, E, K and DHA/EPA
FDA	Food and Drug Administration
GRAS	generally recognized as safe (FDA term regarding formulation excipients)
HLB	hydrophilic lipophilic balance
HLD	hydrophilic lipophilic deviation/difference
HPLC	High Performance Liquid Chromatography
IIG	inactive ingredient (limit for pharmaceutical products)
LCT	long chain triglycerides
LFCS	lipid formulation classification system
MCT	medium chain triglyceride
ME	microemulsion
NIH	National Institutes of Health
O/W	oil-in-water (emulsion)
PDI	polydispersity index
PEO	polyethylene oxide
PIT	phase inversion temperature
PPO	polypropylene oxide
SDHS	dihexyl sodium sulfosuccinate
SDS	sodium dodecyl sulphate
SEDDS	self-emulsifying drug delivery system
S:O:W	surfactant:oil:water (ratio)
TEM	Transmission Electron Microscopy
TPD	ternary phase diagram

TPGS	d-α-tocopherol polyethylene glycol succinate
USP	United States Pharmacopeia
W/O	water-in-oil (emulsion)

Chapter 1: Introduction and Background

Portions of this chapter are reflective of an original manuscript published by the Ph.D. candidate (Shannon P Callender) in the journal International Journal of Pharmaceutics. All pertinent dialogue included in this chapter was written by the Ph.D. candidate. Author contributions are detailed in the 'Copyright Permission' section.

Callender, SP., Mathews, J.A., Kobernyk, K., Wettig, SD. Microemulsion utility in pharmaceuticals: Implications for multi-drug delivery. Int J Pharm 2017; 526: 1-2. doi: 10.1016/j.ijpharm.2017.05.005.[1]

1.1 Nanotechnology Drug Delivery in the 21st Century

The 'magic bullet' approach represents one of the greatest conceptual shifts in drug delivery, beginning in the 20th century and progressing rapidly in the 21st century. Drug delivery tools affording a specific, targeted approach to abnormal cells or disease-causing entities while leaving healthy cells untouched remains the drug delivery gold standard. Nanotechnology tools, in particular, have received increased attention and interest from the scientific community for their potential as effective magic bullet and bioavailability-enhancing agents, due to their small sizes. The term 'nanotechnology' in the context of drug delivery often refers to systems on the scale of 1-100 nm in length[2] though the upper limit may be 200 nm, 300 nm or even 1000 nm. Strictly speaking, 'nano' technology objects possess sizes in the nanometer size range from 1-1000 nanometers. Since the beginning of the nanotechnology revolution in the 1980s, a variety of tools have been developed for effective drug delivery purposes.[3,4]

1.1.1 Current Nanotechnology Drug Delivery Tools

Liposomes, dendrimers, micelles and nanocrystals are just a few of the nanotechnology tools used in the treatment of widespread, chronic diseases such as cancer[5] heart disease[6] and diabetes.[7,8] Other common nanotechnology tools include nanoemulsions, nanotubes, magnetic nanoparticles and pH-, temperature- or electro- sensitive nanoparticles.[9] The potential of these nanotechnology tools for controlled drug release, increased stability, low toxicity and of course, improved absorption via their small sizes[10] renders them invaluable in drug delivery.

Nanotechnology drug delivery tools generally involve a carrier and active ingredient(s) or therapeutic(s). The therapeutic may be the carrier itself, or may be directly coupled to the

carrier through solubilisation, functionalization or entrapment.[11] The addition of proteins, polymers and other material to the surface of each nanoparticle may also enhance targeting efficiency.[9] The amphiphilic nature of many nanotechnology tools such as nanoemulsions, liposomes, micelles etc. affords delivery of both hydrophilic and hydrophobic active pharmaceutical ingredients (APIs) or drugs.[9]

1.1.2 Challenges in Drug Delivery

Nanotechnology tools have the potential to overcome two of the major challenges in drug delivery: drug solubility and permeability.[9] Poor biopharmaceutical properties, in particular, poor water solubility of active ingredients has resulted in the failure of many potentially marketable pharmaceutical products.[12] The Biopharmaceutics Classification System (BCS) adopted by the US Food and Drug Administration (FDA)[13] based on the work of Amidon et al. (1995)[14] classifies orally administered drugs into four classes based on their solubility and permeability (**Table 1.1**).

Table 1.1: Biopharmaceutics classification of drugs based on solubility and permeability. Upward arrows indicate high permeability or solubility while downward arrows indicate low permeability or solubility. Definitions of 'high' and 'low' solubility and permeability are described below.

BCS Class	Solubility	Permeability
I	↑	↑
II	↓	↑
III	↑	↓
IV	↓	↓

A drug is said to demonstrate high permeability when the extent of absorption is greater than 90% of the administered drug, and high solubility when the highest marketed dose is soluble in 250 mL aqueous media across pH 1.2-7.4, the entire gastrointestinal pH range.[14] Based on these criteria, it is evident that hydrophobic and/or lipophilic drugs exhibit low 'solubility' given their incompatibility with aqueous media. Thus, these drugs are often classified as BCS Class II and IV compounds. Given that solubility is an important determinant

of drug concentration in systemic circulation, low solubility often results in low bioavailability. Therefore, lipophilic compounds face unique drug delivery challenges with respect to bioavailability.[15] Nanotechnology carriers, in the form of a hydrophilic shell and hydrophobic core, afford a unique opportunity to solubilize lipophilic material and may improve bioavailability outcomes. The potential of nanotechnology tools in single drug delivery is generally well understood, but their potential in multi-drug delivery is more elusive.

1.1.3 Multi-Drug Delivery

The life expectancy at birth in Canada has increased substantially over the past century.[16] However, with the increase in life expectancy comes an increase in the burden of concurrent, chronic diseases. According to the Public Health Agency of Canada, nearly two thirds of Canadians over the age of 20 suffer from chronic illnesses- in particular, hypertension, mental illness and arthritis.[17] These three chronic diseases tend to occur concurrently with others, resulting in multi-morbidity.[18-24] Multi-drug therapies present an opportunity for better management of these concurrent, chronic diseases, improving patient adherence and reducing the burden on health care systems.[25] However, despite these advantages, multi-drug therapies are often avoided due to formulation complexities.[1] In particular, API-API interactions, instability and insufficient solubility of drugs of varying hydro- and lipophilicity are of primary concern.[1] Nanotechnology emulsion systems with their small droplet sizes, oil and water composition and thermodynamic stability are well suited for the simultaneous solubilisation and delivery both lipophilic and hydrophilic active ingredients.

1.2 Introduction to Emulsion Systems

Emulsion technology is utilized in a variety of industries including the cosmetic, agricultural, food and of course, pharmaceutical industry.[26, 27] Emulsions are metastable colloidal systems comprised of particles of one liquid dispersed in another immiscible liquid.[28] These two immiscible liquids themselves cannot mix and require the presence of emulsifying agents (emulsifiers) or surface-active agents (surfactants).[28,29] Both terms are used interchangeably in this thesis. Surfactants are amphiphilic molecules comprised of a polar, hydrophilic head and a non-polar, hydrophobic tail that orient at the interface of water and oil, respectively. This

reduces the overall interfacial tension between the two immiscible phases, promoting miscibility. **Figure 1.1** depicts the orientation of a typical surfactant molecule at an organic/aqueous interface.

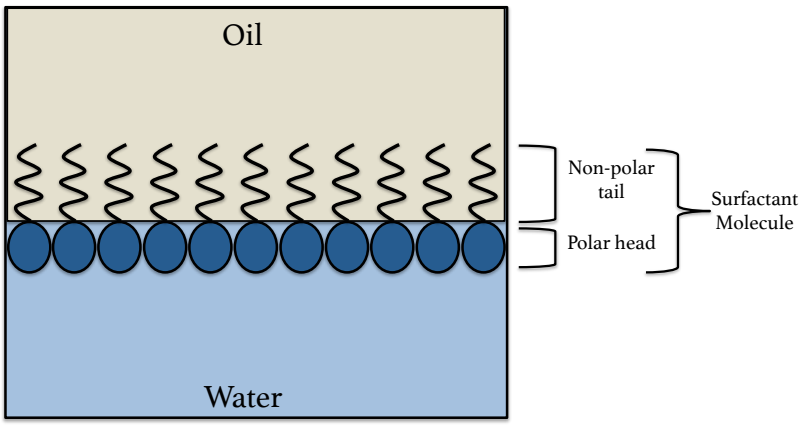

Figure 1.1: Orientation of surfactant molecules at an oil-water interface. The polar head groups of the surfactant orient to face the polar, aqueous phase while the non-polar tail groups of the surfactant orient to face the non-polar, organic phase. This type of orientation reduces the interfacial tension between the two phases, promoting miscibility. Figure taken from Callender et. al. (2017)[1] with permission.

There are three main types of emulsion systems: (i) macroemulsions, (ii) nanoemulsions and (iii) microemulsions. Each system is similar in composition, consisting of oil, water and emulsifying agent. However, they differ with respect to certain characteristics such as droplet size, methods of formation/energetics and stability.

1.2.1 Macroemulsions

Macroemulsions are often referred to as 'coarse' or opaque emulsions due to their relatively large droplet sizes of more than 400 nm in diameter, which result in a turbid solution. [28] This is in contrast to micro- and nanoemulsions, which consist of much smaller droplet sizes and slightly turbid to clear solutions.[28]

In general, there are two main types of macroemulsions: oil-in-water (O/W) and water-in-oil (W/O) emulsions. O/W emulsions consist of oil droplets dispersed in a water continuous phase while W/O emulsions consist of water droplets in an oil continuous phase. In O/W emulsions, the water phase is referred to as the outer, continuous phase while oil is referred to

as the inner, discontinuous phase (and vice versa). The two types of macroemulsions are depicted in **Figure 1.2** and are often referred to as 'single' emulsions.[30] Macroemulsions may also be prepared as multiple emulsions.

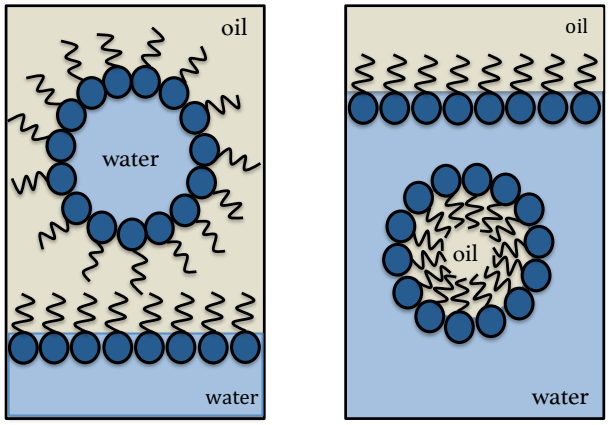

Figure 1.2: Schematic representation of a typical W/O (left) and O/W (right) macroemulsion system. In a water-in-oil macroemulsion system, water is the inner, discontinuous phase dispersed in the outer, oil-continuous phase. The reverse is true for an oil-in-water macroemulsion system. Surfactant molecules concentrate at the interface of each emulsion droplet and orient themselves so that their polar heads face water while their non-polar tails face oil. Upon increased addition of surfactant, the interface becomes saturated and micelle formation begins. O/W systems form 'normal' micelles with a hydrophobic core while W/O systems form 'reversed' micelles with a hydrophilic core. Figure taken from Callender et. al. (2017)[1] with permission.

In particular, there are oil-in-water-in-oil (O/W/O) and water-in-oil-in-water (W/O/W) emulsions where the continuous phases are oil and water, respectively. Multiple emulsions are often used in delayed or controlled release formulations, as the drug must cross an additional phase barrier before it can be released.[31]

With respect to formation, macroemulsions require an input of energy usually in the form of shaking or stirring in order to deform the aqueous/organic interface and produce droplets.[30] The energy input required to do this must be the same as or greater than that of the Laplace pressure of each droplet, i.e. the differential pressure between the outside and inside of a curved surface.[30] Smaller droplets are desired for stability purposes and this can require significant agitation of the macroemulsion system beyond simply shaking or stirring.[30] Because of the energy input required to form these systems, the relatively large droplet sizes, and the

interfacial energy involved, macroemulsions are said to be kinetically, and not thermodynamically, stable. Thus, over time, a macroemulsion will inevitably revert to its phase separated components. Emulsifying agents and the use of strong agitation to introduce energy into the system for macroemulsion formation, simply delay this reversion process for a fixed amount of time.

The most concerning stability factor with macroemulsions is their susceptibility to coalescence and flocculation. Coalescence is the merging of two droplets into one single larger droplet, which eventually leads to phase separation and emulsion 'breaking'. Flocculation is the aggregation of dispersed-phase droplets and can be considered reversible.[30] Both processes depend on the interfacial film surrounding individual droplets and the elasticity or rigidity of this film.[28] Given that this interfacial film is comprised of surfactant molecules, it is the surfactant properties that dictate the system's propensity for coalescence. In general, surfactant molecules at the interface of each droplet provide an elastic mechanical barrier to droplet-droplet collision, reducing the overall probability of coalescence. If the head groups are charged, as in the case of ionic surfactants, an additional barrier is introduced as these charged droplets would repel each other. In the absence of an ionic surfactant, salt may also be added.[28] Temperature and the size range of droplets within the macroemulsion system also affect coalescence.[28] In general, any factor that disturbs the emulsifier and its resulting interfacial film, disrupts stability.

1.2.2 Nanoemulsions

Nanoemulsions are commonly referred to as mini-emulsions or ultrafine emulsions. In comparison to macroemulsions and microemulsions, nanoemulsions are most similar to macroemulsions with the exception of their smaller droplet sizes. Although size is the main differentiating factor between nanoemulsions and macroemulsions, there is much ambiguity in the scientific community regarding the exact droplet size range of nanoemulsions. Articles that *do* specify sizes often fail to mention whether they are referring to diameter or radii measurements. Contrary to their nomenclature and popular belief, however, nanoemulsions do not necessarily contain droplets that are smaller than those found in microemulsions. In fact, droplet sizes in nanoemulsions are usually in the mid-size range between that of macroemulsions and microemulsions, i.e., approximately 100-400 nm in diameter.[28] These

small droplet sizes result in nanoemulsions appearing blue-white to semi-opaque in nature.[28] In terms of types, they are classified according to the same types as macroemulsions; either oil-in-water or water-in-oil.

With respect to formation, nanoemulsions are much like macroemulsions, requiring an energy input and agitation of the system for formation. For this reason, many nanoemulsions are formed by high-pressure processes such as homogenization. Like macroemulsions, nanoemulsions are also kinetically and not thermodynamically stable, meaning that although the components can be sufficiently agitated to overcome an energy barrier for formation, the system will eventually revert to its original phases. This is due to the fact that the free energies of the separate oil and water phases of a nanoemulsion are at a lower energy state than free energy of the colloidal dispersion system, creating a thermodynamically unstable system. This instability may be overcome by ensuring there is a large enough energy barrier between the two phases. The greater the height of the energy barrier between the nanoemulsion and the separated phases, the greater the stability of the nanoemulsion.[32] The smaller particle sizes of nanoemulsions lend improved resistance to coalescence compared to macroemulsions. Therefore, the reversion process is quite slow and some nanoemulsion formulations can therefore remain stable for months and even years.

Content-wise, nanoemulsions are found to generally require less emulsifier than macro or microemulsions, typically on the order of 1-3% of the volume of the oil phase.[28] The length of the co-surfactant (defined in **Section 1.3**) required is also found to be longer than that of microemulsions (at least 12 carbons as compared to the much shorter chain lengths required for microemulsions).[28]

1.2.3 Microemulsions

Microemulsions gained recognition in 1943 after Hoar and Schulman mixed a milky solution with hexanol to produce a uniform single-phase, non-conducting solution.[33] The first commercial application of microemulsions was in the formulation of liquid waxes, discovered by Rodawald in 1928.[27] By 1970, microemulsion research peaked, in part due to its application in enhanced oil recovery[34] where the use of surfactants combined with the ultralow interfacial tensions of microemulsions afforded oil extraction.[28] Microemulsions are transparent,

thermodynamically stable mixtures of oil and water stabilized by emulsifiers. They possess very different properties from nano- and macroemulsions.

Contrary to their terminology, microemulsions consist of the smallest droplet sizes found in emulsion systems. Specifically, microemulsion droplet sizes generally range from 10 to 100 nm in diameter.[28,32] According to Eriksson, Ljunggren, Kegel and Lekkerkerker (2001), one of the most important factors influencing droplet size is the packing density of surfactant molecules in the interfacial film.[35] This curvature and compressibility of the interfacial film then dictates the interfacial tension[35] and contribution to overall free energy. In particular, the more rigid the film, the higher the packing density and the smaller the droplet size.[36]

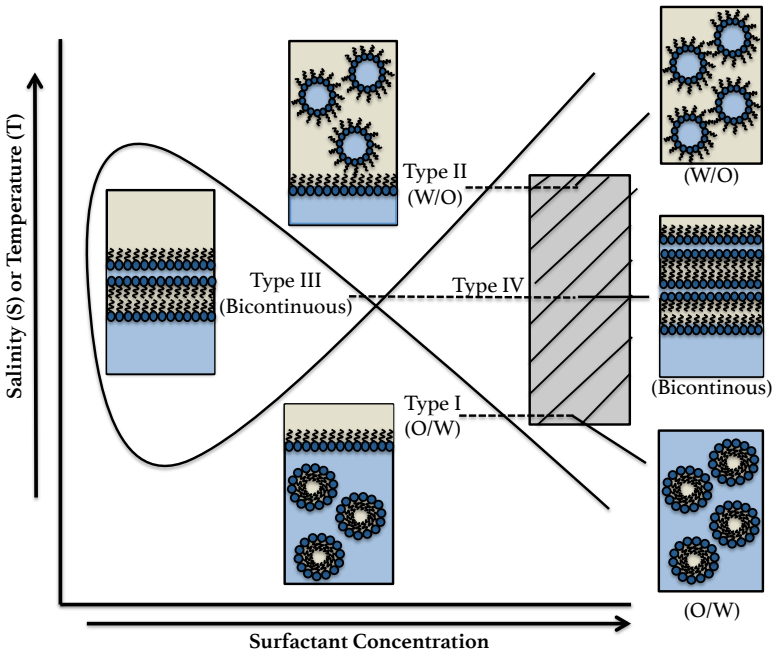

Figure 1.3. Schematic of the effect of temperature (T) or salinity (S) and surfactant concentration on microemulsion type. Spherical structures represent the microemulsion phase, yellow regions represent oil and blue regions represent water. Figure taken from Callender et. al. (2017)[1] with permission.

According to Winsor (1948)[37] there are four types of microemulsions: (i) Type I- biphasic with an upper excess oil phase and lower O/W microemulsion, (ii) Type II- biphasic with an upper W/O microemulsion and lower excess water phase, (iii) Type III- triphasic with upper excess oil phase, middle bicontinuous microemulsion and lower excess water phase, (iv) Type IV- monophasic, single microemulsion phase. Each type can be obtained given different environmental or compositional factors. In general, microemulsions follow trends displayed

in **Figure 1.3,** typically referred to as a fish diagram. A simple change in temperature, T, in the case of a non-ionic surfactant or salinity, S, in the case of an ionic surfactant can result in transition from a Type I→ III→ II microemulsion. An increase in surfactant concentration can also result in the effective solubilization of excess oil or water phases, inducing a transition from any of these microemulsion types to a Type IV microemulsion within temperature and salinity constraints. The rationale behind these trends is explained in **Section 1.5.2**.

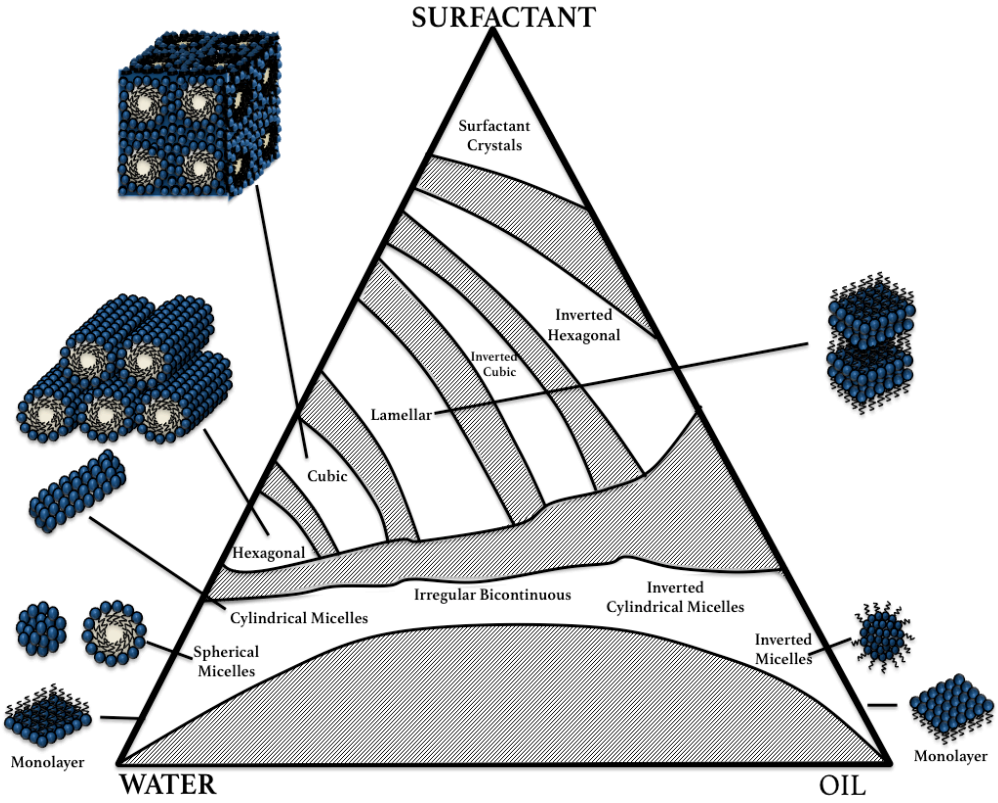

Figure 1.4: Schematic of the various micellar aggregates possible depending on the ratio of water, surfactant and oil utilized. As the water content decreases, structures shift from 'normal', spherical micelles to inverted micelles. As the concentration of surfactant increases, micelles can be seen to aggregate into cubic, lamellar, hexagonal and finally, liquid crystalline structures. Adapted from Brinker (1999).[38] Figure taken from Callender et. al. (2017)[1] with permission.

Each type of microemulsion differs in structural composition. Micellar, rod-like, lamellar and sponge-like structures are all possible depending on the composition of oil, water and surfactant.[32] **Figure 1.4** displays the various structural arrangements that can be obtained depending on the concentration of oil, water and surfactant utilized. In contrast to

nanoemulsions, microemulsions usually require a higher percentage of surfactant or emulsifier (i.e., 15-30% w/w of the oil phase) for formation.[28] Additionally, the co-surfactant required is usually of a shorter carbon chain length than that required in nanoemulsions.[28]

With respect to formation and energetics, microemulsions possess an energy profile opposite to that of macro- and nanoemulsions. In a microemulsion system, little to no energy input is required for formation. This is due to the fact that the oil and water starting components are at a higher energetic state than that of the final microemulsion product. Thus, microemulsion formation is a forward-driven process and formation occurs spontaneously with little to no energy input required. These systems are considered thermodynamically stable; rather than energy being required for microemulsion formation, energy is required for microemulsion dissociation and phase separation. **Figure 1.5** illustrates the energetic profile of microemulsions.

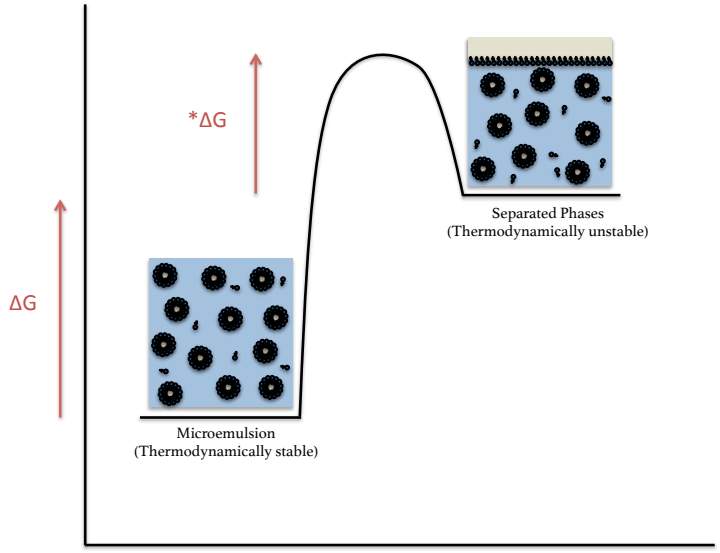

Figure 1.5: Schematic of the energetics involved in a typical microemulsion system (*ΔG= activation energy). The microemulsion product is at a lower energy state than that of its separated phases or starting components, resulting in thermodynamic stability. Nanoemulsions and macroemulsions have the reverse profile with the emulsified systems at a higher energy state that the starting components, resulting in kinetic stability. Adapted from McClements (2012).[32] Figure taken from Callender et. al. (2017)[1] with permission.

1.2.3.1 Advantages of Microemulsion Systems

Microemulsions are uniquely equipped for drug delivery. Specifically, microemulsions are able to: i) present active pharmaceutical ingredients (APIs) in liquid form, ii) improve bioavailability and stability via small droplet sizes, iii) solubilize and deliver both hydrophilic

and lipophilic drugs, simultaneously and (iv) form spontaneously with relatively simple starting ingredients.

i) Presentation of Active Ingredients in Liquid Form

It is generally well established that drugs in solid form must undergo an extra dissolution step before they can be absorbed. There are three main processes necessary for solid drug absorption for oral delivery: a) disintegration, b) dissolution and c) absorption.[39] Disintegration is necessary in order for the solid particles to dissolve in liquid media before being absorbed.[39] Microemulsions are liquid in nature and thus, are able to bypass this additional disintegration step.[39] The overall result is that microemulsions, and liquids in general, experience faster drug absorption rates independent of any effect of disintegration.[39] In the context of drug formulations, this is beneficial for fast-acting relief purposes. Though liquid formulations are often encapsulated in solid dosage forms such as gelatin capsules, dissolution of a solid capsule containing drugs in liquid form is still faster than dissolution of a solid capsule containing drugs in solid form.[39]

The presence of drug in liquid form is also advantageous in terms of transit time.[40] While liquids may take 20-30 minutes to pass completely through the stomach, solids may take up to 3 hours depending on the composition.[40] These solids remain in the stomach for a longer period of time and are thus, exposed to gastrointestinal enzymatic degradation for longer periods of time.[41] This may greatly affect drug stability and cause premature drug degradation.[41]

ii) Small Droplet Sizes

As introduced above, microemulsions generally possess droplet sizes in the diameter range 10-100 nm.[28,32] These small droplet sizes increase the surface area to volume ratio for drug absorption leading to improved bioavailability.[42-45] Additionally, these small droplet sizes are able to resist gravitational sedimentation and enhance the stability of the microemulsion system. The factors influencing droplet sizes in microemulsion systems generally include the type of surfactant used, surfactant chain length, the alkyl chain length of the oil, and the rigidity of the resulting interfacial film. These factors are discussed in **Section 1.3.** Many studies conducted in a five-year period between 2011-2016, have credited the small droplet sizes of microemulsions for the formation of stable and highly bioavailable formulations.[1] In

particular, microemulsions have improved the stability and bioavailability of Aprepitant, a chemotherapy-induced nausea and vomiting preventor[46], Troxerutin, a hydrophilic vasoprotector[47], Fenofibrate, a cholesterol-lowering agent[48], Pranlukast Hemihydrate, an asthma-treating agent[49], Leuprorelin, a hormone-related disorder treatment drug[50], Ritonavir, an HIV anti-retroviral[51], Sirolimus, an immune-suppressant[52] and Gatifloxacin, an antibiotic[53]. **Figure 1.6** depicts the various pathologies treated using microemulsion systems based on publications in the PubMed database from 2011-2016.[1]

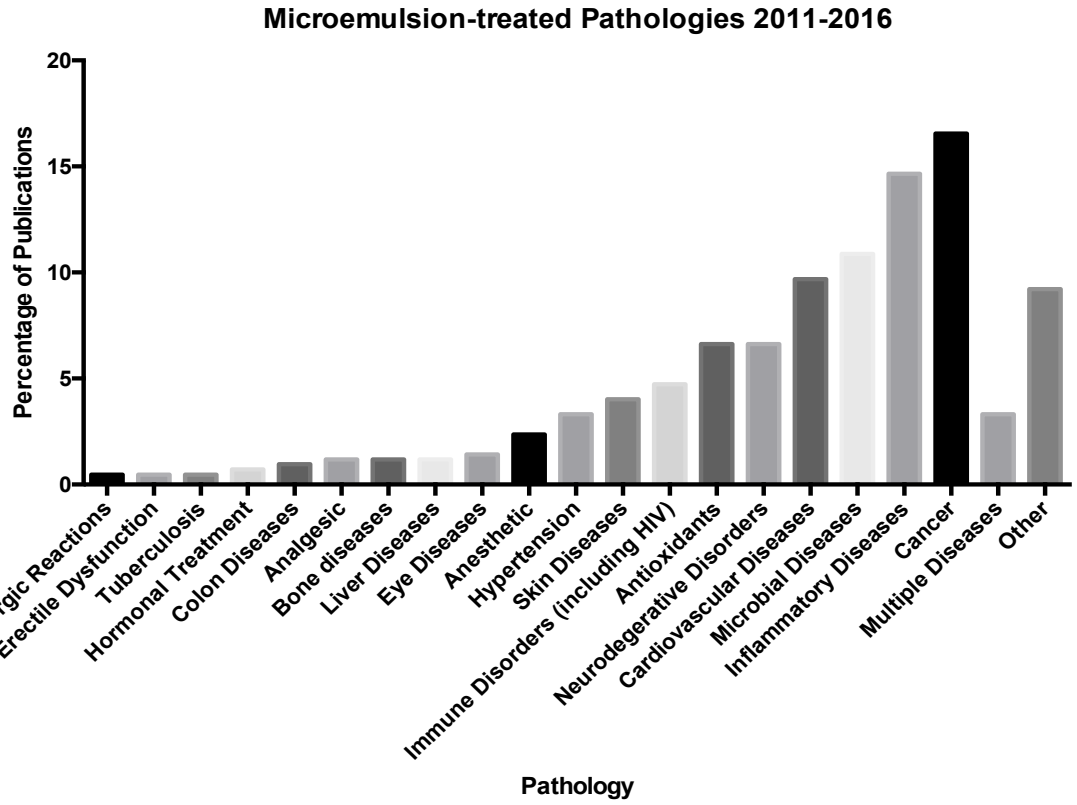

Figure 1.6: Graphic depicting the various pathologies treated by microemulsion systems over a period of five years. Cancer, inflammatory diseases, neurological disorders and cardiovascular diseases are amongst the leading pathologies treated by single drug, microemulsion systems. These diseases typically occur concurrently with a wide variety of other illnesses. Image taken from Callender et. al. (2017)[1] with permission.

Not only have microemulsions been used for the treatment of numerous pathologies, their small droplet sizes also afford delivery via a wide range of administration routes including oral, topical, parenteral and intranasal. **Figure 1.7** depicts the various routes of administration targeted by microemulsion systems based on publications from 2011-2016.[1]

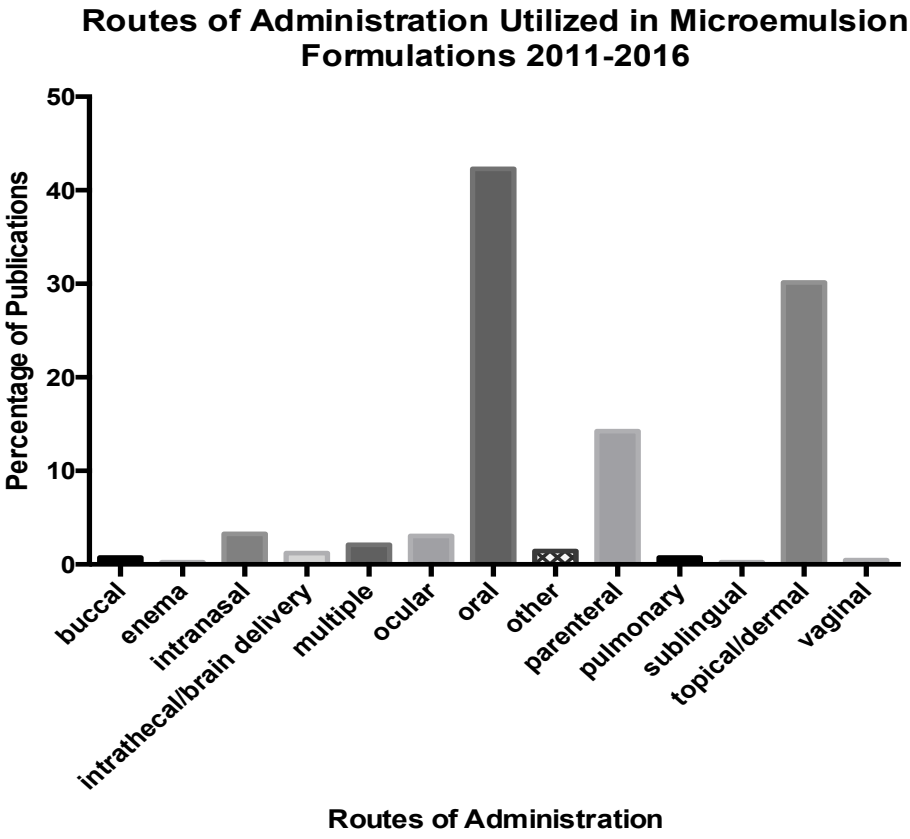

Figure 1.7: Microemulsion drug delivery publications by route of administration. Most microemulsion formulations contain non-ionic surfactants (discussed further in **Section 1.3**) which are generally regarded as the safest type of surfactant for ingestion purposes. Hence, most microemulsions are delivered via the oral route. The small droplet sizes of microemulsions also allow for favourable penetration in topical and parenteral delivery, as well as pulmonary and intranasal delivery to a lesser extent. Figure taken from Callender et. al. (2017)[1] with permission.

iii) Solubilization & Simultaneous Delivery of Hydrophilic and Hydrophobic Drugs

Another major advantage of microemulsion systems is their ability to solubilize poorly water-soluble drugs (PWSDs). More than 40% of drugs in the development phase fail to reach the market due to poor biopharmaceutical properties, including poor water solubility.[12,54,55] PWSDs often experience unfavourable dissolution profiles *in vivo* leading to dissolution being the rate-limiting step with respect to absorption.[56-59] Microemulsions are also able to solubilize hydrophilic APIs given the presence of both a hydrophilic and hydrophobic phase. Thus, the incorporation and delivery of both hydrophilic and hydrophobic APIs, separately and simultaneously is possible using microemulsion systems. Oil-in-water microemulsions are

well suited for lipophilic drug delivery while water-in-oil microemulsions are well suited for hydrophilic drug delivery. Bicontinuous microemulsions of the Type IV Winsor type are well suited to the delivery of both hydrophilic and hydrophobic drugs, simultaneously.

There is an increasing need for multi-drug therapies given the rapidly aging Canadian population and the growing burden of chronic diseases that tend to occur concurrently.[17] In addition, the low patient adherence to concurrent disease treatments due to pill burden, exacerbates the already large burden on the health care system.[25] Thus, the area of combination therapies represents an unfulfilled need that microemulsions may resolve.

However, despite the substantial need for multi-drug therapies in Canada and the potential of microemulsion systems for multi-drug delivery, little research in this area has been performed to date. In a five-year period from 2011-2016 **(Figure 1.8),** microemulsions were predominantly formulated for use in single drug delivery as indicated by over 95% of publications in this period. In contrast, microemulsions formulated for multi-drug therapy purposes accounted for under 5% of publications published in this period. Many of the microemulsions formulated for use in multi-drug delivery consisted of active ingredients of the same degree of hydro- or lipophilicity.[1] In addition, the most common type of microemulsion formulated was Type I, O/W microemulsions due to the predominant delivery of lipophilic active ingredients in comparison to that of hydrophilic active ingredients.[1] **Table 1.2,** below**,** displays a list of microemulsion, multi-drug formulations that have been researched and published between 2011-2016.

iv) Spontaneous Formation and Simple Starting Ingredients

The ability of microemulsions to form spontaneously[32,60] due to the ingredients being driven to an energy state favourable for microemulsion formation[32,45,61-64] results in an economical formation process. This means that in many cases, a high degree of energy is not required for microemulsion formation, unlike in the case of nano- and macroemulsions, resulting in a cost-effective production method. Additionally, the simplicity of the components comprising microemulsion systems renders them suitable for drug delivery of almost every type. Surfactants and oil components are readily available and mostly economical for formulation purposes.

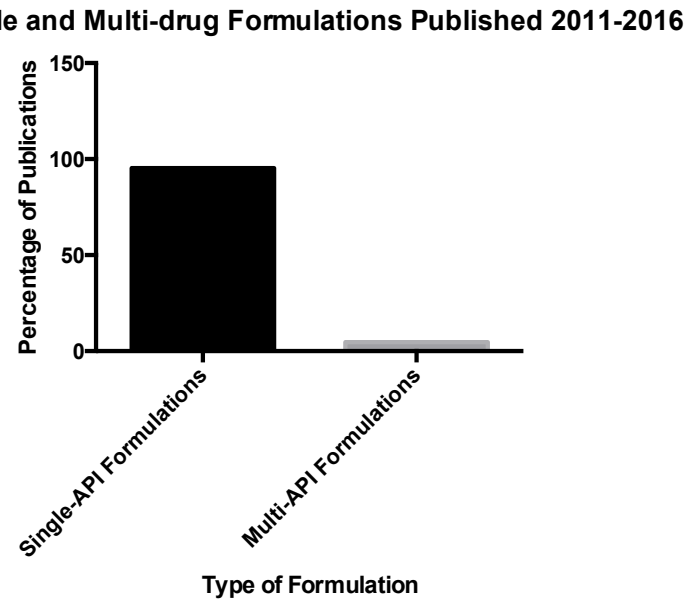

Figure 1.8: The distribution of research involving single and multi-drug microemulsion formulations published in peer-reviewed journals between 2011-2016. Due to their complex nature, multi-drug formulations are rare, comprising a mere 4.6% of total publications in this period. Figure taken from Callender et. al. (2017)[1] with permission.

1.2.3.2 Disadvantages of Microemulsion Systems

Although microemulsions possess a number of advantages, their complex nature does not always make them a viable option for drug delivery. The presence of both an organic and aqueous phase allows for the delivery of both hydrophobic and hydrophilic APIs; however, this becomes problematic when dealing with APIs that do not fall into either category. In the case of prenatal supplements, minerals are a prime example of this. Minerals, metals and other compounds that do not fall into either of these categories, once added to a microemulsion system, would likely result in a suspension. In cases like this, a solid dosage form such as a tablet is likely a better option. Thus, microemulsion systems may not always be a favourable method of delivery for complex ingredients. It is also important to remember that in the case of microemulsions, APIs must be solubilized in their respective phases.

Table 1.2: Publications regarding microemulsion, multi-drug delivery Jan 2011- April 2016. The majority of these publications involved type I oil-in-water microemulsion drug delivery systems. Table taken from Callender et. al. (2017)[1] with permission.

APIs	Function	Formulation Ingredients	Microemulsion Type	Observations	Ref.
Honokiol (p-gp inhibitor) Sirolimus (p-gp substrate)	Immunosuppressant	Cremophor® EL (emulsifier), Propylene glycol (co-emulsifier) and Medium chain triglycerides (MCT) [9:2:9 w/w/w]	I (SMEDDS)	Improved oral absorption and transport of sirolimus	65
Curcumin Silibinin (UGT-mediated clearance inhibitor)	Antioxidant Antiinflammatory	Cremophor® EL (emulsifier) and Carbitol™in 2:1 w/w with Captex®355 as oil (10:1 w/w surfactants to oil)	I (SMEDDS)	Improved curcumin bioavailability in vivo	66
Curcumin Piperine (clearance inhibitor)	Antioxidant Antiinflammatory	Cremophor® RH40 (emulsifier), Transcutol® HP (co-emulsifier), Capryol™ 90 (oil)	I (SMEDDS)	Improved local concentration of curcumin in colonic lesion site	67
Simvastatin Phytosterols (reduce cholesterol absorption)	Statin	Sucrose ester (surfactant) an 1,2-propanediol (co-surfactant) [2:1 w/w] and oleyl lactate as oil (9:1 w/w surfactants to oil)	Lipophilic dispersed in hydrophilic compounds (without water) SMEDDS	Favourable solubilization for both compounds in 1,2-propanediol + nonionic + anionic surfactant	68
Atorvastatin Ezetimibe (inhibits cholesterol uptake)	Statin	Tween® 80 (surfactant), PEG 600 (co-surfactant) [5:1 w/w], ethyl oleate as oil (4:1 w/w surfactants to oil)	I (SMEDDS)	Higher bioavailability and faster dispersion	69
Lycopene Ascorbic acid (protects against lycopene degradation)	Antioxidant UVB- inhibitor	Decylglucoside: propylene glycol (1:1 w/w surfactant blend) and monocaprylin as oil	I or III	Additive rather than synergistic effect observed; monocaprylin as the oil	70

		[50:20:30 w/w/w surfactant:oil:water]		choice increased cutaneous delivery	
Rifampicin Isoniazid Pyrazinamide	Anti-tuberculosis	Brij® 96 (surfactant), butanol (co-surfacatant), ethyl oleate as oil [1.2:2 oil to surfactant w/w]	I	Rifampicin (lipophilic) localized near to oil interface; Isoniazid and pyrazinamide (hydrophilic) near to hydrophilic interface	71
Indomethacin Benzocaine	Anti-inflammatory Anesthetic	Tween® 80 (surfactant), ethanol (co-surfactant), eucalyptus oil and water [30:30:20:20 w/w, respectively]	I	Synergistic effect obtained	72
Evodiamine Rutaecarpine	Anti-inflammatory & antinociceptive	Cremophor® EL (emulsifier), PEG 400 (co-emulsifier) and ethyl oleate [surfactant:co-surfactant:oil:water 30:15:5:50 w/w/w/w]	I	Enhanced permeation and absorption when abdominally applied	73
Lidocaine Prilocaine	Anesthetic	Tween® 80 (surfactant), ethanol (co-surfactant), saturated lipids (Labrasol® and Lauroglycol™ 90); isopropyl myristate as oil; water and API mix [30%:5%:60%:5%, respectively]	I	Enhanced skin permeation and absorption	74
Betamethasone dipropionate Salicylic acid	Antiinflammatory Keratolytic	Tween® 20 (surfactant), isopropyl alcohol (co-surfactant); oleic acid and sefsol (1:1) as oil and water. [Surfactant mix (1:1): oil: water 38:15:47]	I	Enhanced permeation, reduced dosage frequency, sustained drug release	75

Green tea catechins Caffeine	Antimicrobial	Cremophor® EL (emulsifier), glycerol (co-emulsifier) [6:1 w/w] and Labrasol as oil	I	Synergistic effect against *E.coli*	76
Bleomycin Cisplatin Ifosfamide	All chemotherapeutics	Cremophor® RH40 (surfactant): Labrasol® (surfactant): Transcutol® HP (cosurfactant): Capryol™90 (co-surfactant): Isopropyl myristate (oil) (2:2:6:1:1)	I (SMEDDS)	Increased inhibitory effect on human cervical HeLa cells	77
Coix seed oil Etoposide	Ancillary drug for chemotherapeutics to improve undesirable immunologic suppression Chemotherapeutic	Cremophor® RH40 (surfactant); PEG 400 (co-surfactant); Coix seed oil (oil)	I	Enhanced cytotoxicity against A549 cells; promoted significant internalization of etoposide	78
Huperzine A Ligustrazine	Acetylcholine esterase inhibitor for Alzheimer's treatment Antioxidant	Cremophor® RH40 (surfactant), ethanol (co-surfactant), oleic acid (OA), water [12:4:1:80 w/w/w/w]	I	Demonstrated slowed progression of Alzheimer's disease in rats	79
Albendazole sulphoxide Curcumin	Neurocysticercosis treatment Antiinflammatory	Tween® 80 (surfactant), ethanol (co-surfactant), DHA:Capmul 1:1 (oil), water [surfactant:oil:water 60:30:10 w/w/w)	I	Enhanced intranasal delivery when formulated with DHA (docosahexaenoic acid)	80
Bovine serum albumin Cytochrome c	High-molecular weight model hydrophilic proteins	Pluronic F127 (surfactant); monoglyceride, polyglycerol ester, and tetradecane as oil mix	II	Promoted sustained release	81

As a result, the extent of solubilization is limited by the volume of phase available. This could prove to be a limiting factor depending on the amount of API required for delivery.

Microemulsions also require the presence of emulsifiers at a slightly higher concentration than their nanoemulsion counterparts.[32] Some emulsifiers demonstrate toxicity (**Section 1.3.5**), and as a result are heavily regulated. This reduces the list of available surfactants for use in oral formulations. Those surfactants that *are* considered acceptable are only acceptable at certain concentrations. This rule also applies to oils. Finally, microemulsions are sensitive to temperature and salinity changes and may undergo phase changes when exposed to higher or lower than normal temperatures or salinity concentrations. This could lead to 'breaking' of the microemulsion and eventually, phase separation. It is thus, important to identify the temperature and salinity boundaries of the microemulsion system during the formulation stage.

1.2.4 Self-emulsifying Drug Delivery Systems (SEDDS)

SEDDS are a specialized category of emulsions. SEDDS are isotropic mixtures of oil, surfactant and sometimes co-solvent that are able to self-emulsify upon mild agitation and dilution with aqueous media to form O/W emulsions. These fine oil/water dispersions are able to spread throughout the gastrointestinal (GI) tract, as the digestive system provides the agitation needed for the microemulsion to form.[82] SEDDS may be microemulsions (referred to as self-microemulsifying drug delivery systems- SMEDDS) or nanoemulsions (self-nanoemulsifying drug delivery systems- SNEDDS).

According to the lipid formulation classification system (LFCS), SEDDS consisting of water-insoluble surfactants and oil are regarded as Type II LFCS formulations while those with oil, surfactant and a co-solvent are regarded as Type III LFCS formulations with optical clarity and smaller droplet sizes.[82] SEDDS, particularly of the oil-in-water type, are a common emulsion formulation of choice for drug delivery, as demonstrated below in **Figure 1.9.**[1]

Macro-, nano- and microemulsions possess a variety of different properties, which are suitable for various applications. **Figure 1.10** below summarizes the differences discussed in this section between macroemulsions, microemulsions and nanoemulsions.

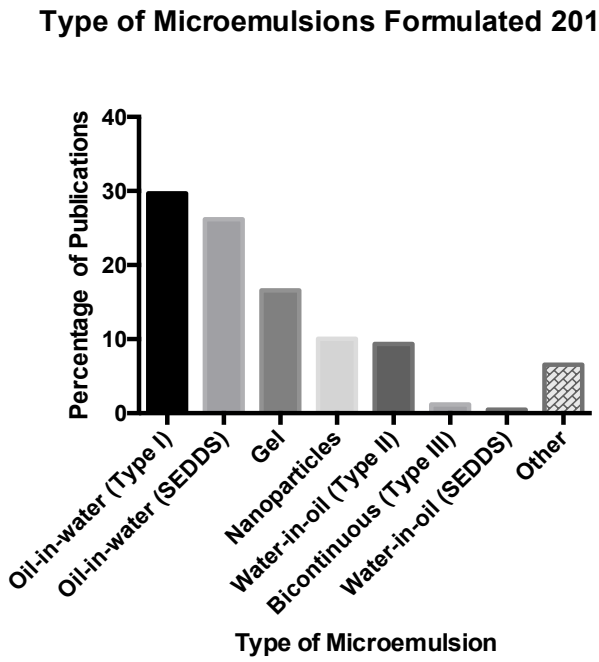

Figure 1.9: Types of microemulsion systems utilized in drug delivery from 2011-2016. Due to the fact that most new chemical entities are lipophilic, oil-in-water microemulsions comprised over 50% of publications in this period. Microemulsion systems have also been used as a basis for nanoparticle formation. Figure taken from Callender et. al. (2017)[1] with permission.

1.3 The Role of Surfactants in Microemulsion Systems

As noted earlier, surfactants and/or emulsifying agents are essential components of any emulsion system. At a simple organic-aqueous interface, there is a difference in the potential energies between the molecules in the bulk liquid and those lying at the interface. Molecules lying at the interface possess higher potential energies as a result of their interactions not only with molecules of their respective phases, but also with molecules of the opposing liquid across the interface.[28] This increase in potential energies represents the minimum work required to form the interface, or the interfacial tension. Upon addition of an amphiphilic emulsifying agent or surfactant, the hydrophilic portions of the molecule orient themselves with the molecules of the aqueous phase (and vice versa for hydrophobic portions with the organic phase). This results in stronger interaction energies between the amphiphile and respective phase, as compared to the system without an emulsifier. As a result, the overall interfacial

tension is reduced, promoting miscibility. Without a surfactant, it would be impossible to sufficiently stabilize such a system.

Emulsion	Types	Particle Size (diameter)	Energy Required?	Type of Stability
Macroemulsion	O/W and W/O	>400 nm	Yes	Kinetic
Nanoemulsion	O/W and W/O	100-400 nm	Yes	Kinetic
Microemulsion	Type I: biphasic O/W; Type II: biphasic W/O; Type III: triphasic bicontinuous Type IV: monophasic	10-100 nm	No	Thermodynamic

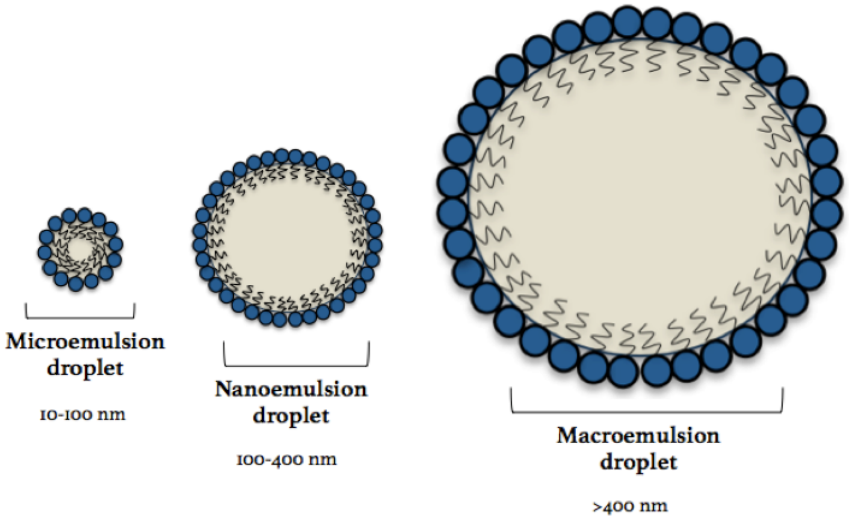

Figure 1.10: Types and typical droplet diameter sizes of macro-, nano- and microemulsions. O/W droplets are depicted here. Image and table taken from Callender et. al. (2017)[1] with permission.

Where very low interfacial tensions are desired, co-surfactants may be added. Co-surfactants act in consort with surfactants to further reduce interfacial tension and introduce an element of flexibility into the interfacial film. This allows the system to adapt a wider variety of curvature values across a wider range of conditions for droplet formation.[83] Medium chain alcohols (8-12 carbons in length) or oils such as ethyl esters of fatty acids are often used as co-surfactants as they reduce interfacial tension as well as introduce flexibility into the interfacial film.[83] Co-surfactants can also have additional effects on an emulsion system. They can change

surfactant-partitioning characteristics, adjusting a parameter called the hydrophilic-lipophilic balance (HLB) (explained in **Section 1.3.2**), which can dictate the type of emulsion formed.[83] Co-surfactants can also curb the formation of gel-like and crystalline phases that inhibit emulsion formation and act to decrease sensitivity to fluctuations in structure.[83]

Surfactants and co-surfactants are typically selected based on the type of emulsion desired, as the type of emulsion formed depends heavily on the type of emulsifier used.[28] According to the well-established Bancroft rule (1913), O/W emulsions are produced by emulsifiers that are more soluble in water than oil while W/O emulsions are produced by emulsifiers that are more soluble in oil than water.[84] In other words, the continuous phase of any emulsion is dictated by the phase in which the emulsifier is most soluble. This rule is counterintuitive, as emulsion formation can often be thought to depend on the relative volumes of oil to water. In addition to the Bancroft rule, several additional theories have been suggested for emulsion formation. Qualitative theories generally involve consideration of the interactions, i.e. interfacial tension and contact angles, between each immiscible phase and the emulsifier. Kinetic theories like those proposed by Davies (1957)[85], as described by Rosen and Kunjappu (2012)[28], rely on the rate of coalescence of each immiscible phase; the phase with a faster coalescence rate becomes the continuous phase of the macroemulsion. Regardless of the theory of emulsion formation proposed, the type of emulsifier plays a key role in the formation of any emulsion system.

1.3.1 Types of Surfactants

Surfactants may be categorized into four broad classes based on the nature of the hydrophilic head group. **Table 1.3** below describes each class of surfactant, the nature of the head group as well as examples of each.[86]

Though there are benefits to each surfactant class, non-ionics are most commonly used in drug delivery applications regardless of the route of administration. Non-ionic surfactants do not possess charged head groups like their ionic or zwitterionic/amphoteric counterparts. This affords them a lower critical micelle concentration (the concentration at which micelles form and thus, can solubilize active ingredients- **Section 1.3.4**) than their ionic counterparts due to an absence of electrostatic repulsion between head groups.[87, 88] Thus, these surfactants are also more resistant to the effect of charge and pH changes compared to the other surfactant

Table 1.3: Types of surfactants based on nature of their head group as well as examples of each.[86]

Type of Surfactant	Nature of Head Group	Examples
Anionic	Negatively-charged	Carboxyls, Sulphates, Sulphonates, Phosphates
Cationic	Positively-charged	Quaternary Ammonium Bromides
Non-ionic	Neutral	Polyoxyethylenes (POEs), R-polyol groups including sugars e.g. Tweens, Spans
Zwitterionic/ Amphoteric	Both negative and positive charges present/ Either negative or positive based on environmental conditions such as pH	Sulfo-betaines

classes.[86] In addition, they are known to have a better oral safety profile than ionic surfactants[89-93] and many are generally recognized as safe (GRAS) by the FDA for ingestion (**Section 1.3.5**). These advantages often result in non-ionics being preferred for use in pharmaceutical formulations. Anionic surfactants are slightly more toxic than non-ionics and thus, less common in pharmaceutical formulations while cationic surfactants are rarely used due to their high toxicity profiles.[91, 94] Near the isoelectric point, zwitterionic surfactants may possess a neutral net charge, leading them to behave in a similar fashion to non-ionic surfactants.[86] **Figure 1.11** depicts the distribution of surfactant class in microemulsion drug formulations from 2011-2016.

As seen below, non-ionic surfactants dominated almost 90% of the microemulsion formulation research between 2011-2016, likely due to their uncharged nature, insensitivity to salt/pH changes and favourable safety profile. Amphoteric surfactants (mainly natural oils such as lecithins and phospholipids) were the second most popular choice comprising almost 7%, likely due to their neutrality attributed to the cancellation of charges near the isoelectric point. Cationic surfactants are considered the most toxic of all the classes due to their positive charges, which interfere with the negative cell membranes of mammalian cells (**Section 1.3.5**). This explains their low occurrence in many microemulsion formulations.

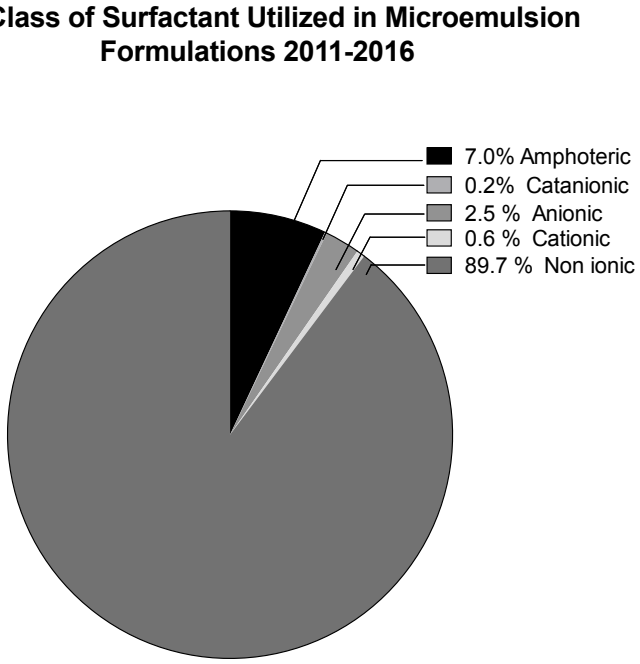

Figure 1.11: Classes of surfactants utilized in microemulsion formulations between 2011-2016. Figure taken from Callender et. al. (2017)[1] with permission.

1.3.2 The Role of Hydrophilic-Lipophilic Balance (HLB)

Hydrophilic-lipophilic balance (HLB) is a surfactant parameter proposed by Griffin in 1949 that relates the structure of a surfactant to its emulsification potential.[95] The proportion of the amphiphilic hydrophilic group to that of the hydrophobic group is classified quantitatively resulting in an arbitrary scale of 0-20 where a HLB value <10 indicates surfactant hydrophobicity and >10 indicates surfactant hydrophilicity.[95] Over the past few decades, HLB has become quite standard in the surfactant field and few commercial surfactants are shipped today without an HLB number on the label. The general equation for HLB[96] is:

$$HLB = 7 + \sum(hydrophilic\ group\ numbers) - \sum(hydrophobic\ group\ numbers) \quad \textbf{(Eq1.1)}$$

From the equation above, it can be seen that a high HLB corresponds to a higher degree of hydrophilic groups while a low HLB corresponds to a lower degree of hydrophilic groups. Thus, a high HLB number corresponds to a hydrophilic surfactant, and tendency to form O/W emulsions or normal micelles while a low HLB number corresponds to a hydrophobic surfactant and tendency to form W/O emulsions or reverse micelles. Given that HLB is a

summative parameter, and that it depends on the relative proportion of hydrophilic groups to hydrophobic ones, it can be seen that the introduction of co-surfactants or linkers into the emulsion system can affect the HLB value. For formulators, the Bancroft rule combined with the HLB number can be used to obtain the desired emulsion system for drug delivery purposes. For example, if delivery of a lipophilic drug is desired, it is best to solubilize the lipophilic drug in an oily micellar core. Thus, an oil-in-water emulsion system would be most suitable and thus, a surfactant with a high HLB can be chosen.

Although HLB is arguably one of the most important surfactant parameters for formulators, two additional surfactant parameters to consider are the efficiency and effectiveness in the formulation in which the surfactant is meant to be active. Efficiency in the context of emulsifiers is the concentration required to reduce the interfacial tension by 20 mN/m. Effectiveness is the maximum reduction in interfacial tension that a surfactant can achieve at a particular concentration. A more effective surfactant is one that lowers the interfacial tension to a greater extent than another. Surfactant efficiency can be improved by increasing the number of carbon atoms in a straight-chain hydrophobic group or through the addition of a fluorocarbon.[28] Branching within the surfactant or the addition of a phenyl group decreases efficiency.[28] Effectiveness can be controlled through the ionic strength of a solution for ionic surfactants, or via the hydrophobic tail for polyethoxylated non-ionic surfactants.[28]

1.3.3 The Critical Packing Parameter (CPP)

The critical packing parameter (CPP) is a quantitative parameter that predicts the degree of surfactant packing at an interface or in the bulk (aqueous) solution.[97] The degree of packing is a function of surfactant structure and greatly influences the type of microemulsion obtained. The equation for CPP is shown below. **Table 1.4** also depicts expected aggregate structures in relation to surfactant CPP, taken from Myers (2005).[96,97]

$$CPP = \frac{V}{al} \qquad \textbf{(Eq. 1.2)}$$

where CPP = critical packing parameter (dimensionless parameter)
V = volume of the hydrophobic portion of the surfactant molecule
a = area of the surfactant head group
l = length of the hydrophobic tail

Surfactants with large head groups tend to form spherical micelles of the O/W type (CPP <0.33) while those with large tail groups tend to form inverse micelles of the W/O type (CPP >1). Surfactants with head and tail groups of relatively equal size demonstrate similar volumes and a × l values resulting in a CPP of close to 1, and the formation of bilayer structures.[96,97] Thus, in addition to surfactant concentration (depicted earlier in **Figure 1.4**), surfactant molecular geometry also plays an important role in the type of aggregates expected.

Table 1.4: Expected aggregate structures on the basis of surfactant CPP. Adapted from Myers (2005).[96,97]

Critical Packing Parameter	Expected Aggregates	General Surfactant Description
< 0.33	Spherical micelles	Single chain surfactants with large head group
0.33-0.5	Cylindrical/ Rod-shaped micelles	Single chain surfactants with small head groups; ionic surfactants in presence of high amounts of electrolyte
0.5-1	Vesicles Bilayer structures	Double chain surfactants with large head groups and flexible chains
1	Planar Bilayer structures	Double chain surfactants with small head groups or rigid chains
> 1	Inverted micelles	Double chain surfactants with small head groups and very large, bulky hydrophobic groups

Recent work by Rodriguez-Abreu (2019) has linked the packing parameter to HLB.[98] Generally, with nonionic, polyethoxylated surfactants, spherical structures were favoured at high HLB values, cylindrical structures at intermediate HLB values and bilayers at low HLB values. [98] With respect to morphological transitions, the HLB required for a transition from bilayers to cylindrical structures (CPP 1 to 0.5) is approximately in the range of 10-15. In addition, the HLB required for further transition from cylindrical structures to spherical (CPP 0.5 to 0.33) is approximately in the range of HLB 12-17. With respect to the effect of surfactant concentration, the HLB required for the transition from bilayer to cylinder to spherical structures increases with increasing surfactant concentration.

1.3.4 The Critical Micelle Concentration (CMC)

Critical micelle concentration (CMC) is the concentration of amphiphile at which micellar aggregates form.[97] At an organic-aqueous interface, upon addition of amphiphilic species, these species concentrate at the interface with their polar heads oriented towards water and their non-polar tails oriented towards oil. However, upon continual addition of amphiphile, the interface becomes saturated such that additional amphiphiles organize themselves into spherical structures called micelles. Thus, at and above the CMC, micellar aggregates are assumed to be the predominant structure.[97] If a hydrophilic surfactant is used, O/W micelles are formed with a polar 'shell' and non-polar 'core'. If a hydrophobic surfactant is used, W/O micelles are formed with a non-polar shell and polar core.

Micelle formation follows two possible models: i) Mass action model where surfactant monomers and micelles are assumed to be in equilibrium and ii) phase separation model where micelles are considered to constitute a new, separate phase at and above CMC. Given the variation in thermodynamic models of micelle formation, there are many methods to determine CMC.[97] Conductivity, dynamic light scattering, fluorescence and tensiometry are just a few of these methods, but each method makes certain assumptions. Thus, absolute experimental CMC values may vary greatly depending on the method, even by an order of magnitude.[97] Therefore, in systems containing low surfactant concentrations, one would ideally conduct surface tension measurements using a variety of methods in order to ensure use above the CMC. This is, however, not a concern in microemulsion systems due to the relatively high surfactant concentrations utilized. Many factors such as the hydrophilic group, hydrophobic group, counterion effects in the case of ionic surfactants and other external factors affect CMC.[97] In general, greater hydrophobicity either through extension of the alkyl chain or reduction of the size of the polyoxyethylene (PEO) head groups in non-ionic surfactants, causes a reduction in CMC.[97] Consequently, an increase in hydrophilicity increases CMC.[97]

Tensiometry is one particular method of measuring CMC. Increasing amounts of surfactant are titrated into an aqueous solution and the tension at the surface is measured using a ring or plate. As surfactant is continuously added to the aqueous solution, a steady decrease in surface tension is seen until the surface becomes saturated with surfactant. At this point, additional surfactant molecules begin to arrange themselves into micelles and the decrease in surface tension becomes negligible or constant. This point is known as the critical micelle

concentration. On a semi-logarithmic plot of surface tension versus surfactant concentration, a linear decrease in surface tension is seen followed by a plateau or negligible further decrease in surface tension. The intersection of these two lines is identifiable as the CMC. Aggregation number, i.e. the number of surfactant monomers comprising each micellar structure, affects this curve as the larger the aggregation number, the sharper the transition from monomers to micelles.[97] The critical micelle concentration of mixed surfactant systems may also be determined in this manner.

In microemulsion systems, more than one surfactant is often used for HLB modification, stability or flexibility purposes in the case of co-surfactants.[1] With respect to mixed surfactant systems, the expected or 'ideal' CMC of a surfactant mixture is obtained with consideration of the mole fraction of each individual surfactant:[99]

$$\frac{1}{\mathrm{CMC}ideal} = \frac{a}{cmc1} + \frac{1-a}{cmc2} \qquad \textbf{(Eq. 1.3)}$$

where a= the mole fraction of surfactant 1
cmc1= critical micelle concentration of surfactant 1
cmc2= critical micelle concentration of surfactant 2

If the ideal CMC is lower than that of the individual CMCs of surfactant 1 and 2, the mixture is considered favourable and synergistic in nature. If the ideal CMC is higher than that of the individual CMCs of each surfactant, the surfactant mixture is considered unfavourable and antagonistic in nature. Synergistic surfactant mixtures afford a lower CMC and thus, a lower amount of surfactant becomes necessary in the pharmaceutical formulation. Considering the variation in absolute CMC values obtained through different experimental methods, the comparison of individual surfactant CMC values with that of the respective surfactant mixture are of greater importance than the absolute CMC values themselves.

1.3.5 Safety Considerations for Surfactant Use

Safety considerations for surfactant use in pharmaceutical products depend largely on the type of surfactant used. In general, charged surfactants such as anionics, cationics and to a lesser extent, zwitterionics, tend to exhibit greater toxicity than their uncharged, non-ionic surfactant

counterparts.[100] Charged surfactants are more able to interact with structural components of the cell membrane including proteins and lipids, causing disruption in their structural integrity.[100] Though non-ionics are also able to interact with structural components of the cell membrane through associations such as hydrophobic interactions, these interactions are generally weaker than charge-charge interactions.[100] Solubilization of cell membrane components is also possible depending on the detergent-protein or detergent-lipid w/v% ratio.[100] It has been noted that the w/v% required for 90% solubilisation of membrane protein is lower for charged species than uncharged species, e.g. 0.9% for sodium dodecyl sulphate (SDS), an anionic surfactant versus 5% for Triton X-100, a non-ionic surfactant.[100]

In terms of absorption, non-ionic alkyl polyoxyethylene esters reported rapid and extensive gastrointestinal absorption of approximately 75%.[100] Cationics, particularly cetyltriammonium bromide (CTAB), reported up to 80% gastrointestinal absorption after 8 hours while anionics of the linear alkyl benzene sulphonates type reported 60% recovery after intraperitoneal injection.[100] With respect to metabolism, it has been reported that the ester link of non-ionic Polysorbate surfactants is easily degraded by intestinal lipase while the polyoxyethylene groups are not well absorbed and are mostly excreted.[100] Cationics and anionics were found to have slower metabolism rates[100], prolonging their effects in the body.

The United States Food and Drug Administration (US FDA) provides useful guidelines for surfactant use in pharmaceuticals based on previously approved drug products. These guidelines are available through their Inactive Ingredient (IIG) Database[101], which lists the names, amounts and GRAS (generally recognized as safe) statuses of surfactants used in FDA-approved drug delivery formulations. Routes of administration as well as dosage forms are also listed. These are used as effective guidelines for acceptable surfactant amounts in drug delivery formulations. It is interesting to note that with respect to oral drug delivery, charged surfactants such as anionics and cationics are virtually non-existent in the IIG database. Instead, these types of surfactants are mostly listed in detergents and shampoos.

1.4 Oral Drug Delivery

Oral drug delivery is often preferred over parenteral routes of administration due to its non-invasive nature, therapeutic efficiency and ease of administration, which result in high patient

compliance.[102-104] The cost-effectiveness, low sterility demand, ease of production and variety of available dosage forms lend further support to this type of drug delivery.[102,104]

The process of oral drug delivery varies based on pharmaceutical properties such as the type of drug or dosage form, and physiological conditions such as gastrointestinal transit time, pH, enzyme activity and microflora.[102] However, in general, the process of oral drug delivery begins in the mouth where mucus, enzymes and saliva (pH 6.2-7.6) act to moisten and even disintegrate the dosage form, depending on its composition.[102,105] The dosage form leaves the mouth and transits the esophagus before reaching the stomach where up to 3 L digestive fluid, comprised of hydrochloric acid, mucus, enzymes such as pepsinogen/pepsin and bicarbonate, are secreted every 24 hours.[102,103,106]

Gastric pH varies based on whether a fed or fasted state is encountered; fasted gastric pH may range from ~ 0.3-1.9 while fed gastric pH may be as high as 5.[102,103] Gastric pH is also a function of regional variations within the stomach itself.[105] The proximal area of the stomach is generally of higher pH (~3) than the distal area due to the presence of fewer parietal cells that secrete hydrochloric acid.[105] Nevertheless, immediate-release dosage forms disintegrate in the stomach, facilitating drug dissolution and possible drug transformation before absorption in the small intestine.[102,103] Contents may remain in the stomach for up to 4 hours[107], where low pH, small surface area and the presence of enzymes and microflora act as barriers to subsequent drug absorption.[102] Release into the small intestine occurs via gastric emptying, which is largely controlled by the nature of the gastric contents; high fat, salt and acidity reduce emptying time.[105] It is also dependent on the size of the dosage form, whether it is ingested in a fasted or fed state and, in the case of the latter, the volume of liquid/food ingested.[105] Once in the small intestine, however, drug remnants are acted upon by enzymes (trypsins, lipases, nucleases), bile/bile salts and sodium bicarbonate, which facilitate lipid digestion and neutralization of stomach contents (chyme) to pH ~8.[106] The exact pH of the small intestine varies by section; the duodenum is approximately neutral at pH 7 while the jejunum and ileum are slightly alkaline above pH 7.[103] Nevertheless, the presence of villi as well as a transit time of up to 6-7 hours facilitates the majority of drug absorption.[102,107] Absorption may occur through simple, passive diffusion or active transport.[108] Most small, hydrophobic drugs are absorbed across intestinal cells through passive, transcellular pathways while their hydrophilic counterparts must be absorbed through receptor-mediated transcellular pathways or paracellular pathways

(in the space between cells).[109] The rate and extent of absorption depends on drug solubility and dissolution as discussed later in **Section 1.7.3.**[102]

The high bacterial population and presence of mucus, fecal matter and dietary residues greatly inhibit further drug absorption in the large intestine.[102,107] These challenges may be slightly offset by the prolonged transit time of at least 17 hours.[102,107] The pH of the colon generally lies between 6-8 depending on regionality[105], and is influenced by the presence of short chain fatty acids (weak acids, pKa 4.8)[102].

Transportation of absorbed drug material to the liver presents perhaps the greatest challenge to oral drug delivery in the form of the first-pass effect.[110,111] Extensive drug metabolization may drastically reduce the amount of active ingredient reaching systemic circulation.[110,111] Such effects may be bypassed through administration of the drug in highly lipophilic form to target the lymphatic rather than the portal route to circulation.[110,111] In addition, pharmaceutical strategies to improve oral drug delivery outcomes include particle size reduction mechanisms, chemical modifications such as pH, drug dispersion in a carrier for protection or solubility purposes (as in the case of emulsions) and complexation/chelation with compounds that increase dissolution or absorption.[102,108]

1.5 Techniques in Microemulsion Formulation

Over the past century, a number of techniques have been used to identify and formulate microemulsion systems. Ternary phase mapping and oil/water titration methods have been employed for years as the most effective manner in which to identify microemulsion phase behaviour. Recently, however, more progressive techniques such as the hydrophilic-lipophilic deviation (HLD) equation have transformed our understanding of microemulsion formation. These two techniques are described in detail below.

1.5.1 Ternary Phase Diagram (TPD) Mapping

Surfactant phase behaviour, including the propensity to form microemulsions, is best represented by phase diagrams and in particular, ternary phase diagrams (TPDs). TPDs consist of three graduated axes ranging from 0% to 100% representing the concentrations of the three main components of microemulsion systems: surfactant, oil and water.[1] Where co-surfactants

are used in combination with surfactants, this surfactant/co-surfactant mixture is treated as a single component and the diagram is referred to as a pseudo-ternary phase diagram (pTPD). The axes are read in a clockwise direction and each point in a TPD plot corresponds to a specific w/w% ratio of surfactant: oil: water (**Figure 1.12**).

TPDs and pTPDs are of tremendous importance in deducing surfactant phase behaviours and types of microemulsions that may be obtained with certain surfactant/co-surfactant, oil and water concentrations. This technique affords identification of specific surfactant:oil:water ratios or regions most useful for a particular application, and their boundaries. In general, as previously explained, hydrophilic surfactants tend to form O/W microemulsions, represented on the TPD in **Figure 1.12** as the region to the bottom left. Hydrophobic surfactants tend to form W/O microemulsions, dominating in the bottom right of the TPD in **Figure 1.12** while higher order structures of greater surfactant concentration tend to dominate at the top of the TPD in **Figure 1.12** as previously alluded to in **Figure 1.4**.

Traditionally, TPDs are generated through oil- and water-titration methods where various ratios of surfactant:water and surfactant:oil are titrated with oil and water, respectively, until a clear, homogenous system, or microemulsion, is obtained. This affords fast formation and deduction of Type IV microemulsion regions but ignores other resulting microemulsion types and phase behaviours. A more comprehensive approach to TPD mapping involves weighing various ratios of surfactant, oil and water into vials, mixing them together by simple manual shaking or stirring and leaving them to settle for a period of time before evaluating phase behaviour. These behaviours may then be plotted on a TPD. Such an approach affords changes along various tie lines to be determined so that care may be taken during formulation to stay within these boundaries and not venture beyond such regions. Therefore, the comprehensive approach to TPD mapping provides a 'snapshot' of surfactant phase behaviour with a particular oil type at a particular temperature. Comparisons of identical systems at increased or decreased temperatures or with varying oil types may then be made in order to deduce microemulsion sensitivity to each factor, along with possible phase transition behaviours.[1] These phase behaviours are imperative in predicting the boundaries and limits of: i) microemulsion application (e.g. coarse emulsions for lotions/creams versus Type IV microemulsions for multi-drug delivery), (ii) microemulsion route of administration (e.g. high water content for oral delivery versus high oil content for topical administration) and (iii)

microemulsion stability (e.g. resistance to change in microemulsion type upon water dilution). Thus, although considered an old and relatively simple technique, TPD mapping, especially when performed in the comprehensive manner described above, introduces invaluable insight and a degree of prediction into microemulsion behaviour and functionality. Although TPD mapping provides a 'snapshot' of microemulsion formation potential at specific conditions, the hydrophilic lipophilic deviation (HLD) equation, in contrast, affords prediction of microemulsion phase behaviour in consideration of multiple conditions, simultaneously.

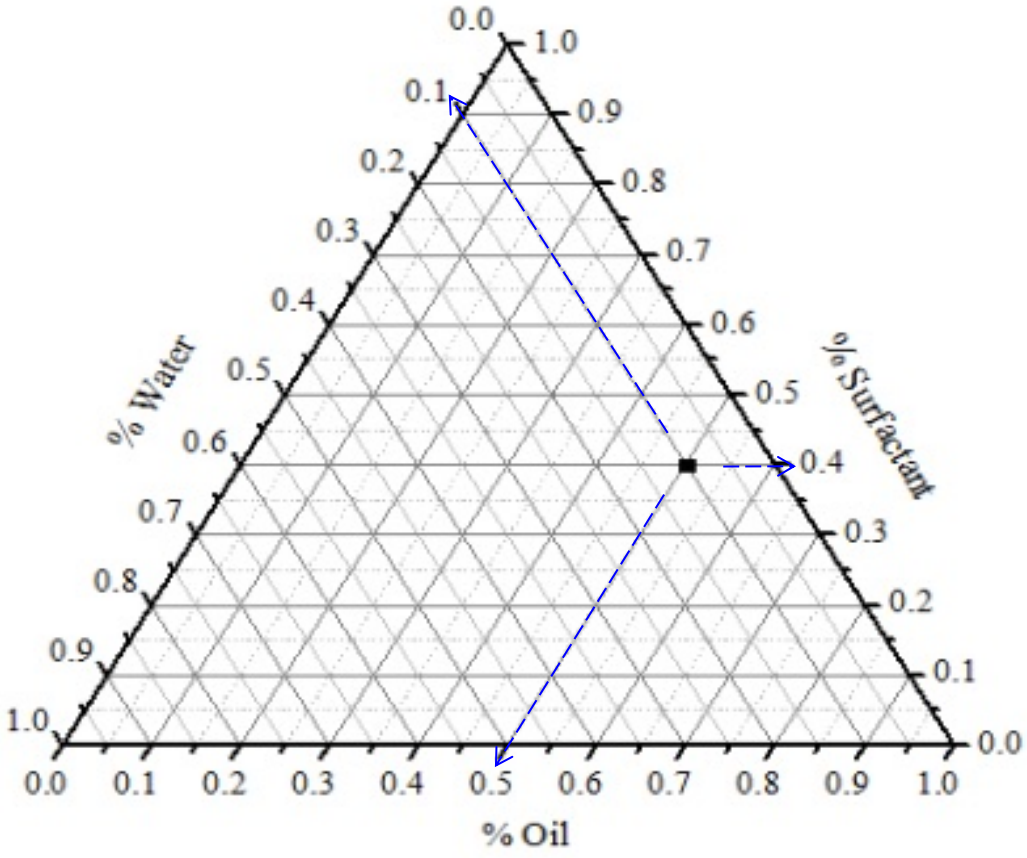

Figure 1.12: Example of ternary phase diagram of surfactant:oil:water. Each axis represents w/w% concentrations from 0-100% and is read in the direction indicated by the blue arrows. Therefore, the square point corresponds to a surfactant:oil:water ratio of 40:50:10.

1.5.2 The Hydrophilic-Lipophilic Deviation (HLD) Equation

In 1979, Salager et al. linked five major variables to microemulsion formation, laying the groundwork for the hydrophilic-lipophilic deviation (HLD) equation.[112] Prior to this, the landscape of microemulsion formation was fairly different, although theories of microemulsion

formation evolved steadily over the previous century. Bancroft's rule of formation in 1913[84] was followed by Winsor's proposal of the R-ratio in 1948[37], Griffin's hydrophilic-lipophilic balance (HLB) classification system in 1949[95] and Shinoda's exploration of the phase inversion temperature (PIT) in 1964.[113] Similar to Bancroft (1913) (discussed in **Section 1.3**), Winsor (1948) also proposed a study of the amphiphile and its interactions with surrounding organic and aqueous solvents as a means of emulsion formation.[37] The Winsor interaction ratio, R, is given by the following equation:

$$R = \frac{A_{CO}}{A_{CW}} \qquad \textbf{(Eq. 1.4)}$$

where A is the solvent attraction between i) amphiphile (c) and oil (o) and ii) amphiphile (c) and water (w). This equation was developed to account for the interaction energies of an amphiphile adsorbed at an oil/water interface.[37] A high R-value corresponds to increased interactions between the amphiphile and organic phase leading to the formation of W/O emulsions.[37] The role of the R-ratio in the modern day HLD equation is described later. Around the same time, Griffin (1949) proposed the HLB as a system of surfactant classification and prediction of microemulsion formation based on the molecular structure of the surfactant[95] (**Section 1.3**). More recently, Shinoda and Arai (1964) identified a particular instance of microemulsion formation possible through a gradual heating of ethoxylated, non-ionic surfactants, resulting in a change from an oil-in-water (O/W) microemulsion to a W/O microemulsion, a parameter called the phase inversion temperature (PIT).[113] The above four theories were sound in their own right and have uniquely contributed to, and advanced our understanding of, emulsion science over the past century. However, these theories possessed a number of limitations including a primary focus on the properties of the amphiphile and immediate organic/aqueous solvent environment, as well as an assumption of the use of pure surfactants. Such focus was considered somewhat short sighted as emulsion formation often occurs in an uncontrolled environment influenced by external factors, using commercially produced surfactants that behave very differently than their pure counterparts.[112] Thus, Salager et al. (1979)[112] using anionic, sulphonate surfactants and a semi-empirical methodology, linked five major variables namely salinity, oil alkane carbon number (ACN), alcohol

type/concentration, surfactant structure and temperature, to optimum microemulsion formation, resulting in the following modern-day HLD equations:

$$HLD = b(S) - K(EACN) - \phi(A) + {}_{CT}\Delta T + CC \quad \textbf{for non-ionic surfactants} \quad (\textbf{Eq. 1.5})$$

$$HLD = \ln(S) - K(EACN) - f(A) - {}_{\alpha T}\Delta T + CC \quad \textbf{for ionic surfactants} \quad (\textbf{Eq. 1.6})$$

where S is the salinity concentration in g/100 ml, EACN is the effective alkane carbon number of the oil (a measure of oil lipophilicity), f(A) and ϕ(A) depend on the type and concentration (w/w%) of co-surfactant or alcohol added, ΔT is the change in system temperature upon heating and CC is the characteristic curvature of the surfactant reflecting its hydrophilic/lipophilic nature. The parameters b, K, αT and CT are empirical constants associated with the type of salt and surfactant used.[114] The parameter 'b' accounts for the addition of electrolytes and the potential salting-out effect on non-ionic, ethoxylated surfactants due to reduced hydration of the polyethoxylated head group.[115] Monovalent and divalent ions partition differently in microemulsions formulated with non-ionic surfactants.[116] Surfactants have been found to be more sensitive to temperatures in solutions containing monovalent ions than divalent ones.[116] Thus, the value for 'b' for non-ionic surfactants has been experimentally determined to be 0.13 for sodium chloride, 0.10 for calcium chloride and 0.09 for potassium chloride as determined by the slope of the graph of optimal salinity versus mole fraction of alkyl polyethoxylated non-ionic test surfactants.[115,117] Originally, the parameter 'k' was determined experimentally to be 0.16 ± 0.01 based on the slope of the natural log of salinity (ln S) versus EACN for alkyl aryl sulphonate surfactants (anionics).[112] It was later determined to be between 0.1 and 0.2 to take into account the induced dipole interactions between the surfactant and oil phase.[115] Today, it is generally accepted that k=0.17 for most surfactants[115,118] with specific examples including sodium dihexyl sulfosuccinate (SDHS) being 0.17, sodium dodecyl sulphate (SDS) being 0.1, and some iso-phenol ethoxylated non-ionic surfactants being 0.15.[115,117,119] Finally, the parameters αT and CT are constants that consider the effect of increasing temperature on the weakening of hydrogen bonds between water molecules only (αT) and between water molecules and oxygen in the ethoxylated surfactant head group (CT). These values have been determined experimentally to be -0.01 K^{-1} for a number of alkyl anionic surfactants (αT) and 0.06 K^{-1} for a number of non-ionic,

polyethoxylated surfactants (CT) based on the slope of the natural log of salinity (ln S) versus temperature.[112,115,117-120] Evidently, the HLD equation takes into account a number of important factors affecting microemulsion formation, affording a greater degree of predictability in the microemulsion formation process.

It is important to note that some of the variables highlighted by Salager et al. (1979) were previously investigated. The relationship between salinity and "optimum" (Type III) microemulsion formation was previously investigated for oil recovery purposes[121,122], as was the relationship between alcohol type / concentration and optimal salinity[123-125], and the relationship between surfactant molecular weight and optimal salinity.[126] Despite these previous works, however, Salager et al. (1979) was the first to correlate these variables into a semi-structured, empirical equation.[112] In fact, Salager et al. (1979) categorized these variables into three types:

i) formulation variables (salinity, oil ACN, alcohol type / concentration and surfactant structure)
ii) external variables (temperature and pressure) and
iii) position variables in ternary phase diagrams (surfactant concentration and oil/water ratio).[112]

In microemulsion science, the practical use of the HLD equation involves the formation of Type III microemulsions, also known as 'optimal' formulations/microemulsions. These Type III microemulsions were considered 'optimal' due to their ultra-low interfacial tensions which originally afforded recovery of petroleum from water-flooded reservoirs.[114] In **Section 1.2.3**, we have described Type III microemulsions as three-phase systems comprised of an upper excess oil phase, a middle bicontinuous microemulsion region and a lower excess water phase. The amphiphilic molecules in these three-phase, bicontinuous systems exhibit no particular preference for either the organic or aqueous phase. Therefore, the interactions between surfactant and water, and surfactant and oil are considered equal, and the hydrophilic-lipophilic deviation or difference (HLD) is said to be zero (0). This mirrors the Winsor R-ratio of 1, which also suggests equal interactions between the surfactant and oil, and the surfactant and water. Thus, an HLD value of 0 or an R-value of 1 corresponds to a Type III microemulsion. In contrast, a negative HLD value or R-value <1 corresponds to a Type I, O/W microemulsion and a positive HLD value or R-value >1 corresponds to a Type II, W/O

microemulsion. Once a Type III microemulsion is formed, either from a Type I or Type II microemulsion as depicted in **Figure 1.13**, one can then set the HLD value to 0 and solve for other equation variables such as EACN and CC. These variables may then be increased or decreased depending on the type of microemulsion system desired, i.e, a shift to a more negative HLD for O/W systems or to a positive HLD for W/O systems.

It can be seen from **Figure 1.13** that a transition from a Type I → Type III → Type II microemulsion is possible through salinity or temperature modifications while a transition from a Type II → Type III → Type I microemulsion is possible through lipophilicity modifications.[114] These transitions can be explained through consideration of the Winsor ratio, R and the interactions between surfactant, oil and water. Recall that the interactive Winsor ratio, R (**Eq. 1.4**) involves 'A_{CO}' which indicates solvent attraction interactions between surfactant and oil molecules, and 'A_{CW}' which indicates solvent attraction interactions between surfactant and water molecules. An increase in parameters such as temperature or salinity results in a decrease in interactions between surfactant molecules and that of water.[127] This leads to an increase in R and thus, a progression from a Type I → III → II microemulsion.[127] An increase in effective alkane carbon number (EACN) or lipophilicity results in an increase in both interactions between surfactant molecules and oil molecules, and interactions between oil molecules, the latter having a greater effect.[127] This leads to a decrease in R and thus, a progression from a Type II → III → I microemulsion.[127] Type IV microemulsions are typically obtained from Type III microemulsions upon an increase in surfactant concentration.

Overall, the modern day HLD equation was conceived through consideration of i) five major variables and ii) the Winsor ratio, R involving interations and chemical potentials via the surfactant affinity deviation (SAD) parameter (a quantification of the free energy of transfer of a surfactant molecule from the aqueous phase to the oil phase).[114] In microemulsion drug delivery, the HLD equation provides a useful way of determining the effects of lipophilicity, temperature and surfactant curvature on drug-loaded formulations. This eliminates the need to re-plot TPDs with drug-loaded oil or water phases and is especially ideal in situations where multiple APIs are involved, as TPD plotting would be quite tedious and impractical in this instance.

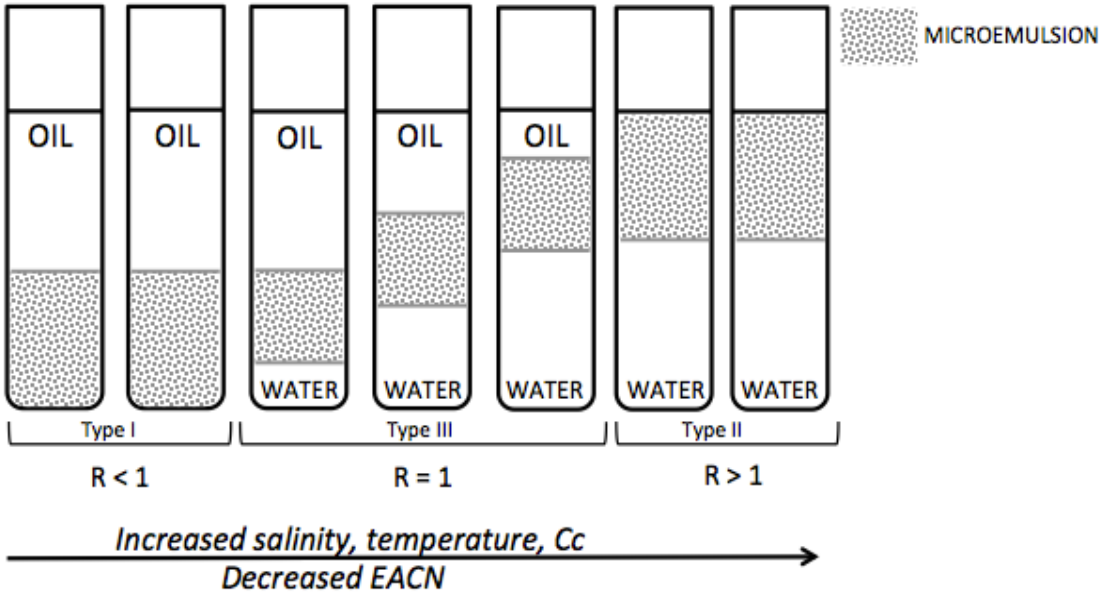

Figure 1.13: Formulation scan expected outcomes for microemulsion phase transitions given changes in salinity, temperature and oil lipophilicity based on the principles of the Winsor ratio, R. 'Oil' and 'water' labels represent excess phases. In the case of excess oil, the microemulsion is of the O/W type while in the case of excess water, the microemulsion is of the W/O type. In the case of both excess oil and water, the microemulsion is of the bicontinuous type.

1.5.2.1 Advantages of the HLD Equation

The development of the HLD equation has afforded a number of advantages in microemulsion science. Perhaps of highest importance, the equation although semi-empirical, considers the effect of a number of formulation, external and position variables, as defined previously, on microemulsion formation. Prior to the development of this equation, the Bancroft rule, Winsor R-ratio, HLB value and PIT were used to predict microemulsion formation behaviour. Though useful, these theories relied heavily on the structure of the amphiphile and its interactions with the surrounding solvents rather than on the effect of other contributing variables. Thus, microemulsion formation was still largely performed on a trial and error basis. The HLD equation eliminates much, though not all, of the trial and error previously associated with microemulsion formation. In addition to the simple consideration of external factors affecting microemulsion formation, the HLD equation affords adjustment of the HLD value itself, once all equation parameters are known. In turn, each equation parameter may also be adjusted once the HLD value is known. Therefore, it is evident that the HLD equation affords a novel

optimization process for microemulsion formation not afforded by previous microemulsion methods.

The HLD equation is also unique in that it accounts for both ionic and non-ionic species. Based on the works of Shinoda and Arai (1964), certain surfactant classes such as non-ionics were well known to be particularly sensitive to the temperature parameter.[113] This is accounted for in the non-ionic HLD equation, as is the salinity parameter in the HLD equation for ionic surfactants. Previous theories of microemulsion formation were often unable to distinguish between ionic and non-ionic amphiphiles. Thus, although the work of Salager (1979)[112] was originally based on the investigative work of sulphonates, a specific surfactant class of anionics, the HLD equation was later refined to account for modifications in surfactant type.[114]

Finally, the use of commercial surfactants in microemulsion formation is not as large a setback as in previous microemulsion theories. The surfactant parameter or characteristic curvature (CC) of commercially utilized surfactants may be determined experimentally so as to reduce the effect of any unpredictability with respect to impure surfactant use, a problem which had plagued many earlier microemulsion formation theories.

1.5.2.2 Limitations of the HLD Equation

Despite the many advantages of the HLD equation, there are limitations that do not completely alleviate the complications of microemulsion formation. It must be noted that first and foremost, the HLD was originally a semi-empirically derived equation.[112] A number of anionic, sulphonate surfactants along with various alcohols were evaluated with salinity, temperature and oil ACN in order to determine the effects of each variable on the system, as well as any correlations amongst them.[112] These correlations were then organized into a structured equation. The semi-empirical nature of the HLD equation suggests that the value of the parameters obtained may not be an exact representation of what is occurring within the system. In addition, the output of the HLD equation has no numerical scale. Values are simply determined to be zero, positive or negative with no understanding of what constitutes a large or small difference in value. Therefore, with respect to optimization, there is no clear numerical boundary or criteria that can be set. Another drawback revolves around how the values themselves are obtained. Certain variables such as temperature and salinity are easily obtained.

However, values such as EACN and CC are complicated, especially when utilizing mixtures of commercial oils and surfactants. These values are largely obtained through formulation scans, which still involve a great deal of trial and error. Such formulation scans also rely heavily on the use of volumes versus that of mass or weight which are more common in microemulsion formation. Hence, the HLD is not only a semi-empirical equation that does not completely eliminate the process of trial and error, but it also requires the values of all parameters to be known which demands the need for a robust library of values for practically infinite surfactant and oil types and combinations.

1.6 Prenatal Multivitamins: A Multi-Drug Model

Prenatal supplements are vitamins and minerals taken by women before, during and even after pregnancy (during breastfeeding) in order to promote healthy fetal development. The United States Food and Drug Administration (US FDA) and Health Canada state that in order to supplement a healthy diet, prenatal supplements may be consumed by women planning on becoming pregnant, women in their first trimester of pregnancy and breastfeeding women.[128,129] Prenatal supplements should contain a variety of essential water-soluble and fat/oil-soluble vitamins and minerals including Vitamins A-E, Vitamin K and calcium and iron.[128] Some of these vitamins and minerals are specifically recommended for inclusion in prenatal supplements due to their importance in fetal development. These include folic acid[130], docosahexaenoic acid (DHA) from Omega-3 fatty acids[131] and iron[129], whose roles in fetal development are described below in **Tables 1.5-1.7**.

Many factors contribute to prenatal supplements acting as an optimal multi-drug model in this thesis work. The primary advantage is that these supplements contain multiple active ingredients of varying hydro- and lipophilicity, often in higher quantities than that of typical multivitamins due to fetal requirements. This provides multiple layers of complexity due to the vastly different physicochemical, solubility and stability properties of each API, as well as the heightened potential for API-API interactions given the increased quantities of each. Considering that the goal of this work is to formulate a microemulsion system capable of complex, multi-API delivery, this pre-natal supplement model satisfies those requirements. In addition, the majority of approved prenatal supplement products are marketed in solid, powder

form (**Section 1.6.3**). As noted earlier, solid formulations may experience inferior absorption when compared to liquid formulations due to the extra dissolution step required. Thus, the formulation of a microemulsion containing these prenatal active ingredients would not only fill a market need, but would be advantageous in terms of comparing any enhanced dissolution effects of the microemulsion formulation with a solid or suspension formulation.

1.6.1 The Role of Prenatal Vitamins and Minerals

Each vitamin and mineral recommended by the US FDA and Health Canada for expectant, pregnant and breastfeeding women plays an important role not only in bodily function but in healthy fetal development. **Tables 1.5-1.7** highlight the structural and functional properties of some of these compounds, including their BCS class and octanol-water partitioning coefficient profiles (log P). In general, it can be seen that the water-soluble vitamins consist of low log P values while the oil-soluble vitamins consist of higher log P values. In addition, due to the high aqueous solubility of the water-soluble vitamins, most are classified as BCS class III compounds while the low aqueous solubility of oil-soluble vitamins leads them to be classified as BCS Class II/IV compounds. All vitamins and minerals are important in the regulation of bodily function but folic acid, docosahexaenoic acid (DHA) via Omega-3 fatty acids and iron are of particular importance in fetal development.

Table 1.5: Physicochemical properties of some water-soluble vitamins typically included in prenatal multivitamin supplements. [130, 132-139]

Water-soluble Vitamins [130,138,139]

Hydrophilic API	Structure	Log P	BCS Class	Function
Vitamin B1 (Thiamine Mononitrate)	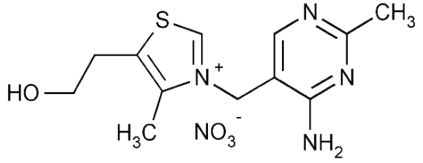	-3.1	III	Co-factor for enzymes involved in energy metabolism (Krebs Cycle) (combines with ATP to metabolize carbohydrates)
Vitamin B2 (Riboflavin)	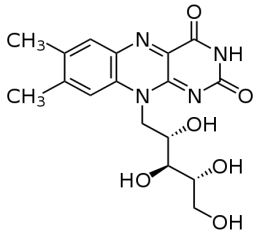	-0.92	III	Precursor for enzymes (flavin electron carriers) involved in energy metabolism (Krebs Cycle)
Vitamin B3 (Niacinamide)	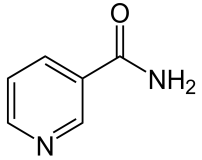	-0.39	III	Precursor for enzymes (NAD+) involved in energy metabolism (Krebs Cycle)
Vitamin B6 (Pyridoxine Hydrochloride)	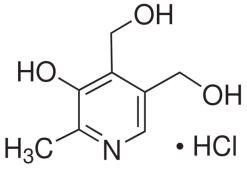	-0.95	III	Co-enzyme involved in aminoacid metabolism

Vitamin B9 (Folic Acid)	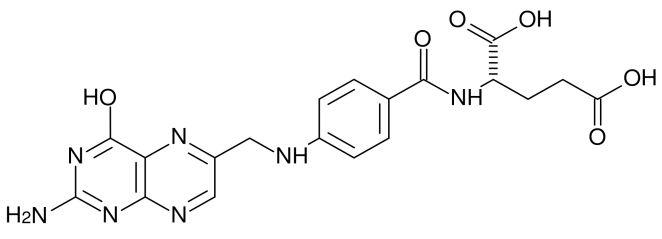	-0.68	IV (high solubility at lowest strength)	• Co-enzyme involved in DNA and RNA metabolism • Aids enzymes in aminoacid catabolism and blood production • In pregnant women (1st trimester) prevents fetal neural tube defects and fetal cardiovascular anomalies
Vitamin B12 (Cyanocobalamin)	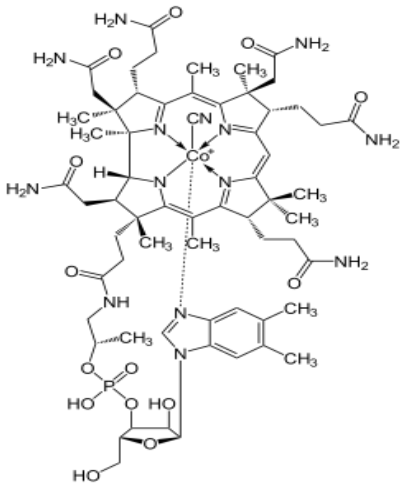	-14	III	Co-enzyme involved in DNA and RNA metabolism Involved in red blood cell production

Table 1.6: Physicochemical properties of oil-soluble vitamins typically included in prenatal multivitamin supplements. [140-145]

Oil-soluble Vitamins [131,138,139]

Hydrophobic API	Structure	Log P	BCS Class	Function
Vitamin A (Beta Carotene: Precursor to Retinal/Retinol)	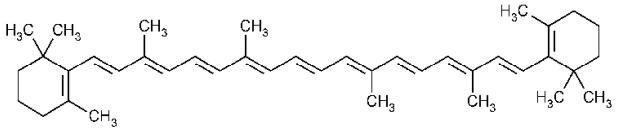	11.12	II/IV	Maintains epithelial tissue Produces visual pigments
Vitamin D_3 (Cholecalciferol)	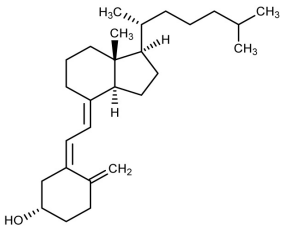	7.13	II/IV	Promotes calcium and phosphorus absorption
Vitamin E (Alpha-d-tocopherol acetate)	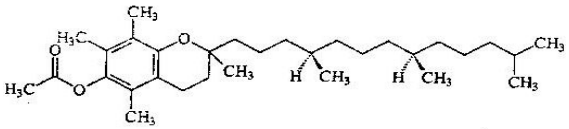	10.42	II/IV	Protects cell membranes due to antioxidant activity
Vitamin K_1 (Phytonadione)	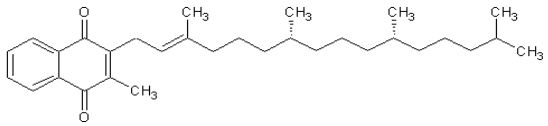	9.7	II/IV	Aids in formation of proteins especially in blood clotting
DHA/EPA Fish Oil	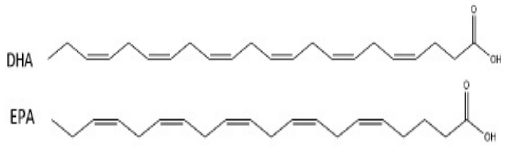	DHA= 6.75 EPA= 6.23	II/IV	During pregnancy, aids overall fetal growth and development including neurodevelopment

Table 1.7: Physicochemical properties of some important minerals needed in the body. Major minerals refer to minerals present in excess of 5 g in the body.
Minerals [138,146]

Classification	Mineral	Function
Major Minerals	Calcium	Aids bone/tooth formation, blood clotting and nerve transmission Produces visual pigments
	Magnesium	Cofactor in multiple enzyme systems regulating energy production; maintains nerve and muscle function
Minor/Trace Minerals	Iron	Major component in haemoglobin and myoglobin Critical in pregnancy due to infant haemoglobin demands; deficiency implicated in low birth weight and infant mortality
	Iodine	Aids in thyroid regulation

1.6.2 Health Canada Requirements

Health Canada has recommended daily allowances of specific vitamins and minerals for expectant and pregnant women.[147-149] These daily recommended amounts, with the exception of minerals, were used as a general guideline for the multi-drug, microemulsion formulation developed in this thesis work (**Table 1.8**).

Table 1.8: Daily recommended amounts of vitamins and minerals suggested for women who are pregnant or who may become pregnant.[147-149]

Class	Vitamin/ Active Pharmaceutical Ingredient (API)	Health Canada Recommended Daily Amount (mg)
Hydrophilic Vitamin	Vitamin B_1 (Thiamine mononitrate)	1.4
	Vitamin B_2 (Riboflavin)	1.4
	Vitamin B_3 (Niacinamide)	18
	Vitamin B_6 (Pyridoxine hydrochloride)	2
	Vitamin B_9 (Folic Acid)	0.6
	Vitamin B_{12} (Cyanocobalamin)	0.0026
Hydrophobic Vitamin	Vitamin A	0.55-0.77
	Vitamin D_3 (Cholecalciferol)	0.015
	Vitamin E	15
	Vitamin K_1 (Phytonadione)	0.09
	Omega-3 Fatty Acid (DHA)	3000
Minerals	Calcium	1000
	Magnesium	350
	Iron	27
	Iodine	0.22

1.6.3 Current Prenatal Supplement Dosage Forms

A variety of dosage forms for prenatal supplementation are currently in existence. According to the National Institute of Health (NIH) Dietary Supplement Label Database, which houses label information of all multivitamins currently marketed in the US, the majority of prenatal supplements are formulated as powders in tablet form.[150] Suspension formulations in caplets were the second most common form followed by liquid formulations in soft gelatin capsules.[150] Edibles such as gummies were the least common.[150] The NIH database produced no results with respect to emulsion prenatal supplements and instead returned only seven (7) emulsion products in total, one of which was a multivitamin in that it contained Vitamins D_3 and K_2.[150] All seven products were formulated as drinkable liquid dosage forms and were not encapsulated.[150] Thus, there is a demand for a microemulsion system capable of delivering both hydro- and lipophilic active ingredients in the form of a multivitamin formulation.

1.7 Microemulsion Evaluation Techniques

Provided the successful development of a microemulsion capable of multi-drug delivery, it is important to evaluate and characterize the resulting formulation. In general, evaluation of a microemulsion formulation involves first determining the solubility of each API in various microemulsion components, followed by characterization and in-vitro analysis via dissolution or disintegration. The techniques associated with these evaluation and characterization procedures are described below.

1.7.1 Saturation Solubility Testing

Solubility is the ability of solute (or drug, in this case) to dissolve in a solvent.[151] Saturation solubility is the maximum solubility of a particular solute in a particular solvent at equilibrium conditions.[151] It also depends on external factors such as temperature.[151] Poorly water-soluble compounds demonstrate low solubility in aqueous or aqueous-related media. Techniques such as concealed delivery in hydrophilic vehicles must, therefore, be employed to improve solubility.[151] In general, saturation solubility tests involve careful addition of measured solute or drug into a specific volume of solvent with stirring until saturation is reached. [152] This is typically indicated by the presence of excess solute at the bottom of the

vessel. The saturated solution is then analyzed using chromatography or spectroscopy, typically high or ultra performance liquid chromatography (HPLC or UPLC)/ ultraviolet (UV) detection.[152] The amount of solute (drug) recovered is compared against a calibration curve of peak area in order to determine the amount of drug dissolved per gram or litre of solvent at saturation. In microemulsion formulation studies, saturation solubility provides insight into drug solubility in the various surfactant, oil and water components in order to determine whether additional solubilization tehcniques may be required.

1.7.2 Characterization

The characterization of microemulsion systems on the basis of properties such as droplet size, charge, conductivity and morphology is crucial in confirming microemulsion type and predicting microemulsion behaviour and stability. Six important microemulsion characteristics are described below:

1.7.2.1 Droplet Size

Microemulsions typically possess small droplet sizes in the range 10-100 nm in diameter[1] but these boundaries are not thoroughly defined.[32] The advantages of such small droplet sizes are numerous, as described in the previous sections of this chapter, but largely include thermodynamic stability and the potential to improve bioavailability through an increased surface area to volume ratio. In addition to the numerical size itself, microemulsions are homogenous in nature, demonstrating uniformity in droplet sizes throughout the system. This homogeneity is another characteristic that may be determined via identification of the size distribution in a microemulsion sample. The two properties of droplet size and size distribution may be determined through light scattering techniques such as dynamic light scattering (DLS).

Dynamic Light Scattering (DLS), also known as Photon Correlation Spectroscopy (PCS), is a light scattering technique involving the irradiation of a sample with a narrow beam of light or laser at a specific angle and temperature. The laser beam, automatically modified by an attenuator based on the size of the particles in the sample, is shone onto a sample and the signal is then passed to a detector, correlator and finally, a computer. DLS

makes use of the natural Brownian motion of particles in a sample, as well as the Stokes-Einstein equation, in which larger particles diffuse or move more slowly than smaller particles.[153] DLS measures the scattering intensity of these particles within a sample using a time correlation function. Larger particles exhibit greater light scattering than that of smaller particles and given Rayleigh's theory that the scattering intensity is proportional to the sixth power of a particle's diameter[153,154], this higher intensity can be converted to a volume and number distribution.[153,155] Given that DLS correlates the movement of a particle with the size of a hard sphere particle that diffuses at the same speed as that of the sample[153], this poses complications for some surfactants, polymers and other surface-bound compounds on a particle, which do not conform to hard sphere morphology. Thus, the size output of the DLS method takes into account the presence of surface-bound compounds on a particular particle. This size output is referred to as hydrodynamic diameter rather than absolute diameter and is therefore, an overestimation of actual droplet size as it accounts for the immediate surrounding layer of solvent or other compounds on a droplet. DLS studies, such as those undertaken in this work, must be interpreted with caution as the current system being studied involves non-ionic surfactants with multiple PEO head groups as well as hydrophilic APIs which may surround the microemulsion droplet being studied. In addition to the measured droplet size, uniformity of size may also be measured using DLS. DLS measures the size distribution of particles using a value called the polydispersity index (PDI). PDI values indicate the homo- or heterogeneity of a sample with values below 0.1 indicating a very narrow, homogeneous droplet size distribution and values above 0.5 indicating a heterogeneous droplet size distribution.[153]

Although DLS is a rapid method for the particle size determination of relatively simple and dilute systems, complex concentrated samples such as microemulsions pose a challenge.[156] Concentrated samples often result in particle-particle interactions and multiple scattering.[157] Thus, dilution of microemulsion samples prior to measurement is often required[157,158], though this may result in changes to the microemulsion itself. Increased addition of aqueous solution to concentrated microemulsion systems causes transitions from higher order structures such as hexagonal, lamellar and cubic structures to spherical micelles.[159] Appropriate dilution, therefore, results in the determination of the size of

spherical micellar structures rather than the native microemulsion. [159] Microscopic methods may offer a more accurate representation of the droplet size of native microemulsion systems.

1.7.2.2 Zeta Potential

Zeta Potential (ζ Potential) is defined as the potential difference between the dispersed medium and the stationary layer of the dispersed medium attached to a dispersed particle or droplet.[153, 160-162] Zeta potential is, thus, an indication of the surface charge of a droplet or particle; however, it is important to distinguish that it is *not* the actual surface potential (i.e. surface charge) which will be larger in absolute value compared to the zeta potential. High zeta potential values, whether negative or positive, are indicative of high stability as electrostatically repulsive forces exceed attractive forces, the latter of which lead to coagulation or flocculation and thus, physical instability. [153, 160-162] Values above +30 mV and below -30 mV are used as an arbitrary scale for particle stability;[153,162] however, studies have shown that a more accurate indicator of stability is to examine the change in zeta potential with time or the zeta potential rate.[1,162] Given that zeta potential is an indication of surface charge, the most important factor affecting zeta potential is pH[153,160] as pH may confer certain charge effects on a particle. Additional factors include ionic strength and additives or impurities.[160] Given that the formulation in this work is pH adjusted in order to accommodate the hydrophilic APIs, it is important to characterize the charge of the droplets in this microemulsion system not only for stability purposes, but in order to deduce any possible charge effects or contributions by certain APIs or other components in the system.

Zeta Potential can also be measured using an appropriate DLS instrument. Samples are placed in a capillary cell containing electrodes on either side. The instrument uses a combination of Electrophoresis and Laser Doppler Velocimetry (LDV) that measures the velocity of a particle in a liquid upon application of an electric field, which is then equated to charge.[153]

1.7.2.3 Conductivity

Electrical conductivity may be used in conjunction with other experimental techniques in order to provide insight on microemulsion type.[155] Conductivity is the measurement of a

medium's ability to 'conduct' or pass electrical flow which is highly dependent on the ions present in solution. In microemulsion science, conductivity provides insight into the type of microemulsion present as water has the ability to conduct charge while oil does not. Thus, in an O/W microemulsion system where water is the continuous phase, conductivity readings are expected to be higher than those of a W/O microemulsion system where oil is the continuous phase.[33,155] Specific values for conductivity are not given and depend on the components of the microemulsion system but Yotsawmimonwat et al. (2006) indicated that some generalizations may be made as W/O emulsions report very low to almost zero conductivity while O/W emulsions report higher conductivities which may be best determined through comparison measurements of the conductivity of water utilized in the system.[163] This is due to the fact that tap, deionized, distilled and MilliQ water are vastly different in their conductivity potential. Conductivity is typically measured using a conductivity probe which measures the ability of the solution to conduct electricity between a pair of electrodes in a probe. The output is given in Siemens per meter or milliSiemens per centimeter and may be of great importance in multi-API formulations comprised of numerous charged species.

1.7.2.4 Rheology

Rheological studies are useful for determination of microemulsion type and even morphology to a limited extent. In terms of microemulsion type, rheology provides insight into Newtonian behaviour and thus, the type of microemulsion obtained.[155] Bicontinuous microemulsions, in particular, exhibit Newtonian behaviour or constant viscosity at low to medium shear rates and shear thinning at high shear rates as the bicontinuous structures are dismantled.[155] Type I and II microemulsions, however, exhibit Newtonian behaviour over a larger range of shear rates.[155] Though rheology provides insight into microemulsion type as well as aggregate type, it must be used in conjunction with other techniques in order to characterize a microemulsion system definitively.[155] Lower viscosity values indicate an O/W microemulsion while higher viscosity values indicate a W/O system.[33] As noted previously in our group, higher viscosities afford greater stability according to the Stokes-Einstein equation as the diffusivity of particles and thus, probability of collisions is low.[1]

In addition to microemulsion type, the morphological behaviour of microemulsion systems may also be deduced to a certain extent using rheological studies. Microemulsion systems are comprised of a number of aggregates of various shape and type. Rheological studies afford insight into the shape and type of aggregates present with larger aggregates resulting in increased viscosity.[155] In fact, rheological studies may enable the characterization of transitions in aggregate structure such as from spherical micelles to bicontinuous channels[155], with changes in certain factors such as water content.

1.7.2.5 Morphology

Morphology is one of the most important properties to be characterized in microemulsion systems. Droplet size measurements often lead to inflated results when light scattering techniques such as DLS are employed. Morphology, usually via microscopic techniques, affords a visual representation of the microstructures present in microemulsion systems. This is particularly important in order to deduce the type of structural properties or aggregates present[82,111,155], especially to confirm the presence of spherical aggregates. Transmission electron microscopy (TEM) is one of the most common microscopic techniques used to image microemulsion systems. A beam of electrons is focused onto a sample and magnified via a projector lens before hitting a fluorescent screen. Contrast studies using various stains are often performed.[155] Microemulsions as dynamic, liquid systems are difficult to image, however, and freeze fracture or cryo-TEM is often used to identify surface characteristics.[82,111,155] TEM and cryo-TEM afford visualization of microemulsions, bicontinuous structures and other mesophases including sponge phases[155] However, electron microscopic techniques have disadvantages with respect to possible artefact imaging and dehydration.[155]

1.7.2.6 Thermoanalytical Behaviour

Differential Scanning Calorimetry (DSC) is a calorimetric technique that measures the thermal properties of a sample. The difference in the amount of heat required to increase the temperature of a sample, with respect to a reference, is measured as the sample is subjected to consecutive heating and cooling cycles. These heating and cooling cycles correspond to

melting and crystallization points unique to each formulation[82], and are displayed as endo- or exothermic processes. Although there is certainly debate about the usefulness of this technique in microemulsion science, the identification of these exo- and endothermic peaks affords insight into the unique energetics of the microemulsion formulation and is most useful when compared to the individual components of the system such as the surfactant, oil and water components. In multi-API formulations, where interactions may be present, DSC profiles may be generated in order to determine the effects on melting and crystallization as well as possible instances of degradation.

1.7.3 Dissolution

In addition to the characterization techniques described above, dissolution is another important part of microemulsion evaluation. Dissolution in the context of pharmaceutics is the process by which a solid drug becomes dissolved in solvent and is a dynamic process. According to Shargel et al. (2012), the dissolution process for solid oral products includes (i) disintegration of the drug product, (ii) dissolution of the drug in aqueous solution and (iii) absorption across cell membranes.[59] The first step in the dissolution of a drug involves the dissolution of drug at the surface of the solid particle, resulting in the formation of a saturated solution around said particle.[59] This is followed by the diffusion of dissolved drug in saturated solution to the bulk solvent, from a region of high drug concentration to one of lower drug concentration.[59] Dissolution testing is, thus, an important precursor and indicator for predicting systemic absorption.[59] For hydrophilic drugs, dissolution is fast while permeation is slow, making the latter a rate-limiting step in absorption. For hydrophobic drugs, dissolution is slow and is considered the rate-limiting step.[59] Thus, the rate at which organic drugs dissolve tends to dictate the rate and extent of systemic absorption.[59] There are many methods for performing dissolution on pharmaceutical products.

1.7.3.1 Dissolution Methods

Dissolution tests are often performed in consideration of United States Pharmacopoeia (USP) guidelines, the standard for dissolution and disintegration regulation in North America, and many countries around the world. According to the USP, there are four (4) possible methods

of dissolution testing acceptable to regulatory agencies, depending on the type of product being tested (**Table 1.9**).[164]

Table 1.9: USP Dissolution Methods I-IV along with their mechanisms and suitability for pharmaceutical dosage forms.

Apparatus Number	Method	Mechanism	Utility
I	Basket	Vessel, drive shaft and rotating cylindrical basket with mesh	Immediate release & extended release tablets and capsules
II	Paddle	Vessel, drive shaft and rotating paddle	Immediate release & extended release tablets and capsules
III	Reciprocating Cylinder	Vessel, reciprocating glass cylinders with mesh (vertical motion)	Extended and controlled release tablets
IV	Flow-through Cell	Reservoir, pump, flow-through cell and water bath	Low-water soluble drug products

Table 1.9 outlines each type of apparatus along with its main components, mechanism of action and suitability for a wide range of dosage forms. In general, Apparatus I and II are considered the most common but each apparatus follows the same general procedure. The dosage form held in a basket, cylinder or reservoir is introduced to a vessel containing dissolution medium and subjected to agitation for a specified period of time. Samples are drawn at specific time intervals and the content is analyzed via spectroscopy and/or chromatography in order to deduce the concentration of drug dissolved at each time interval. Specifications or pass criteria typically include the dissolution of a certain percentage of drug, e.g. 70%, within a certain period of time, e.g. 30 minutes.[59]

1.7.3.2 Importance of IVIVC (In vivo- In Vitro Correlation)

As stated earlier, dissolution testing is a precursor for the prediction of systemic absorption. One of the purposes of dissolution testing is to deduce a relationship between in vitro dissolution testing and in vivo performance, or in vivo- in vitro correlations (IVIVCs).[59]

IVIVC is the relationship between the physicochemical property of a drug, such as dissolution rate, and a biological property of the drug, such as plasma drug concentration.[59] There are various levels of IVIVC; Level A correlations are the highest level and establish a point-to-point relationship between in vitro dissolution testing and absorption rate of the drug from the dosage form, Level B correlations are lower level and establish a relationship between mean in vitro dissolution time and mean in vivo dissolution time and finally, Level C correlations, the lowest level of all, typically demonstrate no statistical correlation and instead, establish a relationship between a single dissolution parameter and a pharmacokinetic parameter. [59] Though dissolution testing is important to establish IVIVC, such correlation studies were not undertaken in this thesis work, but are an important consideration for future analysis.

1.7.3.3 How is it Measured Practically? Pharmaceutical Application

Dissolution testing is typically conducted in accordance with USP standards as outlined in their respective modules. However, there are quite a few considerations. The dissolution test itself is valuable in formulation development but should be discriminating enough to detect changes in formulation variables such as particle size differences as well as manufacturing changes.[59] Thus, this type of testing should be able to distinguish between a pharmaceutically acceptable and non-acceptable dosage form, within the context of USP criteria for acceptable dosage forms.[59] There are numerous factors and conditions that affect dissolution testing including the type of drug itself (size, chemical stability, excipients), the media used (type, pH, concentration), environmental factors (temperature) and of course dissolution apparatus factors (agitation rate, placement of solid dosage in vessel). Nevertheless, the dissolution requirements for formulations containing vitamins and minerals, according to the USP, are outlined below in **Table 1.10.**

Table 1.10: USP dissolution requirements for vitamin-mineral dosage forms

USP Class	Combination of Vitamins or Minerals Present	Dissolution Requirement
I	Oil-soluble vitamins	Not applicable
II	Water-soluble vitamins	One index vitamin; folic acid (if present)
III	Water-soluble vitamins with Minerals	One index vitamin and one index element; folic acid (if present)
IV	Oil- and Water-soluble vitamins	One index water-soluble vitamin; folic acid (if present)
V	Oil- and Water-soluble vitamins with Minerals	One index water-soluble vitamin and one index element; folic acid (if present)
VI	Minerals	One index element

1.7.4 Disintegration

Disintegration as the name suggests, is the process by which any solid dosage form breaks apart in order to release drug material. Disintegration is defined as the state in which no residue, except for fragments of insoluble coating, remains on the screen of the test apparatus.[59] Specifically, this residue must not have a "palpably firm core".[59,165,166] According to the USP, the disintegration test is used to determine whether solid dosage forms such as tablets or capsules can disintegrate within a specified time in liquid medium given certain experimental conditions such as pH and temperature.[165] It is important to note that contrary to dissolution testing, disintegration tests do not provide information regarding the dissolution rate of a drug and thus, no IVIVC can be explicitly implied.[59] Instead, in addition to release time, disintegration tests afford insight into the presence of aggregates or fragments of the solid dosage form and are an important component in the quality control of tablet manufacture.[59]

1.7.4.1 Disintegration Methods

According to the USP, the disintegration apparatus is comprised of a basket rack assembly with 1000 mL low-form beakers of height 138-160 mm and diameter 97-115 nm, a heating

element capable of controlling temperature 35-39°C and a device for raising and lowering the basket in the immersion fluid at a constant rate of 29-32 cycles per minute.[165] There are additional details surrounding the range of motion and distance moved during each stroke, the required distance of the wire mesh and its submersion in the fluid as well as specifications of the basket rack itself in terms of diameter, thickness etc.[165] There is also a specific procedure for the evaluation of tablets and capsules depending on whether they are uncoated or plain-coated, intended for immediate or delayed release or their degree of effervescence.[165]

1.7.4.2 How is it Measured Practically? Pharmaceutical Application

Disintegration is measured in accordance with USP guidelines with consideration of the type of drug product being tested. In short, a certain number of drug product tablets or capsules must disintegrate within a specified period of time in order to obtain a 'pass' result. This period of time, as well as the media of choice, is dependent on the solid dosage form (capsule vs. tablet; coated vs. uncoated), route of administration (oral vs. buccal) and other considerations.[166] For uncoated or plain-coated tablets or capsules (hard-shell), disintegration must occur in 16 of 18 tablets within 30 minutes.[166] Soft gelatin capsules are held to a higher standard and require disintegration of 16 of 18 capsules within 15 minutes.[166] Delayed release tablets require disintegration of at least 16 of 18 tablets within an hour while solid dosage forms administered for buccal delivery, require disintegration within 4 hours.[166] According to Shargel et al. (2012), disintegration of a solid dosage product is usually more rapid than dissolution and absorption, except in the case of controlled release products.[59]

1.8 The Art of Formulation in Microemulsion Science

Despite the progression and advancement of microemulsion formation theories and evaluation techniques over the past century, microemulsion science is still primarily considered an art.[167] According to one of the founding fathers of Colloid and Surface Science, Tharwat F. Tadros (2018), the science of microemulsion has not yet progressed to a place where accurate predictions may be made about resulting phase behaviours when various components are mixed.[167] This is evident as even the most useful theory to date, the HLD equation, bears no numerical scale that can predict microemulsion formation behaviour. The

current approach is still largely based on trial and error and involves: i) determining the type of microemulsion desired, ii) selecting a surfactant based on HLB theory and iii) performing phase mapping via oil- or water-titration methods in order to obtain a suitable surfactant for a given oil and water ratio.

The above limitations may be discouraging but the HLD equation is still the most useful microemulsion formulation tool to date.[118] Abbott (2019) proposes, with good reason, that surfactant curvature may be more important than HLB given its consideration of parameters beyond simple surfactant structure.[118] In addition, surface excess concentration and area per surfactant molecule may be more useful than the CMC[118] given that surfactants are often used above this concentration anyway. Localization of the active ingredient in the micelle is also important as it provides insight into solubilization potential.[118] Regardless of these recommendations, given the sheer number of surfactant and oil combinations, researchers must ensure that published work is as explicit as possible such that a library of HLD, EACN and CC values at specific temperatures and concentrations can be built. In this manner, should one want to use a similar surfactant or oil composition, this can be facilitated.

The aim of this thesis body work is to attempt to improve the current state of the field by reducing the level of trial and error involved in microemulsion science and highlighting properties of emulsifying agents, as the heart of microemulsion systems, that may better predict microemulsion behaviour suitable for multi-drug delivery. In the absence of clear-cut evidence of specific emulsifying agent properties responsible for this type of drug delivery, it is hoped that at the very least, a process for the formulation of a microemulsion, multi-drug system may be obtained.

1.9 Objectives

1.9.1 Short-term Objectives

i) To design, formulate and optimize a basic microemulsion system capable of multi-drug delivery

ii) To incorporate multiple active pharmaceutical ingredients (APIs) of varying hydro- and lipophilicity into this basic microemulsion system

iii) To analyze the multi-drug loaded microemulsion formulation using a variety of microemulsion characterization techniques

1.9.2 Long-term Objectives

i) To develop a stable, multi-drug loaded microemulsion demonstrating superior dissolution over that of a conventional drug delivery form

ii) To identify emulsifying agent properties important in microemulsion, multi-drug delivery

1.9.3 Significance of Study

Life with concurrent, chronic disease is debilitating. In Canada, the increasing life expectancy and rapidly aging population has resulted in a steady increase in the burden of concurrent, chronic disease, resulting in an urgent need for multi-drug therapies. Currently, multi-drug therapies encounter severe challenges with respect to the incorporation of multiple drugs of varying hydro- and lipophilicity. Microemulsions, due to their small droplet sizes, thermodynamic stability and simple oil and water composition are an under-utilized tool for the complex, simultaneous delivery of hydrophilic and lipophilic drugs. Despite their popularity, however, microemulsion formation is still an unpredictable process. In this thesis, emulsifying agents, the heart of microemulsion systems, will be investigated in order to determine the most important properties necessary for multi-drug, microemulsion formation. The significance of this investigation is that through this understanding, microemulsion formation may be better predicted, advancing the development of multi-drug therapies that may reduce the burden of concurrent, chronic disease in Canada and worldwide.

1.10 Hypothesis Statement

Careful selection of structural emulsifying agent properties such as hydrocarbon chain length and polyoxyethylene (POE) content will lead to the development of a microemulsion system, 100 nm in diameter, capable of the simultaneous encapsulation of multiple hydrophilic and hydrophobic active pharmaceutical ingredients.

Chapter 2: Formulating a Microemulsion System: Surfactant Selection

2.1 Introduction

Emulsifying agents or surfactants are the heart of microemulsion systems. Without them, microemulsion formation is practically impossible. Therefore, the choice of surfactant is very important in the development of microemulsion formulations. As outlined in **Chapter 1**, there are generally four classes of surfactants to choose from based on the nature of the hydrophilic head group. However, non-ionic surfactants are most commonly used.

According to Callender et al. (2017), almost 90% of the research conducted on microemulsion drug delivery between 2011-2016 involved the use of non-ionic surfactants in the final microemulsion formulation.[1] This is likely due to the uncharged nature of the head group, low toxicity profile and GRAS status of non-ionics (**Chapter 1, Section 1.3**). As a result, evaluation of specific surfactants utilized in microemulsion drug delivery within this period resulted in mostly non-ionic surfactants being identified (**Figure 2.1**).[1] According to **Figure 2.1**, of the top 10 surfactants used in microemulsion drug delivery between 2011-2016, all were non-ionic with the exception of lecithin, an amphoteric surfactant.[1] Notable commonly used non-ionic surfactants were Polysorbate/Tween 80, Transcutol P and Cremophor RH 40/EL, although Transcutol was primarily used as a co-surfactant.[1]

Many of the surfactants presented in **Figure 2.1** from Callender et al. (2017) were hydrophilic in nature, with HLB values >10.[1] This was not surprising as the authors also found that lipophilic drug delivery accounted for almost 80% of the research publications between 2011-2016.[1] Given the Bancroft rule outlined in **Chapter 1,** and the fact that hydrophilic surfactants facilitate O/W emulsion formation and thus, lipophilic delivery, the use of predominantly hydrophilic surfactants was not surprising. In this thesis work, lipophilic delivery was generally prioritized given that many pharmaceutical products developed today are lipophilic in nature and exhibit poor biopharmaceutical properties.[2-4] Thus, prioritizing this type of delivery would provide insight into overcoming such challenges. For these reasons, O/W microemulsion formation was considered of great importance, requiring the use of hydrophilic surfactants to act as solubilizers.

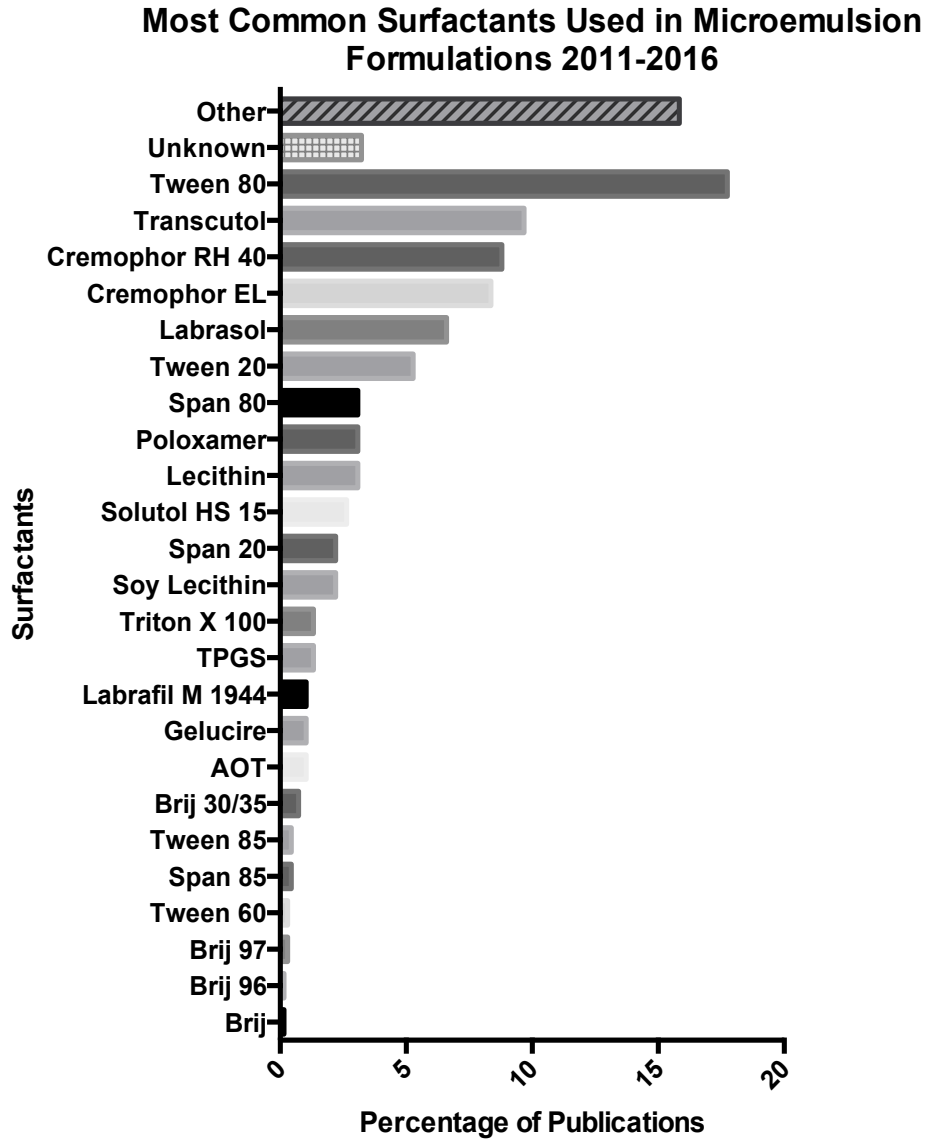

Figure 2.1: Top 25 surfactants utilized in microemulsion drug delivery formulations published in PubMed database between 2011-2016. Figure taken from Callender et al. (2017) with permission.[1]

A variety of non-ionic surfactants of varying classes such as Polysorbates and Poloxamers were desired for further evaluation in this work. Although Polysorbate 80, Transcutol-P, Cremophor RH 40 (PEG-40 hydrogenated castor oil) and Cremophor EL (PEG-35 hydrogenated castor oil) were the most commonly used surfactants in microemulsion drug delivery (**Figure 2.1**), their HLB values were 15, 4.2, 14-16 and 12-14

respectively.[5,6] Given the need for a high HLB surfactant for lipophilic solubilization purposes, Polysorbate 80 and Cremophor RH 40 were selected for further use.

The tri-block copolymer group of surfactants of the type, polypropylene (PPO)-polyethyleneoxide (PEO)- polypropylene (PPO), also known as Poloxamers, are also of interest in drug delivery.[7] These tri-block copolymers have reportedly lower critical micelle concentrations, higher stability and generally narrow micellar size distributions as compared to other surfactant micelles.[8] There are a variety of tri-block copolymers, or Poloxamers, to choose from. However, given that Poloxamer 188 is one of the most commonly used surfactants (**Figure 2.1**) and that the HLB was 29[7], it was selected for further analysis.

Span surfactants, as sorbitan esters, typically have low HLB values and were not considered for further analysis. However, d-α-tocopherol polyethylene glycol succinate (TPGS) has been previously used as an emulsifier, stabilizer and absorption enhancer, with an HLB of 13.2.[9] Based on the emulsifying potential of TPGS and the fact that it is a water-soluble alternative to Vitamin E that may enhance Vitamin E solubility, TPGS was selected for further analysis.[9] The above rationale, combined with literature support in other microemulsion formulations, resulted in the selection of a Polysorbate (Tween 80), a Cremophor (Cremophor RH 40), a tri-block copolymer (Poloxamer 188) and Vitamin E TPGS for further analysis of microemulsion formation potential. Their structures are shown in **Table 2.1.**

With respect to the oil phase of microemulsions, a variety of hydrocarbon oils are available for consideration. However, weakly polar oils such as triglycerides are common.[10,11] Triglycerides consist of three fatty acids attached to a glycerol backbone. The length of this fatty acid determines its classification as a short, medium, long or very long chain triglyceride. Short chain triglycerides (SCTs) consist of fatty acids with less than 8 carbons, medium chain triglycerides (MCTs) 8-12 carbons, long chain triglycerides (LCTs) 13-21 carbons and very long chain triglycerides (VLCTs) more than 22 carbons.[21] MCTs and LCTs have primarily been used in microemulsion drug delivery due to their ability to solubilize and improve lipophilic drug absorption.[22] However, there is much evidence to support the particular use of MCTs for oral microemulsion drug delivery.[23] Medium chain triglycerides are preferred over long chain triglycerides due to their greater water solubility and smaller molecular size.[10,11] These properties have been associated with greater mobility in the lipid-

Table 2.1: Chemical structures of surfactants and medium chain triglyceride used in this work

Surfactant	Chemical Name	MW	HLB	Chemical Structure
Cremophor RH 40	Polyoxyl-40 hydrogenated castor oil	2500[13]	14-16[14]	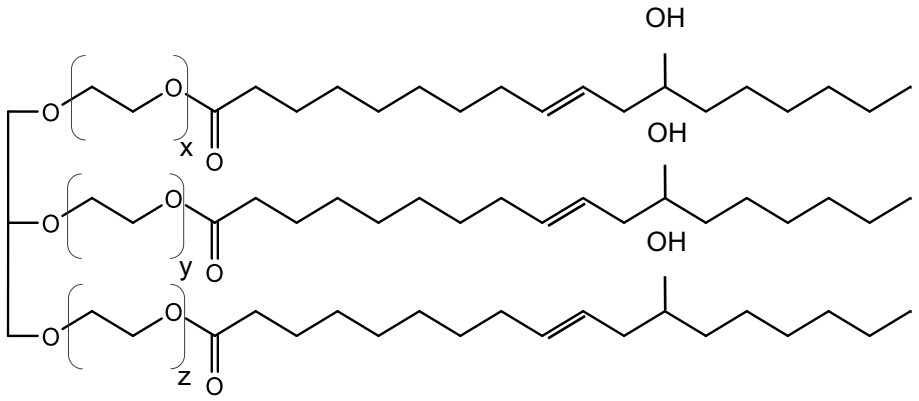 x+y+z= 40[12]
Poloxamer 188	PEO-PPO-PEO block co-polymers	~8400[15]	>24[16]	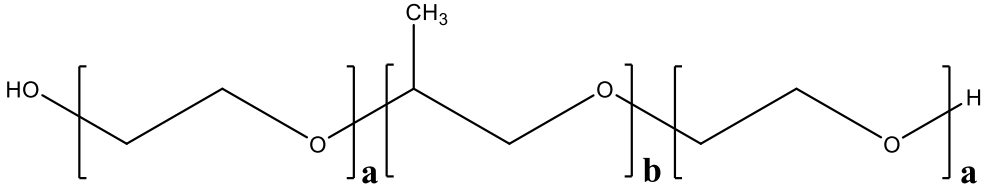 a= 80[16] b= 27[16]

Polysorbate 80	Polyoxyethylene 20 sorbitan monooleate	1309.66[17]	15[18]	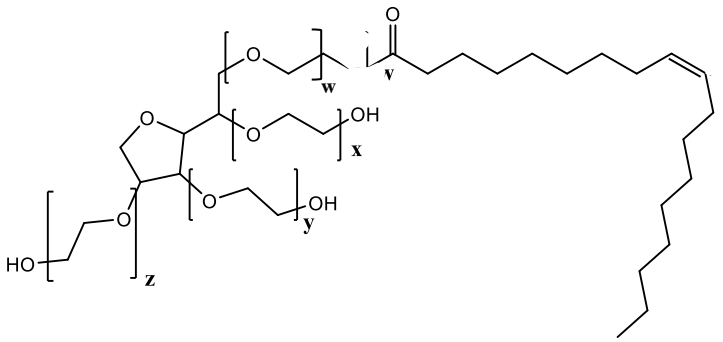 w+x+y+z= 20[19]
Vitamin E TPGS	D-a-tocopherol polyethyleneglycol succinate	1513[9]	13.2[9]	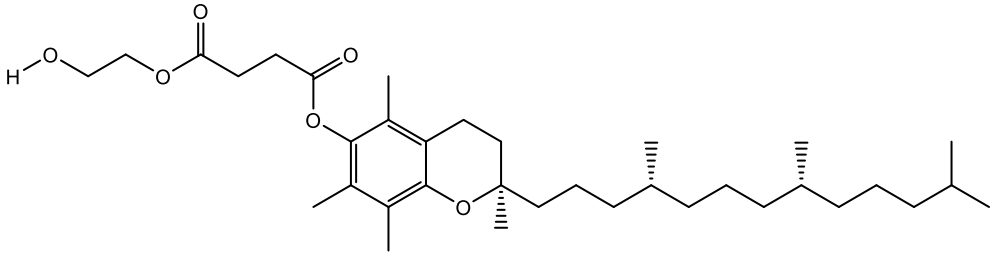
Miglyol 812	C8-C10 Caprylic/capric triglycerides	N/A	15.36[20]	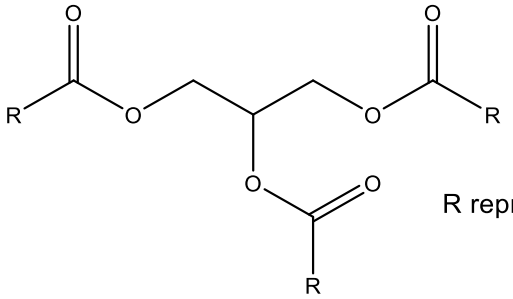 R represents a mixture of C7 to C9 alkanes

water interface, faster lipid hydrolysis, reduced transit times in the gastrointestinal tract and thus, greater ability to improve absorption.[10,11,21] The faster lipid hydrolysis of short and medium-chain triglycerides (less than 12 carbons) is due to the fact that these lipids are able to reach systemic circulation through the portal blood.[21,24] In contrast, LCTs must first be incorporated into chylomicrons[25] leading to slower absorption rates.[24] MCTs have also been reported to enhance drug stability[22] and require less emulsifier than LCTs.[10,11] Within the MCT class itself, i.e. 8-12 carbons, little variation has been reported with respect to microemulsion formation potential. Prajapati et al. (2011) reported minimal differences in phase behaviour when using a C8 versus C12 triglyceride in Cremophor EL surfactant and water systems.[26] An increase in gelling behaviour when using a C12 triglyceride in comparison to C8 was reported.[26] A variety of MCTs such as Neobee M5, Miglyol 810 and Miglyol 812 are commonly used for commercial use.[27] However, Miglyol 812 is a medium chain triglyceride that has been reported to solubilize a large degree of poorly water-soluble drugs.[28] For this reason, Miglyol 812, comprised of 50-65% C_8 and 30-45% C_{10} was selected as the oil solubilizer in this work.[29]

2.2 Study Objectives

Given the major objective of this thesis work, to formulate a microemulsion system capable of multi-drug delivery, the first step involves determining a suitable surfactant(s) and ratio of surfactant:oil:water (S:O:W) necessary for microemulsion formation. Therefore, the objective of **Chapter 2** is to assess the microemulsion formation potential of multiple non-ionic surfactants via TPD mapping. Promising surfactants will be further assessed using tensiometry in order to determine CMC and other important surfactant parameters that may confirm the suitability of each surfactant for microemulsion use.

2.3 Hypothesis

If microemulsions are formulated with Cremophor RH 40, Poloxamer 188, Polysorbate 80 and Vitamin E TPGS, in Miglyol 812 oil, then Type I O/W microemulsion systems are predominantly expected while Type II W/O microemulsions are not, given the surfactant HLB values of ≥ 13.

2.4 Materials and Methods

2.4.1 Materials

All surfactants: PEG-40 hydrogenated castor oil, Poloxamer 188, Polysorbate 80 and D-α-tocopherol polyethylene glycol succinate were generously gifted from Accucaps Industries Limited/Catalent Pharma Solutions Inc. PEG-40 hydrogenated castor oil (Cremophor RH 40), Poloxamer 188 (Kolliphor P188) and Polysorbate 80 (Kolliphor PS80) were supplied by BASF Care Creations (Ontario, Canada) while D-α-tocopherol polyethylene glycol succinate (Vitamin E TPGS) was supplied by Sigma Aldrich Canada (Ontario, Canada). Medium chain triglyceride (MCT) Miglyol 812 was also gifted from Accucaps Industries Limited/Catalent Pharma Solutions Inc. but supplied by IOI Oleochemical (Ontario, Canada). Sudan III 90.0% lipophilic dye was purchased from Fischer Scientific (Ontario, Canada).

2.4.2 Methods

2.4.2.1 Ternary Phase Diagram (TPD) Analysis

Varying ratios of surfactant, MCT and deionized (DI) water were weighed into a 20 mL scintillation vial using a Sartorius Secura 225D-1S analytical balance. Each vial was inverted manually for approximately 20 seconds until the mixture appeared uniform. The vials were stored in the dark at room temperature for a period of 24 hours before phase behaviour was analyzed. For phase analysis at 37ºC, vials were placed in a Fisher Scientific Isotemp GPD 10 water bath set at 37 ºC for a period of 24 hours. Microemulsion phases were primarily identified visually through observation of transparency, turbidity and viscosity. The Tyndall effect was also employed using a red laser beam in order to identify microemulsion phases given that the colloidal particles scatter light. Thus, in all microemulsion phases, the path of the red laser beam was clearly visible. In select samples, conductivity was performed using a SevenEasy Conductivity Meter and In-Lab® 752-6 mm micro-conductivity probe to confirm higher conductivity in the lower O/W microemulsion phase than the upper excess oil phase (Type I microemulsions) and lower conductivity in the upper W/O microemulsion phase than the lower excess water phase (Type II microemulsion). Sudan III red lipophilic dye was also used in selected samples to confirm the presence of an upper excess oil phase in Type I microemulsions. Each phase was recorded and plotted as a single point specific to a certain surfactant:oil:water

(S:O:W) concentration on a ternary phase diagram using OriginLab® 8.5 software. Experiments were conducted in duplicate. **Figure 2.2** represents a simplified illustration of this method.

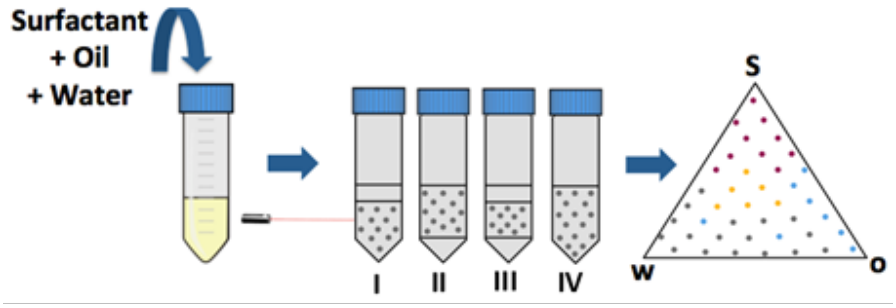

Figure 2.2: Illustration of ternary phase diagram methodology utilized in this work. Microemulsion type was confirmed in two of three ways: visually by identification of phase behaviour, visually via laser detection making use of the Tyndall effect and experimentally through conductivity measurements. Coloured points in the ternary phase diagram indicate that a variety of emulsion structures may be obtained.

2.4.2.2. Tensiometry: Critical Micelle Concentration (CMC) Determination

Critical Micelle Concentrations (CMCs) were determined via tensiometry on a T3 Lauda Tensiometer using the DuNoüy ring method. 40 mL MilliQ water was filtered using a 0.22 μm Sartorius sterile minisart filter and added to a tensiometry glass vessel along with a clean mini stir bar. The DuNoüy ring was immersed 10 times in MilliQ water followed by methanol, then flamed until bright orange to clean off any previous solution. Temperature was controlled at 25°C using a Lauda circulating water bath. Surfactant solutions were carefully titrated into a tensiometry glass vessel followed by stirring for 7 minutes before each surface tension measurement was collected. The instrument recorded a minimum of three surface tension measurements for each titration, until the standard deviation between readings was below 0.1 mN/m. A graph of surface tension versus the logarithm of surfactant concentration was plotted and the breakpoint identified in order to obtain the CMC. Specifically, the CMC was determined by the intersection of the linear trendlines before and after this breakpoint. CMC experiments were performed in triplicate and the results averaged. Additional surfactant parameters, namely surface excess, head group area, micellization energy, critical packing parameter, efficiency,

effectiveness and the beta interaction parameter, as explained later, were obtained using CMC values via the equations listed in **Section 2.5.7**.

2.5 Results and Discussion

The ternary phase plots showed distinct one-, two- and three-phase regions depending on the type of surfactant mixed with water and MCT. In general, biphasic regions (Winsor I and II) were more easily obtained than monophasic and triphasic regions (Winsor IV and III, respectively). In terms of localization, one-phase regions were seen to dominate at higher surfactant concentrations, two-phase O/W regions at higher water concentrations and two-phase W/O regions at higher oil concentrations. These observations are in agreement with surfactant aggregation behaviour.[30,31] All surfactants tested in this work possessed HLB values >13, which according to the Bancroft rule, should result in the production of large O/W microemulsion regions.[32] The following surfactant-specific observations were noted.

2.5.1 PEG-40 Hydrogenated Castor Oil

Cremophors are polyethoxylated castor oils that are synthesized by reacting hydrogenated castor oil with varying amounts of ethylene oxide.[33] In particular, for PEG-40 hydrogenated castor oil, 40 moles of ethylene oxide are reacted with 1 mole of hydrogenated castor oil.[33] The hydrophobic portion of such surfactants consists of glycerol polyethylene ricinoleate while the hydrophilic portion consists of polyethylene glycols and glycerol ethoxylates.[33] In general, PEG-40 hydrogenated castor oil is comprised primarily of hydrophobic constituents of which the main component is glycerol polyethylene glycol 12-hydroxystearate.[33] As a result of the many hydrophilic polyethylene oxide (PEO) groups, however, the HLB value remains high (14-16)[14] and its solubility in water is enhanced. Thus, PEG-40 hydrogenated castor oil is able to act as an oil solubilizer and O/W microemulsion emulsifier[34] as can be seen in **Figure 2.3**.

In general, PEG-40 hydrogenated castor oil primarily demonstrated Winsor Type I microemulsion formation at room temperature. However, its semi-solid, paste-like state at room temperature made phase behaviour interpretations difficult at surfactant concentrations above 20% w/w, resulting in an incomplete phase diagram. Monophasic opaque systems, likely coarse emulsions, dominated at low water concentrations between 15-40% w/w while triphasic

behaviour was particularly seen along the 10% w/w water tie line between 35-50% w/w surfactant concentration. Monophasic Winsor IV microemulsions dominated at surfactant concentrations between 45-80% w/w. As the temperature increased from room temperature to 37ºC, no significant changes in phase behaviour were seen but for small phase changes along the 10% w/w water tie line. The melting temperature of PEG-40 hydrogenated castor oil, which lies around 26 ºC, is a likely explanation for any apparent clarifications in phase behaviour.

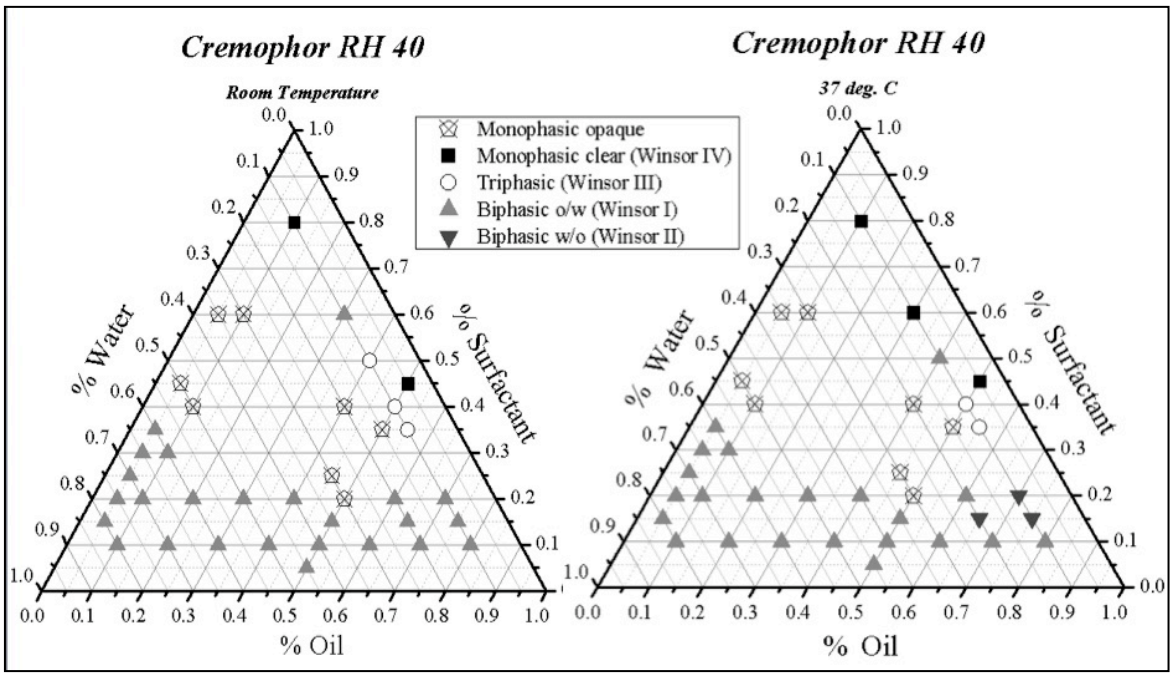

Figure 2.3: Ternary phase diagram for PEG-40 hydrogenated castor oil, Miglyol 812 and water at room temperature (left) and at 37°C (right).

Winsor I microemulsions comprised the primary region in the ternary phase diagrams in this work. In particular, O/W regions dominated at or below 20% w/w surfactant concentration, which has previously been reported by Hasan (2016) in PEG-40 hydrogenated castor oil- Imwitor 308-water systems.[35] These O/W regions also dominated in water-rich regions of the TPD at ≥60% w/w water, which has been previously reported by Zeng et al. (2017) in PEG-40 hydrogenated castor oil-ethyl oleate-water systems.[5] Such observations can be explained structurally. In PEG-40 hydrogenated castor oil micelles, the PEO chains expand to maximise penetration of water into the chains.[5] The branched alkyl chain also enhances

emulsification, increasing oil penetration into the curved surfactant film leading to high flexibility of the oil-water interface and low droplet sizes.[36-38]

The monophasic opaque area was the second most dominating region, particularly between 15-40% w/w water. The physical state of the surfactant is likely responsible for this observation as its waxy consistency attributable to its three C18 tails, likely results in highly turbid solutions. Bicontinuous, Winsor III and Winsor IV microemulsions were the least dominating microemulsion types noted in these PEG-40 hydrogenated castor oil- MCT- water systems. Type III microemulsions were observed along the 10% w/w water line. The propensity of PEG-40 hydrogenated castor oil to form bilayer aggregates has been reported by Hasan (2016).[35] The triple-tailed nature of this surfactant versus that of a single-tailed surfactant, leads to the favouring of spherical or cylindrical aggregates due to consideration of the packing parameter.[31,35] This critical packing parameter (CPP) considers the head group and flexible triple chain area of PEG-40 hydrogenated castor oil which together result in a similar volume to area × length ratio and CPP of between 0.33 and 1.[30] This CPP value affords easy formation of cylindrical structures, as well as vesicles and flexible bilayer structures.[30] The PEO groups are also unable to pack as efficiently as in a single-tailed surfactant due to the three hydrophobic chains in the micelle core (i.e. the cis double bond and the alcohol groups in the ricinoleic acid moiety).[39] Monophasic clear regions were observed at surfactant concentrations above 45% w/w. This is in line with work reported by Suys (2019) who observed monophasic, liquid crystalline regions above 50% w/w PEG-40 hydrogenated castor oil.[39] Winsor Type II microemulsions were only minimally observed at very high oil concentrations of approximately 90% w/w. This is likely due to the high HLB value and packing constraints of the PEG-40 hydrogenated castor oil surfactant molecules.

Gelled regions were observed at particularly high oil concentrations (> 70% w/w) and low water concentrations (< 30% w/w). This is in line with previously reported works. Suys (2019) reported that at >25-30% w/w Cremophor with water, larger structures with higher viscosity were formed rather than typical micelles.[39] Zeng et al. (2017) reported that when used alone with water and oil, PEG-40 hydrogenated castor oil demonstrated large gel-like regions[5] likely due to the triple chain nature of the Cremophor surfactant, which imparts greater viscosity than conventional single chain surfactants. This type of behaviour was also apparent in this work at 0% water content. Thus, although Cremophors are effective at solubilizing hydrophobic

drugs, they are not typically used alone.[33] The semi-solid state of these surfactants also renders them less desirable for drug delivery on their own due to the fact that even if melting is performed, phase separation will still likely occur upon cooling to room temperature.[40] These observations were notable as even upon an increase to 37ºC and slight melting, the phase behaviours only clarified slightly; no significant changes were seen. Triple chain surfactants, though bulkier in nature than their single-chain surfactant counterparts, are also known to produce more stable emulsions than single or double-chained surfactants due to their enhanced viscosity and lower diffusion constant.[41] They have been reported to be more efficient at lowering surface tension as their triple chain helps form stable, branched, threadlike microstructures.[41] These features coupled with Cremophor's ability to inhibit p-glycoprotein and cytochrome enzymes, promoting enhanced permeability[36], make Cremophor a widely used surfactant in oral and parenteral (injectables and intravenous) applications.[33,42] In concentrations of 50 mg/mL and above, Cremophor EL and Cremophor RH 40 have been reported to cause cell damage after 2-3 hours and cell death after 12 hours in endothelial and intestinal epithelial cells.[42] Epithelial cells appeared to be more resilient to surfactant treatment than endothelial cells and Cremophor EL proved to be more toxic than Cremophor RH 40 in both cell types.[42]

2.5.2 Poloxamer 188

Poloxamers, or Pluronics® as trademarked by BASF Corporation, are tri-block copolymers comprised of polyethylene oxide- polypropylene oxide- polyethylene oxide (PEO-PPO-PEO).[16] In particular, Kolliphor P188 (also known as Poloxamer 188 or Pluronic® F-68) is comprised of approximately 27 PO groups flanked by 80 EO groups.[16] The molecular weight of Kolliphor® P188 is approximately 8400 g/mol[40] which is higher than that of typical emulsifying surfactants.[43] In addition, there are two hydrophilic chains unlike typical non-ionic surfactants[43], leading to a PEO/PPO ratio of almost 3[44] and a high HLB value of 29.[16] The oxygen groups present in both hydrophilic and hydrophobic portions of the molecule afford hydrogen bonding with water[43] leading to high water solubility[44] and the propensity to form O/W microemulsions. Structures formed with Poloxamer 188 depend on temperature and concentration.[43] Poloxamer 188 is present as single molecules (unimers) below 50 ºC and above this temperature, polymeric micelles are formed.[43] The variation of microemulsion types obtained through the use of Poloxamer 188 affords usability in many drug delivery applications.[43]

Poloxamer 188 (**Figure 2.4**) at room temperature demonstrated large Winsor I microemulsion formation behaviour at 30% w/w surfactant and below. This surfactant faced similar challenges to PEG-40 hydrogenated castor oil; the solid, powder consistency prevented phase behaviour analysis above 40% w/w Poloxamer 188 as the solubility limit was reached. Triphasic behaviour was concentrated along the 20-30% w/w water line. There was no observable monophasic behaviour and once heated to 37ºC, virtually no change was seen but for slight phase clarification along the 30% water line. This clarification is possible despite the reduced solubility of non-ionic, PEO surfactants at higher temperatures, as both the cloud and melting points of Poloxamer P188 are high (>100°C and 52°C, respectively).[16,40]

Winsor I microemulsions represented the primary phase obtained, as Pluronics can self assemble to form micelles with the PEO groups forming the shell or corona and the PPO groups forming the core of O/W micelles.[45,46] In particular, they assemble at the interface between the oil core and water with the PEO hydrophilic groups pointing outward into the water phase.[47] A single Winsor II microemulsion at 10% surfactant, 80% oil and 10% water was observed due to the high water solubility and HLB of Poloxamer 188, which may be too high to afford oil solubility.

Gel regions were obtained throughout the ternary phase diagram at surfactant concentrations above 30% w/w which has previously been reported by Bodratti (2018).[46] The high PEO to PPO ratio leads to well-hydrated outer shell PEO segments that can stick and stack together to form structures of high viscosity.[46] In general, O/W PEO systems are found to be of high viscosity above 10% w/w concentrations because below this, the droplets are too widely spaced to be bridged by the polymer molecule.[48] Reverse thermal gelation behaviour is typically observed with Poloxamer 188 (Pluronic F68) at surfactant concentrations of 50% w/w and above.[44] However, in this work, surfactant concentrations above 40% w/w were difficult to obtain and thus, this typical reverse gelation behaviour at higher temperatures was not observed.

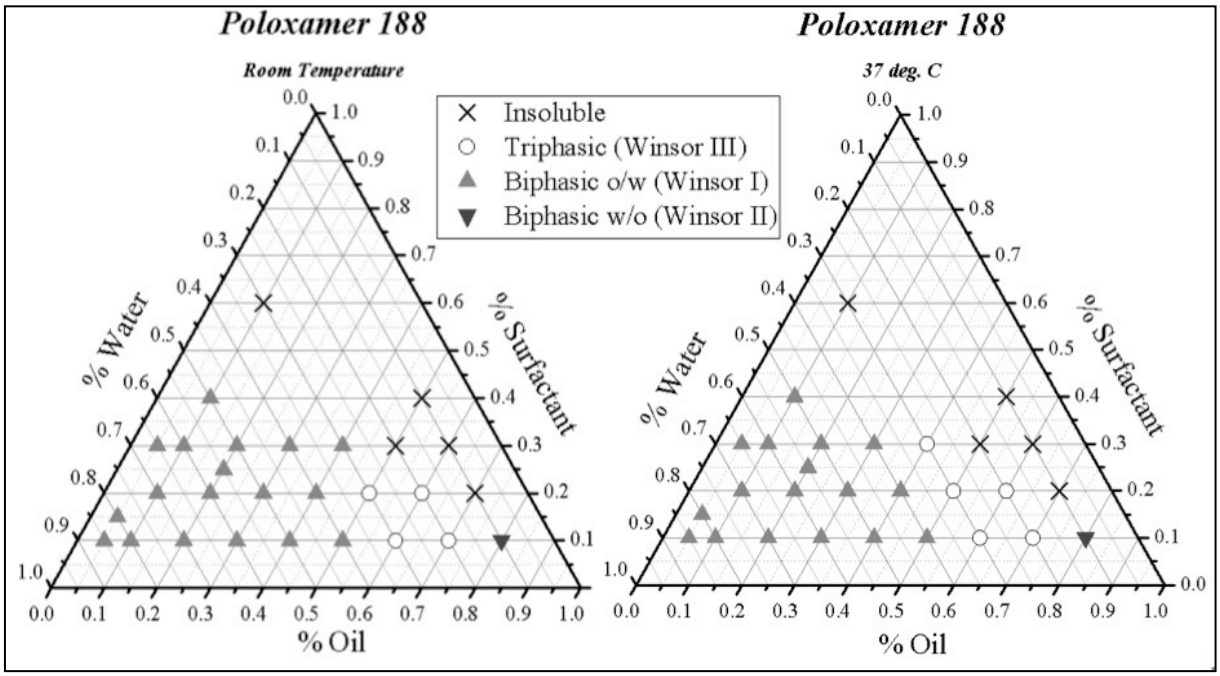

Figure 2.4: Ternary phase diagram for Poloxamer 188, Miglyol 812 and water at room temperature and at 37°C.

2.5.3 Polysorbate 80

Polysorbate 80 is a polyethoxylated (PEO) sorbitan monooleate non-ionic surfactant.[49] It is comprised of an oleate ester of sorbitol and its anhydrides, copolymerized with approximately 20 moles of ethylene oxide for each mole of sorbitol and sorbitol anhydrides.[49] There are four hydrophilic EO head groups, summing to 20, that are attached to a sorbitan ring. The hydrophobic region is comprised of an oleyl, unsaturated tail connected to one PEO group via an ester.[50] The kink present in the hydrophobic tail of Polysorbate 80 affords flexibility, leading to an optimal curvature and packing parameter that promotes microemulsion formation.[51]

Polysorbate 80 (**Figure 2.5**) demonstrated a wide range of mono-, bi- and tri-phasic behaviour across various ratios of surfactant, MCT oil and water. At room temperature, a large monophasic Type IV microemulsion region dominated mainly at surfactant concentrations above 50% w/w. Below 50% w/w surfactant, monophasic opaque, biphasic and triphasic behaviours dominated. Winsor I microemulsions were evident below 40% w/w surfactant and at or above 30% w/w water. Winsor II microemulsions dominated above 70% w/w oil and

Winsor III microemulsions, though rare, were evident along the 10-15% w/w water line. As temperature was increased to 37ºC, virtually no change in phase behaviour was observed.

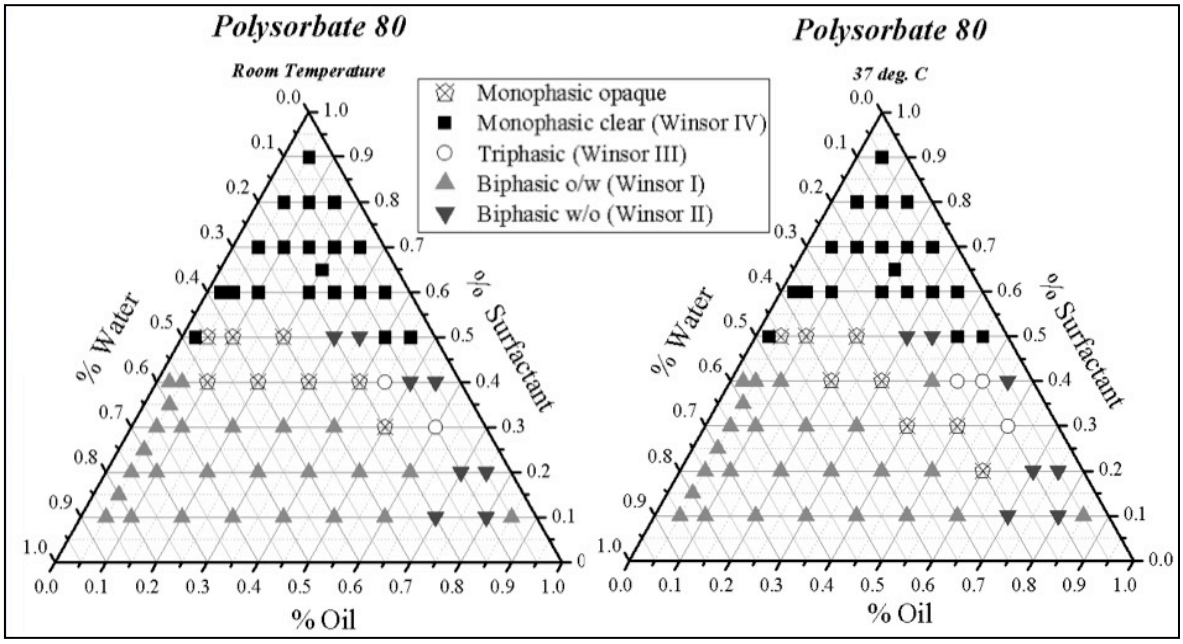

Figure 2.5: Ternary phase diagram for Polysorbate 80, Miglyol 812 and water at room temperature and at 37°C.

The extensive monophasic, microemulsion region observed in this work was previously reported in Polysorbate 80-Captex 355-water systems[52] and Polysorbate 80-isopropyl myristate-water systems.[53] Winsor I microemulsions have also been previously reported in Polysorbate 80-isopropyl myristate-water systems.[53] According to the critical packing parameter, one can expect the relatively large head group and single tail of Polysorbate 80 to form spherical, Type I O/W micelles based on the small volume to area x length ratio (CPP < 0.33).[30] Opaque emulsions obtained between 30-50% w/w surfactant correlate with the previously reported work of Shah et al. (2017) in Polysorbate 80-Captex 355-water systems.[52] Winsor II microemulsion regions, the largest of all surfactants tested in this work, were previously reported by Syed et al. (2014) in Polysorbate 80-isopropyl myristate-water systems.[53] Surfactants with small head groups and large tails have a propensity to form reverse, Type II W/O micelles.[54] Since Polysorbate 80 contains a cis-double bond in the oleyl chain of Polysorbate 80, this leads to a widely spaced tail.[54] This unsaturation also causes kinking[55] and affords flexibility of the surfactant tail to assume an optimum curvature and packing parameter

for many conformations[56] including that of W/O micelles and thus, Type II microemulsions. Winsor III microemulsions observed at 30-40% w/w surfactant were also in good agreement with previous studies using Polysorbate 80-isopropyl myristate- water systems.[53]

Gelling was observed primarily between 10-50% w/w water. This is in good agreement with work by Shah et al. (2017) who studied Polysorbate 80-Captex 355-water systems and observed gelling between 15-60% w/w water.[52] No significant phase changes were seen upon heating to 37°C and gelling regions remained the same. This is in contrast to work by Prieto and Calvo (2013) who reported that in Polysorbate 80-decane-oil systems, when temperatures rose from 25 to 30°C, gel regions decreased due to a reduction in viscosity.[57] However, it should be noted that decane oil is a straight chain oil versus a MCT.

In general, Winsor I O/W microemulsions dominated due to Polysorbate 80 being a hydrophilic surfactant (HLB 15) with a preferred solubility in water than oil, a result of the previously explained Bancroft effect. Phase separated microemulsion regions were seen primarily below 50% w/w surfactant, which correlated with work by Shah et al. 2017.[52] A large spread of microemulsion types was obtained with this surfactant given the common head and tail structure. In Polysorbate 80-palm oil-water systems, Mahdi (2011) previously reported a wide spread of microemulsion types obtained due to the unsaturated nature of the hydrocarbon chain, which affords mobility and flexibility.[58]

2.5.4 D-α-tocopherol Polyethylene Glycol Succinate (TPGS)

TPGS is a water-soluble alternative to fat-soluble vitamin E.[59] Its lipophilic alkyl tail consists of tocopherol succinate (natural vitamin E) while its hydrophilic head consists of polyethylene glycol 1000 (~22 ethylene glycol groups).[59,60] It is a bulky molecule with a molecular weight of ~1513 g/mol that forms low viscosity solutions with water at concentrations of up to 20% w/w surfactant.[59,60]

TPGS (**Figure 2.6**) is a solid wax at room temperature that requires heating prior to phase behaviour analysis. As a result, evaluation at room temperature above 10% w/w surfactant concentrations was difficult. In general, though coarse monophasic emulsions were evident throughout the phase diagram, clear monophasic Type IV microemulsion regions were seen at and above 60% w/w surfactant concentration and Winsor I microemulsions were evident below 50% w/w oil. Winsor II microemulsions were evident at and above 50% w/w oil and at

37ºC, slight decreases of the monophasic opaque emulsion areas were seen, along with an expansion of the monophasic clear, Type IV microemulsion region.

This Winsor IV microemulsion region was previously observed by Ke at al. (2005) who reported monophasic regions in TPGS-MCT-water systems above 30% w/w surfactant.[59] Type I microemulsions were expected at high water concentrations given that the CMC of TPGS is approximately 0.02% w/w at 37°C in water, and that O/W micelles form above this concentration.[60] At 37ºC, many of the opaque emulsion phases clarified and were able to be differentiated into different microemulsion types. This is a result of the melting temperature of TPGS, which is also 37ºC.[60]

Large gelling regions were observed throughout this ternary phase diagram mainly above 60% w/w surfactant concentrations and between 0-50% water. This has previously been reported by Ke et al. (2005).[59] Gelling can be explained due to TPGS' large hydrophobic tocopherol group and long hydrophilic PEG 1000 chain which allows water to be adsorbed to the PEG chains, resulting in a rigid hydrogen bonding structure or gel.[59] Ke et al. (2005) noted that TPGS on its own is unable to form isotropic solutions with water and oil across a broad range of compositions[59] and these observations were evident in this work.

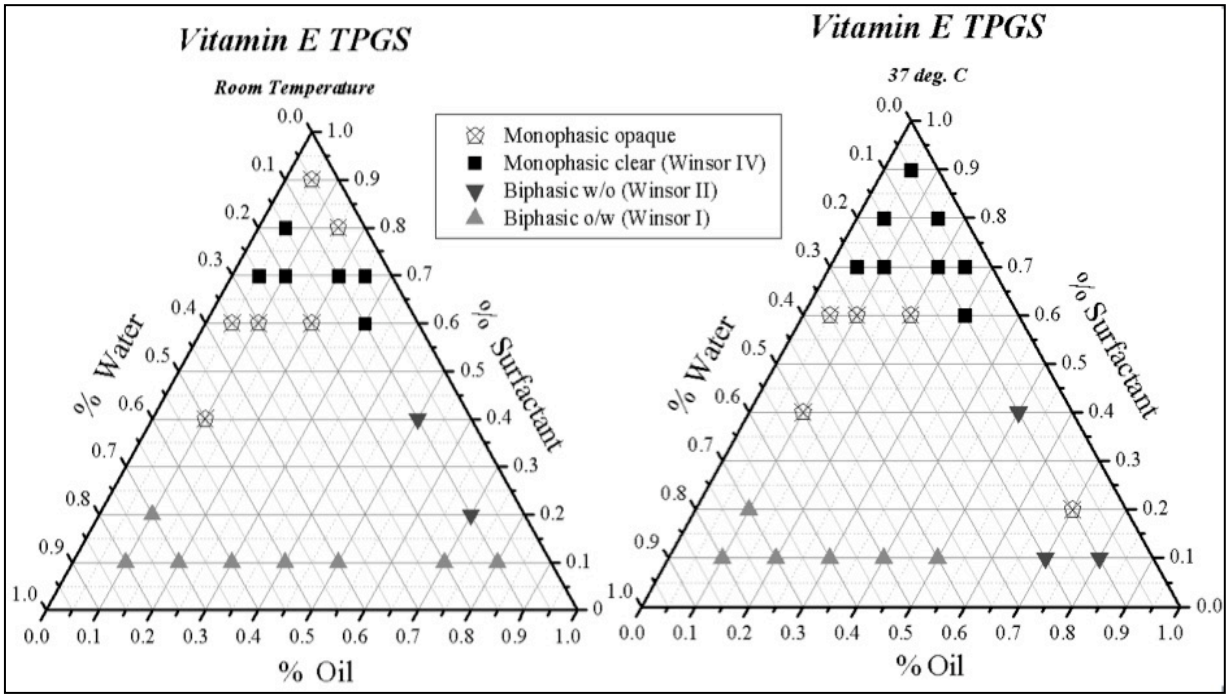

Figure 2.6: Ternary phase diagram for D-α-tocopherol polyethylene glycol succinate, Miglyol 812 and water at room temperature and at 37°C

2.5.5 PEG-40 Hydrogenated Castor Oil, Poloxamer 188, Polysorbate 80 & D-α-tocopherol Polyethylene Glycol Succinate

Based on **Figures 2.3-2.6**, a few observations were noted. In general, Winsor I, O/W microemulsions dominated these ternary phase diagrams irrespective of the solubility challenges faced with solid and wax-based surfactants. This result was expected given that the surfactants used in this work possessed an HLB ≥13. According to the Bancroft rule, the continuous phase is reflective of the phase in which the surfactant is most soluble. Thus, in this case, water dominates as the continuous phase. Winsor II microemulsions of the water-in-oil type were less frequently obtained for this reason as well. Winsor III microemulsions were the most difficult to obtain due to their need for a delicate balance of oil, water and surfactant, no particular preference for a continuous phase and a zero net curvature.[61] Winsor IV microemulsions were primarily present in high surfactant concentrations near 50% w/w or higher.[61] This was particularly evident in Polysorbate 80 but less evident in PEG-40 hydrogenated castor oil due to its waxy nature and Poloxamer 188 due to the water solubility limit being reached.

Opaque emulsions were obtained in the order PEG-40 hydrogenated castor oil = Polysorbate 80 > TPGS > Poloxamer 188. Coarse emulsions are well suited to a number of drug delivery applications, particularly in lotions or creams. They may also be homogenized to produce nanoemulsions, which affords a variety of additional drug delivery applications.

Winsor I, O/W microemulsions were obtained in the order Polysorbate 80 > PEG-40 hydrogenated castor oil > Poloxamer 188 > TPGS. Although Polysorbate 80, PEG-40 hydrogenated castor oil and Poloxamer 188 demonstrated large Winsor I microemulsion regions, TPGS demonstrated a much smaller region. This may be attributed to the solid state of TPGS, which required significant heating before phase regions could be observed. It should also be noted that while a relatively complete ternary phase diagram was obtained for Polysorbate 80, this was not necessarily the case with the other surfactants studied in this work. Nevertheless, O/W microemulsions in general are well suited for lipophilic drug delivery.[62]

Winsor II microemulsions were obtained in the order Polysorbate 80 > PEG-40 hydrogenated castor oil = TPGS > Poloxamer 188. The high HLB value of the surfactants tested in this work may be responsible for decreasing the tendency to form W/O microemulsions given the Bancroft rule. Winsor III microemulsions were obtained in the order Poloxamer 188 > PEG-

40 hydrogenated castor oil = Polysorbate 80 > TPGS. Type III microemulsions are uncommon in drug delivery applications but are useful for oil-recovery methods.

Type IV microemulsions were obtained in the order Polysorbate 80 > TPGS > PEG-40 hydrogenated castor oil > Poloxamer 188. Polysorbate 80 demonstrated a Type IV microemulsion region up to 5X larger than that of the other surfactants. This type of microemulsion is homogenous and uniform and thus, well suited for many types of drug delivery especially multi-drug delivery. In addition, the typically higher viscosity of these microemulsions renders them especially suitable for other types of drug delivery applications such as ocular, topical and rectal delivery.

2.5.6 PEG-40 Hydrogenated Castor Oil: Polysorbate 80

Multi-drug delivery represents an unmet need given the burden of chronic disease in Canada.[1] The demand for this type of drug delivery requires further exploration of the Type IV microemulsion region, as these microemulsions are able to facilitate simultaneous delivery of both hydrophilic and lipophilic drug compounds. Based on **Figures 2.3-2.6**, Polysorbate 80 demonstrated the largest Winsor Type IV microemulsion region. However, there is literature support for the use of PEG-40 hydrogenated castor oil as a solubilizer, particularly for hydrophobic active pharmaceutical ingredients (APIs).[33] The high HLB value of PEG-40 hydrogenated castor oil affords lipophilic drug delivery due to the propensity to form O/W micelles and solubilize lipophilic drug material.[34] PEG-40 hydrogenated castor oil has also been reported to be efficient at lowering surface tension[41] and promoting enhanced permeability of drugs.[36] Despite these advantages, PEG-40 hydrogenated castor oil is unable to form large Type IV microemulsion regions. Given the high propensity for Polysorbate 80 to form Type IV microemulsions, PEG-40 hydrogenated castor oil was combined with Polysorbate 80 in order to determine whether expansion of the Type IV microemulsion region in PEG-40 hydrogenated castor oil was possible.

Polysorbate 80 and PEG-40 hydrogenated castor oil were mixed in increasing ratios of Polysorbate 80 from 1:2, 1:1 and 3:1 Polysorbate 80: PEG-40 hydrogenated castor oil (**Figures 2.7-2.9**). As the concentration of Polysorbate 80 increased and that of PEG-40 hydrogenated castor oil decreased, there was a clear reduction in monophasic opaque emulsion areas and promotion and expansion of clear, monophasic, Type IV microemulsion regions. Of particular

note is that monophasic formation was scarce below 60% w/w surfactant in 1:1 and 1:2 Polysorbate 80: PEG-40 hydrogenated castor oil. However, in 3:1 and Polysorbate 80: PEG-40 hydrogenated castor oil systems, monophasic behaviour can be seen at as low as 50% w/w surfactant. Heating these samples to 37°C appears to somewhat afford expansion of this Type IV, monophasic microemulsion region. These results prove that expansion of the Type IV microemulsion region in PEG-40 hydrogenated castor oil is possible with the combination of Polysorbate 80 and that this combination may be well suited for multi-drug delivery.

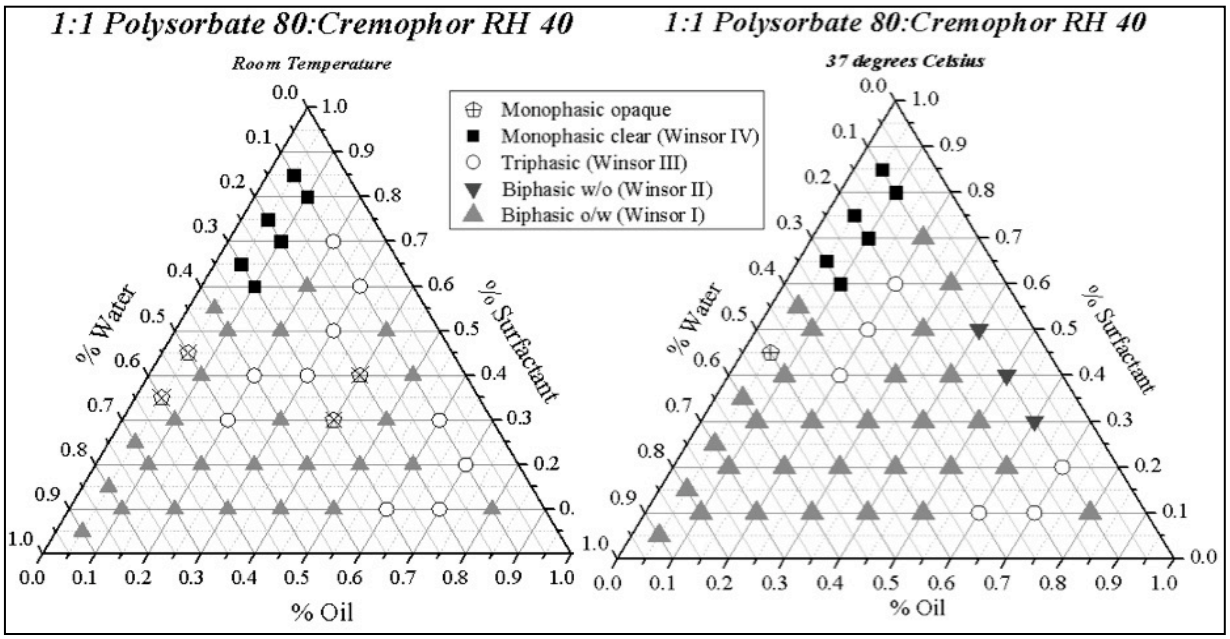

Figure 2.7: Ternary phase diagram for 1:1 Polysorbate 80:PEG-40 hydrogenated castor oil, Miglyol 812 and water at room temperature and at 37°C.

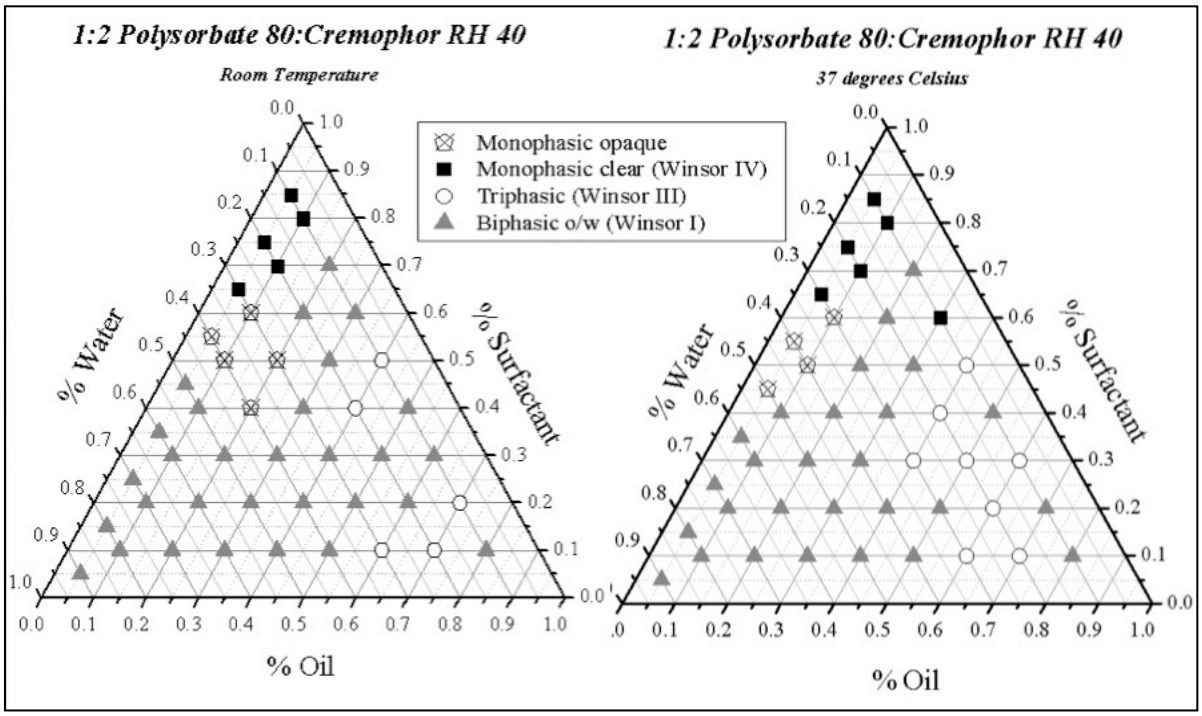

Figure 2.8: Ternary phase diagram for 1:2 Polysorbate 80:PEG-40 hydrogenated castor oil, Miglyol 812 and water at room temperature and at 37°C.

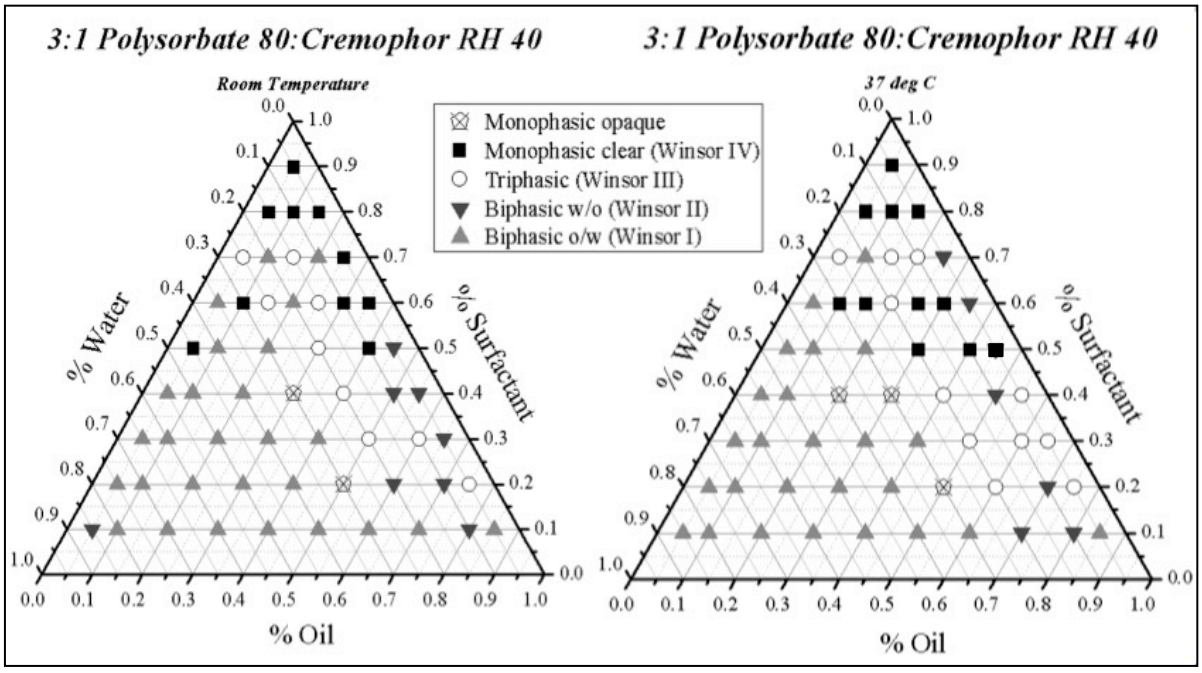

Figure 2.9: Ternary phase diagram for 3:1 Polysorbate 80: PEG-40 hydrogenated castor oil, Miglyol 812 and water at room temperature and at 37°C.

The ability of Polysorbate 80 to afford expansion of the Winsor IV microemulsion region in PEG-40 hydrogenated castor oil can be explained through examination of various surfactant characteristics and packing properties, both individually and upon mixing. **Figures 2.7-2.9** demonstrate a gradual expansion in the variety of microemulsion types produced upon mixing PEG-40 hydrogenated castor oil with increased concentrations of Polysorbate 80. Thus, it can be inferred that the mixing of these two surfactants is favourable with respect to microemulsion formation potential. In terms of packing, Polysorbate 80 micelles in water contain three hydrophilic heads with terminal OH groups and a fourth PEO segment attached to an 18-carbon alkyl tail.[63] This results in a 'cactus-type' orientation with two heads assuming a V-shape, perpendicular to the third head and fourth tail in an almost linear backbone.[63] Polysorbate 80 micelles assemble very quickly in water, with the OH groups covering the surface of the micelle, while the hydrophobic tails remain within the micelle core.[63] The tails of Polysorbate 80 do not assume a straight or 180° angle; rather, they assume a conformation between 50 and 180°, peaking at approximately 140°.[63] Thus, these tails do not point to the centre of the micelle but are somewhat slanted at approximately 25° rather than at 0°.[63]

The packing of Cremophor surfactant micelles in water is slightly different and highly dependent on concentration. Below 25% w/w, micelles are the dominant form but above 25% w/w larger, gel-like structures are seen.[39] In water, Cremophor surfactant molecules aggregate with glycerol and its three connected PEO chains on the outer micellar core in a relatively expanded conformation to maximize water penetration.[39] The hydrophobic ricinoleic acid moieties concentrate in the core of micellar structures, but the presence of a cis double bond in these moieties leads to inefficient packing of the PEO chains.[39] Thus, micelles of Cremophor are found to be larger than that of Polysorbate 80.[39]

In a study of mixed micelles containing POE (10) stearyl ether and either Polysorbate 20 or Polysorbate 60, it was found that when the length of the alkyl tail of the ether and that of the Polysorbate surfactant were the same, the two hydrophobic chains tended to remain elongated within the micelle, rather than tangling and becoming globular in the case of unequal alkyl chain lengths.[64] This is supported by the investigative work of Weerapol et al. (2014) on Cremophor RH 40 and Span 80 micelles, who found that surfactants with similar alkyl chain lengths pack favourably, leading to small droplet sizes.[37] Given that PEG-40 hydrogenated castor oil and Polysorbate 80 have the same number of carbons in their hydrophobic alkyl tails,

it is possible that the hydrophobic tails pack well together, remaining somewhat linear and elongated in the core of the micelle in contrast to a tangled or globular orientation. In addition, there is the possibility of a type of symmetry in the packing of Polysorbate 80:PEG-40 hydrogenated castor oil mixed micelles at an interface, due to the fact that Polysorbate 80 consists of three hydrophilic heads and one lipophilic tail while PEG-40 hydrogenated castor oil consists of one hydrophilic head (with three interconnected PEO chains) and three hydrophobic tails. The interactions between Polysorbate 80 and PEG-40 hydrogenated castor oil leading to this favourable packing may be further explained through consideration of CMC, surface excess, efficiency, effectiveness and the β interaction parameter (**Table 2.2**).

2.5.7 Tensiometry

Mixed surfactant systems may be characterized through examination of their ideal and experimental CMCs. The ideal CMC is the calculated CMC of a surfactant mixture using molar fractions and CMC values of each individual surfactant. If the experimental CMC is lower than that of the ideal as predicted by **Eq. 2.1**, the surfactant mixture is said to behave synergistically. If the ideal CMC is greater than the experimental CMC, the surfactant mixture behaves antagonistically. Using the following equation proposed by Clint (1975)[65] for mixed micelle formation, the ideal CMC is given by:

$$\frac{1}{\mathrm{CMC}1,2} = \frac{a}{cmc1} + \frac{1-a}{cmc2} \qquad \textbf{(Eq. 2.1)}$$

where $CMC_{1,2}$ is the ideal CMC, a and (1-a) are the mole fractions of surfactant 1 and surfactant 2, respectively, and cmc_1 and cmc_2 are the CMCs of surfactant 1 and 2, respectively. Using **Eq. 2.1**, the ideal CMC for 3:1 Polysorbate 80: PEG-40 hydrogenated castor oil is 4.77 μM (**Appendix A**). The results in **Table 2.2** indicate that the experimental CMC for 3:1 Polysorbate 80: PEG-40 hydrogenated castor oil (**Figures A6-A8**, **Appendix A**) was lower than that of the ideal CMC, which was 3.59 μM. This is despite the fact that the experimental CMCs for the individual surfactants were higher than that of the literature values, an occurrence that has previously been reported.[66] The low experimental CMC confirms the presence of attractive forces between these two surfactants and thus, a degree of synergism. CMC plots may be found in **Figures A-1 – A-8, Appendix A.**

Table 2.2: Surfactant parameters for Polysorbate 80, PEG-40 hydrogenated castor oil and a mixture of 3:1 Polysorbate 80: PEG-40 hydrogenated castor oil as obtained via tensiometry studies.

Surfactant	Experimental CMC ± SD (μM)	Surface Excess x 10^{-6} ± SD (mol/m^2)	A_0± SD (nm^2/molecule)	ΔG_{mic} x 10^3 ± SD (kJ/mol)	CPP± SD	Efficiency (± SD mM)	Effectiveness ± SD	CMC/C_{20} ± SD (mN/m)
Polysorbate 80*	4.73	2.45	0.68	-40.3	0.31	2.86	27.00	3.41
PEG-40 hydrogenated castor oil	4.91 ±0.00	1.95 ±0.00	0.85 ±0.01	-40.3 ±0.33	0.25 ±0.00	2.76 ±0.10	24.81 ±0.73	2.86 ±0.40
3:1 Polysorbate 80/PEG-40 hydrogenated castor oil	3.59 ±0.00	2.22±0.00	0.75 ±0.03	-41.0 ±0.35	0.28 ±0.01	2.74 ±0.08	23.84 ±1.55	2.00 ±0.56

* standard deviations not computed for Polysorbate 80 due to absence of replicates

Surface excess (Γ) is a measure of the amount of "excess" surfactant molecules per unit area at the interface relative to that present in the bulk.[67] It is given by the following equation[67]:

$$\Gamma = -\frac{1}{2.303nRT}\left(\frac{\delta Y}{\delta \log C}\right) \qquad \textbf{(Eq. 2.2)}$$

where R is the gas constant in J/K.mol, T is the temperature in K and $\left(\frac{\delta \gamma}{\delta \log C}\right)$ is the slope of the initial decreasing surface tension line (line 1). A positive surface excess value indicates that a surfactant decreases surface tension and vice versa.[68] Based on **Eq. 2.2** and the results from **Table 2.2**, all surface excess values are positive, indicating surface activity and surface tension lowering capacity in all surfactants investigated. PEG-40 hydrogenated castor oil has a lower surface excess value than that of Polysorbate 80. This can be explained structurally, as PEG-40 hydrogenated castor oil is quite bulky with a large hydrophilic head and three unsaturated hydrophobic chains, leading to steric limitations and thus, a lower amount of surfactant molecules that are able to pack per unit area of the interface.[69] Polysorbate 80 has the largest surface excess of all surfactants tested, indicating close packing at the interface and little

repulsive forces between the Polysorbate head groups.[66] 3:1 Polysorbate 80: PEG-40 hydrogenated castor oil has lower surface excess values than that of Polysorbate 80 alone, likely due to the presence of larger PEG-40 hydrogenated castor oil molecules which are able to pack less efficiently between the Polysorbate 80 surfactant molecules.

A_0 is the molecular area (in nm^2/molecule) occupied by each surfactant molecule at the interface and is therefore, an indication of the amount of space each surfactant head group occupies at said interface.[67] It is given by the following equation:[70]

$$A_0 = \frac{10^{18}}{N_A.\Gamma} \qquad \textbf{(Eq. 2.3)}$$

where N_A is Avogadro's number and Γ is the surface excess in mol/m^2. As expected, PEG-40 hydrogenated castor oil molecules occupy a larger area than that of Polysorbate 80 molecules **(Eq. 2.3, Table 2.2).** 3:1 Polysorbate 80: PEG-40 hydrogenated castor oil surfactant molecules occupy an area that is between that of the individual surfactant molecules.

$\Delta G°_{mic,}$ the Gibbs free energy of micellization, is a measure of the tendency of surfactant molecules to form micelles and is measured in $KJmol^{-1}$.[70] It is calculated via the equation:

$$\Delta G°mic = RTln(cmc)$$
$$\text{Therefore, } \Delta G°mic = RTln\left(\frac{c}{55.5+c}\right) \qquad \textbf{(Eq. 2.4)}$$

where R is the gas constant in J/K, T is the temperature in K, C is the concentration of surfactant in M and the CMC is expressed as a mole fraction in bulk water. Large and negative ΔG values indicate spontaneous micelle formation and a thermodynamically stable micellar solution at the tested temperature[70], in this case, 25°C. The results in **Table 2.2** from the use of **Eq. 2.4** indicate similar spontaneity of micellization in Polysorbate 80 and PEG-40 hydrogenated castor oil individually, and more favourable spontaneity upon the mixing of these surfactants in 3:1 Polysorbate 80: PEG-40 hydrogenated castor oil systems. This lends further support to the use of Polysorbate 80: PEG-40 hydrogenated castor oil mixed micelle systems in drug delivery.

CPP, the critical packing parameter, is an indication of the packing geometry of surfactant molecules in water.[67] It relates the volume of the hydrophobic portion of the

surfactant molecule to that of the area occupied by the head group multiplied by the length of the hydrocarbon tail. It is given by the following equation[67] :

$$CPP = \frac{v}{a_0 l_c} \quad \textbf{(Eq. 2.5)}$$

where v is the volume of the hydrophobic portion of the surfactant molecule in nm^3, a_0 is the area occupied by the head group in nm^2 and l_c is the length of the hydrocarbon tail in m. The values of v and l were obtained using Tanford's equations[67]:

$$v = 0.0274 + (0.0269 * n_c) \text{ and} \quad \textbf{(Eq. 2.6)}$$

$$l = 0.15 + (0.1265 * n_c) \quad \textbf{(Eq. 2.7)}$$

where n_c is the number of carbons in the surfactant hydrocarbon chain. The CPP values listed in **Table 2.2**, as obtained from **Eqs. 2.5-7**, are below 0.33 and consistent with spherical micelle formation, as is expected for each surfactant given its head and tail structures. Surfactant efficiency and effectiveness are indicators of surfactant performance. Efficiency is the concentration of surfactant required to reduce the surface tension by a specified amount of 20 mN/m, while effectiveness is the maximum reduction of surface tension that can be obtained with a particular surfactant.[67] Surfactant efficiency is given by the equation[67]:

$$Efficiency = -\log C_{20} \quad \textbf{(Eq. 2.8)}$$

where C_{20} is the concentration of surfactant, typically in mM, required to reduce the surface tension by 20 mN/m. In contrast, surfactant effectiveness is given by the equation[67]:

$$\Delta^{\circ}_{cmc} = \pi_{cmc} + 2.3nR\Gamma.\log\left(\frac{cmc}{c_1}\right) \quad \textbf{(Eq. 2.9)}$$

where π_{cmc} is the surface pressure as calculated by the difference between the surface tension of water and that of the system at the critical micelle concentration (typically in N/m), R is the gas constant in J/K.mol, T is the temperature in K, Γ is the surface excess in mol/m^2, cmc is the critical micelle concentration (typically in M) and C_1 is the lowest surfactant concentration

(M) obtained from line 1 in the semi-log plot of surface tension versus surfactant concentration. According to **Table 2.2** and **Eqs. 2.8-9**, 3:1 Polysorbate 80: PEG-40 hydrogenated castor oil proved to be an efficient surfactant mixture while effectiveness appeared to decrease upon mixing the two surfactants. The highest surfactant effectiveness was seen in Polysorbate 80, likely due to its small hydrophilic head group, which is able to pack neatly at the interface as has been previously reported.[69] This small hydrophilic head also leads to relatively large CMC/C_{20} and Γ values[69] as seen in this work. PEG-40 hydrogenated castor oil with its multi-hydrophobic tail structure had a smaller effect on efficiency than effectiveness as has been previously reported for multi-chain surfactants.[71] CMC/C_{20} sheds insight into the micellization and adsorption processes, where CMC is the critical micelle concentration and C_{20} is the concentration of surfactant required to reduce the surface tension by 20 mN/m.[69] An increase in CMC/C_{20} indicates that micellization is inhibited more than adsorption while a decrease in this parameter indicates that micellization is facilitated more than adsorption. 3:1 Polysorbate 80: PEG-40 hydrogenated castor oil demonstrated lower CMC/C_{20} values in comparison to that of the individual surfactants, indicating that this surfactant mixture exhibits a strong tendency for micellization. This lends further support to the use of Polysorbate 80 and PEG-40 hydrogenated castor oil mixed micelle systems for multi-drug delivery.

The β interaction parameter is an indicator of the nature and strength of an interaction between two different surfactants in a mixed micelle system.[72,73] The value of this parameter is dimensionless and relates to the free energy change between mixed and unmixed systems.[72,73] A negative β value indicates more attractive or less repulsive forces between the two surfactants and thus, synergism.[72] Consequently, a positive β value indicates less attractive or more repulsive forces between the two surfactants and thus, antagonism. A β value of 0 indicates little to no change in interaction.[72,74] The equation for calculating the β interaction parameter and its variables was given by Rubingh in 1979[75]; the value itself depends heavily on surfactant structure including the bulkiness of head and tail groups as well as the mole fraction of each surfactant used.[72] The β parameter is valid assuming: 1) a lack of solution impurities, 2) an absence of counterion effects and 3) an absence of free water in all mixed micelle systems.[72] It is given by the following equation:[73]

$$\beta = \ln\left(\frac{cmc.a_1}{cmc_1.x_1}\right)/(1 - X_1)^2 \qquad \textbf{(Eq. 2.10)}$$

where a_1 is the mole fraction of surfactant 1, cmc is the critical micelle concentration of the surfactant mixture, cmc_1 is the critical micelle concentration of surfactant 1 and X_1 is the micellar composition (solved iteratively) using the following equation:[73]

$$\frac{x_1^2 \ln(\frac{cmc.a_1}{cmc_1.x_1})}{[(1-x_1)^2.\ln(\frac{cmc\,(1-a_1)}{cmc_2.(1-x_1)})]} = 1 \qquad \textbf{(Eq. 2.11)}$$

where all variables are as defined above with cmc_2 being the critical micelle concentration of surfactant 2.

According to **Table 2.3** and based on **Eqs. 2.10 and 2.11**, 3:1 Polysorbate 80: PEG-40 hydrogenated castor oil mixtures resulted in negative β values that deviate from zero, indicating attractive interactions between these two surfactants and thus, synergism. This could possibly be due to the facilitated packing of Polysorbate 80 between the bulky PEG-40 hydrogenated castor oil molecules. Nevertheless, it is evident that Polysorbate 80 and PEG-40 hydrogenated castor oil exhibit attractive tendencies, leading to synergism and thus, favourable microemulsion formation, which may find application in a variety of drug delivery spheres.

Table 2.3: Mole fraction (α_1), ideal CMC, experimental CMC, mixed micellar composition (X_1) and interaction parameter (β) for 3:1 Polysorbate 80: PEG-40 hydrogenated castor oil mixed surfactant systems.

Surfactant Mixture	α_1	Ideal CMC (μM)	Experimental CMC (μM)	X_1	β
3:1 Polysorbate 80: PEG-40 hydrogenated castor oil	0.75	4.77	3.59 ± 0.00	0.67	-2.2

2.6 Conclusion

The phase mapping performed in this work demonstrated that despite the similarities in HLB value amongst the non-ionic surfactants utilized, a broad range of microemulsion types, unique to each surfactant, was obtained. In general, all surfactants used in this work demonstrated high Winsor I, O/W microemulsion formation potential at increased water concentrations, and low Winsor II W/O microemulsion formation potential at increased oil concentrations, as

hypothesized. This is a direct result of the high HLB value and propensity to form O/W emulsions in accordance with the Bancroft rule. Winsor III microemulsions were generally concentrated in the middle of each ternary phase diagram while Winsor IV monophasic microemulsions were concentrated primarily at high surfactant concentrations above 40% w/w.

Given that all surfactants tested in this work had the tendency to form O/W microemulsions, it can be concluded that PEG-40 hydrogenated castor oil, Poloxamer 188, Polysorbate 80 and TPGS are suitable for lipophilic drug delivery. Type II W/O microemulsions were difficult to obtain. However, of the surfactants tested in this work, Polysorbate 80 demonstrated the largest W/O microemulsion potential rendering it suitable for hydrophilic drug delivery. Type IV microemulsion drug delivery was notable in all surfactant systems but most prominent in Polysorbate 80. Type IV microemulsions were formed at higher surfactant concentrations and thus, are well suited for a multitude of drug delivery applications including multi-drug delivery. Overall, Polysorbate 80 demonstrated the highest versatility in terms of microemulsion formation type, most likely due to its large hydrophilic head and hydrocarbon tail structure, which was able to assume a variety of conformations.

This work also demonstrated the promotion of Type IV microemulsion formation in PEG-40 hydrogenated castor oil upon mixing with Polysorbate 80. The propensity of Polysorbate 80 to induce Type IV microemulsion formation in PEG-40 hydrogenated castor oil is a direct result of the molecular structures and packing arrangements afforded by each surfactant. It appears that Polysorbate 80 with its triple PEO head group and monooleate alkyl tail was able to pack efficiently between the large head group and triple monooleate tail structure of PEG-40 hydrogenated castor oil. An investigation of important mixed surfactant parameters such as CMC, $\Delta G°_{mic}$ and the β interaction parameter proved that these two surfactants have a particular affinity for each other, leading to synergistic tendencies and an ability to form a myriad of microemulsion types. Thus, this work has determined that Polysorbate 80 and PEG-40 hydrogenated castor oil are a novel, non-ionic surfactant pair that may be further investigated for drug delivery applications, particularly with respect to multi-drug delivery.

Chapter 3: Optimization of Microemulsion Formulation Using HLD Equation and Active Pharmaceutical Ingredient (API) Incorporation

3.1 Introduction

In **Chapter 2**, a microemulsion system comprised of 3:1 Polysorbate 80:Cremophor RH 40, Miglyol 812 and water was identified for further analysis and incorporation of active pharmaceutical ingredients (APIs). Given that the proof-of-concept in this work is a multi-vitamin comprised of multiple APIs of varying hydro- and lipophilicity, the challenge involves developing a strategy for incorporating them into the existing microemulsion formulation.

3.1.1 Lipophilic versus Hydrophilic API Incorporation

As noted in **Chapter 1** of this work, literature regarding multi-drug delivery and specifically, microemulsion, multi-drug delivery is limited. Research involving this type of multi-drug delivery has typically focused on the incorporation of drugs of similar hydro- or lipophilicity, such that similar solubilisation conditions were used.[1] The type of multi-drug delivery necessary in this work, where drugs of varying hydro- and lipophilicity are used, presents greater challenges.

The involvement of more than one API results in complications not only in solubility, but upon exposure to temperature, salinity and lipophilicity as these parameters may affect various APIs in solution as well as the resulting microemulsion. One approach to this problem is to group APIs based on their hydro- or lipophilicity and treat this multi-API group as a single entity. In this manner, complex, multi-drug delivery is simplified and similar incorporation conditions may be used for each group of APIs; this is the approach that has been used in this work. The lipophilic API component was comprised of beta-carotene (precursor to Vitamin A), cholecalciferol (Vitamin D_3), d-α-tocopherol acetate (Vitamin E acetate), phytonadione (Vitamin K_1) and docosahexaenoic/eicosapentaenoic acid (DHA/EPA) while the hydrophilic API component was comprised of thiamine mononitrate (Vitamin B_1), riboflavin (Vitamin B_2), niacinamide (Vitamin B_3), pyridoxine hydrochloride (Vitamin B_6), folic acid (Vitamin B_9) and

cyanocobalamin (Vitamin B_{12}). Amounts were added in accordance with Health Canada requirements, adjusting for potency as outlined in **Table B-1**, **Appendix B**. Minerals were not considered for future formulation due to their inability to be solubilized and the fact that they would simply remain suspended in solution. This suspension may present further complications with respect to stability due to gravitational separation and potential metal incompatibility with the aqueous component of the formulation.

As noted in **Chapter 1, Section 1.5.2**, lipophilicity impacts the type of microemulsion obtained and shifts the HLD value to the left.[2] Incorporation of highly lipophilic APIs into the oil phase of a microemulsion can result in a change in lipophilicity of the system, affecting the ability of the surfactant to sufficiently solubilize the oil component and produce a microemulsion. Incorporation of hydrophilic, charged APIs into the water phase of the microemulsion, while unlikely to produce as large an effect as lipophilic API incorporation, may also affect ionic strength and the type of microemulsion produced. In addition, the presence of slightly surface-active APIs may affect partitioning into either aqueous or organic phase and may act along with the emulsifying agent to either decrease or increase the interfacial tension, affecting microemulsion type. Therefore, optimizing such a system for drug delivery involves solubilizing the lipophilic APIs in oil, the hydrophilic APIs in water, and examining the overall effect on the microemulsion. The HLD equation may be used to examine this effect.

3.1.2 Optimization of Microemulsion Formulation via the HLD Equation

In **Chapter 1**, **Section 1.5.2** the HLD equation was identified as a powerful tool for microemulsion formulation that not only considers structural properties of the surfactant, but also environmental factors that greatly impact microemulsion formation such as temperature and lipophilicity, as depicted by the equations below[2] :

$$\mathrm{HLD} = \mathrm{b}(\mathrm{S}) - \mathrm{K}(\mathrm{EACN}) - \phi(\mathrm{A}) + {}_{\mathrm{CT}}\Delta\mathrm{T} + \mathrm{CC} \quad \textbf{for non-ionic surfactant} \qquad \textbf{(Eq. 3.1)}$$

$$\mathrm{HLD} = \ln(\mathrm{S}) - \mathrm{K}(\mathrm{EACN}) - \mathrm{f}(\mathrm{A}) - {}_{\alpha\mathrm{T}}\Delta\mathrm{T} + \mathrm{CC} \quad \textbf{for ionic surfactants} \qquad \textbf{(Eq. 3.2)}$$

One way to evaluate the effect of lipophilic API incorporation on microemulsion formation is to determine the value of the effective alkane carbon number (EACN) term in the HLD equation. EACN has practical relevance given that formulation studies are not often

performed with straight chain oils. Rather, oils that are commercially available contain a mixture of structurally related oils.[3] In addition, complications may arise from commercial, non-ionic surfactants that tend to preferentially partition into oil[4] or polar oils that tend to partition into water.[5,6] Thus, the EACN is a practical approach to quantifying many of the non-linear oils most commonly used today, though impure oils must be used with caution.[5,7] EACN assigns a straight-chain carbon number to non-linear oils but the assignment of an EACN to a particular oil does not necessarily mean that the oil behaves analogously to its straight chain counterpart. It merely means that there is a way to quantitatively determine the degree of lipophilicity of complex oils typically used in microemulsion formulations, and to adjust the HLD value accordingly as a formulation optimization tool. The EACN of the oil phase before and after API incorporation may be compared in order to determine any differences in microemulsion formation potential. The higher the EACN, the more lipophilic the oil phase and the more negative the HLD or propensity to form O/W microemulsion systems.

Characteristic curvature (CC) is another term unique to each surfactant, essential in determining the HLD value. CC is a surfactant parameter like HLB that takes into account the structure of the head and tail groups of a surfactant.[4] It describes the tendency of a surfactant to curve towards a particular interface.[4] A negative CC refers to a hydrophilic surfactant with a tendency to form O/W micelles while a positive CC refers to a hydrophobic surfactant with a tendency to form W/O micelles.[4] Oleic acid with 18 carbons including a carboxylic acid group and unsaturated double bond, has been determined to possess a CC value of 0.[8] Thus, a CC value above or below 0 indicates a surfactant more hydrophobic or hydrophilic than oleic acid, respectively.[8] As can be seen from the HLD equation, the lower the CC, the lower the HLD. This increases the tendency to form O/W microemulsion systems.

Oil EACN and surfactant CC are two of the most difficult values to obtain in the HLD equation. Both EACN and CC are determined via formulation scans which involve keeping all parameters but one, constant. Typically, oil, water and surfactant ratios are kept constant while one variable such as salt concentration or temperature or oil alkane carbon number is varied. For EACN determination, temperature is varied in the case of non-ionic surfactants, while salinity is varied in the case of ionic surfactants. For CC determination, oil EACN is varied. Formulation scans often involve a large degree of trial-and-error in order to obtain the right conditions to observe a shift from a Type I→ III→ II microemulsion. However, despite these

difficulties, formulation scans afford the determination of how microemulsion behaviour changes upon API incorporation. Once these changes are determined, the plotting of ternary phase diagrams (TPDs) with each individual API to determine microemulsion behaviour may not be necessary.

In this work, lipophilic APIs are likely to demonstrate an ease of solubility in oil versus that of hydrophilic APIs in water, given the low water solubilities of some B vitamins. As a result, saturation solubility testing (**Chapter 1, Section 1.7.1)** will be performed on the hydrophilic B vitamins with the microemulsion components identified in **Chapter 2** i.e., Miglyol 812, Polysorbate 80 and Cremophor RH 40. Components in which the B vitamins demonstrate favourable solubility will be confirmed for use as the microemulsion into which both hydrophilic and lipophilic APIs may be incorporated.

3.2 Study Objectives

Ternary Phase Diagram (TPD) analysis in **Chapter 2** culminated in the selection and finalization of a basic microemulsion system comprised of 3:1 Polysorbate 80:Cremophor RH 40 surfactant, Miglyol 812 oil and water. The broad aim of this chapter, **Chapter 3**, is to incorporate all lipophilic and hydrophilic APIs, treating each as a separate group in order to assess potential impacts of each type of incorporation on the microemulsion system. Specific aims include:

i) To assess the solubility of hydrophilic APIs in individual microemulsion components via saturation solubility testing
ii) To assess the effect of lipophilic API incorporation on microemulsion formation via EACN determination
iii) To determine the HLD value of the lipophilic drug-loaded microemulsion system in order to facilitate O/W delivery
iv) To incorporate all hydrophilic B vitamins into the water phase of the microemulsion system

3.3 Hypotheses

3.3.1 Hydrophilic API Solubility

All water-soluble B vitamins (thiamine mononitrate, riboflavin, niacinamide, pyridoxine hydrochloride, folic acid and cyanocobalamin) will demonstrate greater solubility in water than in Miglyol 812 oil or Polysorbate 80/Cremophor RH 40 surfactant. Riboflavin and folic acid will exhibit the lowest saturation solubility results due to their low water solubilities.

3.3.2 Lipophilic API Incorporation

The addition of five lipophilic APIs (beta-carotene, cholecalciferol, d-α-tocopherol acetate, phytonadione and docosahexaenoic/eicosapentaenoic acid) to Miglyol 812 will result in an increase of EACN by at least 1 carbon unit, relative to the EACN value of Miglyol 812 alone.

3.4 Materials and Methods

3.4.1 Materials

Unless explicitly stated, all materials were generously gifted by Catalent Pharma Solutions Inc., formerly Accucaps Industries Limited (Ontario, Canada), and were used without purification. Thiamine mononitrate, riboflavin, niacinamide, pyridoxine hydrochloride, folic acid, cyanocobalamin, beta-carotene, cholecalciferol, d-α-tocopherol acetate and phytonadione were produced by DSM Nutritional Products (Ontario, Canada). Omega-3 fatty acid ester (20% eicosanopentaenoic acid/ 60% docosahexaenoic acid) was produced by Huatai Biopharm Inc. (Sichuan, China). Miglyol 812 was produced by IOI Oleochemical (Ruhr, Germany), PEG-40 hydrogenated castor oil (Cremophor/Kolliphor RH 40) was produced by BASF Care Creations (New Jersey, USA) and Polysorbate 80 was produced by BASF (Ontario, Canada). Chemical structures and log P values of all APIs are outlined in **Chapter 1**: **Table 1.5** and **Table 1.6.** *All water-soluble vitamins were present in solid powder form while all oil-soluble vitamins, surfactants and Miglyol 812 were present in liquid form. Cremophor RH 40 surfactant was semi-solid in nature.*

Dihexyl sodium sulphosuccinate (SDHS) (80% in water), hexane (HPLC grade ≥ 98.5%), hexadecane (reagent plus 99%), sodium chloride (ACS reagent, ≥99%) and sodium hydroxide pellets (≥97%) were purchased from Sigma-Aldrich (Ontario, Canada). Dodecane (99% pure, ACROS organics) and ethyl caprate (99%) were purchased from Thermo Fisher Scientific (Ontario, Canada). Toluene (certified ACS ≥99.5%) was purchased from Chemstores at the University of Waterloo and manufactured by Fisher Scientific (Ontario. Canada). 100% pure sunflower and canola oil were obtained from PC Organics (Ontario, Canada).

3.4.2 Methods

A series of Health Canada-recommended vitamins and minerals for prenatal supplementation were selected as APIs. Each API was literature-screened for stability, toxicity and performance in previous microemulsion formulations. Alternative forms of each API were also considered. A final list ranking the suitability of each API and its alternate form was completed and the formulation was built around these ingredients. **Tables 1.5-1.6** in **Chapter 1** contain the list of final ingredients and structures.

3.4.2.1 Saturation Solubility

An empty weighing boat was placed onto a Mettler AT261 Delta Range Analytical Balance and its weight recorded. The scale was tared and between 0 and 1 g ± 0.1 mg of water-soluble API was added to the weighing boat. The weighing boat and its contents were then reweighed and some of the API was carefully transferred to a 20 mL scintillation vial containing 15 g ± 0.1 mg solvent and a magnetic stir bar. The scintillation vial was placed onto a stir plate and set to stir at 300 RPM until all API was dissolved. The time taken for dissolution was recorded in minutes. The weighing boat containing the remaining API was reweighed and subtracted from the original weight of the weighing boat and its contents, giving an accurate weight of API added to each vial. When all APIs appeared dissolved, the above steps were repeated until saturation was observed or until excess API was seen at the bottom of the scintillation vial. This saturation test was repeated for all water-soluble APIs in 15 g ± 0.1 mg deionized (DI) water, 15 g ± 0.1 mg Miglyol 812, 15 g ± 0.1 mg Polysorbate 80 and 15 g ± 0.1 mg Cremophor

RH 40. Each solution of API and solvent was centrifuged, filtered and diluted for Ultra Performance Liquid Chromatography (UPLC). Calibration curves of concentration versus peak area were obtained for pure API and used to quantify the amount of API recovered from each saturated sample. A Waters Acquity H-Class UPLC instrument was used along with a C18 silica column. The mobile phases consisted of 0.1% phosphoric acid and acetonitrile at 55°C with 2 μL injection volume at wavelengths 275, 260 and 192 nm. Saturation solubility tests were only performed on the hydrophilic APIs given the low water solubilities of many of these compounds. The lipophilic APIs exhibited high log P values and thus, an ease of solubility was expected in Miglyol 812. As a result, these lipophilic APIs were instead evaluated using temperature, salinity and lipophilicity scans.

3.4.2.2 Formulation Scan: Temperature

Polysorbate 80 aqueous solution (10% w/w) was prepared in a scintillation vial by weighing 1 g ± 0.1 mg surfactant into 10 g DI water using a Mettler AT261 Delta Range Analytical Balance and/or Sartorius Secura225D1S Analytical Balance. The solution was inverted manually until dissolved. 5 g ± 0.1 mg of this surfactant stock solution was added to a scintillation vial containing 5 g of oil phase*. The solution was inverted manually 20-25 times and left to settle for a period of 24 hours in a dark cupboard before evaluating phase behaviour. Each sample was heated for a period of 24 hours at each respective temperature point in 2-5ºC increments from 25 ± 0.1ºC to 80 ± 0.1ºC mg using a Fisher Scientific Isotemp GPD 10 water bath and a hot plate with a temperature controlled beaker of water. At each temperature increment, the mixes were removed from the water-bath, visually observed for any changes in phase behaviour using a red laser pointer (Tyndall effect), photographed and then replaced into the water bath at a higher temperature. Temperature scans were performed in triplicate.

**two oil phases were prepared for comparison purposes: 5 g Miglyol 812 and 5 g 50% w/w Miglyol 812: oil-soluble actives (drug-loaded Miglyol 812)*

3.4.2.3 Formulation Scan: Salinity and Conductivity

Dihexyl sodium sulphosuccinate (SDHS) aqueous surfactant solution (32.5% w/w) was prepared and added to equal volumes of deionized water and oil. SDHS is a commonly-used

surfactant for salinity scans due to its ionic nature and well-characterized characteristic curvature (CC) value.[8] The oil phases were the same as mentioned previously and consisted either of Miglyol 812 or 50% w/w Miglyol 812:oil-soluble APIs. All surfactant, water and oil mixtures were exposed to increasing amounts of 20% sodium chloride solution from 1 g/100 mL to 19 g/100 mL. The aqueous surfactant concentration in each vial was maintained at 10%. Following manufacture, each sample was left to settle in a dark cupboard for a period of 24 hours before conductivity was measured using a Mettler Toledo InLab 752-6 mm microconductivity probe and SevenEasy conductivity meter. Conductivity readings were also recorded after 48 and 72 hours in milli Siemens per cm (mS/cm) ± 0.1. Graphs of conductivity versus sodium chloride concentration were generated in Graphpad Prism 6 software. Salinity scans were performed in duplicate.

3.4.2.4 Formulation Scan: Lipophilicity

1 mL 3:1 Polysorbate 80:Cremophor RH 40 surfactant mixture, 2.5 mL DI water, 10 mL 25-30% NaCl solution and 10 mL oil ranging from EACN 1-18 were weighed to ± 0.1 mg using a Sartorius Secura225D1S Analytical Balance into a 30 mL scintillation vial and mixed manually by inverting. Therefore, all conditions were kept constant except for that of lipophilicity or EACN, affording a shift to a Type III microemulsion. The samples were left to settle for a period of 24 hours in a dark cupboard before phase behaviour was visually analyzed and examined using a red laser pointer. Given that the EACN value is additive, oils of known EACN value were mixed together in varying proportions in order to obtain the desired EACN. Lipophilicity scans were performed in duplicate.

3.4.2.5 Tensiometry

Tensiometry to determine the critical micelle concentration (CMC) was conducted using a T3 Lauda Tensiometer and DuNoüy ring, in the same manner as described in **Chapter 2**. Briefly, the surfactant solution was carefully titrated into a glass vessel containing 40 mL MilliQ water with stirring for 7 minutes. A semi-log graph of surface tension versus surfactant concentration was generated and the breakpoint identified. The CMC was determined by the intersection of

the linear trendlines before and after this breakpoint in the plot. Tensiometry experiments were performed in triplicate.

3.4.2.6 Hydrophilic API Incorporation

A number of approaches were employed in an effort to solubilize all water-soluble active ingredients, riboflavin and folic acid being the most challenging due to their low water solubility. These approaches included: i) an increase in temperature, ii) an increase in pH, iii) a change in solvent, iv) dissolution of riboflavin and folic acid in the oil-soluble API phase and v) dissolution of riboflavin and folic acid in the fully formulated microemulsion. Approach ii) was most successful.

The final protocol for successful incorporation of all six hydrophilic APIs involved first tarring a section of weigh paper on a Sartorius Secura225D1S Analytical Balance. Desired amounts of each vitamin (**Table B-1, Appendix B**) were then added individually to the weighing paper, the weight recorded, and the contents transferred to a beaker of (pre-measured) MilliQ water on a hot/stir plate set to stir at 300 RPM using a magnetic stir bar. The weighing paper with the empty contents was reweighed in order to determine the exact amount of each API added to the water phase. This process was first carried out for the easily soluble water-soluble vitamins, i.e. thiamine mononitrate (B_1), niacinamide (B_3), pyridoxine hydrochloride (B_6) and cyanocobalamin (B_{12}). Riboflavin (B_2) and folic acid (B_9) were then added where insolubility was immediately evident. 1 M sodium hydroxide solution was added in small increments of 100 μL until riboflavin and folic acid were dissolved. The final pH of the microemulsion formulation was approximately 8.5. All measurements were conducted in light-restricted conditions.

3.5 Results and Discussion

3.5.1 Saturation Solubility

The amount of hydrophilic API added to 15 g of solvent, until the point of saturation, is displayed in **Table 3.1**. As expected, the solvents most and least able to accommodate the majority of hydrophilic APIs were water and Miglyol 812 oil, respectively. Many of the APIs

also demonstrated high solubility in Cremophor RH 40 which, in some cases, surpassed their solubility in water. Polysorbate 80 was less accommodating, with vitamins recording low solubilities similar to that of Miglyol 812.

With respect to water, the order of solubility was Vitamin B_3> Vitamin B_6> Vitamin B_{12}> Vitamin B_1> Vitamin B_2> Vitamin B_9. This is generally comparable to solubilities reported in the literature for each form of vitamin used in this work- 500 mg/g[9], 220 mg/g[10], 12.5 mg/g[11], 27 mg/g[12], 0.657 mg/g[13] and 0.0761 mg/g[14], respectively. Cremophor RH 40 also acted as a favourable solvent for many hydrophilic APIs with the ranking following a similar pattern to that of water: Vitamin B_3> Vitamin B_{12}> Vitamin B_1> Vitamin B_6> Vitamin B_2> Vitamin B_9. In Polysorbate 80, API solubility was generally low and in the order Vitamin B_3> Vitamin B_{12}> Vitamin B_6> Vitamin B_2> Vitamin B_9> Vitamin B_1 while in Miglyol 812, the same trend applied with the Vitamins B_1, B_2 and B_6 exhibiting practically equal solubility followed by B_9. These results are depicted in **Figure 3.1.**

The reasons for the varying solubilities may be explained through consideration of the physicochemical structures of the B vitamins outlined in **Chapter 1** in **Table 1.5.** The water solubility of all vitamins followed literature trends except in the case of Vitamin B_1 and B_{12} where solubility trends were reversed. This is attributable to the low potency of cyanocobalamin (1%) used in this work. The other 99% is likely comprised of stability-enhancing sugar components[15], resulting in higher water-solubility values in comparison to Vitamin B_1.

With respect to API solubility in the surfactants, Cremophor RH 40 and Polysorbate 80, Vitamins B3 and B12 demonstrated the greatest degree of solubility. Vitamin B_3, niacinamide, consists of a single pyridine ring and amide bond as well as one hydrogen donor and two hydrogen acceptors.[9] These donors and acceptors may afford hydrogen bonding with the ethoxylated head groups of Cremophor RH 40 and Polysorbate 80. The high water solubility, low log P value (-0.39)[9] and low permeability results in niacinamide being classified as a BCS Class III compound.[16]

Table 3.1: Saturation solubility results (to 3 significant figures) of water-soluble APIs in 15 g water, oil or surfactant.

API	Solvent	API added (± 0.1 mg) per 15 g Solvent
Vitamin B_1 (Thiamine mononitrate)	Water	108
	Miglyol 812	8.90
	Polysorbate 80	3.70
	Cremophor RH 40	95.7
Vitamin B_2 (Riboflavin)	Water	33.7
	Miglyol 812	9.00
	Polysorbate 80	9.70
	Cremophor RH 40	46.4
Vitamin B_3 (Niacinamide)	Water	2370
	Miglyol 812	38.3
	Polysorbate 80	54.6
	Cremophor RH 40	383
Vitamin B_6 (Pyridoxine hydrochloride)	Water	921
	Miglyol 812	8.90
	Polysorbate 80	16.6
	Cremophor RH 40	82.9
Vitamin B_9 (Folic Acid)	Water	3.20
	Miglyol 812	3.80
	Polysorbate 80	6.30
	Cremophor RH 40	23.4
Vitamin B_{12} (Cyanocobalamin)	Water	306
	Miglyol 812	17.2
	Polysorbate 80	29.8
	Cremophor RH 40	122

Despite its generally low log P value, however, niacinamide possesses the highest log P value of all the B vitamins tested in this work. In other words, it is the most lipophilic of all the B vitamins. This may be attributed to its small molecule structure and low molecular weight of approximately 122 g/mol[9], which allows the contribution of the lipophilic pyridine ring to be greater than expected for a pyridine ring present in a larger molecule. This degree of lipophilicity versus that of the other B vitamins tested in this work, may enable interactions with the hydrogenated trioleate castor oil tail of Cremophor RH 40 and the monooleate tail of

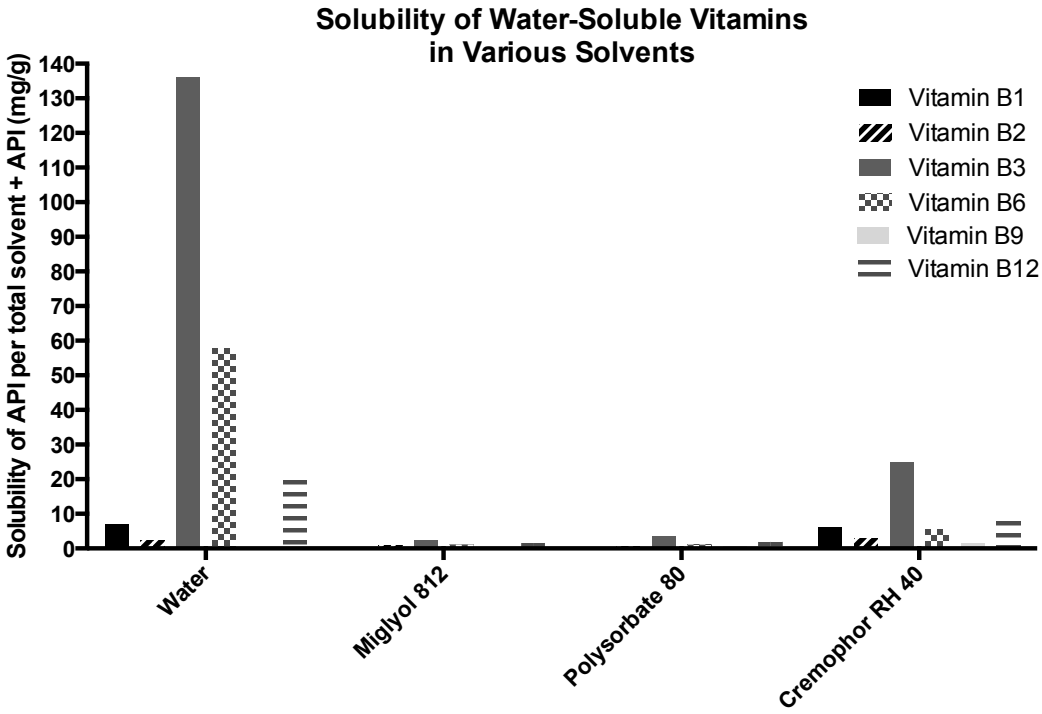

Figure 3.1: Solubility (mg/g) of vitamins, B_1, B_2, B_3, B_6, B_9 and B_{12} in water, Miglyol 812, Polysorbate 80 and Cremophor RH 40 as determined by saturation solubility test, categorized by solvent.

Polysorbate 80, resulting in high solubility in these surfactants, as well as in Miglyol 812 (a medium chain triglyceride). Vitamin B_{12} is an organometallic compound with a cobalt (Co^{3+}) corrin ring at its center, along with multiple, amide side chains, a ribose-3-phosphate sugar and a benzimidazole ring. It has the most complex structure of all the B vitamins with approximately 9 hydrogen donors and 19 hydrogen acceptors, which are likely able to interact with the polyethoxylated head groups of Cremophor RH 40 and Polysorbate 80. This is further compounded by the solubility-enhancing sugars likely present in its structure as a result of its low potency. These hydrogen donors and acceptors result in cyanocobalamin having the lowest log P of all the B vitamins, -14.[11] This high water solubility and low permeability makes cyanocobalamin a BCS class III compound.[17] Its low permeability is likely a result of both its high water solubility and high molecular weight of 1355.37 g/mol.[11] However, the complex corrin ring structure may have offered an advantage over B_1, B_2, B_6 and B_9 with respect to Miglyol 812 solubility.

In contrast to Vitamins B_3 and B_{12}, Vitamins B_1, B_2, B_6 and B_9 demonstrated lower solubilities in Cremophor RH 40 and Polysorbate 80. The main difference in the order of solubility in both surfactants involved Vitamin B_1, which was most soluble in Cremophor RH 40 and least soluble in Polysorbate 80. Given that Polysorbate 80 contains half as many hydrophilic, ethylene oxide groups as Cremophor RH 40, resulting in a slightly higher lipophilic profile[18-20], it is not surprising that the solubility of hydrophilic Vitamin B_1 was lower in Polysorbate 80. Pyridoxine hydrochloride, the salt form of Vitamin B_6 consists of an associated hydrochloride and pyrimidine ring with multiple side groups including two methanol groups, one hydroxyl and one methyl group. Its slightly lower log P value of -0.95[21], along with a total of approximately 4 hydrogen acceptors and donors on a small molecule with molecular weight of only 205.64 g/mol, leads to higher hydrogen bonding potential with the head groups of Cremophor RH 40 and Polysorbate 80, as compared to Vitamins B_2 and B_9. As a result of its high water solubility and low permeability, Vitamin B_6 is a BCS Class III compound.[22]

With respect to solubility in oil, trends would generally be expected to be the reverse of those seen in water. However, in the case of Miglyol 812, the most and least soluble APIs were the same as those in water- B_3 and B_9, respectively. This is likely due to the fact that Miglyol 812, as a medium chain triglyceride, is a polar oil.[23,24] Therefore, though the lipophilic rings of Vitamin B_9 appeared to confer an advantage with respect to solubility in Polysorbate 80, this advantage was not seen in Miglyol 812. Due to its poor solubility and permeability, folic acid is classified as BCS Class IV compound.[25]

In general, based on the results in **Table 3.1** and **Figure 3.1,** Vitamins B_3, B_{12}, B_6 and B_1, respectively, were the easiest to dissolve across all solvents while Vitamins B_2 and Vitamin B_9 were the most difficult; Vitamin B_2 exhibited slightly less difficulty than Vitamin B_9. Vitamin B_2, riboflavin, is comprised of an isoalloxazine ring and ribityl group with multiple electronegative (hydrogen acceptor) groups such as nitrogen and oxygen and multiple hydroxyl (hydrogen donor) groups. Although these groups theoretically promote hydrogen bonding with water, the additional lipophilic ring restricts solubility in water, resulting in the low values seen in **Table 3.1** and **Figure 3.1**. Consequently, the log P of riboflavin is higher than that of Vitamin B_1 at -0.92[13], indicating greater lipophilicity. With respect to Vitamin B_9 (folic acid), though multiple hydrogen donors and acceptors are able to participate in hydrogen bonding

with water, the pyrimidine and benzene rings which outnumber those in B_1, result in lower water solubility. This is confirmed in the log P of -0.68[14] similar to that of Vitamin B_2.

In addition to the solubility results contained in **Table 3.1** and **Figure 3.1**, UPLC analysis was performed on the APIs in this work in an effort to determine whether each API could be recovered from its respective solvent, once solubilized. As noted in **Chapter 1** (**Section 1.7.1**), saturation solubility via liquid chromatography (LC) confirms whether the amount of API introduced into a system can be recovered and quantified. This is especially important in the case of vitamins, which as discussed later on in this Chapter, are susceptible to degradation upon exposure to a variety of conditions and as a result, present many analytical challenges.[26] Given the unique LC conditions also required for each vitamin with respect to column choices, mobile phases and detection wavelengths, it was important to establish an appropriate recovery method.[27,28]

The results in **Figure 3.2** illustrated that despite the low solubilities in Miglyol 812 oil and Polysorbate 80, recovery of the APIs in these solvents was still possible and, in cases such as that of Vitamin B_3, very high. The highest recovery for all APIs was noted in Cremophor RH 40 where five of the six water-soluble APIs demonstrated over 60% recovery with Vitamin B_6 and B_{12}, in particular, exhibiting over 90% recovery. Water also demonstrated high recoveries with four of the six vitamins exhibiting 90% or higher recovery. Not surprisingly, the most difficult vitamins to recover in water were riboflavin (B_2) and folic acid (B_9). Similar to **Figure 3.1**, not only were water and Cremophor RH 40 able to demonstrate the highest solubility for the water-soluble APIs tested in this work, but according to **Figure 3.2** they were also the easiest solvents to recover dissolved APIs from. As in **Figure 3.1,** Vitamin B_3 had the highest recovery in consideration of all solvents. Recovery was highest in Polysorbate 80 (100%) followed by water (91%) then Miglyol 812 and Cremophor RH 40. Vitamin B_6 also exhibited a high degree of recovery in almost all solvents. 100% recovery was seen in water, and approximately 90% was seen in both Polysorbate 80 and Cremophor RH 40 but less than 2% was recovered in Miglyol 812. Vitamin B_{12} was similar to Vitamin B_1 in that high recovery percentages were obtained in water and Cremophor RH 40 but virtually none in Miglyol 812 oil as well as Polysorbate 80. Vitamins B_2 and B_9 demonstrated very low recoveries in all solvents tested. However, it is worth noting that at least some degree of recovery was obtained even in Miglyol 812 oil. The results in **Figure 3.2** as compared to

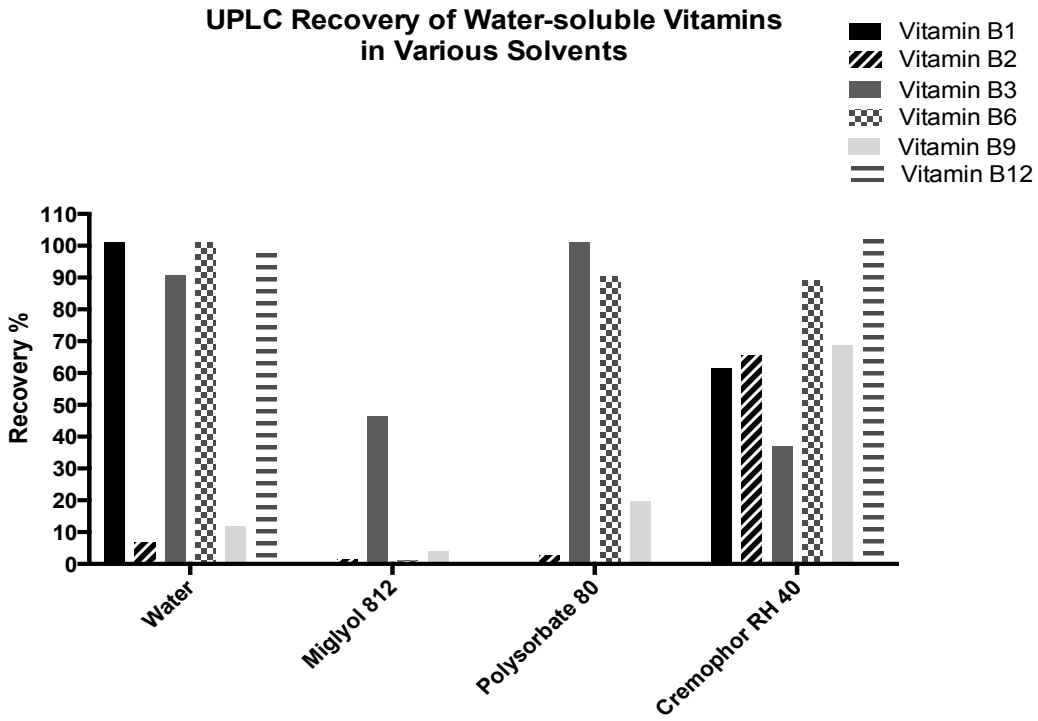

Figure 3.2: Recovery percentages of Vitamins, B_1, B_2, B_3, B_6, B_7, B_9 and B_{12} in water, Miglyol 812, Polysorbate 80 and Cremophor RH 40 as determined by UPLC.

Figure 3.1, show that API solubility in a particular solvent does not necessary reflect its ability to be analytically recovered. Analytical methods are complex when dealing with multi-component drug formulations and care must be taken when developing them.[26,29] Thus, despite the suitability of liquid chromatography techniques for multivitamin recovery due to their high sensitivity and selectivity[30], each vitamin has specific physiochemical properties and stability requirements (re: pH, temperature, light and oxidation) that must be accounted for.[27,30]

With respect to the water-soluble vitamins, riboflavin is relatively hydrophobic, folic acid is acidic and pyridoxine and thiamine are generally basic.[31] Thiamine must often be oxidized to thiochrome prior to LC detection and even then, its UV absorption range is pH-dependent.[27] Riboflavin and its vitamers may possess similar UV absorbance but riboflavin is extremely photosensitive and care must be taken during extraction and analysis, as with pyridoxine and cyanocobalamin.[27,28] Nicotinamide is less stable than nicotinic acid and extraction techniques involving dilute acid are typically required, while folic acid is susceptible to oxidation often requiring the use of antioxidants.[27,28] For the fat-soluble vitamins, isomerization is common in oxygen-sensitive beta-carotene, and recovery of trans- vs. cis-

isomers must often be resolved during LC analysis.[26,28,32] Vitamin D recovery is complicated due to the presence of pre-D forms, and the OH group which requires elution with a more polar solvent than many other fat-soluble vitamins.[28,32] Vitamin E has up to eight homologs (tocopherols and tocotrienols) that may be detected, while Vitamin K is sensitive to saponification.[28,32] These unique requirements and challenges highlight the fact that API solubility is not necessarily reflected analytically as is evident in **Figure 3.2**.

In **Chapter 2**, Polysorbate 80 and Cremophor RH 40 were selected as surfactants given their propensity to form Type IV microemulsions. These saturation solubility results demonstrate the additional advantage of adding Cremophor RH 40 to the formulation, as many APIs exhibited preferred solubility in this surfactant.

3.5.2 Effective Alkane Carbon Number (EACN) Determination

3.5.2.1 Lipophilic API Incorporation

All lipophilic APIs (beta-carotene, cholecalciferol, d-α-tocopherol acetate, phytonadione and docosahexaenoic/eicosapentaenoic acid) were easily incorporated into Miglyol 812 with simple stirring, given their lipophilicity. Amounts were added based on the daily recommended dosages provided by Health Canada (**Chapter 1: Table 1.8**) and potencies as provided by the manufacturer (**Table B-1**, **Appendix B**).

3.5.2.2 Formulation Scan: Temperature

The results of the temperature scan conducted on Miglyol 812 and 50% w/w Miglyol 812:Oil-soluble actives are seen in **Figure 3.3.** Vials containing white or clear solutions represent Miglyol 812, while amber vials or yellow formulations represent 50% w/w Miglyol 812:Oil-soluble API mixtures. It can be seen from **Figure 3.3** that Type I microemulsions were obtained from 25ºC to 57ºC. At 59ºC, however, a shift was seen in the samples containing Miglyol 812, from a Type I microemulsion with two phases to a Type III microemulsion with three phases. This shift occurred later in samples containing 50% w/w Miglyol 812: Oil soluble actives, at 61ºC. Beyond this point and until 67ºC, Type III microemulsions were evident. However, at 80ºC, all samples clearly shifted from a Type III microemulsion to a Type II microemulsion.

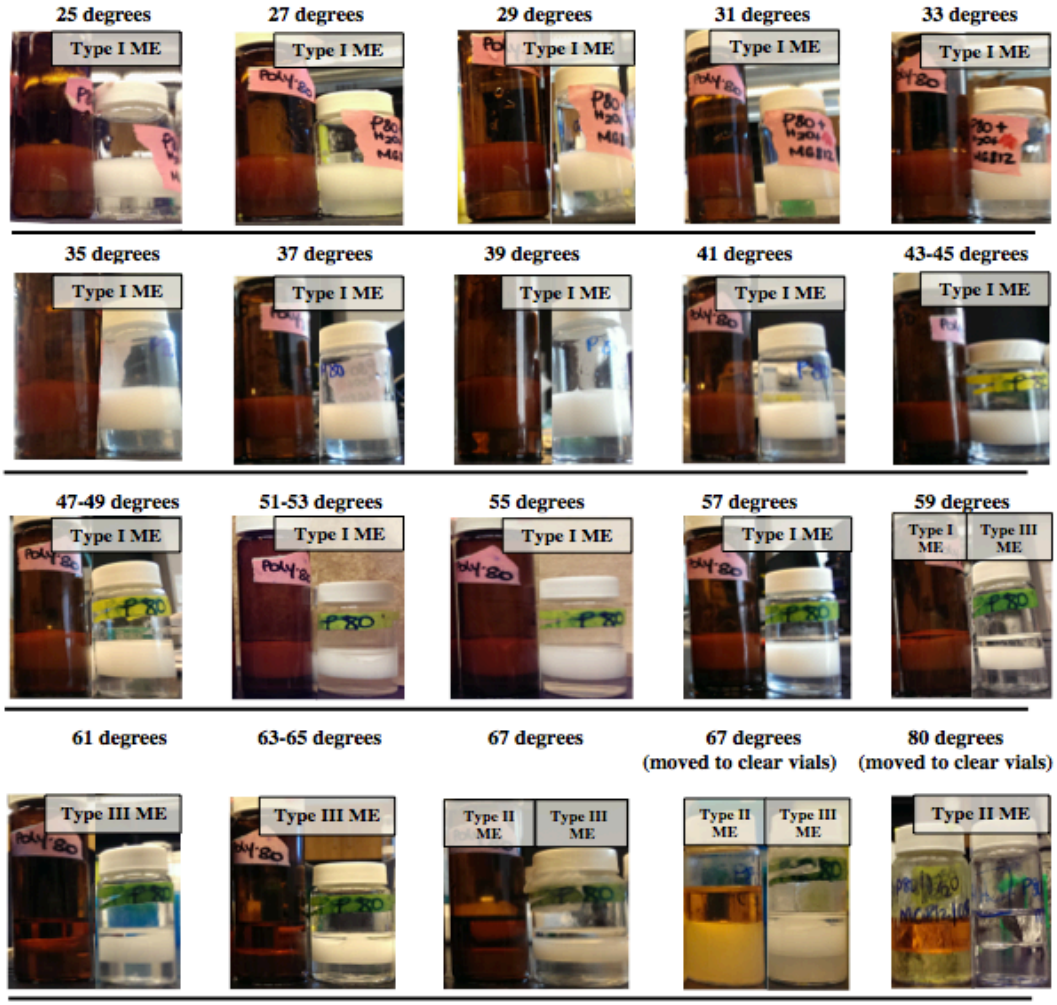

Figure 3.3: Temperature scan performed on Miglyol 812 and a 50/50 mixture of Miglyol 812 and five oil-soluble APIs in order to determine the EACN value of both oils.

The temperature scan was repeated and the results are depicted in **Figure 3.4.** White samples contained Polysorbate 80 and Miglyol 812 while orange samples contained Polysorbate 80 and 50% w/w Miglyol 812:oil-soluble APIs. Results indicated the presence of Type I microemulsions from room temperature to 63ºC (not pictured). At 65ºC, a transition from Type I to Type III microemulsions was seen in both Miglyol 812 and drug-loaded Miglyol 812. These Type III microemulsions persisted until 80ºC where a transition to a Type II microemulsion occurred.

Setting the HLD to 0 at the temperature at which a Type III microemulsion occurs, the HLD equation was rearranged in order to calculate the EACN of Miglyol 812 and 50% w/w Miglyol 812:Oil-soluble APIs. Therefore, using the HLD equation for non-ionic surfactants:

$$HLD = b(S) - K(EACN) - \phi(A) + {}_{CT}\Delta T + CC \qquad \textbf{(Eq. 3.1)}$$

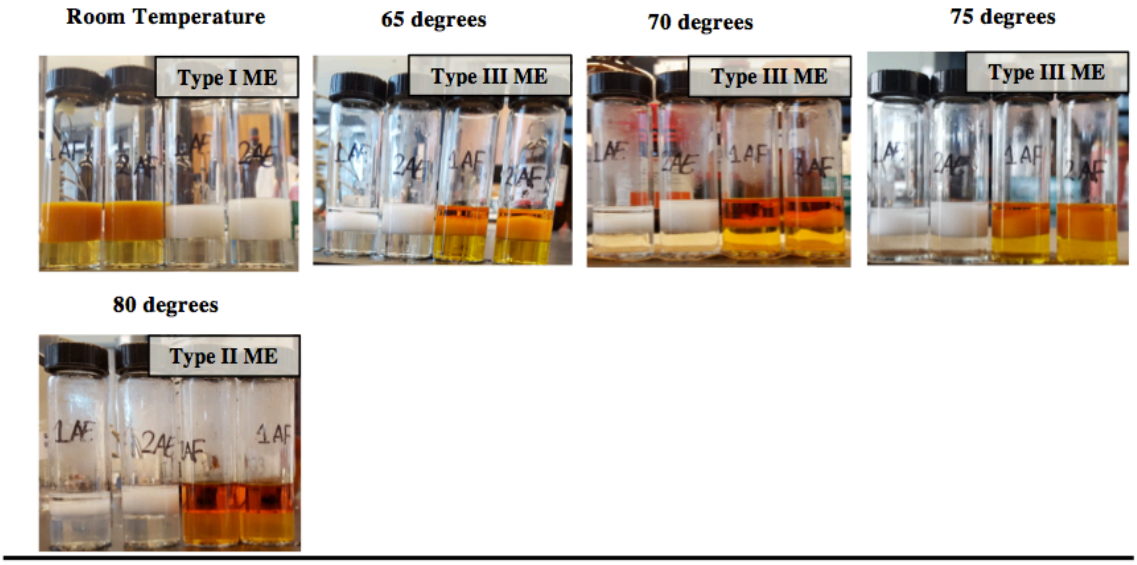

Figure 3.4: Replicates of temperature scan performed with Polysorbate 80 only on Miglyol 812 and a 50/50 mixture of Miglyol 812 and five oil-soluble APIs in order to determine the EACN value of both oils. White samples (AE) contain Polysorbate 80 and Miglyol 812 while orange samples (AF) contain Polysorbate 80 and drug-loaded Miglyol 812.

When HLD=0, as in the case of a Type III microemulsion, then,

$$EACN = \frac{b(S) - \phi(A) + {}_{CT}\Delta T + CC}{K} \qquad \textbf{(Eq. 3.3)}$$

where EACN is unknown

b(S)= the salt/electrolyte concentration; 0 g/100 mL as no salt was used

ϕ (A)= the alcohol concentration; 0 g/mL as no alcohol was used

$_{CT}$= constant associated with the effect of temperature on surfactant; 0.06 for non-ionic ethoxylated surfactants[4, 33, 34]

ΔT= the change in temperature from 25ºC

CC= the characteristic curvature of surfactant; -3.7 for Polysorbate 80

k= slope of ln (S) vs EACN; 0.17 for most surfactants[34,35]

Based on **Figures 3.3** and **3.4**, the results from the temperature scan are summarized in **Table 3.2.**

Table 3.2: Replicated temperature scan results of Miglyol 812 and a 50/50 mixture of Miglyol 812 and five oil-soluble APIs in Polysorbate 80 surfactant.

Replicate	**Temperature (ºC) at transition from Type I→ III microemulsion**	
	Miglyol 812	**Miglyol 812:Oil-soluble APIs**
1	59	61
2	65	65
3	65	65
Average ± SD	**63 ± 3.4**	**64 ± 2.3**

Thus, using **Eq. 3.3**, the calculated EACNs for Miglyol 812 and Miglyol 812:oil-soluble APIs are:

Miglyol 812:

$$EACN = \frac{0 - 0 + (0.06\,(63\,ºC - 25\,ºC) + (-3.7)}{0.17}$$

$EACN_{MG\ 812}$ = 8.4

Miglyol 812: Oil-soluble APIs:

$$EACN = \frac{0 - 0 + (0.06\,(64\,ºC - 25\,ºC) + (-3.7)}{0.17}$$

$EACN_{MG\ 812:OSA}$ = 8

Therefore, it can be concluded that Miglyol 812 and 50% w/w Miglyol 812:Oil-soluble APIs have EACN values of 8.4 and 8, respectively, equating to approximately an 8 carbon oil. Thus, the lipophilicity of Miglyol 812 upon incorporation of five oil-soluble APIs does not appear to vary remarkably. Further confirmation of these results was determined via salinity scanning as described below.

3.5.2.3 Formulation Scan: Salinity and Conductivity

In order to supplement temperature scan results, salinity scans were also performed on Miglyol 812 and 50% w/w Miglyol 812:Oil-soluble actives using an ionic surfactant, sodium dihexyl sulphosuccinate (SDHS). A visual shift in Type I→III→ II microemulsions, followed by conductivity measurements in order to ascertain this shift, afforded the obtaining of a Type III microemulsion (HLD=0), which was then used to calculate the EACN using the HLD equation. Salinity scan results are seen in **Figure 3.5.**

Figure 3.5: Salinity scan from 0.5-8 g/100 mL (labelled in white) performed with dihexyl sodium sulphosuccinate (SDHS) on Miglyol 812 and a 50/50 mixture of Miglyol 812 and five oil-soluble APIs in order to determine the EACN value of both oils. White samples contain Miglyol 812 only (image A) while orange samples contain a mixture of 50:50 Miglyol 812/oil-soluble APIs (image B).

In **Figure 3.5**, a shift in microemulsion type from a Type I microemulsion to a Type III microemulsion occurred at approximately 8 g/100 mL sodium chloride salinity for both

Miglyol 812 and the 50:50 Miglyol 812:Oil-soluble APIs phase. These results are in agreement with theoretical results shown in **Figure 3.6** using the Steven Abbott HLD calculator.[36]

Figure 3.6: Theoretical EACN results for an oil of EACN 8 as estimated by the Steven Abbott HLD calculator[34] for salinities from 0.5- 8 g/100 mL.

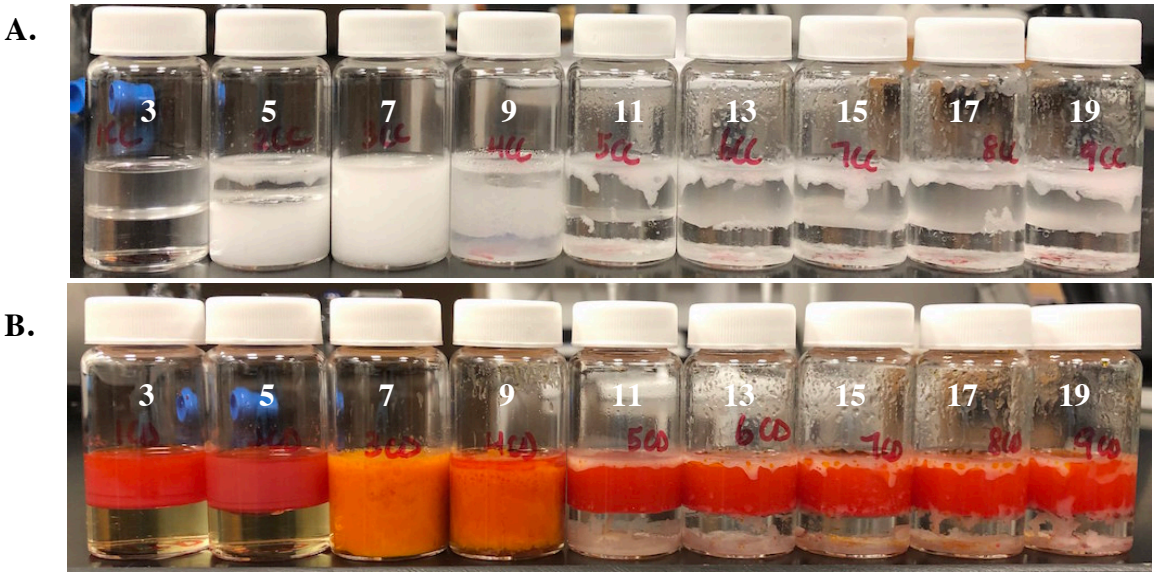

Figure 3.7: Salinity scan from 3-19 g/100 mL (labelled in white) performed with dihexyl sodium sulphosuccinate (SDHS) on Miglyol 812 and a 50/50 mixture of Miglyol 812 and five oil-soluble APIs in order to confirm the EACN value of both oils. White samples contain Miglyol 812 only (image A) while orange samples contain a mixture of 50:50 Miglyol 812/oil-soluble APIs (image B).

The salinity scan was replicated as shown in **Figure 3.7**, with an increase in salinity to confirm the results obtained in **Figure 3.5**. A visible shift in microemulsion type from a Type I to a Type III microemulsion was observed at 9 g/100 mL and 11 g/100 mL salinity for Miglyol 812 and Miglyol 812:Oil-soluble API-containing samples, respectively. These results were also in line with predicted EACN results as depicted in **Figure 3.8.**[36]

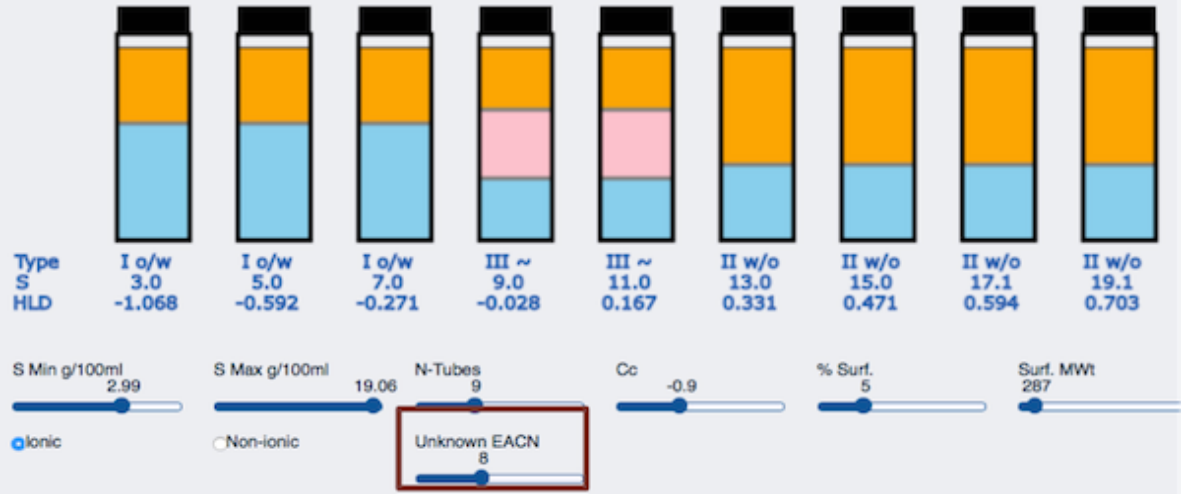

Figure 3.8: Theoretical EACN results for an oil of EACN 8 as estimated by the Steven Abbott HLD calculator for salinities ranging from 3-19 g/100 mL. These theoretical samples align with the results obtained in **Figure 3.7**.

The conductivity results from the salinity scans in **Figure 3.5** and **Figure 3.7** are depicted in **Figure 3.9**. For the first replicate, a drop in conductivity from approximately 15-16 mS/cm to 0 mS/cm at a salinity of 8 g/100 mL for both Miglyol 812 and 50% w/w Miglyol 812:Oil-soluble APIs was seen. For the second replicate, a drop in conductivity from approximately 19 mS/cm to 0 mS/cm at a salinity of 9 g/100 mL and 11 g/100 mL for Miglyol 812 and 50% w/w Miglyol 812:Oil-soluble APIs, respectively, was seen. This decrease in conductivity occurred upon an increase in lipophilicity as the system transitioned from a Type I→III→II microemulsion. Though the decrease in conductivity between replicates appears large, this difference is minimal once the EACN is computed.

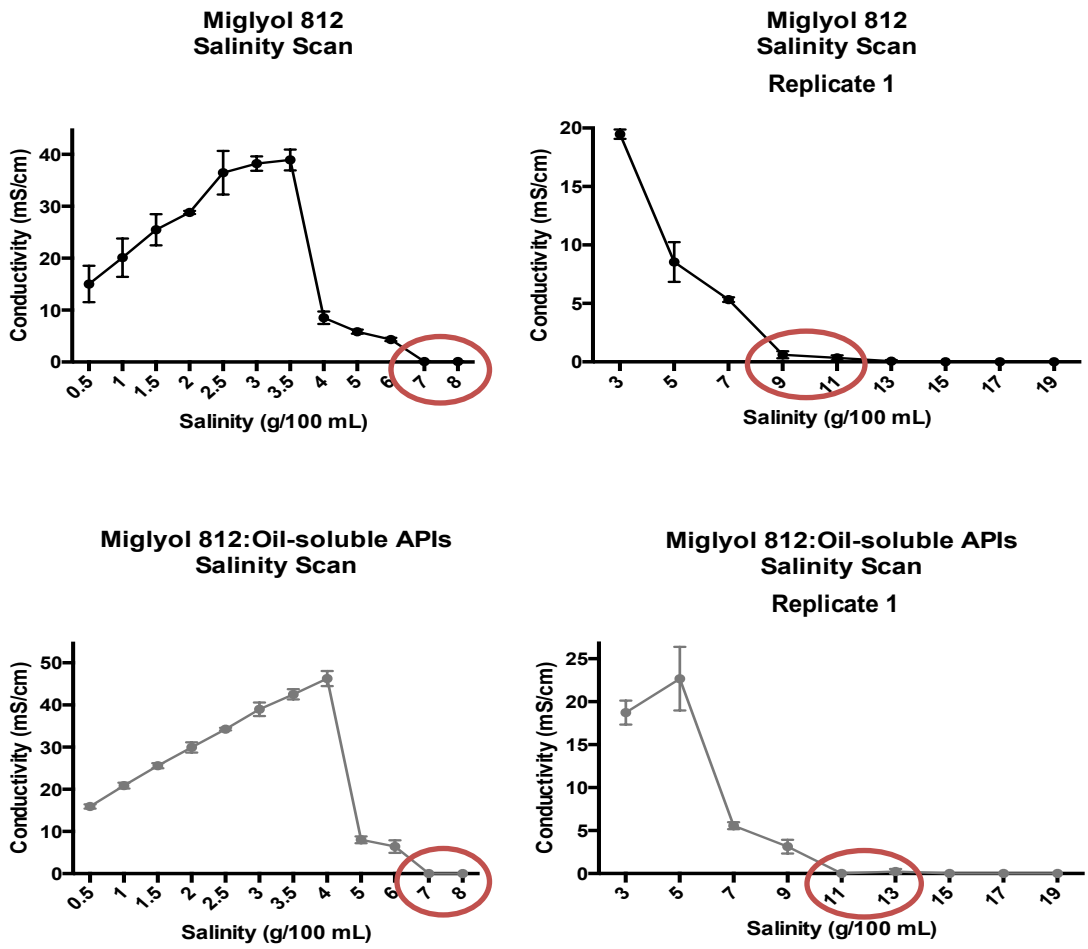

Figure 3.9: Conductivity results from salinity scans performed on Miglyol 812 and Miglyol 812: Oil soluble API phases. A drop in conductivity indicates a shift in microemulsion type as indicated by the red circles.

Using the HLD equation for ionic surfactants:

$$HLD = \ln(S) - K(EACN) - f(A) - {}_{\alpha T}\Delta T + CC \qquad \textbf{(Eq. 3.2)}$$

When HLD=0, as in a Type III microemulsion, then:

$$EACN = \frac{\ln(S) - f(A) - {}_{\alpha T}\Delta T + CC}{K} \qquad \textbf{(Eq. 3.4)}$$

where EACN is unknown

ln(S)= the natural logarithm of the salt/electrolyte concentration; various depending on whether samples are Miglyol 812 or 50:50 Miglyol 812: oil-soluble APIs

ϕ (A)= the alcohol concentration; 0 g/mL as no alcohol was used

$_{\alpha T}\Delta T$= constant associated with the effect of temperature on surfactant/change in temperature from 25ºC; 0 as no change in temperature occurred

CC= the characteristic curvature of surfactant; -0.92 for dihexyl sodium sulphosuccinate (SDHS)

k= slope of ln (S) vs EACN; 0.17 for most surfactants[34,35]

Based on results from **Figures 3.5-3.9**, the calculated EACNs for Miglyol 812 and Miglyol 812:oil-soluble APIs are summarized in **Table 3.3**:

Table 3.3: Duplicated salinity scan results of Miglyol 812 and a 50/50 mixture of Miglyol 812 and five oil-soluble APIs in SDHS surfactant.

Replicate	**Salinity (g/100 mL) at transition from Type I→ III microemulsion**	
	Miglyol 812	**Miglyol 812:Oil-soluble APIs**
1	8	8
2	9	11
Average ± SD	**8.5 ± 0.7**	**9.5 ± 2**

Thus, using **Eq. 3.4**, the calculated EACNs for Miglyol 812 and Miglyol 812:oil-soluble APIs are:

Miglyol 812:

$$\text{EACN} = \frac{\ln(8.5) - 0 - 0 + (-0.92)}{0.17}$$

$\text{Av.EACN}_{\text{MG 812}} = 7.2$

Miglyol 812: Oil-soluble APIs:

$$\text{EACN} = \frac{\ln(9.5) - 0 - 0 + (-0.92)}{0.17}$$

$Av.EACN_{MG\ 812:OSA}$ = 7.8

Therefore, combining *both* temperature and salinity scan results, the EACN values are best represented by **Table 3.4**:

Table 3.4: Overall EACN results of Miglyol 812 and 50:50 Miglyol 812: oil-soluble APIs confirmed via both temperature and salinity scanning with non-ionic and ionic surfactants, respectively.

Type of Scan	**EACN Miglyol 812**	**EACN 50:50 Miglyol 812:Oil-soluble APIs**
Temperature	8.4	8.0
Salinity	7.2	7.8
Average ± SD	**7.8 ± 0.8**	**7.9 ± 0.1**

Consideration of both temperature and salinity scans confirmed that overall, both Miglyol 812 and 50:50 Miglyol 812:oil-soluble APIs possessed an EACN value of approximately 8 carbons. It can be concluded then, that both oils tend to behave in a similar fashion to that of a straight-chain alkyl oil with 8 carbons, or octane. In terms of temperature, it has been previously discussed that the hydrophilic polyethoxylated head groups of non-ionic surfactants are temperature sensitive and become dehydrated upon exposure to increased temperatures, forcing a shift from a Type I→ III→ II microemulsion.[37] With respect to the Winsor interactive ratio, $R = A_{CO}/A_{CW}$, this increase in temperature leads to a decrease in interactions between the amphiphilic species and water (A_{CW}) and high R value, resulting in a transition to a Type II microemulsion.[38] According to Shinoda (1964)[37], the more soluble a hydrocarbon in a non-ionic surfactant species, the lower the phase inversion temperature (PIT). Given the PIT of 63ºC and 64ºC for Miglyol 812 and 50% w/w Miglyol 812:oil-soluble APIs, respectively, and the overall EACN values of 7.8 and 7.9 for Miglyol 812 and 50:50 Miglyol

812:oil-soluble APIs, respectively, it can be concluded that both oils behave in a similar fashion with respect to solubility in the non-ionic surfactant species.

Some of the lipophilic APIs tested in this work are temperature-sensitive. However, it is generally accepted that fat/oil-soluble vitamins are less heat-labile than that of their water-soluble vitamin counterparts.[39] **Table 3.5** contains information regarding the effect of temperature on each lipophilic API based on previous literature works. Based on the various degradation studies reported in the literature for the lipophilic APIs, no significant degradation was expected for any lipophilic APIs at the PIT of 63 and 64ºC.

In terms of salinity, it has been previously discussed and reported that an increase in salinity decreases the interactions between surfactant and water, forcing a shift from a Type I→ III→ II microemulsion.[7] In consideration of the Winsor interactive ratio, $R = A_{CO}/A_{CW}$, A_{CW} is reduced leading to a high R value, resulting in a transition to a Type II microemulsion.[7,38] This effect may also be explained in terms of surfactant packing as the monovalent cation in the salt shields the anionic surfactant head group of SDHS, reducing the head group area and increasing the packing parameter value (recall CPP= v/al).[2] An increase in this packing parameter consequently results in a negative curvature or formation of W/O micelles.[2] Salager et al. (1979) reported an increase in oil lipophilicity or alkane carbon number (ACN) with an increase in salinity.[40] This relationship is linear when plotting the natural logarithm of the salinity in g/100 mL (ln (S)) against oil ACN.[40] Given the salinity scan results indicating a transition from a Type I microemulsion to a Type III microemulsion at 8.5 g/100 mL sodium chloride and 9.5 g/100 mL sodium chloride for Miglyol 812 and 50:50 Miglyol 812:oil-soluble APIs, respectively, it can be concluded that the 50% w/w Miglyol 812:oil-soluble APIs phase demonstrates a higher lipophilicity than that of Miglyol 812. This is expected as the five fat-soluble vitamins, although considered small molecules, exhibit very high log P values: 11 for beta-carotene[41] 7.1 for Vitamin D_3[42] 10 for Vitamin E acetate[43] 9.7 for Vitamin K_1[44] 6.8 for DHA[45] and 6.2 for EPA[46]. These high log P values are not surprising given the structural compositions of these compounds, which primarily consist of multiple cyclic rings and lengthy alkyl chains. Beta-carotene has a molecular weight of 536.9 g/mol and consists of two cyclohexene rings connected via an unsaturated, methyl-branched C_{20} chain with no hydrogen donors or acceptors leading to the highest log P of the fat-soluble vitamins.[41] Vitamin D_3 consists of a molecular weight of 384.6 g/mol and has a structure similar to cholesterol. The

Table 3.5: Effect of temperature on oil-soluble vitamins based on previous literature

Vitamin	Melting/Boiling Point (MP/BP)	Temperature Effects
Beta Carotene: (Precursor to Retinal/ Retinol)	MP: 176ºC[41] BP: 577ºC[41]	• 180ºC (2h): cis-isomers & oxidation products[47,48] • 97ºC (3h): epoxide, cyclohexanone and carboxaldehyde products[47,49] • 100ºC: degradation in soybean oil[50] • 85ºC (2h); 130ºC (8 mins); degradation in olive oil[51]
Vitamin D_3 (Cholecalciferol)	MP: 85ºC[42]	• 150ºC: degradation in canola oil[52] • 200-210ºC (10 mins): 24% degradation in sunflower oil[53]
Vitamin E Acetate (D-α-tocopherol acetate)	MP: 10ºC[43]	Stable to very high temperatures in absence of oxygen [54] • 180ºC (1h): 6% degradation in triolein oil[54] • 60ºC (1h);100ºC (9h): degradation in olive oil[54]
Vitamin K_1 (Phytonadione)	MP: -20ºC[44]	• 185-190ºC (40 mins): 15% degradation in peanut, corn and olive oil; 6% degradation in safflower, sunflower, rapseed and soybean[55]
DHA/EPA Fish Oil	N/A	Depends on fish source • 180ºC: minor degradation [56] • 40-60ºC (1.5h) followed by 85ºC (30 mins): 30% degradation DHA/EPA in trout; 50% degradation DHA/EPA in carp[57] • 50-150ºC: degradation seen in salmon oil[58] • 60ºC (2h), 100ºC (2h), 160ºC (2h): no degradation EPA/DHA in rainbow trout and European; 25% EPA/DHA degradation at 1.5-2h.[59]

fused cyclohexane and cyclopentane along with the C_6branched, saturated chain are conserved. However, an unsaturated C_2 chain connects to a third cyclohexane.[42] It consists of 1 hydrogen donor and 1 hydrogen acceptor leading to the lowest log P of the fat-soluble vitamins.[42] Vitamin E acetate has a molecular weight of 472.2 g/mol and is comprised of a tetrahydropyran

and benzene ring along with a C_{13} saturated, branched chain. Its structure yields 2 hydrogen acceptors and 3 hydrogen donors.[43] This results in a log P of 10.[43] Vitamin K_1 has a molecular weight of 450.7 g/mol and is comprised of a 1,4-naphthoquinone. In addition, it consists of a C_{17} chain that is branched and saturated for the most part leading to its high log P of 9.7.[44] DHA and EPA both consist of carboxylic acids attached to a C_{22} and C_{20} unsaturated chain, respectively and molecular weights of 328.5 g/mol and 302.5g/mol, respectively.[46] The carboxylic acid group provides a degree of hydrophilicity leading them both to have log p values around 6- the lowest of the lipophilic APIs used in this work.[45,46] Salt concentration, in general, has little effect on oils and can be assumed to generally not affect the lipophilic APIs in this work. The physiological charges of beta-carotene, Vitamin D_3, Vitamin E acetate and Vitamin K_1 are 0.[41-44] Miglyol 812 is also noted to be a neutral oil.[60] The physiological charge of DHA and EPA are -1 given their carboxylic acid group so these are the lipophilic APIs likely most affected by the salt concentration.[45,46]

Based on the overall temperature and salinity scan results, the EACNs of Miglyol 812 and 50% w/w Miglyol 812: Oil-soluble APIs were determined to be practically equal: 7.8 versus 7.9. Given the hydrophobicity of the lipophilic APIs as described above, these results may seem counterintuitive. However, Miglyol 812, comprised of C_8 and C_{10} caprylic and capric triglycerides[60] has been utilized as a medium chain triglyceride (MCT) solubilizer for the oil-soluble APIs, in a very high concentration of 50% w/w. In addition, it has been previously reported that oils comprised of cyclical structures, in particular, aromatic structures, contribute to low EACN values.[7] In fact, benzene is known to possess an EACN of 0, and toluene is said to possess an EACN of 1.[7,35] Given this information, it is logical to assume that the lipophilic APIs in this work possessing aromatic rings, Vitamin E acetate and Vitamin K_1, contribute to a lowering of the EACN that brings the overall value of the 50% w/w Miglyol 812:Oil-soluble API phase close to that of Miglyol 812. Given that Miglyol 812 is comprised of 50-65% C_8, a result of EACN 8 is expected.

3.5.3 Characteristic Curvature (CC) Determination

3.5.3.1 Formulation Scan: Lipophilicity

With the determination of the EACN of Miglyol 812 and the 50% w/w Miglyol 812:oil-soluble API oil phase, all of the variables in the HLD equation are now complete except for that of

characteristic curvature (CC). 3:1 Polysorbate 80:Cremophor RH 40 was selected as the surfactant phase for our microemulsion system based on the results in **Chapter 2**. However, although the CC value of Polysorbate 80 is known (-3.7), that of Cremophor RH 40 is unknown and must be determined. Determining the CC allows for all variables in the HLD equation to be known such that the HLD may be calculated and adjusted or optimized for multi-drug delivery, based on **Eq. 3.1.**

A lipophilicity scan, keeping all variables constant but varying the EACN of numerous oils, is the most efficient way to determine the characteristic curvature of a surfactant.[4,35] Lipophilicity scans were performed with oils of known EACN value; two such results are shown here. **Figure 3.10** depicts a lipophilicity scan of 3:1 Polysorbate 80:Cremophor RH 40 where all other variables, including temperature and salinity were kept constant. A shift from a Type I→ Type III → Type II microemulsion was seen at EACN 18→EACN 16→ EACN 1, respectively.

The scan depicted in **Figure 3.10** was expanded by including all EACN values between EACN 18 (Canola oil) and EACN 1 (Toluene), in increments of 1. Two oils of known EACN may be combined in order to produce an oil of a particular EACN. This was performed in **Figure 3.11.** In general, **Figure 3.11** depicted a transition from a Type I → III → II microemulsion given a decrease in oil EACN. There were a number of outliers in this scan, which may be due to the use of impure oils. Specifically, samples of EACN 7, 8 and 13 should have indicated triphasic behaviour or Type III microemulsion behaviour. Nevertheless, a shift from a Type I microemulsion to a Type III microemulsion was seen to occur at EACN 16, consistent with the results in **Figure 3.10**. Using the theoretical lipophilicity scan calculator proposed by Abbott[61] these results coincided with a CC value of between -0.5 and -0.6 (**Figure 3.12**).

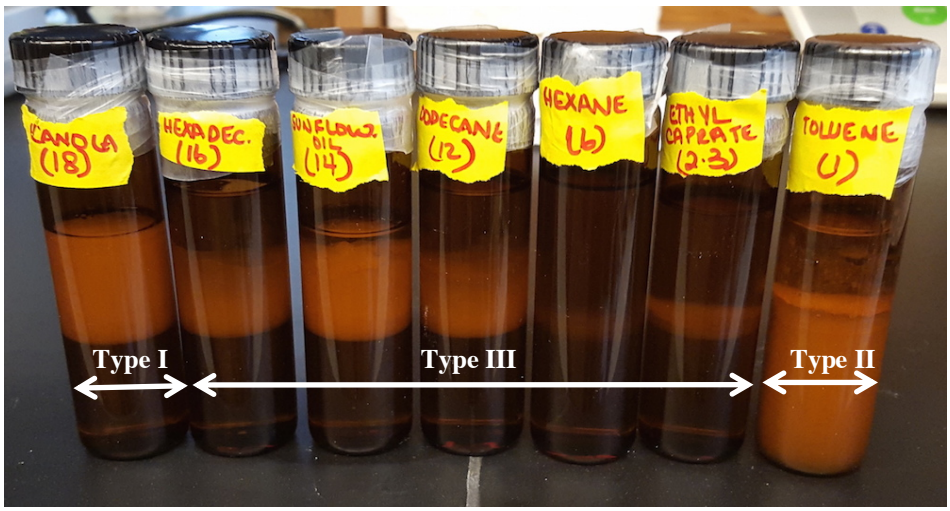

Figure 3.10: Lipophilicity scan conducted on 3:1 Polysorbate 80:Cremophor RH 40 using a variety of oils of known EACN[37]: Canola (18), Hexadecane (16), Sunflower oil (14*), Dodecane (12), Hexane (6), Ethyl Decanoate/Caprate (2.3) and Toluene (1) at fixed surfactant concentration, temperature and salinity (25 g/100 mL).
The literature EACN value of Sunflower oil is 14 but given its similarity in appearance to EACN 18, an independent EACN scan of sunflower oil was conducted and found to be 17. (see **Figure B-1, Appendix B) This EACN value better fits the scan.*

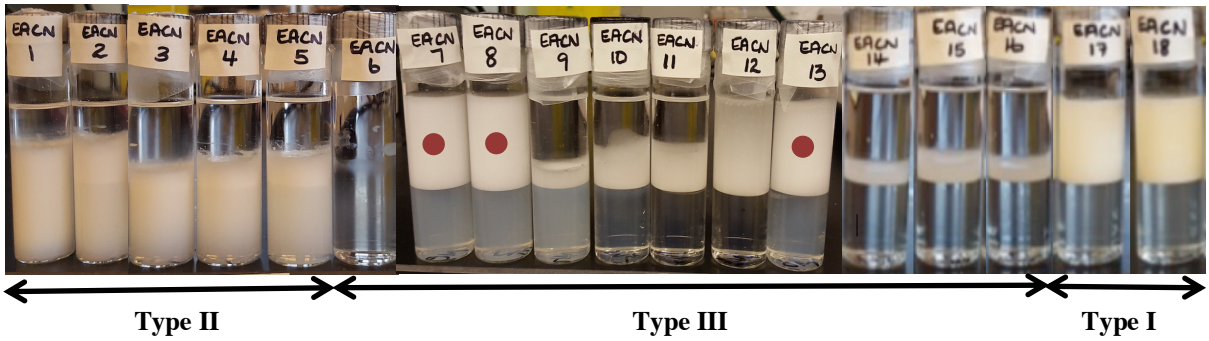

Figure 3.11: Lipophilicity scan conducted on 3:1 Polysorbate 80:Cremophor RH 40 using a variety of oils from EACN 1 to EACN 18 at fixed surfactant concentration, temperature and salinity (25 g/100 mL). The red dots indicate possible outliers. EACN 1= toluene, EACNs 2-5 were manufactured through mixtures of toluene (1) and dodecane (12), EACN 6= hexane, EACNs 7-11 were also manufactured through mixtures of toluene (1) and dodecane (12), EACN 12= dodecane, EACN 13 was manufactured through mixtures of toluene (1) and hexadecane (16), EACNs 14-15 were manufactured through mixtures of dodecane (12) and hexadecane (16), EACN 16= hexadecane, EACN 17= sunflower oil, EACN 18= canola oil.

Figure 3.12: Theoretical CC results for a non-ionic surfactant using oils ranging from EACN 18 to EACN 1 keeping all other variables constant including surfactant concentration, temperature and salinity (25 g/100 mL). Results show that this unknown surfactant has a CC value of between -0.5 and -0.6.

Given that this CC value is representative of a surfactant mixture of 3:1 Polysorbate 80:Cremophor RH 40, and that the CC value of Polysorbate 80 is -3.7[63], the CC value of Cremophor RH 40 may be determined using weight % properties. Using **Eq. 3.1** and rearranging for HLD=0, as in a Type III microemulsion, then:

$$CC = -(b(S) - K(EACN) - \phi(A) + CT\,\Delta T) \qquad \textbf{(Eq. 3.5)}$$

where CC of Cremophor RH 40 is unknown; CC Polysorbate 80= -3.7**

EACN = 16 (hexadecane)

b(S)= 0.13 (25 g/100 mL)[33,34]

ϕ (A)= 0 g/mL as no alcohol was used

$_{CT}\Delta T$= 0° C as there was no change in temperature

k= 0.17, a constant for most surfactants (slope ln (S) versus EACN)[34,35]

CC of Polysorbate 80 was verified separately using EACN scan (see **Figure B-2, Appendix B)

Based on the results of the lipophilicity scan, the calculated CCs for Polysorbate 80 and Cremophor RH 40 are listed in **Table 3.6**:

Table 3.6: Lipophilicity scan results aimed at determining the characteristic curvature of Polysorbate 80 and Cremophor RH 40.

Replicate	**EACN value at transition from Type I→ III microemulsion**	
	Polysorbate 80	**Cremophor RH 40**
1	16	16
2	16	16
Average	**16 ± 0.0**	**16 ± 0.0**

Based on **Eq. 3.5**, the calculated CCs for Polysorbate 80 and Cremophor RH 40 are:

$$\mathrm{CC} = -(0.13(25\ \mathrm{g} / 100\ \mathrm{mL}) - 0.17\ (16) - 0 + 0)$$

$CC_{3:1\ P80:C40}$ = -0.53 ± 0.0

Therefore, CC of Cr40:

$3{:}1\ P80{:}C40 = 0.75\%\ P80 + 0.25\%\ C40$

$$CC_{3:1\ P80:C40} = 0.75 * CC_{P80} + 0.25 * CC_{C40} \quad \textbf{(Eq. 3.6)}$$

$$-0.53 = (0.75 * (-3.7)) + (0.25 * (8.98))$$

Av. CC_{CR40}: 8.98 ± 0.0

The calculation above based on **Eq. 3.6** demonstrated a characteristic curvature value of 8.98 for Cremophor RH 40. As described earlier, characteristic curvature considers the structural composition of a surfactant and its tendency to curve towards an oil or water interface. A negative characteristic curvature indicates a hydrophilic surfactant with a tendency

to curve towards oil, while a positive characteristic curvature indicates a hydrophobic surfactant with a tendency to curve towards water. Acosta et al. noted that a general characteristic curvature scale from -4 to +4 supports a linear correlation between HLB and CC for most non-ionic surfactants, especially as it pertains to surfactants with very high HLB values (above HLB 25).[8] The characteristic curvature of +8.98 obtained for Cremophor RH 40 is highly positive which suggests a very hydrophobic surfactant, despite its high HLB value of 14-16. However, these linear correlations and other associations between CC and HLB are difficult to predict in complex surfactants. The structure of Cremophor RH 40 is atypical of many non-ionic surfactants and relatively complex. It consists of three ricinoleic fatty acid chains which together with glycerol, form castor oil. This castor oil is hydrogenated and substituted with polyethoxylated chains. Each ricinoleic fatty acid chain is comprised of 18 carbons with an unsaturation at the C9 and C10 position. Therefore, this triple chain surfactant closely resembles a triglyceride versus that of a typical single chain, linear surfactant. As a result, there are complications with fitting this surfactant to typical non-ionic surfactant models. For comparison, Polysorbate 80, of HLB 15, possesses a single 18 carbon unsaturated tail and polyethoxylated head group but consists of a CC value of -3.7.

To examine this disparity, it is worth considering the CC values for similar surfactants of high HLB value which have been tabulated by Abbott.[62] One such surfactant is lecithin which, despite its lipid structure, has been stated to have as high a HLB as 12.[63] Lecithin is a phospholipid comprised of two fatty acids, one of which is also an 18 carbon, unsaturated chain. Although lecithin has the potential to act as a hydrophilic surfactant (given a HLB of 12), the CC value of +4 would indicate that this surfactant is hydrophobic. Sucrose distearate is another surfactant that possesses a CC value of +4 yet has a HLB value of 8, which is not strongly hydrophobic.[64] Sucrose distearate surfactant is also comprised of two C18 unsaturated fatty acid tails but with a sucrose head group. An additional example of the discrepancy between CC and HLB can be found in sophorolipid lactone, purported to have a CC value of +4.5 despite the HLB of sophorolipids which has been found to be 8-10.[65] Sophorolipid is comprised of a C17, unsaturated fatty acid chain as well as a lactonic group yet the CC is found to be highly hydrophobic. These three surfactants may be considered complex due to the presence of more than one hydrophobic tail and extensive head groups, resulting in a disparity between quoted CC values and HLB. Therefore, the concept of CC as it relates to multi-chain

surfactants is an area that requires further investigation by researchers. Nevertheless, given the CC value of 8.98 for Cremophor RH 40, the HLD value for a system containing 3:1 Polysorbate 80:Cremophor RH 40, five oil-soluble APIs in Miglyol 812 and water may be calculated using **Eq. 3.1** and the following variables:

HLD= unknown
b(S)= 0 g/100 mL as no salt was used in this final microemulsion, multi-drug formulation
k*EACN = 0.17*7.9 for Miglyol 812 containing 50% oil-soluble APIs
ϕ (A)= 0 g/mL as no alcohol was used in this final microemulsion, multi-drug formulation
$_{CT}\Delta T$= 0ºC as there was no change in temperature since all mixes were performed at room temperature
CC= -0.53 for a 3:1 Polysorbate 80:Cremophor RH 40 mixture where CC Polysorbate 80 = -3.7 and CC Cremophor 40= +8.98

The calculated HLD value for a microemulsion, multi-drug delivery system comprised of 3:1 Polysorbate 80:Cremophor RH 40 surfactant, Miglyol 812 oil, 5 lipophilic APIs (fat-soluble vitamins) and water was -1.9 ± 0.02. According to Salager et al. (2005), a negative HLD results in the production of a Type I, O/W microemulsion.[2] It can also be seen that the HLD is proportional to the CC such that an increase in CC results in an increase in HLD and vice versa.

Given that the CC value of 3:1 Polysorbate 80:Cremophor RH 40 was only slightly negative at -0.5, a more negative CC value and consequently, a more negative HLD value for O/W microemulsion formation, was explored. The goal was to determine whether an increase in negative HLD would result in an increase in O/W microemulsion formation, despite there being no objective scale of HLD values readily available in the literature. An arbitrary value of four times the CC value of 3:1 Polysorbate 80:Cremophor RH 40, from -0.5 to -2, was selected in order to determine whether the resulting shift in HLD would be enough to produce a larger O/W microemulsion than originally seen in 3:1 Polysorbate 80:Cremophor RH 40. A CC value of -2 equates to a Polysorbate 80:Cremophor RH 40 ratio of approximately 8:1.

Ternary Phase Diagram (TPD) mapping was performed on this 8:1 Polysorbate 80:Cremophor RH 40 surfactant mixture, Miglyol 812 and water at room temperature and

37ºC, as in the case of 3:1 Polysorbate 80:Cremophor RH 40 in **Chapter 2**. Results are shown in **Figure 3.13** and indicated that despite the increased negative CC value of -2 in 8:1 Polysorbate 80:Cremophor RH 40, no increased benefit in terms of an expansion of the O/W microemulsion region was seen. Given that the EACN value of Miglyol 812 was similar to that of drug-loaded Miglyol 812, it can be inferred that these TPDs are also reflective of lipophilic API incorporation. Therefore, an increase in CC from -0.5 to -2 and thus, an increase

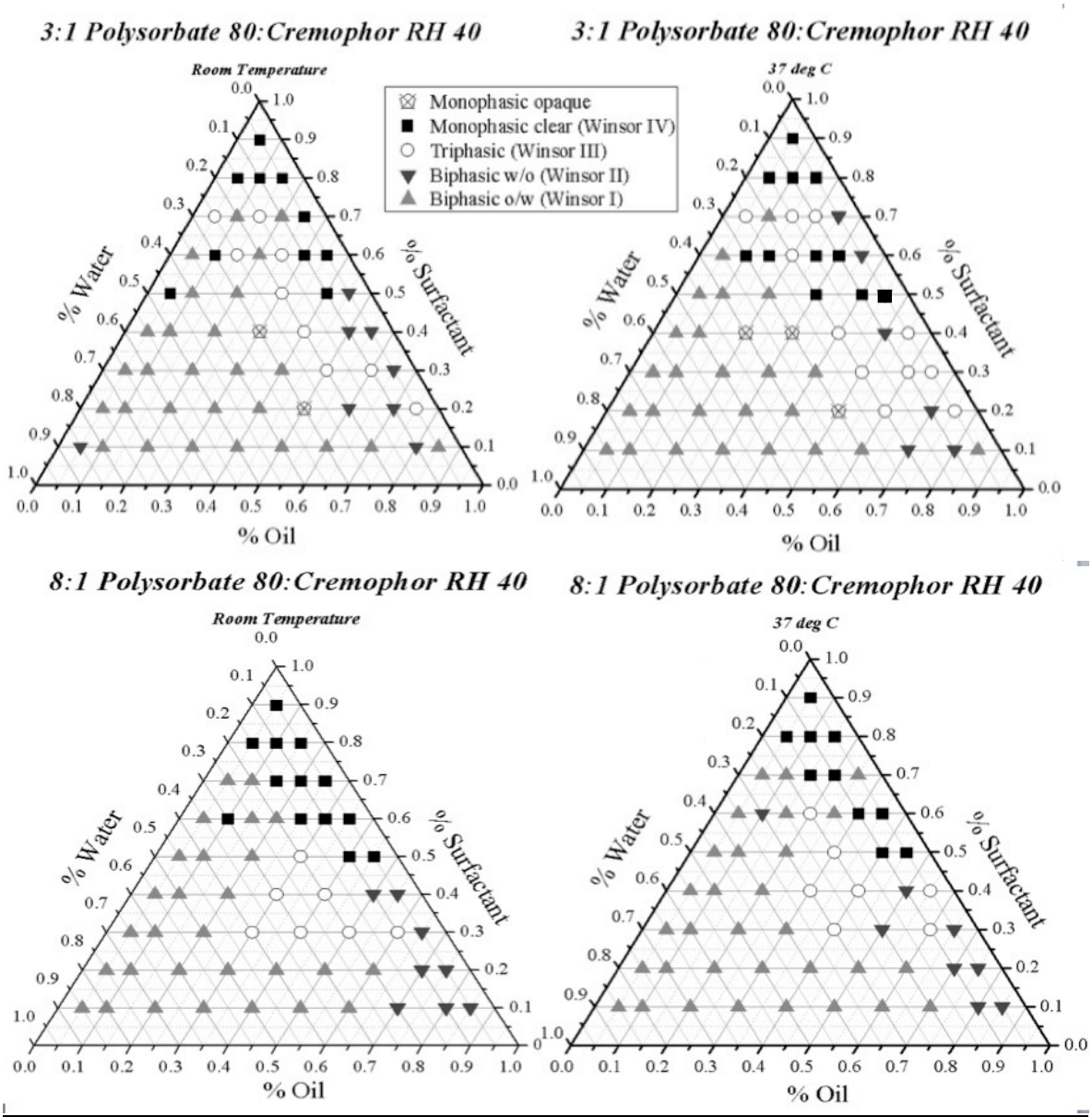

Figure 3.13: Ternary Phase Diagram (TPD) results of 3:1 Polysorbate 80:Cremophor RH 40 (CC= -0.53) as compared to 8:1 Polysorbate 80:Cremophor RH 40 (CC= -2.3) at room temperature and 37ºC.

in HLD from -2 to -4 did not appear to confer any additional benefit of Type I microemulsion formation potential in this multi-drug delivery system.

Tensiometry performed on 3:1 Polysorbate 80:Cremophor RH 40 (**Figure 3.14A, reproduced from Chapter 2**) and 8:1 Polysorbate 80:Cremophor RH 40 (**Figure 3.14B**), surfactant solutions resulted in average CMC values of 0.0036 ± 0.001 mM (**Chapter 2**) and 0.0028 ± 0.001 mM, respectively. As in the case of 3:1 Polysorbate 80:Cremophor RH 40 (**Chapter 2**), the experimental CMC for 8:1 Polysorbate 80:Cremophor RH 40 was below that of the ideal CMC (0.0048 mM, **Appendix B**) indicating synergism. However, the degree of synergism for both 3:1 and 8:1 Polysorbate 80:Cremophor RH 40, as determined by the Rubingh β interaction parameter (**Appendix B**), was -2.2 and -2.8, respectively. Given that the CMCs for both ratios were within the standard deviations of each other, and that their degrees of synergism was similar, no notable advantage to using a higher percentage of Polysorbate 80 in this formulation was observed. As a result, the final microemulsion system was determined to consist of 3:1 Polysorbate 80: Cremophor RH 40 as the surfactant component, Miglyol 812 as the oil component into which five lipophilic APIs may be incorporated, and water as the aqueous component into which six hydrophilic APIs may be incorporated.

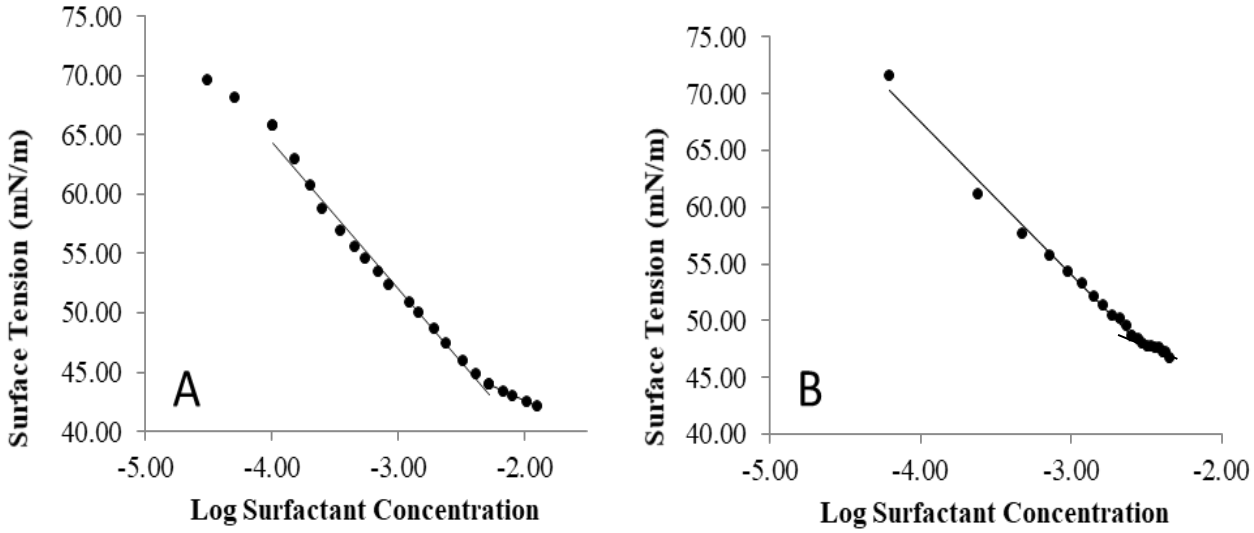

Figure 3.14: Tensiometry results for 3:1 (A) and 8:1 (B) Polysorbate 80:Cremophor RH 40 in water at 25ºC.

3.5.4 Hydrophilic API Incorporation

The process of hydrophilic API incorporation was found to be more complicated than that of lipophilic API incorporation. Where high log P values and generally neutral charges prevailed in the case of the lipophilic APIs, the hydrophilic APIs exhibited a number of challenges including poor water solubility in the cases of Vitamins B_2 and Vitamin B_9 (0.7 mg/ml[13] and 0.08 mg/mL[14] respectively), light sensitivity (Vitamin B_1[66], Vitamin B_2[67-69], Vitamin B_6[66,67], Vitamin B_9[66] and Vitamin B_{12}[66,69]), oxygen sensitivity (Vitamin B_1[66,70], Vitamin B_{12}[66,70]), acid sensitivity (Vitamin B_9[66,67] and Vitamin B_{12}[66,67]) and alkaline sensitivity (Vitamin B_1, Vitamin B_2 and Vitamin B_{12}).[66,67,69] The B vitamins are generally stable to dry heat but rapidly degrade when subjected to an additional factor such as pH or light exposure.[66,67]

The high water solubilities of thiamine mononitrate (Vitamin B_1), niacinamide (Vitamin B_3), pyridoxine hydrochloride (Vitamin B_6) and cyanocobalamin (Vitamin B_{12}) resulted in easy water incorporation in the amounts listed in **Table 3.7.** However, riboflavin (Vitamin B_2) and folic acid (Vitamin B_9) remained insoluble and required pH adjustment as described earlier in **Materials and Methods.** This adjustment resulted in a final pH of the microemulsion formulation of approximately 8.5. The effect of this pH adjustment on all APIs is outlined here.

Table 3.7: The water-soluble APIs were incorporated in the following Health Canada amounts according to their individual potencies.[71,72] (potencies listed in **Table B-1**, **Appendix B**)

Hydrophilic API	Health Canada Recommended Daily Allowance (mg)
Vitamin B_1 (Thiamine mononitrate)	1.4
Vitamin B_2 (Riboflavin)	1.4
Vitamin B_3 (Niacinamide)	18
Vitamin B_6 (Pyridoxine hydrochloride)	2
Vitamin B_9 (Folic Acid)	0.6
Vitamin B_{12} (Cyanocobalamin)	0.0026

At physiological pH, all APIs except for thiamine mononitrate, riboflavin and folic acid remain neutral or uncharged. Thiamine mononitrate exhibits a charge of +1 at physiological pH[73] given the positive nitrogen in the thiazole ring.[74] Riboflavin exhibits a charge of -1 at physiological pH[13] due to protonation of the nitrogen on the pyrazine ring (pKa 10)[13] subsequently leading to a resonance shift which causes a negative charge on the adjacent oxygen atom.[75] Finally, folic acid exhibits a charge of -2 at physiological pH[14] due to its four pKa values of 2.4, 3.4, 4.8 and 8 at the N_1, α-COOH, γ-COOH and N_3 positions, respectively.[76] At physiological pH, both COOH moieties are deprotonated leading to a charge of -2. Upon an increase from physiological pH to a more alkaline pH, changes in some of the APIs can be seen.

For thiamine mononitrate, its pKa_1 and pKa_2 values are 4.8 and 9.2, respectively.[74] Thus at a pH above 9.2, the nitrogen on the thiol ring becomes deprotonated leading to an uncharged intermediate that later results in a negatively charged thiol upon further addition of base.[74] For riboflavin at alkaline pH above 10.2, deprotonation of the nitrogen on the pyrazine ring would occur, leading to a restoration of the carbonyl bond and overall neutrality in the molecule. Studies involving the sole effect of pH on riboflavin have rarely been conducted; many studies tend to focus on the effect of pH upon light or heat exposure. Upon exposure to light and/or oxygen at pH 7-12, the ribityl side chain of riboflavin is oxidized to form lumiflavin.[68] In acidic conditions upon exposure to light and/or oxygen, riboflavin degrades to lumichrome.[68] For folic acid, its four pKa values dictate the charge of the molecule at alkaline pHs. Given its fourth pKa value, at pH values above 8, the molecule would be negatively-charged as the hydrogen on the nitrogen would simply be deprotonated. As is the case with riboflavin, pH studies with folic acid were often conducted in combination with factors such as light and temperature. Gazzalli et al (2016) found that below pH values of 5, folic acid was very unstable while pH values of 5-12 rendered stability.[77] Between pH 4 and 12, folic acid was found to shift between its acidic and basic form, i.e. from an amide at approximately pH 5 to a phenolate at approximately pH 10.[77] At alkaline pHs above 8, the degradation of folic acid was only seen to be approximately 7% in contrast to >45% at pHs below 6.[77] The authors also found that folic acid was heat stable even when heated at 100˚C for an hour, and stable to degradation below 180˚C.[77] The degradation of folic acid in alkaline pHs with exposure to UV

light or temperature has been recorded[77] but little evidence of the degradation of folic acid upon exposure to pH alone has been recorded.[77]

The pKa of niacinamide 3.3.[78] Thus, below pH 3, the nitrogen in the pyridine ring is protonated and positively charged.[78] However, above pH 3, as in this formulation, the nitrogen is deprotonated and the molecule remains neutral.[78] Pyridoxine hydrochloride is stable to heat, acid and alkali but in the presence of light, rapidly degrades in alkaline conditions.[67] It has a pKa_1 value of 5.6 and a pKa_2 value of 8.6[21,79] pKa_1 is located at the nitrogen position while pKa_2 is located at the phenolic position. Thus, at high alkaline pHs above that of 8.6, it can be expected that the phenolic group is deprotonated while that of nitrogen remains neutral. The large, complex structure of cyanocobalamin provides many opportunities for degradation. The acetamide and propionamide side chains in the corrin ring are susceptible to hydrolysis by both acids and bases, to carboxylic acids.[66] In highly acidic conditions, the phosphate bond in ribose-3 phosphate is cleaved to produce an amide and nucleotide moiety that can be further broken down.[66] In highly alkaline conditions, lactam formation of the acetamide side chain in the corrin ring occurs.[66] Given the above analysis, the APIs most susceptible to interference at a final microemulsion pH of 8.5 are thiamine mononitrate, riboflavin and folic acid.

3.5.5 API-API Interactions

Following the successful development of a methodology for lipophilic and hydrophilic API incorporation into Miglyol 812 and water, respectively, it is imperative to be wary of any potential API-API interactions within these systems. Both water-soluble and fat-soluble APIs consist of a number of functional groups that may interact with each other. For example, lipophilic APIs such as Vitamin E acetate and Vitamin K_1 are comprised of a number of aromatic pi-bonds which may participate in pi-pi stacking or even $–CH_2–$pi stacking with nearby methyl groups. These chemical interactions, though not previously reported in the literature to our knowledge, are expanded further in **Chapter 4**. Here, their biological interactions are discussed.

With respect to lipophilic API interactions, Vitamin E has been reported to prevent the oxidation of Vitamin A, enhancing absorption.[80,81] Inversely, Vitamin A/beta-carotene has been reported to decrease serum levels of Vitamin E[80] and excess levels of Vitamin A may increase

the requirement for Vitamin E.[81] High levels of Vitamin A have also been reported to decrease Vitamin D uptake[80] and Vitamin K absorption.[81] Medium to high levels of Vitamin E have been reported to reduce Vitamin D absorption[81] and uptake by up to 14%.[80] Similarly, Vitamin D has been reported to reduce the intestinal uptake of Vitamin E.[80] High doses of Vitamin E have also been reported to affect the absorption and metabolism of Vitamin K_1[81-83] and similarly, large doses of Vitamin K_1 have been reported to inhibit the intestinal absorption of Vitamin E.[80] The uptake of Vitamins E and K_1 has been reported to follow a common pathway used in Vitamin D uptake, thus explaining their interference with Vitamin D absorption.[84]

Hydrophilic API interactions are more complex. Vitamin B_1 was reported to interfere with the absorption of Vitamin B_2.[81] The decomposition products of Vitamin B_1 have also been reported to affect the breakdown of Vitamin B_9 (accelerated through the presence of hydrogen sulphide especially from pH 5.9-7) and Vitamin B_{12}[66] (accelerated though the cleavage of thiamine resulting in the breakdown from cyanocobalamin to 4-methyl-5-ß-hydroxyethyl thiazole.[69,70]). Vitamin B_1 has also been found to inhibit biosynthesis of Vitamin B_6.[81] Conversely, Vitamin B_1 has been reported to be necessary for Vitamin B_3 formation.[81]

Riboflavin may lead to the partial reduction of Vitamin B_1[70] through possible oxidative effects leading to the formation of thiochrome.[69] Riboflavin may also degrade Vitamin B_9/folic acid[70] through cleavage of the methylene link resulting in the release of aromatic amide, i.e. p-aminobenzoyl glutamic acid[77] despite the report that riboflavin is required to convert folic acid to its co-enzyme.[81] This is especially evident in the presence of light and at pH 6.5.[69] Riboflavin has also been reported to degrade Vitamin B_{12}/cyanocobalamin.[66] Despite the negative effects of riboflavin on Vitamins B_1, B_9 and B_{12}, riboflavin has been reported to be needed for the metabolism of Vitamin B_6 and Vitamin B_3.[69,81] Riboflavin is an essential component of two co-enzymes, flavin mononucleotide (FMN) and flavin adenine dinucleotide (FAD) that play an important role in energy production[85] ; FMN is required for the conversion of Vitamin B_6 to the co-enzyme pyridoxal 5'-phosphate while FAD is required for the conversion of tryptophan to niacin.[85]

Niacinamide/Vitamin B_3 has been reported to degrade cyanocobalamin (B_{12}) and thiamine (B_1)[66] but acts as a solubilizer for Vitamins B_2 and B_9[69]. It is also necessary in the conversion of Vitamin B_6.[81] Although Vitamin B_6 may inhibit the biosynthesis of B_1 in the case of excess levels of the latter, it is also necessary for Vitamin B_1 absorption.[81] Similarly,

although Vitamin B_6, affects the absorption of Vitamin B_3, it is necessary for its metabolism[81], as enzymes in the metabolic pathway of B_6 are involved in the conversion of tryptophan to B_3.[86] Vitamin B_6 has also been reported to be necessary for the optimum absorption of Vitamin B_{12}[81] and leads to an increased requirement of Vitamin B_9.[81]

Vitamin B_9 has been reported to increase the need for Vitamin B_{12} due the former's ability to obscure deficiency in the latter.[81] Vitamin B_9 has also been reported to be needed for optimal absorption of Vitamin B_1[81] as a depletion in folic acid reduces thiamine absorption through a down-regulation of transporters on polarized absorptive epithelial cells.[87] Vitamin B_{12} has been reported to be necessary for the optimum absorption of Vitamin B_1[81] yet is a contributor to the destruction of Vitamin B_6.[81]

In terms of cross API-API interactions between both hydrophilic and lipophilic APIs, Vitamin E appears to be necessary for metabolism of Vitamin B_{12}.[81] This is due to possible assistance of Vitamin E in the conversion of cyanocobalamin to its coenzyme form (B_{12} to 5'-deoxyadenosylcobalamin and thus, the metabolism of methyl malonyl co-enzyme A to succinyl co-enzyme A).[88] These API-API interactions are important considerations for future reference, especially in the characterization stages of the microemulsion.

3.6 Conclusion

This chapter has presented a methodology for the API incorporation and possible optimization of a microemulsion system capable of multi-drug delivery. Miglyol 812 and lipophilic drug-loaded Miglyol 812 exhibited a similar degree of lipophilicity as demonstrated by EACN values of 7.8 and 7.9, respectively. This was in opposition to what was hypothesized. The characteristic curvature of Cremophor RH 40 was much larger than that of Polysorbate 80 (+8.98 versus -3.7), despite their similar HLB values. This is likely due to greater lipophilicity in the case of Cremophor RH 40 attributed to its triple tailed structure.

Upon determination of the EACN and CC values of the microemulsion components, the HLD was shifted to the left (to a more negative value) in order to deduce any possible advantages of O/W microemulsion formation. Results indicated that an 8:1 Polysorbate 80:Cremophor RH 40 surfactant mixture demonstrated no appreciable advantage over a 3:1 Polysorbate 80:Cremophor RH 40 surfactant mixture in terms of microemulsion formation

potential, critical micelle concentration or degree of synergism. Thus, a simple shift in HLD from -2 to -4 conferred no apparent advantage in terms of microemulsion formation. This is important because unlike HLB, there is no quantifiable HLD scale currently in existence that indicates boundaries for microemulsion formation. The results of this Chapter led to the development of a final microemulsion formulation comprised of 3:1 Polysorbate 80: Cremophor RH 40 surfactant, Miglyol 812 oil and water. This served as the basis into which eleven active pharmaceutical ingredients were incorporated.

Chapter 4: Characterization and Stability of Multi-Drug Loaded 3:1 Polysorbate 80:Cremophor RH 40, Miglyol 812 and Water Microemulsion Systems

4.1 Introduction

4.1.1 Characterization

The process of microemulsion formation is often performed on a trial-and-error basis with the main objective being to obtain a clear, homogenous solution- the hallmark of microemulsion formation. However, the presence of a clear, homogenous microemulsion formulation provides little in the way of information about the properties of such a system. Thus, characterization techniques are an essential part of elucidating these unique properties. Scattering, microscopic and thermo-analytic techniques provide important insight into critical properties of a microemulsion system including size, charge, morphology and droplet energetics (**Chapter 1, Section 1.7.2**).

4.1.1.1 Droplet Size

As noted earlier, droplet size is an important property of microemulsion systems. However, the technique employed in this work, Dynamic Light Scattering (DLS) involves some considerations before results may be interpreted. Given that DLS correlates the movement of a particle with the size of a hard sphere particle that diffuses at the same speed as that of the sample[1], this poses complications for surface-bound compounds on a particle, which do not conform to hard sphere morphology. In this particular formulation, the PEO groups of Polysorbate 80 and Cremophor RH 40 surfactant, and the localization of some hydrophilic active pharmaceutical ingredients (APIs) around these PEO head groups, may inflate the size output of the microemulsion using this technique. Therefore, the hydrodynamic diameter output of this particular technique must be interpreted with caution.

4.1.1.2 Zeta Potential

Zeta potential, as noted earlier, is an important indicator of droplet charge and thus, propensity for coagulation, flocculation or general, physical instability.[1-4] The droplet charge for core-shell structures is generally straightforward given that API is contained within the core. However, in the case of this microemulsion formulation, PEO head groups as well as hydrophilic APIs that prefer to localize around these surfactant head groups may contribute to the charge values obtained in zeta potential measurements. Therefore, zeta potentials results must also be interpreted with caution.

4.1.2 Stability

One of the major advantages of microemulsion systems is their thermodynamic stability. The free energy of a microemulsion's colloidal droplets is lower than that of the microemulsion starting components, oil and water.[5] This difference in energy drives microemulsion formation forward and confers thermodynamic stability.[5] Thermodynamic stability is advantageous in drug delivery and pharmaceutical formulations as delayed phase separation leads to drug uniformity and increased shelf life, respectively. However, the incorporation of active ingredients may impart instability by shifting the free energies between the microemulsion and its separated phases. In particular, the free energy involved in microemulsion formation may be affected by the presence of lipophilic and surface-active APIs in solution, and possible interactions of these ingredients with the microemulsion starting components.[6,7] This may result in a less thermodynamically stable microemulsion as compared to the native system in the absence of API. Thus, in microemulsion systems, stability studies after API incorporation are essential in deducing formulation fitness for drug delivery applications.

The stability mechanisms most important in pharmaceutical formulations include: a) physical stability, b) chemical stability and c) microbiological stability.[8] Physical stability involves the physical attributes of the formulation, particularly appearance. Odour, the presence of precipitate, a change in rheology and phase separation in the case of emulsion systems, are important indicators of physical instability.[8] Chemical stability is often the most important indicator of formulation instability that limits the shelf life of pharmaceutical products[9], and refers to chemical reactions that occur among components within a formulation. Hydrolysis, oxidation, photochemical and thermal degradation reactions occurring between

pharmaceutical components are important indicators of chemical instability within a formulation.[8] Finally, microbiological stability refers to the presence of microbial entities such as bacteria, yeast and mold in pharmaceutical formulations.[8] Physical, chemical and microbiological factors pose great risk not only to the stability of the formulation, but more importantly, to patient safety.[8]

In **Chapter 3**, a number of factors were shown to affect microemulsion systems-namely temperature, salinity and the presence of additives. However, additional factors that affect API stability must also be taken into consideration such as light and pH. Therefore, the physical stability of the selected formulation, F1A (comprised of 50% 3:1 Polysorbate 80:Cremophor RH 40 surfactant, 40% Miglyol 812 loaded with beta carotene, cholecalciferol, vitamin E acetate, phytonadione, docosahexaenoic acid and eicosapentaenoic acid and 10% water loaded with thiamine mononitrate, riboflavin, niacinamide, pyridoxine hydrochloride, folic acid and cyanocobalamin) was evaluated on the basis of temperature, light, pH, conductivity and accelerated gravitational separation via centrifugation. Many of these factors do not affect the microemulsion components themselves, but are rather a stability concern for the APIs present in the system. Each factor and its relevance in drug-loaded microemulsion systems are outlined below. In all cases, droplet sizes and zeta potentials were measured before and after exposure to each condition.

4.1.2.1 Temperature

Microemulsion systems are greatly affected by changes in temperature. As previously discussed in **Chapter 3**, temperature has unique effects on non-ionic surfactants in microemulsion systems due to dehydration of the PEO head groups. In addition, an increase in temperature results in a transition from a Type I→III→ II microemulsion. However, with the incorporation of API, the chemical effect of temperature is more pronounced given the number of temperature sensitive APIs present in F1A. As noted earlier in **Chapter 3**, the lipophilic APIs are generally heat stable. The hydrophilic APIs are also stable to dry heat, but rapidly degrade when simultaneously exposed to additional factors such as pH and light. Nevertheless, exposure to changes in temperature provides useful insight into the physical and chemical stability of this pharmaceutical formulation. There are two well-established methods of

determining the effect of temperature on the stability of emulsion systems: freeze-thaw cycling and heat cycling.

4.1.2.1.1 Freeze-thaw Cycle

Freeze-thawing, as the name suggests, is the process of freezing and thawing at set temperatures for specific periods of time, typically 24 hours per condition, in order to deduce possible changes in emulsion behaviour. Emulsion systems tend to phase separate and often become "grainy and watery" upon thawing.[10] This phase separation occurs not only as a result of the freeze-thawing conditions, but primarily as a result of the individual components of the emulsion system.[10] Lipid crystallization is one of the main determinants of a freeze-stable emulsion system.[10] Upon freezing, lipid crystals may form leading to partial coalescence of the semi-frozen emulsion which, upon subsequent heating, fully coalesces leading to phase separation.[10] Emulsions with higher oil compositions, because of the increased probability of crystallization, tend to be more susceptible to phase separation or freeze-thaw instability than those with lower oil compositions.[10] Emulsifying agent selection is also important as these provide a layer of protection around emulsion droplets that may delay crystallization processes.[10] Cryo-protectants and other materials that alter the crystallization of water may be added to the emulsion system in order to increase freeze-thaw stability and improve shelf life.[1]

4.1.2.1.2 Heat Cycle

High temperatures affect microemulsion stability as we have seen in **Chapter 3** where phase transitions may occur. This effect is especially important in systems that contain non-ionic surfactants. In order to deduce the effect of heat on microemulsion systems, samples are typically subjected to increasing temperatures for specific periods of time in order to evaluate possible physical and chemical changes including changes in phase behaviour, colour, viscosity and degradation. This enables the boundaries of temperature stability to be identified. The results of both the freeze-thaw cycle and heating cycles are often compared to calorimetry results in order to confirm possible similarities and differences in heating or cooling on the microemulsion system.

4.1.2.2 Light

Light exposure is an important chemical stability factor in formulations containing light-sensitive APIs. The water-soluble vitamins B_1, B_2, B_6, B_9, B_{12} and the fat-soluble vitamins A and K_1 are light sensitive (**Chapter 3**), requiring reduced visible light or amber light conditions. Thus, exposure of a microemulsion system containing light-sensitive APIs to visible light for specified periods of time provides insight into possible chemical degradation behaviours that may destabilize the formulation.

4.1.2.3 pH

A change in pH, similar to light exposure, is also an important indicator of chemical stability in pharmaceutical formulations. In the current formulation, two water soluble APIs in F1A, riboflavin and folic acid, were unable to be incorporated without pH adjustment of the water phase to alkaline conditions. Thus, there is a possibility of a change in pH with time as the microemulsion system slowly equilibrates. In **Chapter 3,** vitamins B_1, B_2, B_9 and B_{12} in particular, were noted to possess alkaline sensitivity, undergoing chemical degradation in some cases. In addition, at pH 8.5, Vitamins B_2, B_9 and DHA/EPA possess negative charges. Thus, measuring any effect of pH on the microemulsion formulation may afford insight into possible API mobilization behaviours, degradation or destabilization.

4.1.2.4 Conductivity

Conductivity provides insight into microemulsion type, and enables changes in phase behaviour to be determined if evaluated over a period of time. The nature of F1A as a bicontinuous microemulsion should result in low conductivity values given the presence of interconnected oil and water channels. However, the presence of charged APIs, some of which may be attached to droplet surfaces, could impart charges into solution and must be measured by conductivity in order to determine the full spectrum of stability, including shelf life and storage requirements.

4.1.2.5 Centrifugation

Centrifugation stress testing, similar to the freeze-thaw cycle, is one of the only other established microemulsion thermodynamic stability indicators noted in the literature.[11] Microemulsions are thermodynamically stable and not greatly susceptible to phase separation. However, centrifugation stress testing where microemulsion samples are subjected to centrifugal force for a prolonged period of time is an indicator of accelerated gravitational sedimentation.[10] Phase separations can then be measured and quantified in order to determine the degree of physical stability of a microemulsion formulation.

4.2 Study Objectives

Chapter 2 culminated in the selection of the surfactant phase of 3:1 Polysorbate 80:Cremophor RH 40 while **Chapter 3** outlined the process of API incorporation as well as system optimization. Given the finalization of the microemulsion components, the aims of this chapter, **Chapter 4** are:

i) To characterize the finalized microemulsion formulation(s) on the basis of several properties including droplet size at various stages of drug-loading, charge, rheology and morphology

ii) To assess the stability of the finalized microemulsion formulation on the basis of temperature and centrifugation, the two tests most indicative of thermodynamic stability.[11] An additional aim is to assess specific, API-affecting stability factors such as light exposure in order to identify the most critical formulation stability factors

4.3 Hypotheses

4.3.1 Characterization

If a combination of 3:1 Polysorbate 80:Cremophor RH 40, Miglyol 812 and water results in the formation of a multi-drug loaded, Type IV microemulsion, then the following characteristics are expected: droplet sizes of approximately 100 nm and zeta potential values below -30 mV (after 100x dilution with water), conductivity values above 0 mS/cm, Newtonian behaviour below 100 RPM and the presence of interconnected bicontinuous channels as visualized microscopically.

4.3.2 Stability

If F1A is exposed to three freeze thaw cycles, heat exposure beyond 60°C‡ and light exposure for 24 hours, droplet size changes of greater than 50%* are expected due to droplet rupture, phase separation and degradation of Vitamins A, K_1 and the B_1, B_2, B_6, B_9, B_{12}, respectively. In addition, if the pH and conductivity of F1A are tested, changes of at least 1 pH unit over the period of one month and 10 uS/cm over the period of one week are expected, given increased API mobility with time.

4.4 Materials and Methods

4.4.1 Materials

Surfactant and active ingredient materials were the same as those used in **Chapter 3**.

4.4.2 Methods

4.4.2.1 Characterization

4.4.2.1.1 Droplet Size

Microemulsion formulations were prepared by weighing respective amounts of 3:1 Polysorbate 80:Cremophor RH 40 surfactant, drug-incorporated Miglyol 812 oil (containing beta carotene, cholecalciferol, d-a-tocopherol acetate, phytonadione, docosahexaenoic acid and eicosapentaenoic acid) and drug-incorporated water (containing thiamine mononitrate, niacinamide, pyridoxine hydrochloride, cyanocobalamin- and riboflavin and folic acid in later measurements) into a 20 mL scintillation vial using a Sartorius Secura225D1S Analytical Balance. Each vial was inverted manually 20-25 times and left to settle for a period of 72 hours in a dark cupboard before size measurements were conducted. Droplet size measurements were performed using a Malvern Zetasizer Nano ZS. Samples were diluted 100x with water based on instrument recommendations that particle sizes in the range of 10-1000 nm be prepared as 1% w/w solutions that are slightly turbid.[1] In addition, this

---

‡Changes expected at 60°C given cloud point of Polysorbate 80 (60°C)[12] and Cremophor RH 40 (80°C)[13]

*The emulsion stability index (ESI) is an indicator of stability measured by the change in droplet size with time, expressed as a percentage.[14] There is no acceptable ESI range but the closer the value to 1 (100%), the more stable the emulsion. 50% was selected as this is representative of a poor stability index.[15]

dilution factor affords easier facilitation of size measurements in the optimal count rate range (200-500 kcps or kilo counts (of photons) per second).[16] Size measurements of F1A placebo at 100x, 500x and 1000x showed no notable differences (**Figure C-1, Appendix C**). The use of a 100x dilution factor for droplet size and zeta potential measurements has also been previously reported for microemulsion systems.[17,18] 500 μL sample was pipetted into a Fisherbrand 1.5 mL polystyrene cuvette and inserted into the cuvette holder. Samples were left to equilibrate for 300 seconds at 25ºC (and 37ºC in some cases) before readings were taken at a scattering angle of 173º. Three measurements were taken per sample. No replicates were prepared in the initial droplet size studies but after incorporation of all eleven active ingredients, samples were prepared and measured in triplicate at the very least. Graphs were plotted in Graphpad Prism 6 software.

4.4.2.1.2 Zeta Potential

Zeta potential measurements were performed using a Malvern Zetasizer Nano ZS. 700 μL sample was introduced via syringe into a primed Malvern folded capillary zeta cell and inserted into the cuvette holder. Samples were left to equilibrate for 300 seconds at 25ºC before readings were taken. pH was measured with a Fisher Scientific Accumet AB15 pH meter and probe. Samples were prepared in triplicate at the very least, with three measurements taken per sample. Graphs were plotted in Graphpad Prism 6 software.

4.4.2.1.3 Conductivity

Conductivity measurements on formulation samples were performed using an InLab 752-6 mm micro-conductivity probe connected to a SevenEasy Conductivity meter. The probe was calibrated with 0.01 M potassium chloride calibration solution before each measurement was taken. Temperature was set to automated control at 25ºC. Conductivity measurements for water diluted samples were performed with a Malvern Zetasizer Nano ZS using the same protocol as that for zeta potential measurements. Measurements were performed in duplicate for the microemulsion formulation and using ten replicates for diluted samples. Graphs were plotted in Graphpad Prism 6 software.

4.4.2.1.4 Rheology

Rheological measurements were carried out using an m-VROC RheoSense rheometer. 800 μL sample was introduced into a 1 mL Hamilton glass syringe and carefully placed into the syringe jacket. The lid of the syringe jacket was tightened and the drive nut knob adjusted to approximately 2 cm from the syringe end. The instrument was set to run at increasing shear rate values and the viscosity and shear stress recorded using Rheosense Inc. m-VROC software. Measurements were performed in duplicate with ten measurements per sample. Graphs were plotted in Graphpad Prism 6 software.

4.4.2.1.5 Morphology

5 μL sample was carefully pipetted onto a copper grid held with tweezers. The underside of the copper grid was blotted with filter paper. 1 drop of 1% phosphotungstic acid was added to the grid and left for 15 seconds before the underside of the grid was blotted again with filter paper. The copper grid containing stained sample was placed into a protective case and left in a fume hood to dry for 24 hours. Samples were imaged on a Philips CM10 Transmission Electron Microscope (TEM) at 60 kV.

4.4.2.1.6 Thermoanalytic Behaviour

A Perkin Elmer Differential Scanning Calorimeter (DSC) 4000 was set to a heating and cooling cycle from -50 to 25ºC. Approximately 2-6 mg of sample was placed into a standard aluminum sample pan, sealed and placed in the instrument sample holder. An empty aluminum pan was used as a reference. Each sample was held for 1 minute at 25 ºC, then cooled from 25ºC to -50ºC at a rate of 5ºC per minute. The sample was then held for 3 minutes at -50ºC then heated from -50ºC to 25ºC at a rate of 10ºC per minute. Experiments were carried out under nitrogen gas. Surfactant and microemulsion formulation measurements were performed twice on one sample of each. DSC graphs of heat flow vs. temperature were generated using Pyris software.

4.4.2.1.7 Statistical Analysis: Characterization

An independent, two-tailed, two-sample Student's t-test was performed on the size and zeta potential measurements of placebo and drug-loaded samples in order to determine whether any statistically significant differences existed. Test assumptions included a normal distribution

with equal variance at 95% confidence intervals (p-value ≤ .05). All data were analyzed using Graphpad Prism 6 software.

4.4.2.2 Stability

10 g final formulation (F1A) was prepared and added to an amber scintillation vial. The formulation was subjected to various stability tests as described below, before measurement of droplet size and zeta potential using the methodology described earlier (**Sections 4.1.1.1 and 4.1.1.2**). Samples were measured in duplicate with three measurements per sample. All graphs were plotted in Graphpad Prism 6 software.

4.4.2.2.1 Temperature: Freeze-thaw Cycle

F1A was placed in a -25°C Thermo Fischer Forma freezer, removed after 24 hours and left to thaw to room temperature with limited light exposure for an additional 24 hours. This represented one cycle. The test was repeated until three cycles were completed. Experiments were performed in duplicate with three measurements per sample.

4.4.2.2.2 Temperature: Heat Cycle

F1A was left for 24 hours at room temperature in a dark cupboard before being placed into a Fisher Scientific Isotemp GPD 10 water bath set at 37, 50, 60 and 70°C and held for 24-48 hours at each temperature. Samples were taken at each temperature point before dilution and size/zeta potential measurement. Experiments were performed in duplicate with three measurements per sample.

4.4.2.2.3 Light Exposure Test

F1A was left for 24 hours and 1 week at room temperature in a flow-controlled fume hood with exposure to fluorescent light. Samples were taken at each time point before dilution and size/zeta measurement. Experiments were performed in duplicate with three measurements per sample.

4.4.2.2.4 pH Test

After 24 hours at room temperature in restricted lighting, the pH of F1A was measured with a Fisher Scientific Accumet AB15 pH meter and probe three times and the measurements recorded. The pH was continually measured at 48, 72, 96, 120 and 164 hours as well as at 2, 3 and 4 weeks. One sample was measured, with three readings of said sample per time point.

4.4.2.2.5 Conductivity Test

After 24 hours at room temperature in restricted lighting, the conductivity of F1A was measured with an InLab 752-6 mm micro-conductivity probe connected to a SevenEasy Conductivity meter three times and the measurements recorded. Conductivity and temperature were measured immediately after manufacture and at 24 hours, 48 hours and 1 week after manufacture. One sample was measured, with three readings of said sample per time point.

4.4.2.2.6 Centrifugation Stress Testing

Approximately 5 g F1A was placed into two graduated centrifuge tubes and subjected to centrifugation using a Beckman Coulter floor centrifuge with JA-12 rotor at 5000 RPM for 30 minutes and 10000 RPM for 30 minutes. The volume of intact phase was compared to that of the entire sample and quantified as a percentage in order to determine stability. One sample was measured.

4.4.2.2.7 Statistical Analysis: Stability

A dependent, two-tailed, two-sample Student's t-test was performed on the size and zeta potential measurements of F1A samples before and after subjection to three freeze-thaw cycles in order to determine whether any statistically significant differences existed. Test assumptions included a normal distribution with equal variance at 95% confidence intervals (p-value $\leq$.05). For all other stability samples, a matched, one-way Analysis of Variance (ANOVA) was conducted along with a Dunnett's multiple comparisons test, where samples after treatment were compared to those before treatment. Test assumptions included a normal distribution with no equal variability of differences (sphericity). As a result of the latter, the Geisser-Greenhouse correction was used. 95% confidence intervals (p-value $\leq$ .05) were used. All data were analyzed using Graphpad Prism 6 software.

4.5 Results and Discussion

4.5.1 Characterization

4.5.1.1 Droplet Size

4.5.1.1.1 Lipophilic Active Pharmaceutical Ingredient (API) Incorporation

Droplet sizes of three potential microemulsion formulations were evaluated at 25ºC and 37ºC. Given that a Type IV microemulsion was preferred, the ternary phase diagram for 3:1 Polysorbate 80:Cremophor RH 40, Miglyol 812 and water (**Chapter 2**) was assessed and three surfactant:oil:water (S:O:W) ratios selected based on their ability to form Type IV microemulsions: i) 50:40:10 (Formulation F1A), ii) 50:45:5 (Formulation F2A) and iii) 60:30:10 (Formulation F3A). According to the TPD plot in **Chapter 2**, 50:40:10 and 50:45:5 possessed the lowest surfactant concentration for Type IV microemulsion formation, while 60:30:10 required a slightly higher (10% w/w) surfactant concentration than its counterparts. Thus, the latter provides insight into the effect of increased surfactant concentration on droplet size. Hydrodynamic diameter results are shown in **Figure 4.1** at 100x dilution with water. Given that the critical micelle concentration of the 3:1 Polysorbate 80 and Cremophor RH 40 surfactant phase was 0.0036 mM, this aqueous dilution still afforded use of the surfactant phase above the CMC (see **Appendix C** for calculation). Therefore, micelles were still present at 100x aqueous dilution for DLS measurements.

Based on the results in **Figure 4.1**, some general trends were noted. Overall, drug-free microemulsion formulations F1A, F2A and F3A possessed sizes of 110 ± 0.3 nm, 142 ± 0.3 nm and 54 ± 0.7 nm, respectively while drug-loaded samples possessed sizes of 56 ± 0.0 nm, 63 ± 0.2 nm and 28 ± 0.2 nm, respectively. Thus, it can be seen that droplet size in both drug-free and drug-loaded formulations followed the order F2A>F1A>F3A, where F2A recorded the largest sizes and F3A, the smallest. Based on these results, four general observations were noted. First, all formulations demonstrated a two-fold reduction in droplet size upon incorporation of the lipophilic active ingredients. Though microemulsions typically experience an increase in droplet size upon most types of API incorporation, a decrease in size upon API incorporation has been previously reported.[19-21]

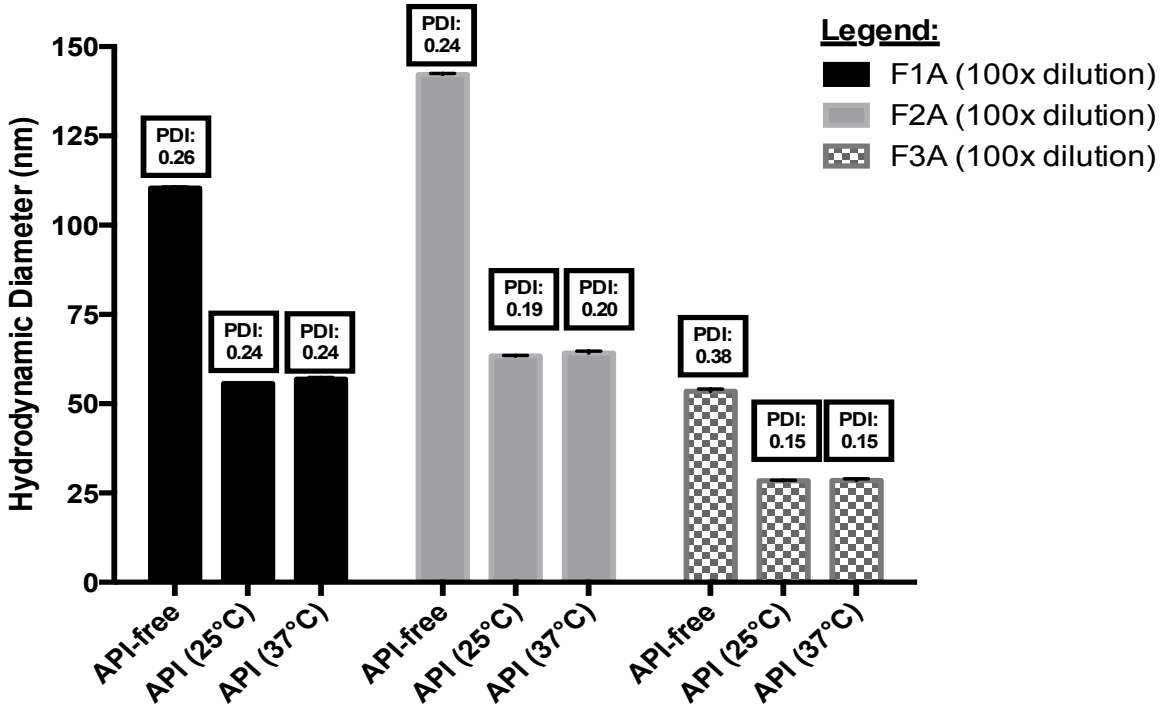

Figure 4.1: Droplet size and polydispersity indices (PDIs) of three microemulsion formulations before and after lipophilic API incorporation of A, D_3, E acetate, K_1 and Omega-3 fatty acids DHA/EPA upon 100x dilution with water.

These previous studies by Nikolakakis et al. (2015), Patel et al. (2013) and Shahba et al. (2016) utilized medium chain mono-, di- and triglycerides and a Cremophor surfactant for incorporation of lipophilic APIs. The proposed mechanism for the reduction in droplet size upon incorporation of lipophilic drug material in medium chain oil and Cremophor surfactant systems largely involved effects and interactions of the drugs themselves with other system components. Nikolakakis et al. (2015) proposed that the API of choice tested in their work, furosemide, acted as a co-surfactant reducing the interfacial tension and causing a reduction in droplet size. Patel et al. (2013) proposed that droplet sizes decreased in their study because of the interactions between the amine group in their drug, lumefantrine, and the carboxylic acid group in oleic acid, which was also present in their formulation. Finally, Shahba et al. (2016) proposed a reduction in droplet sizes in their work due to an interaction between the amine group in cinnarizine, their lipophilic drug, and the carboxylic acid group of oleic acid also present in the formulation, leading to the formation of an ion-pairing complex.

With respect to API-surfactant/polymer interactions responsible for size decreases, Ahmad at al. (2014) observed a decrease in droplet size upon incorporation of lipophilic drug, meta-tetraphenyl porphyrin (mTPP), due to an interaction between the phenyl group of mTPP and the alkyl group of its surfactant, polyethyleneglycol 500- distearoyl phosphatidyl ethanolamine (PEG 5000- DSPE). Such –CH - pi bond interactions may be explained by previously reported works such as that of Brunner et al. (2014).[22] Desale et al. (2013) also reported a decrease in droplet size upon incorporation of cisplatin into polymer PEG-glutamic acid-phenylalanine micelles due to complexation via neutralization and condensation of cisplatin with the glutamic acid moiety.[23] Similarly, Chen at al. (2012) reported a decrease in droplet size upon incorporation of lipophilic norcantharidin in polymeric PEG-polycaprolactone micelles due to Van der Waals interactions of the drug with the polycaprolactone moiety.[24] Additional explanations for a reduction in droplet size upon API incorporation, include the ability of the API to decrease micelle aggregation number[25,26] and the ability of the API to induce erosion or hydrolysis in core-shell systems.[27,28]

In this work, the decrease in droplet size upon incorporation of Vitamins A (beta-carotene), D_3 (cholecaliferol), E acetate, K_1 (phytonadione) and omega-3 fatty acids DHA and EPA, implies evidence of interactions between the APIs and other system component(s). These interactions though not explicitly examined in this work, may be deduced by structural considerations of each component. Of great consequence may be the presence of slightly surface-active APIs in this formulation. DHA and EPA consist of 22 and 20-carbons, respectively, which present as cis-unsaturated alkyl chains with a terminal carboxylic acid group. These molecules may concentrate at the droplet interface, acting in a similar manner to co-surfactants, thereby reducing the interfacial tension and resulting in smaller droplets. Triglyceride molecules themselves are also surface-active, although this fact is rarely addressed.[29] Surface tensions of 30 mN/m at 20ºC have been previously reported for tricaprylin[30] leading to the assumption that Miglyol 812 is also slightly surface-active, given its glycerol head and fatty acid tails. Thus, Miglyol 812 while largely concentrated in the core of O/W micelles, may also be present in some concentration, albeit a low one, at the interface. These surface-active APIs in Miglyol 812, which itself is slightly surface-active, may be one mechanism responsible for the reduction in droplet size upon API incorporation as seen here.

Additional interactions may arise as a result of cyclic π-systems contained in some API structures. Vitamin E acetate is comprised of a phenyl ring with a methyl group at the *para*-position and Vitamin K_1 is comprised of a naphthoquinone. It is possible that π -π stacking interactions, or even –CH- π interactions, though weak in nature, may occur given the proximity of the methyl groups in Vitamin E acetate to the benzene ring. Weak -CH- π interactions may also occur between the methyl groups in the tails of Cremophor RH 40 and Polysorbate 80 and the π systems of Vitamin E acetate and K_1. The carboxylic acid groups of DHA/EPA and the hydroxyl groups of Cremophor RH 40 may also act as proton donors to the carbonyl groups in Vitamin E acetate and Vitamin K_1 phytonadione resulting in a degree of hydrogen bonding that furthers such interactions. DHA and EPA, in addition to being surface-active, are also comprised of cis-unsaturated alkyl chains, which are more readily available for interactions versus that of trans-unsaturated alkyl chains as in the case of beta-carotene. In general, all lipophilic APIs examined in this work are of high octanol/water partition coefficient values (< 5) and consist of alkyl tails and aromatic structures that likely localize in the lipophilic core of the microemulsion droplets. The presence of such a large amount of hydrophobic material within a confined space would undoubtedly lead to a number of hydrophobic and additional weak interactions which may be responsible for the reduction in droplet size.

The second general observation was that there was no notable difference in droplet size at 25ºC and 37ºC. As noted in **Chapter 3**, the lipophilic APIs in this work are heat tolerant and unlikely to experience degradation effects at this temperature. The third general observation was that a higher surfactant concentration as in the case of F3A, led to a reduction in droplet size and increased homogeneity as indicated by the PDI values. This is understandable in consideration of emulsification principles. An increase in surfactant concentration with a simultaneous decrease in concentration of the oil phase to be solubilized leads to greater emulsification power and smaller droplet sizes. Even though measurements were conducted above CMC, the presence of 30% w/w oil in formulation F3A versus 40% and 45% oil w/w in F2A and F1A, respectively, likely leads to smaller, more monodisperse droplet sizes. In general, all PDI values fell below 0.4, the threshold value for a polydisperse sample[1] and it can be seen that PDI values decreased and samples became more monodisperse and homogenous

upon lipophilic API incorporation. This is demonstrated by the size histograms of F1A, F2A and F3A in **Figures C-2, C-3** and **C-4,** respectively in **Appendix C**.

4.5.1.1.2 Hydrophilic Active Pharmaceutical Ingredient (API) Incorporation

Figure 4.2 shows droplet size results of F1A, F2A and F3A after 100x dilution with water upon incorporation of the most soluble B-vitamins: B_1 (thiamine mononitrate), B_3 (niacinamide), B_6 (pyridoxine hydrochloride), and B_{12} (cyanocobalamin). Overall, drug-free microemulsion formulations of F1A, F2A and F3A exhibited sizes of 110 ± 0.3 nm, 142 ± 0.3 nm and 54 ± 0.7 nm, respectively while drug-loaded samples exhibited sizes of 224 ± 4 nm, 199 ± 4 nm and 107 ± 6 nm, respectively. Thus, it can be seen that droplet sizes in drug-loaded formulations followed the order F1A>F2A>F3A, where F1A recorded the largest sizes and F3A, the smallest. These results led to two general observations. The first is that, in contrast to lipophilic API incorporation, droplet sizes were not reduced upon hydrophilic API incorporation. In fact, droplet sizes were doubled in most cases. These results were expected, as hydrophilic APIs are not typically incorporated into O/W droplets, but rather align themselves with the surfactant head groups around the circumference of O/W droplets as previously observed.[31]

The original microemulsions formulated in this work were bicontinuous in nature, where both aqueous and organic phases acted as the continuous phase. Upon 100x dilution with water, however, as in this case of droplet size determination, these bicontinuous microemulsions dilute to O/W microemulsions and the O/W droplets are unable to facilitate the incorporation of hydrophilic material. Thus, these hydrophilic APIs concentrate around the droplet. Though interactions between the hydrophilic APIs and the surfactant head groups have not been experimentally determined in this work, inferences may be made from the chemical structures of these hydrophilic APIs. It is notable that of the six hydrophilic APIs incorporated in this work, four of them namely Vitamins B_2, B_3, B_6 and B_9 consisted of log P values between -0.3 and -0.95. Given that log P values of 1 indicate equal partitioning between the organic and aqueous phases, it can be deduced that although these negative partition coefficients indicate preferential aqueous solubility, these compounds may arguably be considered weakly hydrophilic in comparison to their counterparts Vitamins B_1 and B_{12}, which exhibit log P values

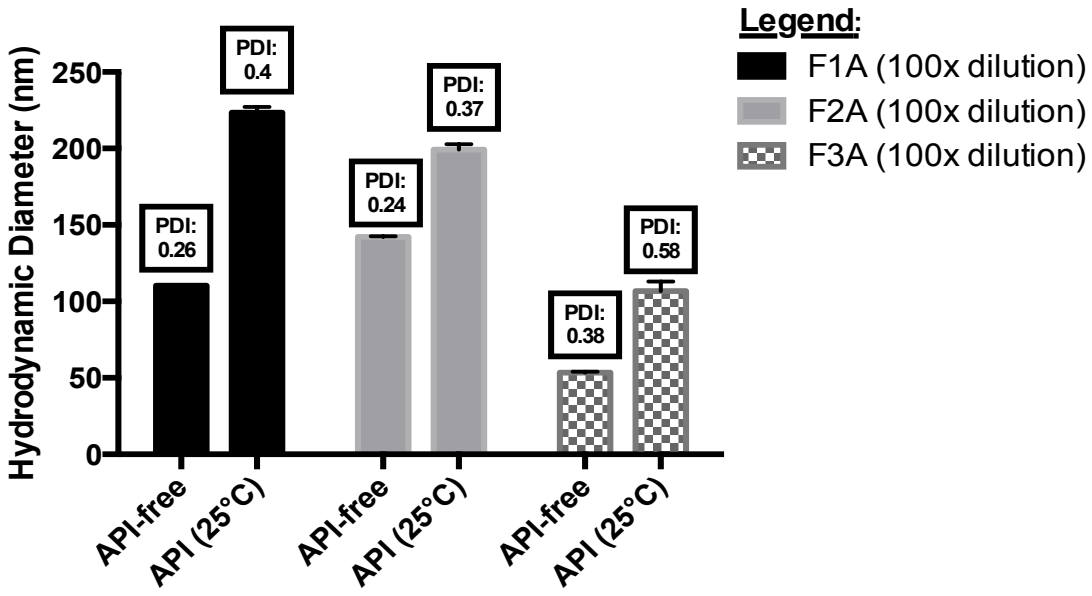

Figure 4.2: Droplet size and polydispersity indices (PDIs) of three microemulsion formulations before and after hydrophilic API incorporation of Vitamins B_1, B_3, B_6 and B_{12} upon 100x dilution with water.

of -3.1 and -14, respectively. Thus, it can be hypothesized that Vitamins B_1 and B_{12} are most likely to concentrate near the outer layer of the O/W droplet near the surfactant heads given their highly negative log P values while Vitamins B_3 and B_6 are also likely to concentrate near the surfactant head groups, but closer to the palisade layer due to their weakly hydrophilic nature. All APIs, however, possess a number of hydrogen donor groups as detailed in **Chapter 3,** with Vitamin B_{12} possessing the most (at least 11 hydrogen donor groups). These hydrogen donor groups may also participate in hydrogen bonding with surfactant PEO head groups. The concentration of hydrophilic APIs around the circumference of the O/W droplet, regardless of the specific interactions, may explain the increase in hydrodynamic diameter upon hydrophilic API incorporation.

The second observation in **Figure 4.2** is that, again in contrast to lipophilic API incorporation, PDI values increased upon hydrophilic API incorporation leading to a more polydisperse sample as demonstrated in the size histograms of F1A, F2A and F3A in **Figure C-5, Appendix C**. The explanation hypothesized for the increase in droplet size upon hydrophilic API incorporation is also relevant in explaining this observation. The four Vitamin B APIs here consist of a number of hydrogen bond donors, which are able to engage in

hydrogen bonding to varying degrees with the PEO groups of Polysorbate 80 and Cremophor RH40. These interactions are likely irregular due to the sheer number of APIs and surfactant head groups in a confined space. Thus, these interactions may be responsible for the increase in size variations of the droplets. It must be noted that all hydrodynamic diameter results plotted in **Figure 4.2** are z-average values, which are considered a reliable indicator of size in instances of PDI values 0.4 and below.[1] In the case of F3A where the PDI value was 0.58, the main peak demonstrated a hydrodynamic diameter closer to 250 nm rather than 107 nm indicated by the multi-modal size histogram of F3A in **Figure C-5, Appendix C.**

All three formulations demonstrated similarities in size after lipophilic (30-60 nm diameter) and hydrophilic API incorporation (~200 nm diameter). Given these similarities, the size results alone were not sufficient to select a final microemulsion formulation for further studies. Rather, the surfactant content in the formulation was considered the determining factor. Despite promising results, F3A was eliminated as a potential candidate due to the fact that 60% w/w surfactant is above the acceptable safety limit for Polysorbate 80 and Cremophor RH 40, according to the US Food and Drug Administration (FDA) inactive ingredient limit (IIG) database (418.37 mg per unit dose for an oral capsule containing P80 (CAS#9005656 | Unique Ingredient Identifier or UNII 6OZP39ZG8H)[32] and 414.83 mg per unit dose for an oral capsule containing Cremophor RH 40 (CAS# 61788850 | UNII 7YC686GQ8F)).[33] F2A and F1A contain the same % w/w surfactant but F1A contains a higher percentage of water than F2A (10% w/w vs 5% w/w). Thus, preference was given to F1A due to the consideration that both hydrophilic and lipophilic API incorporation were of importance. This was the final formulation selected for further investigation.

4.5.1.1.3 Lipophilic and Hydrophilic Active Pharmaceutical Ingredient (API) Incorporation

Figure 4.3 shows the results of F1A (S:O:W 50:40:10) upon incorporation of all lipophilic APIs (Vitamins A, D_3, E acetate, K_1 and Omega-3 fatty acids DHA/EPA) and four hydrophilic APIs (B_1, B_3, B_6 and B_{12}). Despite inclusion of up to nine (9) APIs, droplet sizes of 65 ± 0.5 nm were recorded as compared to sizes of 56 ± 0.0 nm and 224 ± 4 nm after incorporation of lipophilic APIs or hydrophilic APIs, respectively. Thus, the results in **Figure 4.3** indicate the possible presence of interactions between hydrophilic and lipophilic APIs, barring interactions

occurring amongst lipophilic APIs alone (including pi-pi interactions) and hydrophilic APIs alone (including API-surfactant head group interactions and hydrogen bonding). Though not experimentally determined in this work, these interactions may be inferred through structural considerations.

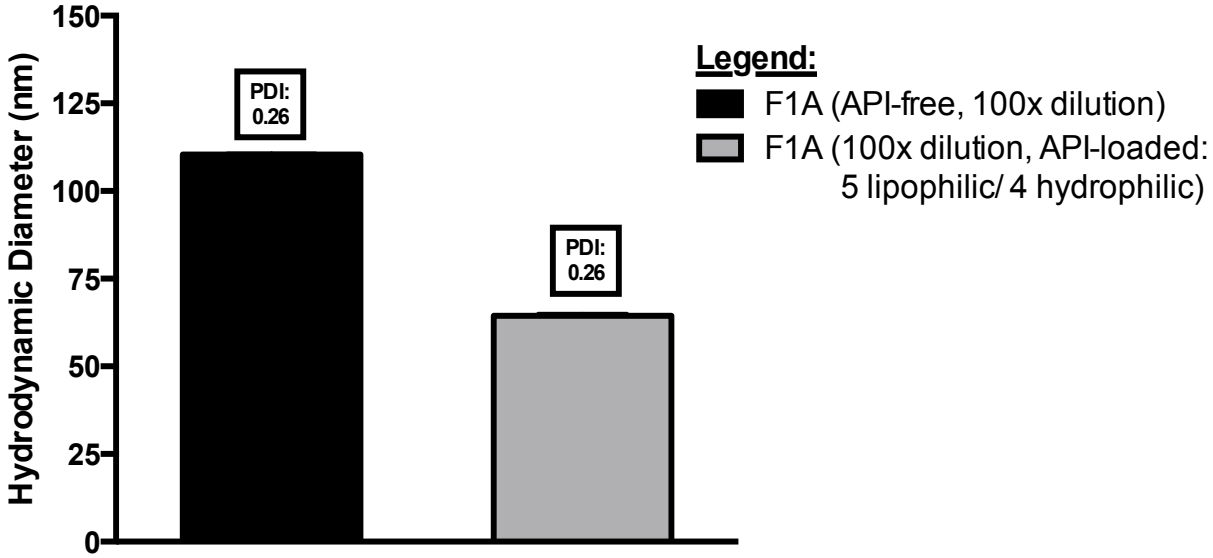

Figure 4.3: Droplet size and polydispersity indices (PDIs) of F1A before and after incorporation of all lipophilic APIs (Vitamins A, D_3, E acetate, K_1 and Omega-3 fatty acids DHA/EPA) along with the four hydrophilic APIs B_1, B_3, B_6 and B_{12} upon 100x dilution with water.

The low surface activity of DHA and EPA affords exposure of their carboxylic acid groups (near the surfactant head groups) to hydrogen bonding with any of the hydrogen donor groups present in the hydrophilic APIs. This may result in a 'tightening' or constricting of the droplet in comparison to the absence of lipophilic API material. Vitamin E acetate has an ester functional group in its acetate moiety and a C_{14} carbon alkyl chain. This may result in an orientation of the Vitamin E acetate molecule such that the alkyl tail projects into the core of the O/W droplet while the ester moiety orients closer to the surfactant head group. This proximity, again, could lead to possible hydrogen bonding with hydrogen donor groups present in many of the hydrophilic APIs. The type of interaction between Vitamin E acetate and the hydrogen bond donors of the hydrophilic APIs may also be possible with Vitamin K_1 given its dione structure and long C_{17} alkyl tail. However, the presence of the neighbouring benzene ring near the dione group of Vitamin K_1 makes this type of interaction less likely. In addition, the

possibility of low surface activity in triglycerides such as Miglyol 812, adds another layer of possible interactions between the ester groups in Miglyol 812 and the hydrogen bond donor groups in Vitamins B_1, B_3, B_6 and B_{12}. It is also possible that the presence of pyridine rings in Vitamins B_3 and B_6, a pyrimidine ring in Vitamin B_1 and an aromatic benzene ring in Vitamin B_{12} leads to additional interactions of weak pi-CH type with the surfactant tails or tails of slightly surface-active lipophilic APIs (DHA/EPA) in the formulation. PDI values before and after incorporation were the same and passed criteria as a homogenous, monodisperse sample (< 0.4).[1]

Subsequent to incorporation of the easily water-soluble vitamins, Vitamins B_2 and B_9 were successfully incorporated into the formulation via pH adjustment of the water-soluble API phase from pH 6.5 to pH 11. **Figure 4.4** shows the results of F1A before and after incorporation of all lipophilic APIs (Vitamins A, D_3, E acetate, K_1 and Omega-3 fatty acids DHA/EPA) and all hydrophilic APIs B_1, B_2, B_3, B_6, B_9 and B_{12}. It can be seen that after the addition of all eleven (11) active ingredients, droplet sizes were approximately 164 ± 37 nm in diameter. Using the two-sample, T-test where API-free microemulsions (N=4) possessed average sizes of 150 nm (SD±37) and drug-loaded microemulsions (N=14) possessed average sizes of 164 nm (SD±37), no statistically significant difference in size, $t(16)=.62$, $p=.547$, was seen between samples. The assumption of equal variances was satisfied using the F-test, $F(16)= 1.04$, $p>0.999$. (**Table C-1, Appendix C**). This non-significant increase in hydrodynamic diameter was observed despite the concentration of hydrophilic APIs at the surface of the droplet around the surfactant head groups.

In comparison to the hydrodynamic diameter results for F1A containing lipophilic material only, the presence of all six hydrophilic APIs resulted in an increase of approximately 100 nm. Despite this increase, the droplet sizes upon dilution with water of F1A containing all eleven (11) active ingredients, were still below 200 nm in diameter or 100 nm in radius, the generally accepted boundary for true nanotechnology vehicles and microemulsion systems.[5] Literature evidence of multi-drug incorporation in microemulsion systems is poor, and never to the extent of 11 APIs to the best of our knowledge. Ding et al. (2015) loaded two hydrophobic drugs, honokiol and sirolimus, into a self-emulsifying system and recorded droplet sizes of 20-30 nm upon 200x dilution with water.[34] Ujhelyi et al (2015) loaded three hydrophilic drugs, bleomycin, cisplatin and ifosfamide into a self-emulsifying microemulsion

with sizes between 68 to 149 nm in diameter, although the dilution factor was not specified.[35] Kaur (2014) loaded one lipophilic drug, rifampicin, and two hydrophilic drugs, isoniazid and pyrazinamide into a microemulsion system with sizes of 20 nm, though the formulation was mostly comprised of water (56%).[36] Given these studies, the hydrodynamic diameter results for this type of drug-saturated system is promising.

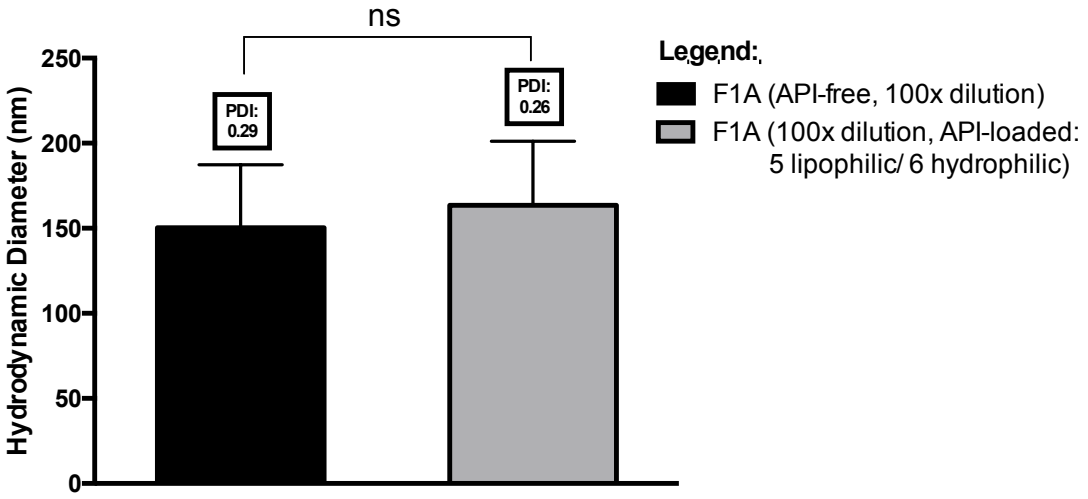

Figure 4.4: Droplet size and polydispersity indices (PDIs) of F1A before and after incorporation of all lipophilic APIs (Vitamins A, D_3, E acetate, K_1 and Omega-3 fatty acids DHA/EPA) and all hydrophilic APIs (B_1, B_2, B_3, B_6, B_9 and B_{12}) upon 100x dilution with water. Size histograms are depicted in **Figure C-6, Appendix C.** A two-sample T-test showed no significant difference in size (p=.547) between drug-free and drug-loaded samples.

4.5.1.2 Zeta Potential

The zeta potential of F1A (pH 8.5) at 100x aqueous dilution is depicted in **Figure 4.5**. The zeta potential value before incorporation of all APIs was -10.5 ± 4 mV while the zeta potential after incorporation of all APIs was -14 ± 2 mV. This small increase in absolute magnitude of zeta potential (to a more negative value) indicates that the incorporation of APIs has a stabilizing effect for the microemulsion droplets. Given that zeta potential values typically +/- 30 mV have been reported to confer stability and delay phase separation as discussed earlier, it can be deduced that this formulation is not, in strict terms, electrostatically stable. However, it has been suggested that rather than considering an absolute zeta potential value as an indicator of

physical stability in emulsion systems, it may be more practical to consider a change in zeta potential value upon subjection to a specific parameter.[2]

Using the two-sample T-test where API-free microemulsions (N=4) recorded average zeta potential values of -10.5 mV (SD±4) and drug-loaded microemulsions (N=12) recorded average zeta potential values of -14 mV (SD±2), a statistically significant difference in charge, $t(14)=2.36$, $p=.033$, was observed between samples. The assumption of equal variances was satisfied using the F-test, $F(14)= 2.88$, $p=.168$ (**Table C-1, Appendix C**). Non-ionic surfactants do not carry a charge and theoretically, should not confer a charge in emulsion droplets. However, droplets formed with Tweens (Polysorbates) and Spans have been reported to exhibit a negative charge due to the presence of free fatty acids and possible contaminants present in impure, commercial surfactants.[4] The change in zeta potential from -10.5 ± 4 mV to -14 ± 2 mV implied a direct effect of APIs on the surface charge of the droplet. At pH 8.5, a number of APIs carry a negative charge based on their pKa values discussed in **Chapter 3**. Vitamin B_2, riboflavin, carries a negative charge of -1 due to its pKa value of 10.2. Below this value, the nitrogen on the pyrazine ring becomes protonated, leading to a resonance shift and negative charge imparted on the neighbouring oxygen. Vitamin B_9, folic acid, carries a negative charge of -2 due to its pKa values of 3.4 and 4.8 on the glutamic acid moiety leading to negative charges on both carboxylic acids. DHA and EPA also carry one negative charge each due to the deprotonation of their carboxylic acid groups given pKa values of 4.9 and 4.8, respectively.[37,38] These negative charges corroborate the previous hypothesis regarding droplet size- that vitamins riboflavin, and folic acid tend to concentrate at the surfactant head groups around the circumference of the O/W droplet, increasing the negative zeta potential of the system. DHA and EPA have been previously reported to be slightly surface-active and in this case, the carboxylic acid moieties may concentrate around the O/W droplet near the surfactant head groups while the alkyl tails localize in the oily core of O/W droplets. Given that the carboxylic acid groups are negatively charged at pH 8.5, this theory is plausible given the increased negative charge of the O/W droplets as evidenced by zeta potential.

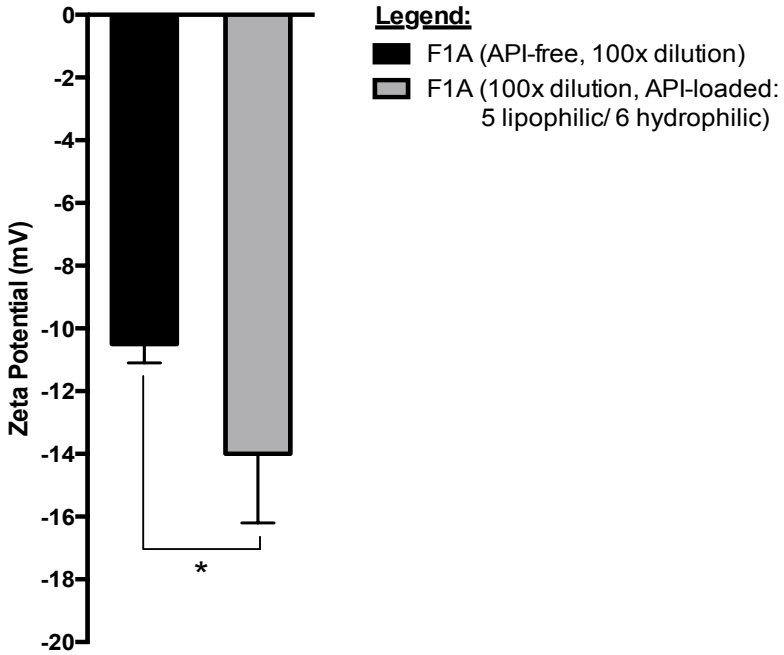

Figure 4.5: Zeta potential values of F1A before and after incorporation of all lipophilic APIs (Vitamins A, D_3, E acetate, K_1 and Omega-3 fatty acids DHA/EPA) and all hydrophilic APIs (B_1, B_2, B_3, B_6, B_9 and B_{12}) upon 100x dilution with water. Zeta potential curves are depicted in **Figure C-7, Appendix C.** A two-sample T-test showed a statistically significant difference (p=.033) in zeta potential between drug-free and drug-loaded samples.

4.5.1.3 Conductivity

Trends in conductivity were similar to those obtained via zeta potential after 100x dilution with water as depicted below in **Figure 4.6.** Prior to API addition, conductivity values were approximately 10 ± 0.1 μS/cm; after incorporation, this increased to 58 ± 21 μS/cm. The increase in conductivity is likely due to the presence of charged APIs as explained in the previous section (**Section 4.5.1.2**). Although there are no strict agreed-upon threshold values for conductivity that define microemulsion type, high conductivities are indicative of O/W droplets while conductivities of zero or close to zero are typically indicative of W/O droplets (although bicontinuous microemulsions may also be represented at near zero conductivity values).[39] A trend or shift in conductivity values, especially in comparison to water, has been purported to be valuable. In this case, a shift and increase in conductivity in the presence of API suggested a charge effect of hydrophilic APIs, in line with zeta potential and droplet size results.

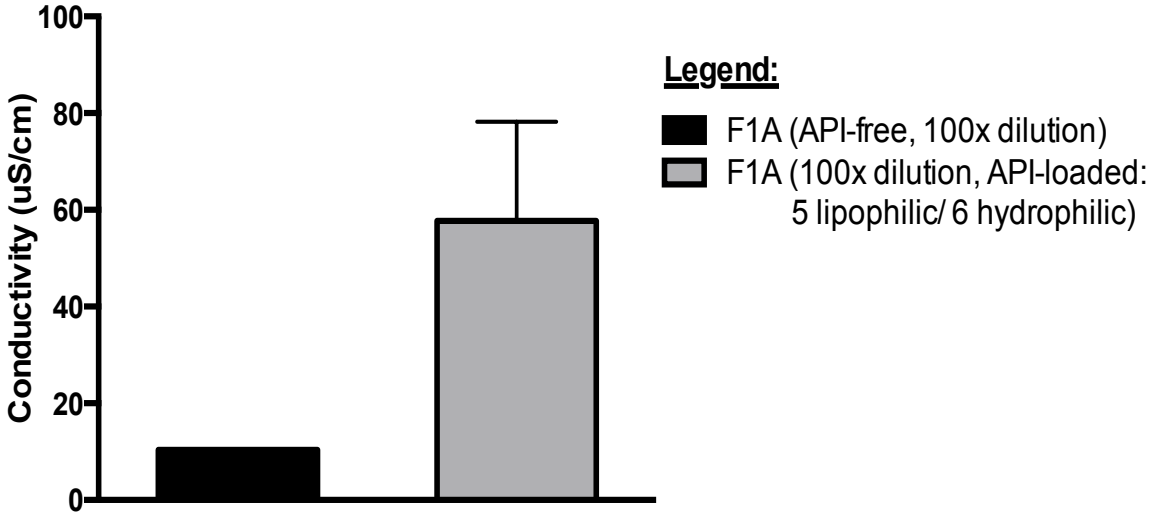

Figure 4.6: Conductivity values of F1A before and after incorporation of all lipophilic APIs (Vitamins A, D_3, E acetate, K_1 and Omega-3 fatty acids DHA/EPA) and all hydrophilic APIs (B_1, B_2, B_3, B_6, B_9 and B_{12}) upon 100x dilution with water

According to Acharya et al. (2012), conductivity is best evaluated in conjunction with other techniques rather than in isolation.[40] It is important to note that in microemulsion formulations containing low water concentrations such as the one in this work, conductivity measurements upon dilution with water are inflated, even in the absence of API, due to the hydration effect of the PEO head groups of Polysorbate 80.[41] Conductivity measurements of MilliQ water used to dilute these samples have been previously measured in our lab to be 4.35 μS/cm while measurements of F1A before dilution with MilliQ water have been measured to be 4.78 μS/cm. Bicontinuous microemulsions due to the presence of interconnected oil and water channels are expected to have lower conductivities than their O/W microemulsion counterparts where water is the continuous phase. This was observed here, as the conductivity of F1A before and after 100x dilution with water exhibited a ten-fold increase.

4.5.1.4 Rheology

Similar to conductivity, rheological measurements for emulsion systems are best interpreted in conjunction with other techniques.[41] However, they are useful in elucidating important microemulsion characteristics such as microemulsion type and stability. As discussed earlier,

microemulsions may exhibit either Newtonian (lamellar) or non-Newtonian (non-lamellar) flow behaviours[42], where Newtonian behaviour results in constant viscosity with increasing shear rate as well as a linear relationship between shear stress and shear rate. Winsor Type I and II microemulsions tend to demonstrate Newtonian behaviour while bicontinuous microemulsions tend to exhibit non-Newtonian (weak shear thinning) behaviours at high shear rates[42], especially if their low-shear viscosities exceed approximately 10 cP or mPa/s.[43] At low shear rates, however, bicontinuous microemulsions are reported to be Newtonian.[40] The rheological results for F1A at 100 and 1000x dilution with MilliQ water are depicted in **Figure 4.7**. MilliQ water can be seen to be Newtonian given the linear relationship (R^2= 0.999) between shear rate and shear stress and the constant viscosity despite increasing shear rates. Water is known to possess a dynamic viscosity value of 0.89 mPa/s at 25°C and 1.002 mPa/s at 20°C.[44] The results in **Figure 4.7** show a water viscosity of approximately 0.95 ± 0.02 mPa/s across all shear rates at room temperature. With respect to F1A, similar trends were seen. Newtonian behaviour as demonstrated by a linear relationship (R^2= 0.996 at 100x dilution; R^2= 0.999 at 1000x dilution) between shear stress and shear rate, and a constant viscosity despite increases in shear rate, was observed at room temperature. The viscosity of F1A at 100x and 1000x aqueous dilution and room temperature was 1.04 ± 0.04 mPa/s and 1.02 ± 0.05 mPa/s, respectively. Thus, both MilliQ water and F1A upon dilution with water exhibited Newtonian behaviours, lending credence to the existence of an O/W microemulsion, in the case of the latter. The viscosity of F1A at room temperature prior to aqueous dilution was recorded using a ViscoQC 300/100 Rotational Viscometer. The instrument indicated a viscosity of 447 mPa/s at 40-100 RPM and Newtonian behaviour. This corroborated work by Acharya et al (2012) in that bicontinuous microemulsions tend to remain Newtonian at low shear rates.40 Thus, it was concluded that F1A was bicontinuous in its native form but upon dilution with water, transitioned to an O/W microemulsion. This phenomenon has been previously reported.[45,46]

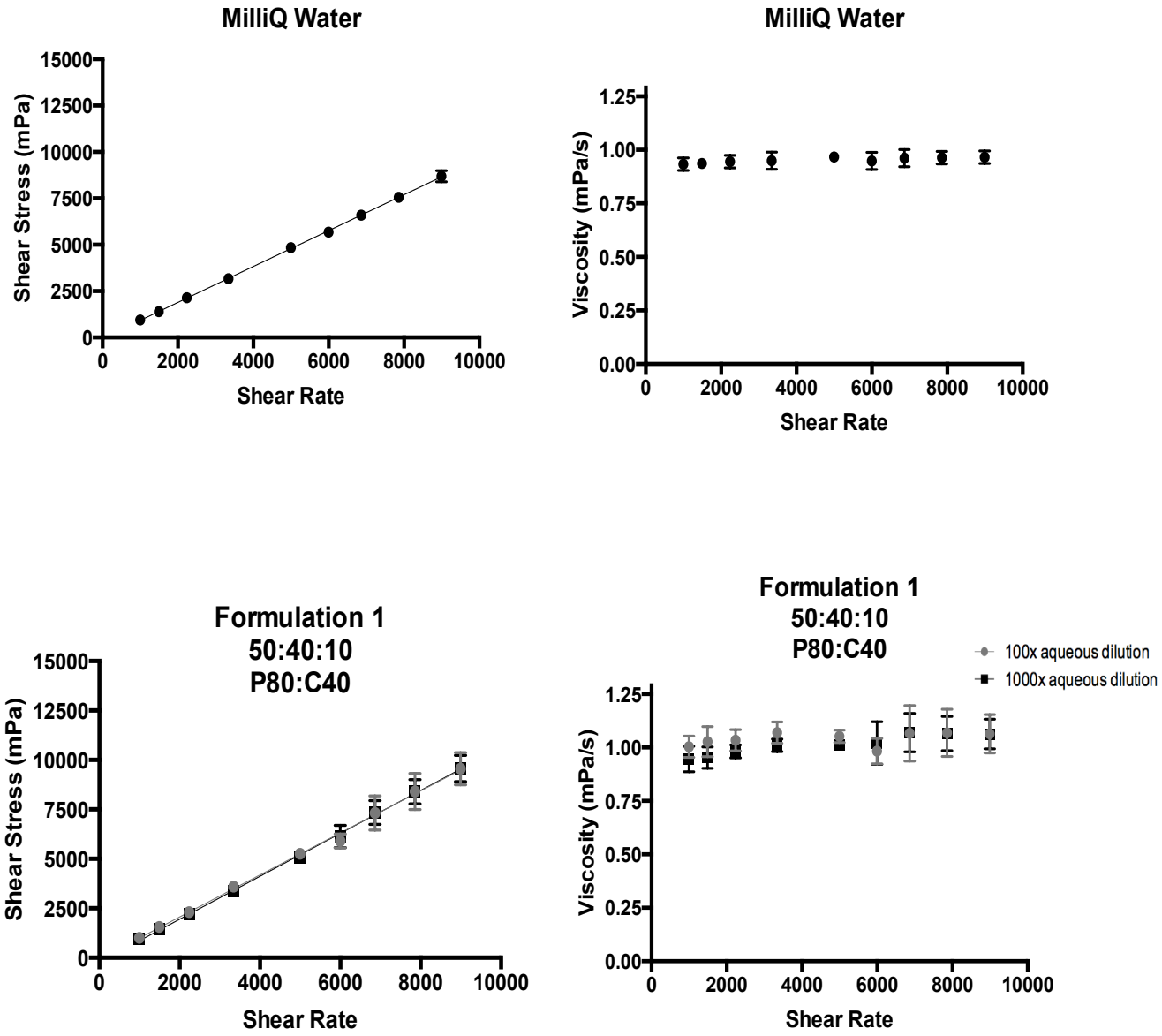

Figure 4.7: Viscosity values of water and F1A after incorporation of all lipophilic APIs (Vitamins A, D_3, E acetate, K_1 and Omega-3 fatty acids DHA/EPA) and all hydrophilic APIs (B_1, B_2, B_3, B_6, B_9 and B_{12}) upon dilution with water.

4.5.1.5. Morphology

Figure 4.8 depicts the TEM images obtained for Formulation F1A. **Panels A** and **B** illustrate F1A in its native, bicontinuous, Type IV microemulsion form. Interconnected channels of oil and water were seen throughout both panels with individual structures averaging 30 nm (**Panel A**) and 38 nm (**Panel B**) in diameter. These interconnected channels are similar to previous vitamin microemulsion studies conducted by Salimi at el. (2013).[47] At 10x dilution with water (**Panel C**), the tight interconnected structures disappeared as droplets became diluted with aqueous solution. Here, droplet sizes ranged from 50-200 nm in diameter and finally in **Panel D**, upon 100x dilution with water, the droplets assumed a defined, spherical shape characteristic of O/W droplets. It was noted that the droplets were not completely monodisperse and ranged in sizes from 25 nm to 150 nm in diameter. Compared to the hydrodynamic diameter results of 164 ± 37 nm for F1A (**Figure 4.4**), even accounting for the standard deviation, this is still an appreciable size difference. It is likely, then, that the PEO chains and presence of hydrophilic APIs around the surfactant head groups contributes to an inflation of the size value as obtained by DLS, given that hydrodynamic diameter also accounts for the surrounding layer of solvent and/or surfactant.

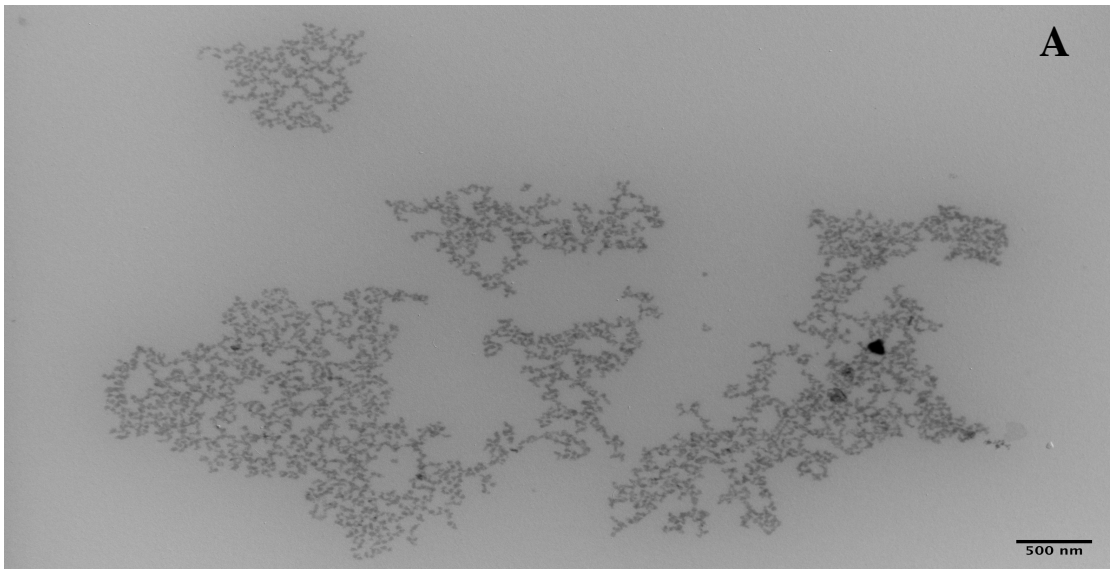

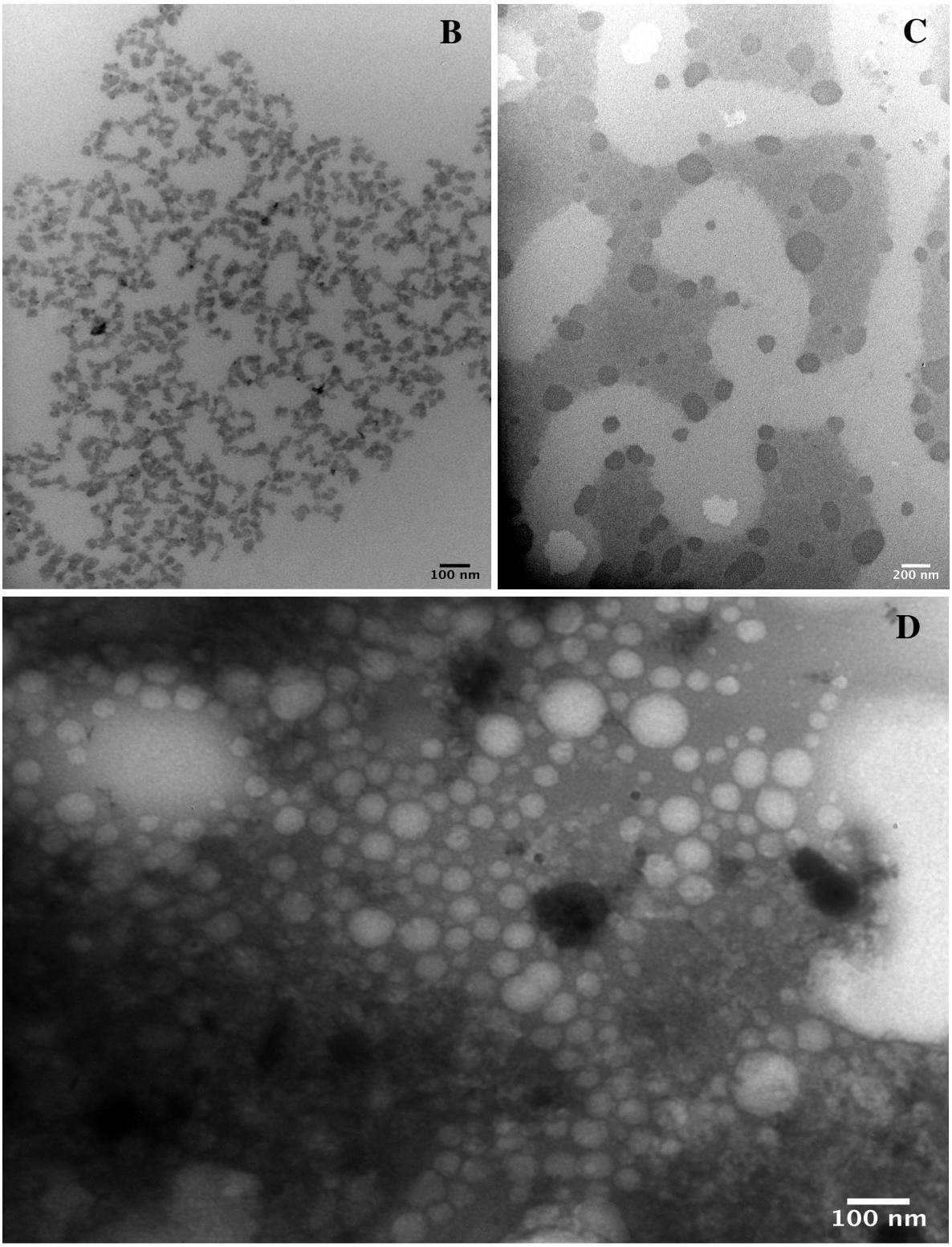

Figure 4.8: TEM images of S:O:W 50:40:10 microemulsion formulation after incorporation of all lipophilic APIs (Vitamins A, D_3, E acetate, K_1 and Omega-3 fatty acids DHA/EPA) and all hydrophilic APIs (B_1, B_2, B_3, B_6, B_9 and B_{12}) in its native state (a) and (b) and after dilution at 10X (c) and 100X (d) with water.

4.5.1.6 Thermoanalytic Behaviour

DSC results are depicted in **Figure 4.9.** Heat flow is dependent on whether a process is endothermic or exothermic. Freezing is an exothermic process as less heat is required to raise the sample temperature at the same rate as that of the reference.[48] Melting, however, is an endothermic process and heating of the sample is required in order to raise the temperature at the same rate as that of the reference.[48] Endothermic peaks in this work, indicating heat absorption, are facing down and are shown in an 'upside down' orientation. Pure water (**Panel A**) showed a gradual cooling with a sharp exothermic, crystallization peak occurring at approximately -18ºC as previously reported[49], and a gradual heating until the appearance of an endothermic, melting peak at 0-8ºC, also previously reported.[50] Although the melting peak is intuitive, the crystallization peak is more obscure. This is explained by Dalmazzone et al. (2009) who noted that for pure compounds, the melting temperature does not appear to depend on sample size while the crystallization or freezing temperature does.[50] Thus, for bulk water with a volume of 1cm^3, freezing appears to occur at approximately -14ºC while for 1 mm^3, freezing appears to occur around -24ºC.

For systems containing oil such as emulsions, investigations of the endothermic and exothermic profiles of bulk oil have been suggested.[50] **Figure 4.9, Panel B** depicts the DSC results of Miglyol 812 oil. Upon cooling, a crystallization peak was observed at approximately -45ºC. This crystallization peak is bell shaped and symmetrical indicating a monodisperse sample in which all droplets freeze at approximately the same time. Upon heating, a second crystallization peak albeit smaller and broader, is seen at -31ºC. A pronounced melting peak is then seen at approximately -2ºC. In Miglyol 812-containing PEG oil systems, it has been previously reported that the increased incorporation of Miglyol 812 led to slight decreases in enthalpy.[51] The presence of a small crystallization peak in Miglyol 812 upon heating is unique and will be discussed below.

The DSC graph of the surfactant phase, 3:1 Polysorbate 80:Cremophor RH 40, is depicted in **Panel C**. The results of this DSC graph were clearly more complex than that of pure water and Miglyol 812. A crystallization or freezing peak was seen at approximately -28ºC. Heating resulted in a second large, symmetrical crystallization peak at approximately -42ºC, although the peak is broad indicating a degree of polydispersity.

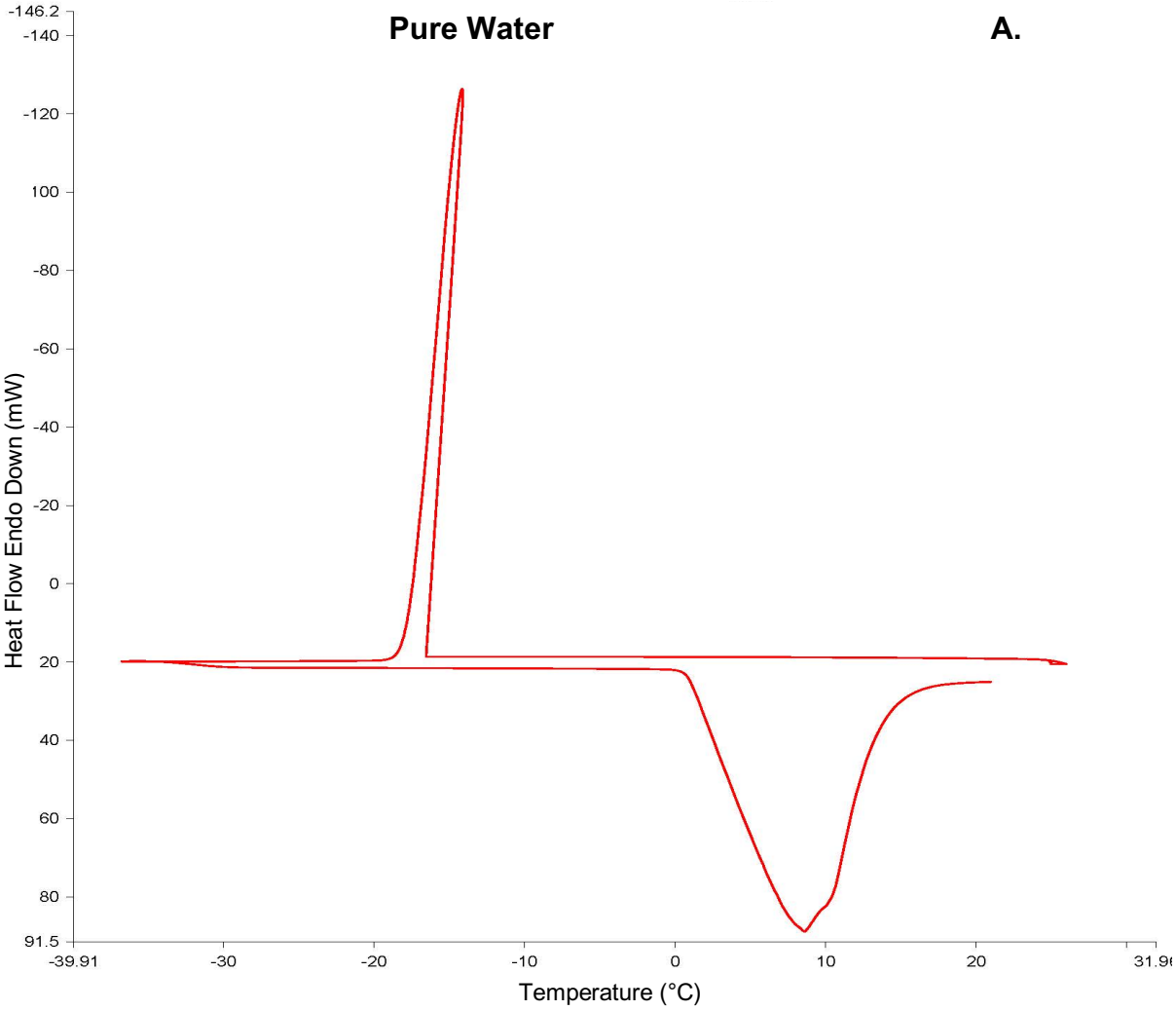
Pure Water
A.
-146.2
-140
-120
100
-80
-60
-40
-20
0
20
40
60
80
91.5
Heat Flow Endo Down (mW)
-39.91
-30
-20
-10
0
10
20
31.9
Temperature (°C)

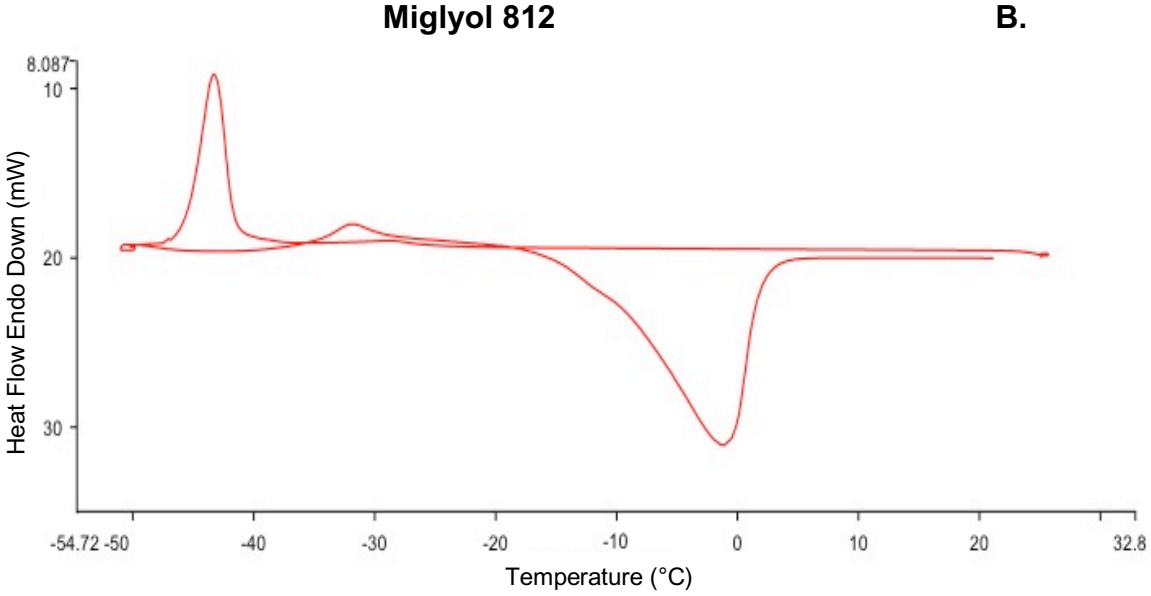
Miglyol 812
B.
8.087
10
20
30
Heat Flow Endo Down (mW)
-54.72
-50
-40
-30
-20
-10
0
10
20
32.8
Temperature (°C)

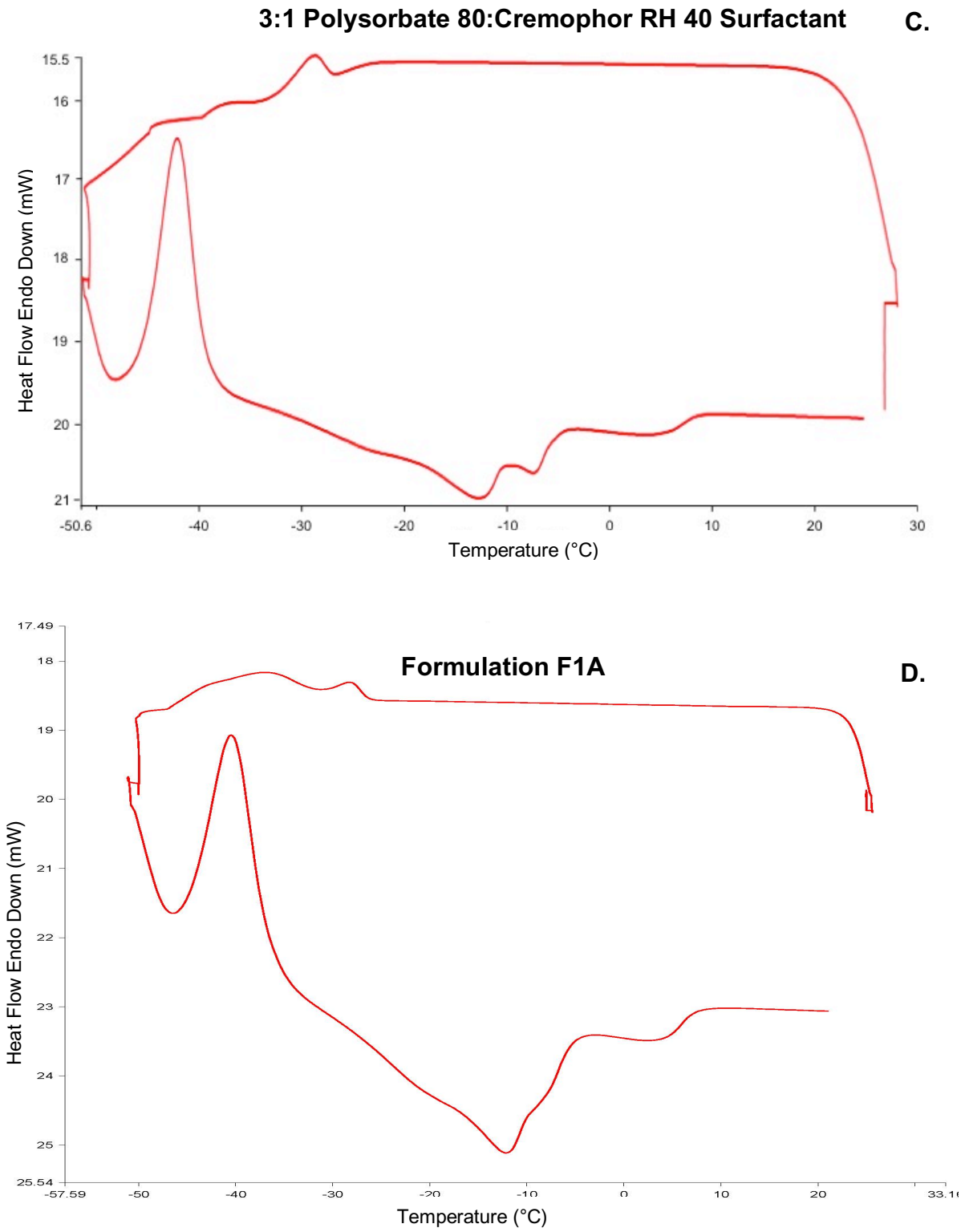

Figure 4.9: DSC graphs of A) pure water, B) Miglyol 812, C) 3:1 Polysorbate 80:Cremophor RH40 and D) S:O:W 50:40:10 microemulsion formulation after incorporation of all lipophilic APIs (Vitamins A, D_3, E acetate, K_1 and Omega-3 fatty acids DHA/EPA) and all hydrophilic APIs (B_1, B_2, B_3, B_6, B_9 and B_{12}).

Additional heating resulted in two small, broad melting peaks at approximately -14ºC and -8ºC. A small increase in heat flow is seen around 7ºC, though it cannot be definitively characterized as a peak. Rather it is likely a slight change in heat capacity due to a parameter change like viscosity, rather than a true phase change.[52] Both Miglyol 812 and the surfactant phase (Cremophor RH 40, specifically) consist of triglycerides. Thus, it is possible that this commonality may be responsible for coinciding peaks, particularly the crystallization peak at -45ºC.

The DSC graph of F1A is depicted in (**Figure 4.9, Panel D**). It was immediately evident that the peaks were remarkably similar to that of the surfactant phase, 3:1 Polysorbate 80:Cremophor RH 40. Upon cooling, there was a small, broad crystallization peak at approximately -28ºC. Upon heating, a second crystallization peak that is large and symmetrical, similar to that of the surfactant phase, was seen at approximately -38ºC. Additional heating resulted in one small, broad peak at approximately -12ºC. Slight changes in heat flow were also seen at approximately -7ºC and 5ºC. The small melting peak at -12ºC and the heat flow change at -7ºC coincide with that of the surfactant phase at -14ºC and -8ºC, respectively. The heat change of F1A at 5ºC is also similar to that of the surfactant phase at 7ºC.

The DSC graphs of Miglyol 812 (albeit to a low extent), 3:1 Polysorbate 80:Cremophor RH 40 and F1A demonstrated a unique characteristic with respect to the crystallization peaks; they all occurred upon heating rather than cooling. The presence of a crystallization peak at approximately –45ºC, -42ºC or -38ºC in the case of oil, surfactant or microemulsion phase, respectively, has been previously described as the possibility of 'bound' water in contrast to free water.[50,53] This is plausible in the case of the F1A microemulsion as there is 'bound' water via interconnected bicontinuous channels but in the case of oil and surfactant, this may indicate the presence of water as an impurity (or possibly other chemical impurities). Although crystallization typically occurs during the cooling phase, crystallization that occurs during the heating phase such as in the case of Miglyol 812, 3:1 Polysorbate 80:Cremophor RH 40 and F1A before the melting peak, indicates that the sample being measured is in a non-equilibrium state.[54] This non-equilibrium state is reasonable given that these peaks were obtained in impure, mixed components: Miglyol 812 (containing varying percentages of C_6, C_8, C_{10} and C_{12} fatty acids), the surfactant phase containing both Polysorbate and Cremophor and the final

microemulsion formulation containing Miglyol 812, two surfactants and eleven active ingredients. This type of crystallization has also been referred to as 'cold crystallization', often seen in polymers where the system is cooled too rapidly to afford crystallization such that only subsequent heating affords such formation.[55]

Overall, it can be noted that F1A exhibited a thermal profile most similar to the surfactant phase, which is not surprising given the fact that surfactant is the main component in this formulation (at 50% w/w composition in the microemulsion). In addition, despite the presence of 11 APIs in F1A, no new or unidentified peaks not seen in either the surfactant, oil or water components were observed, indicating no obvious evidence of degradation. Evidence of chemical reactions including decomposition, are typically notable in the exothermic curves.[54] The exothermic curves in this case do not show a high degree of variance between that of the surfactant phase and that of the microemulsion. However, it should also be cautioned that microemulsion analysis at sub-zero temperatures is not reliable given the presence of multiple components which may phase separate.[53] Finally, the DSC curves of Miglyol 812, the surfactant phase and F1A did not exhibit the high exothermic heat flows values seen in the DSC graph of pure water. This may be explained by the lack of water in these systems resulting in a lack of freezing ability.

4.5.2 Stability

4.5.2.1 Temperature

4.5.2.1.1 Temperature: Freeze-thaw Cycle

After three consecutive cycles of freezing at -25°C for 24 hours followed by thawing to room temperature for 24 hours, no evidence of phase separation was seen in F1A. However, tiny precipitates yellow/orange in colour were seen when examined closely. The results in **Figure 4.10** below, demonstrate changes in hydrodynamic diameter and zeta potential after three freeze-thaw cycles. Droplet sizes greatly reduced by almost 50% from 200 ± 59 nm to 125 ± 61 nm while zeta potential values increased (i.e. became less negative, which is consistent with decreased stability) from -15 ± 2 mV to -10 ± 0.3 mV. Using the paired, two-sample T-test, F1A (N=2 pairs) demonstrated a statistically significant difference t(1)=77, p=.008 in average size before, 203 nm (SD±59) and after, 126 nm (SD±61) exposure to three freeze-thaw cycles.

In contrast, there was no statistically significant difference t(1)=3.5, p= .177 in average zeta potential before, -14 mV (SD±2) and after, -10 mV (SD±0.2) treatment. (**Table C-2, Appendix C**).

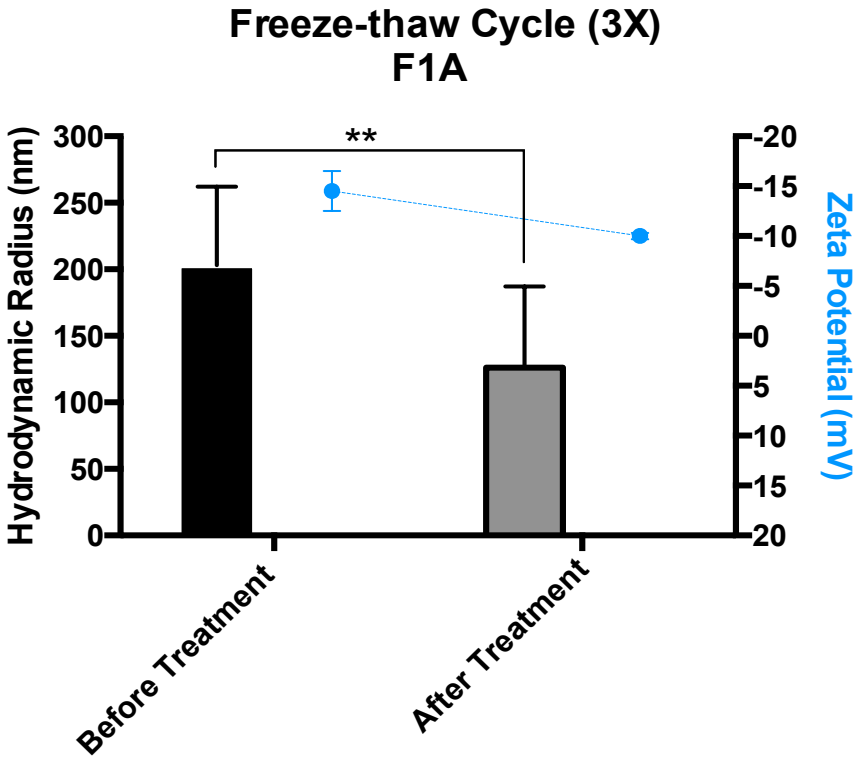

Figure 4.10: Hydrodynamic diameters and zeta potentials of drug-loaded microemulsion formulation F1A before and after three consecutive freeze-thaw cycles from -25°C to room temperature at 24 hours each. PDI values before and after treatment were 0.28 and 0.24, respectively. Size histograms and zeta potential curves can be found in **Figure C-8** (**Appendix C**). A paired two-sample T-test indicated a statistically significant difference (p=.008) in size but not zeta potential (p=.177) after exposure to three freeze-thaw cycles. A paired two-sample T-test indicated a statistically significant difference in size (p=.008) but not zeta potential (p=.177) before and after exposure to three freeze-thaw cycles.

Though no phase separation was visibly apparent, the presence of yellow/orange precipitates suggests the precipitation of riboflavin and folic acid. Thus, it is possible that these APIs, which are likely localized near the hydrophilic surfactant head groups at the oil/water boundary, became displaced upon water crystallization and thawing. DSC studies, as discussed earlier, revealed that water crystallized before, and melted after, Miglyol 812 leading to the possible forcing out of some API from the frozen water phase to the oil phase. Upon thawing,

it is further possible that these APIs did not completely revert to their original state in the aqueous phase, resulting in precipitation. Although the temperature ranges studied in DSC were wider than that of the freeze-thaw cycle, we suggest that the crystallization and melting of both water and Miglyol 812 were still possible here; the crystallization and melting peaks of water, according to DSC, were both within range of this freeze-thaw cycle (-25°C to +25°C) and although the crystallization peak of Miglyol 812 was slightly outside this range (-32°C), the peak was not fully depressed until -18°C. Thus, some crystallization activity of Miglyol 812 may still have occurred upon freeze-thawing at -25°C to +25°C, leading to the presence of both Miglyol 812 and water crystals, and the forcing out of respective APIs.

The large reduction in droplet size before and after exposure to three freeze-thaw cycles was unexpected as freeze-thaw cycling in microemulsion systems tends to lead to droplet rupture[56] and phase separation.[10] Theoretically, this should result in an increase in droplet size as has been previously reported throughout the literature. Instead, this reduction in droplet size suggests a possible release of API material. Tcholakova et al. (2017) previously reported that the crystallization of both water and oil at separate temperatures, as in this case, could lead to possible rupture of the interface and release of API, resulting in a decrease in droplet size.[56] A previous study of an amphotericin B-loaded microemulsion comprised of glyceryl monooleate oil and PEG-40 stearate/PEG-15 hydroxy stearate surfactants also demonstrated an almost 50% reduction in droplet size after three freeze thaw cycles from -20 to +32°C.[57] In F1A, droplet sizes were approximately 164 ± 37 nm when loaded with all eleven APIs and approximately 65 ± 0.5 nm when loaded with nine APIs, excluding riboflavin and folic acid. Thus, given the final droplet size of 126 ± 61 nm after these three freeze-thaw cycles, it is possible that some of these APIs, likely riboflavin and folic acid, were released. This is corroborated by the yellow/orange precipitates seen in F1A after freeze-thawing.

The increase in zeta potential was indicative of destabilization and the possible release of interface-associated, negatively-charged APIs. Given that freezing and melting has previously been reported to result in rupture and bursting of droplets[56], it is possible that this disruption of the surfactant layer resulted in a disruption of APIs bound near the surface of the droplet. Given the increase in zeta potential to a less negative charge, this may coincide with a release of negatively charged APIs riboflavin (-1) and folic acid (-2) from the droplet surface.

4.5.2.1.2 Temperature: Heat Cycle

Upon exposure to heat at 37°C for 48 hours, there were indications of potential phase separations beginning in F1A. This phase separation and API precipitation was particularly pronounced at 70°C and a gradual darkening of sample from red-brown to dark brown/black was also seen, beginning at 50°C. **Figure 4.11** below illustrates changes in hydrodynamic diameter and zeta potential after 48-hour consecutive heating cycles at 37°C, 50°C, 60°C and 70°C. Size decreases of approximately 35% from approximately 180 ± 37 nm to 115 ± 25 nm were seen at the first temperature point, i.e. after two consecutive days of heating at 37°C. The droplet sizes never seem to recover after this point, varying only slightly between 120-140 nm as the temperature was increased from 37 to 60°C. Similar trends in zeta potential were seen where values increased (became less negative) from -16 ± 1 mV to between -14 ± 3 mV and -18 ± 6 mV as samples were heated from 37°C to 70°C. A matched one-way ANOVA, however, indicated no statistically significant difference in size $F(1,1)=16.9$, $p=.152$ or zeta potential $F(1,1)=1.91$, $p=.399$ of individually treated samples as compared to samples before treatment (**Table C-3, Appendix C**). Nevertheless, it is important to make the distinction between statistical and practical significance here as such changes in droplet size and charge pose stability concerns for the drug formulation.

It was evident based on **Figure 4.11** that prolonged heating of F1A at 37°C for 48 hours led to a decrease in droplet size of approximately 65 nm. Given that the lipophilic APIs in F1A are generally heat-stable (**Chapter 3**), the cause for this size decrease may be attributed to i) surfactant behaviour and ii) hydrophilic APIs and their potential precipitation. In terms of surfactant behaviour, we previously explained the effect of increasing temperatures on the dehydration of non-ionic, polyethylene oxide head groups in **Chapter 3**. Small increases in temperature have been reported to reduce hydration of the PEO head group of Polysorbate 80 resulting in a more lipophilic head group and lower interfacial tension between oil and water.[58] This small temperature increase favours micellization[58] and the production of small droplet sizes.[59] With larger increases in temperature, however, a breakdown of the structure of surrounding water disfavours micellization[58] which may result in larger droplet sizes. This temperature 'sweet spot' of Polysorbate 80 where a minimum in critical micelle concentration and low in droplet size is experienced, has been reported to be 40°C.[58] This would align with

the minimum droplet sizes recorded at 37°C. Above 37°C, droplet size behaviour may be attributable to hydrophilic APIs and their precipitates.

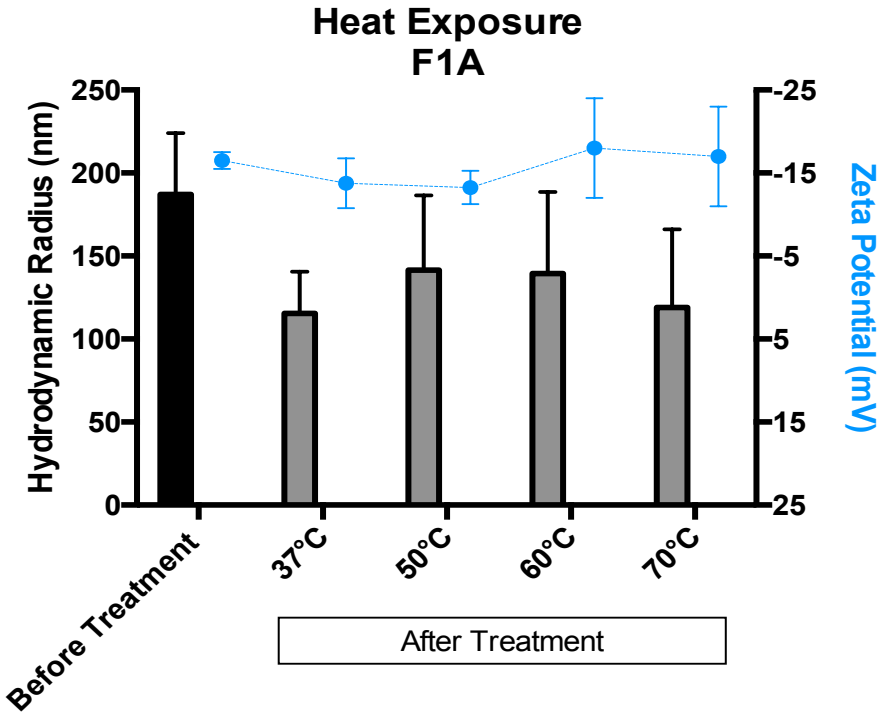

Figure 4.11: Hydrodynamic diameters and zeta potentials of drug-loaded microemulsion formulation F1A before and after consecutive heating for 48 hours at each temperature point. PDI values before treatment were 0.27 and remained between 0.22-0.27 after treatment. Size histograms and zeta potential curves can be found in **Figure C-9** (**Appendix C**). A matched one-way ANOVA with Dunnett's post-hoc test indicated no statistically significant differences in size (p=.152) or zeta potential (p=.399) before and after treatment.

Prolonged heating combined with the alkaline pH of F1A may have degraded folic acid as explained in **Chapter 3.** In addition, it has been previously reported that in high alkaline conditions, riboflavin experiences degradation between 50°C and 70°C.[60] These degradation behaviours in addition to increased dehydration of the surfactant head groups with increasing temperatures may have resulted in a dissociation of APIs (such as riboflavin and folic acid) affiliated with these head groups. Such observations would corroborate the yellow-orange precipitate increasingly seen at the bottom of these vials as the temperature increased, as well as the increased clarity of F1A upon heating as these APIs precipitated out. In addition, the size histograms in **Figure C-9, Appendix C** illustrate polydispersity and the presence of two

peaks beginning at 60°C. The greatest degree of clarity and precipitation (phase separation) was seen at 70°C, where the lowest droplet sizes were recorded as this sample likely contained the highest amount of precipitated API.

The transition in colour of F1A from red-brown to brown-black was first observed at 50°C and may be a result of a number of thermal oxidation processes of various APIs in solution. In terms of fat-soluble APIs, it has previously been reported that oxidation (including thermal oxidation) results in the degradation of essential fatty acids and Vitamins A, D, E and K as well as colour changes such as the darkening of some of these fats and oils.[61] Heat favours oxidation of beta-carotene[62] and possible cis-trans isomerization behaviours[63] which may result in red-brown colour changes.[64] Vitamin E and tocopherols have been reported to darken upon oxidation, an effect that may also be seen upon exposure to air and light.[64,65] DHA and EPA in Omega-3 Fatty Acids are also said to degrade in temperatures as low as 50°C.[66] In terms of hydrophilic APIs, the cobalt in cyanocobalamin, originally pink-red, may have undergone oxidation to cobalt (III) oxide which is black in colour.

Finally, with respect to zeta potential, the change from -16 ± 1 mV to between -14 ± 3 mV and -18 ± 6 mV after treatment was not significant and was likely a result of dehydration of the surfactant head group as well as loss of negatively charged API (riboflavin and folic acid) at the droplet interface.

4.5.2.2 Light Exposure Test

The beginnings of API precipitation were immediately seen upon exposure to fluorescent light after just 24 hours and this became more pronounced after 1 week. **Figure 4.12** below depicts droplet sizes and zeta potentials of F1A before and after exposure to fluorescent light for 24 hours and one week. After 24 hours, droplet sizes decreased by almost 30% from 180 ± 40 nm to 130 ± 8 nm while zeta potentials experienced just over 40% reduction from -14 ± 5 mV to -8 ± 4 mV. Exposure to light for 1 week had virtually the same effect as exposure for 24 hours, except in the case of zeta potential where charge was restored after one week. A matched, one-way ANOVA indicated no statistically significant difference in either size $F(1,1)= 6.44$, $p= .239$ or zeta potential $F(1,1)= 1.16$, $p= .476$ between treated and untreated samples. However, practically, it is evident that F1A and its contents are quite sensitive to light degradation. (**Table C-4, Appendix C**).

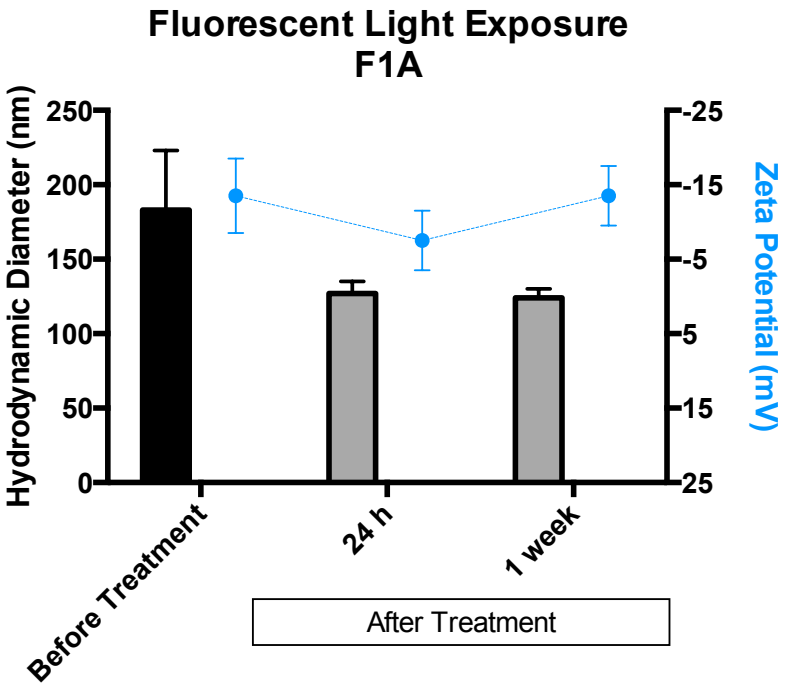

Figure 4.12: Hydrodynamic diameters and zeta potentials of drug-loaded microemulsion formulation F1A before and after exposure to fluorescent light after 24 hours and one week. PDI values were 0.29 (before treatment), 0.33 (24 h treatment) and 0.28 (1 week treatment), respectively. Size histograms and zeta potential curves can be found in **Figure C-10** (**Appendix C**). A matched one-way ANOVA with Dunnett's post-hoc test indicated no statistically significant differences in size (p=.239) or zeta potential (p=.476) before and after treatment.

The phase separation observations along with the droplet size reduction and zeta potential increase after only 24 hours of light exposure were a clear indication of the light sensitivity of the APIs present in F1A. The fact that these results remained virtually unchanged one week later suggested that the greatest degree of degradation occurred at the 24-hour mark and continued degradation was negligible one week later. The size histograms in **Figure C-10, Appendix C** illustrate gradual polydispersity and the development of a bimodal distribution after light exposure for 24 hours and 1 week. Over 50% of the APIs in F1A have been reported to possess light sensitivity as highlighted previously in **Chapter 3**. In terms of lipophilic active ingredients, exposure of beta-carotene to fluorescent light was reported to result in 50% loss at 24 hours, although this rate was found to decrease in the presence of α-tocopherol.[67] Light was also reported to cause cis-trans isomerization in beta-carotene.[63]

Although degradation in visible light was not observed, exposure to UV light was previously reported to degrade the quinone moiety in Vitamin K_1.[68] In terms of hydrophilic APIs, Vitamin B_2, riboflavin, may be degraded into various photoproducts upon light exposure including lumichrome, lumiflavin, formylmethylflavin and carboxymethylflavin.[60] In a recent study, upon one hour exposure to combined visible and UV light, B_3, B_6, B_9 and B_{12} were also degraded by over 50% but the degradation products could not be identified.[69] Folic acid (Vitamin B_9) was recently reported to degrade in the presence of light to 6-formylpterin and *para*-aminobenzoic acid (PABA)- glutamic acid.[70] In cyanocobalamin, Vitamin B_{12}, the formation of hydroxocobalamin was recently reported as a light degradation product.[70] In addition, complete degradation of cyanocobalamin was seen in formulations also containing vitamins B_1 and B_6 after exposure to normal laboratory light for 5 days.[71] This was reportedly due to possible degradation products of B_1 and B_6 acting on B_{12}.[71] Unlike in the case of the heating cycle, no apparent change in colour of F1A was observed after 1 week of light exposure.

4.5.2.3 pH Test

Figure 4.13 depicts the change in pH of F1A over the course of 1 month. The pH remained stable with a slight downward trend beginning at the 7-day mark. These small decreases continued until the 28-day mark. A decrease in pH of approximately 1 unit (0.9 ± 0.0) over the period of one month, from 8.8 ± 0.0 to 7.8 ± 0.0 was recorded at room temperature. The consistency in pH over the course of this 1-month time frame was highly unexpected given the multi-component nature of F1A, and the absence of any compounds with buffering capacity in F1A. A change of -1 unit was not concerning given that the system appeared to approach physiological pH. The low water composition in F1A, however, suggests that any further pH changes may be minimal in nature, given that this is the phase in which many of the charged components reside.

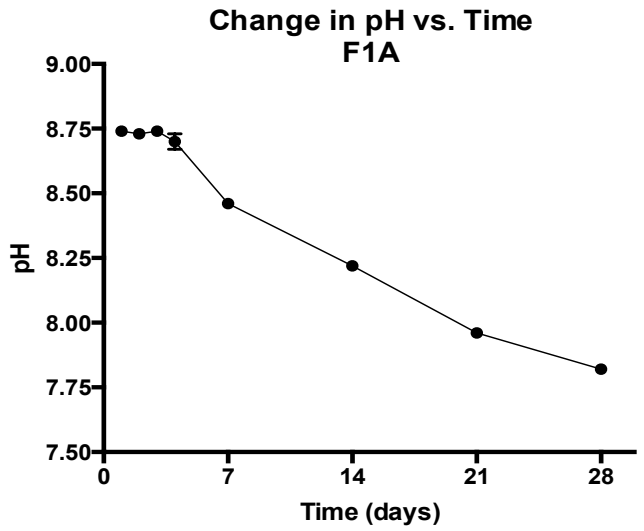

Figure 4.13: pH changes in drug-loaded F1A at room temperature over the course of 4 weeks on a pH scale of 0-14 (left).

4.5.2.4 Conductivity Test

Figure 4.14 presents the change in conductivity of F1A from immediately after formulation to 1 week after formulation. Conductivity remained low at just under 5 μS/cm from the time of manufacture to one week later with values ranging between 4.78 uS/cm and 3.32 uS/cm. Conductivity values were within expected ranges for bicontinuous microemulsions where both oil and water serve as the continuous phases as noted earlier. The consistency in conductivity was surprising given the presence of many charged species in F1. However, the

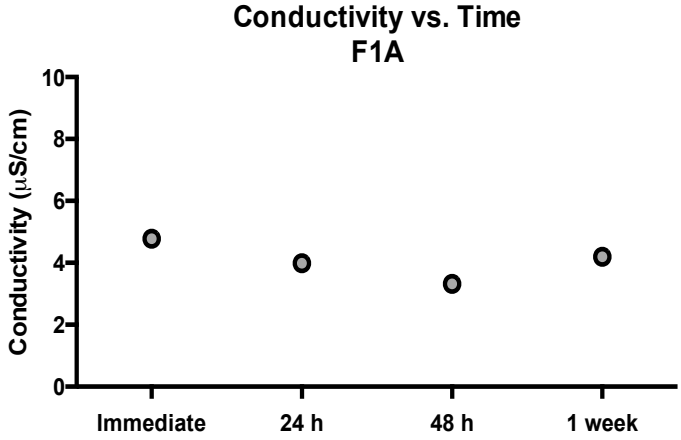

Figure 4.14: Conductivity changes in drug-loaded F1A over the course of 1 week. Values remained relatively constant and under 5 us/cm.

low conductivity was surprising given the presence of many charged species in F1. However, the low variation in conductivity values suggest that despite any observations in phase behaviour, there is no shift in microemulsion type from bicontinuous Type IV to Type I O/W or Type II W/O over the period of one week. It follows that if the conductivity of F1A was consistent across the period of one week, zeta potentials should also remain consistent over this time period. This was corroborated by a F1A control kept in the dark at room temperature for one week which exhibited a slight decrease in size (30 nm) from the original microemulsion, but no change in zeta potential. (**Figure C-11, Appendix C**)

4.5.2.5 Centrifugation Stress Test

Figure 4.15 depicts results before (left) and after centrifugation at 5000 RPM for 30 minutes (middle) and 10000 RPM for 30 minutes (right). An equal volume of water was used as a balance. There was notable phase separation after centrifugation at 5000 and 10000 RPM. This phase separation can be quantified in terms of volume [72] and this phase volume may also be equated to the height of liquid in the vial or centrifuge tube. The emulsion stability may be calculated as follows[10,15,73] :

$$Emulsion\ Stability\ (ES) = \frac{Volume\ of\ Intact\ Emulsion\ Layer}{Total\ Volume\ of\ Emulsion\ Layer} \qquad \textbf{(Eq. 4.1)}$$

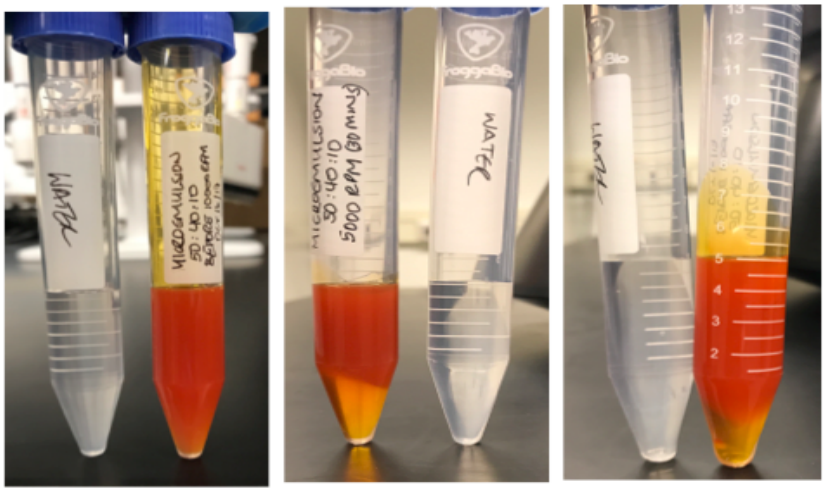

Figure 4.15: Effects of centrifugation on drug-loaded F1A before (A), after centrifugation at 5000 RPM for 30 minutes (B) and after centrifugation at 10000 RPM for 20 minutes (C).

Based on the results obtained for these centrifugation studies, and on **Eq. 4.1**, the emulsion stability percentages were as follows:

5000 RPM at 30 minutes

$$Emulsion\ Stability\ \%\ (ES) = \frac{3.45\ mL}{5\ mL} * 100$$
$$= \mathbf{69\%}$$

10000 RPM at 30 minutes

$$Emulsion\ Stability\ \%\ (ES) = \frac{4.25\ mL}{5\ mL} * 100$$
$$= \mathbf{85\%}$$

Despite the presence of eleven APIs, subjection to high centrifugal force demonstrated 69% stability at 5000 RPM for 30 minutes and 85% stability at 10000 RPM for 30 minutes. These results were in contrast to expected results where low stabilities <10% were anticipated given this multi-component system and the extensive pH adjustment required for API incorporation.

4.6 Conclusion

A 50:40:10 microemulsion comprised of 50% w/w surfactant, 40% w/w oil and 10% w/w water was selected as the optimal formulation given IIG limits for surfactant content as well as water content considerations. The surfactant phase was comprised of 3:1 Polysorbate 80:Cremophor RH 40, the oil phase was comprised of Miglyol 812 and 5 lipophilic APIs (Vitamins A, D, E, K and Omega-3-fatty acids) and the water phase contained 6 hydrophilic APIs (Vitamins B_1, B_2, B_3, B_6, B_9 and B_{12}). The droplet size of this formulation, F1A, was approximately 164 nm after 100x aqueous dilution (larger than hypothesized) and the zeta potential was -14 mV, which fell short of the widely accepted -30 mV value purported to impart stability, as hypothesized. Conductivity values of just under -5 µS/cm for F1A and 57 µS/cm after 100x dilution of F1A with water, were in line with the low conductivity values characteristic of bicontinuous microemulsions and the higher conductivity values as a result of the presence of water, respectively. Rheology measurements indicated a viscosity of F1A of approximately 447 cP but closer to 1 cP upon dilution with 100 and 1000x with water. Newtonian behaviour characteristic of bicontinuous microemulsions (at low shear rates) and O/W microemulsions

was also observed, as hypothesized. TEM images illustrated bicontinuous, interconnected oil and water channels and small droplets with sizes closer to 25-150 nm in diameter, given removal of the effect of surface-bound APIs and PEO groups as determined by DLS. DSC results exhibited a lack of exothermic peaks typically characteristic of system degradation. Rather, the DSC graph of F1A was akin to that of the surfactant phase, 3:1 Polysorbate 80:Cremophor RH 40, which is unsurprising given the high surfactant content in this formulation but surprising given the number of active ingredients in the formulation which we hypothesized, would have resulted in numerous outlier peaks.

With respect to the stability of F1A, temperature appeared to be the factor with the greatest impact on microemulsion instability. Results indicated that the largest decreases in droplet size (35-50%, lower than hypothesized) and increases in zeta potential (to a less negative value) occurred during subjection to three freeze-thaw cycles and subsequent heating at increasing temperatures. The second most important factor impacting microemulsion stability was light exposure, with droplet size reductions of 30% experienced, lower than hypothesized. In terms of pH, a decrease of 1 unit was seen over the period of 1 month as was hypothesized. Conductivity also remained constant over the period of 1 week as did zeta potential which was contrary to our hypothesis that there would be a fluctuation in charge due to the presence of charged APIs. Centrifugation studies indicated 69% stability after 5000 RPM for 30 minutes and 85% stability after 10000 RPM at 30 minutes. Given these results, it can be concluded that F1A, as a Type IV, bicontinuous microemulsion containing eleven (11) successfully incorporated APIs of varying hydro- and lipophilicity, is best maintained in cool temperatures away from light sources. It may also be beneficial to consider inclusion of a buffer and stabilizer to assist with pH changes and centrifugation phase separation, respectively.

Chapter 5: Identification of Emulsifying Agent Properties Necessary for Microemulsion Formation and Dissolution/ Stability Testing

5.1 Introduction

Emulsifying agents and surfactants play an important role in microemulsion formation. Throughout this work, it has been shown that the formation of a microemulsion system suitable for multi-drug delivery relies on successful surfactant selection, along with a multitude of factors. These factors include phase behaviour as determined by ternary phase diagram mapping, critical micelle concentration, hydrophilic-lipophilic balance (HLB), characteristic curvature (CC), hydrophilic-lipophilic deviation (HLD) of the microemulsion system and effective alkane carbon number (EACN) of the oil (**Chapters 2** and **3**). Following the formulation of F1A, a Type IV microemulsion suitable for the incorporation of both hydro- and lipophilic active ingredients (**Chapter 4**), one major goal of this thesis work was to identify additional surfactants, or alternatives to Polysorbate 80 and Cremophor RH 40, also suitable for multi-drug microemulsion formation. To achieve this, formulations containing surfactants of varying head and tail groups will be prepared and their emulsification potential, as well as their ability to act synergistically in mixed surfactant systems, will be evaluated via droplet size and tensiometry measurements, respectively. This will allow for the identification of emulsifying agent properties suitable for multi-drug, microemulsion formation.

Upon formulation of these additional microemulsion systems, the final goal of this thesis work- to determine the pharmaceutical relevance of each formulation- will be pursued. One of the greatest drivers for the use of microemulsion systems in drug delivery is their potential to improve bioavailability due to their small droplet sizes and large surface area to volumes, as reported previously.[1-4] Dissolution testing determines whether a formulation is readily dissolvable in physiologically relevant media, such that inferences about bioavailability may be made. Disintegration of the pharmaceutical dosage form is also important, as drug material cannot be physiologically absorbed otherwise. Finally, stability studies provide insight into formulation integrity as well as pharmaceutically relevant storage conditions.

Dissolution, disintegration and stability have been described previously in **Chapter 1: Section 1.7.3, Chapter 1: Section 1.7.4** and **Chapter 4**, respectively.

5.1.1 Emulsifying Agents

5.1.1.1 Surfactant Head Groups

In contrast to surfactant tail groups, which typically consist of alkyl chains and possible variations such as branching, an almost infinite variety of surfactant head groups may be utilized in emulsion systems. Anionic surfactants may be comprised of sulphate, sulphonate, carboxylic or phosphate head groups that impart a negative charge, cationic surfactants may be comprised of quaternary ammonium or amine salts that impart a positive charge and amphoteric surfactants may be comprised of betaines or phosphatides that impart both negative and positive charges.[5] Non-ionic surfactants on the other hand, are arguably less variable and mainly consist of ethoxylated groups, polyglycerols/polyols or block co-polymers.[5] Given the low variability of the non-ionic surfactant class, polyethyleneoxide (PEO) groups are less challenging to work with as a simple increase or decrease in the number of ethylene oxide (EO) units results in an increase or decrease in water solubility, respectively. Thus, one can attempt to control the emulsification potential of a non-ionic surfactant for a particular application through manipulation of the number of ethylene oxide units.

In this work, non-ionic surfactants analogous to Polysorbate/Tween 80 (a sorbitan fatty acid ester) with the same hydrocarbon chain length, but different number of ethylene oxide units, were selected for further analysis of emulsification potential. Sorbitan fatty acid ester surfactants with 0, 5, 10, 15, 20 and 40 ethylene oxide units were initially selected to evaluate the effect of PEO number on microemulsion droplet size and formation. However, only three such surfactants were commercially available from reputable manufacturing sources- Span 80, Tween 81 and Tween 80 (Polysorbate 80) with a degree of polyethoxylation of 0, 5 and 20, respectively. Given that Polysorbate 80 was already present in the current formulation (F1A), Span 80 and Tween 81 were selected for further analysis. (**Table 5.1**)

Sorbitan Ester-based Surfactants (Tween Class)

Table 5.1: Structural properties of sorbitan esters, Span 80, Polysorbate 81 and Polysorbate 80, tested in this work as a substitute for Polysorbate 80 in 3:1 Polysorbate 80:Cremophor surfactant mix. Hydrocarbon chain length remained constant at 18 carbons while EO content was varied.

Surfactant	EO Content (w+x+y+z)	Molecular Weight (g/mol)	HLB
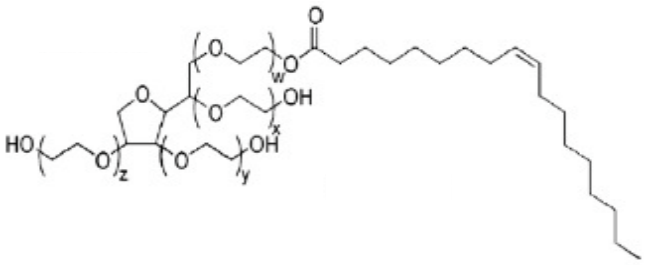			
Span 80 (Sorbitan monooleate) [10]	0	428.62	4.3[11]
Polysorbate 81 (EO (5) sorbitan monooleate) [10]	5	648.85	10[12]
Polysorbate 80 (EO (20) sorbitan monooleate) [10]	20	1309.6	15[11]

Ethers represent another important class of non-ionic surfactants, similar in nature to esters as they are both considered weak hydrophiles.[5] The Brij class of surfactants consists of polyethoxylated alkyl ethers with low toxicity.[6] Given the similarities between the Tween and Brij surfactant classes, Brij surfactants with differing PEO content but the same C18 hydrocarbon tail as that of Polysorbate 80, were selected for further evaluation**. (Table 5.2)** The higher the PEO number, the more hydrophilic the surfactant and the more likely the formation of an O/W emulsion.[7] Thus, the amount of aliphatic hydrocarbon that can be solubilized generally decreases with an increase in PEO content.[8] An increase in PEO chain also results in a decrease in both efficiency and effectiveness of adsorption.[9] These effects may be reflected in the emulsification potential of both Tween and Brij surfactant classes.

Ether-based Surfactants (Brij Class)

Table 5.2: Structural properties of Brij ether-based surfactants, Brij 93, Brij 97, Brij 98 and Brij S 100 tested in this work as a substitute for Polysorbate 80 in 3:1 Polysorbate 80:Cremophor surfactant mix. Hydrocarbon chain length remained constant at 18 carbons while EO content was varied.

Surfactant	EO Content (n)	Molecular Weight (g/mol)	HLB
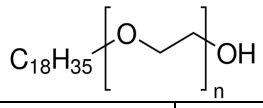			
Brij 93 (EO (2) Oleyl ether)[13]	2	356.6	5[14]
Brij O10/Brij 97 (EO (10) Oleyl ether)[13]	10	709.0	12[15]
Brij O20/Brij 98 (EO (20) Oleyl ether)[13]	20	1149.5	15[16]
Brij S100 (EO (100) Stearyl ether)[13]	100	4675.0	19[17]

5.1.1.2 Surfactant Tail Groups

Surfactant tails are typically comprised of alkyl chains 8-22 carbons in length, as well as their variants.[5] These variants may be unsaturated carbons, fluorocarbons, benzenes, silicones, polyoxypropylenes and in less common instances, hydroxyl groups as in the case of surfactants derived from castor oil.[5] The complexities of alkyl branching and saturation, render surfactant classification via head group a more practical approach. In the context of emulsions, hydrophobic tail groups play an important role. Longer alkyl tails reduce critical micelle concentration (CMC) while branching increases CMC.[18] This impact on CMC affects the interfacial tension between oil and water and thus, the resulting droplet size and emulsification potential. Correct selection of the hydrophobic group may also even dictate the type of surfactant structure possible in emulsion systems as branched alkyl systems lead to higher order structures such as bicontinuous and lamellar structures being formed.[19] Thus, for the emulsification purposes necessary in this work, consideration of surfactant hydrophobe is just as important as consideration of PEO content. In order to minimize complexity, variations in alkyl chain length were explored rather than branching or the introduction of reactive functional groups such as fluorine and silicones. Given that the diameter of spherical structures

is roughly twice the length of the hydrocarbon chain[19], it can be inferred that the longer the hydrocarbon chain, the larger the diameter and thus, the larger the droplet size. Polysorbates 20, 40 and 60 with 12, 16 and 18 carbons were selected for further analysis. (**Table 5.3**)

Table 5.3: Structural properties of Polysorbate 20, Polysorbate 40, Polysorbate 60 and Polysorbate 80 tested in this work as a substitute for Polysorbate 80 in 3:1 Polysorbate 80:Cremophor surfactant mix. EO content remained constant at 20 groups while hydrocarbon chain length was varied.

Surfactant	Carbon # (Chain)	Structure	Mol. Weight (g/mol)	HLB
Polysorbate 20 (EO (20) Sorbitan monolaurate)[10]	12	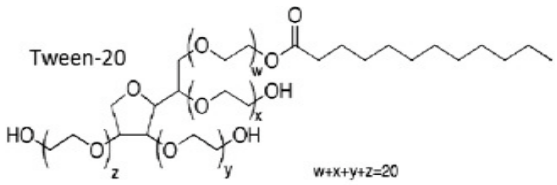	1227.5	16.7[11]
Polysorbate 40 (EO (20) Sorbitan monopalmitate)[10]	16	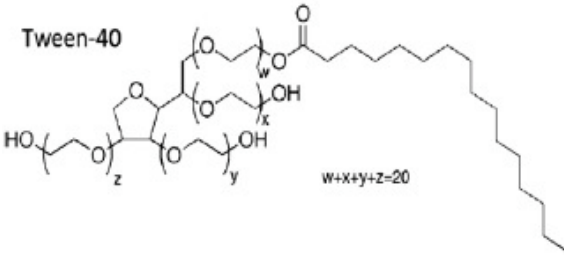	1283.6	15.6[11]
Polysorbate 60 (EO (20) Sorbitan monostearate)[10]	18	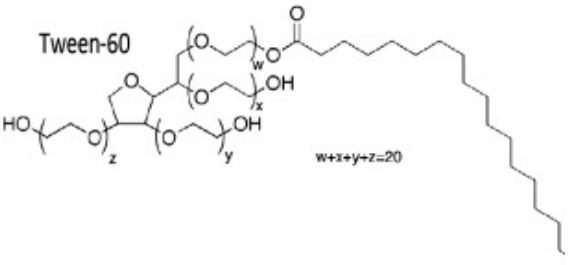	1311.6	14.9[11]
Polysorbate 80 (EO (20) Sorbitan monooleate)[10]	18	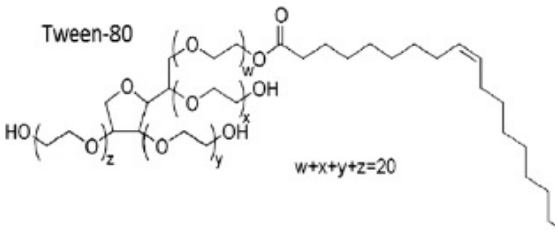	1309.6	15[11]

5.1.1.3 Other Substitutions

In addition to evaluating surfactants similar in nature to Polysorbate 80, a surfactant similar in nature to Cremophor RH 40 was also selected for further analysis. As outlined in **Chapter 2**, Cremophor RH 40 is a polyethoxylated, hydrogenated castor oil amphiphile comprised of 40 PEO groups and three C18 hydrocarbon chains. Cremophor RH 60 is analogous to Cremophor RH 40 but contains 60 PEO groups instead of 40. Thus, this surfactant was evaluated as a substitute for Cremophor RH 40 in 3:1 Polysorbate 80:Cremophor RH 40 surfactant mixtures. The increase in PEO content of 20 is expected to have the same impact on oil solubilization as outlined earlier. (**Table 5.4**)

Table 5.4: Structural properties of Cremophor RH 60 surfactant as a substitute for Cremophor RH 40. The hydrocarbon chain length is the same as that of Cremophor RH 40 and Polysorbate 80 but the EO number is 60.

Surfactant	EO # (x+y+z)	Carbon # (Chain)	Structure	Mol.Weight (g/mol)	HLB
PEG-60 Hydrogenated Castor Oil[20]	60	18	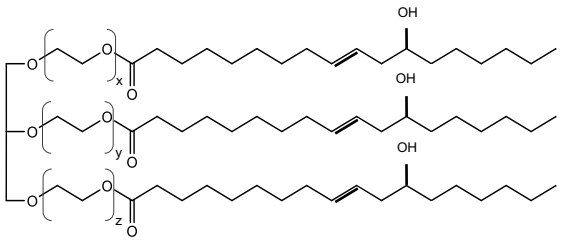 x+y+z= 60	3578[21]	16

An additional single surfactant was screened in order to determine whether it could replace 3:1 Polysorbate 80:Cremophor RH 40 altogether. Tween 85 is a polyethoxylated sorbitan trioleate amphiphile comprised of 20 EO units and a triple oleate (C18) surfactant chain with a double bond at the C9-C10 position, similar to that of Polysorbate 80 and Cremophor RH 40. (**Table 5.5**) Tween 85 possesses a molecular weight of approximately 1839 g/mol which is higher than that of the other surfactants tested in this work, except for Brij S100 and the Cremophors. According to Myers (2006), higher molecular weight surfactants increase oil capacity in microemulsion systems.[22]

Table 5.5: Structural properties of Polysorbate 85 surfactant information tested in this work as a substitute for 3:1 Polysorbate 80: Cremophor RH 40. The hydrocarbon chain length is the same as that of Cremophor RH 40 and Polysorbate 80 and the PEO number is the same as that of Polysorbate 80.

Surfactant	EO Content (n)	Carbon # (Chain)	Structure	Mol.Weight (g/mol)	HLB
Polysorbate 85 (EO (20) Sorbitan trioleate[23]	20	18	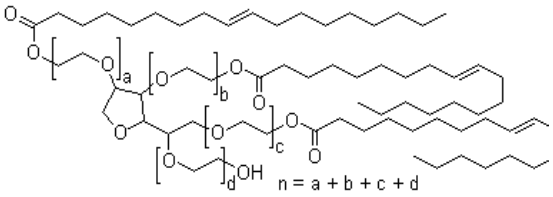	1838.5	11[24]

5.1.2 Pharmaceutically Relevant Tests

5.1.2.1 Dissolution

Dissolution testing of multi-drug formulations is complex. In multivitamin formulations, to simplify this process, the United States Pharmacopeia (USP) requires quantification of an 'index' vitamin instead.[25] An 'index' vitamin is typically used as a single indicator of dissolution for all other compounds of its kind in a formulation. As required by the USP, this vitamin must be riboflavin.[25] Riboflavin has poor water solubility and as such, its dissolution is likely to be much lower than that of other hydrophilic vitamins. Thus, if riboflavin is dissolved to an appreciable degree, it is an indicator that this is also likely for the other hydrophilic vitamins present in the formulation.

Given that folic acid is essential for prenatal development[25], the USP also requires quantification of this vitamin. With respect to fat-soluble vitamins, beta-carotene presents the greatest challenge due to its high lipophilicity and sensitivity to light and oxygen. Therefore, although fat-soluble dissolution is not required by the USP, the dissolution of beta-carotene will be tested in this Chapter as an 'index' fat-soluble vitamin. Dissolution testing is typically performed with filled formulation dosage forms such as tablets or capsules. However, in the absence of a filled dosage form as in this case, dissolution testing solely with the fill

formulation may provide insight into the dissolution potential of the microemulsion formulation.

5.1.2.2. Disintegration

According to the USP, a drug product undergoes successful disintegration when after 30 minutes, 89% of the dosage form shows no residue (with a palpably firm core) on the dissolution apparatus mesh.[25] Disintegration is not an indicator of drug dissolution rate.[26] However, it is still an important parameter given that rupture of the dosage form is the first step in drug dissolution and absorption. In addition, disintegration provides insight into the quality of the manufacturing process for a pharmaceutical dosage form.[26] Disintegration testing may be performed on a number of dosage forms including tablets and capsules. In this work, the disintegration of filled hard-gelatin capsules will be tested. This is in contrast to dissolution testing where filled dosage forms were not used.

5.1.2.3 Stability

The importance of stability testing on microemulsion pharmaceutical formulations was previously described in **Chapter 4**. Upon microemulsion formation with the newly identified emulsifying agents, stability will be tested on the basis of temperature, light, pH, conductivity and accelerated gravitational separation as in **Chapter 4**. The results of this study, along with dissolution testing, will provide insight into whether careful surfactant selection leads to the identification of favourable microemulsion formulations analogous to F1A or F1.

5.2 Study Objectives

At this stage, Polysorbate 80 and Cremophor RH 40 have been identified as a successful surfactant pair for microemulsion formation (**Chapter 2**), multiple hydro- and lipophilic active ingredients have been incorporated (**Chapter 3**) and F1A, a successful microemulsion formulation, was identified, characterized and tested for stability (**Chapter 4**). The objectives of this chapter, **Chapter 5**, are:

(i) To identify additional emulsifying agents suitable for microemulsion formulation, based on droplet size and zeta potential measurements

(ii) To determine emulsifying agent properties implicated in microemulsion formulation based on results from (i)

(iii) To perform dissolution, disintegration and stability testing of all microemulsion formulations to deduce pharmaceutical relevance and practical application

5.3 Hypothesis

If surfactant head groups are increased from 0-20 ethylene oxide (EO) groups, and hydrocarbon chain lengths are decreased from 18 to 12 carbons, then a general decrease in droplet size of the resulting microemulsions is expected, as the amount of aliphatic hydrocarbon that can be solubilized decreases.[18]

It was hypothesized that all selected microemulsion formulations would achieve >75% dissolution of riboflavin in water within 60 minutes. Dissolution of <75% folic acid in water within 60 minutes was expected for all microemulsions given the low water solubility of folic acid in comparison to riboflavin.

5.4 Materials and Methods

5.4.1 Materials

Polysorbate 80, Cremophor RH 40, Miglyol 812 and all APIs were generously gifted from Accucaps Industries Limited/Catalent Pharma Solutions (Ontario, Canada) as stated earlier. The BRIJ class of surfactants, BRIJ 93 (BRIJ O2-MBAL-LQ- (AP)-098), BRIJ 97 (BRIJ O10-LQ- (AP)), BRIJ 98 (BRIJ O20-SO- (AP)) and BRIJ S100 (BRIJ S100-MBAL-SO- (AP)), along with Polysorbate 81, were generously gifted from Croda Canada Limited (Ontario, Canada). Polysorbate 20, 40, 60 and 85 were obtained from VWR International (Ontario, Canada) and supplied by TCI America. Span 80 and Triton X-100 were obtained from Sigma-Aldrich (Ontario, Canada) and Cremophor RH 60 was generously gifted from BASF. (Ontario, Canada). Potassium dihydrogen monophosphate and dipotassium phosphate were purchased from EMD Millipore (Ontario, Canada) and 99% Citric acid and Tris base were purchased from Fisher Scientific (Ontario, Canada). 18 mm oblong, opaque hard gelatin capsules were

generously gifted from the Flex lab at the University of Waterloo School of Pharmacy for disintegration testing.

5.4.2 Methods

5.4.2.1 Surfactant Screening

Surfactants were screened on the basis of surfactant head group (PEO content), surfactant tail group (length of the hydrocarbon chain) and hydrophilic-lipophilic balance (HLB). Specifically, the head group composition via EO content and the tail group composition via hydrocarbon chain length, were either increased or decreased as systematically as possible. In the majority of cases, Polysorbate 80 in the 3:1 Polysorbate 80:Cremophor RH 40 surfactant mixture was replaced with each Span, Tween or Brij surfactant followed by subsequent formulation with Cremophor RH 40, Miglyol 812, water and all hydro- and lipophilic active ingredients in a surfactant:oil:water (S:O:W) ratio analogous to F1A- 50:40:10. In the case of placebo samples, no active ingredients were incorporated and the formulation simply consisted of surfactant mixture, Miglyol 812 and water in a S:O:W ratio of 50:40:10. Droplet sizes and zeta potentials were determined using Dynamic Light Scattering (DLS) in the same manner as outlined in **Chapter 4**. Surfactants demonstrating favourable droplet sizes were then formulated with Cremophor RH 60, Miglyol 812, water and all active ingredients and again, evaluated on the basis of droplet size and zeta potential. Four approaches to variations in surfactant head and tail groups were taken.

5.4.2.1.1 Consideration of Surfactant Head Group: Variation in EO Content

The effect of surfactant head group was evaluated through a gradual increase in EO content from 0-20, 20 being the EO content in Polysorbate 80. The idea was to increase EO content at a rate of 0, 5, 10 and 20 while keeping the number of carbons in the hydrocarbon chain constant. For the sorbitan ester surfactants, however, only those of EO content 0, 5 and 20 were commercially available from reputable manufacturing sources. For the alcohol ether surfactants, only those of EO 2, 10, 20 and 100 were available. Thus, 5 g 3:1 *x*: Cremophor RH 40 surfactant (where *x* is Span 80, Tween 81, Tween 80, Brij 93, Brij 97, Brij 98 or Brij S100), 4 g Miglyol 812 containing all oil-soluble actives and 1 g water containing all water-soluble

actives were weighed into a glass scintillation vial using a Sartorius Secura 225D Analytical Balance. The vial was inverted manually for approximately 20 seconds until the mixture appeared homogenous. Each microemulsion mixture was placed in a dark cupboard and left to settle for at least 72 hours before dilution with water for droplet size and zeta potential measurements. Droplet size and zeta potential measurements were performed using a Malvern Zetasizer Nano ZS in the same manner as that described in **Chapter 4.** Briefly, for droplet size, 500 μL sample was pipetted into a Fisherbrand 1.5 mL polystyrene cuvette and inserted into the cuvette holder. Samples were left to equilibrate for 300 seconds at 25ºC before readings were taken at a scattering angle of 173º. Measurements were performed in triplicate. Graphs were plotted in Prism 6 software. For zeta potential, 700 μL sample was introduced via syringe into a primed Malvern folded capillary zeta cell and inserted into the cuvette holder. Samples were left to equilibrate for 300 seconds at 25ºC before readings were taken. Measurements were performed in triplicate. Graphs were plotted in Prism 6 software.

5.4.2.1.2 Consideration of Surfactant Tail Group: Variation in Hydrocarbon Chain Length

The effect of hydrocarbon chain length was evaluated through a gradual increase in alkyl chain carbon number from 12-18, 18 being the number of carbons in the alkyl chain of Polysorbate 80. Only Tween surfactants of carbon number 12, 16 and 18, corresponding to Tween 20, Tween 40, Tween 60/80, respectively, were commercially available from reputable manufacturing sources. 5 g 3:1 y: Cremophor RH 40 surfactant (where y is Tween 20, Tween 40, Tween 60 or Tween 80) was combined with the oil and water phases as described above in the previous section, before dilution for size and zeta potential measurements.

5.4.2.1.3 Consideration of Substitution of Cremophor RH 40

Substitution of Cremophor RH 40 was evaluated through consideration of Cremophor RH 60, which is similar in nature to Cremophor RH 40 but with 20 additional EO units. Promising surfactants (derived from **5.4.2.1.1** and **5.4.2.1.2** above) were combined with Cremophor RH 60 in a 3:1 ratio before incorporation of the oil and water phases as described earlier. Size and zeta potential measurements were also carried out as described previously.

5.4.2.1.4 Consideration of Substitution of 3:1 Polysorbate 80:Cremophor RH 40 for a Single Surfactant

Substitution of 3:1 Polysorbate 80:Cremophor RH 40 for a single surfactant was evaluated through consideration of Tween 85 which consists of the same structure as that of Tween 80 but with a triple oleate chain, similar to that of Cremophor RH 40. 5 g of Tween 85, 4 g Miglyol 812 containing all oil-soluble actives and 1 g water containing all water-soluble actives were combined as described previously before dilution for size and zeta potential measurements.

5.4.2.1.5 Tensiometry

Surface tension studies were conducted as outlined in **Chapter 2**.

5.4.2.2 Pharmaceutically Relevant Tests

5.4.2.2.1 Dissolution

Each formulation (1 g) was weighed into black, polytetrafluoroethylene (PTFE) caps using a Sartorius Secura 225D Analytical Balance. Dissolution was conducted using a Hanson Vision 6 Classic Dissolution Apparatus containing six 1 L precision vessels and USP Apparatus II (paddle method). Each vessel was set to heat to 37 ± 0.5ºC before 500 mL dissolution media was introduced. Dissolution media were chosen in accordance with USP guidelines for multivitamin dietary supplements[25] and consisted of water, 0.01 M citric acid (pH 6) and 50 mM phosphate buffer (pH 7.4) for the water-soluble APIs, and 4% Triton X-100 in 50 mM phosphate buffer and 2% Polysorbate 80 in 100 mM tris buffer (pH 8) for the oil-soluble APIs. Once temperature was confirmed with a thermometer, each formulation was introduced to the dissolution vessel, the paddle lowered and the apparatus set to stir at 100 RPM. The timer was set and samples were extracted at 15, 30, 60, 90 and 120 minutes. Samples (3 mL) were extracted using a 5 mL syringe attached to a 0.45 μM GE Whatman or Sartorius filter. In the case of citric acid and phosphate buffer media, studies were conducted in triplicate using newly prepared formulations each time

Samples were analyzed by Accucaps Industries Ltd./Catalent Pharma Solutions (Windsor, Ontario) using a Waters Brand High Performance Liquid Chromatography (HPLC) instrument with Waters Brand C18, 250 x 4.6 mm column, 5 uM particle size. Additional details with respect to run time, flow rate, mobile phases and gradients are outlined in **Table**

D-5, **Appendix D**. The amount of dissolved folic acid and riboflavin was determined in mg/mL and reported as a percentage. The amount of beta-carotene was also determined in this manner, though not required for multivitamin formulations.[25] All graphs were generated with Graphpad Prism 6 software.

5.4.2.2.2 Disintegration

Each formulation (0.7 g) was weighed into six (6) 18 mm oblong red, opaque hard gelatin capsules using a Mettler Toledo MS205DU Analytical Balance. Disintegration testing was conducted with a PharmaTest DIST-3 Standard 3 Position Disintegration Tester comprised of three test baskets connected to a central stroke arm fixed at a height of 55 mm and set at 30 strokes per minute. 750 mL of media (water, 0.1 N hydrochloric acid and 0.05 M acetate buffer, pH 4.5), the latter being the recommended USP medium for hard shell capsules[25] was introduced into each vessel and the temperature set to 37°C. After confirming the temperature with a thermometer, two filled hard gelatin capsules of each formulation were introduced into separate baskets and the apparatus switched on and timer set. The time taken for disintegration of all capsules in each medium was recorded. According to the USP, this type of multivitamin drug product passes disintegration when no residue with a palpably firm core is observed on the apparatus mesh after 30 minutes.[25] All graphs were generated with Graphpad Prism 6 software.

5.4.2.2.3 Stability

Stability was determined in the same manner as outlined in **Chapter 4** on the basis of temperature, light, pH, conductivity and accelerated gravitational separation via centrifugation. All graphs were generated with Graphpad Prism 6 software.

5.4.2.3 Statistical Analysis

An independent, two-tailed, two-sample Student's T-test was performed on the size and zeta potential measurements of placebo and drug-loaded microemulsions in order to determine

whether any statistically significant differences existed between the two. All test assumptions included a normal distribution with equal variance at 95% confidence intervals (p-value ≤ .05). Data were analyzed using Graphpad Prism 6 software.

An ordinary, one-way ANOVA was also performed on size, zeta potential and polydispersity index measurements of various microemulsions as well as on all dissolution data. Test assumptions included a normal distribution with equal variance at 95% confidence intervals (p-value ≤ .05). In the case of equal variance, a Tukey multiple comparisons test was conducted while in the case of unequal variance, the Welch's statistic was used followed by the Games-Howell multiple comparisons test. All data were analyzed using IBM Statistical Product and Service Solutions (SPSS) software.

5.5 Results and Discussion

5.5.1 Surfactant Screening

5.5.1.1. Consideration of Surfactant Head Group: Variation in PEO Content

Sorbitan Ester-based Surfactants (Tween Class)

Figure 5.1 depicts emulsions formulated in a S:O:W ratio of 50:40:10 with the surfactant phase consisting of 3:1 Span 80: Cremophor RH 40, 3:1 Polysorbate 81: Cremophor RH 40 or 3:1 Polysorbate 80:Cremophor RH 40, the oil phase consisting of Miglyol 812 + five oil-soluble APIs and the water phase consisting of six water-soluble APIs. The microemulsion containing 3:1 Polysorbate 80:Cremophor RH 40 is currently the lead formulation, F1A. Formulations comprised of 3:1 Span 80:Cremophor RH 40 exhibited coarse emulsion behaviour, evidenced by highly turbid placebo (white) and active ingredient (orange) samples. In contrast, formulations comprised of Polysorbates 81 and 80 exhibited ideal microemulsion behaviour as indicated by their clarity and apparent homogeneity. Each sample was diluted 100x with water prior to droplet size and zeta potential measurement (**Figure 5.2**). Size histograms and zeta potential curves may be found in **Figure D-1, Appendix D**.

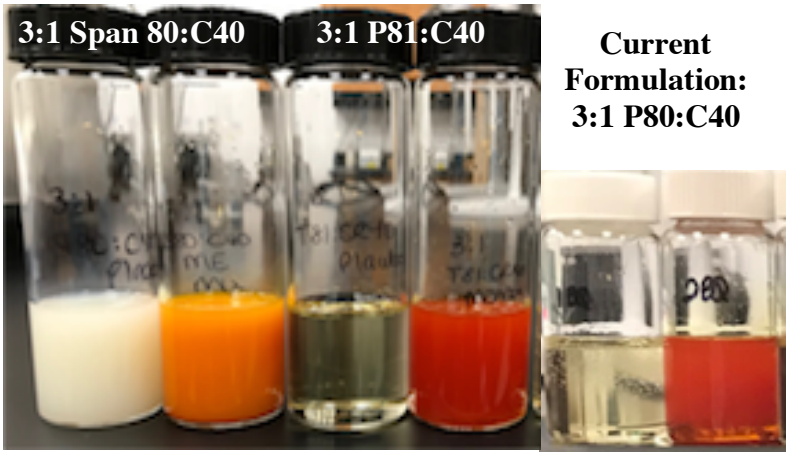

Figure 5.1: Formulations (S:O:W=50:40:10) comprised of 3:1 Span 80/Polysorbate 81/Polysorbate 80: Cremophor RH 40 surfactant, Miglyol 812 oil and water. Drug-loaded samples contain five lipophilic and six hydrophilic APIs, and are red/orange in colour versus placebo samples (clear/white). C40= Cremophor RH 40, P80/81= Polysorbate 80/81

Formulations containing Span 80 were 792 ± 21 nm in size, with an extreme polydispersity index (PDI) of 1. Three separate size populations of over 2000 nm, 500 nm and 200 nm were observed in active ingredient samples. In contrast, formulations containing Polysorbate 81 and 80 were monodisperse with sizes of 80 ± 0.2 nm and 140 ± 1.2 nm, respectively after inclusion of all APIs. Despite the high polydispersity index and large droplet sizes obtained in Span 80 emulsion samples, zeta potential values were -47 ± 0.9 mV after active ingredient addition. Thus, API incorporation appeared to result in a potentially stabilizing effect of the droplets from a strictly electrostatic consideration. Unlike Span 80, the zeta potentials of formulations containing both Polysorbate 81 and Polysorbate 80 did not change by an appreciable degree after API inclusion and were -16 ± 0.6 mV and -14.5 ± 1.1 mV, respectively.

The non-ethoxylated sorbitan head group of Span 80 results in a low degree of hydrophilicity in comparison to that of Polysorbate 81 and 80, as reflected in a HLB value of 4.3 versus 10 and 15 for Polysorbates 81 and 80, respectively.[11,12] The low HLB of Span 80, even when combined with Cremophor RH 40 in a 3:1 ratio, results in a mismatch with the HLB of the oil used in this formulation, Miglyol 812, which possesses an HLB of 15.36.[27]

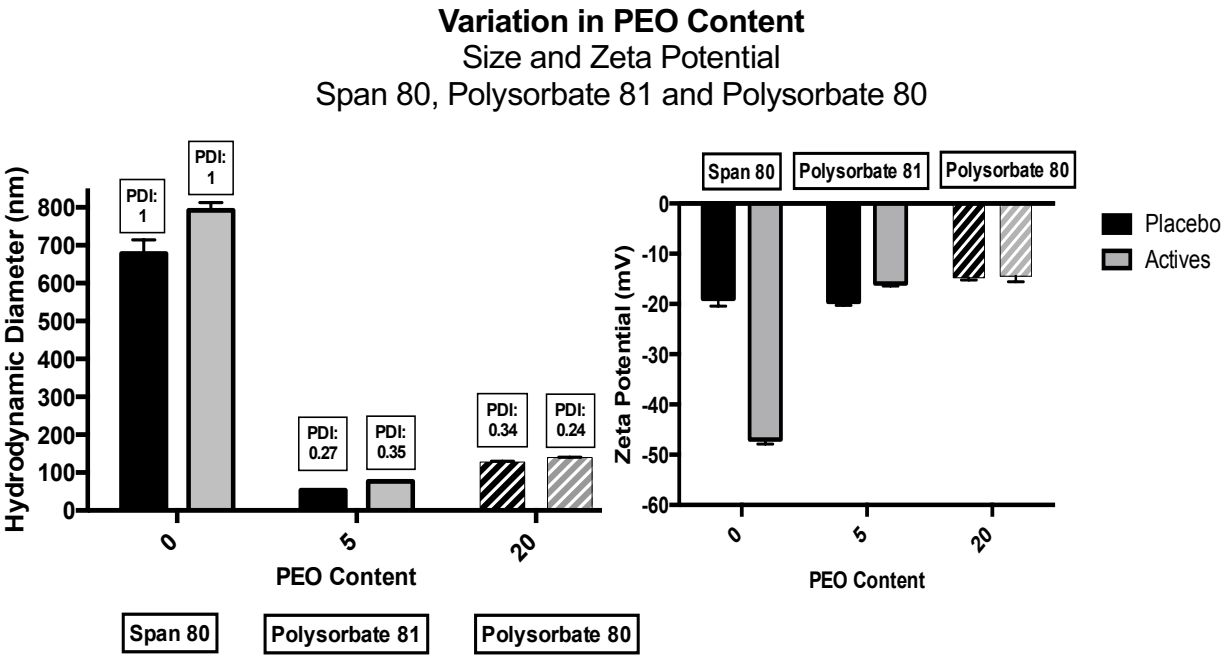

Figure 5.2: Hydrodynamic diameter and zeta potential values for formulations containing 3:1 Span 80/Polysorbate 81/Polysorbate 80:Cremophor RH 40 surfactant. The current formulation, F1A, is depicted by the striped bars (black= placebo; grey= active ingredients).

This mismatch in HLB may be responsible for the formation of large droplets, as it is possible that the interfacial tension between oil and water was not sufficiently reduced. The advantage, however, is that the non-ethoxylated hydrophilic head group is smaller, resulting in less steric hindrance to hydrophilic APIs that prefer to localize around the surfactant head group, such as folic acid and riboflavin. The increased localization of these APIs around the relatively small head group of Span 80 may be responsible for the highly negative zeta potential values recorded after drug loading. This phenomenon of reduced steric hindrance may also be responsible for the more negative zeta potential values seen in Polysorbate 81 (-19 ± 4.2 mV) versus Polysorbate 80 (-14 ± 2.2 mV), given the lower PEO content of the former. Of greater importance, however, are the small droplet sizes of Polysorbate 81-containing microemulsions as compared to Polysorbate 80. This may be attributed to the combined effect of more efficient packing of Polysorbate 81 between Cremophor RH 40 molecules at the interface, as well as more pronounced hydrophobic interactions between Polysorbate 81 and lipophilic API material, given that Polysorbate 81 is more hydrophobic than Polysorbate 80. As one proceeds from Span 80 to Polysorbate 81 to Polysorbate 80, the number of EO units increases from 0 to

5 to 20, respectively. Given that Polysorbate 81 demonstrated the most favourable overall results with respect to droplet size and zeta potential for this group of surfactants, it must be considered that, barring PEO contributions from Cremophor RH 40, an EO content of 5 rather than 20 (as in the case of Polysorbate 80 in F1A), may be sufficient for the production of a homogeneous, microemulsion formulation containing 11 active ingredients. According to Myers (2006), at least 5 to 6 EO units are required for appreciable water solubility.[5] Polysorbate 81 is at this threshold value, suggesting that in a system where both hydrophilic and lipophilic active ingredients must be accommodated, a lower EO content may be an appropriate compromise.

Ether-based Surfactants (Brij Class)

Figure 5.3 depicts emulsions formulated in a surfactant:oil:water ratio of 50:40:10 with the surfactant phase consisting of 3:1 Brij 93: Cremophor RH 40, 3:1 Brij 97: Cremophor RH 40, 3:1 Brij 98:Cremophor RH 40 or 3:1 Brij S100:Cremophor RH 40, the oil phase consisting of Miglyol 812 + five oil-soluble APIs and the water phase consisting of six water-soluble APIs. Size histograms and zeta potential curves may be found in **Figure D-2, Appendix D**. Formulations comprised of 3:1 Brij 93:Cremophor RH 40 and 3:1 Brij S100:Cremophor RH 40 exhibited phase separation, with the latter presenting as a coarse, immovable gel. In

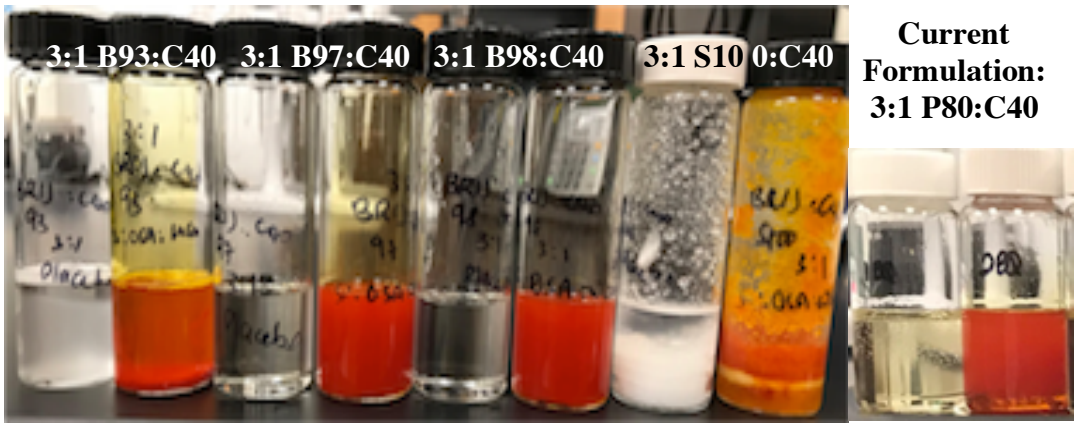

Figure 5.3: Formulations (S:O:W=50:40:10) comprised of 3:1 Brij 93/ Brij 97/ Brij 98/ Brij S100: Cremophor RH 40 surfactant, Miglyol 812 and water. Drug-loaded samples contain five lipophilic and six hydrophilic APIs, and are red/orange in colour versus placebo samples (clear/white). C40= Cremophor RH 40, P80= Polysorbate 80, B93/97/98/S100= Brij 93/97/98/S100

contrast, formulations comprised of 3:1 Brij 97:Cremophor RH 40 and 3:1 Brij 98:Cremophor RH 40 were clear and homogenous, though the latter was viscous in nature. Each sample was diluted 100x with water followed by droplet size and zeta potential determination (**Figure 5.4**).

Active ingredient formulations containing Brij 93 were similar to those of Span 80, possessing large droplet sizes of 421 ± 6 nm with a very polydisperse nature (PDI=1). This was not surprising given that these two surfactants differ by only 2 EO groups. Three size populations of over 3000 nm, 200 nm and 250 nm were also observed in Brij 93 formulations, similar to Span 80. However, these large droplet sizes were smaller than that of Span 80, which was expected given the less turbid nature of the Brij 93 emulsion. Separation of the water-soluble APIs was also apparent, as evidenced by the presence of precipitate on the bottom of the vial in Brij 93 samples. Brij 97 and 98 emulsion formulations were 160 ± 2.6 nm and 219 ± 2.2 nm in size, respectively, after API incorporation. These sizes were comparable to that of Polysorbate 80 but larger than those of Polysorbate 81-containing microemulsions. Size and zeta measurements were not determined for Brij S100 emulsions due to their phase separated and viscous nature, the latter of which is likely due to the saturated stearyl chain that results in a rigid, inflexible interface.

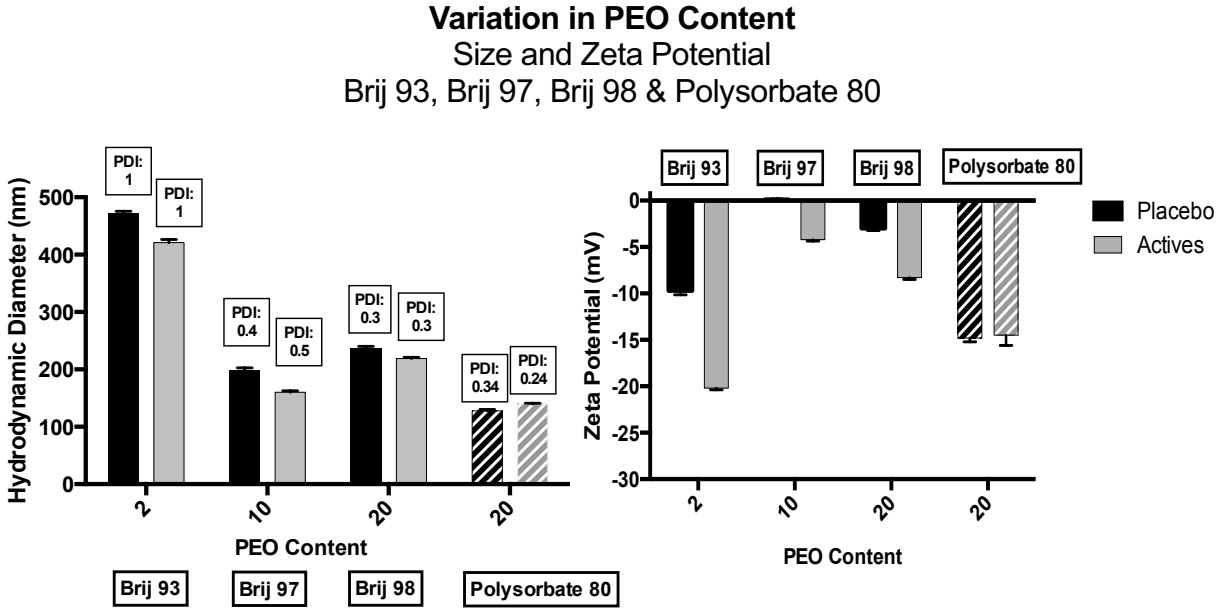

Figure 5.4: Hydrodynamic diameter and zeta potentials for formulations containing 3:1 Brij 93/Brij 97/Brij 98:Cremophor RH 40 surfactant. The current formulation, F1A, is depicted by the striped bars (black= placebo; grey= active ingredients).

With respect to zeta potential, Brij 93 exhibited the largest change in zeta potential, becoming more negative by approximately 10 mV, from –10 ± 0.5 mV to –20 ± 0.2 mV after API incorporation. Smaller changes of approximately 4-5 mV were seen for Brij 97 and 98 after API inclusion. Thus, the Brij class of surfactants appeared to demonstrate a slightly greater shift to more negative zeta potential values upon API incorporation, in comparison to the current formulation, F1A. This suggests that a degree of electrostatic stability was imparted onto the droplets once APIs were introduced into the formulation.

The low degree of polyethoxylation in Brij 93 results in a HLB value of 5. As in the case of Span 80, this represents a mismatch with the HLB of the oil phase resulting in the formation of larger droplets. However, the less sterically hindered head group may have led to possible localization of charged water-soluble APIs, resulting in a decrease in zeta potential after drug loading. This decrease was not as prevalent in Brij 97 and 98 formulations where the PEO content was much higher at 10 and 20, respectively, and the HLB values were closer to that of Miglyol 812 at 12[15] and 15[16], respectively.

Overall, an increase in EO content from 2 to 10 or 20 EO units resulted in a decrease in droplet size, as hypothesized. Similar to the case of the sorbitan esters tested earlier, the smallest droplet sizes of this surfactant group were observed in Brij 97, which has a lower EO content (10 EO units) than that of the current formulation (20 EO units). This, again, suggests that a lower EO content than used in the current formulation may be sufficient for the formation of a homogeneous, Type IV microemulsion. Interestingly, Brij 98 which is remarkably similar to Polysorbate 80 in terms of hydrocarbon chain length and PEO content, but for the absence of a sorbitan head group, possessed larger droplet sizes (219 ± 2 nm) and smaller (less negative) zeta potential values (-8 ± 0.2 mV) than that of F1A. Thus, the presence of a sorbitan head group may be of importance in this type of formulation. In the case of PEO ether surfactants, the phenomenon of better surfactant properties with lower EO content, has been previously explained.[5] PEO ether surfactants with 10 EO units exhibited moderate water solubility and good surfactant properties.[5] However, PEO ether surfactants with 5 EO units exhibited poor water solubility and surfactant usefulness, while those with 20 or more EO units exhibited high water solubility such that most of the good surfactant properties were lost.[5]

The findings of slightly higher droplet sizes in the Brij surfactant class as compared to the Tween surfactant class have been previously reported.[28] In the production of

polyhydroxybutyrate particles with various emulsifiers, Tweens 80, 81 and 85 exhibited lower sizes and size distributions than Brij 35 and Brij 58.[28] Ethers have also been reported to possess higher toxicity than esters due to the fact that the latter are readily hydrolyzed and metabolized, while the former must be degraded by microbial enzyme systems of the liver and intestine.[29] Despite these disadvantages, Brij surfactants appear to trump Tween surfactants with respect to stability. A previous study of ethylene glycol distearate emulsions using Brij L23 and 35P surfactants versus Tween 20 and 80, resulted in emulsion stability for over one month versus only a few hours, respectively.[30] The simple oxyethylene head group of Brij in comparison to the sorbitan ring head group of Tween may have been able to cover the droplet more efficiently leading to a more stable emulsion.[30]

5.5.1.2. Consideration of Surfactant Tail Group: Variation in Hydrocarbon Chain Length

Figure 5.5 depicts emulsions formulated in a surfactant:oil:water ratio of 50:40:10 with the surfactant phase consisting of 3:1 Polysorbate 20: Cremophor RH 40, 3:1 Polysorbate 40: Cremophor RH 40, 3:1 Polysorbate 60:Cremophor RH 40 or 3:1 Polysorbate 80:Cremophor RH 40, the oil phase consisting of Miglyol 812 + five oil-soluble APIs and the water phase consisting of six water-soluble APIs. Size histograms and zeta potential curves are shown in **Figure D-3, Appendix D**. Phase separation was observed in two samples: drug-loaded Polysorbate 20 and the Polysorbate 60 placebo. All other formulations appeared homogenous in nature. The sample containing 3:1 Polysorbate 60:Cremophor RH 40 was highly viscous and gel-like in nature for both placebo and active ingredient-containing samples. Each sample was diluted 100x with water followed by droplet size and zeta potential determination (**Figure 5.6**).

The results in **Figure 5.6** demonstrated no obvious pattern in droplet size differences given an increase in chain length. Overall, droplet sizes in both placebo and active samples for all surfactants tested remained within a narrow range, between 100 and 200 nm. Sizes for drug-loaded formulations containing Polysorbate 20, 40, 60 and 80 were 134 ± 5 nm, 201 ± 3 nm, 147 ± 1 nm and 140 ± 1.2 nm, respectively, and except in the case of Polysorbate 20,

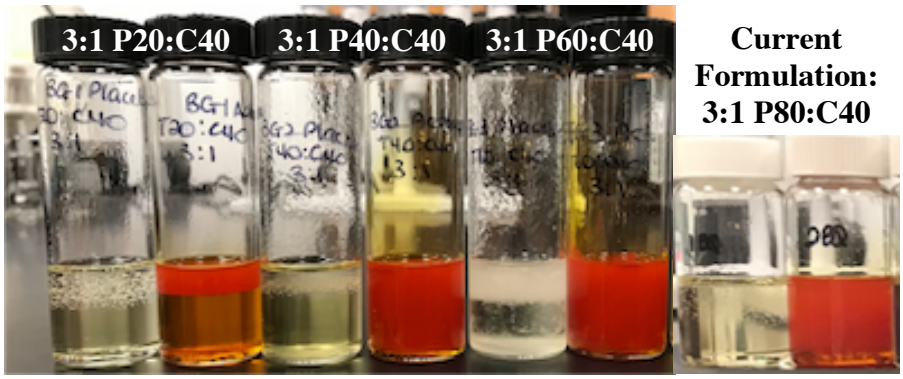

Figure 5.5: Formulations (S:O:W=50:40:10) comprised of 3:1 Polysorbate 20/Polysorbate 40/Polysorbate 60/Polysorbate 80: Cremophor RH 40 surfactant, Miglyol 812 and water. Drug-loaded samples contain five lipophilic and six hydrophilic APIs, and are red/orange in colour versus placebo samples (clear/white). C40= Cremophor RH 40, P20/40/60/80= Polysorbates 20/40/60/80

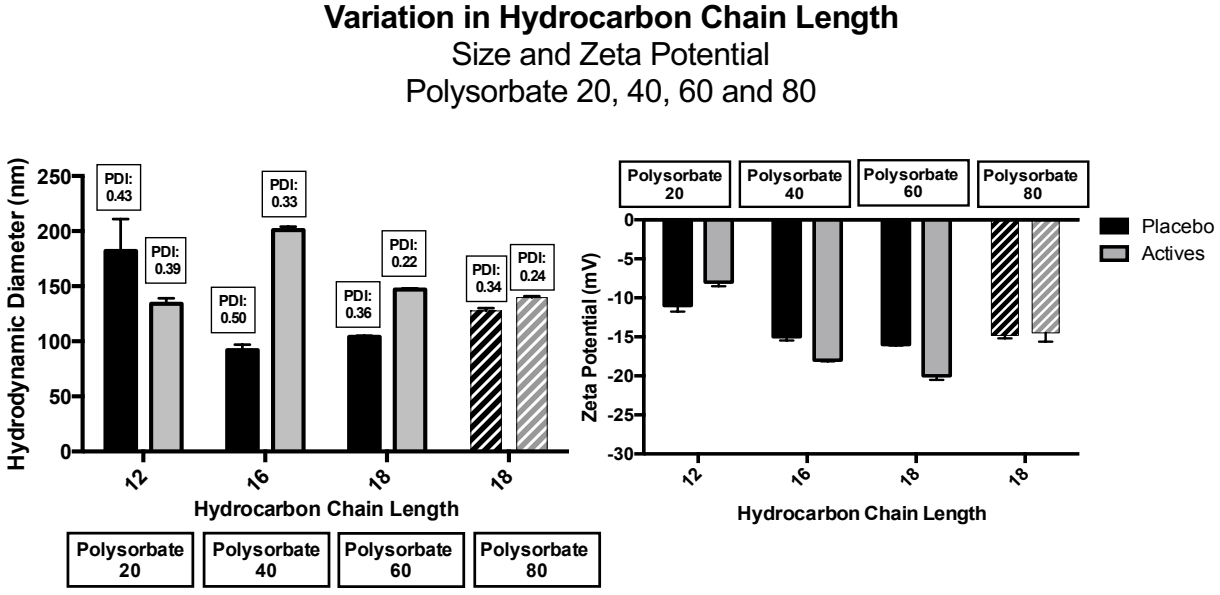

Figure 5.6: Hydrodynamic diameter and zeta potential values for formulations containing 3:1 Polysorbate 20/Polysorbate 40/Polysorbate 60/Polysorbate 80: Cremophor RH 40 surfactant. The current formulation, F1A, is depicted by the striped bars (black= placebo; grey= active ingredients).

droplet sizes increased after API incorporation. The size distribution or polydispersity index also decreased after API incorporation. In terms of zeta potential, a progressively stable droplet of increasing negative charge was generally seen from Polysorbate 20 to Polysorbate 40 to

Polysorbate 60. This continued increase was not seen in the sample containing Polysorbate 80 (F1A). A slight increase in zeta potential to a more negative value (an indicator of stability) was seen upon API incorporation in Polysorbate 40 and 60 samples.

The phase separation in Polysorbate 20-containing formulations may be explained by the relatively short nature of the C12 hydrocarbon tail, which is likely insufficient for lipophilic solubilization. Thus, a layer of phase-separated oil can be seen at the top of the vial in **Figure 5.5**. The gel-like nature of Polysorbate 60-containing formulations, in comparison to that of Polysorbate 80, is likely attributable to its saturated C18 tail which reduces film flexibility and imparts rigidity (unlike the unsaturated tail of Polysorbate 80).

In theory, a longer hydrocarbon chain results in a lower critical micelle concentration and higher aggregation number, such that more non-polar material may be incorporated into the micelle, causing an increase in size.[8] However, a decrease in droplet size with increasing hydrocarbon length has also been previously reported. In the case of nanoparticles containing metal-carbon manufactured with Tweens 20, 40 and 80, nanoparticle size was found to decrease from Tween 20 to Tween 40 to Tween 80.[31] Thus, the longer surfactant (Tween 80) produced smaller nanoparticle sizes than those manufactured with the shorter chain surfactants, Tween 40 and Tween 20.[31] Despite this evidence, neither an increase nor a decrease upon increasing hydrocarbon chain length was clearly seen in this work. Instead, droplet sizes for all samples remained within a narrow size range of approximately 100-200 nm. This may be explained in consideration of the HLB values of these surfactants. The HLB values of Polysorbate 20, Polysorbate 40, Polysorbate 60 and Polysorbate 80 are 16.7, 15.6, 14.9 and 15[11], respectively. As a result, the HLB range is very narrow and only spans a difference of 1.8 units across all four surfactants. Thus, it may be hypothesized that solubilization of all active ingredients occurs to a similar extent across these four surfactants.

In terms of zeta potential, it has previously been reported by Stachurski et al (1996), that alkanes of shorter hydrocarbon chains have less negative values than that of longer hydrocarbon chains.[32] Such a decrease to a more negative zeta potential was very generally seen in this work from Polysorbate 20 to Polysorbate 60, but not in Polysorbate 80. However, the authors of the aforementioned work noted that in subsequent studies with aliphatic hydrocarbons from n-nonane to n-hexadecane, zeta potential values were more dependent on pH rather than solely on hydrocarbon chain length.[32]

In all above surfactant-containing microemulsions, an independent, two-sample T-test was performed in order to determine whether any statistically significant differences existed between the sizes and zeta potentials of drug-free and drug-loaded formulations. Where drug-free formulations (N=10) exhibited average sizes of 244 nm (SD±62) and drug-loaded formulations (N=10) exhibited average sizes of 268 nm (SD±67), no significant difference was noted, $t(18)= 0.27$, $p= .789$. An F-test to compare variances showed no significant difference between drug-free and drug-loaded samples, $F(18)= 1.19$, $p= .800$, satisfying the assumption of equal variance. In addition, where drug-free formulations (N=10) exhibited average zeta potential values of -17.5 mV (SD±6.3) and drug-loaded formulations (N=10), exhibited average zeta potential values of -21.9 mV (SD±5.6), no significant differences were noted, $t(18)= 0.52$, $p= .609$. The assumption of equal variances in this case was also satisfied using the F-test, $F(18)= 1.24$, $p=.754$ (**Table D-1, Appendix D**).

5.5.1.3. Substitution of Cremophor RH 40 with Cremophor RH 60

Based on homogeneity and droplet size, Brij 97 and Polysorbate 81 were selected for further analysis. Brij 98 exhibited gelling behaviour and was discounted for further use while Polysorbate 40 resulted in large and polydisperse droplets, especially with respect to the placebo sample, where the highest PDI of all the Tween surfactants was observed. **Figure 5.7** depicts emulsion formulations containing S:O:W ratios of 50:40:10 with the surfactant phase consisting of 3:1 Polysorbate 80: Cremophor RH 40/60, 3:1 Polysorbate 81:Cremophor RH 40/60, 3:1 or 3:1 Brij 97:Cremophor RH 60, the oil phase consisting of Miglyol 812 + five oil-soluble APIs and the water phase consisting of six water-soluble APIs. A S:O:W ratio of 60:30:10 was also studied for 3:1 Polysorbate 80:Cremophor RH 40 and 3:1 Polysorbate 80:Cremophor RH 60, based on previous formulation studies in **Chapter 4**. No visual differences were observed between samples made with Cremophor RH 40 and Cremophor RH 60. Each sample was diluted 100x with water prior to evaluation of droplet size (**Figure 5.8**), polydispersity index (**Figure 5.9**) and zeta potential (**Figure 5.10**). All size histograms and zeta potential curves may be found in **Figure D-4, Appendix D**.

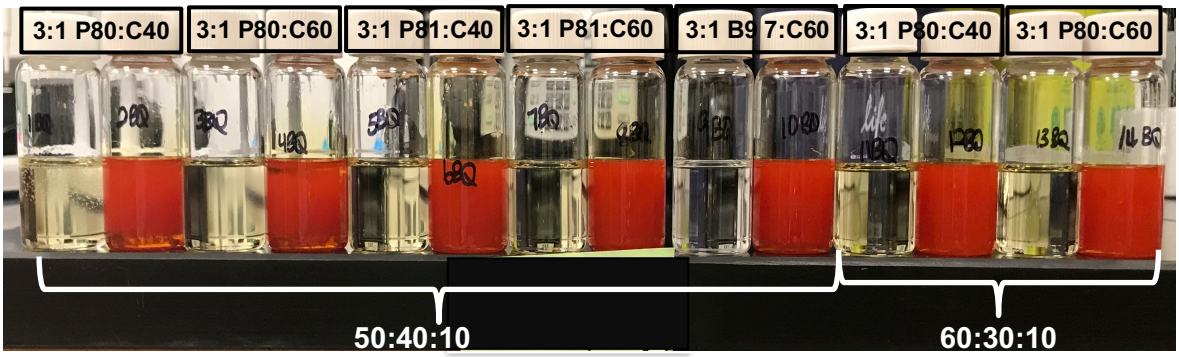

Figure 5.7: Emulsion formulations comprised of S:O:W ratios of 50:40:10 and 60:30:10. The surfactant phase was comprised of (l-r) 3:1 Polysorbate 80: Cremophor RH 40, 3:1 Polysorbate 80: Cremophor RH 60, 3:1 Polysorbate 81: Cremophor RH 40, 3:1 Polysorbate 81: Cremophor RH 60 or 3:1 Brij 97:Cremophor RH 60. Drug-loaded samples contain five lipophilic and six hydrophilic APIs, and are red/orange in colour versus placebo samples (clear). C40/60= Cremophor RH 40/60, P80/81= Polysorbate 80/81

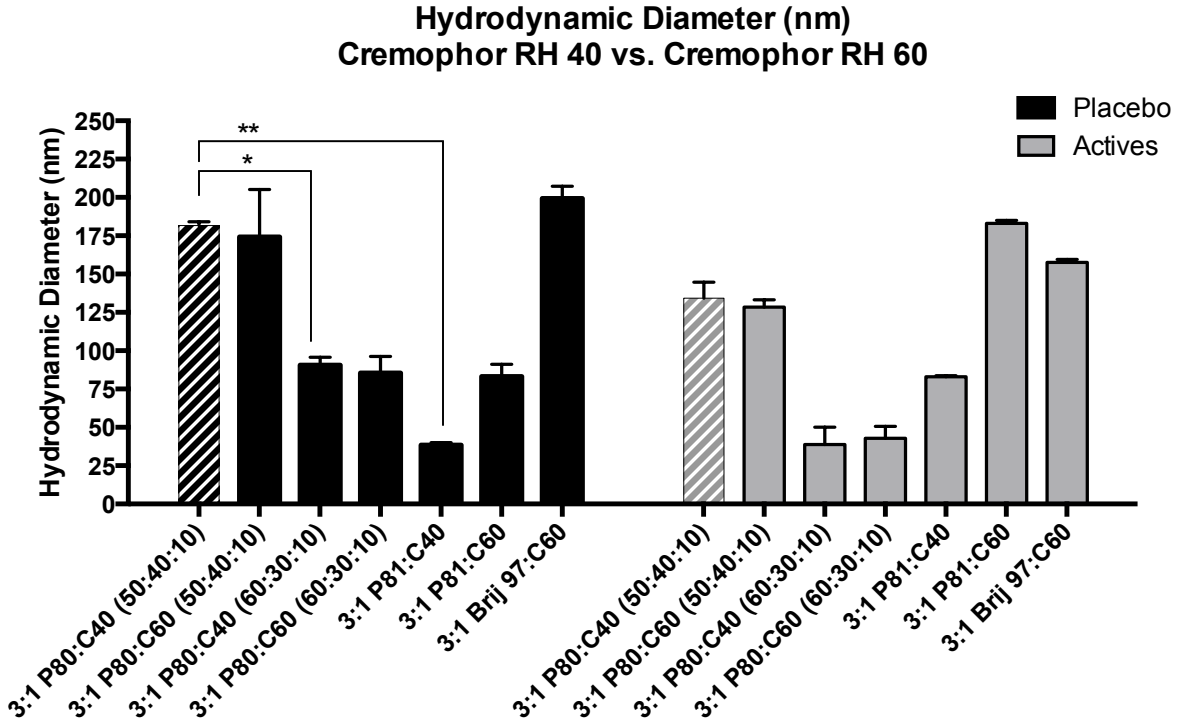

Figure 5.8: Hydrodynamic diameter values for formulations comprised of 3:1 Polysorbate 80: Cremophor RH 40, 3:1 Polysorbate 80: Cremophor RH 60, 3:1 Polysorbate 81:Cremophor RH 40, 3:1 Polysorbate 81:Cremophor RH 60 or 3:1 Brij 97:Cremophor RH 60 surfactant. The current formulation, F1A, is depicted by the striped bars (black= placebo; grey= active ingredients). Statistical significance from the Welch's statistic and Games-Howell post-hoc test, involving F1A microemulsions *only,* are depicted here.

Polysorbate 80 and Polysorbate 81 produced the smallest droplet sizes, especially at S:O:W ratios of 60:30:10 for the former and 50:40:10 for the latter (**Figure 5.8**). Brij 97 formulations exhibited the largest droplet sizes and overall, no difference in size was observed between formulations manufactured with Cremophor RH 40 and Cremophor RH 60. The exception to this was Polysorbate 81, where an increase of approximately 100 nm was seen in active ingredient samples manufactured with Cremophor RH 60 rather than Cremophor RH 40. An ordinary, one-way ANOVA comparing the effect of surfactant type on droplet size revealed a statistically significant effect for both placebo [$F(6,2.95) = 270.59$, $p < .001$] and active ingredient [$F(6,2.7)=826.56$, $p<.001$] samples. Given that homogeneity of variance, as calculated by Levene's F-statistic, was violated in both drug-free ($F(6,7)= 2.2*10^{30}$, $p<.001$) and drug-loaded ($F(6,7)= 1.5*10^{29}$, $p<.001$) data, reported p-values were obtained using the Welch's test. A Games-Howell post-hoc analysis revealed statistically significant differences in droplet size between F1A (134 ± 13.6 nm) and 3:1 Polysorbate 80:Cremophor RH 40 60:30:10 placebo formulations (38.8 ± 6.3 nm), and F1A and 3:1 Polysorbate 81:Cremophor RH 40 placebo formulations (83.0 ± 0.01 nm) (depicted in **Figure 5.8**). No statistically significant differences were noted between F1A and any other formulation with respect to active ingredient samples. All other statistically significant differences are reported in **Table D-2, Appendix D**.

With respect to polydispersity (**Figure 5.9**), 3:1 Polysorbate 80:Cremophor RH 40 (F1A) and 3:1 Polysorbate 81:Cremophor RH 40 exhibited the lowest polydispersity indices-between 0.17 and 0.29. The highest polydispersity indices were observed in formulations containing 3:1 Polysorbate 80:Cremophor RH 40 (S:O:W 60:30:10), 3:1 Polysorbate 80:Cremophor RH 60 (S:O:W 50:40:10) and Brij 97. A one-way ANOVA comparing the effect of surfactant type on polydispersity index revealed a statistically significant effect for both placebo [$F(6,2.72)=44.14$, $p=.008$] and active ingredient [$F(6,2.7)=102$, $p=.003$] samples. Homogeneity of variance, as computed by Levene's F-statistic, was violated in both drug-free ($F(6,7)= 1.1*10^{30}$, $p<.001$) and drug-loaded samples ($F(6,7)= 1.1*10^{31}$, $p<.001$). Therefore, all reported p-values were obtained using the Welch's test. A Games-Howell post-hoc analysis revealed no statistical differences between F1A and any of the tested microemulsions. Other statistically significant differences are reported in **Table D-3, Appendix D.**

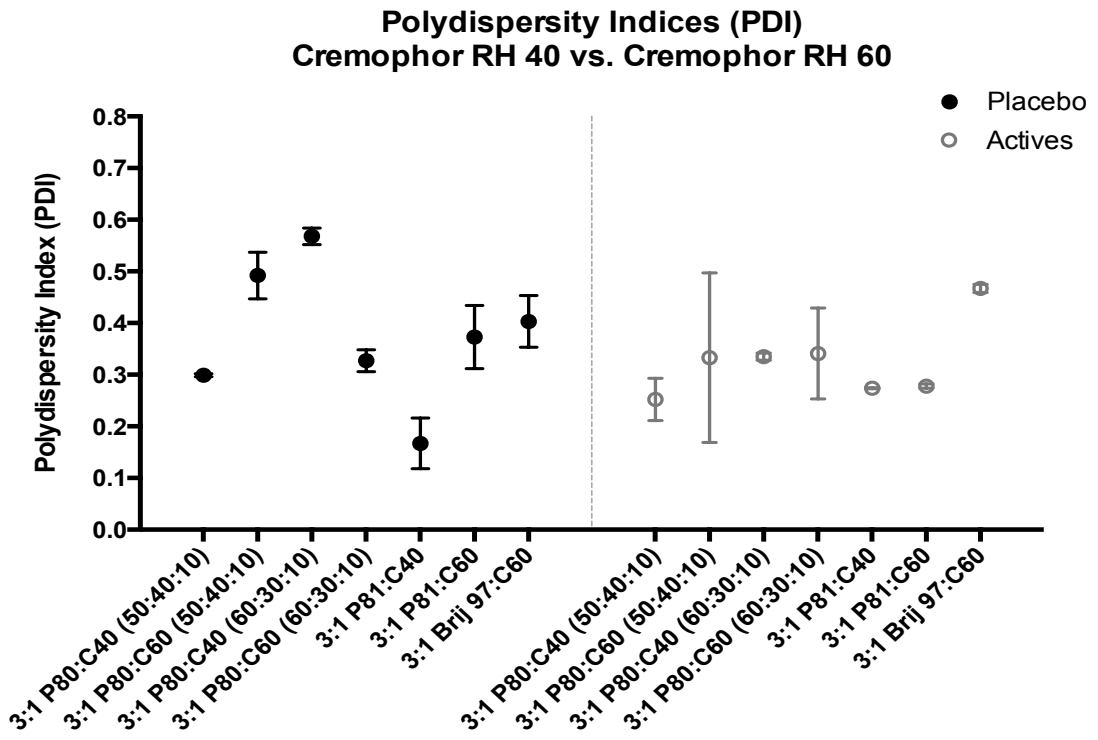

Figure 5.9: Polydispersity indices for formulations comprised of 3:1 Polysorbate 80: Cremophor RH 40, 3:1 Polysorbate 80: Cremophor RH 60, 3:1 Polysorbate 81:Cremophor RH 40, 3:1 Polysorbate 81:Cremophor RH 60 or 3:1 Brij 97:Cremophor RH 60 surfactant. No statistically significant differences were noted between the PDI values of F1A and the other formulations. Statistical significance involving F1A microemulsions *only*, are depicted here (none, this case).

In terms of zeta potential (**Figure 5.10**), samples containing Polysorbate 81 and Brij 97 exhibited the most and least negative values, respectively. Thus, of all surfactants tested, Polysorbate 81 possessed the highest stability and Brij 97, the lowest. Zeta potential values mainly decreased or became more negative upon API-incorporation and no large differences were seen between Cremophor RH 40 and Cremophor RH 60-containing samples, even for Polysorbate 81, which had previously recorded a 100 nm size increase in samples formulated with Cremophor RH 60 rather than Cremophor RH 40. A one-way ANOVA comparing the effect of surfactant type on zeta potential revealed a statistically significant difference in both placebo [$F(6,3.03)=339$, $p<.000$] and active ingredient [$F(6,2.96)=17.18$, $p=.021$] samples. Homogeneity of variance, as determined by Levene's F-statistic, was violated in both placebo ($F(6,7)= 3.1*10^{29}$, $p<.001$) and active ingredient ($F(6,7)= 1.4*10^{30}$, $p<.001$) samples.

Therefore, the reported p-values were obtained using the Welch's test. A Games-Howell post-hoc analysis revealed statistically significant differences between F1A (-10.6 ± 0.9 mV) and 3:1 Polysorbate 81:Cremophor RH 60 (-26.3 ± 0.3 mV), and F1A and 3:1 Brij 97:Cremophor RH 60 (-0.53± 0.5 mV) placebo samples. No further statistically significant differences were noted between the zeta potential values of F1A and the other formulations. All other statistically significant differences are reported in **Table D-4, Appendix D**.

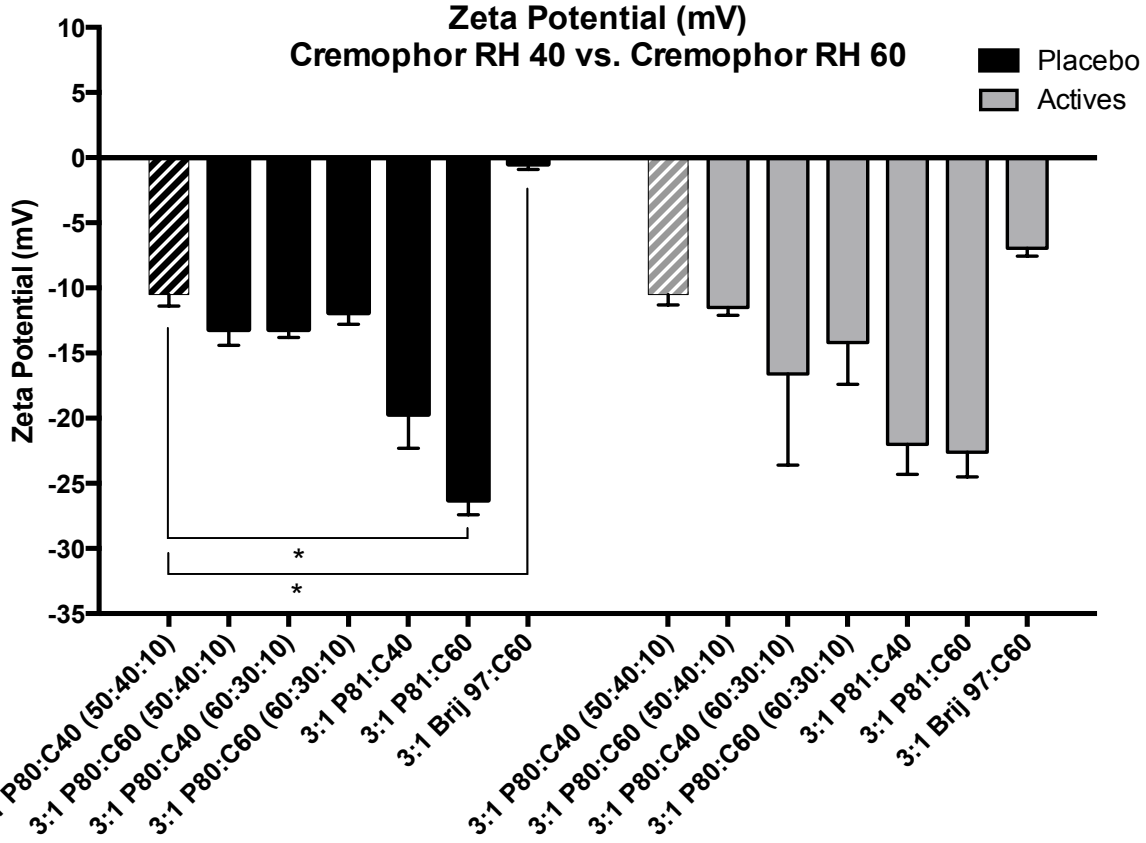

Figure 5.10: Zeta potential values for formulations comprised of 3:1 Polysorbate 80: Cremophor RH 40, 3:1 Polysorbate 80: Cremophor RH 60, 3:1 Polysorbate 81:Cremophor RH 40, 3:1 Polysorbate 81:Cremophor RH 60 or 3:1 Brij 97:Cremophor RH 60 surfactant. The current formulation, F1A, is depicted by the striped bars (black= placebo; grey= active ingredients). Statistical significance from the Welch's statistic and Games-Howell post-hoc test, involving F1A microemulsions *only*, are depicted here.

The fact that no large difference in droplet size or zeta potential was seen between samples manufactured with either Cremophor RH 40 or Cremophor RH 60, except for in the case of Polysorbate 81, lends credence to the loss of importance of PEO content above a certain value. Cremophor RH 60 has a total of 60 EO units in comparison to 40 in Cremophor RH 40. This PEO increase of 20 is likely not beneficial to any further solubilization of APIs. In addition, the use of a surfactant ratio of 3:1 results in a low concentration of Cremophor RH 60 in each formulation, such that any contribution to size or zeta potential may be masked. These results suggest no benefit to including Cremophor RH 60 in future formulations.

5.5.1.4. Substitution of 3:1 Polysorbate 80:Cremophor RH 40 for a Single Surfactant

Figure 5.11 depicts S:O:W 50:40:10 formulations comprised of Tween/Polysorbate 85 surfactant, Miglyol 812 oil and water. Tween 85 was used as a single surfactant substitute for the 3:1 Polysorbate 80:Cremophor RH 40 mixture of the current formulation, F1A. Although the placebo demonstrated near perfect homogeneity and clarity, there were indications of phase separation upon API incorporation. Each sample was diluted 100x with water followed by droplet size and zeta potential determination (**Figure 5.12**). Size histograms and zeta potential curves may be found in **Figure D-5, Appendix D**.

Figure 5.11: Formulations comprised of Polysorbate 85 surfactant, Miglyol 812 and water. Drug-loaded samples are red/orange in colour versus placebo samples (clear/pale yellow). C40= Cremophor RH 40, P80/81= Polysorbate 80/81

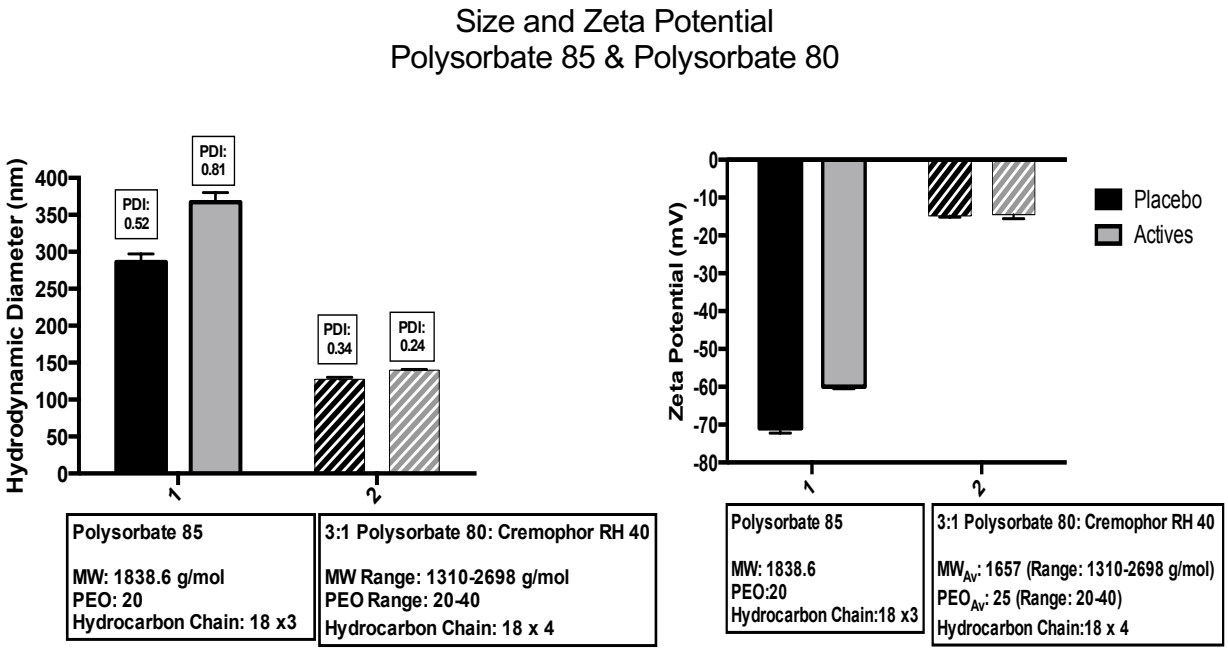

Figure 5.12: Hydrodynamic diameter and zeta potential values for microemulsion formulations comprised of Polysorbate 85 surfactant, Miglyol 812, water and all active ingredients. Results for the current formulation, F1A, are indicated by the striped bars (black= placebo; grey= active ingredients).

Given the similarity in structure of Polysorbate 85 to both Polysorbate 80 and Cremophor RH 40, the large droplet sizes observed were unexpected. Both placebo and active ingredient samples exhibited sizes of 367 ± 13 nm, twice that of F1A. In addition, the sample was quite polydisperse resulting in multiple size populations (**Figure D-5, Appendix D**). Active ingredient samples contained size populations over 1000 nm and 250 nm. These large, polydisperse droplets were surprising given that Polysorbate 85 possesses an HLB value of 11, which is remarkably similar to the HLB value of 3:1 Polysorbate 81: Cremophor RH 40 (12). However, the latter produced sizes in the range of 80 nm after active ingredient incorporation.

Despite unfavourable droplet sizes, zeta potential values were extremely favourable at -60 ± 0.5 mV after drug loading. Thus, droplets containing Polysorbate 85 are expected to be highly stable from an electrostatic standpoint. The large droplet sizes of Polysorbate 85 may be attributed to the lower PEO content relative to the 3:1 Polysorbate 80:Cremophor RH 40 surfactant mixture of F1A. It is possible that this lower PEO content affords greater oil incorporation and larger droplet sizes. A more likely explanation, however, is that the

replacement of a Polysorbate 80 and Cremophor RH 40 surfactant mixture with a single surfactant like Polysorbate 85, evidently changes the packing behaviour and film flexibility afforded by a surfactant-co-surfactant system. Consequently, the large droplet sizes and polydispersity of Tween 85-containing formulations resulted in this surfactant being discounted for further use.

5.5.1.5. Tensiometry

Surfactants demonstrating favourable droplet sizes were selected for critical micelle concentration (CMC) analysis via tensiometry in order to determine whether synergism with Cremophor RH 40 was a possible criterion for the formation of homogenous, emulsion systems capable of multi-drug delivery. The selected surfactants were Polysorbate 81, Brij 97, Brij 98 and Polysorbate 40. The CMC of 3:1 Polysorbate 80:Cremophor RH 60 was also evaluated.

Tensiometry results are shown in **Table 5.6.** All CMC graphs and concentration tables are located in **Figures D-6** to **D-13, Appendix D.** Brij 97 and 98, as well as

Table 5.6: Critical micelle concentration (CMC) experimental and ideal results via tensiometry for Brij 97, Brij 98, Polysorbate 40, Polysorbate 81 and Polysorbate 80 in Cremophor RH 40/60. Synergism occurs when experimental CMC values are below those of the ideal. All calculations are located in **Appendix D**.

Surfactant Mixture	Experimental CMC ± SD (mM)	Ideal CMC (mM)
3:1 Brij 97:Cremophor RH 40*	0.0015	0.019
3:1 Brij 98:Cremophor RH 40*	0.0016	0.019
3:1 Polysorbate 40:Cremophor RH 40*	0.0022	0.012
3:1 Polysorbate 80:Cremophor RH 40	0.0036 ± 0.0	0.0048
3:1 Polysorbate 80:Cremophor RH 60*	0.0047	0.0056-0.0062
3:1 Polysorbate 81:Cremophor RH 40	0.0059 ± 0.0	0.0057

* standard deviations not computed due to absence of replicates

Polysorbate 40, demonstrated synergism with Cremophor RH 40 as indicated by experimental CMC values that were below those of the calculated ideal (**Appendix D**).

Synergism was also seen in 3:1 Polysorbate 80:Cremophor RH 40 (**Chapter 2**) and 3:1 Polysorbate 80:Cremophor RH 60 samples, while in the case of 3:1 Polysorbate 81:Cremophor RH 40, the experimental CMC was consistent with that of the ideal. Given that thus far, the greatest microemulsion formation potential was seen with Polysorbate 81, it is possible that in terms of CMC, synergism is not an important emulsifying agent property in microemulsion, multi-drug delivery. Instead, it may be more important that surfactants simply not exhibit antagonistic behaviour, but tensiometry studies would have to be performed on the unsuccessful surfactants used in this Chapter in order to state this with certainty. In addition, tensiometry experiments would have to be repeated in order to garner sufficient statistical power to confirm this trend.

5.5.2 Pharmaceutically Relevant Tests

Despite the promising results observed with Brij 97, Brij 98, Polysorbate 40, Polysorbate 81 and Cremophor RH 60, a number of considerations were necessary before subjecting these formulations to dissolution, disintegration and stability testing. Brij 97 exhibited very low zeta potentials that were significantly different from the current formulation, F1A. Thus, it was inferred that this surfactant would perform poorly in stability tests. Brij 98, though homogenous in nature, exhibited larger droplet sizes than that of the current formulation as well as viscous behaviour to the point of gelling, which would inhibit proper solubilization of active ingredients. Polysorbate 40 demonstrated favourable droplet sizes, but high polydispersity in the placebo sample. Finally, there appeared to be no benefit to using Cremophor RH 60 in place of Cremophor RH 40, as droplet sizes and zeta potentials remained relatively the same, except in the case of Polysorbate 81 where droplet sizes increased. The use of a 60:30:10 S:O:W ratio for Polysorbate 80:Cremophor RH 40 microemulsion samples, though exhibiting smaller sizes than that of the current formulation (S:O:W 50:40:10), was also not possible given the inactive ingredient (IIG) limits of Polysorbate 80 (**Chapter 4**). Based on the above observations, Polysorbate 81 was selected as the sole surfactant for future investigation due to its small droplet sizes, negative zeta potential value and microemulsion formation potential.

5.5.2.1. Ternary Phase Diagram (TPD) Mapping

The ternary phase diagram for 3:1 Polysorbate 81:Cremophor RH 40 is depicted below in **Figure 5.13**. A variety of phase behaviours were obtained at room temperature and 37ºC with Miglyol 812 oil and water. At room temperature, the majority of monophasic, Type IV microemulsion behaviour was observed at high surfactant concentrations ≥ 60% w/w. Below 60% w/w surfactant, biphasic behaviour was primarily observed. Similar to the case of Polysorbate 80, Type I, O/W microemulsions dominated both TPDs at and below 40% w/w surfactant while Type II, W/O microemulsions were observed across a wide range of surfactant concentrations from 10-60% w/w but particularly at low water (10-30% w/w) and high oil (70-90% w/w) concentrations. Monophasic, opaque (coarse) emulsion regions were also observed largely between 20-30% w/w surfactant. As the temperature increased to 37ºC, no major phase changes were observed but for a slight reduction in opaque emulsion areas. Type III microemulsions were primarily observed at 37ºC.

Type I O/W regions were dominant, as expected for a non-ionic, hydrophilic surfactant. Though monophasic, Type IV microemulsions were present at high surfactant concentrations, a Type IV microemulsion was repeatedly observed at a relatively low surfactant concentration of 40% w/w at S:O:W 40:50:10. This phenomenon was not seen previously in the surfactant systems evaluated in **Chapter 2**. TPD results of F1A, comprised of 3:1 Polysorbate 80:Cremophor RH 40, indicated that at least 50% w/w surfactant was required for monophasic, microemulsion formation. The ability of 3:1 Polysorbate 81:Cremophor RH 40 to form a Type IV microemulsion at this relatively low surfactant concentration of 40% w/w (S:O:W 40:50:10) may be explained through consideration of the low EO content of Polysorbate 81 in comparison to that of Polysorbate 80. The low EO content of Polysorbate 81 affords higher lipophilicity of the surfactant mixture, possibly enhancing its amenability to Miglyol 812, present at a 50% w/w concentration. This is also likely responsible for the larger Type II, W/O microemulsion region observed here in comparison to 3:1 Polysorbate 80:Cremophor RH 40. Almost 50% of samples demonstrated gelling at room temperature, typically between 20-30% w/w surfactant. Upon heating to 37ºC, this behaviour was reduced and accounted for just under 30% of all samples, typically at higher surfactant concentrations (40-60% w/w). The reduction in gelling behaviour is likely attributable to the action of heat on Cremophor RH 40 which has a low melting temperature as explained in **Chapter 2**.

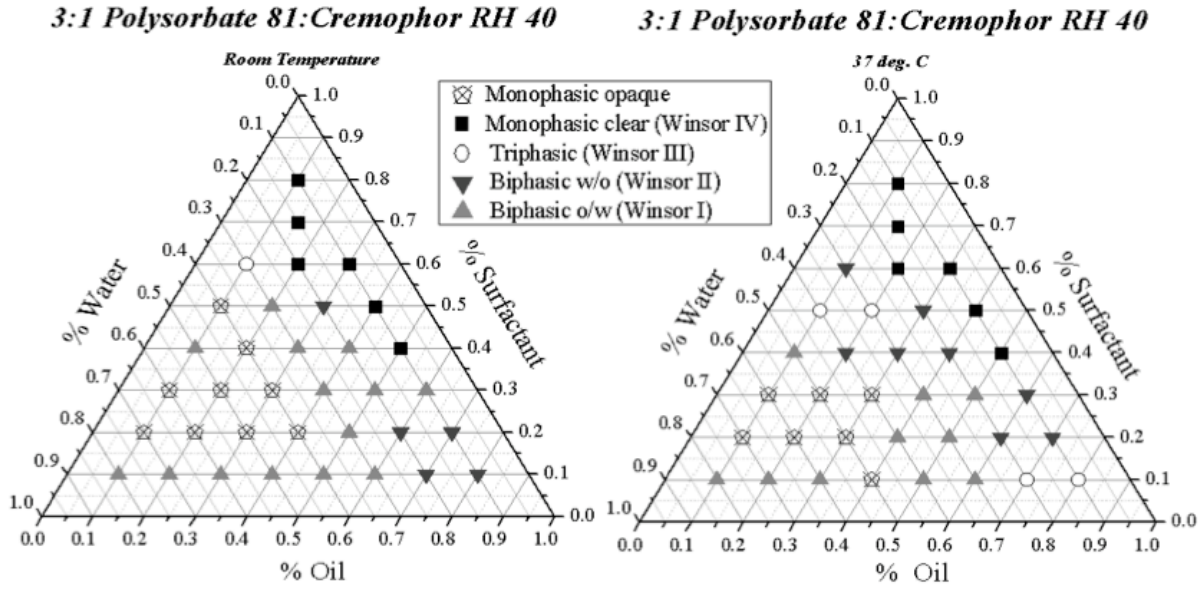

Figure 5.13: Ternary phase diagram for 3:1 Polysorbate 81:Cremophor RH 40, Miglyol 812 and water at room temperature (left) and at 37°C (right).

The main difference in microemulsion phase behaviour between 3:1 Polysorbate 81:Cremophor RH 40 and 3:1 Polysorbate 80:Cremophor RH 40 (**Chapter 2**) lies in the large Type I, O/W microemulsion region obtained in the latter. In 3:1 Polysorbate 81:Cremophor RH 40, this region is much smaller and instead, coarse emulsions dominate at the S:O:W ratios where Type I O/W microemulsions are observed in 3:1 Polysorbate 80:Cremophor RH 40. The low EO content of Polysorbate 81 in comparison to that of Polysorbate 80 evidently reduces the propensity to form Type I, O/W microemulsions and increases the ability of the former to form Type II, W/O microemulsions. Other differences include a much larger bicontinuous, Type III microemulsion region in 3:1 Polysorbate 80:Cremophor RH 40, and lower instances of gelling than seen in 3:1 Polysorbate 81:Cremophor RH 40.

Despite the differences observed between 3:1 Polysorbate 81:Cremophor RH 40 and 3:1 Polysorbate 80:Cremophor RH 40, TPD mapping led to the selection of two additional microemulsion formulations for further analysis via dissolution, disintegration and stability testing, both containing 3:1 Polysorbate 81:Cremophor RH 40 in S:O:W ratios: i) 40:50:10 and ii) 50:40:10.

5.5.2.2. Dissolution

In total, three samples were subjected to dissolution testing:

i) Formulation 1 (F1*): S:O:W= 50:40:10
   3:1 Polysorbate 80:Cremophor RH 40, Miglyol 812, Water and all Actives
   (**same as F1A in previous Chapters*)
ii) Formulation 2 (F2): S:O:W= 40:50:10
   3:1 Polysorbate 81:Cremophor RH 40, Miglyol 812, Water and all Actives
iii) Formulation 3 (F3): S:O:W= 50:40:10
   3:1 Polysorbate 81:Cremophor RH 40, Miglyol 812, Water and all Actives

Figure 5.14 depicts droplet sizes and zeta potential measurements of F1, F2 and F3 as determined by DLS. As discussed previously, F1 (N=14) possessed droplet size and zeta potential values of 164 ± 37 nm and -14 ± 2.2 mV, respectively. In contrast, F2 (N=4) and F3 (N=6) possessed size and zeta potential measurements of 94 ± 15 nm, -16.5 ± 4 mV and 80.7 ± 2.4 nm, -23 ± 6 mV, respectively. An ordinary one-way ANOVA conducted in order to determine the presence of statistically significant differences in droplet size and zeta potential amongst all tested formulations, revealed a statistically significant difference in both size [$F(2,6.7)=31.6$, $p< .001$] and zeta potential [$F(2,5.9)=6.10$, $p= .037$] with surfactant type. Homogeneity of variance, as evaluated by Levene's F-test, was violated in all cases. As a result, all p-values reported are derived from the Welch's Equality of Means test rather than a standard ANOVA, with a Games-Howell post-hoc analysis. All values are fully reported in **Table D-6, Appendix D.** Rheological measurements performed on aqueous dilutions of F2 and F3 were analogous to that of F1 (**Chapter 4**) and confirmed Newtonian behaviour (and thus, the presence of O/W droplets) at 100x aqueous dilution. (**Figure D-15, Appendix D**).

These results of this Chapter have led to the successful procurement of two microemulsion systems possessing smaller droplet sizes and higher electrostatic stability than the current formulation, due to careful, methodical surfactant selection. For dissolution testing, all formulations were compared to an existing prenatal supplement reference. This

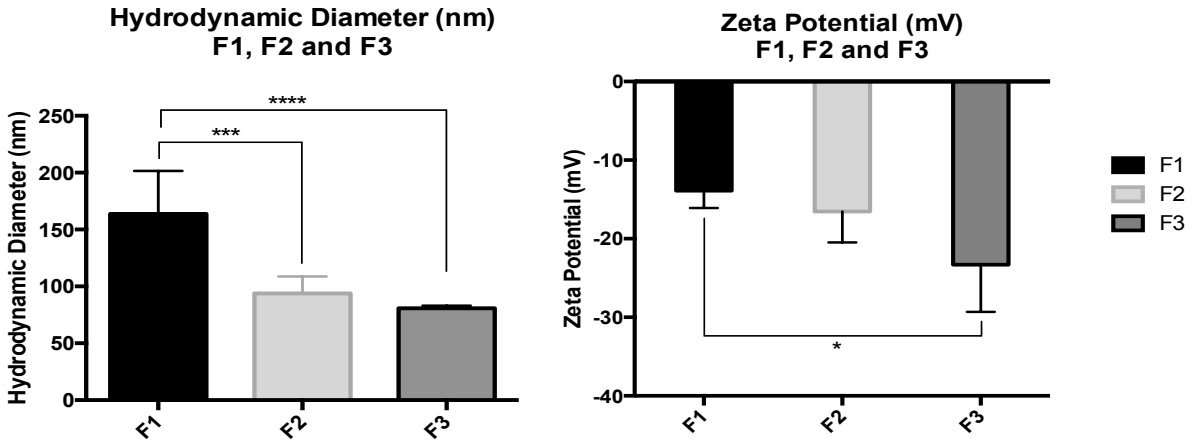

Figure 5.14: Droplet size and zeta potential values of F1, F2 and F3 depicting statistically significant results from Welch's Equality of Means test and Games-Howell post-hoc analyses. Statistically significant differences in size were seen between F1 and F2 (p=.0002) and F1 and F3 (p=.000004) while significant differences in zeta potential were seen between F1 and F3 (p=.03) Size histograms and zeta potential curves are depicted in **Figure D-14, Appendix D**.

suspension reference, though not a control in the true sense of the word, represents the pharmaceutical standard for prenatal supplement gelatin capsules currently on the market. To the best of our knowledge, there is no prenatal formulation currently in existence in microemulsion form. Thus, this suspension reference was compared against that of F1, F2 and F3 in order to determine any possible advantages to utilizing prenatal formulations in microemulsion form. In this manner, though not an *in vivo* test by any means, inferences regarding oral absorption may be made.[26] The reference used in this work is currently marketed as a commercial supplement and contains all the active ingredients of the current formulation, along with some additional active ingredients such as minerals. Details of the prenatal supplement reference along with its label claim may be found in **Table D-7**, **Appendix D**. Given that Formulations 1, 2 and 3 were unable to be filled into soft gelatin capsules, dissolution studies were conducted using 1 g of each formulation, along with an amount of the prenatal supplement reference equal to that of the label claim (1.556 g). Each formulation was introduced into black, PTFE caps, placed in the dissolution vessel then the apparatus set to stir. HPLC chromatograms for vitamin recovery via dissolution may be found in **Figure D-16, Appendix D.**

Water-soluble Active Ingredients

According to the USP[25], folic acid dissolution should be performed for 60 minutes using water as the medium. At least 75% of folic acid should be dissolved within 60 minutes. If this fails, the dissolution test should be repeated in 10 mM citric acid (pH 6). **Figure 5.15** displays the dissolution results for solely folic acid (Vitamin B_9) in water while **Figure 5.16** displays the dissolution results for both riboflavin (Vitamin B_2) and folic acid (Vitamin B_9) in water.

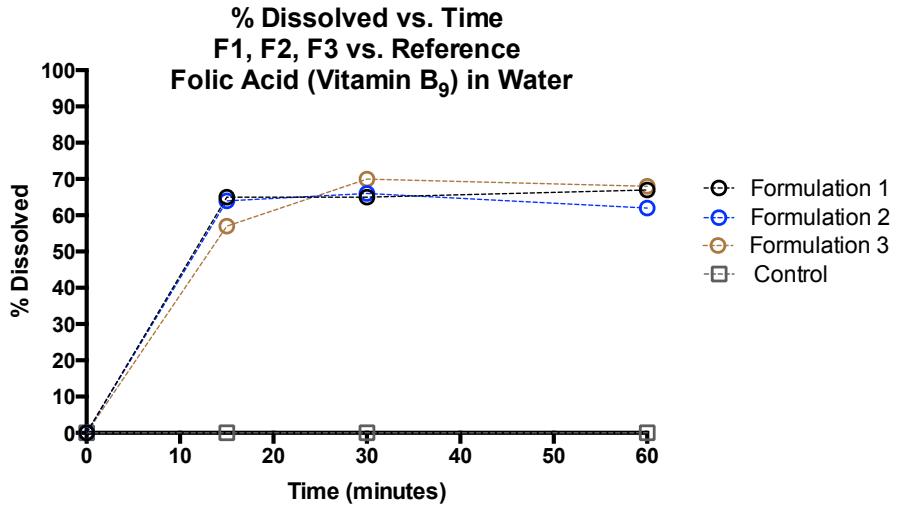

Figure 5.15: Dissolution results for folic acid (Vitamin B_9) in water from F1, F2, F3 and a suspension reference using USP Apparatus II (Paddle Method) at 100 RPM.

According to **Figure 5.15**, the percentage of folic acid dissolved in water after 60 minutes was 67%, 62% and 68% for Formulations 1, 2 and 3, respectively. In contrast, 0% folic acid was dissolved in and recovered from the prenatal suspension reference. These observations were supplemented by the cloudy, yellow dissolution media seen after 60 minutes in Formulations 1, 2 and 3 and the clear dissolution medium seen after 60 minutes with the suspension reference. A gradual increase in dissolved folic acid with time was observed with Formulation 1. However, for Formulations 2 and 3, the amount of dissolved folic acid reached its peak at 30 minutes with 66% and 70%, respectively. After this point, a decline in dissolved folic acid was noted. In all instances, within 15 minutes, 65% of the folic acid was dissolved in the case of Formulation 1 followed by 64% in Formulation 2 and 57% in Formulation 3. All results fell short of the USP required dissolution of at least 75% within one hour.[25] These results were not unexpected given the difficulty in dissolving folic acid (**Chapter 3**), as

well as its low water solubility (0.0761 mg/g).[33] However, more favourable dissolution results may have been obtained through the use of 0.1 N hydrochloric acid, as suggested by the USP.[25]

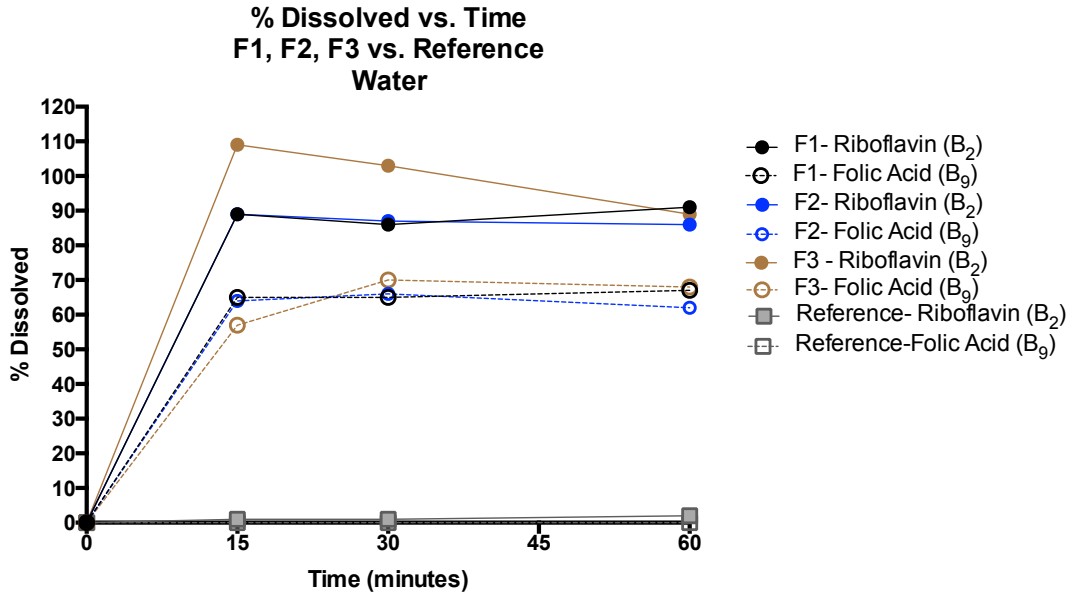

Figure 5.16: Dissolution results of riboflavin (Vitamin B_2) and folic acid (Vitamin B_9) in water from F1, F2, F3 and a suspension reference using USP Apparatus II (Paddle Method) at 100 RPM. Riboflavin= solid lines and closed circles; folic acid= broken lines and open circles.

Despite the unfavourable dissolution results for folic acid, riboflavin (Vitamin B_2) (**Figure 5.15)** exhibited highly satisfactory dissolution results in water as depicted in **Figure 5.16**. Within the first 15 minutes, 89%, 89% and 109% of riboflavin was dissolved in water from Formulations 1, 2 and 3 respectively. At the 60-minute mark, these values increased in the case of F1 to 91%, and decreased in the case of F2 and F3 to 86% and 89%, respectively. In the case of the suspension reference, the dissolution of riboflavin was slightly higher than seen in folic acid, with 2% dissolved within 60 minutes. Therefore, with the exception of the reference formulation, all microemulsion formulations passed USP acceptable criteria of at least 75% riboflavin dissolution within 60 minutes.

The improved dissolution of riboflavin, in comparison to folic acid, was not unexpected given the higher water solubility of the former, 0.657 mg/g[33]. In the case of both folic acid and riboflavin, though F1 demonstrated a steady increase in dissolution from 0 – 60 minutes, the dissolution of F3 was highly variable. Given that F1 and F3 differ only with respect to

surfactant type, this fluctuation must be attributed to Polysorbate 81, which is less hydrophilic than Polysorbate 80. In general, all microemulsion formulations demonstrated superior dissolution as compared to the suspension reference, lending credibility to claims of potentially improved bioavailability using microemulsion systems.

Given that the dissolution of folic acid was unfavourable in water, dissolution studies were re-performed in 10 mM citric acid buffer (pH 6), as suggested by the USP.[25] **Figure 5.17** displays dissolution results for both riboflavin (Vitamin B_2) and folic acid (Vitamin B_9) in 10 mM citric acid buffer (pH 6) for F1, F2, F3 and the suspension reference. The dissolution of folic acid was greatly improved through the use of citric acid medium. After 60 minutes, the percentage of dissolved folic acid in F1, F2 and F3 was 80 ± 8%, 73 ± 9% and 76 ± 14%, respectively. This increased to 84%, 86% and 85%, respectively after 120 minutes. No folic acid was dissolved in the reference formulation, even after 120 minutes. The dissolution curves for folic acid appeared less stable than those of riboflavin, especially in Formulations 2 and 3. Nevertheless, F1 and F3 passed USP criteria of at least 75% dissolution of folic acid within 60 minutes. Formulation 2 fell just 2% short of this threshold. However, 30 minutes later at the 90-minute mark, F1, F2 and F3 demonstrated large increases to 85%, 84% and 87% dissolution, respectively, which well exceeded the 75% dissolution criteria outlined by the USP. Overall, F1 demonstrated the highest degree of folic acid dissolution after 60 minutes at 80 ± 8%, likely as a result of the presence of the more hydrophilic surfactant, Polysorbate 80, which disperses favourably in the polar medium.

With respect to riboflavin, higher dissolution values than those of folic acid were obtained. The dissolution of riboflavin in F1, F2 and F3 after 60 minutes was 107 ± 10%, 99 ± 14 % and 107 ± 3%, respectively. In contrast, the dissolution of riboflavin in the reference suspension was close to 1 ± 0% dissolution after 60 minutes. The recovery of riboflavin in excess of 100% may be attributable to impurities. As evident in **Figure 5.17**, the majority of riboflavin was dissolved within the first 15 minutes. F1 and F3 also exhibited the smoothest and most stable dissolution curves for riboflavin in comparison to F2, where fluctuations were noted. This result is new for F3, which exhibited large fluctuations upon dissolution with water, suggesting that F3 with its less hydrophilic surfactant favours this slightly less polar medium. Overall, F1 and F3 equally demonstrated the highest degree of riboflavin dissolution after

60 minutes and all formulations passed USP criteria of at least 75% dissolution within 60 minutes.

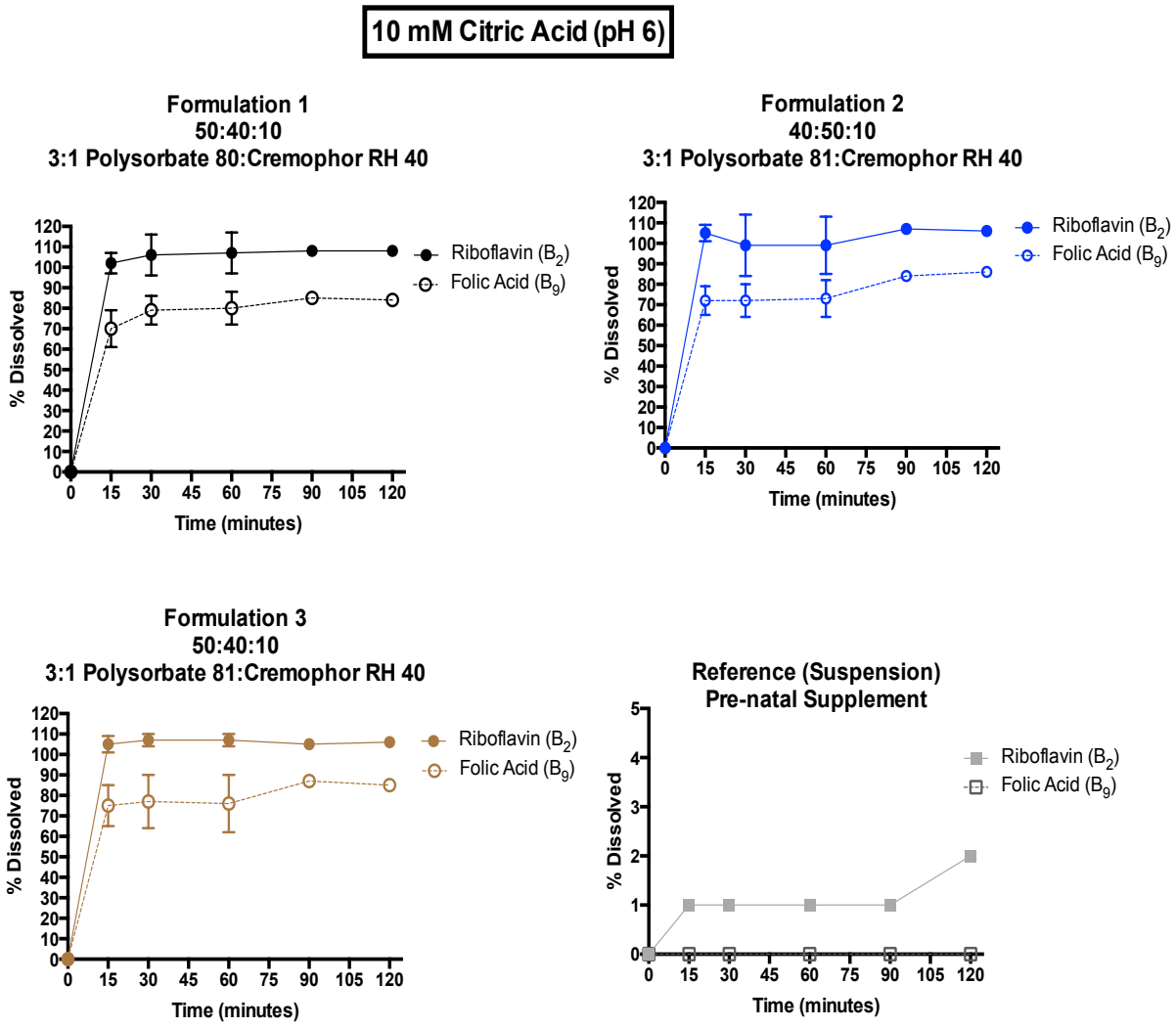

Figure 5.17: Dissolution results of riboflavin (Vitamin B_2) and folic acid (Vitamin B_9) in 10 mM citric acid buffer (pH 6) from F1, F2, F3 and a suspension reference using USP Apparatus II (Paddle Method) at 100 RPM.

An ordinary, one-way ANOVA comparing the effect of microemulsion formulation type on drug dissolution percentage in 10 mM citric acid (pH 6) medium revealed statistically significant differences in the dissolution of riboflavin (B_2) in F1, F2 and F3 samples at 15 [$F(3,1.7)= 699$, $p= .004$], 30 [$F(3,1.7)= 1180$, $p= .002$], and 60 minutes [$F(3,1.7)= 1641$, $p= .002$], as compared to the reference in 10 mM citric acid with 1% sodium dodecyl sulphate (SDS) surfactant. With respect to folic acid (B_9), a statistically significant effect of

microemulsion formulation type on drug dissolution percentage was also observed in F1, F2 and F3 samples at 15 [F(3,1.7)= 84.85, p= .021], 30 [F(3,1.7)= 64.74, p= .027], and 60 minutes [F(3,1.7)= 54.05, p= .031], as compared to the reference formulation in 10 mM citric acid in 1% SDS. Homogeneity of variance, as evaluated by Levene's F-test, was violated in all cases due to the near zero dissolution percentages and variance of the reference formulation. As a result, all p-values reported were derived from the Welch's test rather than a standard ANOVA, with a Games-Howell post-hoc analysis. The results from the post-hoc analyses, including statistical significance, are depicted in **Figure 5.18**. Statistics are fully reported in **Table D-8, Appendix D.**

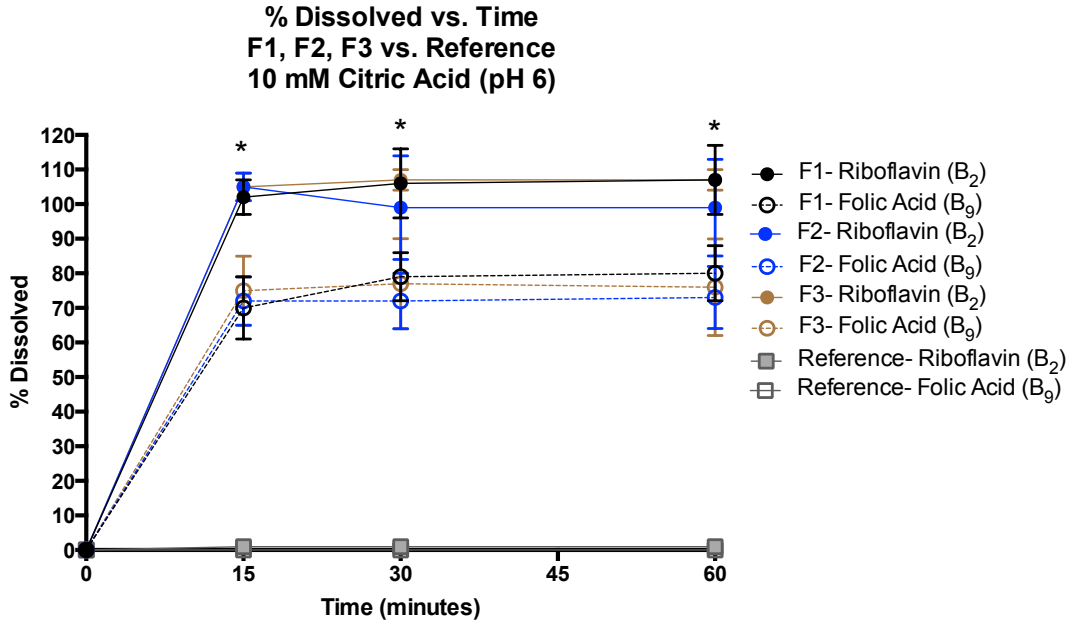

Figure 5.18: Combined dissolution results of riboflavin (Vitamin B_2) and folic acid (Vitamin B_9) in 10 mM citric acid buffer (pH 6) from F1, F2, F3 and a suspension reference using USP Apparatus II (Paddle Method) at 100 RPM. Statistical differences using the Welch's test with Games-Howell post-hoc analysis are depicted here. Significance stars are representative of F1, F2 and F3 as a collective, in comparison to the reference formulation. Compared to the reference formulation, all formulations demonstrated statistically significant differences at 15 (p=.021), 30 (p=.027) and 60 (p=.031) minutes.

The differences in the dissolution of folic acid as compared to riboflavin are visually evident in **Figure 5.18.** A degree of fluctuation was seen from 15 to 60 minutes in F2 and F3. The dissolution curve of F1 by comparison, appeared more stable. In all microemulsion samples, dissolution values plateaued and stabilized from the 90 to 120-minute mark. This

stabilization was not seen in the suspension reference, however. Rather, a small increase in dissolved riboflavin was seen at the 120-minute mark suggesting that this suspension formulation may require additional time for complete dissolution of both riboflavin and folic acid.

Although all microemulsion formulations demonstrated favourable dissolution of riboflavin, only F1 and F3 demonstrated USP-acceptable dissolution criteria of folic acid in 10 mM citric acid buffer (pH 6). Thus, dissolution was also performed using phosphate buffer, as previously outlined in the USP.[34] **Figure 5.19** depicts the dissolution results of riboflavin and folic acid from F1, F2, F3 and the suspension reference in 50 mM phosphate buffer (pH 7.4). In comparison to water and citric acid, dissolution curves in phosphate buffer were remarkably more stable. In addition, favourable dissolution results were obtained for folic acid. Within the first 15 minutes, 75 ± 1%, 76 ± 8% and 82 ± 4% of folic acid was dissolved from F1, F2 and F3 respectively, meaning that all microemulsion formulations passed USP dissolution criteria within the first 15 minutes. At the 60-minute mark, 81 ± 8%, 75 ± 10% and 80 ± 8% folic acid was dissolved in F1, F2 and F3, respectively. Aside from F3, the dissolution curves for folic acid were smooth and steady. Unfortunately, the reference suspension still exhibited 0% dissolution of folic acid even after 120 minutes.

With respect to riboflavin, 93 ± 5%, 95 ± 2% and 102 ± 1% dissolution was observed within the first 15 minutes for F1, F2 and F3, respectively. This increased to 98 ± 5%, 92 ± 12% and 104 ± 0% after 60 minutes. The dissolution of riboflavin was 1 ± 0% at the 15- and 60- minute mark, but this increased to 1.5 ± 1% at the 90-minute mark and 2 ± 0% at the 120-minute mark.

An ordinary, one-way ANOVA comparing the effect of microemulsion formulation type on drug dissolution percentage in 50 mM phosphate buffer (pH 7.4), revealed statistically significant differences in the dissolution of riboflavin (B_2) in F1, F2 and F3 samples at 15 [$F(3,1.7)= 8341$, $p< .001$], 30 [$F(3,1.7)= 8255$, $p< .001$], 60 [$F(3,2)= 4.2*10^7$, $p< .001$] and 90 minutes [$F(3,1.8)= 6968$, $p< .001$], as compared to the reference formulation. With respect to folic acid (B_9), a statistically significant effect of microemulsion formulation type on drug dissolution percentage was also observed in F1, F2 and F3 samples at 15 [$F(3,1.7)= 12.81$, $p= .002$], 30 [$F(3,1.7)= 163.4$, $p= .012$], 60 [$F(3,1.7)= 89.88$, $p= .020$] and 90 minutes [$F(3,1.7)= 77.4$, $p= .023$], as compared to the reference. Homogeneity of variance was violated in all cases

due to the near zero variance of the reference formulation. As a result, all p-statistics reported are derived from the Welch's test with Games-Howell post-hoc analysis. The results from the post-hoc analyses of F1, F2 and F3 versus the reference formulation are depicted in **Figure 5.19**. All statistical values are fully reported in **Table D-9, Appendix D.**

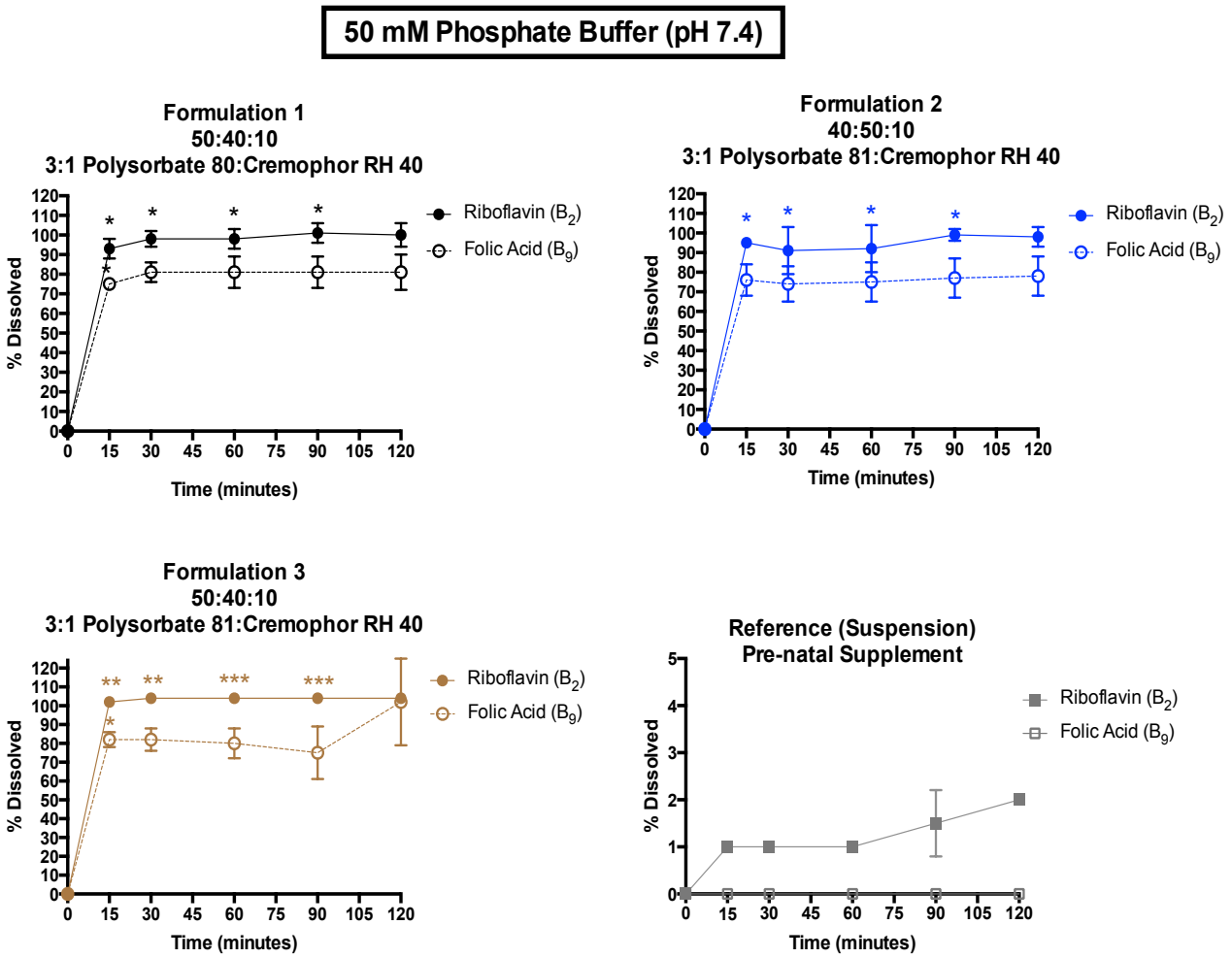

Figure 5.19: Dissolution results of riboflavin (Vitamin B_2) and folic acid (Vitamin B_9) in 50 mM phosphate buffer (pH 7.4) from F1, F2, F3 and a suspension reference using USP Apparatus II (Paddle Method) at 100 RPM. Statistical significance using the Welch's test with Games-Howell post-hoc analysis is depicted here. Significance stars are representative of F1, F2 and F3 as compared to the reference formulation.

Combined dissolution curves of both riboflavin and folic acid for F1, F2, F3 and the reference are depicted below in **Figure 5.20**. A reduced distance, and thus, smaller difference between dissolution curves of riboflavin and folic acid, in comparison to those in water and

citric acid media, was evident. In addition, the steadiness and smoothness of the dissolution curves were superior. Overall, dissolution of riboflavin was highest in F3 (102 ± 1%) while dissolution of folic acid was highest and similar in both F1 and F3 (81 ± 4% and 82 ± 5%, respectively). Considering both dissolution profiles for riboflavin and folic acid, the dissolution medium demonstrating the most promising dissolution results was 50 mM phosphate buffer (pH 7.4). The higher pH of this medium in comparison to that of water and citric acid buffer (pH 6), likely resulted in enhanced dissolution of these APIs, given that higher pH values were required for solubility.

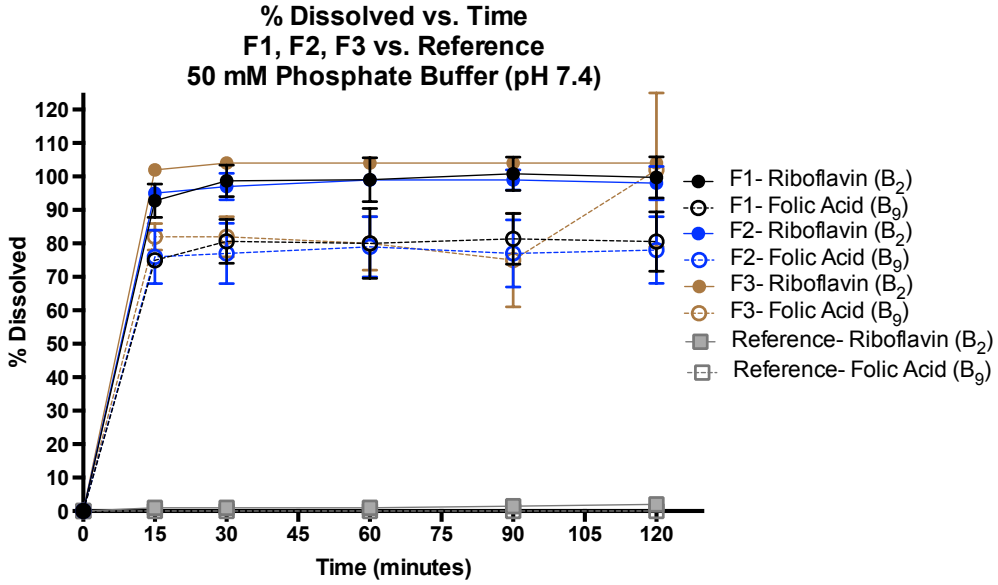

Figure 5.20: Conglomerated dissolution results of riboflavin (Vitamin B_2) and folic acid (Vitamin B_9) in 50 mM phosphate buffer (pH 7.4) from F1, F2, F3 and a suspension reference formulation using USP Apparatus II (Paddle Method) at 100 RPM.

Overall, Formulations 1, 2 and 3 exhibited similar drug dissolutions in citric acid and phosphate buffer media. One way of quantifying the similarities and differences in dissolution curves is through the use of the $f1$ difference factor and $f2$ similarity factor. Developed by Moore and Flanner (1996)[35], $f1$ and $f2$ are a simple model independent approach to comparing two dissolution profiles at every dissolution sample time point.[36] The difference factor, $f1$, calculates the difference in percent between two dissolution curves at each time point:[35,36]

$$f1 = [\Sigma_{t=1}^{n} \left(\frac{|R-T|}{R}\right)) * 100] \qquad \textbf{(Eq. 5.1)}$$

where n is the number of time points, t is time (typically, minutes), R is the percentage of drug dissolved in the reference formulation (%) and T is the percentage of drug dissolved in the test formulation (%).

In contrast, the similarity factor $f2$, is a measurement of the similarity in percent between two dissolution curves.[36] It is the logarithmic reciprocal square root transformation of the sum of the squared error.[35,36]

$$f2=50 * log\left[\frac{100}{\sqrt{1+\left(\frac{\sum_{t=1}^{n}(R-T)^2}{n}\right)}}\right] \quad \textbf{(Eq. 5.2)}$$

where all variables are the same as defined above.

In general, the mean dissolution values from both reference and test curves at each time interval are used; two curves are determined to be similar or equivalent when $f1$ is less than 15% and $f2$ is greater than 50%.[36] In addition, the FDA stipulates that only one measurement over 85% dissolution be considered, as this is the threshold for acceptable dissolution.[36] Therefore, in this work, values above 85% were excluded. **Table 5.7** presents $f1$ and $f2$ values for all formulations tested in this work, as compared to the reference formulation and Formulation 1 (F1). Only folic acid curves were considered given that more than 85% dissolution was achieved for riboflavin.

In the case of citric acid medium, the dissolution curve with the largest difference when compared to the prenatal reference formulation was F1, followed by F3 then F2. F3 was also more similar to the current formulation (F1) than F2. With respect to phosphate buffer medium, the dissolution curve with the highest deviation from that of the prenatal reference formulation was F3 followed by F1 and F2. In addition, the formulation most similar to F1 was F2 followed by F3. In general, all microemulsion formulations (F1, F2 and F3) exhibited equivalence ($f1$ <15%, $f2$ >50%). Thus, the process of surfactant selection for microemulsion, multi-drug delivery culminated in the manufacture of three successful formulations with similar dissolution profiles. $f1$ values for the reference formulation could not be computed due to the fact that the dissolution of folic acid was 0% was in both media. All raw and calculated values are reported in **Table D-10, Appendix D**.

Table 5.7: $f1$ and $f2$ factor values for all tested formulations after folic acid dissolution. The prenatal suspension reference formulation is labeled as the 'control'.

Media	Reference Sample	Test Sample	Time Points Analyzed (mins)	$f1$ Difference Factor	$f2$ Similarity Factor
10 mM Citric Acid (pH 6)	F1	F2	0-60	6.98	61.4
	F1	F3	0-60	4.80	69.9
	Control	F1	0-60	N/A	5.82
	Control	F2	0-60	N/A	7.03
	Control	F3	0-60	N/A	5.96
50 mM Phosphate Buffer (pH 7.4)	F1	F2	0-120	3.17	75.9
	F1	F3	0-90	4.68	65.5
	Control	F1	0-120	N/A	4.97
	Control	F2	0-120	N/A	5.56
	Control	F3	0-90	N/A	1.77

Oil-soluble Active Ingredients

As stated previously in **Section 5.1.2.1**, with respect to multivitamin supplements there is no USP requirement for the dissolution of fat-soluble vitamins as it is well-known that these active ingredients are highly lipophilic and do not dissolve well in polar media. In addition, low permeation is generally not of concern with organic compounds and is not considered the rate-limiting step of absorption.[26] Nevertheless, dissolution testing was performed in an attempt to determine whether fat-soluble APIs could be dissolved and recovered. Given that the water-soluble active ingredients performed well in phosphate buffer, 50 mM phosphate buffer as well as 100 mM tris buffer were selected as the dissolution media. Beta-carotene was selected as the 'index' vitamin given that it was the most lipophilic API used in this work, and sensitive to degradation via light and oxygen (**Chapter 3**). Non-ionic surfactants were introduced to the dissolution media given the high lipophilicity of beta-carotene, as suggested by de Souza Anselmo et al. (2016).[37] **Figure 5.21** depicts the percentage of dissolved beta-carotene after 60 minutes in F1 and F2, the formulations that yielded the most and least favourable dissolution results thus far, respectively.

In general, higher recoveries of beta-carotene were seen in F1 than in F2. This was interesting given that F2 contains 50% w/w oil versus 40% w/w oil in F1. However, the use of a less hydrophilic surfactant, Polysorbate 81, in a lower concentration (40% w/w) than that of

F1, may likely have led to a lower degree of oil solubilization. Nevertheless, the lowest dissolution value obtained was still quite high, at 81% after 60 minutes. Given that beta-carotene was successfully dissolved, it was inferred that other less lipophilic APIs in F1 and F2 could also be dissolved.

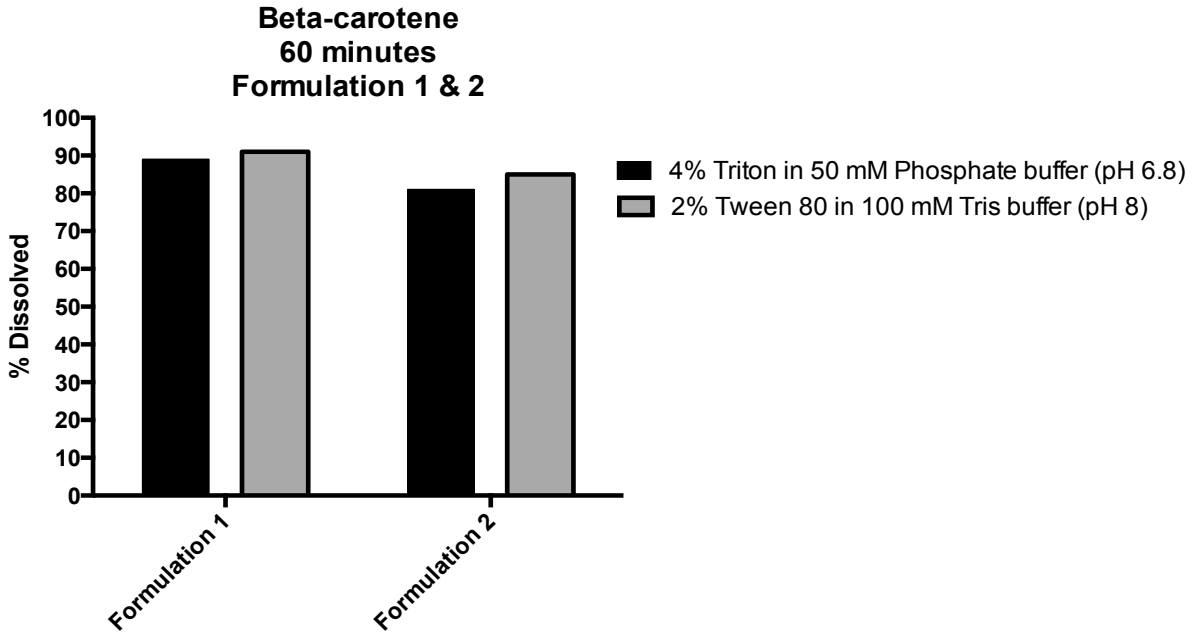

Figure 5.21: Dissolution results of beta-carotene (Vitamin A) in 4% Triton-X-100 50 mM phosphate buffer (pH 6.8) and 2% Polysorbate 80 in 100 mM Tris buffer (pH 8) from F1 and F2 using USP Apparatus II (Paddle Method) at 100 RPM.

Figures 5.15 to **5.21** illustrated results from multiple dissolution trials performed on F1, F2 and F3. Despite variations in dissolution media, some generalizations were noted. In all cases, riboflavin demonstrated a much higher degree of dissolution than folic acid. This was not surprising given the low water solubility of folic acid in comparison to riboflavin. The dissolution media producing the best result was 50 mM phosphate buffer (pH 7.4). This was expected given the slightly alkaline favorability demonstrated by both riboflavin and folic acid, and the fact that this medium possessed the highest pH value of all media tested. Of all microemulsion formulations tested, F1 and F3 demonstrated the highest recoveries while F2 demonstrated the lowest. The inability of the suspension reference to surpass 2% dissolution was unexpected. It is evident that the dissolution media and conditions utilized in this work were insufficient to afford the dissolution of riboflavin or folic acid in this reference

formulation. However, it was interesting to note that given the presence of lecithin in the suspension formulation, a surface active molecule by nature, greater dissolution of either active ingredient was not observed. The low HLB value of lecithin may have been insufficient to solubilize all actives in the dissolution media. Although dissolution media are not an absolute reflection of physiological conditions due to variations in the GI tract such as flora, digestive enzymes, pH, transit time and whether in fed or fasted state[26], the results from these dissolution studies indicate a potential benefit to the use of microemulsion systems for this type of multi-drug delivery.

5.5.2.3. Disintegration

Originally, microemulsion formulations were to be developed and filled into soft gelatin capsules for dissolution and disintegration testing. However, given the water content of this formulation and the possible risk of water migration into the shell of the soft gelatin capsule along with other factors, this process was unable to be performed. Instead, each microemulsion formulation was filled into 18 mm oblong, red, opaque hard-gelatin capsules before disintegration testing. **Figure 5.22** depicts the disintegration test and apparatus in progress (in amber lighting) while **Figure 5.23** presents the disintegration results for F1 and F2, the microemulsion formulations demonstrating the most and least favourable dissolution results, respectively.

Upon introduction of F1 and F2-filled capsules, a colour change was seen in the vessel containing hydrochloric acid. (**Figure 5.22**) This colour change was likely due to isomerization of beta-carotene in the presence of strong acid[38] leading to a reduction in colour intensity.[39] From **Figure 5.23,** both dosage forms successfully achieved disintegration within 30 minutes, as required by the USP.

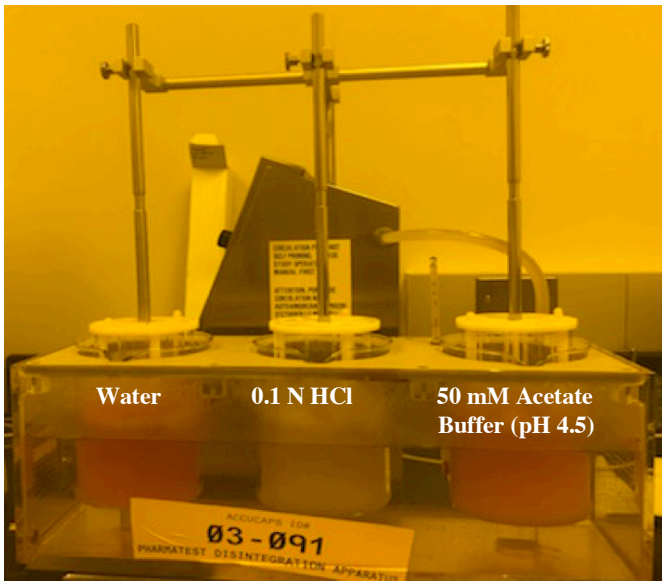

Figure 5.22: Disintegration test in progress for hard-shell gelatin capsules filled with F1 and F2. Three media were tested: i) water, ii) 0.1N hydrochloric acid and iii) 50 mM acetate buffer (pH 4.5)

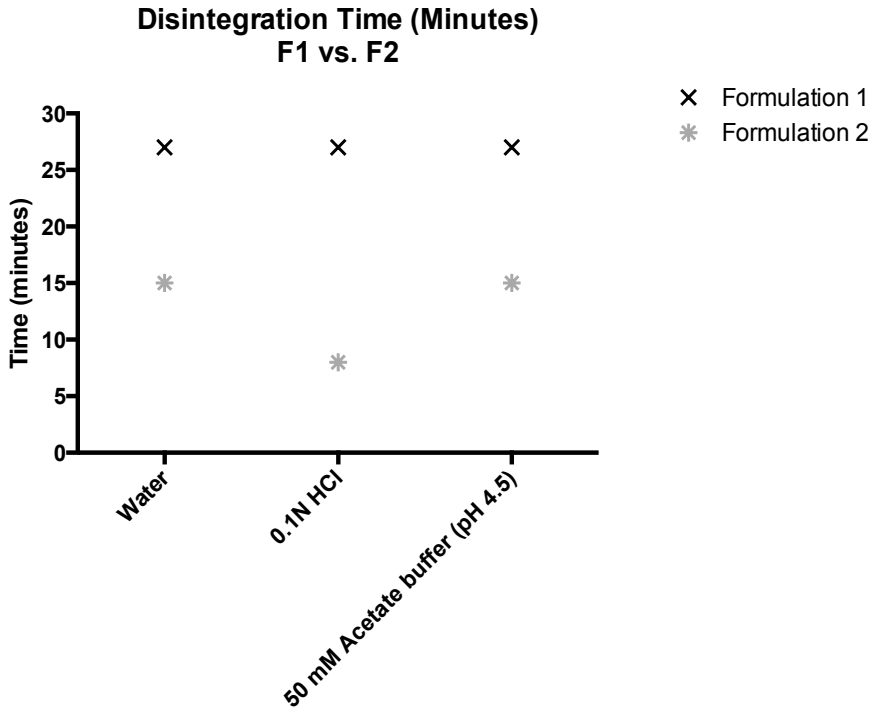

Figure 5.23: Disintegration results of hard-shell gelatin capsules filled with F1 and F2 tested in three media: i) water, ii) hydrochloric acid and iii) acetate buffer

5.5.2.4. Stability

5.5.2.4.1. Temperature: Freeze-thaw Cycle

After three consecutive cycles of freezing at -25°C for 24 hours, followed by thawing to room temperature for 24 hours, no evidence of phase separation was seen in F1, F2 or F3. Despite no evidence of phase separation, F1 appeared progressively cloudy after each consecutive cycle, with tiny yellow/orange precipitates dispersed throughout upon close examination. No such changes were observed in F2 and F3. **Figure 5.24** depicts changes in hydrodynamic diameter and zeta potential after exposure to three freeze-thaw cycles. F1 showed a droplet size reduction of just over 30% while zeta potential values increased by more than 3 mV and became less negative, indicating decreased stability. In contrast, F3 showed a droplet size increase of over 40% while zeta potential values remained relatively constant. F2 showed stable droplet size and zeta potential values before and after treatment. Size histograms and zeta potential curves are depicted in **Figure D-17, Appendix D**.

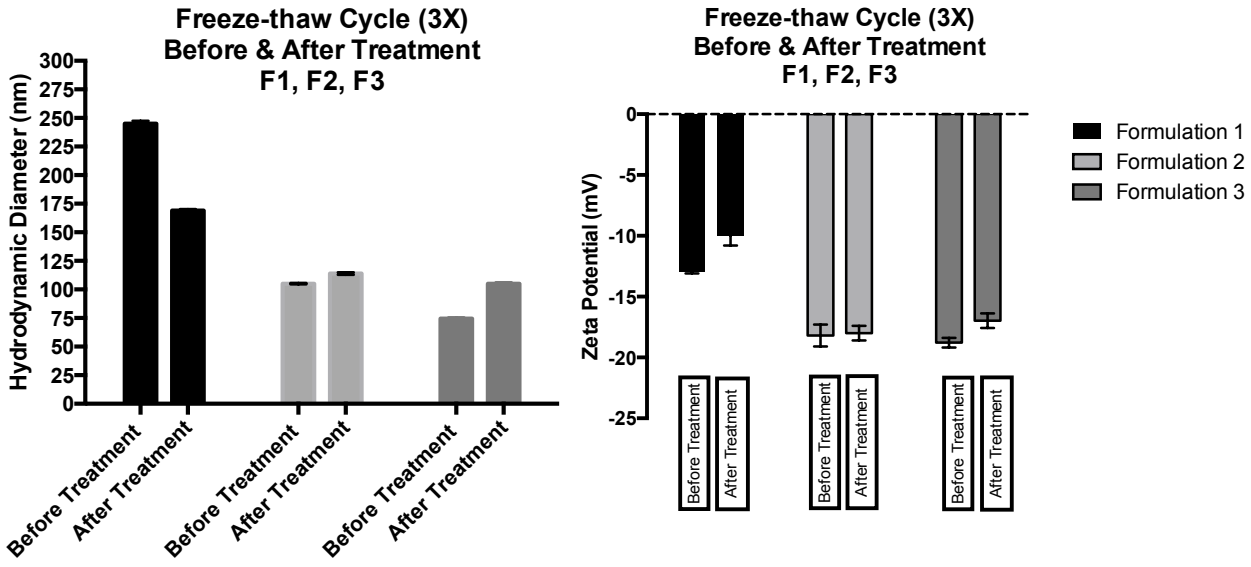

Figure 5.24: Hydrodynamic diameters (left) and zeta potentials (right) of microemulsion formulations F1, F2 and F3 before and after three consecutive freeze-thaw cycles from -25°C to room temperature.

The rationale for the decrease in droplet size and increase in zeta potential in F1 has been previously explored in **Chapter 4**. However, the increase in droplet size experienced in F3 (and F2 to a low degree), is consistent with literature reports that freeze-thawing in microemulsion systems may lead to eventual phase separation.[40] This drive towards phase

separation leads to a gradual increase in droplet size as droplets coalesce.[40] Despite these observations, there was no visual evidence of phase separation after three freeze-thaw cycles in F2 and F3. The stability of the zeta potential values in F2 and F3 was also surprising despite the occurrence of possible phase separation. However, it could be that droplet sizes increased at a slow rate so as to not affect the charged APIs localized around the surfactant head groups. Overall stability appeared to follow the trend F2> F3> F1, with F2 exhibiting the greatest resistance to size and zeta potential changes.

5.5.2.4.2. Temperature: Heat Cycle

After exposure to 48 hours of heating at 37°C, there were indications of cloudiness in all formulations with F1 being the most turbid. This turbidity decreased in all samples at 50°C as the formulations began to phase separate; an upper clear, orange phase and lower phase containing precipitate were observed. At this temperature, a gradual darkening of sample from red-brown to brown-black was also seen until 80°C. At 60°C-70°C, phase separation was evident and the presence of solid, yellow precipitate was observed at the bottom of the vial in F1. At 80°C, this lower layer of solid API appeared to disappear completely, likely due to degradation. In addition, lower amounts of yellow precipitate were evident in F2 and F3. **Figure 5.25** depicts changes in hydrodynamic diameter after 48-hour consecutive heating cycles at 37°C, 50°C, 60°C, 70°C and 80°C. It is evident that F1 experienced a larger variation in size from room temperature to 80°C than F2 and F3. In F1, a size decrease of 37% was experienced at the first temperature point. The droplet sizes remained depressed throughout additional heating cycles with a final size reduction of approximately 28% (60 nm) at 80°C. F2 and F3 experienced less droplet size fluctuations than F1 upon consecutive heating. F2 exhibited a 13% decrease in size after the first temperature point, culminating in a final size at 80°C that was equivalent to room temperature. F3 exhibited virtually no change in size after the first temperature point and a final droplet size increase of 24% (21 nm) at 80°C.

Prolonged heating of all formulations resulted in colour changes and eventual phase separation beginning at 50°C and reaching its maximum at 70°C. Possible explanations for the droplet size trends and colour changes obtained have been previously explored for F1 in **Chapter 4** and may be extended to F2 and F3 given the similarity in formulation. However, from room temperature to 80°C, the droplet size differences of 2 nm and 21 nm experienced

by F2 and F3, respectively, were considered negligible. Both formulations demonstrated greater heat stability than F1.

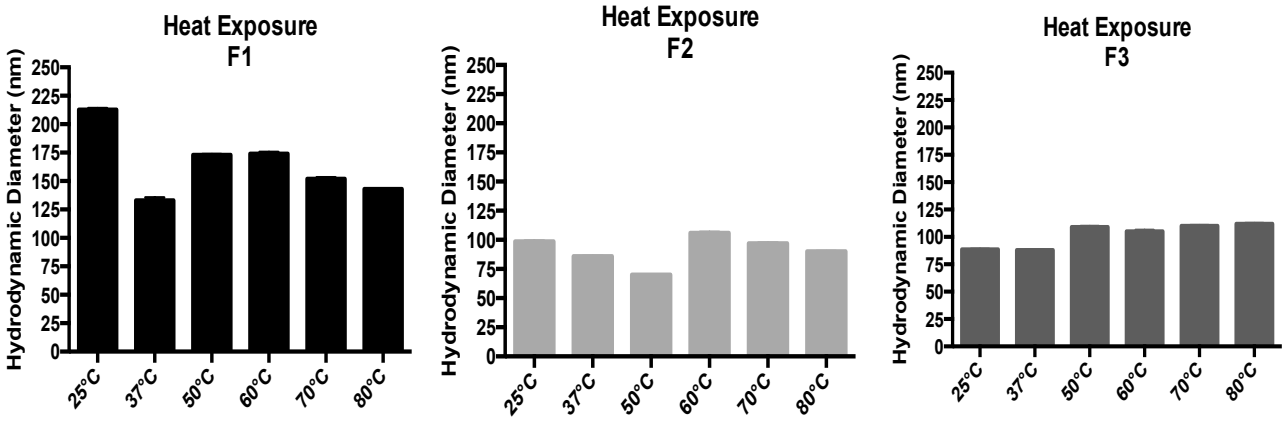

Figure 5.25: Hydrodynamic diameters of microemulsion formulations F1, F2 and F3 before and after consecutive heating from 25°C - 80°C. Size histograms are depicted in **Figures D-18 – D-20, Appendix D**.

Figure 5.26 depicts the change in zeta potential of F1, F2 and F3 upon heating. In general, zeta potential values increased or became less negative for F1 as described in **Chapter 4**. However, F2 and F3 experienced a steady decrease in zeta potential, becoming more negative and eventually plateauing between 60-70°C before increasing (becoming less negative) at 80°C. Particularly around 60-70°C, zeta potential values for all formulations were observed to be at their lowest (most negative), indicating greatest stability from a colloidal perspective. At these temperatures, formulations demonstrated notable colour changes and phase separation. It is, thus, possible that thermal oxidation of some of the lipophilic APIs occurred resulting in the increased presence of negatively-charged fatty acid products[41] as described in **Chapter 4.**

Overall, F1 experienced a maximum zeta potential change of 8 mV throughout all heating cycles while F2 and F3 experienced a maximum change of 20 mV and 15 mV, respectively. Thus, based on this consideration, it would appear that F1 demonstrated greater resistance to zeta potential changes upon heating while F2 and F3 demonstrated greater resistance to size changes upon heating.

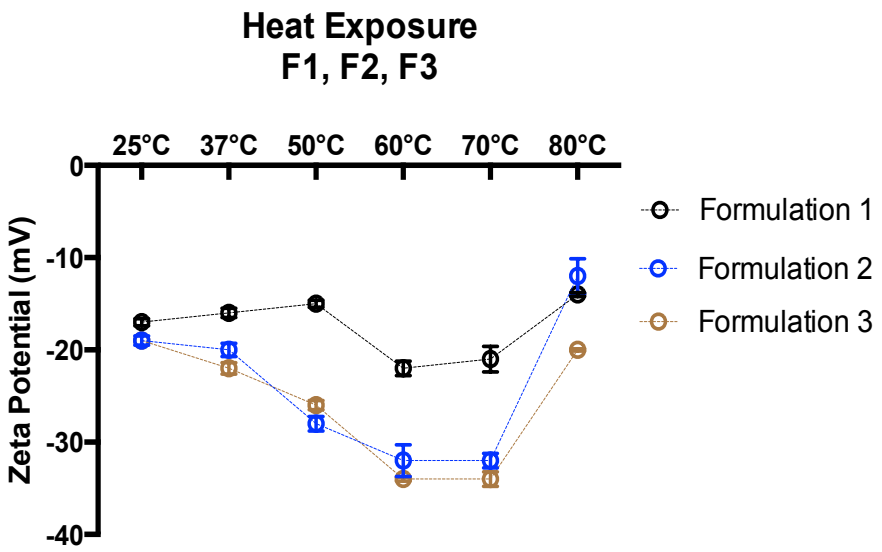

Figure 5.26: Zeta potential values of microemulsion formulations F1, F2 and F3 before and after consecutive heating from 25°C - 80°C. Zeta potential curves are depicted in **Figures D-18- D-20, Appendix D**.

5.5.2.4.3. Light Exposure Test

The beginnings of phase separation were immediately observed upon exposure to fluorescent light after just 24 hours, and this became more pronounced at day 5. From this point forward, phase separation was observed in all samples at the one-week, two-week and one-month marks- the latter of which demonstrated the greatest separation. A gradual darkening in colour was also seen beginning at the two-week mark though not to the extent of that seen during the heating cycle. **Figure 5.27** illustrates the gradual phase separation experienced by F1, F2 and F3 after exposure to light over a one-month period.

Figure 5.28 depicts droplet sizes and zeta potentials of F1, F2 and F3 before and after exposure to fluorescent light for one month. Droplet sizes reduced by 37% after 24 hours for F1, but by only 12% for F2 and 17% for F3. In all formulations, zeta potential values were least negative 24 hours after exposure to fluorescent light. F1 experienced a reduction of 5 mV, F2 6 mV and F3 13 mV, indicating peak instability at this time point. In general, all formulations showed the largest fluctuations in droplet size during the first five days of exposure to light. After this point, droplet size values appeared to stabilize and plateau. The fluctuation in droplet size and zeta potential up to day 5 corresponds to the phase separation seen in all formulations beginning at day 5 as depicted in **Figure 5.27**. Zeta

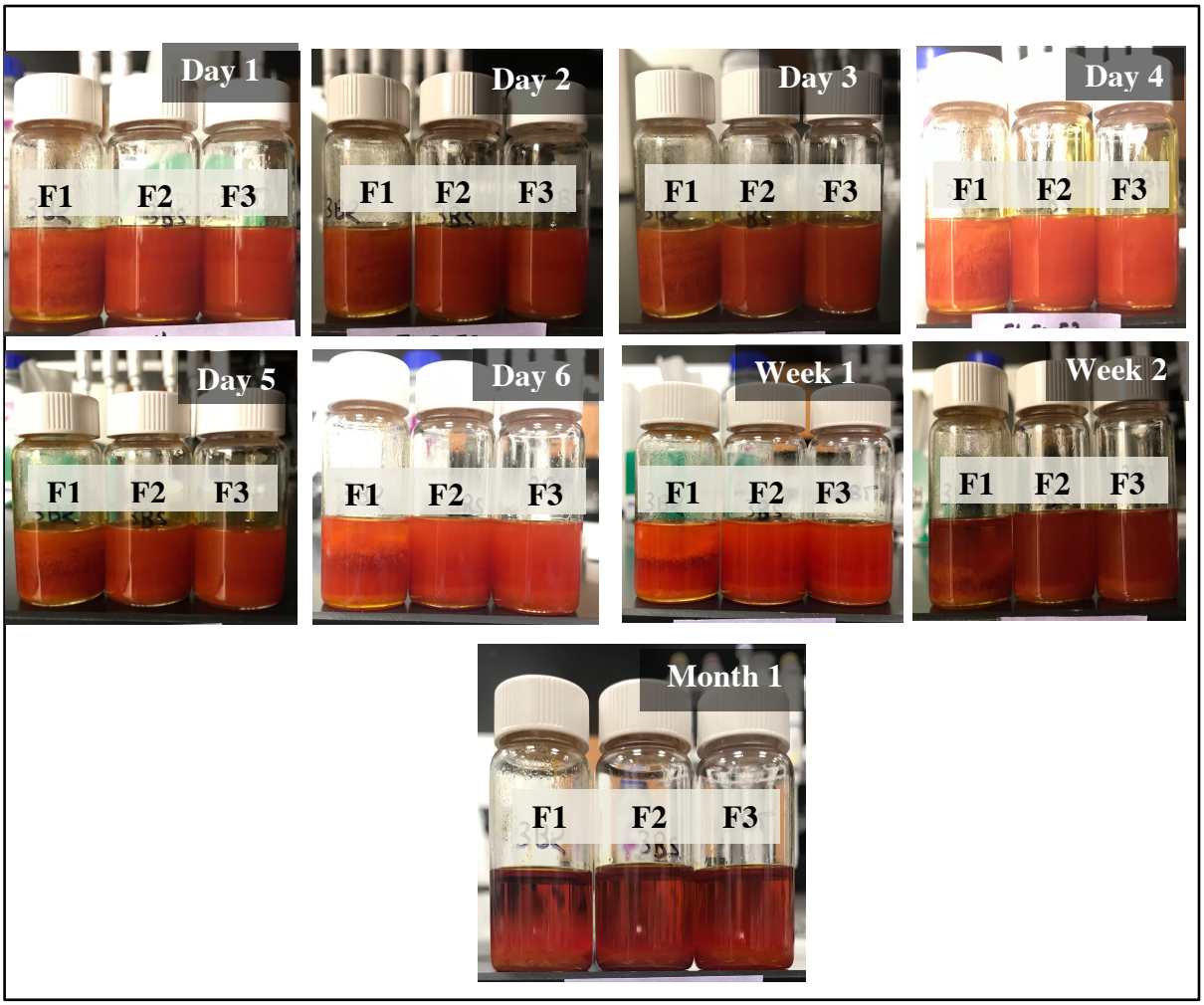

Figure 5-27: Phase separation in microemulsion formulations F1, F2 and F3 after exposure to light over the period of one month.

potential values also exhibited this trend with the exception of day 14 results, which show an increase in negatively charged droplets. This coincides with the darkening of samples also observed at day 14 (**Figure 5.27**), which could correspond to the oxidation of fatty acids, yielding more negative charges in the same manner as seen during the heating cycle. In addition, many active ingredients in this formulation have been reported to undergo colour changes upon light exposure. With respect to water-soluble vitamins, Vitamin B_1 has been reported to form thiochrome upon exposure to light and Vitamins B_2 and B_{12} have been reported to undergo decolouration due to photolysis.[42] With respect to fat-soluble vitamins, tocopherols have been reported to oxidize and darken upon exposure to air and light.[43] The presence of multiple light-sensitive APIs in F1, F2 and F3, results in vulnerability to light exposure as

described in **Chapter 4**. However, overall, F3 exhibited the highest tolerability to light exposure given its moderate droplet size and zeta potential fluctuations, followed by F2 then F1.

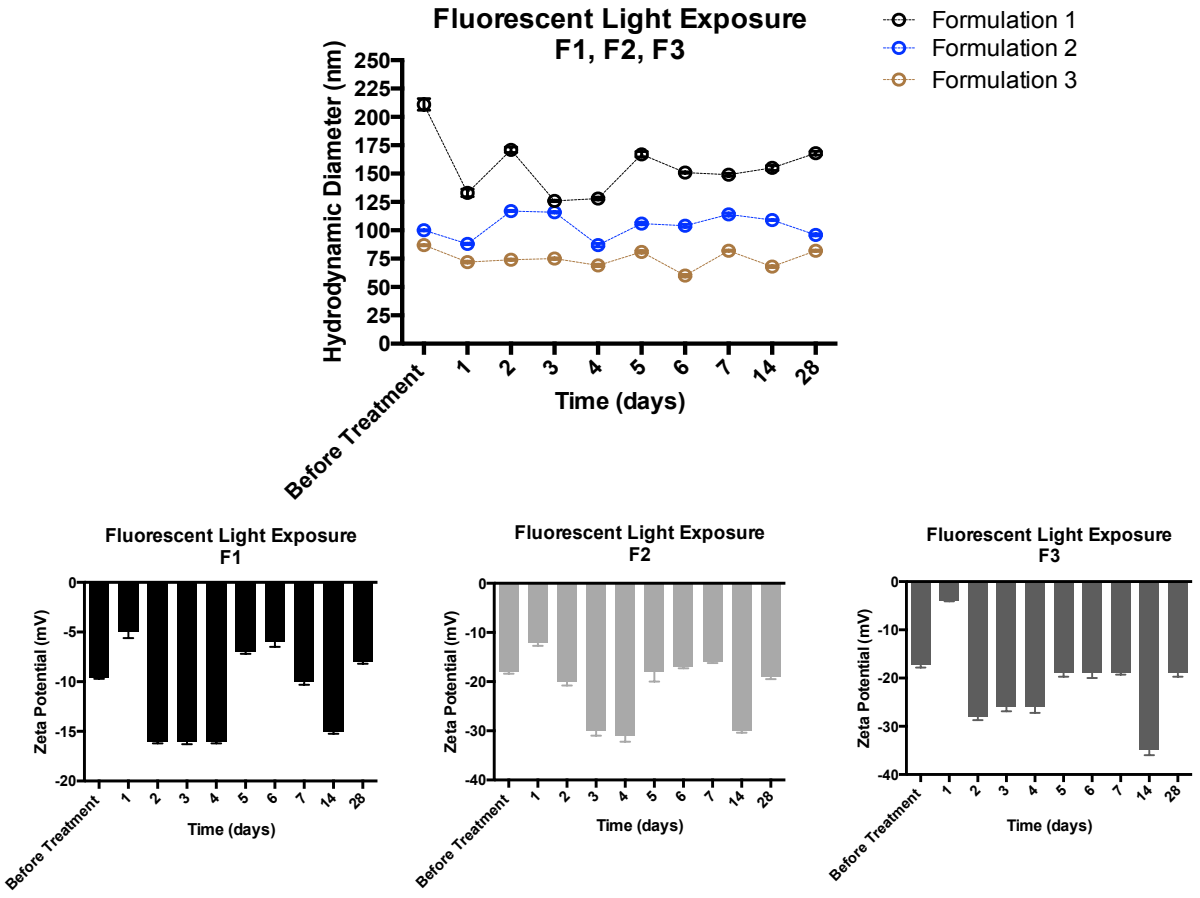

Figure 5.28: Hydrodynamic diameters and zeta potential values for microemulsion formulations F1, F2 and F3 after exposure to light over the period of one month. Size histograms are depicted in **Figures D-21 – D-23, Appendix D**.

5.5.2.4.4. pH Stability

Figure 5.29 depicts pH changes in F1, F2 and F3 over the course of 1 month. According to **Panel A**, pH values were not only stable throughout this time period, but remarkably close to each other despite the differences in surfactant composition. A slight downward trend in pH was seen beginning at the 7-day mark, similar to that seen in F1 in **Chapter 4.** These small decreases continued until the 28-day mark as depicted by **Panel B**, where the y-axis is

expanded. A decrease in pH of approximately 0.92 units for F1, 1.23 units for F2 and 1.12 unit for F3 was noted. The initial pHs for F1, F2 and F3 were 8.8, 9.0 and 9.0, respectively, while the pHs at the end of one month were 7.8, 7.7 and 8.0. This decrease in pH is not surprising given the presence of a pH-adjusted, drug-loaded water phase and the absence of buffer. Therefore, this decrease may be attributed to the formulation equilibrating itself.

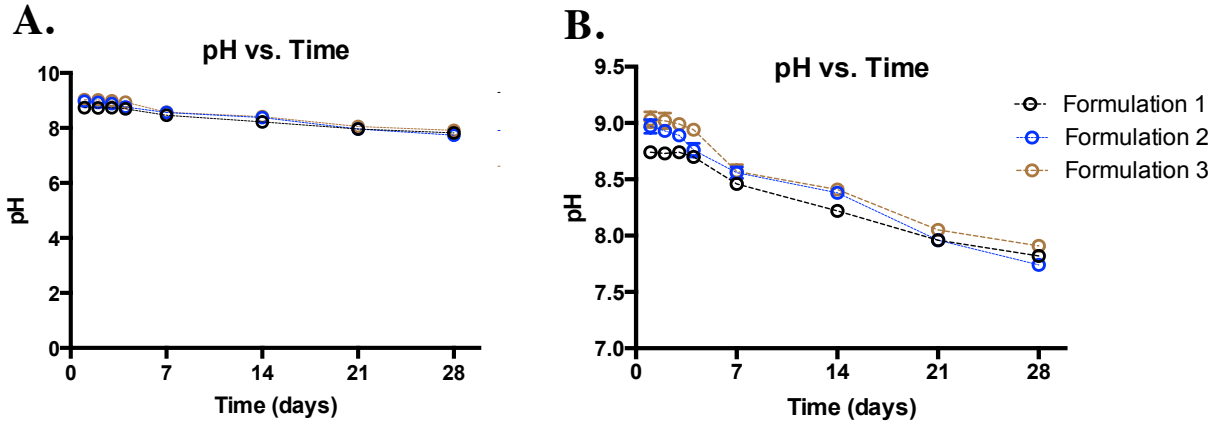

Figure 5.29: pH changes in F1, F2 and F3 at room temperature over the course of 4 weeks on a pH scale of 0-14 (Panel A). This scale was expanded (B) in order to better visualize changes.

F1 exhibited the smallest change in pH over the course of one month versus that of F2 and F3. Nevertheless, all formulations displayed pH resilience and stability, despite the presence of differing surfactants in each formulation. These results suggested that the surfactant phase plays little role in the pH stability of these microemulsion formulations, and that the active ingredients, themselves, were likely of greater importance.

5.5.2.4.5. Conductivity Test

Figure 5.30 depicts the change in conductivity of F1, F2 and F3 immediately after formulation to one week later. Conductivity of all formulations remained low, below 5 µS/cm, from the time of manufacture to one week later. However, despite these overall low conductivity values, F1 possessed a higher value than that of F2 and F3. The average conductivity of F1 was 4.07 µS/cm with a maximum difference of 1.47 µS/cm experienced over the course of one week. In contrast, the average conductivities of F2 and F3 were 0.01 µS/cm and 0.00 µS/cm, respectively. Upon 100x aqueous dilution, however, conductivities of F1, F2 and F3 were 58

± 21 µS/cm, 46 ± 28 µS/cm and 35 ± 25 µS/cm, respectively. In general, conductivity values of F2 and F3 were consistent and did not exhibit any observable fluctuations in value.

Similar to results in **Chapter 4**, conductivity values for F1, F2 and F3 were within expected ranges for bicontinuous microemulsions where both oil and water serve as the continuous phase. However, the lower conductivity values of F2 and F3 may be attributable to the presence of the less hydrophilic surfactant, Polysorbate 81, in the formulation. This less hydrophilic surfactant possesses a lower HLB value and as such, is less likely to favour oil-in-water systems and more likely to favour water-in-oil systems leading to lower conductivity values. These results were consistent with the ternary phase diagram results for 3:1 Polysorbate 81:Cremophor RH 40 presented earlier (**Figure 5.13**) where the tendency to form W/O systems was clear. After 100x aqueous dilution, however, F2 and F3 demonstrated higher conductivity values indicating a possible reversion to O/W systems as seen in F1 (**Chapter 4**). Regardless of the actual values, conductivity values were consistent across the period of one week suggesting no phase changes or shifts in microemulsion type throughout this period.

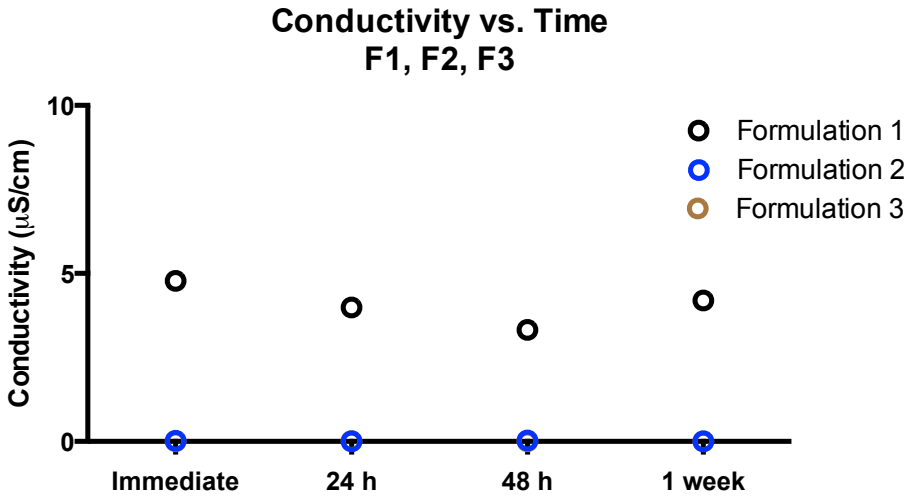

Figure 5-30: Conductivity changes in F1, F2 and F3 over the course of 1 week.

5.5.2.4.6. Centrifugation Stress Test

Figure 5.31 depicts results for F1, F2 and F3 after centrifugation at 5000 and 10000 RPM for 30 minutes. An equal volume of water was used as a balancer. Unlike the clear phase separation observed in F1 in **Chapter 4**, no large phase separation was evident in F1, F2 and F3 samples. In F1, after 5000 RPM for 30 minutes, the appearance of solid precipitate (active ingredient residue) was evident along the side of the centrifugation tube. This was not the case for F2, although F3 exhibited precipitate at the bottom of the tube. At 10000 RPM after 30 minutes, all formulations demonstrated a pellet of solid precipitate at the bottom of each tube.

As explained in the previous chapter, emulsion stability may be inferred through consideration of the volume of the separated phase in emulsion formulations[44], using the following equation:

$$Emulsion\ Stability\ (ES) = \frac{Volume\ of\ Intact\ Emulsion\ Layer}{Total\ Volume\ of\ Emulsion\ Layer} \qquad \textbf{(Eq. 5.3)}$$

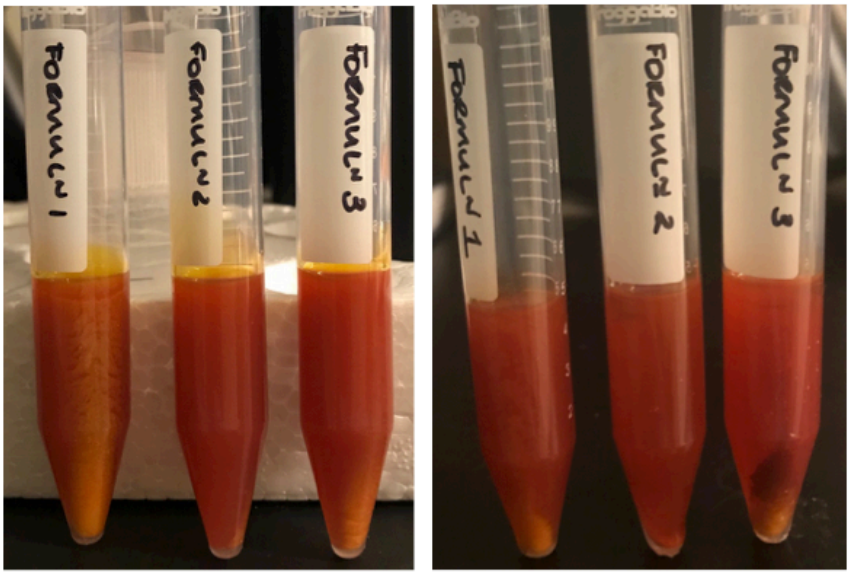

Figure 5.31: Effects of centrifugation on F1, F2 and F3 after centrifugation at 5000 RPM for 30 minutes (left) and after centrifugation at 10000 RPM for 30 minutes (right).

Given that no clear, measureable phase separation was observed, aside from the presence of precipitate along the bottom and sides of each tube, it was not possible to calculate an estimation of emulsion stability for F1, F2 and F3. However, the presence of yellow/orange precipitate supports the fact that the water-soluble APIs, riboflavin and folic acid, are

insufficiently incorporated into the current microemulsion systems especially for Formulations 1 and 3. Thus, despite an effort to employ pH adjustment in order to incorporate these poorly water-soluble active ingredients, the accelerated gravitational separation results indicated that these formulations fell short of being truly stable in nature.

5.5.2.4.7. Long-term Droplet Size and Zeta Potential Test

Given the presence of multiple emulsifiers, oils and active ingredients in these formulations, measurements of droplet size and zeta potential were obtained over the period of one month in order to deduce any trends or changes that may impact stability (**Figure 5.32**). In general, F1 possessed higher droplet sizes and zeta potential values than F2 and F3, which exhibited very similar droplet size and zeta potential results. However, no major fluctuations in size were seen. Average droplet sizes over the course of one month for F1, F2 and F3 were 146 ± 12 nm, 92 ± 14 nm and 75 ± 11 nm, respectively. This amounts to total droplet size changes of 18 nm in F1, 22 nm in F2 and 13 nm in F3 after one month.

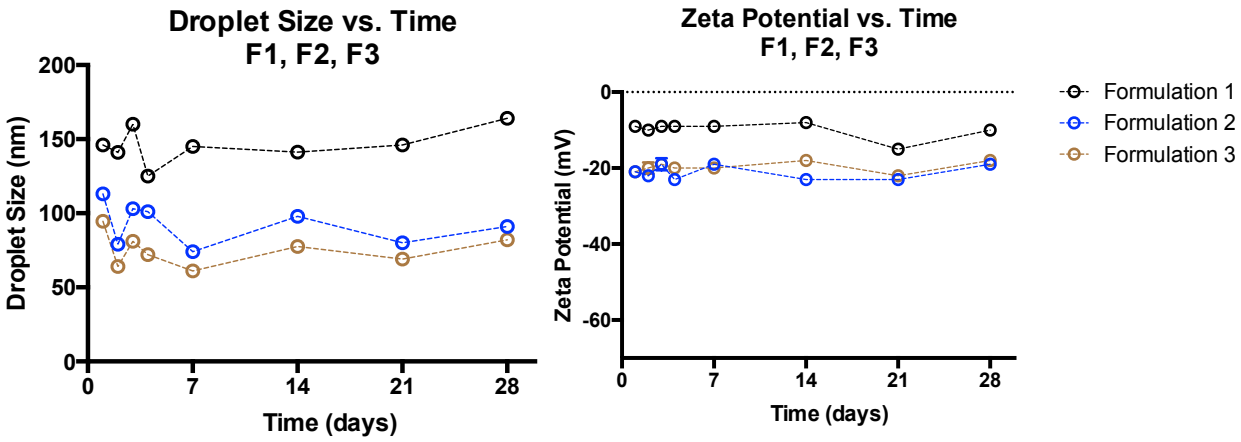

Figure 5.32: Droplet size and zeta potential measurements of F1, F2 and F3 over the course of 1 month.

Zeta potential values for F1, F2 and F3 remained stable and consistent over the period of one month. No major fluctuations in charge were observed. Average zeta potential values over the course of one month were -10 ± 2 mV for F1, -21 ± 2 mV for F2 and -20 ± 1 mV for F3. F1 experienced a maximum difference in charge of 7 mV while the maximum charge differences experienced by F2 and F3 were both 4 mV. Given the droplet size and zeta potential

results in **Figure 5.32**, it appeared that Formulation 1, strictly on the basis of droplet size and zeta potential, was a less favourable microemulsion than Formulations 2 and 3. Formulations 2 and 3 appeared to depict a higher degree of stability than Formulation 1. Generally, the greatest fluctuation in droplet size occurred within the first three to four days after which results appeared to stabilize. Size histograms and zeta potential curves are depicted in **Figures D-24 – D-26, Appendix D**.

5.6 Conclusion

A number of surfactants with the potential to replace Polysorbate 80 in the current formulation (F1A) were identified in this Chapter. However, Polysorbate 81 was selected as the most promising surfactant based on size and zeta potential results. The ability of Polysorbate 81 (and Brij 97) to produce homogeneous microemulsion formulations, with favourable droplet sizes, was surprising given the low EO content of both surfactants when compared to that of Polysorbate 80. These results suggest that an optimal number of EO units exists for a given surfactant when formulating a microemulsion, above which these optimal effects become less evident. This effect was previously proposed by Myers (2006) in EO-containing ether surfactants.[5] In this particular case, it appears that the optimal EO number for this formulation, barring EO contributions from Cremophor RH 40, may lie around 5 rather than 20 as in the case of F1A. Given that Polysorbate 80 and 81 possess the same number of carbons in the hydrophobic tail, this property may also be one of the most important considerations in the development of this type of multi-drug delivery system. Tensiometry studies indicated no particular importance of CMC, except for the fact that interactions between the two surfactants used in a microemulsion formulation should be synergistic at best and ideal at worst.

In microemulsions formulated with Polysorbate 80 and 81 (F1, F2 and F3), riboflavin was successful in meeting USP dissolution requirements of at least 75% dissolution within one hour in all tested media. Folic acid proved more difficult, owing to its poor water solubility, and only met dissolution criteria using 50 mM phosphate buffer (pH 7.4) medium. The most favourable results were observed in phosphate buffer where all formulations demonstrated almost 100% dissolution of riboflavin and approximately 80% dissolution of folic acid. The

successful dissolution of beta-carotene suggested that less lipophilic active ingredients would also be dissolved. F1 and F2 filled in hard gelatin capsules met disintegration criteria.

With respect to stability, the factors of greatest importance were the same as those observed in **Chapter 4**: temperature and light exposure. Reductions in size were observed at the first temperature point of 37°C while light exposure resulted in phase separation commencing at approximately day 5. These factors tended to affect Formulation 1 to a greater extent than Formulations 2 and 3, as greater size reductions and measurement fluctuations were observed. pH and conductivity of all formulations remained stable throughout the evaluation period of one month and one week, respectively. Accelerated gravitational separation testing via centrifugation was unable to yield any results with respect to emulsion stability due to unclear phase separation. However, the presence of precipitate at the bottom of each tube suggested insufficient solubilization of riboflavin and folic acid in this microemulsion formulation. Droplet size and zeta potential measurements over the course of one month indicated fluctuations in measurements in the first three to four days, but a plateau or stabilization after this period. Given these results, it can be concluded that all formulations are best maintained in cool, dark storage conditions. Similar to results in **Chapter 4**, the addition of a buffer or stabilizer to assist with the pH change of approximately 1 unit in all formulations could be beneficial.

Overall, Formulations 1 and 3 performed best during dissolution studies, but Formulations 2 and 3 outperformed Formulation 1 with respect to stability. All microemulsion formulations performed significantly better than the prenatal suspension formulation, lending support to the use of microemulsion systems for improved drug dissolution. In general, considering both dissolution and stability data, Formulation 3 appeared to be the most promising microemulsion candidate for this type of multi-drug delivery. The results of this Chapter in its entirety suggest that careful consideration of emulsifying agent properties can result in the development of additional microemulsion formulations superior to that of the original formulation. This highlights a novel process for the development of a microemulsion system capable of the simultaneous delivery of both hydrophilic and hydrophobic active pharmaceutical ingredients.

Chapter 6: Conclusions & Future Directions

This thesis work consisted of four main objectives: i) to design and formulate a microemulsion system capable of delivering multiple active ingredients of varying hydro- and lipophilicity, ii) to identify additional emulsifying agents suitable for this type of multi-drug delivery, iii) to determine emulsifying agent properties, based on results from (ii), necessary in this type of microemulsion formulation and iv) to use information from (i-iii) to develop microemulsion formulations capable of superior dissolution when compared to a prenatal, suspension reference. Objective (i) was accomplished through a process of careful surfactant selection, ternary phase diagram (TPD) mapping, optimization via the hydrophilic-lipophilic deviation (HLD) equation and active pharmaceutical ingredient (API) solubility enhancement using pH adjustment (**Chapters 2-4**). Objectives (ii) and (iii) were accomplished through methodical surfactant screening and variation of head and tail groups, specifically polyoxyethylene (PEO) content and hydrocarbon chain length, on the basis of size, charge, homogeneity and critical micelle concentration studies (**Chapter 5**) and finally, objective (iv) was accomplished through evaluation of dissolution, disintegration and stability as compared to a commercially available, prenatal suspension reference formulation (**Chapter 5**).

6.1 Conclusions

TPD mapping resulted in the identification of a 3:1 Polysorbate 80:Cremophor RH 40 surfactant mix to be used in conjunction with Miglyol 812 oil and water for microemulsion formation. This surfactant ratio was further optimized through the use of the HLD equation. Eleven (11) active pharmaceutical ingredients (APIs), five lipophilic and six hydrophilic, were successfully incorporated and further surfactant screening resulted in an additional surfactant selection of 3:1 Polysorbate 81:Cremophor RH 40. Overall, three microemulsion formulations: F1, F2 and F3 with surfactant:oil:water (S:O:W) ratios of 50:40:10, 40:50:10 and 50:40:10, respectively, were used. F1 contained 3:1 Polysorbate 80:Cremophor RH 40 surfactant while F2 and F3 contained 3:1 Polysorbate 81:Cremophor RH 40. Sizes for F1, F2 and F3 after 100x aqueous dilution were 164 ± 37 nm, 94 ± 15 nm and 81 ± 2.4 nm, respectively and all formulations exhibited >95% dissolution improvement of riboflavin compared to that of a commercial standard prenatal supplement. Stability

of all formulations with respect to pH, droplet size and zeta potential for a period of 1 month was demonstrated.

Based on these results, microemulsion formulations comprised of 3:1 Polysorbate 80:Cremophor RH 40 and 3:1 Polysorbate 81:Cremophor RH 40 acted as effective solubilizers for lipophilic APIs loaded in Miglyol 812 with an EACN of 8. The difference in PEO content (~15 EO groups) yet equivalence in hydrocarbon chain length (18 carbons) of Polysorbate 80 and 81 led to the finding that differences in PEO content may be better tolerated than differences in hydrocarbon chain length for this specific multi-drug, microemulsion formulation. In other words, the optimal range of PEO content for this particular formulation comprised of five lipophilic and six hydrophilic APIs, was larger and less restrictive than that of hydrocarbon chain length. Critical micelle concentration was determined to be of low importance in microemulsion systems, where surfactant concentration is inherently high. In addition, hydrophilic lipophilic balance (HLB) appeared to be a poor predictor of microemulsion formation given the difference in HLB between Polysorbate 80 and 81 (15 versus 10). The results of this thesis work support the hypothesis that the development of a microemulsion system with droplet sizes close to 100 nm in diameter, capable of multi-drug delivery, is possible through the identification of structural emulsifying agent properties, in this case hydrocarbon chain length and a well-defined PEO range. Overall, it is evident that careful and methodical surfactant screening and optimization are crucial in the development of such systems.

Though this work led to the development of three successful formulations capable of multi-drug delivery, a number of limitations are evident. The identification of 3:1 Polysorbate 80/81:Cremophor RH 40 surfactant for this type of microemulsion, multi-drug formulation is specific to a system comprised of an oil component of EACN 8. In addition, the characteristic curvature of additional promising surfactants was not experimentally evaluated, ignoring a potentially critical emulsifying agent property necessary in this type of drug delivery. Dissolution studies were not performed with filled soft gelatin capsules (the intended dosage form) or in hydrochloric acid, the latter of which would have shed insight into dissolution in the stomach and may have improved dissolution of the commercial pre-natal supplement reference. The nature of the APIs employed in this work also resulted in formulations with extreme sensitivity to temperature and fluorescent light exposure. Finally, additional replicates and controls are necessary to confirm trends noted in this work, particularly regarding droplet sizes as a result of surfactant screening and formulation stability. For the latter, chromatographic studies for the identification of possible API-API, API-surfactant and

API-oil interactions, degradants and related substances are likely of greater importance than the evaluation of droplet size changes as conducted in this work.

6.2 Future Directions

Future directions may involve two broad approaches: i) advancing our understanding of critical factors important in microemulsion, multi-drug delivery and ii) bridging the gap between this thesis work and clinical applicability. In terms of advancing our understanding of critical factors important in microemulsion, multi-drug delivery, a number of areas of exploration are possible. First, it is important to note that formulators are often limited by emulsifying agents that are commercially available. A truly robust approach would include synthesizing surfactants of consistent head and tail group variations prior to microemulsion formulation and investigation. The effect of oil type on microemulsion formulation would also provide insight into a much-neglected area of microemulsion investigation. Perhaps of greater importance is the determination of characteristic curvature values for the emulsifying agents employed in this work, as this is evidently an important parameter in microemulsion formation and optimization. The use of more appropriate physicochemical properties may also be explored. Particularly, in this work, log P values used to make assumptions about the partitioning of active ingredients into the respective microemulsion components, may be replaced by log D (distribution) values that take into account partitioning at a particular pH which given the pH-adjusted nature of this formulation, would be most useful. A methodology such as that utilized by Lu et al. (2012) [1] may be explored using a software such as MarvinView by ChemAxon Ltd. [2] Finally, a high throughput methodology for the screening of factors most important in microemulsion, multi-drug formulation is key to advancing this work. Typically, the slow utility of artificial intelligence (AI) systems in the pharmaceutical industry has been attributed to a combined lack of investment and insufficient skillset.[3] However, a recent review by Damiati (2020) evaluated the use of multiple machine learning (ML) techniques, particularly artificial neural networks (ANN), for pharmaceutical pre-formulation studies.[3] Damiati et al. (2017) developed a ML model using ANN for the prediction of solubility enhancers for indomethacin.[4] Factors under consideration included log P, pKa and hydrotrope concentration.[4] Rodriguez-Dorado et al. (2018) also utilized ANN to dictate formation of microemulsion-alginate core-shell systems for drug delivery.[5] The authors were able to predict oil and surfactant concentrations, along with other properties, contributing to optimal microparticle size and shape.[5] Employing a similar methodology to deduce the surfactant, oil and API properties most

critical for microemulsion, multi-drug formulation would afford rapid and efficient advancement of this technology. The data upon which this AI screening is based, however, must be reliable, accurate and reproducible[3] and thus, may present a challenge when trying to obtain surfactant parameter values such as characteristic curvature (CC).

In terms of bridging the gap between this thesis work and clinical applicability, further *in-vitro* and *in vivo* testing to ascertain an *in vitro-in vivo* correlation with the dissolution results obtained in this work, would be an excellent avenue for further investigation. Use of the Caco-2 cell line, widely used as a model of the intestinal epithelial barrier, may also be explored especially as it relates to the toxicity and safety of the surfactants employed in this work. This is particularly important for the most promising formulation in this work, Formulation 3 (F3) as there are no guidance limits for Polysorbate 81 tolerability on the US Food and Drug Administration (FDA) inactive ingredient (IIG) database presenting a barrier to commercialization. Another approach to bridging the gap between this thesis work and clinical applicability involves replacing the APIs used in this formulation with drugs of similar physicochemical properties used in common chronic disease treatment. Finally, enhancing microemulsion formulation stability through the development of a lyophilization process, previously proven to be effective through slow and careful reconstitution [6, 7], is worth investigating.

6.3 Scientific Contribution

With respect to contribution of this work to microemulsion science, the results demand a shift in focus to surfactant characteristics most useful in microemulsion formulation development. This translates to a reduced focus on properties such as HLB and an increased focus on potentially important surfactant factors such as hydrocarbon chain length, surfactant mixing behaviour, PEO content and even characteristic curvature. In addition, a renewed interest in ternary phase mapping should be employed, especially as it gives the formulator a range of surfactant: oil: water ratios in which to operate (and avoid). Finally, a transparent body of literature including EACN results for multiple oil mixtures, CC results for multiple surfactants and HLD results for ensuing microemulsion formulations, is imperative to the advancement of this field. Efforts to develop a repository of EACN and CC values, such as the one undertaken by Steven Abbott [8], are imperative in affording the rapid development and reduced stagnation of microemulsion formulation science. Such a library may require increased collaboration, cooperation and time; however, the potential to alleviate the burden

of concurrent, chronic disease through multi-drug microemulsion development, not only in Canada but around the world, is one that is worth the effort.

Copyright Permission

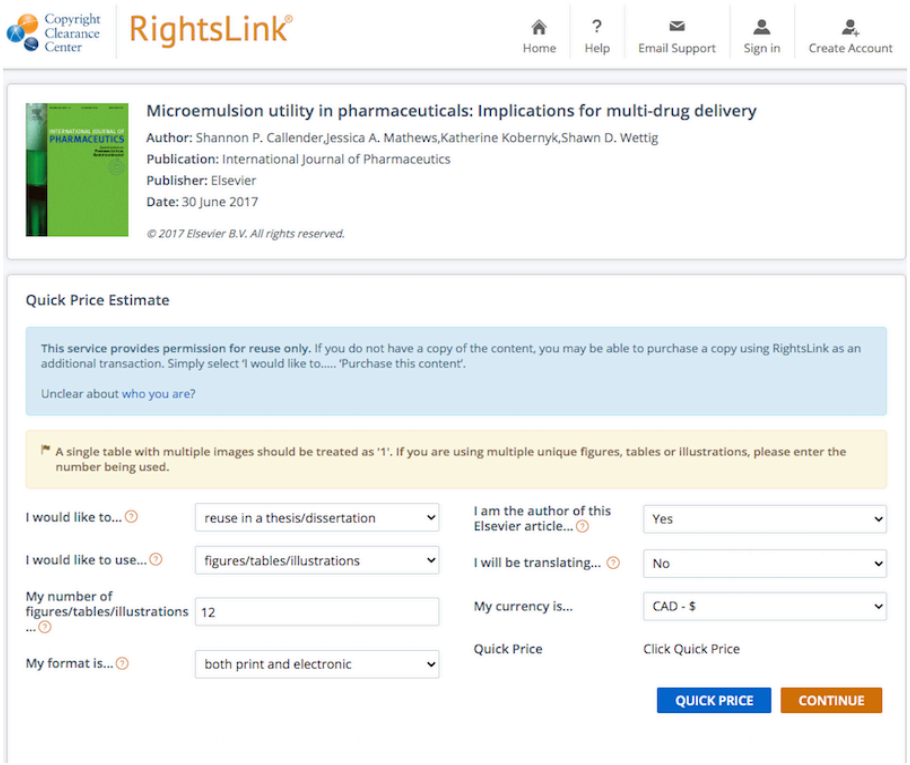

References

Chapter 1

1. Callender S, Mathews J, Kobernyk K, Wettig S. Microemulsion utility in pharmaceuticals: Implications for multi-drug delivery. *International Journal of Pharmaceutics*.2017;**526**:425-442. DOI: 10.1016/j.ijpharm.2017.05.005
2. Kim S, Kwon IK, Kwon IC, Park K. Chapter 19: Nanotechnology in drug delivery: Past, present and future. In: de Villiers MM, Aramwit P, Kwon GS, eds. *Nanotechnology in Drug Delivery*. New York, USA: Springer; 2009:581.
3. Park K. Facing the truth about nanotechnology in drug delivery. *ACS Nano*. 2013;**7**:7442-7447. DOI: 10.1021/nn404501g
4. Park K. Nanotechnology: What it can do for drug delivery. *Journal of Controlled Release*. 2007;**120**:1-3. DOI: 10.1016/j.jconrel.2007.05.003
5. Tran S, DeGiovanni P, Piel B, Rai P. Cancer nanomedicine: A review of recent success in drug delivery. *Clinical and Translational Medicine*. 2017;**6**:1-22. DOI: 10.1186/s40169-017-0175-0
6. Kumar N, Kumar R. Chapter 5: Nanomedicine for treatment of cardiovascular diseases and stroke. In: *Nanotechnology and Nanomaterials in the Treatment of Life-Threatening Diseases*. Massachusetts, USA: Elsevier; 2014:248-291.
7. Fonte P, Andrade F, Araujo F, Andrade C, das Neves J, Sarmento B. Chapter 15: Chitosan-coated solid lipid nanoparticles for insulin delivery. In: Duzgunes N, ed. *Methods in Enzymology:Nanomedicine-Cancer, Diabetes, and Cardiocascular, Central Nervous System, Pulmonary and Inflammatory Diseases Volume 508*. California, USA: Elsevier; 2012:295-312.
8. Reis CP, Damge C. Chapter 14: Nanotechnology as a promising strategy for alternative routes of insulin delivery. In: Duzgunes N, ed. *Methods in Enzymology:Nanomedicine- Cancer, Diabetes, and Cardiocascular, Central Nervous System, Pulmonary and Inflammatory Diseases Volume 508*. California, USA: Elsevier; 2012:271-290.
9. Mishra RK, Tiwari SK, Mohapatra SS, Thomas S. Chapter 1: Efficient nanocarriers for drug delivery systems: Types and fabrication. In: Mohapatra SS, Ranjan S, Dasgupta N, Mishra RK, Thomas S, eds. *Nanocarriers for Drug Delivery: Nanoscience and Nanotechnology in Drug Delivery*. Netherlands: Elsevier; 2019.
10. Wilczewska AZ, Niemirowicz K, Markiewicz KH, Car H. Nanoparticles as drug delivery systems. *Pharmacological Reports*. 2012;**64**:1020-1037. DOI: 10.1016/ S1734-1140(12)70901-5
11. Bawa R. Chapter 6: What's in a name? Defining "nano" in the context of drug delivery. In: Bawa R, Audette GF, Rubinstein I, eds. *Handbook of Clinical Nanomedicine: Nanoparticles, Imaging, Therapy and Clinical Applications*. Singapore: Pan Stanford Publishing; 2016.
12. Dahan A, Hoffman A. Chapter 6: Enhanced gastrointestinal absorption of lipophilic drugs. In: Touitou E, Barry B, eds. *Enhancement in Drug Delivery*. USA: CRC Press; 2011:111.
13. US Food and Drug Administration (FDA). Waiver of In-vitro Bioavailability and Bioequivalent Studies for Immediate Release Solid Oral Dosage Forms Based on a Biopharmaceutics Classification System: Guidance for Industry. Available at: https://www.fda.gov/downloads/Drugs/GuidanceComplianceRegulatoryInformation/Guidances/UCM070246.pdf. Accessed September 19, 2018.
14. Amidon GL, Lennernas H, Shah VP, Crison JR. A theoretical basis for a biopharmaceutic drug classification: The correlation of in-vitro drug product dissolution and in-vivo bioavailability. *Pharmaceutical Research*. 1995;**12**:413-420. DOI: 10.1023/a:1016212804288
15. Vimalson C, Sundararajan P, Jeganathan NS, Anbazhagan S. Techniques to enhance solubility of hydrophobic drugs: An overview. *Asian Journal of Pharmaceutics*. 2015;**10**:S67-S75. DOI: 10.22377/ajp.v10i2.625
16. Bushnik T, Tjepkema M, Martel L. Statistics Canada health report: Health-adjusted life expectancy in Canada. 82-003-X. 2018;1209-1367:1.
17. Public Health Agency of Canada. Chronic diseases and injuries in Canada. Public Health Agency of Canada. 2014.

18. Innala L, Sjöberg C, Möller B, et al. Co-morbidity in patients with early rheumatoid arthritis - inflammation matters. *Arthritis Research and Therapy*. 2016;**18**:1-8. DOI: 10.1186/s13075-016-0928-y
19. Sajatovic M, Gunzler D, Einstadter D, et al. A preliminary analysis of individuals with serious mental illness and comorbid diabetes. *Archives of Psychiatric Nursing*. 2016;**30**:226-229. DOI: 10.1016/j.apnu.2015.11.004
20. Lee S, Rothbard A, Choi S. Effects of comorbid health conditions on healthcare expenditures among people with severe mental illness. *Journal of Mental Health*. 2015:**25**;291-296. DOI: 10.3109/09638237.2015.1101420.
21. Ogdie A, Schwartzman S, Eder L, Maharaj A, Zisman D, Raychaudhuri S. Comprehensive treatment of psoriatic arthritis: Managing comorbidities and extraarticular manifestations. *Journal of Rheumatology*. 2014;**41**:2315-2322. DOI: 10.3899/jrheum.140882
22. Uutela T, Kautiainen H, Järvenpää S, Salomaa S, Hakala M, Häkkinen A. Patients with rheumatoid arthritis have better functional and working ability but poorer general health and higher comorbidity rates today than in the late 1990s. *Scandinavian Journal of Rheumatology*. 2014;**44**:173-181. DOI: 10.3109/03009742. 2014.957240
23. Nousen EK, Franco JG, Sullivan EL. Unraveling the mechanisms responsible for the comorbidity between metabolic syndrome and mental health disorders. *Neuroendocrinology*. 2013;**98**:254-266. DOI: 10.1159/000355632
24. Michaud K, Wolfe F. Comorbidities in rheumatoid arthritis. *Best Practice & Research Clinical Rheumatology*. 2007;**21**:885-906. DOI: 10.1016/j.berh.2007.06. 002.
25. Lehmann A, Aslani P, Ahmed R, et al. Assessing medication adherence: Options to consider. *International Journal of Clinical Pharmacy*. 2014;**36**:55-69. DOI: 10.1007/ s11096-013-9865-x
26. Bibette J, Calderon FL, Poulin P. Emulsions: Basic principles. *Reports on Progress in Physics*. 1999;**62**:969-1033. DOI:10.1088/0034-4885/62/6/203
27. Prince LM. *Microemulsions Theory and Practice*. Elsevier; 1977.
28. Rosen MJ, Kunjappu JT. Chapter 8: Emulsification by surfactants. In: Rosen MJ, Kunjappu JT, eds. Surfactants and Interfacial Phenomena, 4th Edition. New Jersey, USA: John Wiley & Sons Publisher; 2012:336.
29. Leal-Calderon F, Schmitt V, Bibette J. *Emulsion Science: Basic Principles*. Paris, France: Springer Science and Business Media; 2007.
30. Sharma MK, Shah DO. Introduction to macro- and microemulsions. In: Shah DO, ed. *Macro and Microemulsions: Theory and Applications Volume 272*. American Chemical Society; 1985:1.
31. Sharma S, Shukla P, Misra A, Mishra PR. Chapter 8: Interfacial and colloidal properties of emulsified systems: Pharmaceutical and biological perspective. In: Ohshima H, Makino K, eds. *Colloid and Interface Science in Pharmaceutical Research and Development*. Oxford, UK: Elsevier B.V.; 2014:149.
32. McClements DJ. Nanoemulsions versus microemulsions: Terminology, differences and similarities. *Soft Matter*. 2012;**8**:1719-1729. DOI: 10.1039/C2SM06903B
33. Gibaud S, Attivi D. Microemulsions for oral administration and their therapeutic applications. *Expert Opinion on Drug Delivery*. 2012;**9**:937-951. DOI: 10.1517/ 17425247.2012.694865
34. Langevin D. Microemulsions. *Accounts of Chemical Research*. 1988;**21**:255-260. DOI: 10.1021/ar00151a001
35. Eriksson JC, Ljunggren S, Kegel WK, Lekkerkerker HNW. Entropy and droplet size distributions of Winsor I and II microemulsions. *Colloids and Surfaces A: Physicochemical and Engineering Aspects*. 2001;**183-185**:347-360. DOI: 10.1016/ S0927-7757(01)00526-X
36. Lang J, Lalem N, Zana R. Droplet size and dynamics in water-in-oil microemulsions. *Colloids and Surfaces*. 1992;**68**:199-206. DOI: 10.1016/0166-6622(92)80205-G
37. Winsor PA. Hydrotropy, solubilisation and related emulsification processes. *Transactions of the Faraday Society*. 1948;**44**:376-398. DOI: 10.1039/TF9484400376
38. Brinker CJ, Lu Y, Sellinger A, Fan H. Evaporation-induced self-assembly: Nanostructures made easy. *Advanced Materials*. 1999;**11**:579. DOI: 10.1002/ (SICI)1521-4095(199905)11:7<579::AID-ADMA579>3.0.CO;2-R
39. McCuistion LE, Kee J, Hayes E, R. *Pharmacology: A Patient-Centered Nursing Process Approach 8th Edition*. USA: Elsevier Saunders; 2014.
40. Brandlin C. *Your Body, Your Genes, Your Digestion, and Your Metabolism*. USA: Xlibris LLC; 2013.
41. Paradkar AR, Bakliwal S. Chapter 2: Drug absorption. In: *Biopharmaceutics & Pharmacokinetics 3rd Edition*. India: Nirali Prakashan; 2008:**2**.16.

42. Liu W, Zhai Y, Heng X, et al. Oral bioavailability of curcumin: Problems and advancements. *Journal of Drug Targeting*. 2016;**24:**694-702. DOI: 10.3109/ 1061186X.2016.1157883
43. Cerpnjak K, Zvonar A, Gasperlin M, Vrcer F. Lipid-based systems as a promising approach for enhancing the bioavailability of poorly water-soluble drugs. *Acta Pharmaceutica*. 2013;**63**:427-445. DOI: 10.2478/acph-2013-0040
44. He C, He Z, Gao J. Microemulsions as drug delivery systems to improve the solubility and the bioavailability of poorly water-soluble drugs. *Expert Opinion on Drug Delivery*. 2010;**7**:445-460. DOI: 10.1517/17425241003596337
45. McClements DJ. Nanoscale nutrient delivery systems for food applications: Improving bioactive dispersibility, stability, and bioavailability. *Journal of Food Science*. 2015;**80**:1602-1611. DOI: 10.1111/1750-3841.12919
46. Kamboj S, Sharma R, Singh K, Rana V. Aprepitant loaded solid preconcentrated microemulsion for enhanced bioavailability: A comparison with micronized aprepitant. *European Journal of Pharmaceutical Sciences*. 2015;**78**:90-102. DOI: 10.1016/j.ejps.2015.07.008
47. Xu M, Yu Q, Zhao Q, Chen W, Lin Y, Jin Y. Development and in vitro-in vivo evaluation of a water-in-oil microemulsion formulation for the oral delivery of troxerutin. *Drug Development and Industrial Pharmacy*. 2016;**42**:280-287. DOI: 10.3109/03639045.2015.1047849
48. Hu L, Wu H, Niu F, Yan C, Yang X, Jia Y. Design of fenofibrate microemulsion for improved bioavailability. *International Journal of Pharmaceutics*. 2011;**420**:251-255. DOI: 10.1016/j.ijpharm.2011.08.043
49. Baek MK, Lee JH, Cho YH, Kim HH, Lee GW. Self-microemulsifying drug-delivery system for improved oral bioavailability of pranlukast hemihydrate: Preparation and evaluation. *International Journal of Nanomedicine*. 2013;**8**:167-176. DOI: 10.2147/ ijn.s37338
50. Hintzen F, Perera G, Hauptstein S, Müller C, Laffleur F, Bernkop-Schnürch A. In vivo evaluation of an oral self-microemulsifying drug delivery system (SMEDDS) for leuprorelin. *International Journal of Pharmaceutics*. 2014;**472**:20-26. DOI: 10.1016/j.ijpharm.2014.05.047
51. Deshmukh A, Kulkarni S. Solid self-microemulsifying drug delivery system of ritonavir. *Drug Development and Industrial Pharmacy*. 2014;**40**:477-487. DOI: 10.3109/03639045.2013
52. Cho W, Kim MS, Kim JS, et al. Optimized formulation of solid self-microemulsifying sirolimus delivery systems. *International Journal of Nanomedicine*. 2013;**8**:1673-1682. DOI: 10.2147/IJN.S43299
53. Kalam MA, Alshamsan A, Aljuffali IA, Mishra AK, Sultana Y. Delivery of gatifloxacin using microemulsion as vehicle: Formulation, evaluation, transcorneal permeation and aqueous humor drug determination. *Drug Delivery*. 2016;**23**:896-907. DOI: 10.3109/10717544.2014.920432
54. Gullapalli RP. Soft gelatin capsules. *Journal of Pharmaceutical Sciences*. 2010;**99**:4107-4148. DOI:10.1002/jps.22151
55. Jambhekar SS, Breen PJ. Drug dissolution: Significance of physicochemical properties and physiological conditions. *Drug Discovery Today*. 2013;**18**:1173-1184. DOI: 10.1016/ j.drudis.2013.08.013
56. Kwon Y. Handbook of Essential Pharmacokinetics, Pharmacodynamics and Drug Metabolism for Industrial Scientists. USA: Kleuwer Academic Publishers; 2002.
57. Niazi SK. *Handbook of Bioequivalence Testing 2nd Edition*. USA: CRC Press; 2015.
58. Gupta S, Kesarla R, Omri A. Formulation strategies to improve the bioavailability of poorly absorbed drugs with special emphasis on self-emulsifying systems. *ISRN Pharmaceutics*. 2013:1-16. DOI:10.1155/2013/848043
59. Shargel L, Wu-Pong S, Yu ABC. *Applied Biopharmaceutics & Pharmacokinetics 6th Edition*. USA: McGraw-Hill Education; 2012.
60. Mason TG, Wilking JN, Meleson K, Chang CB, Graves SM. Nanoemulsions: Formation, structure, and physical properties. *Journal of Physical and Condensed Matter*. 2006;**18**:R635-666. DOI:10.1088/0953-8984/18/41/R01
61. Tong K, Zhao C, Sun Z, Sun D. Formation of concentrated nanoemulsion by W/O microemulsion dilution method: Biodiesel, Tween 80, and water system. *ACS Sustainable Chemistry and Engineering*. 2015;**3**:3299-3306. DOI:10.1021/ acssuschemeng.5b00903
62. Fast J, Mecozzi S. Chapter 15: Nanoemulsions for intravenous drug delivery. In: de Villiers MM, Aramwit P, Kwon GS, eds. *Nanotechnology in Drug Delivery Volume X*. USA: American Association of Pharmaceutical Scientists Press; 2009:461.

63. Ngan CL, Basri M, Tripathy M, Karjiban RA, Abdul-Malek E. Physicochemical characterization and thermodynamic studies of nanoemulsion-based transdermal delivery system for fullerene. *The Scientific World Journal*. 2014:1. DOI:10.1155/ 2014/219035
64. Lawrence MJ, Warisnoicharoen W. Chapter 7: Recent advances in microemulsions as drug delivery vehicles. In: Torchillin V, ed. *Nanoparticulates as Drug Carriers*. UK: Imperial College Press; 2006.
65. Ding W, Hou X, Cong S, et al. Co-delivery of honokiol, a constituent of magnolia species, in a self-microemulsifying drug delivery system for improved oraltransport of lipophilic sirolimus. *Drug Delivery*. 2015;**1**: 2513-2523. DOI:10.3109/ 10717544.2015.1020119
66. Grill AE, Koniar B, Panyan J. Co-delivery of natural metabolic inhibitors in a self-microemulsifying drug delivery system for improved oral bioavailability of curcumin. *Drug Delivery and Translational Research*. 2014;**4**:344-352. DOI: 10.1007/s13346-014-0199-6
67. Li Q, Zhai W, Jiang Q, et al. Curcumin–piperine mixtures in self-microemulsifying drug delivery system for ulcerative colitis therapy. *International Journal of Pharmaceutics*. 2015;**490**:22-31. DOI: 10.1016/j.ijpharm.2015.05.008
68. Fisher S, Wachtel E, Aserin A, Garti N. Solubilization of simvastatin and phytosterols in a dilutable microemulsion system. *Colloids and Surfaces B: Biointerfaces*. 2013;**107**:35-42. DOI: 10.1016/j.colsurfb. 2013.01.036
69. Hwang K, Park S, Kim J, Park C, Rhee Y, Park E. Formulation and in vitro evaluation of self-microemulsifying drug delivery system containing fixed-dose combination of atorvastatin and ezetimibe. *Chemical and Pharmaceutical Bulletin*. 2015;**63**:423-430. DOI: 10.1248/cpb.c14-00814
70. Pepe D, Phelps J, Lewis K, et al. Decylglucoside-based microemulsions for cutaneous localization of lycopene and ascorbic acid . *International Journal of Pharmaceutics*. 2012;**434**:420-428. DOI: 10.1016/j.ijpharm.2012.06.016
71. Kaur G, Mehta S. Probing location of anti-TB drugs loaded in Brij 96 microemulsions using thermoanalytical and photophysical approach. *Journal of Pharmaceutical Sciences*. 2014; **103**:937-944. DOI:10.1002/jps.23857.
72. El Maghraby G, Arafa M, Osman M. Microemulsion for simultaneous transdermal delivery of benzocaine and indomethacin: In vitro and in vivo evaluation. *Drug Development and Industrial Pharmacy*. 2014;**40**:1637-1644. DOI: 10.3109/03639045. 2013.841186
73. Zhang Y, Zhao J, Zhong S, et al. Enhanced transdermal delivery of evodiamine and rutaecarpine using microemulsion. *International Journal of Nanomedicine*. 2011;**6**:2469-2482. DOI: 10.2147/IJN.S25258
74. Negi P, Singh B, Sharma G, Beg S, Raza K, Katare O. Phospholipid microemulsion-based hydrogel for enhanced topical delivery of lidocaine and prilocaine: QbD-based development and evaluation. *Drug Delivery*. 2016;**23**:941-957. DOI:10.3109/ 10717544.2014.923067
75. Baboota S, Alam M, Sharma S, Sahni J, Kumar A, Ali J. Nanocarrier-based hydrogel of betamethasone dipropionate and salicylic acid for treatment of psoriasis. *International Journal of Pharmaceutical Investigation*. 2011;**1**:139-147. DOI: 10.4103/2230-973X.85963
76. Gupta S, Bansal R, Ali J, Gabrani R, Dang S. Development and characterization of polyphenon 60 and caffeine microemulsion for enhanced antibacterial activity. *Boomed Research International*. 2014:1-7. DOI: https://doi.org/10.1155/2014/932017
77. Ujhelyi Z, Kalantari A, Vecsernyes M, et al. The enhanced inhibitory effect of different antitumor agents in self-microemulsifying drug delivery systems on human cervical cancer HeLa cells. *Molecules*. 2015;**20**:13226-13239. DOI: 10.3390/ molecules200713226
78. Qu D, Ma Y, Sun W, et al. Microemulsion-based synergistic dual-drug codelivery system for enhanced apoptosis of tumor cells. *International Journal of Nanomedicine*. 2015;10:1173.
79. Shi J, Cong W, Wang Y, Liu Q, Luo G. Microemulsion-based patch for transdermal delivery of huperzine A and ligustrazine phosphate in treatment of Alzheimer's disease. *Drug Development and Industrial Pharmacy*. 2012;**38**:752-761. DOI:10. 3109/03639045.2011.625031
80. Shinde R, Bharkad G, Devarajan P. Intranasal microemulsion for targeted nose to brain delivery in neurocysticercosis: Role of docosahexaenoic acid. *European Journal of Pharmaceutics and Biopharmaceutics*. 2015;**96**:363-379. DOI:10.1016/j.ejpb.2015. 08.008
81. Chemelli A, Maurer M, Geier R, Glatter O. Optimized loading and sustained release of hydrophilic proteins from internally nanostructured particles. *Langmuir*. 2012;**28**:16788-16797. DOI: 10.1021/la303373q

82. Rahman MA, Hussain A, Hussain MS, Mirza MA, Iqbal Z. Role of excipients in successful development of self-emulsifying/microemulsifying drug delivery system (SEDDS/SMEDDS). *Drug Development and Industrial Pharmacy*. 2013;**39**:1-19. DOI:10.3109/03639045.2012.660949
83. Talegaonkar S, Negi LM. Chapter 14: Nanoemulsion in drug targeting. In: Devarajan P, Jain S, eds. *Targeted Drug Delivery: Concepts and Design*. London UK: Springer; 2015:433.
84. Bancroft WD. The theory of emulsification. *Journal of Physical Chemistry*. 1913;**17**:501-519. DOI:10.1021/j150141a002
85. Davies JT. A quantitative kinetics theory of emulsion type. I. Physical chemistry of the emulsifying agent in gas/liquid and liquid/liquid interfaces. *Proceedings of the 2nd International Congress of Surface Activity*. 1957:426-438.
86. Myers D. Chapter 2: The organic chemistry of surfactants. In: *Surfactant Science and Technology 3rd Edition*. USA: Wiley Interscience; 2005:29.
87. Attwood D, Florence AT. Chapter 4: Surfactants. In: *Physical Pharmacy 2nd Edition*. UK: Pharmaceutical Press; 2012:43.
88. Tadros TF. Chapter 2: Physical chemistry of surfactant solutions. In: *Applied Surfactants: Principles and Applications*. UK: Wiley-VCH; 2005:19.
89. Malmsten M. Chapter 5: Microemulsions in pharmaceuticals. In: Kumar P, Mittal KL, eds. *Handbook of Microemulsion Science and Technology*. USA: Marcel Dekker Inc; 1999:755.
90. Grove M, Mullertz A, eds. Oral Lipid Based Formulations- Enhancing the Bioavailability of Poorly Water Soluble Drugs. Chapter 5- Liquid Self-Microemulsifying Drug Delivery Systems. USA: Informa Healthcare; 2007. Hauss D. J., ed. *Drugs and the Pharmaceutical Sciences Volume 170*.
91. Liu R, Dannenfelser RM, Li S. Chapter 12: Micellization and drug solubility enhancement pg 296. In: Liu R, ed. *Water-Insoluble Drug Formulation 2nd Edition*. USA: CRC Press; 2008.
92. Hauss DJ. Oral lipid-based formulations. *Advanced Drug Delivery Reviews*. 2007;**59**: 667-676. DOI:10.1016/j.addr.2007.05.006
93. Balazs O. Preclinical formulation in early drug research. In: Tihanyi K, Vastag M, eds. *Solubility, Delivery and ADME Problems of Drugs and Drug-Candidates*. Bentham Science Publishers; 2011:68.
94. Atwood JL, Steed JW. *Encyclopedia of Supramolecular Chemistry Volume 2*. USA: CRC Press; 2004.
95. Griffin WC. Classification of surface active agents by "HLB". *Journal of the Society of Cosmetic Chemists*. 1949;**1**:311-326.
96. Myers D,. Chapter 9: Emulsions. In: Myers D, ed. *Surfactant Science and Technology 3rd Edition*. New Jersey, USA: Wiley Interscience; 2006:280.
97. Myers D. Chapter 4: Surfactants in solution: Monolayers and micelles. In: Myers D, ed. *Surfactant Science and Technology 3rd Edition*. USA: John Wiley & Sons Inc; 2006:107-157.
98. Rodriguez- Abreu C. On the relationships between the hydrophilic-lipophilic balance and the nanoarchitecture of nonionic surfactant systems. *Journal of Surfactants and Detergents*. 2019;**22**:1001-1010. DOI:10.1002/jsde.12258
99. Clint JH. Micellization of mixed nonionic surface active agents. *Journal of Chemical Society, Faraday Transactions 1: Physical Chemistry in Condensed Phases*. 1975;**71**:1327-1334.
100. Attwood D, Florence AT. Chapter 10: Aspects of surfactant toxicity. In: Attwood D, Florence AT, eds. *Surfactant Systems: Their Chemistry, Pharmacy and Biology*. Springer; 1983:698-777.
101. United States Food and Drug Administration (US FDA). Inactive Ingredient Database. Available at: https://www.accessdata.fda.gov/scripts/cder/iig/index.Cfm. Accessed Jan 20, 2020.
102. Viswanathan P, Muralidaran Y, Ragavan G. Chapter 7: Challenges in oral drug delivery: A nano-based strategy to overcome. In: Andronescu E, Grumezescu AM, eds. *Nanostructure for Oral Medicine: Micro and Nano Technologies*. Elsevier; 2017:173-197.
103. Homayun B, Lin X, Choi H,J. Challenges and recent progress in oral drug delivery systems for biopharmaceuticals. *Pharmaceutics*. 2019;**11**:129-158. DOI:10.3390/ pharmaceutics11030129
104. Keservani RK, Kesharwani RK, Sharma AK. Chapter 1: Introduction to nanotechnology in drug delivery. In: Keservani RK, Kesharwani RK, Sharma AK, eds. *Drug Delivery Approaches and Nanosystems: Volume 1- Novel Drug Carriers Volume 1*. ON, Canada: Apple Academic Press; 2018.
105. Wilson CG. Chapter 2: The organization of the gut and the oral absorption of drugs: Anatomical, biological and physiological considerations in oral formulation development. In: Wilson CG, Crowley PJ, eds. *Controlled Release in Oral Drug Delivery*. UK: Springer; 2011:27-48.
106. Chiras DD. Chapter 5: Nutrition and digestion. In: *Human Biology 7th Edition*. U.S.A: Jones and Bartlett Learning; 2012:89-117.

107. Allen C, Harper V. Digestive system: Structure and function. In: *Laboratory Manual for Anatomy and Physiology 6th Edition*. USA: John Wiley and Sons Inc.; 2017:571-598.
108. Talevi A, Bellera CL. Chapter 2: Drug absorption. In: Talevi A, Quiroga PAM, eds. *ADME Processes in Pharmaceutical Sciences: Dosage, Design and Pharmacotherapy Success*. Switzerland: Springer; 2018:11-32.
109. Laksitorini M, Prasasty VD, Kiptoo PK, Siahaan TJ. Pathways and progress in improving drug delivery through the intestinal mucosa and blood-brain barriers. *Therapeutic Delivery*. 2015;**5**:1143-1163. DOI: 10.4155/tde.14.67
110. Ahn H, Park J,. Liposomal delivery systems for intestinal lymphatic drug transport. *Biomaterials Research*. 2016;**20**:36-42. DOI: 10.1186/s40824-016-0083-1
111. Kohli K, Chopra S, Dhar D, Arora S, Khar RK. Self-emulsifying drug delivery systems: An approach to enhance oral bioavailability. *Drug Discovery Today*. 2010; **15**:958-965. DOI:10.1016/j.drudis.2010.08.007
112. Salager JL, Morgan JC, Schechter RS, Wade WH, Vasquez E. Optimum formulation of Surfactant/Water/Oil systems for minimum interfacial tension or phase behavior. *Society of Petroleum Engineers Journal*. 1979;**19**:107-115. DOI:10.2118/7054-PA
113. Shinoda K, Arai H. The correlation between phase inversion temperature in emulsion and cloud point in solution of nonionic emulsifier. *The Journal of Physical Chemistry*. 1964;**68**:3485-3490. DOI:10.1021/j100794a007
114. Salager JL, Anton R, E., Sabatini DA, Harwell JH, Acosta EJ, Tolosa EI. Enhancing solubilization in microemulsions: State of the art and current trends. *Journal of Surfactants and Detergents*. 2005;**8**:3-21. DOI: 10.1007/s11743-005-0328-4
115. Acosta EJ. The HLD-NAC equation of state for microemulsions formulated with nonionic alcohol ethoxylate and alkylphenol ethoxylate surfactants. *Colloids and Surfaces A: Physicochemical Engineering Aspects*. 2008;**320**:193-204. DOI:10.1016/ j.colsurfa.2008.01.049
116. Aarra MG, Hoiland H, Skauge A. Phase behaviour and salt partitioning in two- and three- phase anionic surfactant microemulsion systems: Part II, partitioning of salt. *Journal of Colloid and Interface Science*. 1999;**215**:216-225. DOI:10.1006/jcis.1999.6228.
117. Salager JL, Anton R, Anderez JM, Aubry JM. Formulation des microemulsions par la methode du HLD. *Techniques de l'ingenieur*. 2001;**157**:1-19.
118. Abbott S. Surfactant Science: Principles and Practice. Creative Commons BY-ND; 2019.
119. Acosta EJ, Yuan J, Bhakta A. The characteristic curvature of ionic surfactants. *Journal of Surfactants and Detergents*. 2008;**11**:145-158. DOI:10.1007/s11743-008-1065-7
120. Zarate-Munoz S, Vasconcelos FT, Myint-Myat K, Minchom J, Acosta E. A simplified methodology to measure the characteristic curvature (cc) of alkyl ethoxylate non-ionic surfactants. *Journal of Surfactants and Detergents*. 2016;**19**:249-263. DOI:10. 1007/s11743-016-1787-x
121. Healy RN, Reed RL. Physicochemical aspects of microemulsion flooding. *Society of Petroleum Engineers Journal*. 1974;**14**:491-501. DOI:10.2118/4583-PA
122. Healy RN, Reed RL, Carpenter CW. A laboratory study of microemulsion flooding. *Society of Petroleum Engineers Journal*. 1975;**15**:87-100. DOI:10.2118/4752-PA
123. Hsieh WC, Shah DO. The effect of chain length of oil and alcohol as well as surfactant to alcohol ratio on the solubilization, phase behaviour and interfacial tension of Oil/Brine/Surfactant/Alcohol systems. *Society of Petroleum Engineers Journal*. 1977. DOI:10.2118/6594-MS
124. Jones SC, Dreher KD. Co-surfactants in micellar systems used for tertiary oil recovery. *Society of Petroleum Engineers Journal*. 1976;**16**:161-167. DOI:10.2118/ 5566-PA
125. Salter SJ. The influence of type and amount of alcohol on surfactant-oil-brine phase behaviour and properties. *Society of Petroleum Engineers Journal*. 1977. DOI:10. 2118/6843-MS
126. Puerto MC, Gale WW. Estimation of optimal salinity and solubilization parameters for alkyl orthoxylene sulfonates mixtures. *Society of Petroleum Engineers Journal*. 1977;**17**:193-200.
127. Salager JL, Forgiarini AM, Bullon J. How to attain ultralow interfacial tension and three-phase behavior with surfactant formulation for enhanced oil recovery: A review. part 1. optimum formulation for simple surfactant-oil-water ternary systems. *Journal of Surfactants and Detergents*. 2013;**16**:449-472. DOI:10.1007/s11743-013-1485-x
128. US Food and Drug Administration (FDA). Fortify Your Knowledge About Vitamins. Available at: https://www.fda.gov/consumers/consumer-updates/fortify-your-knowledge-about-vitamins. Accessed February 28, 2020.

129. Government of Canada. Prenatal Nutrition. Available at: https://www.canada.ca/en/health-canada/services/canada-foodguide/resources/ prenatal-nutrition.html. Accessed February 28, 2020.
130. Government of Canada. Prenatal Nutrition Guidelines for Health Professionals- Folate Contributes to a Healthy Pregnancy. Available at: https://www.canada.ca/en/health-canada/services/publications/food-nutrition/prenatal-nutrition-guidelines-health-professionals-folate-contributes-healthy-pregnancy-2009.html. Accessed February 28, 2020.
131. Government of Canada. Prenatal Nutrition Guidelines for Health Professionals- Fish and Omega-3 Fatty Acids. Available at: https://www.canada.ca/en/health-canada/services/publications/food-nutrition/prenatal-nutrition-guidelines-health professionals-fish-omega-3-fatty-acids-2009.html. Accessed February 28, 2020.
132. DrugBank. Thiamine Mononitrate. Available at: https://www.drugbank.ca/salts/ DBSALT001495. Accessed November 21, 2019.
133. DrugBank. Riboflavin. Available at: https://www.drugbank.ca/drugs/DB00140. Accessed November 21, 2019.
134. DrugBank. Nicotinamide. Available at: https://www.drugbank.ca/drugs/DB02701. Accessed November 21, 2019.
135. DrugBank. Pyridoxine Hydrochloride. Available at: https://www.drugbank.ca/salts/ DBSALT000151. Accessed November 21, 2019.
136. DrugBank. Folic Acid. Available at: https://www.drugbank.ca/drugs/DB00158. Accessed November 21, 2019.
137. DrugBank. Cyanocobalamin. Available at: https://www.drugbank.ca/drugs/DB00115. Accessed November 21, 2019.
138. Chiras DD. Part 2: Human body systems: Homeostasis and health. In: Human Biology- 9th Edition. USA: Jones and Bartlett Learning; 2019:137-177.
139. Patton KT, Thibodeau GA. Unit 5: Respiration, nutrition and excretion. In: Anatomy and Physiology- 9th Edition. USA: Elsevier; 2016:930-961.
140. DrugBank. Beta Carotene. Available at: https://www.drugbank.ca/drugs/DB06755. Accessed November 21, 2019.
141. DrugBank. Cholecalciferol. Available at: https://www.drugbank.ca/drugs/DB00169. Accessed November 21, 2019.
142. DrugBank. Phytonadione. Available at: https://www.drugbank.ca/drugs/DB01022. Accessed November 21, 2019.
143. DrugBank. Doconexent. Available at: https://www.drugbank.ca/drugs/DB03756. Accessed November 21, 2019.
144. DrugBank. Icosapent. Available at: https://www.drugbank.ca/drugs/DB00159. Accessed November 21, 2019.
145. DrugBank. D-alpha Tocopherol Acetate. Available at: https://www.drugbank.ca/ drugs/DB14002. Accessed November 21, 2019.
146. Government of Canada. Prenatal Nutrition Guidelines for Health Professionals- Iron Contributes to a Healthy Pregnancy. Available at: https://www.canada.ca/en/health-canada/services/publications/food-nutrition/prenatal-nutrition-guidelines-health-professionals-iron-contributes-healthy-pregnancy-2009.html. Accessed February 28, 2020.
147. Health Canada. Omega-3 Fatty Acids and Fish During Pregnancy 2014. Available at: https://www.canada.ca/en/public-health/services/pregnancy/omega-3-fatty-acids-fish-during-pregnancy.html#a3. Accessed January 8, 2020.
148. Health Canada. Prenatal Nutritional Guidelines for Health Professionals 2009: Background on Canada's Food Guide. Available at: https://www.canada.ca/content/dam/hc-sc/migration/hc-sc/fn-an/alt_formats/hpfb-dgpsa/pdf/pubs/guide-prenatal-eng.pdf. Accessed January 8, 2020.
149. Health Canada. Dietary Reference Intakes 2010. Available at: https://www.canada.ca/ en/health-canada/services/food-nutrition/healthy-eating/dietary-reference-intakes/ tables/reference-values-vitamins-dietary-reference-intakes-tables-2005.html.Accessed January 8, 2020.
150. National Institute of Health (NIH). Dietary Supplement Label Database. Available at: https://www.dsld.nlm.nih.gov/dsld/lstProducts.jsp?item=PRENATAL. Accessed February 28, 2020.
151. Perrie Y, Rades T. Chapter 2: Immediate-release drug delivery systems I: Increasing the solubility and dissolution rate of drugs. In: *Pharmaceutics- Drug Delivery and Targeting*. Vol 2nd Edition. United Kingdom: Pharmaceutical Press; 2012:25-58.

152. Kong R. LC/MS application in high-throughput ADME screen. In: Ahuja S, Dong M, eds. *Handbook of Pharmaceutical Analysis by HPLC Volume 6*. The Netherlands: Elsevier Academic Press; 2005:413-439.
153. Malvern Instruments, ed. Zetasizer Nano Series User Manual. ; 2004.
154. Qiu L, Itzjan I, Perelman LT. Light scattering spectroscopy. In: Boas DA, Pitris C, Ramanujam N, eds. *Handbook of Biomedical Optics*. Florida, USA: CRC Press; 2011:165-180.
155. Acharya DP, Hartley PG. Progress in microemulsion characterization. *Current Opinion in Colloid and Interface Science*. 2012;**17**:274-280. DOI:10.1016/ j.cocis.2012.07.002
156. Fanun M. Chapter 5: Microemulsions with mixed non-ionic surfactants. In: Fanun M, ed. *Microemulsions: Properties and Applications Volume 144*. USA: CRC Press; 2009:1.
157. Tadros TF. Chapter 7: Microemulsions- V. characterization of microemulsions. In: *Surfactants in Agrochemicals Volume 54*. USA: Marcel Dekker Inc; 1995.
158. Fulton JL. Chapter 20: Structure and reactions in microemulsions formed in near-critical and supercritical fluids. In: Kumar P, Mittal KL, eds. *Handbook of Microemulsion Science and Technology*. USA: Marcel Dekker Inc; 1999.
159. Goddeeris C, Cuppo F, Reynaers H, Bouwman WG, Van den Mooter G. Light scattering measurements on microemulsions: Estimation of droplet sizes. *International Journal of Pharmaceutics*. 2006;**312**:187-195. DOI:10.1016/j.ijpharm. 2006.01.037
160. Lu GW, Gao P. Emulsions and microemulsions for topical and transdermal drug delivery. In: Kulkarni VS, ed. *Handbook of Non-Invasive Drug Delivery Systems: Non-Invasive and Minimally-Invasive Drug Delivery Systems for Pharmaceutical and Personal Care Products*. UK; USA: Elsevier; 2010:59-94.
161. Vo-Dinh T. Bioconjugated nanoparticles for biotechnology and bioanalysis. In: Vo-Dinh T, ed. *Nanotechnology in Biology and Medicine: Methods, Devices and Applications*. Florida, USA: CRC Press; 2007.
162. Parthasarathi S, Anandharamakrishnan C. Chapter 11: Stability and viability of food nanoparticles. In: Anandharamakrishnan C, Parthasarathi S, eds. *Food Nanotechnology: Principles and Applications*. Florida, USA: CRC Press; 2019:239-258.
163. Yotsawmimonwat S, Okonoki S, Krauel K, Sirithunyalug J, Sirithunyalug B, Rades T. Characterisation of microemulsions containing orange oil with water and propylene glycol as hydrophilic components. *Pharmazie*. 2006;**61**:920-926.
164. United States Pharmacopeia (USP). <711> Dissolution. Available at: http://www.usp.org/sites/default/files/usp_pdf/EN/USPNF/20110225711DISSOLUTION.pdf. Accessed September 30, 2016.
165. United States Pharmacopeia (USP). <701> Disintegration. Available at: https://www.usp.org/sites/default/files/usp/document/harmonization/gen-chapter/april-2019m99460.pdf. Accessed February 12, 2020.
166. United States Pharmacopeia (USP). <2040> Disintegration and Dissolution of Dietary Supplements Available at: https://www.uspnf.com/sites/default/files/usp_pdf/EN/USPNF/revisions/genChapter 2040 .pdf. Accessed February 13, 2020.
167. Tadros TF. Chapter 6: Formulation of microemulsions. In: *Formulation Science and Technology: Basic Principles of Formulation Types Volume 2*. Germany: De Gruyter; 2018:183-204.

Chapter 2

1. Callender S, Mathews J, Kobernyk K, Wettig S. Microemulsion utility in pharmaceuticals: Implications for multi-drug delivery. *International Journal of Pharmaceutics*. 2017; ;**526**:425-442. DOI: 10.1016/j.ijpharm.2017.05.005
2. Dahan A, Hoffman A. Chapter 6: Enhanced gastrointestinal absorption of lipophilic drugs. In: Touitou E, Barry B, eds. Enhancement in Drug Delivery. USA: CRC Press; 2011:111.
3. Gullapalli RP. Soft gelatin capsules. *Journal of Pharmaceutical Sciences*. 2010;**99**:4107-4148. DOI:10.1002/jps.22151
4. Jambhekar SS, Breen PJ. Drug dissolution: Significance of physicochemical properties and physiological conditions. *Drug Discovery Today*. 2013;**18**:1173-1184. DOI: 10.1016/j.drudis.2013.08.013
5. Zeng L, Xin X, Zhang Y. Development and characterization of promising Cremophor EL-stabilized O/W nanoemulsions containing short-chain alcohols as a cosurfactant. *RSC Advances*. 2017;**32**:19815-19827. DOI: 10.1039/C6RA27096D
6. Shah BM, Misra M, Shishoo CJ, Padh H. Nose to brain microemulsion-based drug delivery system of rivastigmine: Formulation and *ex-vivo* characterization. *Drug Delivery*. 2015;**22**:918-930. DOI: 10.3109/10717544.2013.878857
7. Sekhon B. Surfactants: Pharmaceutical and medicinal aspects. *Journal of Pharmaceutical Technology, Research and Management*. 2013;**1**:11-36. DOI: 10.15415/jptrm.2013.11004
8. Kataoka K, Harada A, Nagasaki Y. Block copolymer micelles for drug delivery: Design, characterization and biological significance. *Advanced Drug Delivery Reviews*. 2012;**64**:37-48. DOI: 10.1016/s0169-409x(00)00124-1
9. Zhang Z, Tan S, Feng SS. Vitamin E TPGS as a molecular biomaterial for drug delivery. *Biomaterials*. 2012;**33**:4889. DOI: 10.1016/j.biomaterials.2012.03.046
10. Hauss DJ. Oral lipid-based formulations. *Advanced Drug Delivery Reviews*. 2007;**59**: 667-676. DOI:10.1016/j.addr.2007.05.006
11. Mullertz A, Grove M. Chapter 5: Liquid self-microemulsifying drug delivery systems. In: Hauss DJ, ed. *Oral Lipid-Based Formulations: Enhancing the Bioavailability of Poorly Water-Soluble Drugs Volume 170*. USA: Informa Healthcare; 2007:107-127.
12. Kamboj S, Singh K, Rana V. Chapter 10: Recent developments in the microemulsion-based targeted delivery of neurotherapeutics. In: Kumar P, Pillay V, Choonara Y, eds. *Advances in Neurotherapeutic Delivery Technologies*. OMICS International; 2015.
13. Matsaridou I, Barmpalexis P, Salis A, Nikolakakis I. The influence of surfactant HLB and the Oil/Surfactant ratio on the formation and properties of self-emulsifying pellets and microemulsion reconstitution. *AAPS PharmSciTech*. 2012;**13**:1319-1330. DOI: 10.1208/s12249-012-9855-7
14. BASF. Kolliphor RH 40. Technical Information. 2011.
15. DrugBank. Poloxamer 188. Available at: https://www.drugbank.ca/drugs/DB11333. Accessed October 20, 2018.
16. BASF. Kolliphor P grades. Technical Information. 2013.
17. Millipore Sigma. Polysorbate 80 USP Reference Standard. Available at: https://www.sigmaaldrich.com/catalog/product/usp/1547969?lang=en&region=CA. Accessed October 20, 2018.
18. Hollis G. Non-ionics: Polysorbate 80. In: Hollis G, ed. *Surfactants Europa Third Edition*. UK: Royal Society of Chemistry; 1995:224.
19. Zhang R, Wang Y, Tan L, Zhang HY, Yang M. Analysis of Polysorbate 80 and its related compounds by RP-HPLC with ELSD and MS detection. *Journal of Chromatographic Science*. 2012;**50**:598-607. DOI: 10.1093/chromsci/bms035
20. Macedo JPF, Fernandes LL, Formiga FR, Reis MF, Nagashima T, Soares LAL. Micro-emultocrit technique: A valuable tool for determination of critical HLB value of emulsions. *AAPS PharmSciTech*. 2006;**7**:E1. DOI: 10.1208/pt070121
21. Shah ND, Limketkai BN. The use of medium-chain triglycerides in gastrointestinal disorders. *Practical Gastroenterology*. 2017;**41**:20-28.

22. Cerpnjak K, Zvonar A, Gasperlin M, Vrcer F. Lipid-based systems as a promising approach for enhancing the bioavailability of poorly water-soluble drugs. *Acta Pharmaceutica*. 2013;**63**:427-445. DOI: 10.2478/acph-2013-0040
23. Fanun M. Biocompatible microemulsions. In: Fanun M, ed. *Colloids in Biotechnology Volume 152*. USA: CRC Press; 2011:423.
24. Rahman MA, Hussain A, Hussain MS, Mirza MA, Iqbal Z. Role of excipients in successful development of self-emulsifying/microemulsifying drug delivery system (SEDDS/SMEDDS)**.** *Drug Development and Industrial Pharmacy*. 2013;**39**:1-19. DOI:10.3109/03639045.2012.660949
25. Sung M, Liao F, Chien Y. Medium chain triglycerides lower blood lipids and body weight in streptozotocin-induced type 2 diabetes in rats. *Nutrients*. 2018;**10**:1-11. DOI: 10.3390/nu10080963
26. Prajapati H, Patel D, Patel N, Dalrymple D, Serajuddin A. Effect of difference in fatty acid chain length of medium chain lipids on lipid/ surfactant/ water phase diagrams and drug solubility. *Journal of Excipients and Food Chemicals*. 2011;**2**:73-88.
27. Lawrence MJ. Medium-chain triglycerides. In: Rowe RC, Sheskey PJ, Owen SC, eds. *Handbook of Pharmaceutical Excipients Fifth Edition*. UK: Pharmaceutical Press; 2006.
28. Spitler R, Zanganeh S, Jafari T, et al. Chapter 1: Drug delivery systems: Possibilities and challenges. In: Pieter S, Morteza M, eds. *Drug Delivery Systems Volume 1*. Singapore: World Scientific Publishing Co.; 2018:1-52.
29. Cremer Care. Miglyol 810, 812 INCI: Caprylic/Capric Triglyceride. Available at: http://s3.amazonaws.com/petercremerna/products/spec_sheets/159/339/301/original/MIGLYOL_810_ __812_TDS.pdf?1389204445. Accessed November 1, 2019.
30. Myers D. Chapter 4: Surfactants in solution: Monolayers and micelles. In: Myers D, ed. *Surfactant Science and Technology, 3rd Edition*. USA: John Wiley & Sons Inc; 2006:107-157.
31. Myers D, ed. Chapter 5: Higher-Level Surfactant Aggregate Structures: Liquid Crystals, Continuous Biphases and Microemulsions. In: *Myers D, ed. Surfactant Science and Technology, 3rd Edition*. New Jersey, USA: Wiley Interscience; 2006
32. Bancroft WD. The theory of emulsification. *Journal of Physical Chemistry*.1913;**17**:501-519. DOI:10.1021/j150141a002
33. Strickley RG. Solubilizing excipients in oral and injectable formulations. *Pharmaceutical Research*. 2004;**21**:201-230. DOI: 10.1023/b:pham.0000016235. 32639.23
34. Myers D,. Chapter 9: Emulsions. In: Myers D, ed. *Surfactant Science and Technology, 3rd Edition*. New Jersey, USA: Wiley Interscience; 2006:280.
35. Hasan NMY. Effect of a model lipophilic compound on the phase behaviour of hydrophilic self-microemulsifying lipid formulations. *Journal of Pharmacy Research*. 2016;10:647-654.
36. Negi JS. Chapter 6: Nanolipid materials for drug delivery systems: A comprehensive review. In: Mohapatra SS, Ranjan S, Dasgupta N, Mishra RK, Thomas S, eds. *Characterization and Biology of Nanomaterials for Drug Delivery: Nanoscience and Nanotechnology in Drug Delivery*. Elsevier; 2019.
37. Weerapol Y, Limmatvapirat S, Nunthanid J, Sriamornsak P. Self-nanoemulsifying drug delivery system of nifedipine: Impact of hydrophilic-lipophilic balance and molecular structure of mixed surfactants. *AAPS PharmSciTech*. 2014;**15**:456-464. DOI: 10.1208/s12249-014-0078-y
38. Bandivadekar M, Shyamsundar P, Kaul-Ghanekar R, Choudhari A, Koppikar S. Single non-ionic surfactant based self-nanoemulsifying drug delivery systems: Formulation, characterization, cytotoxicity and permeability enhancement study. *Drug Development and Industrial Pharmacy*. 2013;**39**:696-703. DOI:10.3109/ 03639045.2012.687745.
39. Suys EJA, Warren DB, Pham AC, et al. A non-ionic polyethylene oxide (PEO) surfactant model: Experimental and molecular dynamics studies of Kolliphor EL. *Journal of Pharmaceutical Sciences*. 2019;**108**:193-204. DOI: 10.1016/j.xphs.2018.11.028
40. Shah AV, Serajuddin A. Development of solid self-emulsifying drug delivery system (SEDDS) I: Use of poloxamer 188 as both solidifying and emulsifying agent for lipids. *Pharmaceutical Research*. 2012;**29**:2817-2832. DOI: 10.1007/s11095-012-0704-x
41. Li S, Madan P, Lin S. Application of Capmul MCM and caprylic acid for the development of danazol-loaded SEDDS. *Pharmaceutical Development and Technology*. 2015;**20**:886-896. DOI: 10.3109/10837450.2014.943408

42. Kiss L, Walter FR, Bocsik A, et al. Kinetic analysis of the toxicity of pharmaceutical excipients Cremophor EL and Cremophor RH 40 on endothelial and epithelial cells. *Journal of Pharmaceutical Sciences*. 2013;**102**:1173-1181. DOI: 10.1002/jps.23458
43. Schmolka IR. Chapter 10: Polymers in the pharmaceutical industry. In: Tarcha PJ, ed. *Polymers for Controlled Drug Delivery*. Florida, USA: CRC Press; 1991:189-214.
44. Zhao X, Xiao R. Rheological properties of thermo-responsive microemulsion-based gels formed by Pluronic F68. *Journal of Chemical and Pharmaceutical Research*. 2014;**6:**2067-2072.
45. Capek I. Chapter 26: Novel inorganic and metal nanoparticles prepared by inverse microemulsion. In: Starov VM, ed. *Nanoscience: Colloidal and Interfacial Aspects Volume 147*. CRC Press, USA; 2010.
46. Bodratti AM, Alexandridis P. Formulation of Poloxamers for drug delivery. *Journal of Functional Biomaterials*. 2018;**9**:1-24. DOI: 10.3390/jfb9010011
47. Partch R, Stamper A, Ford E, Al Bawab A, Odeh F. Chapter 11: Medicine in reverse. In: Matijevic E, ed. *Fine Particles in Medicine and Pharmacy*. USA: Springer; 2012:309-341.
48. Gradzielski M, Hoffman H. Chapter 11: Rheological properties of microemulsions. In: Mittal KL, ed. *Handbook of Microemulsion Science and Technology*. USA: Marcel Dekker Inc; 1999:1-30.
49. Christiansen A, Backensfeld T, Weitschies W. Stability of the non-ionic surfactant Polysorbate 80 investigated by HPLC-MS and charged aerosol detector. *Pharmazie*. 2011;**66**:666-671.
50. Tang X, Huston KJ, Larson RG. Molecular dynamics simulations of structure-property relationships of Tween 80 surfactants in water and at interfaces. *The Journal of Physical Chemistry B*. 2014;**118**:12907-12918. DOI: 10.1021/jp507499k
51. Aboumanei MH, Abdelbary AA, Ibrahim IT, Tadros MI, El-Kolaly MT. Design and development of microemulsion systems of a new antineoplaston A10 analog for enhanced intravenous antitumor activity: In vitro characterization, molecular docking, 125I-radiolabelling and in vivo biodistribution studies. *International Journal of Pharmaceutics*. 2018;**545**:240-253. DOI: 10.1016/j.ijpharm.2018.05.010
52. Shah A, Thool P, Sorathiya K, Prajapati H, Dalrymple D, Serajuddin ATM. Effect of different polysorbates on development of self-microemulsifying drug delivery systems using medium chain lipids. *Drug Development and Industrial Pharmacy*. 2017;**44**:1-9. 10.1080/03639045.2017.1386202
53. Syed HK, Peh KK. Identification of phases of various oil, surfactant/cosurfactants and water system by ternary phase diagram. *Acta Poloniae Pharmaceutica Drug Research*. 2014;**71**:301-309.
54. Gaonkar AG, Bagwe RP. Chapter 20: Microemulsions in foods: Challenges and applications. In: Mittal KL, Shah DO, eds. *Adsorption and Aggregation of Surfactants in Solution Volume 109*. New York: Marcel Dekker Inc; 2003:368-388.
55. Singh SM, Bandi S, Jones DNM, Mallela KMG. Effect of Polysorbate 20 and Polysorbate 80 on the higher-order structure of a monoclonal antibody and its fab and fc fragments probed using 2D nuclear magnetic resonance spectroscopy. *Journal of Pharmaceutical Sciences*. 2017;**106**:3486-3498. DOI: 10.1016/j.xphs.2017.08.011
56. Komaiko JS, McClements DJ. Formation of food-grade nanoemulsions using low-energy preparation methods: A review of available methods. *Comprehensive Reviews in Food Science and Food Safety*. 2016;**15**:331-352. DOI: 10.1111/1541-4337.12189
57. Prieto C, Calvo L. Performance of the biocompatible surfactant tween 80 for the formation of microemulsions suitable for new pharmaceutical processing. *Journal of Applied Chemistry*. 2013:1-10. DOI: 10.1155/2013/930356
58. Mahdi ES, Sakeena MHF, Abdulkarim MF, Abdullah GZ, Sattar MA, Noor AM. Effect of surfactant and surfactant blends on pseudoternary phase diagram behaviour of newly synthesized palm kernel oil esters. *Drug Design, Development and Therapy*. 2011**;5**:311-323. DOI: 10.2147/DDDT.S15698
59. Ke WT, Lin SY, Ho HO, Sheu MT. Physical characterization of microemulsion systems using tocopherol polyethylene glycol 1000 succinate (TPGS) as a surfactant for the oral delivery of protein drugs. *Journal of Controlled Release*. 2005;**102**:489-507. DOI: 10.1016/j.jconrel.2004.10.030
60. Robin Y. Using tocophersolan for drug delivery: A natural vitamin E derivative is an innovative excipient. *Pharmaceutical Technology*. 2015;**39**:48-52.
61. Myers D. Chapter 5: Higher-level surfactant aggregate structures: Liquid crystals, continuous biphases and microemulsions. In: *Surfactant Science and Technology 3rd Edition*. USA: John Wiley and Sons Inc; 2006:160-189.
62. Lawrence MJ, Warisnoicharoen W. Chapter 7: Recent advances in microemulsions as drug delivery vehicles. In: Torchillin V, ed. *Nanoparticulates as Drug Carriers*. UK: Imperial College Press; 2006.

63. Amani A, York P, de Waard H, Anwar J. Molecular dynamics simulation of a polysorbate 80 micelle in water. *Soft Matter*. 2011;**7**:2900-2908. DOI: 10.1039/C0SM00965B
64. Tepavcevic V, Posa M, Obradovic S. Binary mixed micelles of polyoxyethylene (10) stearyl ether with Polysorbate 20 and Polysorbate 60: Thermodynamic description. *Journal of Surfactants and Detergents*. 2017;**20**:379-389.
65. Clint JH. Micellization of mixed nonionic surface active agents. *Journal of Chemical Society, Faraday Transactions 1: Physical Chemistry in Condensed Phases*. 1975;**71**:1327-1334. DOI: 10.1039/F19757101327
66. Szymczyk K, Zdziennicka A, Janczuk B. Adsorption and aggregation properties of some polysorbates at different temperatures. *Journal of Solution Chemistry*. 2018;**47**:1824-1840.
67. Myers D. Chapter 3: Fluid surfaces and interfaces. In: *Surfactant Science and Technology, 3rd Edition*. USA: John Wiley and Sons Inc; 2006:80-105.
68. Mitropoulos AC. What is a surface excess? *Journal of Engineering Science and Technology Review* 1. 2008:1-3.
69. Rosen MJ, Kunjappu JT. Chapter 3: Micelle formation by surfactants. In: *Surfactants and Interfacial Phenomena*. Canada: John Wiley and Sons; 2012:171.
70. Tadros TF. Part II: Colloid and interface science in cosmetics and personal care 6- surfactants used in cosmetic and personal care formulations, their properties and surfactant-polymer interaction. In: *Handbook of Colloid and Interface Science Volume 3: Industrial Applications 1: Pharmaceuticals, Cosmetics and Personal Care*. Germany: DeGruyter; 2018:109-120.
71. Myers D. Physical properties of surfactants used in cosmetics. In: Rieger M, ed. *Surfactants in Cosmetics Volume 68*. New York, USA: Marcel Dekker Inc; 1997:29-82.
72. Rosen MJ. Chapter 11: Molecular interactions and synergism in mixtures of two surfactants. In: *Surfactants and Interfacial Phenomenon 3rd Edition*. New Jersey, USA: Wiley-Interscience; 2004:379-409.
73. Holland PM, Rubingh DN. Chapter 4: Cationic surfactants in mixed surfactant systems. In: Rubingh DN, Holland PM, eds. *Cationic Surfactants: Physical Chemistry Volume 37*. New York, USA: Marcel Dekker Inc.; 1991:142-183.
74. Negm NA, El Sabagh AM. Interaction between cationic and conventional non-ionic surfactants in the mixed micelle and monolayer formed in aqueous medium. *Quimica Nova*. 2011;**34**:1007-1013. DOI: 10.1590/S0100-40422011000600018.
75. Rubingh, D. N. Surface concentrations and molecular interactions in binary mixtures of surfactants. *In Solution Chemistry of Surfactants*, Vol.1; Mittal, K. L., Ed.; Plenum Press: New York,1979; 337–359

Chapter 3

1. Callender S, Mathews J, Kobernyk K, Wettig S. Microemulsion utility in pharmaceuticals: Implications for multi-drug delivery. *International Journal of Pharmaceutics*. 2017;**526**:425-442. DOI: 10.1016/j.ijpharm.2017.05.005
2. Salager JL, Anton R, E., Sabatini DA, Harwell JH, Acosta EJ, Tolosa EI. Enhancing solubilization in microemulsions: State of the art and current trends. *Journal of Surfactants and Detergents*. 2005;**8**:3-21. DOI: 10.1007/s11743-005-0328-4
3. Thakur RK, Villette C, Aubry JM, Delaplace G. Spectrophotometric method associated with formulation scans for application of hydrophilic-lipophilic deviation concept in food emulsions. *Colloids and Surfaces A: Physicochemical Engineering Aspects*. 2007;**301**:469-474. DOI: 10.1016/j.colsurfa.2007.01.028
4. Zarate-Munoz S, Vasconcelos FT, Myint-Myat K, Minchom J, Acosta E. A simplified methodology to measure the characteristic curvature (CC) of alkyl ethoxylate non-ionic surfactants. *Journal of Surfactants and Detergents*. 2016;**19**:249-263. DOI: 10.1007/s11743-016-1787-x
5. Queste S, Salare JL, Strey R, Aubrey JM. The EACN scale for oil classification revisited thanks to fish diagrams. *Journal of Colloid and Interface Science*. 2007; **312**:98-107. DOI: 10.1016/j.jcis.2006.07.004
6. Hegde RR, Verma A, Ghosh A. Microemulsion: New insights into the ocular drug delivery. *ISRN Pharmaceutics*. 2013:1-11. doi:10.1155/2013/826798.
7. Salager JL, Forgiarini AM, Bullon J. How to attain ultralow interfacial tension and three-phase behavior with surfactant formulation for enhanced oil recovery: A review. part 1. optimum formulation for simple surfactant-oil-water ternary systems. *Journal of Surfactants and Detergents*. 2013;**16**:449-472. DOI:10.1007/s11743-013-1485-x
8. Acosta EJ, Yuan J, Bhakta A. The characteristic curvature of ionic surfactants. *Journal of Surfactants and Detergents*. 2008;**11**:145-158. DOI: 10.1007/s11743-008-1065-7
9. DrugBank. Nicotinamide. Available at: https://www.drugbank.ca/drugs/DB02701. Accessed November 21, 2019.
10. FooDB Canada. Pyridoxine Hydrochloride. Available at: http://foodb.ca/compounds/ FDB000575. Accessed November 25, 2019.
11. DrugBank. Cyanocobalamin. Available at: https://www.drugbank.ca/drugs/DB00115. Accessed November 21, 2019.
12. European Food Safety Authority. Scientific opinion on the safety and efficacy of vitamin B1 (thiamine mononitrate) as a feed additive for all animal species based on a dossier submitted by VITAC EEIG1. *EFSA Journal*. 2011;**9**:1-14.
13. DrugBank. Riboflavin. Available at: https://www.drugbank.ca/drugs/DB00140. Accessed November 21, 2019.
14. DrugBank. Folic Acid. Available at: https://www.drugbank.ca/drugs/DB00158. Accessed November 21, 2019.
15. Kondepudi N. Stability of vitamins in pharmaceutical preparations: A review. *International Journal for Research in Applied Science and Engineering Technology*. 2016;**4**:499-503.
16. Drug Delivery Foundation, Amidon GL. Biopharmaceutical Classification System (BCS) Database: Nicotinamine. Available at: http://www.ddfint.net/results.cfm. Accessed November 21, 2019.
17. United Kingdom Medicines & Healthcare Products Regulatory Agency. Public Assessment Report: Cyanocobalamin. Available at: http://www.mhra.gov.uk/ home/groups/par/documents/websiteresources/con793807.pdf. Accessed November 21, 2019.
18. BASF. Kolliphor RH 40. Technical Information. 2011.
19. BASF. Kolliphor P grades. Technical Information. 2013.
20. Zhang R, Wang Y, Tan L, Zhang HY, Yang M. Analysis of polysorbate 80 and its related compounds by RP-HPLC with ELSD and MS detection. *Journal of Chromatographic Science*. 2012;**50**:598-607. DOI: 10.1093/chromsci/bms035
21. DrugBank. Pyridoxine Hydrochloride. Available at: https://www.drugbank.ca/ salts/DBSALT000151. Accessed November 21, 2019.

22. Drug Delivery Foundation, Amidon GL. Biopharmaceutical Classification System (BCS) Database: Pyridoxine Hydrochloride. Available at: http://www.ddfint.net/ results.cfm. Accessed November 21, 2019.
23. Hauss DJ. Oral lipid-based formulations. *Advanced Drug Delivery Reviews*. 2007;**59**: 667-676. DOI:10.1016/j.addr.2007.05.006
24. Mullertz A, Grove M. Chapter 5: Liquid self-microemulsifying drug delivery systems. In: Hauss DJ, ed. *Oral Lipid-Based Formulations: Enhancing the Bioavailability of Poorly Water-Soluble Drugs Volume 170*. USA: Informa Healthcare; 2007:107-127.
25. Drug Delivery Foundation, Amidon GL. Biopharmaceutical Classification System (BCS) Database: Folic Acid. Available at: http://www.ddfint.net/results.cfm. Accessed November 21, 2019.
26. Bates CJ. Vitamin analysis. *Annals of Clinical Biochemistry*. 1997;**34**:599-626. DOI: 10.1177/000456329703400604
27. Russell LF. Chapter 10: Quantitative determination of water-soluble vitamins. In: Nollet LML, ed. *Food Analysis by HPLC, 2nd Edition*. USA: Marcel Dekker Inc.; 2000:403.
28. Eitenmiller RR, Landen WO, Ye (Jr.) L. Chapter 14: Multi-analyte methods for analysis of the fat- and water-soluble vitamins. In: *Vitamin Analysis for the Health and Food Sciences Volume 2*. USA: CRC Press; 2008.
29. Otles S, Karaibrahimoglu Y. Chapter 9: Analysis of vitamins for health, pharmaceutical and food sciences. In: Otles S, ed. *Methods of Analysis of Food Components and Additives*. USA: CRC Press; 2012:211.
30. Kim YN, Giraud DW, Driskell JA. Chapter 24: Vitamins. In: Nollet LML, Toldra F, eds. *Handbook of Muscle Foods Analysis*. USA: CRC Press; 2009:419.
31. Choi CK, Dong MW. Chapter 5: Sample preparation for HPLC analysis of drug products. In: Ahuja S, Dong M, eds. *Handbook of Pharmaceutical Analysis by HPLC Volume 6*. The Netherlands: Elsevier; 2005:123.
32. Ball GFM. The fat-soluble vitamins. In: Nollet LML, ed. *Food Analysis by HPLC, 2nd Edition*. USA: Marcel Dekker Inc.; 2000.
33. Salager JL, Anton R, Anderez JM, Aubry JM. Formulation des microemulsions par la methode du HLD. Techniques de l'ingenieur. 2001;157:1-19.
34. Acosta EJ. The HLD-NAC equation of state for microemulsions formulated with nonionic alcohol ethoxylate and alkylphenol ethoxylate surfactants. *Colloids and Surfaces A: Physicochemical Engineering Aspects*. 2008;**320**:193-204. DOI: DOI:10.1016/ j.colsurfa.2008.01.049
35. Abbott S. Surfactant Science: Principles and Practice. Creative Commons BY-ND; 2019.
36. Abbott S. Online HLD Calculator: EACN. Available at: https://www.stevenabbott.co.uk/practical-surfactants/measure-eacn.php. Accessed December 3, 2019.
37. Shinoda K, Arai H. The correlation between phase inversion temperature in emulsion and cloud point in solution of nonionic emulsifier. *The Journal of Physical Chemistry*. 1964;**68**:3485-3490. DOI: 10.1021/j100794a007
38. Winsor PA. Hydrotropy, solubilisation and related emulsification processes. *Transactions of the Faraday Society*. 1948;**44**:376-398. DOI: 10.1039/ TF9484400376
39. Karimian-Khosroshahi N, Hosseini H, Rezaei M, Khaksar R, Mahmoudzadeh M. Effect of different cooking methods on minerals, vitamins and nutritional quality indices of rainbow trout (*oncorhynchus mykiss*). *International Journal of Food Properties*. 2016;**19**:2471-2480. DOI: 10.1080/ 10942912.2015.1039028
40. Salager JL, Morgan JC, Schechter RS, Wade WH, Vasquez E. Optimum formulation of Surfactant/Water/Oil systems for minimum interfacial tension or phase behavior. *Society of Petroleum Engineers Journal*. 1979;**19**:107.
41. DrugBank. Beta Carotene. Available at: https://www.drugbank.ca/drugs/DB06755. Accessed November 21, 2019.
42. DrugBank. Cholecalciferol. Available at: https://www.drugbank.ca/drugs/DB00169. Accessed November 21, 2019.
43. DrugBank. D-alpha Tocopherol Acetate. Available at: https://www.drugbank.ca/ drugs/DB14002. Accessed November 21, 2019.
44. DrugBank. Phytonadione. Available at: https://www.drugbank.ca/drugs/DB01022. Accessed November 21, 2019.

45. DrugBank. Doconexent. Available at: https://www.drugbank.ca/drugs/DB03756. Accessed November 21, 2019.
46. DrugBank. Icosapent. Available at: https://www.drugbank.ca/drugs/DB00159. Accessed November 21, 2019.
47. Boon CS, McClements DJ, Weiss J, Decker EA. Factors influencing the chemical stability of cartenoids in foods. *Critical Reviews in Food Science and Nutrition*. 2010;**50**:515-532. DOI: 10.1080/10408390802565889
48. Marty C, Berset C. Factors affecting the thermal degradation of all trans-beta-carotene. *Journal of Agricultural and Food Chemistry*.1990;**38**:1063-1067. DOI: 10.1021/jf00094a033
49. Kanasawud P, Crouzet JC. Mechanism of formation of volatile compounds by thermal degradation of carotenoids in aqueous medium. 1. Beta-carotene degradation. *Journal of Agricultural and Food Chemistry*. 1990;**38**:237-243. DOI: 10.1021/jf00091a052
50. Dutra-de-Oliveira JE, Favaro RM, Junqueira-Franco MV, Carvalho CG, Jordao Junior AA, Vannucchi H. Effect of heat treatment on the biological value of beta-carotene added to soybean cooking oil in rats. *International Journal of Food Science and Nutrition*. 1998;**49**:205-210. DOI: doi.org/10.3109/09637489809086413
51. Knockaert G, Pulissery SK, Lemmens L, Buggenhout SV, Hendrickx M, Loey AV. Carrot beta-carotene degradation and isomerization kinetics during thermal processing in the presence of oil. *Journal of Agricultural and Food Chemistry*. 2012;**60**:10312-10319. DOI: 10.1021/jf3025776
52. Zareie M, Abbasi A, Faghih S. Thermal stability and kinetic study on thermal degradation of vitamin D3 in fortified canola oil. *Journal of Food Science*. 2019;**84**:2475-2481. DOI: 10.1111/1750-3841.14764
53. Loznjak P, Jakobsen J. Stability of vitamin D3 and vitamin D2 in oil, fish and mushrooms after household cooking. *Food Chemistry*. 2018;**254**:144-149. DOI: 10.1016/j.foodchem.2018.01.182
54. Sabilov CM, Fronczek CF, Astete C, Khachaturyan M, Khachatryan L, Leonardi C. Effects of temperature and UV light on degradation of alpha-tocopherol in free and dissolved form. *Journal of the American Oil Chemists' Society*. 2009;**86**:895-902. DOI: 10.1007/s11746-009-1411-6
55. Ferland G, Sadowski JA. Vitamin K1 (phylloquinone) content of edible oils: Effects of heating and light exposure. *Journal of Agricultural and Food Chemistry*. 1992;**40**: 1869-1873. DOI: 10.1021/jf00022a028
56. Fournier V, Destaillats F, Juaneda P, et al. Thermal degradation of long-chain polyunsaturated fatty acids during deodorization of fish oil. *European Journal of Lipid Science and Technology*. 2006;**108**:33-42. DOI: 10.1002/ejlt.200500290
57. Bienkiewicz G, Tokarczyk G, Czerniejewska-Surma B, Suryn J. Changes in the EPA and DHA content and lipids quality parameters of rainbow trout (*cyprinus carpio, L.*) at individual stages of hot smoking. *Heliyon*. 2019;**5**:1-7. DOI: 10.1016/ j.heliyon.2019.e02964
58. Hadaruga DI, Unlusayin M, Gruia AT, Birau C, Rusu G, Hadaruga NG. Thermal and oxidative stability of atlantic salmon oil (*salmo salar L.*) and complexation with B-cyclodextrin. *Beilstein Journal of Organic Chemistry*. 2016;**12**:179-191. DOI: 10.3762/bjoc.12.20
59. Domiszewski Z. Effect of heating fatty fish: Baltic herring (*clupea harengus membras*), european sprat (*sprattus sprattus*) and rainbow trout (*oncorhynchus mykiss)* on lipid oxidation and contents of eicosapentaenoic and docosahexaenoic acids. *International Journal of Food Science and Technology*. 2013;**48**:786-793. DOI: 10.1111/ijfs.12028
60. Cremer Care. Miglyol 810, 812 INCI: Caprylic/Capric Triglyceride. Available at: http://s3.amazonaws.com/petercremerna/products/spec_sheets/159/339/301/original/MIGLYOL_810__812_TDS.pdf?1389204445. Accessed November 1, 2019.
61. Abbott S. Online HLD Calculator: CC. Available at: https://www.stevenabbott.co.uk/ practical-surfactants/measure-cc.php. Accessed December 3, 2019.
62. Abbott S. Practical Surfactants: HLD Basics- Cc Values. Available at: https://www.stevenabbott.co.uk/practical-surfactants/cc.php. Accessed December 4, 2019.
63. Ash M, Ash I. *Handbook of Green Chemicals, 2nd Edition*. NY, USA: Synapse Info Resources; 2004.
64. Ruiz CC. *Sugar-Based Surfactants: Fundamentals and Applications Volume 143*. NY, USA: CRC Press; 2009.
65. Kim HS, Kim YB, Lee BS, Kim EK. Sophorolipid production by *candida bombicola* ATCC 22214 from a corn-oil processing byproduct. *Journal of Microbiological Biotechnology*. 2005;**15**:55-58. DOI: 10.3389/fmicb.2015.01324

66. Schnellbaecher A, Binder D, Bellmaine S, Zimmer A. Vitamins in cell culture media: Stability and stabilization strategies. *Biotechnology and Bioengineering*. 2019;**116**:1537-1555. DOI: 10.1002/bit.26942
67. Halver JE. Chapter 6: The vitamins. In: United Nations Development Programme: Fish Feed Technology. Rome, Italy: Food and Agriculture Organization of the United Nations; 1980.
68. Sheraz MA, Kazi SH, Ahmed S, Anwar Z, Ahmad I. Photo, thermal and chemical degradation of riboflavin. *Beilstein Journal of Organic Chemistry*. 2014;**10**:1999-2012. DOI: 10.3762/bjoc.10.208
69. Ottaway PB. Stability of vitamins in food. In: Ottaway PB, ed. *The Technology of Vitamins in Food*. England, U.K.: Springer Science and Business Media Dordrecht; 1993:90-112.
70. Lovander MD, Lyon JD, Parr IV DL, Wang J, Parke B, Leddy J. Critical review: Electrochemical properties of 13 vitamins- A critical review and assessment. *Journal of the Electrochemical Society*. 2018;**165**:G18-G49. DOI: 10.1149/2.1471714jes
71. Health Canada. Prenatal Nutritional Guidelines for Health Professionals 2009: Background on Canada's Food Guide. Available at: https://www.canada.ca/ content/dam/hc-sc/migration/hc-sc/fn-an/alt_formats/hpfb-dgpsa/pdf/pubs/guide prenatal-eng.pdf. Accessed January 8, 2020.
72. Health Canada. Dietary Reference Intakes 2010. Available at: https://www.canada.ca/ en/health-canada/services/food-nutrition/healthy-eating/dietary-reference-intakes/tables/reference-values-vitamins-dietary-reference-intakes-tables-2005.html. Accessed January 8, 2020.
73. DrugBank. Thiamine Mononitrate. Available at: https://www.drugbank.ca/salts/DBSALT001495. Accessed November 21, 2019
74. Edwards KA, Tu-Maung N, Cheng K, Wang B, Baeumner AJ, Kraft CE. Thiamine assays- advances, challenges and caveats. *Chemistry OPEN*. 2017;6:178-191. 10.1002/open.201600160
75. Bailey MR, Schultz ZD. SERS speciation of the electrochemical oxidation-reduction of riboflavin. *Analyst*. 2016;**141**:5078-5087. DOI: 10.1039/C6AN01054G
76. Szakacs Z, Noszal B. Determination of dissociation constants of folic acid, methotrexate, and other photolabile pteridines by pressure-assisted capilliary electrophoresis. *Electrophoresis*. 2006;**27**:3399-3409. DOI: 10.1002/elps.200600128
77. Gazzali AM, Lobry M, Colombeau L, et al. Stability of folic acid under several parameters. *European Journal of Pharmaceutical Sciences*. 2016;**93**:419-430. DOI: 10.1016/j.ejps.2016.08.045
78. Dryhurst G. Chapter 9: Pyridines and pyridine nucleotides. In: *Electrochemistry of Biological Molecules*. New York, USA: Academic Press; 1977:473-570.
79. Dos Santos TAD, Da Costa DO, Pita SSR, Semaan FS. Potentiometric and conductimetric studies of chemical equilibria for pyridoxine hydrochloride in aqueous solutions: Simple experimental determination of pKa values and analytical applications to pharmaceutical analysis. *Ecletica Quimica*. 2010;**35**:81-86. DOI: 10.1590/S0100-46702010000400010.
80. Albahrani AA, Greaves RF. Fat-soluble vitamins: Clinical indications and current challenges for chromatographic measurement. *The Clinical Biochemist Reviews*. 2016;**37**:27-47.
81. Machlin LJ, Langseth L. Vitamin-vitamin interactions. In: Bodwell CE, Erdman Jr. JW, eds. *Nutrient Interactions*. New York, USA: Marcel Dekker Inc; 1988:287-306.
82. Booth SL, Golly I, Sacheck JM, et al. Effect of vitamin E supplementation on vitamin K status in adults with normal coagulation status. *The American Journal of Clinical Nutrition*. 2004;**80**:143-148. DOI: 10.1093/ajcn/80.1.143
83. Traber MG. Vitamin E and K interactions- A 50-year-old problem. *Nutrition Reviews*. 2008;**66**:624-629. DOI: 10.1111/j.1753-4887.2008.00123.x
84. Maurya VK, Aggarwal M. Factors influencing the absorption of vitamin D in GIT: An overview. *Journal of Food Science and Technology*. 2017;**54**:3753-3765. DOI: 10.1007/s13197-017-2840-0
85. National Institute of Health (NIH). Riboflavin. Available at: https://ods.od.nih.gov/ factsheets/Riboflavin-HealthProfessional/. Accessed January 6, 2019.
86. National Institute of Health (NIH). Niacin. Available at: https://ods.od.nih.gov/ factsheets/Niacin-HealthProfessional/. Accessed January 6, 2020.
87. Ettinger S. Chapter 7: Diabetic nephropathy, chronic kidney disease. In: *Nutritional Pathophysiology of Obesity and its Comorbities: A Case-Study Approach*. UK: Elsevier; 2017:161-189.
88. Unknown. Possible role of vitamin E in the conversion of cyanocobalamin to its coenzyme form. *Nutrition Reviews*. 1979;**37:**332-333. DOI: 10.1111/j.1753-4887.1979.tb06633.x

Chapter 4

1. Malvern Instruments. Zetasizer Nano Series User Manual; 2004.
2. Lu GW, Gao P. Emulsions and microemulsions for topical and transdermal drug delivery. In: Kulkarni VS, ed. *Handbook of Non-Invasive Drug Delivery Systems: Non-Invasive and Minimally-Invasive Drug Delivery Systems for Pharmaceutical and Personal Care Products*. UK; USA: Elsevier; 2010:59-94.
3. Vo-Dinh T. Bioconjugated nanoparticles for biotechnology and bioanalysis. In: Vo-Dinh T, ed. *Nanotechnology in Biology and Medicine: Methods, Devices and Applications*. Florida, USA: CRC Press; 2007.
4. Parthasarathi S, Anandharamakrishnan C. Chapter 11: Stability and viability of food nanoparticles. In: Anandharamakrishnan C, Parthasarathi S, eds. *Food Nanotechnology: Principles and Applications*. Florida, USA: CRC Press; 2019:239-258.
5. McClements DJ. Nanoemulsions versus microemulsions: Terminology, differences and similarities. *Soft Matter*. 2012;8:1719. DOI:10.1039/C2SM06903B
6. Harini Chowdary V, Prasanna Raju Y, Basaveswara Rao MV, Sundaresan CR. Insights of microemulsions- A thermodynamic comprehension. *Jordan Journal of Pharmaceutical Sciences*. 2017;**10**:23-40.
7. Muller RH. Biodegradable fat emulsion carriers. In: *Colloidal Carriers for Controlled Drug Delivery and Targeting: Modification, Characterization, in Vivo Distribution*. Germany: CRC Press; 1991:175-201.
8. Marshall P. Chapter 49: Product stability and stability testing. In: Aulton ME, Taylor KMG, eds. *Aulton's Pharmaceutics E-Book: The Design and Manufacture of Medicines*. Elsevier; 2017.
9. Barnes AR. Chapter 47: Chemical stability in dosage forms. In: Aulton ME, Taylor KMG, eds. *Aulton's Pharmaceutics E-Book: The Design and Manufacture of Medicines*. Elsevier; 2017:836- 849.
10. Wahlgren M, Bergenstahl B, Nilsson L, Rayner M. Formulation of microemulsions. In: Rayner M, Dejmek P, eds. *Engineering Aspects of Food Emulsification and Homogenization*. Florida, USA: CRC Press; 2015:58.
11. Ali KA, Roy S. Emulsification technology for cosmetic preparation. In: Mazumder B, Ray S, Pal P, Pathak Y, eds. *Nanotechnology: Therapeutic, Nutraceutical and Cosmetic Advances*. Florida, USA: CRC Press; 2019:413.
12. Prieto C, Calvo L. Performance of the biocompatible surfactant Tween 80 for the formation of microemulsions suitable for new pharmaceutical processing. *Journal of Applied Chemistry*. 2013:1-10. DOI:10.1155/2013/930356
13. Bandivadekar M, Shyamsundar P, Kaul-Ghanekar R, Choudhari A, Koppikar S. Single non-ionic surfactant based self-nanoemulsifying drug delivery systems: Formulation, characterization, cytotoxicity and permeability enhancement study. *Drug Development and Industrial Pharmacy*. 2013;**39**:696-703. DOI:10.3109/03639045. 2012.687745.
14. McClements DJ. Chapter 11: Characterization of emulsion properties. *In: Food Emulsions: Principles, Practices and Techniques 2nd Edition*. Florida, U.S.A: CRC Press; 2005:464.
15. Yang S, Baldwin RE. Chapter 16: Functional properties of eggs in foods. In: Stadelman WJ, Newkirk D, Newby L, eds. *Egg Science and Technology, 4th Edition*. USA, UK: Food Products Press; 1995:405-450.
16. Malvern Panalytical. Derived Count Rate- What Is It? Available at: https://www.materials-talks.com/blog/2015/06/11/derived-count-rate-what-is-it/. Accessed April 8, 2020.
17. Xia L, Zhang S, Ma H, et al. In situ monitoring of the structural change of microemulsions in simulated gastrointestinal conditions by SAXS and FRET. *Acta Pharmaceutica Sinica B*. 2018;**8**:655-665. DOI:10.1016/j.apsb.2018.05.008
18. Ben Yehuda Greenwald M, Frusic-Zlotkin M, Soroka Y, et al. Curcumin protects skinagainst UVB-inducted cytotoxicity via the Keap1-Nrf2 pathway: The use of a microemulsion delivery system. *Oxidative Medicine and Cellular Longevity*. 2017;**6**:1-17. DOI: 10.1155/2017/5205471

19. Nikolakakis I, Panagopoulou A, Salis A, Malamataris S. Relationships between the properties of self-emulsifying pellets and of the emulsions used as massing liquids for their preparation. *AAPS PharmSciTech*. 2015;**16**:129-139. DOI:10.1208/s12249-014-0214-8.
20. Patel K, Vavia P, Sarma V. Design and evaluation of lumefantrine- oleic acid self-nanoemulsifying ionic complex for enhanced dissolution. *Daru Journal of Pharmaceutical Sciences*. 2013;**21**:1-10. DOI:10.1186/2008-2231-21-27.
21. Shahba A, Mohsin K, Alanzi FK, Abdel-Rahman SI. Optimization of self-nanoemulsifying formulations for weakly basic lipophilic drugs: Role of acidification and experimental design. *Brazilian Journal of Pharmaceutical Sciences*. 2016;**52**:653- 667.DOI:10.1590/s1984- 82502016000 400009.
22. Brunner H, Tsuno T, Balazs G, Bodensteiner M. Methyl/Phenyl attraction by CH/Pi interaction in 1,2-substitution patterns. *Journal of Organic Chemistry*. 2014;**79**:11454-11462. DOI:10.1021/jo5020454 |.
23. Desale SS, Cohen SM, Zhao Y, Kabanov AV, Bronich TK. Biodegradable hybrid polymer micelles for combination drug therapy in ovarian cancer. *Journal of Controlled Releas*e. 2013;**171**:339-348. DOI:10.1016/j.jconrel.2013.04.026.
24. Chen SF, Lu WF, Wen ZY, Li Q, Chen JH. Preparation, characterization and anticancer activity of norcantharidin-loaded poly(ethylene glycol)-poly(caprolactone) amphiphilic block co-polymer micelles. *Pharmazie*. 2012;**67**:781-788. DOI:10.1691/ph.2012.1151.
25. Sharma PK, Bhatia SR. Effect of anti-inflammatories on Pluronic F127: Micellar assembly, gelation and partitioning. *International Journal of Pharmaceutics*. 2004;**278**:361-377. DOI:10.1016/j.ijpharm.2004.03.029.
26. Basak R, Bandyopadhyay R. Encapsulation of hydrophobic drugs in pluronic F127 micelles: Effects of drug hydrophobicity, solution temperature and pH. *Langmuir*.2013;**29**:4350-4395. DOI:10.1021/a304836e.
27. Ahmad Z, Shah A, Siddiq M, Kraatz BH. Polymeric micelles as drug delivery vehicles. *RSC Advances*. 2014;**4**:17028-17038. DOI:10.1039/C3RA47370H
28. Jalil R, Nixon JR. Biodegradable poly(lactic acid) and poly(lactide-co-glycolide) microcapsules: Problems associated with preparative techniques and release properties. *Journal of Microencapsulation*. 1990;**7**:297-325. DOI:10.3109/02652049 009021842.
29. Sjoblom J. *Emulsions- A Fundamental and Practical Approach*. Netherlands: Kluwer Academic Publishers; 1992.
30. Chumpitaz LDA, Coutinho LF, Meirelles AJA. Surface tension of fatty acids and triglycerides. *Journal of the American Oil Chemists' Society*. 1999;**76**:379-382. DOI:10.1007/s11746-999-0245-6.
31. Shaker DS, Ishak RAH, Ghoneim A, Elhuoni MA. Nanoemulsion: A review on mechanisms for the transdermal delivery of hydrophobic and hydrophilic drugs. *Scientia Pharmaceutica*. 2019;**87**:17. DOI:10.3390/scipharm87030017.
32. United States Food and Drug Administration (US FDA). Drug Databases: Inactive Ingredient Search- Polysorbate 80 Oral Capsule. Available at: https://www.accessdata.fda.gov/scripts/cder/iig/index.cfm?event=BasicSearch.page. Accessed January 29, 2020.
33. United States Food and Drug Administration (US FDA). Drug Databases: Inactive Ingredient Search- Polyoxyl 40 Hydrogenated Castor Oil Oral Capsule. Available at: https://www.accessdata.fda.gov/scripts/cder/iig/index.cfm?event=BasicSearch.page. Accessed January 29, 2020.
34. Ding W, Hou X, Cong S, et al. Co-delivery of honokiol, a constituent of magnolia species, in a self-microemulsifying drug delivery system for improved oral transport of lipophilic sirolimus. *Drug Delivery*. 2015;**1**: 2513-2523. DOI:10.3109/10717544.2015.1020119
35. Ujhelyi Z, Kalantari A, Vecsernyes M, et al. The enhanced inhibitory effect of different antitumor agents in self-microemulsifying drug delivery systems on human cervical cancer HeLa cells. *Molecules*. 2015;**20**:13226-13239. DOI:10.3390/ molecules200713226.
36. Kaur G, Mehta S. Probing location of anti-TB drugs loaded in Brij 96 microemulsions using thermoanalytical and photophysical approach. *Journal of Pharmaceutical Sciences*. 2014;**103**:937-944. DOI:10.1002/jps.23857
37. DrugBank. Doconexent. Available at: https://www.drugbank.ca/drugs/DB03756. Accessed November 21, 2019.

38. DrugBank. Icosapent. Available at: https://www.drugbank.ca/drugs/DB00159. Accessed November 21, 2019.
39. Wang Z, Pal R. Microemulsions and their applications in drug delivery. In: Birdi KS, ed. *Handbook of Surface and Colloid Chemistry 4th Edition*. USA: CRC Press; 2016:583-600.
40. Acharya DP, Hartley PG. Progress in microemulsion characterization. *Current Opinion in Colloid and Interface Science*. 2012;**17**:274-280. DOI: 10.1016/j.cocis.2012.07.002
41. Yotsawmimonwat S, Okonoki S, Krauel K, Sirithunyalug J, Sirithunyalug B, Rades T. Characterisation of microemulsions containing orange oil with water and propylene glycol as hydrophilic components. *Pharmazie*. 2006;**61**:920-926.
42. Paul BK, Moulik SP. The viscosity behaviours of microemulsions: An overview. *Proceedings of the Indian National Science Academy*. 2000;**66**:499-519.
43. Chen CM, Warr GG. Rheology of ternary microemulsions. *The Journal of Physical Chemistry*. 1992;**96**:9492-9497. DOI:10.1021/j100202a077
44. Engineer's Edge. Physics: Water- Density Viscosity Specific Weight. Available at: https://www.engineersedge.com/physics/water__density_viscosity_specific_weight_13146.htm. Accessed January 28, 2020.
45. Kogan A, Shalev DE, Raviv U, Aserin A, Garti N. Formation and characterization of ordered bicontinuous microemulsions. *The Journal of Physical Chemistry B*. 2009;**113**:10669-10678. DOI:10.1021/jp901617g
46. Gradzielski M, Hoffman H. Chapter 11: Rheological properties of microemulsions. In: Mittal KL, ed. *Handbook of Microemulsion Science and Technology*. USA: Marcel Dekker Inc; 1999:1-30.
47. Salimi A, Moghimipour E, Sharif B. Preparation and characterization of cyanocobalamin (Vit. B12) microemulsion properties and structure for topical and transdermal application. *Iranian Journal of Basic Medical Science*. 2013;**16**:865-872.
48. Fleming D. Differential Scanning Calorimetry and Thermo-Gravimetric Analysis. Available at: http://www.flemingptc.co.uk/our-services/dsc-tga/. Accessed January 29, 2020.
49. Basheer HS, Noordin MI, Ghareeb MM. Characterization of microemulsions prepared using isopropyl palmitate with various surfactants and cosurfactants. *Tropical Journal of Pharmaceutical Research*. 2013;**12**:305-310. DOI:10.4314/tjpr.v12i3.5
50. Dalmazzone C, Noik C, Clausse D. Application of DSC for emulsified system characterization. *Oil and Gas Science and Technology*. 2009;**64**:543-555. DOI: 10.2516/ogst:2008041
51. Hasan NMY. Preparation of solid self-micro-emulsified lipid systems for the delivery of hydrophobic drugs. *International Journal of Pharmaceutical Research*. 2015;**7**:75-84.
52. John A Dutton e-Education Institute. MATSE 202: Introduction to Polymer Materials Thermal Transitions and Differential Scanning Calorimetry. Available at: https://www.e-education.psu.edu/matse202/node/845. Accessed January 28, 2020.
53. Garti N, Aserin A, Tiunova I, Fanun M. A DSC study of water behaviour in water-in-oil microemulsions stabilized by sucrose esters and butanol. *Colloids and Surfaces A: Physicochemical Engineering Aspects*. 2000;**170**:1-18. DOI:10.1016/S0927- 7757(00)00486-6
54. Hohne GWH, Hemminger WF, Flammershein HJ. *Differential Scanning Calorimetry, 2nd Edition*. New York, USA: Springer; 2003.
55. Xin J, Meng X, Xu X, Zhu Q, Naveed HB, Ma W. Cold crystallization temperature correlated phase separation, performance, and stability of polymer solar cells. *Matter*. 2019;**1**:1316-1330. DOI:10.1016/j.matt.2019.06.011
56. Tcholakova S, Valkova Z, Cholakova D, et al. Efficient self-emulsification via cooling-heating cycles. *Nature Communications*. 2017;**8**:15012. DOI:10.1038/ncomms15012.
57. Darole PS, Hegde DD, Nair HA. Formulation and evaluation of microemulsion based drug delivery system for amphotericin B. *AAPS PharmSciTech*. 2008;**9**:122-128. DOI:10.1208/s12249-007-9022-8.
58. Mohajeri E, Noudeh GD. Effect of temperature on the critical micelle concentration and micellization thermodynamic of nonionic surfactants: Polyoxyethylene sorbitan fatty acid ester. *E-Journal of Chemistry*. 2012;**9**:2268-2274. DOI:10.1155/2012/961739
59. Su R, Yang L, Wang Y, et al. Formulation, development and optimization of a novel octyldodecanol-based nanoemulsion for transdermal delivery of ceramide IIIB. *International Journal of Nanomedicine*. 2017;**12**:5203-5221. DOI:10.2147/IJN.S139975

60. Sheraz MA, Kazi SH, Ahmed S, Anwar Z, Ahmad I. Photo, thermal and chemical degradation of riboflavin. *Beilstein Journal of Organic Chemistry*. 2014;**10**:1999-2012. DOI:10.3762/bjoc.10.208
61. Arab-Tehrany E, Jacquot M, Gaiani C, Imran M, Desobry S, Linder M. Beneficial effects and oxidative stability of omega-3 long-chain polyunsaturated fatty acids. *Trends in Food Science & Technology*. 2012;**25**:24-33. DOI:10.1016/j.tifs.2011.12.002
62. Penichaud C, Achir N, Dhuique-Meyer C, Dornier M, Bohuon P. Degradation of B-carotene during fruit and vegetable processing or storage: Reaction mechanisms and kinetic aspects- A review. *Fruits*. 2011;**66**:417-420. DOI:10.1051/fruits/2011058
63. Ashikawa I, Miyata A, Koike H, Inoue Y, Koyama Y. Light-induced structural change of B-carotene in thylakoid membranes. *Biochemistry*. 1986;**25**:6154-6160. DOI:10.1021/bi00368a049
64. Buhler V. *Vademecum for Vitamin Formulations 2nd Edition*. Germany: Wissenschaftliche Verlagsgesellschaft mbH; 2001.
65. US Cosmetic Ingredient Review. Final report on the safety assessment of tocopherol, tocopheryl acetate, tocopheryl linoleate, tocopheryl Linoleate/Oleate, tocopheryl nicotinate, tocopheryl succinate, dioleyl tocopheryl methylsilanol, potassium ascorbyl tocopheryl phosphate, and tocophersolan. *International Journal of Toxicology*. 2002;**21**:116. DOI:10.1080/10915810290169819
66. Hadaruga DI, Unlusayin M, Gruia AT, Birau C, Rusu G, Hadaruga NG. Thermal and oxidative stability of atlantic salmon oil (*salmo salar L.*) and complexation with B-cyclodextrin. Beilstein *Journal of Organic Chemistry*. 2016;**12**:179-191. DOI:10.3762/bjoc.12.20
67. Scita G. The stability of B-carotene under different laboratory conditions. *Journal of Nutritional Biochemistry*. 1992;**3**:124-128. DOI:10.1016/0955-2863(92)90104-Q
68. Ewing DT, Tomkins FS, Kamm O. The ultraviolet absorption of vitamin K1 and the effect of light on the vitamin. *Journal of Biological Chemistry*. 1943;**147**:233-241.
69. Yessaad M, Bernard L, Bourdeaux D, Chennell P, Sautou V. Development of a stability indicating method for simultaneous analysis of five water-soluble vitamins by liquid chromatography. *Pharmaceutical Technology in Hospital Pharmacy*. 2018;**3**:207-218. DOI:10.1515/pthp-2018-0026
70. Schnellbaecher A, Binder D, Bellmaine S, Zimmer A. Vitamins in cell culture media: Stability and stabilization strategies. *Biotechnology and Bioengineering*. 2019;**116**:1537-1555. DOI:10.1002/bit.26942
71. Monajjemzadeh F, Ebrahimi F, Zakeri-Milani P, Valizadeh H. Effects of formulation variables and storage conditions on light protected vitamin B12 mixed parenteral formulations. *Advanced Pharmaceutical Bulletin*. 2014;**4**:329-338. DOI:10.5681/apb.2014.048
72. Damodaran S. Chapter 5: Amino acids, peptides and proteins. In: Damodaran S, Parkin KL, eds. *Fennema's Food Chemistry 5th Edition*. Florida, USA: CRC Press; 2017:301.
73. Zayas JF. *Functionality of Proteins in Food*. Germany: Springer; 1997.

Chapter 5

1. Liu W, Zhai Y, Heng X, et al. Oral bioavailability of curcumin: Problems and advancements. *Journal of Drug Targeting*. 2016;**24**:694-702. DOI: 10.3109/1061186X.2016.1157883
2. Cerpnjak K, Zvonar A, Gasperlin M, Vrcer F. Lipid-based systems as a promising approach for enhancing the bioavailability of poorly water-soluble drugs. *Acta Pharmaceutica*. 2013;**63**:427-445. DOI: 10.2478/acph-2013-0040
3. He C, He Z, Gao J. Microemulsions as drug delivery systems to improve the solubility and the bioavailability of poorly water-soluble drugs. *Expert Opinion on Drug Delivery*. 2010;**7**:445. DOI; 10.1517/17425241003596337
4. McClements DJ. Nanoscale nutrient delivery systems for food applications:Improving bioactive dispersibility, stability, and bioavailability. *Journal of Food Science*. 2015;**80**:1602-1611. DOI: 10.1111/1750-3841.12919
5. Myers D. Chapter 2:The organic chemistry of surfactants . In: *Surfactant Science and Technology, 3rd Edition*. USA: Wiley Interscience; 2005:29.
6. Ribeiro MENP, de Moura CL, Vieira MGS, et al. Solubilization capacity of brij surfactants. *International Journal of Pharmaceutics*. 2012;**436**:631-635. 10.1016/j.ijpharm.2012.07.032
7. Bancroft WD. The theory of emulsification. *Journal of Physical Chemistry*. 1913;**17**:501-519. DOI:10.1021/j150141a002
8. Myers D. Chapter 6: Solubilization and micellar and phase transfer catalysis. In: *Surfactant Science and Technology, 3rd Edition*. USA: John Wiley and Sons Inc; 2006:191-218.
9. Myers D. Chapter 10: Solid surfaces and dispersions. In: *Surfactant Science and Technolog,3rd Edition*. USA: John Wiley and Sons Inc; 2006:323-367.
10. Sannaningannavar FM, Patil SN, Melavanki RM, Navati BS, Ayachit NH. Ultrasonic study of thermo-acoustic parameters of the Polysorbate 20, 40, 60 and 80 liquid surfactants at different temperatures. *Journal of Molecular Liquids*. 2014;**196**:244-248. DOI: 10.1016/j.molliq.2014.03.039
11. Brunaugh AD, Smyth HDC, Williams III RO. Chapter 7: Disperse systems. In: *Essential Pharmaceutics*. Switzerland: AAPS/Springer; 2019:111-121.
12. CRODA. Tween 81. Available at: https://www.crodacropcare.com/en-gb/products-and-applications/product-finder/product/255/Tween_1_81. Accessed February 22, 2020.
13. Millipore Sigma. Brij 93. Available at: https://www.sigmaaldrich.com/catalog/product/aldrich/388866?lang=en&region=CA. Accessed February 18, 2020.
14. CRODA. Brij O2. Available at: https://www.crodacropcare.com/en-gb/products-and-applications/product-finder/product/15/Brij_1_O2. Accessed February 22, 2020.
15. CRODA. SP BRIJ O10 MBAL. Available at: https://www.crodacropcare.com/en-gb/products-and-applications/product-finder/product/16/SP_1_Brij_1_O10_1_MBAL Accessed February 22, 2020.
16. CRODA. SP BRIJ O20 MBAL. Available at: https://www.crodacropcare.com/en-gb/products-and-applications/product-finder/product/17/SP_1_Brij_1_O20_1_MBAL Accessed February 22, 2020.
17. CRODA. BRIJ S100. Available at: https://www.crodacropcare.com/en-gb/products-and-applications/product-finder/product/10/Brij_1_S100. Accessed February 22, 2020.
18. Myers D. Chapter 3: Fluid surfaces and interfaces. In: *Surfactant Science and Technology, 3rd Edition*. USA: John Wiley and Sons Inc; 2006:80-105.
19. Myers D. Chapter 4: Surfactants in solution: Monolayers and micelles. In: Myers D, ed. *Surfactant Science and Technology, 3rd Edition*. USA: John Wiley & Sons Inc; 2006:107-157.
20. Kamboj S, Singh K, Rana V. Chapter 10: Recent developments in the microemulsion-based targeted delivery of neurotherapeutics. In: Kumar P, Pillay V, Choonara Y, eds. *Advances in Neurotherapeutic Delivery Technologies*. OMICS International; 2015.
21. Matsaridou I, Barmpalexis P, Salis A, Nikolakakis I. The influence of surfactant HLB and the oil/surfactant ratio on the formation and properties of self-emulsifying pellets and microemulsion reconstitution. *AAPS PharmSciTech*. 2012;**13**:1319. DOI: 10.1208/s12249-012-9855-7
22. Myers D. Chapter 5: Higher-level surfactant aggregate structures: Liquid crystals, continuous biphases and microemulsions. In: *Surfactant Science and Technology, 3rd Edition*. USA: John Wiley and Sons Inc; 2006:160-189.

23. ChemSrc. Tween 85. Available at: https://www.chemsrc.com/en/cas/9005-70-3_1198859.html. Accessed February 18, 2020.
24. CRODA. Tween 85. Available at: https://www.crodacropcare.com/en-gb/products-and-applications/product-finder/product/256/Tween_1_85. Accessed February 22, 2020.
25. United States Pharmacopeia (USP). <2040> Disintegration and Dissolution of Dietary Supplements. Available at: https://www.uspnf.com/sites/default/files/usp_pdf/EN/USPNF/revisions/genChapter2040.pdf. Accessed February 13, 2020.
26. Shargel L, Wu-Pong S, Yu ABC. *Applied Biopharmaceutics & Pharmacokinetics 6th Edition*. USA: McGraw-Hill Education; 2012.
27. Macedo JPF, Fernandes LL, Formiga FR, Reis MF, Nagashima T, Soares LAL. Micro-emultocrit technique: A valuable tool for determination of critical HLB value of emulsions. *AAPS PharmSciTech*. 2006;**7**:E1. DOI: 10.1208/pt070121
28. Muller RH. Chapter 5: Biodegradable polymeric carriers. In: *Colloidal Carriers for Controlled Drug Delivery and Targeting: Modification, Characterization and in Vivo Distribution*. Germany: CRC Press; 1991:155-172.
29. Conacher M, Alexander J, Brewer JM. Chapter 10: Niosomes as immunological adjuvants. In: Uchegbu IF, ed. *Synthetic Surfactant Vesicles: Niosomes and Other Non-Phospholipid Vesicular Systems*. The Netherlands: Harwood Academic Publishing; 2000:204-227.
30. dos Santos EC, Fernandez-Ronco MP, Mazzotti M. Crystallization of phase change emulsions. In: *BIWIC 2014: 21st International Workshop on Industrial Crystallization*. France:2014:328.
31. Cho SJ, Uddin MJ, Alaboina P. Review of nanotechnology for cathode materials in batteries. In: Rodriguez-Martinez LM, Omar N, eds. *Emerging Nanotechnologies in Rechargeable Energy Storage Systems*. Netherlands: Elsevier; 2017:83-127.
32. Stachurski J, MichaLek M. The effect of the zeta potential on the stability of a non-polar oil-in-water emulsion. *Journal of Colloid and Interface Science*. 1996;184:433-436. DOI: 10.1006/jcis.1996.0637
33. DrugBank. Riboflavin. Available at: https://www.drugbank.ca/drugs/DB00140. Accessed November 21, 2019.
34. United States Pharmacopeia (USP). <711> Dissolution. Available at: http://www.usp.org/sites/default/files/usp_pdf/EN/USPNF/2011-02-25711DISSOLUTION.pdf. Accessed September 30, 2016.
35. Moore JW, Flanner HH. Mathematical comparison of dissolution profiles. *Pharmaceutical Technology*. 1996;**20**:64-74.
36. United States Food and Drug Administration (US FDA). Guidance for industry: Dissolution testing of immediate release solid oral dosage forms. 2019;BP 1:1-17.
37. de Souza Anselmo C, de Carvalho Mendes T, da Silva Honorio T, Almada do Carmo A, Cabral LM, Pereira de Sousa V. Development and validation of a dissolution test for lutein tablets and evaluation of intestinal permeability. *Food Chemistry*. 2016;**210**:63-69. DOI: 10.1016/j.foodchem.2016.04.081
38. Zechmeister L. *Cis-Trans Isomeric Cartenoids, Vitamin A and Arylpolyenes*. New York, U.S.A: Springer Verlag Vienna; 1962.
39. Khoo HE, Prasad KN, Kong KW, Jiang Y, Ismail A. Cartenoids and their isomers: Colour pigments in fruits and vegetables. *Molecules*. 2011;**16**:1710-1738. DOI: 10.3390/molecules16021710
40. Wahlgren M, Bergenstahl B, Nilsson L, Rayner M. Formulation of microemulsions. In: Rayner M, Dejmek P, eds. *Engineering Aspects of Food Emulsification and Homogenization*. Florida, USA: CRC Press; 2015:58.
41. Arab-Tehrany E, Jacquot M, Gaiani C, Imran M, Desobry S, Linder M. Beneficial effects and oxidative stability of omega-3 long-chain polyunsaturated fatty acids. *Trends in Food Science & Technology*. 2012;25:24-33. DOI: 10.1016/j.tifs.2011.12.002
42. Buhler V. *Vademecum for Vitamin Formulations, 2nd Edition*. Germany: Wissenschaftliche Verlagsgesellschaft mbH; 2001.
43. US Cosmetic Ingredient Review. Final report on the safety assessment of tocopherol, tocopheryl acetate, tocopheryl linoleate, tocopheryl Linoleate/Oleate, tocopheryl nicotinate, tocopheryl succinate, dioleyl tocopheryl methylsilanol, potassium ascorbyl tocopheryl phosphate, and tocophersolan. *International Journal of Toxicology*. 2002**;21**:116. DOI: 10.1080/10915810290169819
44. Damodaran S. Chapter 5: Amino acids, peptides and proteins. In: Damodaran S, Parkin KL, eds. *Fennema's Food Chemistry, 5th Edition*. Florida, USA: CRC Press; 2017:301.

Chapter 6

1. Lu D, Chambers P, Wipf P, Xie XQ, Englert D, Weber S. Lipophilicity screening of novel drug-like compounds and comparison to cLogP. *Journal of Chromatography A*. 2012;**1258**:161-167. DOI: 10.1016/j.chroma.2012.07.078
2. ChemAxon Ltd. MarvinView Software. Available at: https://chemaxon.com/products/marvin. Accessed September 4, 2020.
3. Damiati SA. Digital pharmaceutical sciences. *AAPS PharmSciTech*. 2020;**21**:1-12. DOI: 10.1208/s12249-020-01747-4
4. Damiati SA, Martini LG, Smith NW, Lawrence MJ, Barlow DJ. Application of machine learning in prediction of hydrotrope-enhanced solubilisation of indomethacin. International *Journal of Pharmaceutics*. 2017;**530**:99-106. DOI: 10.1016/j.ijpharm.2017.07.048
5. Rodriguez-Dorado R, Landin M, Altai A, Russo P, Aquino RP, Del Gaudio P. A novel method for the production of core-shell microparticles by inverse gelation optimized with artificial intelligent tools. *International Journal of Pharmaceutics*. 2018;**538**:97-104. DOI: 10.1016/j.ijpharm.2018.01.023
6. Wu HY, Sun CB, Liu N. Effects of different cryoprotectants on microemulsion freeze-drying. *Innovative Food Science and Emerging Technologies*. 2019;**54**:28-33. DOI: 10.1016/j.ifset.2018.12.007
7. Morais ARVM, Xavier Jr. FH, Alencar EN, et al. Optimization of the freeze-drying process for microemulsion systems. *Drying Technology*. 2018;**37**:1745-1756. DOI:10.1080/07373937.2018.1536883
8. Abbott S. Practical Surfactants. Available at: https://www.stevenabbott.co.uk/practical-surfactants/. Accessed September 4, 2020.

Appendices

Appendix A

Critical Micelle Concentration (CMC) Plots

Polysorbate 80:

Surfactant Concentration (mM)	Log Surfactant Concentration	Average Surface Tension (mN/m)	Standard Deviation
0	-4.30	68.61	0.25
0.0001	-3.90	64.20	0.08
0.0002	-3.60	58.75	0.04
0.0005	-3.30	54.57	0.07
0.0012	-2.91	48.86	0.09
0.0017	-2.76	46.91	0.05
0.0024	-2.61	45.06	0.07
0.0036	-2.44	43.10	0.05
0.0048	**-2.32**	**41.61**	**0.03**
0.0070	-2.16	40.79	0.01
0.0091	-2.04	40.22	0.03
0.0111	-1.95	39.72	0.02
0.0140	-1.85	39.50	0.01
0.0167	-1.78	39.31	0.03
0.0200	-1.70	39.29	0.11
0.0259	-1.59	39.28	0.02
0.0322	-1.49	39.29	0.03
0.0403	-1.39	40.20	0.04
0.0452	-1.34	40.34	0.02

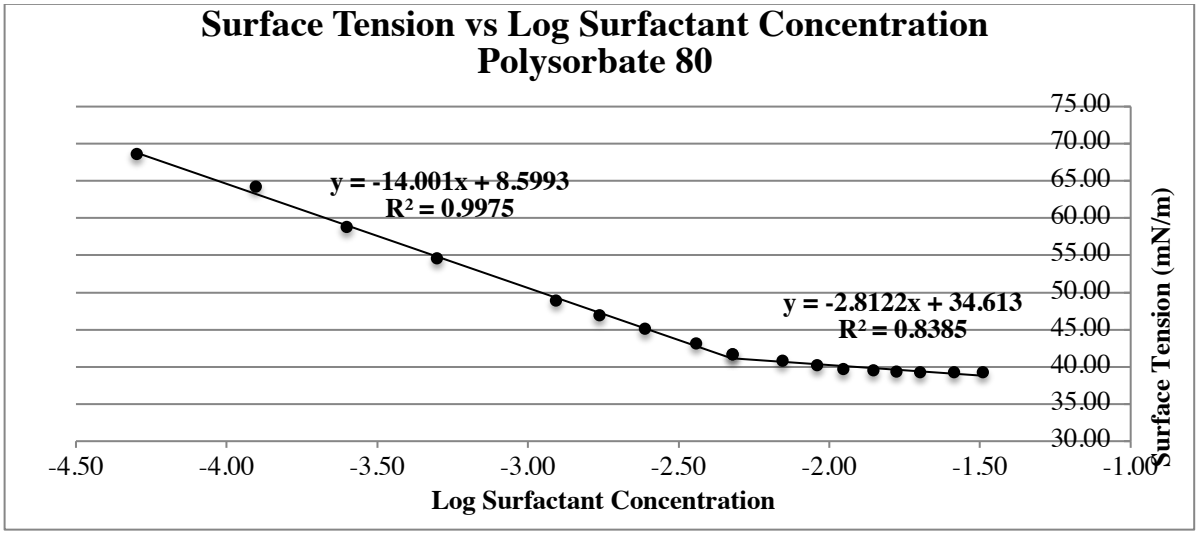

Figure A-1: Surface tension values versus surfactant concentration for Polysorbate 80 (CMC bolded)

PEG-40 hydrogenated castor oil
Replicate 1

Surfactant Concentration (mM)	Log Surfactant Concentration	Average Surface Tension (mN/m)	Standard Deviation
0	-4.50	69.54	0.13
0.0004	-3.45	58.03	0.10
0.0005	-3.28	55.78	0.05
0.0007	-3.16	54.94	0.05
0.0010	-2.99	53.23	0.05
0.0014	-2.87	52.08	0.06
0.0017	-2.78	50.75	0.04
0.0023	-2.64	49.31	0.05
0.0029	-2.54	48.17	0.06
0.0034	-2.46	47.24	0.05
0.0040	-2.40	46.11	0.03
0.0050	**-2.30**	**45.03**	**0.01**
0.0064	-2.20	44.46	0.01
0.0080	-2.10	44.31	0.01
0.0101	-2.00	43.40	0.00
0.0127	-1.90	44.89	0.05
0.0158	-1.80	44.36	0.04
0.0181	-1.74	43.76	0.03

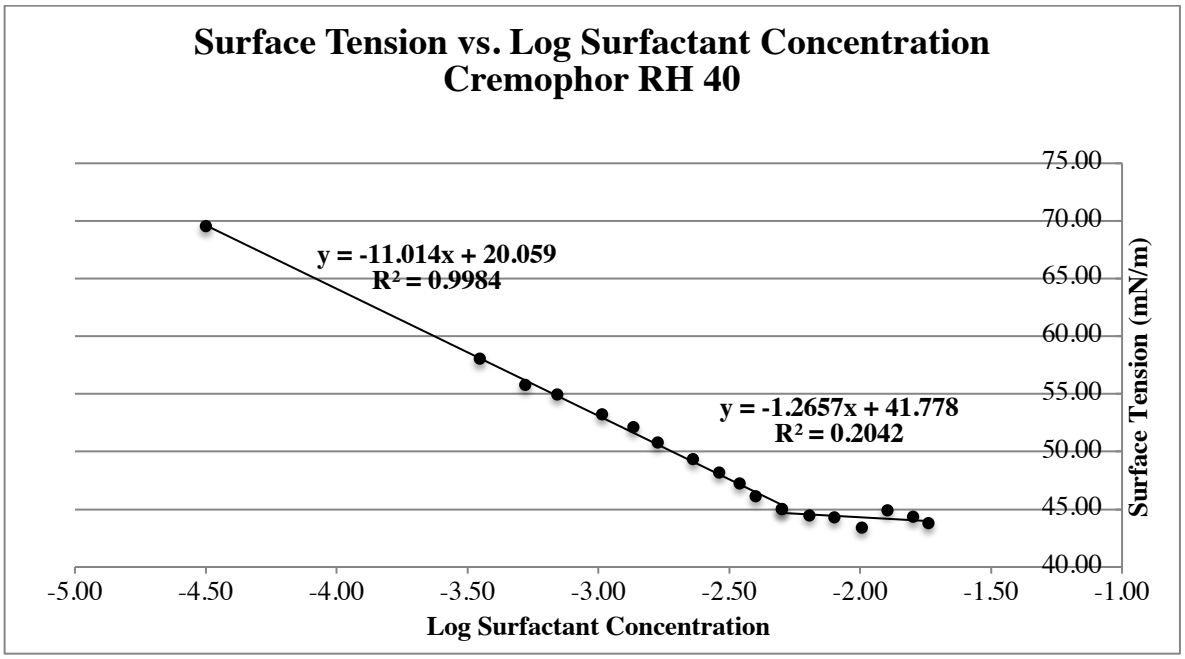

Figure A-2: Surface tension values versus surfactant concentration for PEG-40 hydrogenated castor oil (Replicate 1) (CMC bolded)

PEG-40 hydrogenated castor oil
Replicate 2

Surfactant Concentration (mM)	Log Surfactant Concentration	Average Surface Tension (mN/m)	Standard Deviation
0.0000	-7.00	70.29	0.09
0.0005	-3.34	55.15	0.03
0.0009	-3.04	53.32	0.03
0.0014	-2.86	51.48	0.05
0.0018	-2.74	49.60	0.05
0.0023	-2.64	48.16	0.04
0.0027	-2.56	47.05	0.05
0.0032	-2.50	46.26	0.06
0.0036	-2.44	45.79	0.07
0.0041	-2.39	45.39	0.06
0.0045	**-2.35**	**45.11**	**0.06**
0.0050	-2.31	44.91	0.07
0.0054	-2.27	44.66	0.06
0.0058	-2.23	44.49	0.06
0.0063	-2.20	44.37	0.07
0.0067	-2.17	44.28	0.09
0.0071	-2.15	44.29	0.08
0.0075	-2.12	44.14	0.08
0.0080	-2.10	44.18	0.09
0.0084	-2.08	44.08	0.08
0.0088	-2.06	44.10	0.09

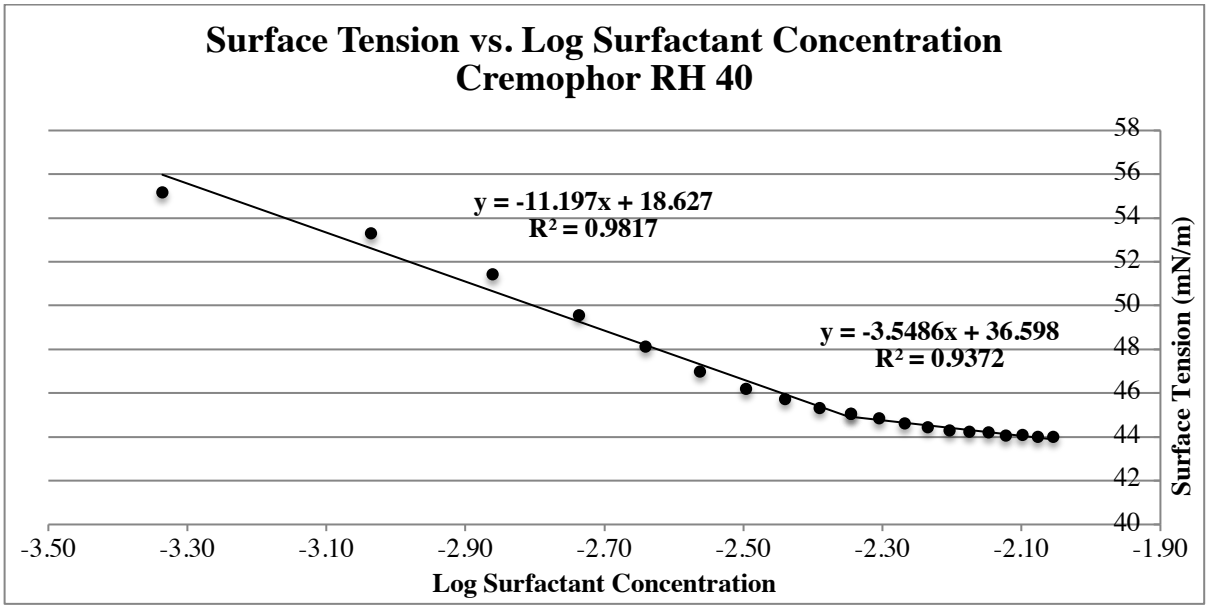

Figure A-3: Surface tension values versus surfactant concentration for PEG-40 hydrogenated castor oil (Replicate 2) (CMC bolded)

PEG-40 hydrogenated castor oil
Replicate 3

Surfactant Concentration (mM)	Log Surfactant Concentration	Average Surface Tension (mN/m)	Standard Deviation
0.0000	-7.00	70.29	0.09
0.0005	-3.34	56.61	0.02
0.0009	-3.04	54.92	0.08
0.0014	-2.86	53.16	0.10
0.0018	-2.74	51.34	0.08
0.0023	-2.64	49.83	0.08
0.0027	-2.56	48.74	0.08
0.0032	-2.50	47.79	0.08
0.0036	-2.44	47.29	0.08
0.0041	-2.39	46.73	0.09
0.0045	**-2.35**	**46.34**	**0.08**
0.0050	-2.31	46.12	0.08
0.0054	-2.27	45.87	0.08
0.0058	-2.23	45.66	0.09
0.0063	-2.20	45.51	0.09
0.0067	-2.17	45.35	0.09
0.0071	-2.15	45.19	0.10
0.0075	-2.12	45.04	0.09
0.0080	-2.10	44.90	0.10
0.0084	-2.08	44.78	0.10
0.0088	-2.06	44.79	0.14
0.0092	-2.03	44.71	0.10
0.0096	-2.02	44.57	0.10
0.0101	-2.00	44.41	0.09
0.0105	-1.98	44.35	0.10
0.0109	-1.96	44.31	0.10

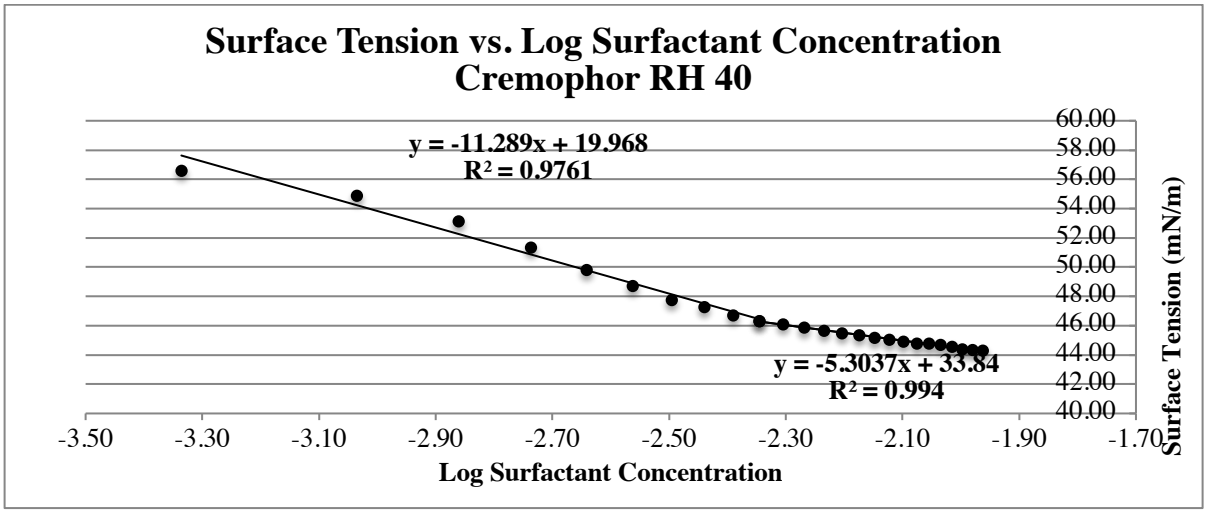

Figure A-4: Surface tension values versus surfactant concentration for PEG-40 hydrogenated castor oil (Replicate 3) (CMC bolded)

PEG-40 hydrogenated castor oil
Replicate 4

Surfactant Concentration (mM)	Log Surfactant Concentration	Average Surface Tension (mN/m)	Standard Deviation
0.0000	-7.00	71.04	0.01
0.0005	-3.34	55.55	0.01
0.0009	-3.04	53.52	0.06
0.0014	-2.86	51.60	0.08
0.0018	-2.74	49.87	0.08
0.0023	-2.64	48.45	0.09
0.0027	-2.56	47.33	0.08
0.0032	-2.50	46.62	0.09
0.0036	-2.44	46.08	0.09
0.0041	-2.39	45.72	0.08
0.0045	**-2.35**	**45.44**	**0.09**
0.0050	-2.31	45.14	0.08
0.0054	-2.27	44.95	0.09
0.0058	-2.23	44.75	0.09
0.0063	-2.20	44.61	0.09
0.0067	-2.17	44.52	0.09
0.0071	-2.15	44.44	0.09
0.0075	-2.12	44.33	0.09
0.0080	-2.10	44.22	0.09
0.0084	-2.08	44.13	0.08
0.0088	-2.06	44.04	0.09
0.0092	-2.03	43.96	0.08
0.0096	-2.02	43.87	0.09
0.0101	-2.00	43.78	0.09
0.0105	-1.98	43.74	0.09
0.0109	-1.96	43.71	0.10

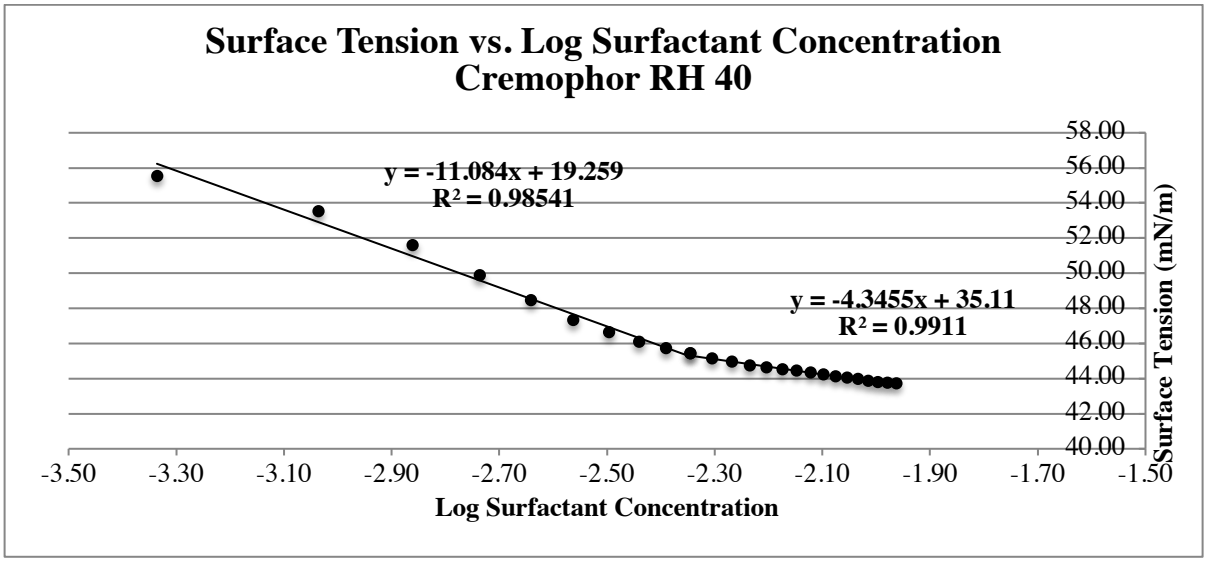

Figure A-5: Surface tension values versus surfactant concentration for PEG-40 hydrogenated castor oil (Replicate 4) (CMC bolded)

3:1 Polysorbate 80: PEG-40 hydrogenated castor oil
Replicate 1

Surfactant Concentration (mM)	Log Surfactant Concentration	Average Surface Tension (mN/m)	Standard Deviation
0	-4.50	69.61	0.11
0.0001	-4.29	68.19	0.03
0.0001	-3.99	65.84	0.05
0.0002	-3.81	62.91	0.07
0.0002	-3.69	60.76	0.03
0.0003	-3.59	58.80	0.01
0.0004	-3.45	56.92	0.05
0.0005	-3.34	55.52	0.04
0.0006	-3.25	54.55	0.03
0.0007	-3.15	53.48	0.04
0.0009	-3.07	52.29	0.06
0.0012	-2.91	50.88	0.04
0.0015	-2.83	49.98	0.05
0.0020	-2.71	48.69	0.05
0.0024	-2.62	47.44	0.04
0.0033	-2.48	45.88	0.04
0.0041	-2.38	44.84	0.03
0.0054	**-2.27**	**43.98**	**0.04**
0.0068	-2.16	43.38	0.04
0.0082	-2.09	43.01	0.02
0.0106	-1.97	42.54	0.04
0.0127	-1.89	42.13	0.07

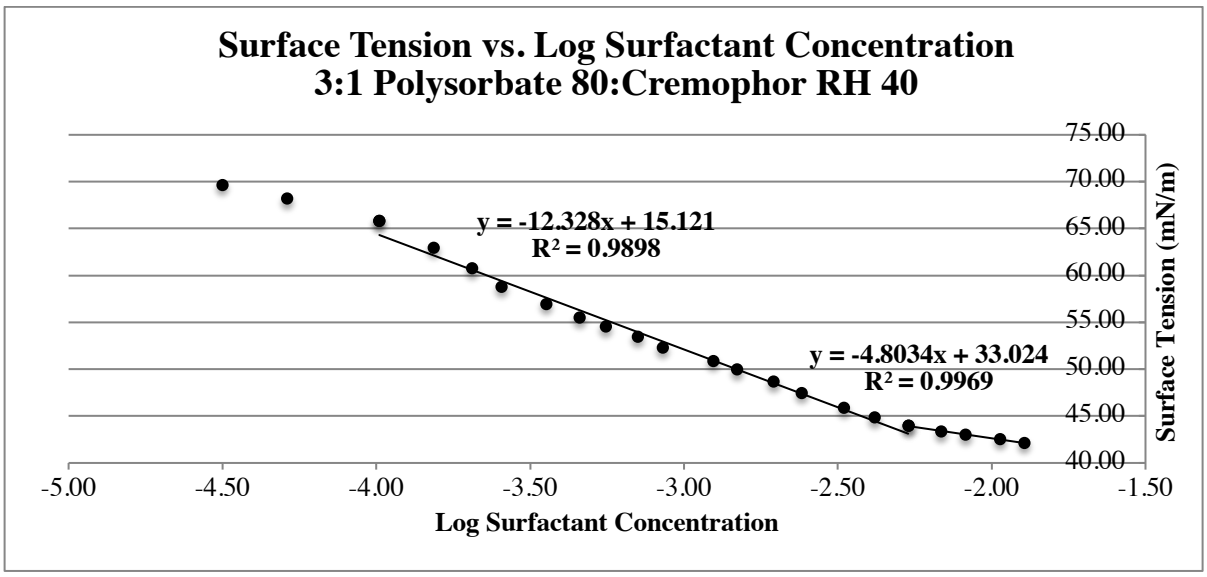

Figure A-6: Surface tension values versus surfactant concentration for 3:1 Polysorbate 80: PEG-40 hydrogenated castor oil (Replicate 1) (CMC bolded)

3:1 Polysorbate 80: PEG-40 hydrogenated castor oil
Replicate 2

Surfactant Concentration (mM)	Log Surfactant Concentration	Average Surface Tension (mN/m)	Standard Deviation
0	-4.50	68.67	0.13
0.0001	-4.29	68.02	0.01
0.0002	-3.69	61.60	0.06
0.0003	-3.59	59.81	0.04
0.0003	-3.51	58.05	0.12
0.0004	-3.45	57.18	0.12
0.0004	-3.39	56.69	0.02
0.0005	-3.30	55.80	0.02
0.0006	-3.22	54.86	0.02
0.0007	-3.15	54.05	0.04
0.0008	-3.09	53.00	0.02
0.0010	-3.00	51.92	0.04
0.0013	-2.89	49.63	0.05
0.0016	-2.80	48.57	0.03
0.0020	-2.71	47.65	0.03
0.0024	-2.62	46.34	0.01
0.0033	**-2.48**	**45.81**	**0.03**
0.0046	-2.34	44.03	0.03
0.0065	-2.19	43.34	0.02
0.0098	-2.01	44.66	0.10
0.0148	-1.83	42.23	0.01
0.0184	-1.74	43.66	0.09

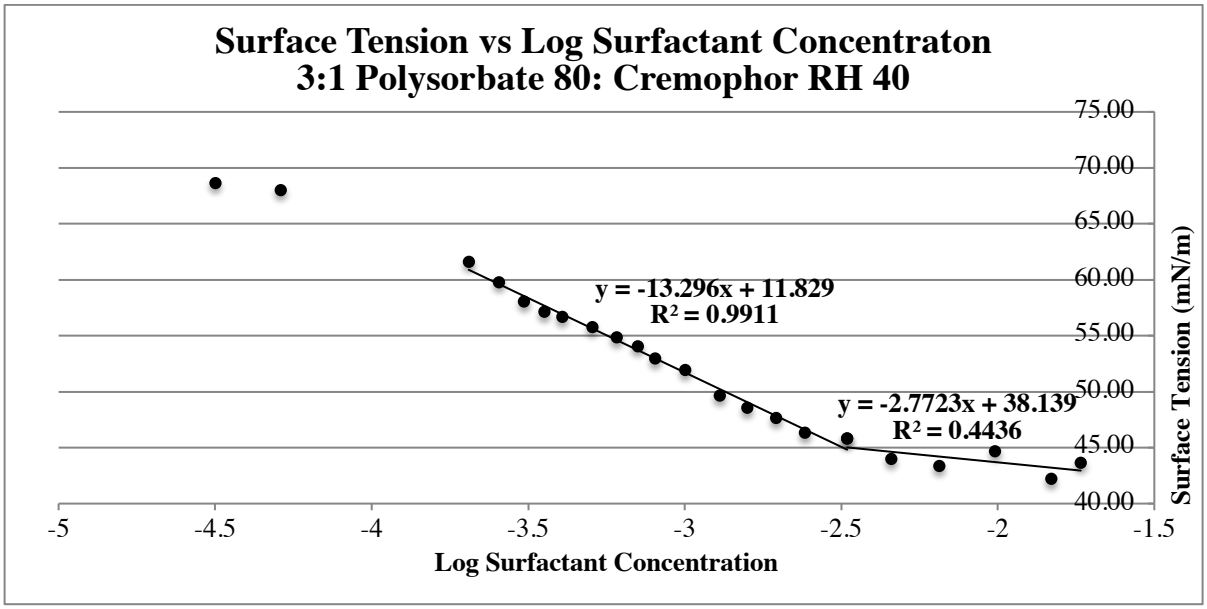

Figure A-7: Surface tension values versus surfactant concentration for 3:1 Polysorbate 80: PEG-40 hydrogenated castor oil (Replicate 2) (CMC bolded)

3:1 Polysorbate 80: PEG-40 hydrogenated castor oil
Replicate 3

Surfactant Concentration (mM)	Log Surfactant Concentration	Average Surface Tension (mN/m)	Standard Deviation
0	-4.50	68.75	0.17
0.0001	-4.29	67.84	0.01
0.0001	-3.99	66.31	0.03
0.0002	-3.81	64.31	0.07
0.0003	-3.51	59.58	0.14
0.0005	-3.30	56.86	0.10
0.0010	-3.00	53.40	0.11
0.0015	-2.83	50.93	0.09
0.0020	-2.71	48.94	0.04
0.0024	-2.62	48.05	0.05
0.0033	-2.48	46.98	0.07
0.0041	-2.38	45.73	0.05
0.0054	-2.27	45.10	0.05
0.0068	**-2.16**	**44.41**	**0.07**
0.0085	-2.07	44.05	0.08
0.0112	-1.95	42.90	0.03
0.0137	-1.86	42.13	0.02
0.0176	-1.75	41.46	0.02
0.0205	-1.69	42.87	0.06
0.0228	-1.64	41.94	0.02

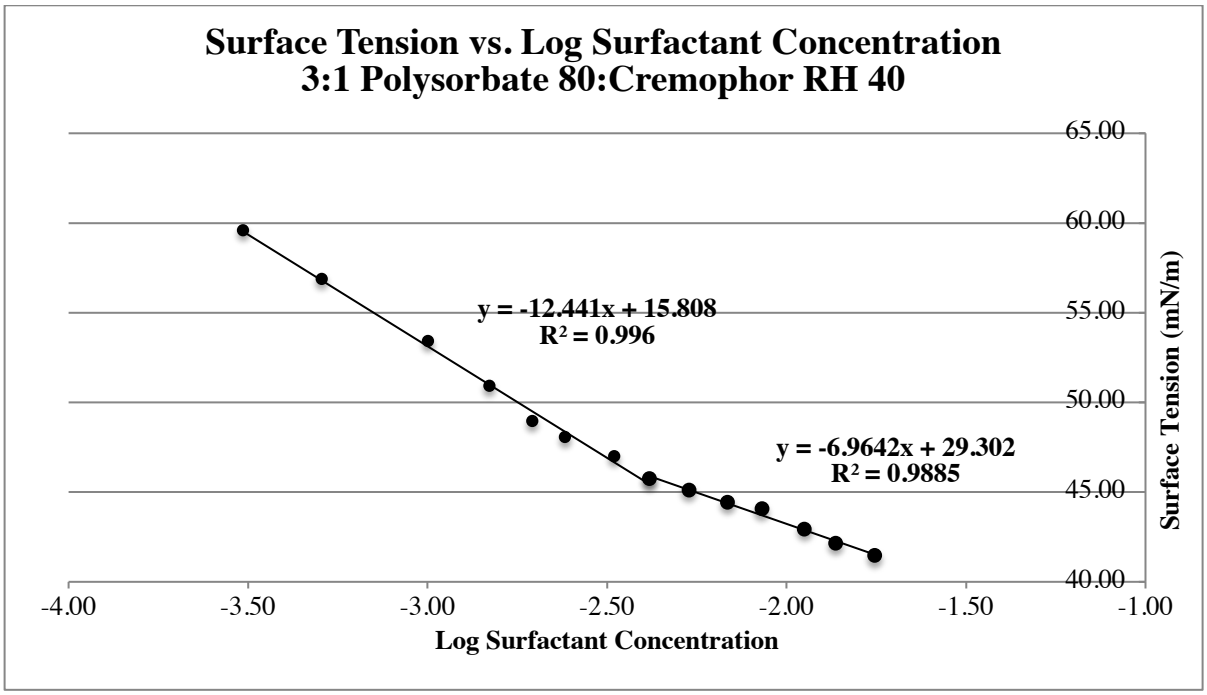

Figure A-8: Surface tension values versus surfactant concentration for 3:1 Polysorbate 80: PEG-40 hydrogenated castor oil (Replicate 3) (CMC bolded)

Appendix B

Table B-1: Health Canada recommended amounts of hydrophilic and lipophilic APIs based on raw material potencies

Vitamin Class	API	Potency (%)	Health Canada Recommended Amount (mg)	Amount Required based on Potency & Health Canada Requirements (mg)
Hydrophilic	Vitamin B_1 (Thiamine mononitrate)	100	1.4	1.4
	Vitamin B_2 (Riboflavin)	100	1.4	1.4
	Vitamin B_3 (Niacinamide)	100	18	18
	Vitamin B_6 (Pyridoxine hydrochloride)	82.3	2	2.43
	Vitamin B_9 (Folic Acid)	94.8	0.6	0.63
	Vitamin B_{12} (Cyanocobalamin)	1	0.0026	0.26
Lipophilic	Vitamin A	30	0.55-0.77	1.84-2.57
	Vitamin D_3 (Cholecalciferol)	2.5	0.015	0.6
	Vitamin E	98.8	15	15.2
	Vitamin K_1 (Phytonadione)	100	0.09	0.09
Fish Oil	Omega-3 Fatty Acid (DHA)	60	3000	5000

A salinity test was performed using Sunflower Oil using the following conditions:

HLD= 0 (at Type III microemulsion)
S= 21 g/100 mL sodium chloride concentration
EACN= unknown
T= 25ºC
CC= 0.18 using 1-dodecanol surfactant

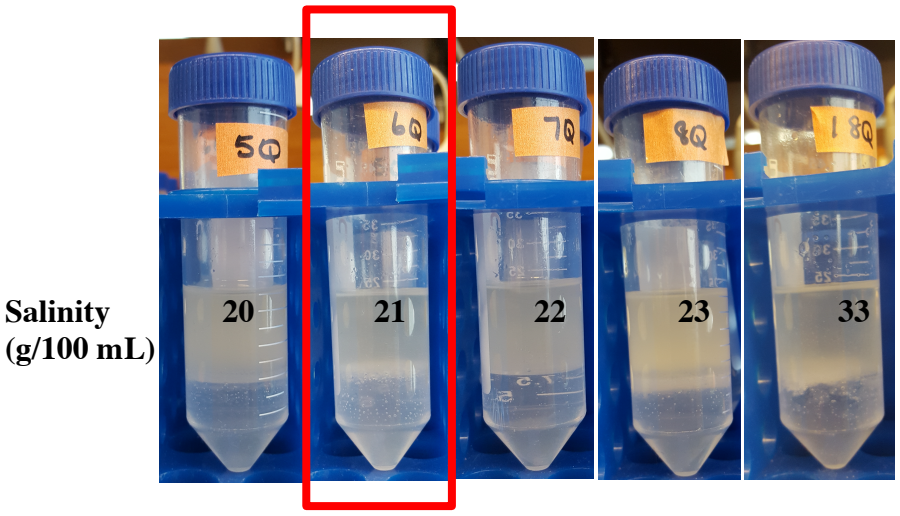

$$HLD = F(S) - k.\,\mathbf{EACN} - \alpha\,(T-25) + CC$$

$$0 = (0.13^{*}\ 21\ g/100mL) - 0.17\,(\mathbf{EACN}) - 0 + 0.18$$

$$0 = 2.91 - 0.17\,(\mathbf{EACN})$$

$$\mathbf{EACN} = 17.12$$

Confirmation using Abbott Online Simulator:

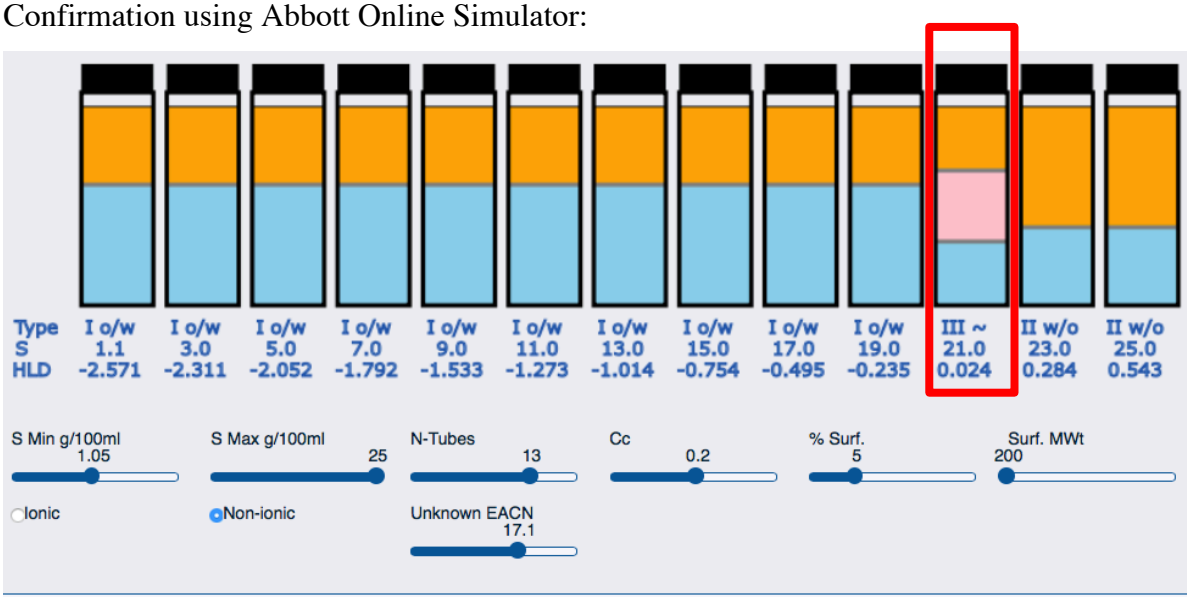

Figure B-1: Effective Alkane Carbon Number (EACN) calculation of sunflower oil

An EACN test was performed on Polysorbate 80 using the following conditions:

HLD= 0 (at Type III microemulsion)
S= 30 g/100 mL sodium chloride concentration
EACN= 2.3 (Type III microemulsion shift obtained using sodium decanoate oil, EACN 2.3)
T= 25ºC
CC= unknown

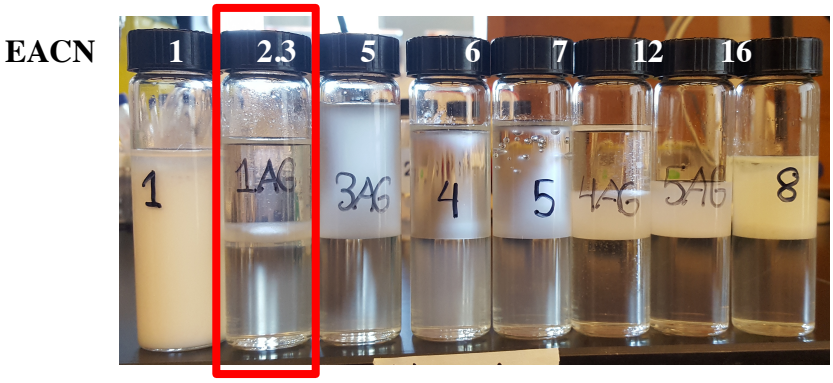

$$HLD = F(S) - k.EACN - \alpha(T-25) + \mathbf{CC}$$

$$0 = (0.13 * 30\ g/100mL) - 0.17(2.3) - 0 + \mathbf{CC}$$

$$0 = 3.9 - 0.391 + \mathbf{CC}$$

$$\mathbf{CC} = \underline{\mathbf{-3.509}}$$

Confirmation using Abbott Online Simulator:

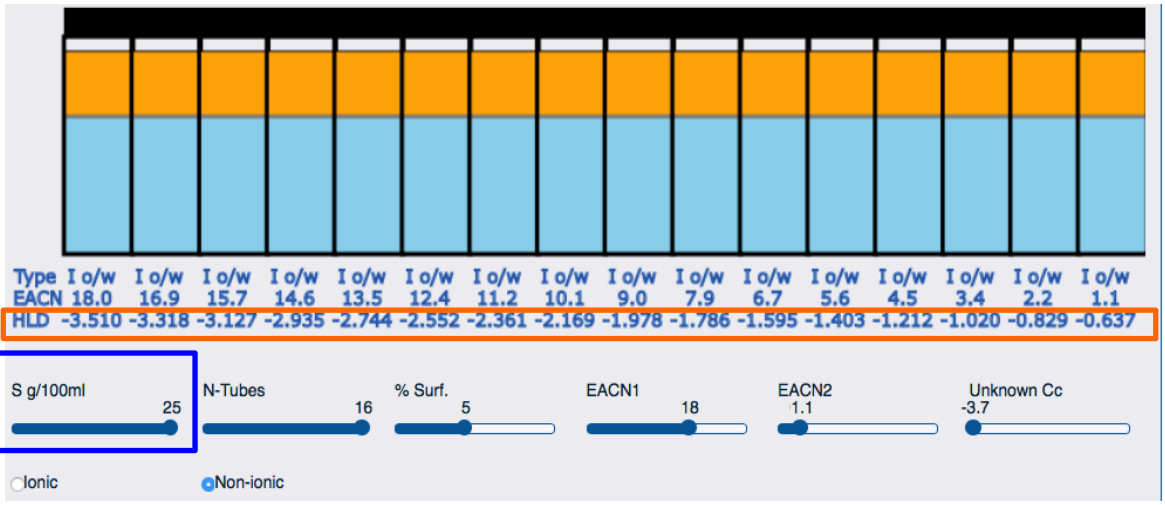

Figure B-2: Characteristic Curvature (CC) of Polysorbate 80

Although maximum salinity of online simulator is 25 g/100 mL, (blue box) we can see the HLD approaching near zero close to EACN 1 (orange box). Given that 30 g/100 mL salinity was used in this case, it is safe to assume that a shift to a Type III microemulsion was indeed seen at EACN 2.3

Surfactant Parameter Calculations/Equations

- *Critical Micelle Concentration (CMC) for Mixed Surfactant Systems:*

$$\frac{1}{CMC_{MIXED}} = \frac{a}{cmc_1} + \frac{1-a}{cmc_2}$$

where CMC_{MIXED} is the critical micelle concentration of the mixed system
a is the molar fraction of surfactant 1
cmc_1 is the critical micelle concentration of surfactant 1
1-a is the molar fraction of surfactant 2
cmc_2 is the critical micelle concentration of surfactant 2

8:1 Polysorbate 80:Cremophor RH 40

$$\frac{1}{CMC_{MIXED}} = \frac{0.89}{0.00473\ mM} + \frac{0.11}{0.00491\ mM}$$

$$= 0.00475\ mM$$

where cmc_1= Polysorbate 80= 0.00473 mM (**Chapter 2)**
cmc_2= Cremophor RH 40= 0.00491 mM (**Chapter 2)**

– – – – – – –

- *β Interaction Parameter:*

$$\beta = \ln\left(\frac{cmc.a_1}{cmc_1.X_1}\right) / (1-X_1)^2$$

where a_1= mole fraction of surfactant 1
cmc_1= cmc of surfactant 1
X_1= micellar composition (solved iteratively)

- X_1*:*

$$\frac{X_1^2 \ln(cmc.a_1/ cmc_1.X_1)}{\{(1-X_1)^2.\ln(cmc\,(1-a_1)/cmc_2(1-X_1))\}} = 1$$

Surfactant Mixture	**α_1**	**Ideal CMC (μM)**	**Experimental CMC (μM)**	**X_1**	**β**
3:1 Polysorbate 80: PEG-40 hydrogenated castor oil	0.75	4.77	3.59 ± 0.00	0.67	**-2.2**
8:1 Polysorbate 80: PEG-40 hydrogenated castor oil	0.89	4.75	2.77 ± 0.00	0.66	**-2.8**

Appendix C

Calculation demonstrating F1A is above CMC at 100x aqueous dilution

F1A- 3:1 Polysorbate 80:Cremophor RH 40: Experimental CMC 0.0036 mM (**Chapter 2**)
$MW_{POLYSORBATE\ 80}$: 1309.66 g/mol
$MW_{CREMOPHOR\ RH40}$: 2698 g/mol
$MW_{AVERAGE\ 3:1\ P80:CR40}$: (3*1309.66 g/mol)+ (1*2698 g/mol)= 6628 g/mol

1 mole= 6628 g
1g = 1/6628 mol
In F1A, there is 5 g surfactant per 10 mL formulation
Therefore, 5 g= 1/6628 * 5 mol
= 0.0008 moles of surfactant per 10 mL formulation
= 0.08 M

At 100x aqueous dilution, 1 mL F1A in 100 mL water
$C_1V_1=C_2V_2$
0.08 M*0.001 L= C_2*0.1 L
C_2= 0.00008 M/0.1 L
C_2= 0.0008 M

Given that CMC= 3.6 x 10^{-6} M and C_2= 8 x 10^{-4} M, aqueous dilution at 100X still ensures measurement above CMC

Table C-1: Two sample, t-test results for size and zeta potential measurements of F1A before and after drug loading.

Parameter	**Sample**	**Mean ± SEM, N**	**Difference between means**	**t, df**	**p-value, p-value summary**	**F-test to compare variance F, DFn, DFd**
Size (nm)	API-free	150.4 ± 18.5, 4	13.1 ± 21.3	t=0.6156 df= 16	0.5468, ns (not significant)	F=1.039 DFn= 13 DFd=3 p-value: >0.99 ns
	API	163.5 ± 10.1, 14				
Zeta Potential (mV)	API-free	-10.5 ± 1.89, 4	-3.61 ± 1.53	t=2.361 df= 14	0.0333, * (significant)	F=2.884 DFn= 3 DFd=11 p-value: 0.168 ns
	API	-14.1 ± 0.64 12				

Table C-2: Two sample, t-test results for size and zeta potential measurements of F1A before and after exposure to three freeze-thaw cycles

Parameter	**Sample**	**Mean ± SEM, N**	**Mean of Differences**	**t, df**	**p-value, p-value summary**
Size (nm)	Before Treatment	203 ± 59, 2	77 ± 1.4	t=77 df= 1	0.0083, ** (significant)
	After 3X Freeze-thaw Cycles	126 ± 61, 2			
Zeta Potential (mV)	Before Treatment	-14.4 ± 2, 2	-4.2 ± 1.7	t= 3.5 df= 1	0.1772, ns (not significant)
	After 3X Freeze-thaw Cycles	-10.15 ± 0.2, 2			

Table C-3: One-way ANOVA results for size and zeta potential measurements of F1A before and after exposure to various heating cycles.

Parameter	Sample	Mean ± SD, N	Sum of Squares	F, df	p-value, summary
Size (nm)	Before Treatment	187 ± 37, 2	6503	F= 16.89 df= 4	0.152, ns (not significant)
	37°C	116 ± 25, 2			
	50°C	142 ± 45, 2			
	60°C	140 ± 49, 2			
	70°C	119 ± 47, 2			
Zeta Potential (mV)	Before Treatment	-16.5 ± 1, 2	34.85	F= 1.91 df= 4	0.399, ns (not significant)
	37°C	-13.75 ± 3, 2			
	50°C	-13.25 ± 3, 2			
	60°C	-18 ± 6, 2			
	70°C	-17 ± 6, 2			

Table C-4: One-way ANOVA results for size and zeta potential measurements of F1A before and after light exposure

Parameter	Sample	Mean ± SD, N	Sum of Squares	F, df	p-value, summary
Size (nm)	Before Treatment	183 ± 40, 2	4459	F= 6.44 df= 2	0.239, ns (not significant)
	24 h	127 ± 8, 2			
	1 week	124 ± 6, 2			
Zeta Potential (mV)	Before Treatment	-13.5 ± 5, 2	48	F= 1.16 df= 2	0.476, ns (not significant)
	24 h	-7.5 ± 4, 2			
	1 week	-13.5 ± 4, 2			

Size measurements of F1A microemulsion placebo at various dilution factors

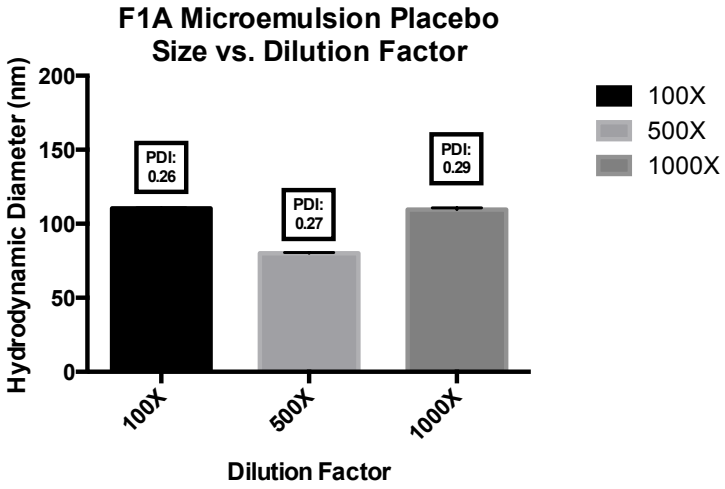

Figure C-1: Hydrodynamic diameters of F1A after various aqueous dilutions.

No notable difference in size was seen in samples at 100x and 1000x aqueous dilution. Therefore, 100x aqueous dilution was selected for all droplet size and zeta potential measurements.

Size Histograms and Zeta Potential Curves (Zetasizer)

Lipophilic API Incorporation (Size)
F1A

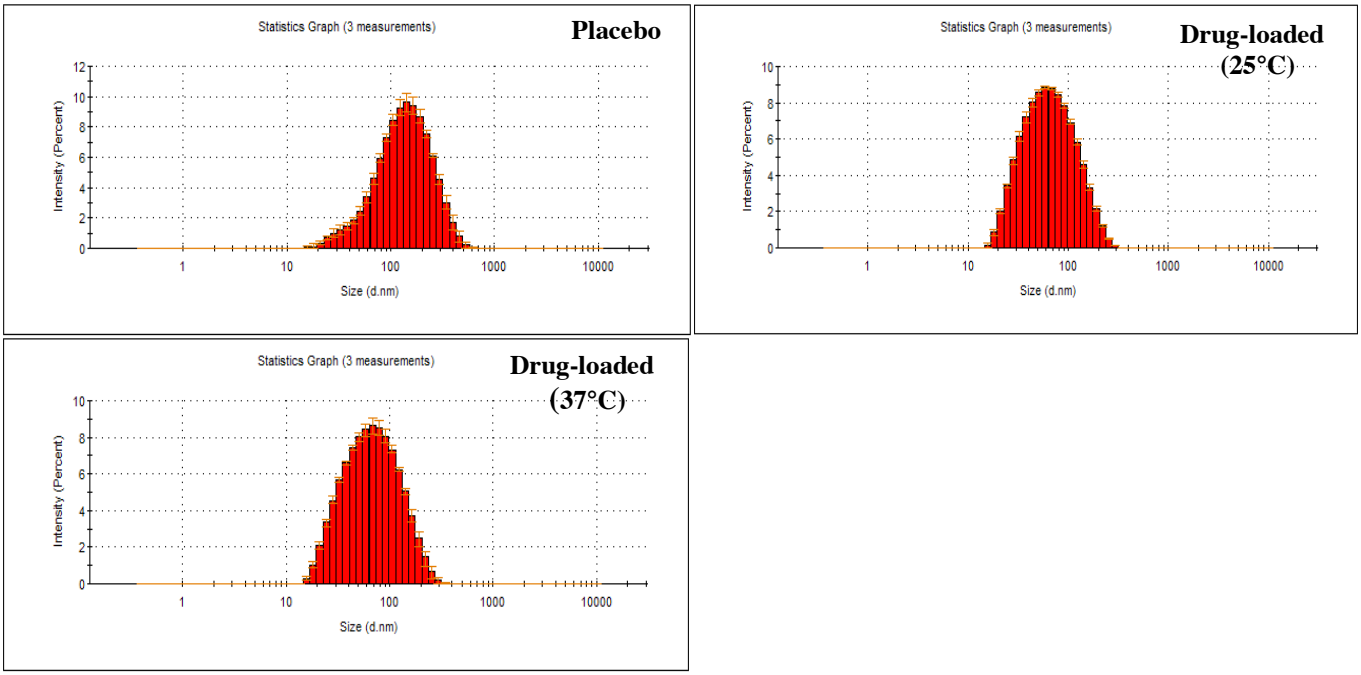

Figure C-2: Size histograms of F1A before and after lipophilic API incorporation at 25 and 37°C.
F2A

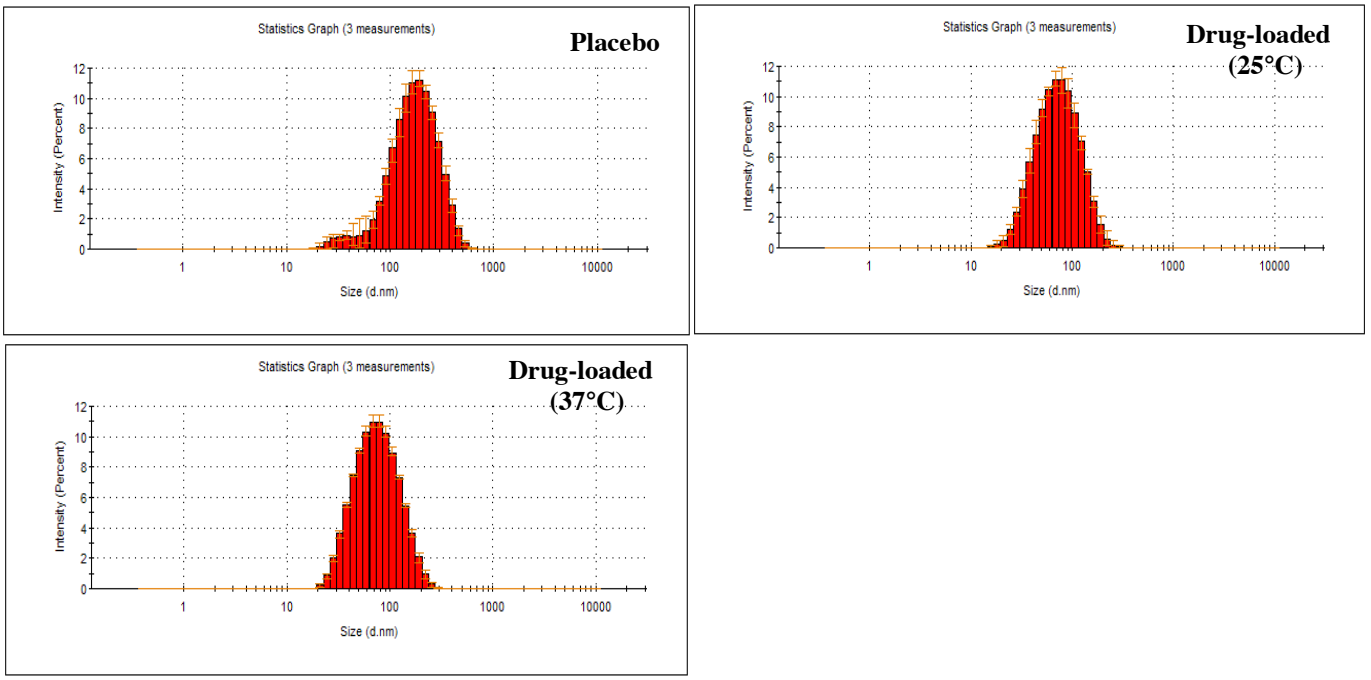

Figure C-3: Size histograms of F2A before and after lipophilic API incorporation at 25 and 37°C.

F3A

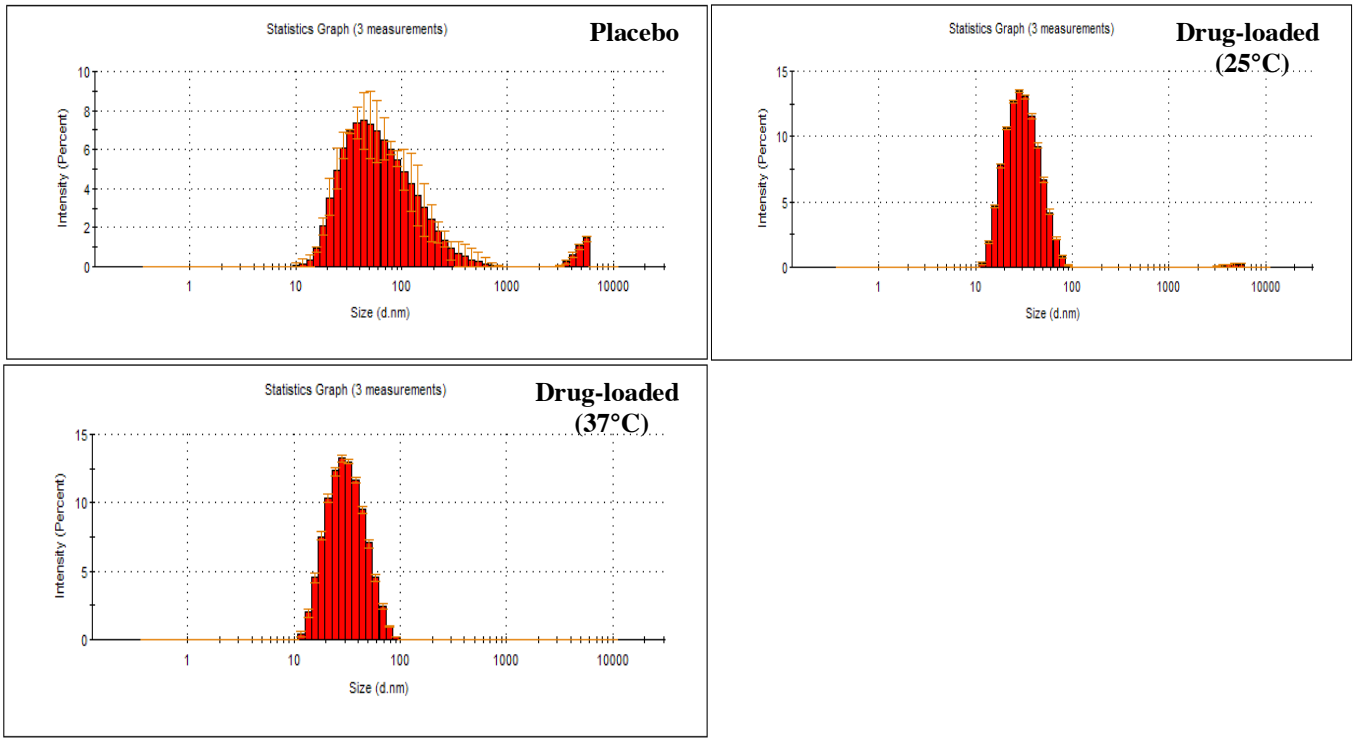

Figure C-4: Size histograms of F3A before and after lipophilic API incorporation at 25 and 37°C.

Hydrophilic API Incorporation (Size)

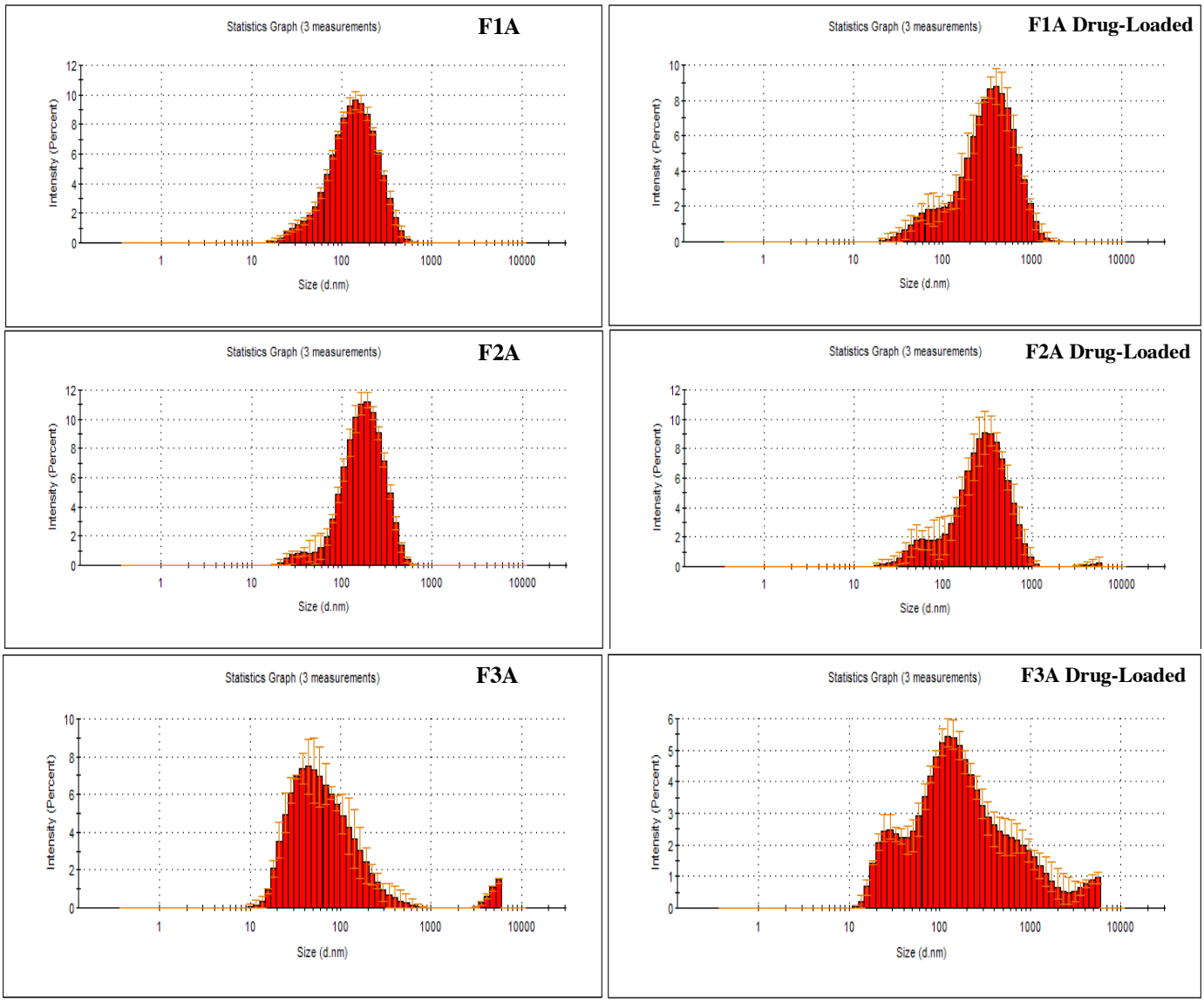

Figure C-5: Size histograms of F1A, F2A and F3A before and after hydrophilic API incorporation.

Lipophilic and Hydrophilic API Incorporation (Size)

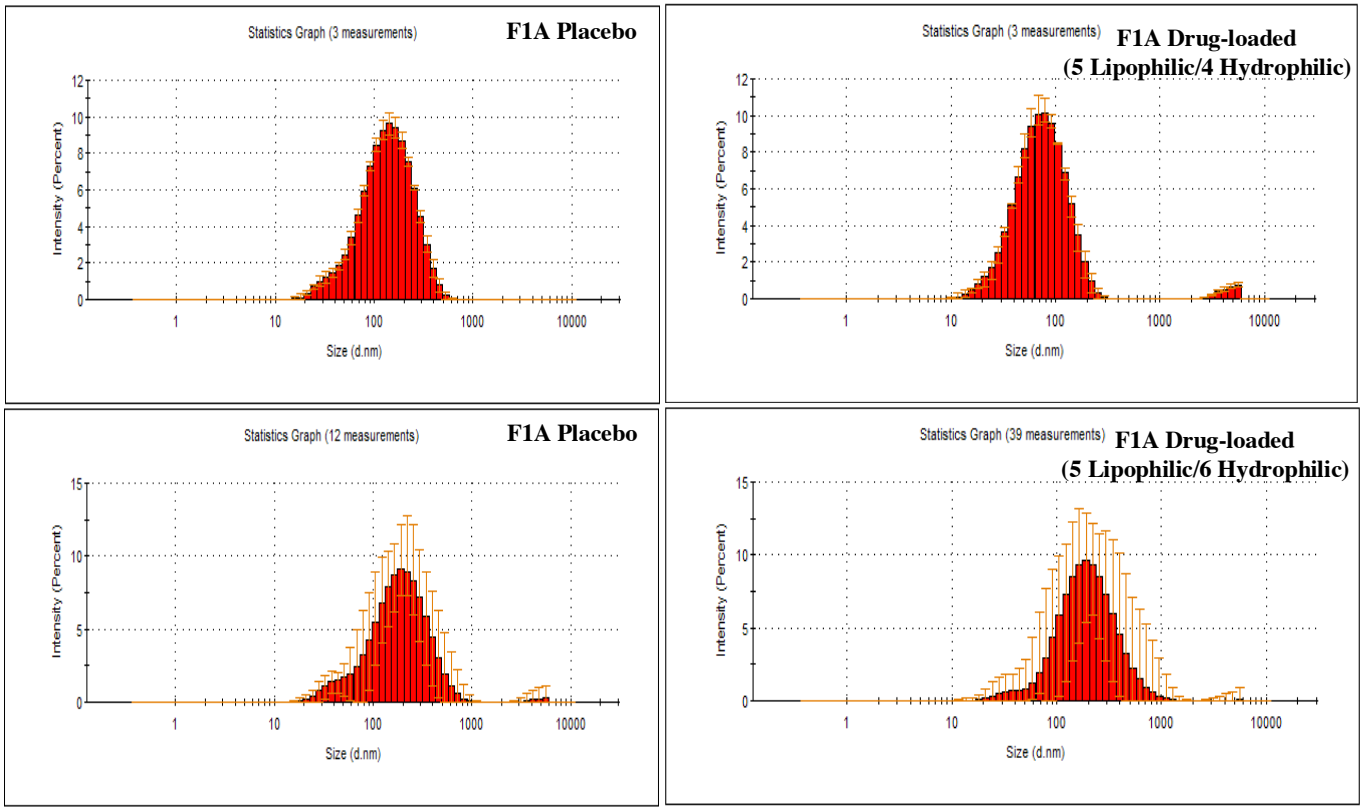

Figure C-6: Size histograms of F1A before and after multi-API incorporation.

Lipophilic and Hydrophilic API Incorporation (Zeta)

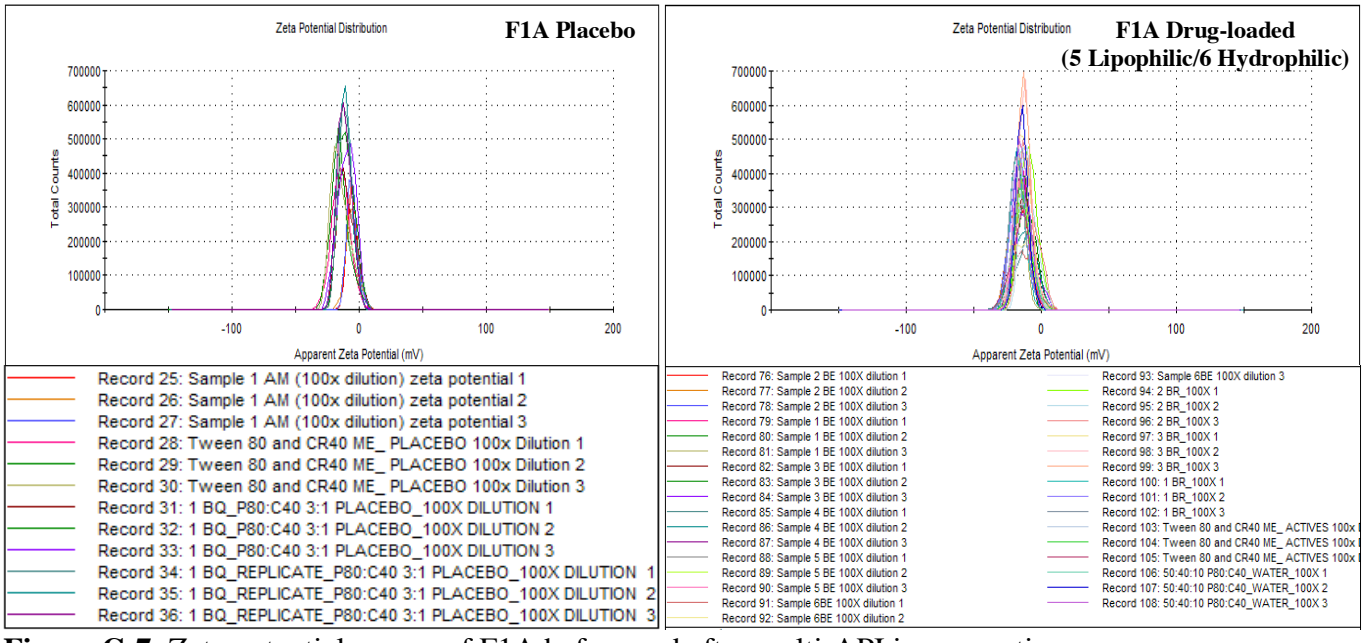

Figure C-7: Zeta potential curves of F1A before and after multi-API incorporation

Freeze-thaw Cycle

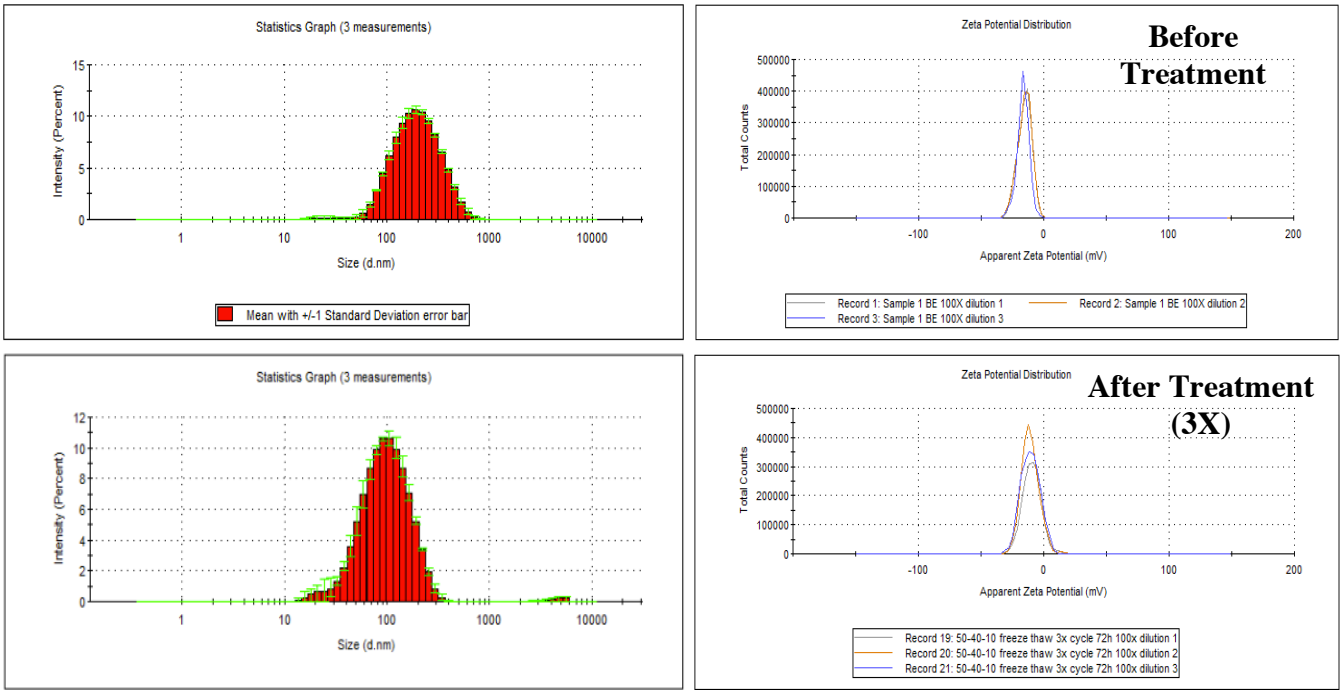

Figure C-8: Size histograms and zeta potential curves of F1A before (top) and after (bottom) subjection to three freeze-thaw cycles.

Heat Cycle

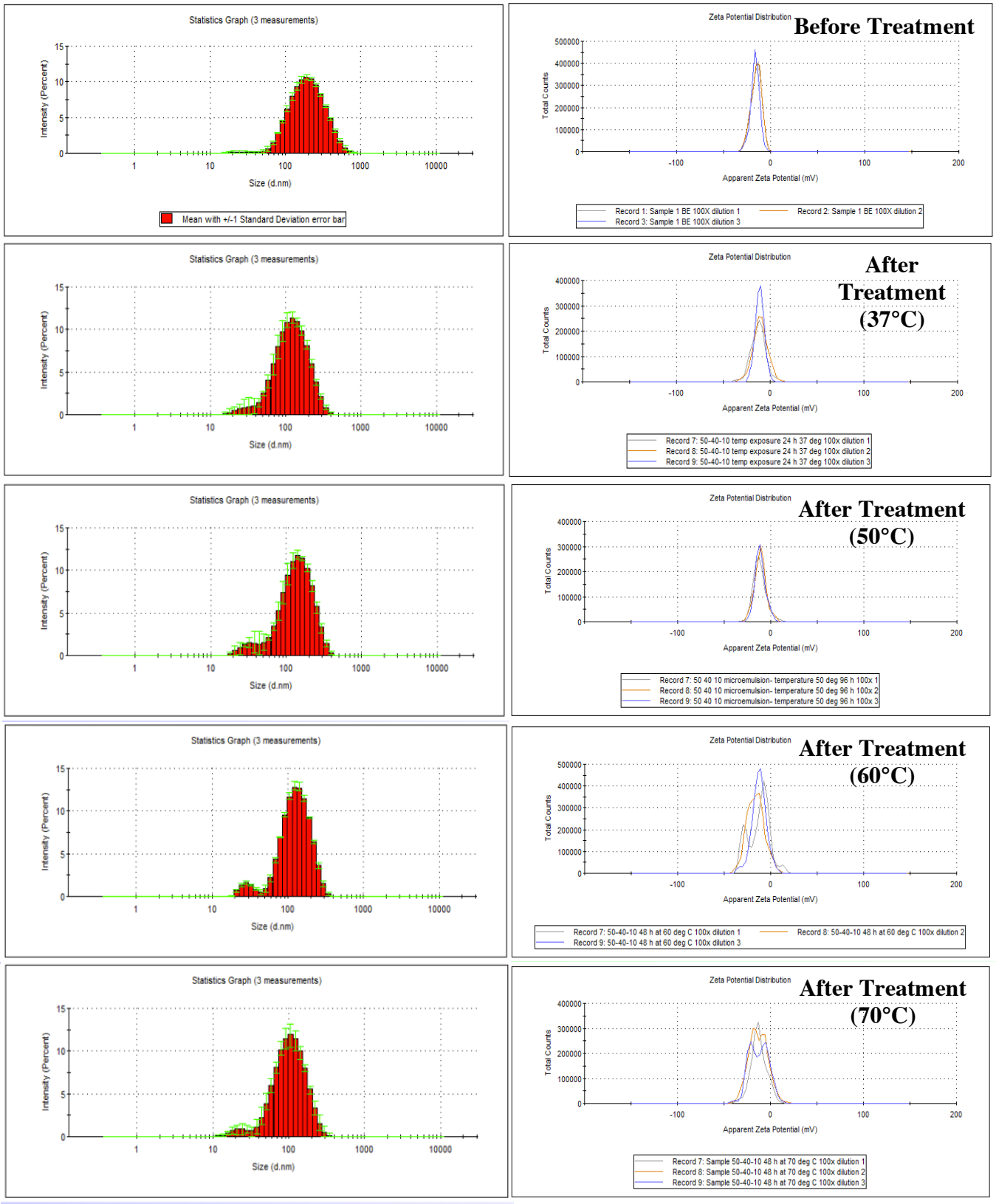

Figure C-9: Size histograms and zeta potential curves of F1A before and after heating cycles.

Light Exposure

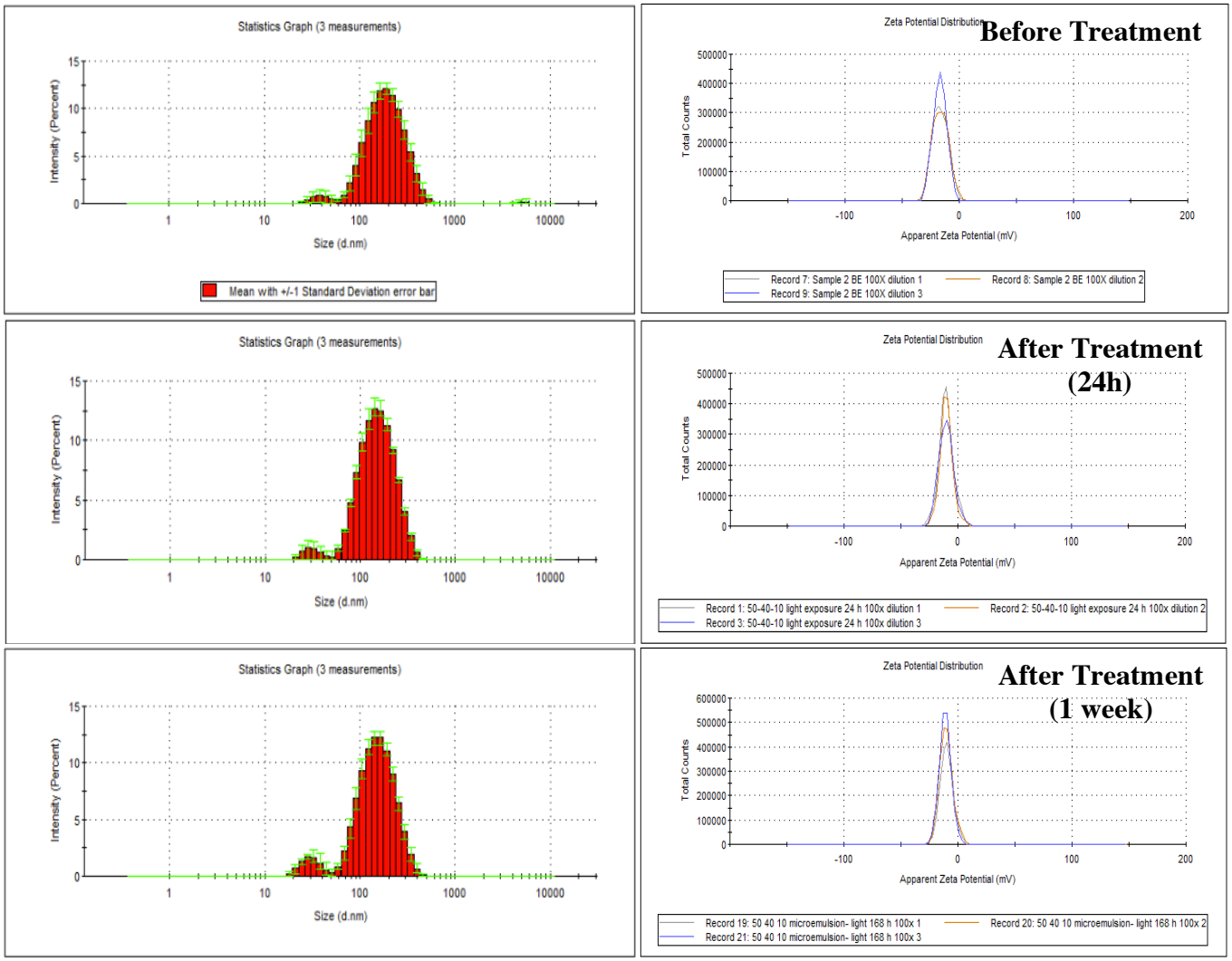

Figure C-10: Size histograms and zeta potential curves of F1A before and after light exposure.

Conductivity

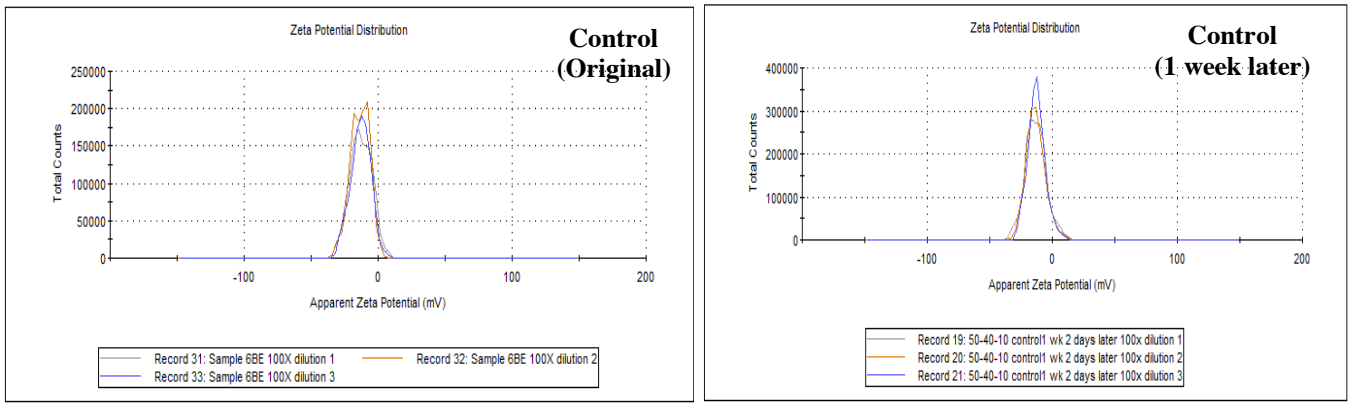

Figure C-11: Zeta potential curves of F1A at manufacture and one week later.

Appendix D

Table D-1: Two sample, t-test results for size and zeta potential measurements of F1A before and after drug-loading.

Parameter	Sample	Mean ± SD, N	Difference between Means	t, df	p-value, p-value summary	F-test to compare variance F, DFn, DFd
Size (nm)	Drug-free	244 ± 62, 10	24.8 ± 91	t=0.2723 df= 18	0.7885, ns (not significant)	F=1.19 DFn= 9 DFd=9 p-value: 0.7995,ns
	Drug-loaded	268 ± 67, 10				
Zeta Potential (mV)	Drug-free	-17.5 ± 6.28, 10	-4.4 ± 8.4	t= 0.5205 df= 18	0.6090, ns (not significant)	F=1.24 DFn= 9 DFd=9 p-value: 0.7537,ns
	Drug-loaded	-21.9 ± 5.64, 10				

Table D-2: One-way Welch's Equality of Means test with Games-Howell post-hoc for the effect of surfactant type on droplet size for both placebo and drug-loaded samples. Only statistically significant results ($p<.05$) are presented.

Parameter	Label	Sample: Microemulsion (S:O:W)	Mean ± SD, N	Mean Difference (nm)	Games-Howell Multiple Comparisons	
					vs. Subject 2	p-value, signif.
Size (nm) Placebo	A	F1A- 3:1 P80:C40 (50:40:10)	182 ± 2.9, 2	91.1	C	0.037, *
				143	E	0.002, **
	B	3:1 P80:C60 (50:40:10)	174 ± 39, 2			
	C	3:1 P80:C40 (60:30:10)	90.7 ± 6.4, 2	109	G	0.033,*
	D	3:1 P80:C60 (60:30:10)	85.4 ± 14, 2			
	E	3:1 P81:C40 (50:40:10)	38.5 ± 2.1, 2			
	F	3:1 P81:C60 (50:40:10)	83.2 ± 10, 2	116	G	0.029,*
	G	3:1 B97:C60 (50:40:10)	199 ± 10, 2			
Size (nm) API-loaded	A	F1A- 3:1 P80:C40 (50:40:10)	182 ± 2.9, 2			
	B	3:1 P80:C60 (50:40:10)	182 ± 2.9, 2	92.2	C	0.048, *
				88.2	D	0.049,*
	C	3:1 P80:C40 (60:30:10)	182 ± 2.9, 2	144.2	F	0.024, *
				118.8	G	0.049, *
	D	3:1 P80:C60 (60:30:10)				
	E	3:1 P81:C40 (50:40:10)		99.9	F	0.027, *
				74.5	G	0.017, *
	F	3:1 P81:C60 (50:40:10)				
	G	3:1 B97:C60 (50:40:10)				

Table D-3: One-way Welch's Equality of Means test with Games-Howell post-hoc for the effect of surfactant type on polydispersity indices for both placebo and drug-loaded samples. Only statistically significant results (p<.05) are presented.

Parameter	Label	Sample: Microemulsion (S:O:W)	Mean ± SD, N	Mean Difference	Games-Howell Multiple Comparison	
					vs. Subject 2	p-value, signif.
PDI Placebo	A	F1A- 3:1 P80:C40 (50:40:10)	0.29 ± 0.00, 2			
	B	3:1 P80:C60 (50:40:10)	0.49 ± 0.05, 2			
	C	3:1 P80:C40 (60:30:10)	0.57 ± 0.02, 2	109	D	0.027,*
	D	3:1 P80:C60 (60:30:10)	0.33 ± 0.02, 2			
	E	3:1 P81:C40 (50:40:10)	0.17 ± 0.05, 2			
	F	3:1 P81:C60 (50:40:10)	0.37 ± 0.06, 2			
	G	3:1 B97:C60 (50:40:10)	0.40 ± 0.13, 2			
PDI API-loaded	A	F1A- 3:1 P80:C40 (50:40:10)	0.25 ± 0.04, 2			
	B	3:1 P80:C60 (50:40:10)	0.33 ± 0.16, 2			
	C	3:1 P80:C40 (60:30:10)	0.34 ± 0.01, 2			
	D	3:1 P80:C60 (60:30:10)	0.34 ± 0.09, 2			
	E	3:1 P81:C40 (50:40:10)	0.27 ± 0.00, 2			
	F	3:1 P81:C60 (50:40:10)	0.28 ± 0.00, 2			
	G	3:1 B97:C60 (50:40:10)	0.47 ± 0.01, 2	0.13	C	0.013, *
				0.19	E	0.042, *
				0.19	F	0.013, *

Table D-4: One-way Welch's Equality of Means test with Games-Howell post-hoc for the effect of surfactant type on zeta potential values for both placebo and drug-loaded samples. Only statistically significant results (p<.05) are presented.

Parameter	Label	Sample: Microemulsion (S:O:W)	Mean ± SD, N	Mean Difference (mV)	Games-Howell Multiple Comparison	
					vs. Subject 2	p-value, signif.
Zeta Potential (mV) Placebo	A	F1A- 3:1 P80:C40 (50:40:10)	-10.6 ± 0.9, 2	15.7	F	0.038, *
				10.2	G	0.048, *
	B	3:1 P80:C60 (50:40:10)	-13.2 ± 1.4, 2			
	C	3:1 P80:C40 (60:30:10)	-13.3 ± 0.5, 2	13.0	F	0.008,**
				12.7	G	0.006, **
	D	3:1 P80:C60 (60:30:10)	-11.9 ± 1.1, 2			
	E	3:1 P81:C40 (50:40:10)	-19.7 ± 2.0, 2			
	F	3:1 P81:C60 (50:40:10)	-26.3 ± 0.3, 2			
	G	3:1 B97:C60 (50:40:10)	-0.53 ± 0.5, 2	25.7	F	0.002, **
Zeta Potential (mV) API-loaded	A	F1A- 3:1 P80:C40 (50:40:10)	-10.5 ± 0.4, 2			
	B	3:1 P80:C60 (50:40:10)	-11.5 ± 0.3, 2			
	C	3:1 P80:C40 (60:30:10)	-16.6 ± 4.8, 2			
	D	3:1 P80:C60 (60:30:10)	-14.2 ± 2.5, 2			
	E	3:1 P81:C40 (50:40:10)	-22.0 ± 3.0, 2			
	F	3:1 P81:C60 (50:40:10)	-22.7 ± 2.3, 2			
	G	3:1 B97:C60 (50:40:10)	-6.7 ± 0.5, 2			

Table D-5: HPLC method development for quantification of water-soluble and fat-soluble vitamins in microemulsion solution

<table>
<tr><td rowspan="2">Parameters</td><td colspan="4">Specifications</td></tr>
<tr><td colspan="2">INITIAL METHOD</td><td colspan="2">FINAL METHOD</td></tr>
<tr><td>Waters Symmetry</td><td colspan="2">C18, 250 x 4.6 mm, 5 uM</td><td colspan="2">C18, 250 x 4.6 mm, 5 uM</td></tr>
<tr><td>Column Temp.</td><td colspan="2">25 ºC</td><td colspan="2">35-55 ºC</td></tr>
<tr><td>Mobile Flow Rate</td><td colspan="2">0.5-1 mL/min</td><td colspan="2">0.5-1 mL/min</td></tr>
<tr><td>Wavelength</td><td colspan="2">280 nm</td><td colspan="2">265-270 nm</td></tr>
<tr><td>Injection Volume</td><td colspan="2">10 uL</td><td colspan="2">10- 60 uL</td></tr>
<tr><td>Run Time</td><td colspan="2">40-60 min</td><td colspan="2">60 min</td></tr>
<tr><td>Mobile Phases and Elution Gradients</td><td colspan="2">A: KH2PO4/Methanol
B: Acetonitrile/Isopropyl Alcohol

<table>
<tr><td>Time</td><td>%A</td><td>%B</td></tr>
<tr><td>0</td><td>95</td><td>5</td></tr>
<tr><td>4</td><td>95</td><td>5</td></tr>
<tr><td>10</td><td>2</td><td>98</td></tr>
<tr><td>30</td><td>2</td><td>98</td></tr>
<tr><td>35</td><td>95</td><td>5</td></tr>
<tr><td>40</td><td>95</td><td>5</td></tr>
</table></td><td colspan="2"><u>Water Solubles:</u>
A: 0.15% Hexansulfonate Sodium Monohydrate (pH 2.8),19% Glacial Acetic Acid
B: Methanol/Acetonitrile

<table>
<tr><td>Time</td><td>%A</td><td>%B</td></tr>
<tr><td>0</td><td>99</td><td>1</td></tr>
<tr><td>5</td><td>99</td><td>1</td></tr>
<tr><td>20</td><td>35</td><td>65</td></tr>
<tr><td>21</td><td>99</td><td>1</td></tr>
<tr><td>26</td><td>99</td><td>1</td></tr>
<tr><td>60</td><td>99</td><td>1</td></tr>
</table>
<u>Fat Solubles:</u>
A: Tetrahydrofuran
B: Acetonitrile

<table>
<tr><td>Time</td><td>%A</td><td>%B</td></tr>
<tr><td>0</td><td>60</td><td>40</td></tr>
<tr><td>5</td><td>60</td><td>40</td></tr>
<tr><td>35</td><td>4</td><td>96</td></tr>
<tr><td>40</td><td>4</td><td>96</td></tr>
<tr><td>50</td><td>4</td><td>96</td></tr>
<tr><td>60</td><td>60</td><td>40</td></tr>
</table></td></tr>
</table>

Table D-6: One-way Welch's Equality of Means test with Games-Howell post-hoc for the effect of surfactant type on microemulsion droplet size and zeta potential. Only statistically significant values ($p<0.05$) listed.

Parameter	Formulation	Mean ± SD, N	Homogeneity of Variance & Welch's Statistic	Mean Difference (% dissol.)	Games-Howell Multiple Comparisons	
					vs.	p-value, signif.
Size (nm)	F1	163.5 ± 38, 14	Levene's F-test: F(2,21)=4.26, p= .028 Welch's Equality of Means: F(2,6.7)=31.6, p< .001	69.66	F2 F3	.0002, *** .000004, ****
	F2	93.8 ± 15, 4		82.75		
	F3	80.7 ± 2.4, 6				
Zeta Potential (mV)	F1	-14.1 ± 2.2, 12	Levene's F-test: F(2,19)=6.06, p= .009 Welch's Equality of Means: F(2,5.9)=6.10, p= .037	9.18	F3	.030, *
	F2	-16.5 ± 4, 4				
	F3	-23.3 ± 5, 6				

Reference

Brand: Jamieson Prenatal + DHA (All-in-one)
Package count: 60 units
Dosage form: Soft gelatin capsules
Dosage fill: Liquid

Table D-7: Active ingredient list and amounts for Jamieson Pre-natal Supplement with DHA in softgel dosage forms.

Vitamin	Amount per Serving/Capsule	Amount per 1g F1A
Active Ingredients Present in F1A		
Beta-carotene	1500 mcg	
Vitamin B1 (Thiamine Mononitrate)	1.4 mg	1.4 mg
Vitamin B2 (Riboflavin)	1.6 mg	1.4 mg
Vitamin B3 (Niacinamide)	18 mg	18 mg
Vitamin B6 (Pyridoxine Hydrochloride)	5 mg	2.4 mg
Vitamin B9 (Folic Acid)	1000 mcg	800 mcg
Vitamin B12 (Cyanocobalamin)	2.8 mcg	2.6 mcg
Vitamin D3 (Cholecalciferol)	15 mcg/600 IU	15 mcg
Vitamin E (d-Alpha Tocopherol))	19 mg AT/28 IU	15 mg
Vitamin K1	90 mcg	90 mcg
Active Ingredients NOT Present in F1A		
Vitamin A (Palmitate)	1050 mcg	N/A
Vitamin B5 (Calcium d-Pantothenate)	7 mg	N/A
Vitamin B7 (Biotin)	35 mg	N/A
Vitamin C (Ascorbic Acid)	120 mg	N/A

'Inactive' Ingredients:

Medium chain triglycerides
Gelatin
Glycerin
Yellow Beeswax
Lecithin (Soy)
Titanium Dioxide
Natural Vanilla Flavour

Table D-8: One-way Welch's Equality of Means test with Games-Howell post-hoc for the effect of formulation type on vitamin recovery using 10 mM Citric Acid (pH 6). The medium for the reference formulation was 10 mM Citric Acid in 1% SDS. Only statistically significant values ($p<0.05$) listed.

	Dissolution Time (mins)	Formulation	Mean ± SD, N	Homogeneity of Variance & Welch's Statistic	Mean Difference (% dissol.)	Games-Howell Multiple Comparisons	
						vs. Subject 2	p-value, signif.
B2	15	F1	102 ± 5, 2	Levene's F-test: F(3,4)=7.8E+32, p<0.001	100.5	Reference	.040, *
		F2	105 ± 4, 2		104.0	Reference	.033,*
		F3	106 ± 4, 2		104.5	Reference	.028,*
		Reference	1.02 ± 0.01, 2	Welch's Equality of Means: F(3,1.7)=699, p= .004			
	30	F1	111 ± 6, 2	Levene's F-test: F(3,4)=8.6E+32, p<0.001	110	Reference	.042, *
		F2	107 ± 3, 2		106	Reference	.022,*
		F3	107 ± 3, 2		106	Reference	.022,*
		Reference	1.01 ± 0.01, 2	Welch's Equality of Means: F(3,1.7)=1180, p= .002 116			
	60	F1	113 ± 5, 2	Levene's F-test: F(3,4)=6.7E+32, p<0.001	111.5	Reference	.036, *
		F2	108 ± 2, 2		106.5	Reference	.016,*
		F3	107 ± 3, 2		106.0	Reference	.022,*
		Reference	1.02 ± 0.01, 2	Welch's Equality of Means: F(3,1.7)=1641, p= .002			
B9	15	F1	70 ± 8, 2	Welch's Equality of Means: F(3,1.7)=84.85, p= .021			
		F2	72 ± 7, 2				
		F3	75 ± 10, 2				
		Reference	0.01 ± 0.01, 2				
	30	F1	77 ± 8, 2	Welch's Equality of Means: F(3,1.7)=64.74, p= .027			
		F2	74 ± 10, 2				
		F3	77 ± 13, 2				
		Reference	0.01 ± 0.01, 2				
	60	F1	77 ± 8, 2	Welch's Equality of Means: F(3,1.7)=54.05, p= .031			
		F2	75 ± 13, 2				
		F3	76 ± 14, 2				
		Reference	0.01 ± 0.01, 2				

Table D-9: One-way Welch's Equality of Means test with Games-Howell post-hoc for the effect of formulation type on vitamin recovery using 50 mM Phosphate Buffer (pH 7.4). The medium for the reference formulation was 10 mM Citric Acid in 1% SDS. Only statistically significant values ($p<0.05$) listed.

	Dissolution Time (mins)	Formulation	Mean ± SD, N	Homogeneity of Variance & Welch's Statistic	Mean Difference (% dissol.)	Games-Howell Multiple Comparisons	
						vs. Subject 2	p-value, signif.
B2	15	F1	92.5 ± 5, 2	Levene's F-test: F(3,4)=7.7E+32, p<.001 Welch's Equality of Means: F(3,1.7)=8341, p< .001	91.5	Reference	.044, *
		F2	95.5 ± 2, 2		94.5	Reference	.018,*
		F3	102 ± 1, 2		100.5	Reference	.006,**
		Reference	1.01 ± 0.01, 2				
	30	F1	99 ± 4, 2	Levene's F-test: F(3,4)=7E+32, p<0.001 Welch's Equality of Means: F(3,1.7)=8255, p< .001	98.0	Reference	.035, *
		F2	97.5 ± 4, 2		96.5	Reference	.030,*
		F3	104 ± 1, 2		102.5	Reference	.006,**
		Reference	1.01 ± 0.01, 2				
	60	F1	99.8 ± 6, 2	Levene's F-test: F(3,4)=4.4E+29, p<0.001 Welch's Equality of Means: F(3,2)=42436150, p< .001	98.8	Reference	0.05,*
		F2	99 ± 3, 2		98	Reference	.024,*
		F3	104 ± 0.01, 2		103	Reference	.000,***
		Reference	1.01 ± 0.01, 2				
	90	F1	100.5 ± 5, 2	Welch's Equality of Means: F(3,1.8)=6968, p< .001	98.8	Reference	.040, *
		F2	99 ± 3, 2		97.3	Reference	.022,*
		F3	104.5 ± 1, 2		103.8	Reference	.001,***
		Reference	1.01 ± 0.5, 2				
B9	15	F1	75 ± 1, 2	Welch's Equality of Means: F(3,1.7)=1281, p=.002	75.0	Reference	.015, *
		F2	76 ± 7, 2				
		F3	81 ± 4, 2		81.5	Reference	.036,*
		Reference	0.01 ± 0.01, 2				
	30	F1	80.5 ± 6, 2	Welch's Equality of Means: F(3,1.7)=163.4, p= .012			
		F2	77.5 ± 9, 2				
		F3	82 ± 6, 2				
		Reference	0.01 ± 0.01, 2				
	60	F1	80 ± 10, 2	Welch's Equality of Means: F(3,1.7)=89.88, p= .020			
		F2	78.5 ± 9, 2				
		F3	79.5 ± 8, 2				
		Reference	0.01 ± 0.01, 2				
	90	F1	81.5 ± 8, 2	Welch's Equality of Means: F(3,1.7)=77.4, p=.023			
		F2	77.5 ± 9, 2				
		F3	75 ± 14, 2				
		Reference	0.01 ± 0.01, 2				

Table D-10: Difference ($f1$) and similarity ($f2$) factors for F1, F2, F3 and the reference formulation.

Media	Reference vs. Test	Time (mins) (n = # of points)	% Dissolved Reference (R)	% Dissolved Test (T)	|R-T|	$R\text{-}T^2$
Citric Acid	F1 vs. F2	15	70± 9.0	72± 7.0	2.00	4
		30	79± 7.0	72± 8.0	7.00	49
		60	80± 8.0	73± 9.0	7.00	49
		Sum (Σ)	**229**		**16**	**102**
	F1 vs. F3	15	70± 9.0	75± 10.0	5.00	25
		30	79± 7.0	77± 13.0	2.00	4
		60	80± 8.0	76± 14.0	4.00	16
		Sum (Σ)	**229**		**11**	**45**
	Control vs. F1	15	0± 0.0	70± 9.0	70.00	4900
		30	0± 0.0	79± 7.0	79.00	6241
		60	0± 0.0	80± 8.0	80.00	6400
		Sum (Σ)	**0**		**229**	**17541**
	Control vs. F2	15	0± 0.0	72± 7.0	72.00	5184
		30	0± 0.0	72± 8.0	72.00	5184
		60	0± 0.0	73± 9.0	73.00	5329
		Sum (Σ)	**0**		**217**	**15697**
	Control vs. F3	15	0± 0.0	75± 10.0	75.00	5625
		30	0± 0.0	77± 13.0	77.00	5929
		60	0± 0.0	76± 14.0	76.00	5776
		Sum (Σ)	**0**		**228**	**17330**
Phosphate Buffer	F1 vs. F2	15	75± 1.0	76± 8.0	1	1
		30	81± 6.0	77± 9.0	4	13
		60	80± 11.0	79± 9.0	1	1
		90	81± 8.0	77± 10.0	4	19
		120	81± 9.0	78± 10.0	3	6
		Sum (Σ)	**398**		**13**	**40**
	F1 vs. F3	15	75± 1.0	82± 4.0	7	50
		30	81± 6.0	82± 6.0	1	2
		60	80± 11.0	80± 8.0	0	0
		90	81± 8.0	75± 14.0	6	41
		Sum (Σ)	**398**		**14**	**93**
	Control vs. F1	15	0 ± 0.0	75± 1.0	75	5617
		30	0 ± 0.0	81± 6.0	81	6504
		60	0 ± 0.0	80± 11.0	80	6396
		90	0 ± 0.0	81± 8.0	81	6625
		120	0 ± 0.0	81± 9.0	81	6486
		Sum (Σ)	**0**		**398**	**31628**
	Control vs. F2	15	0 ± 0.0	76± 8.0	76	5776
		30	0 ± 0.0	77± 9.0	77	5929
		60	0 ± 0.0	79± 9.0	79	6241
		90	0 ± 0.0	77± 10.0	77	5929
		120	0 ± 0.0	78± 10.0	78	6084
		Sum (Σ)	**0**		**387**	**29959**
	Control vs. F3	15	0 ± 0.0		82	6724
		30	0 ± 0.0		82	6724
		60	0 ± 0.0		80	6400
		90	0 ± 0.0		75	5625
		Sum (Σ)	**0**		**319**	**25473**

f1 (difference factor): $[\left(\frac{\Sigma|R-T|}{\Sigma R}\right)) * 100]$

f2 (similarity factor): $50 * log\ [\frac{100}{\sqrt{1+(\frac{\Sigma(R-T)^2}{n})}}]$

Size Histograms and Zeta Potential Curves

Span 80, Polysorbate 81, Polysorbate 80

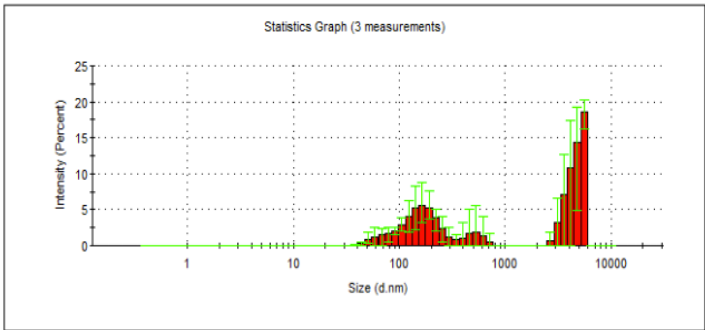

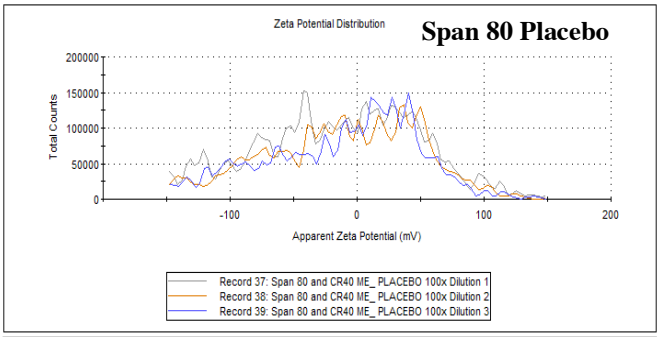

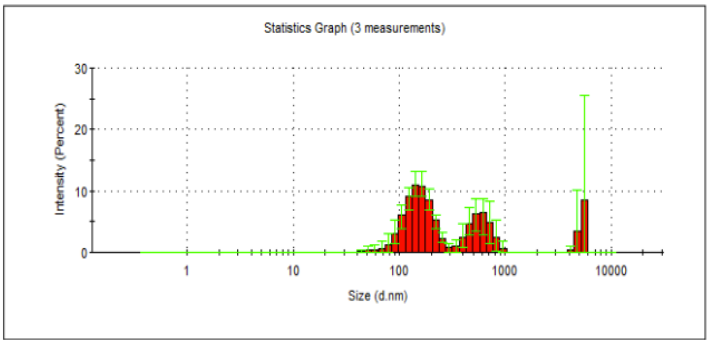

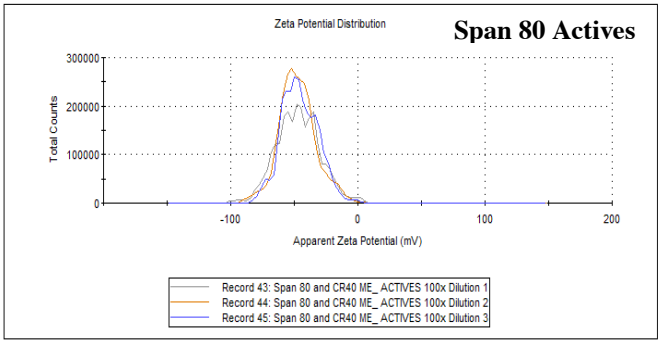

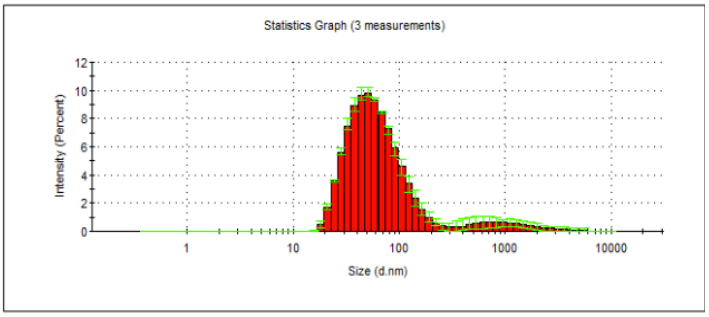

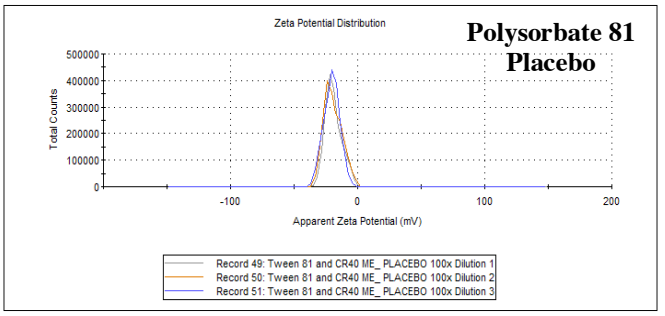

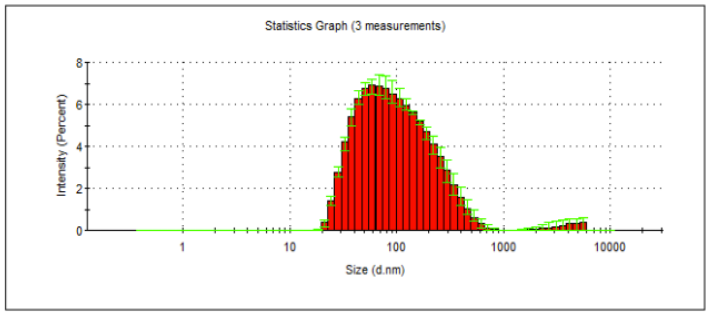

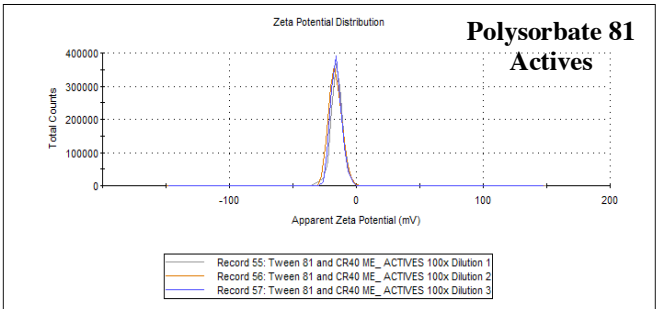

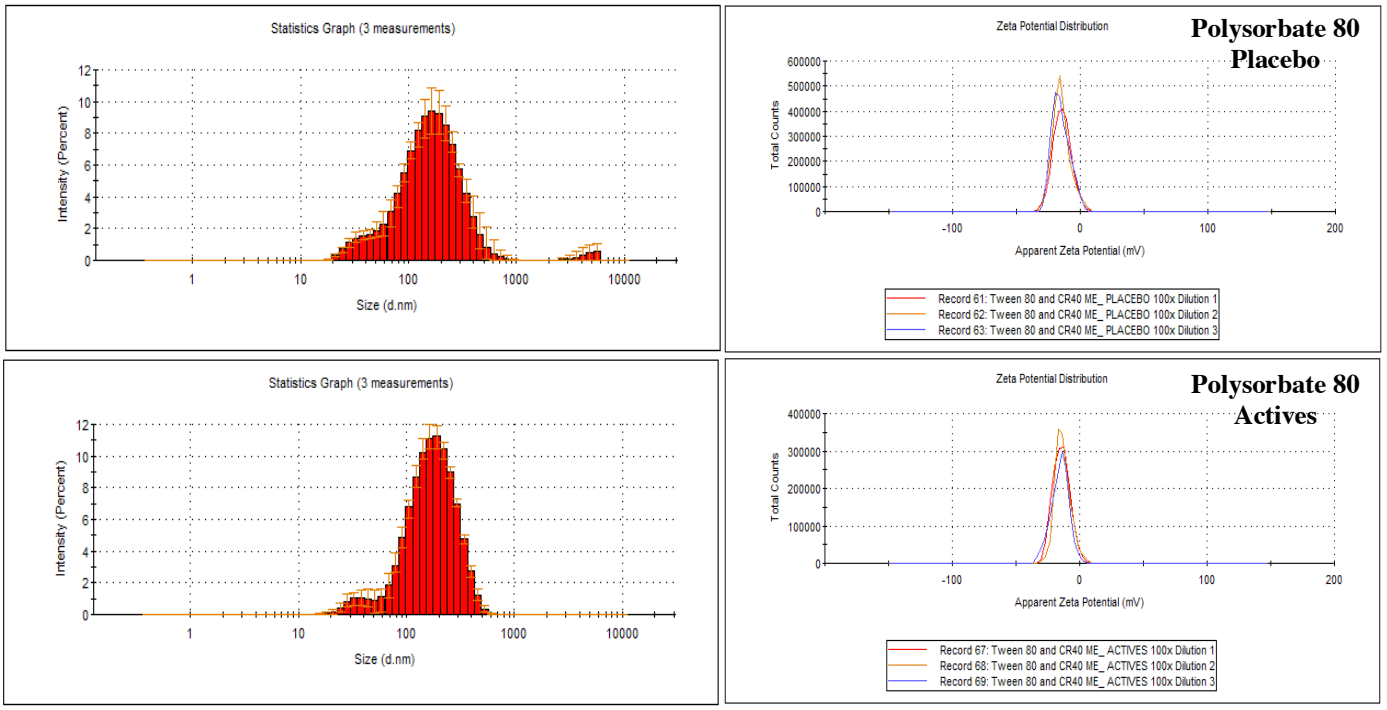

Figure D-1: Size histograms and zeta potential curves of Span 80, Polysorbate 81 and Polysorbate 80-containing microemulsions before and after API incorporation

Brij 93, Brij 97 and Brij 98

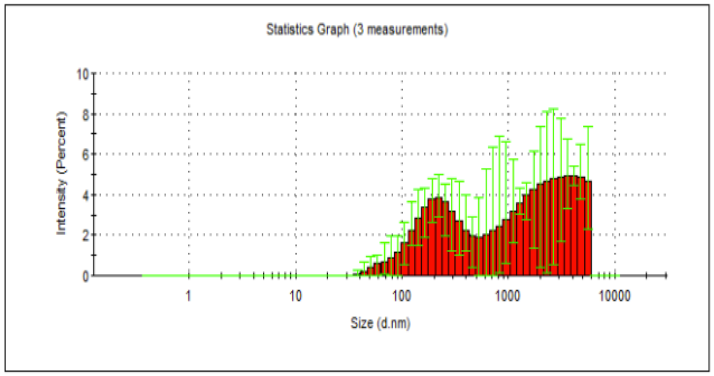

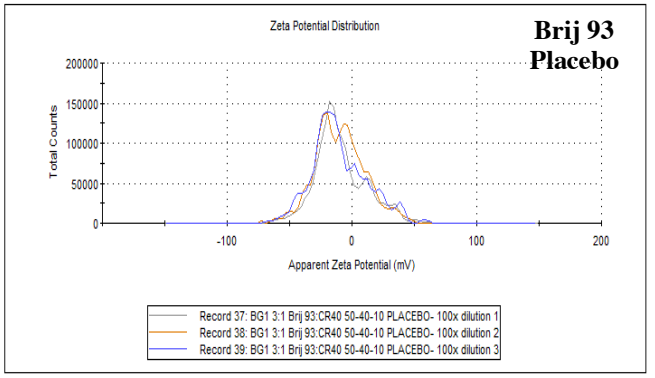

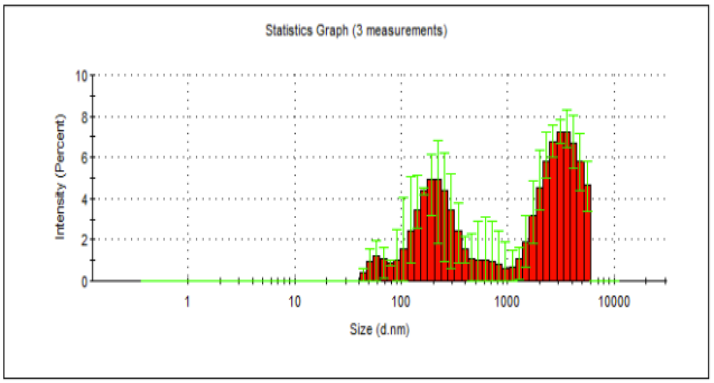

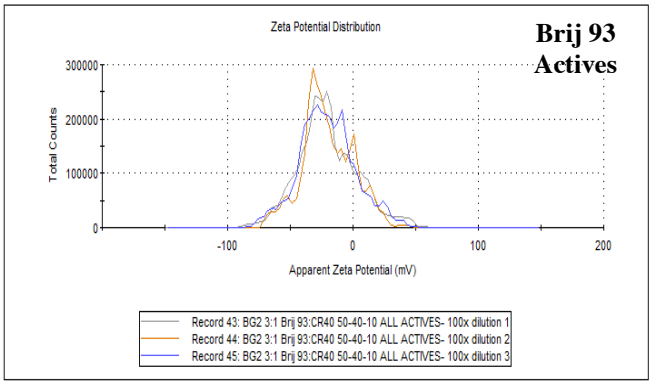

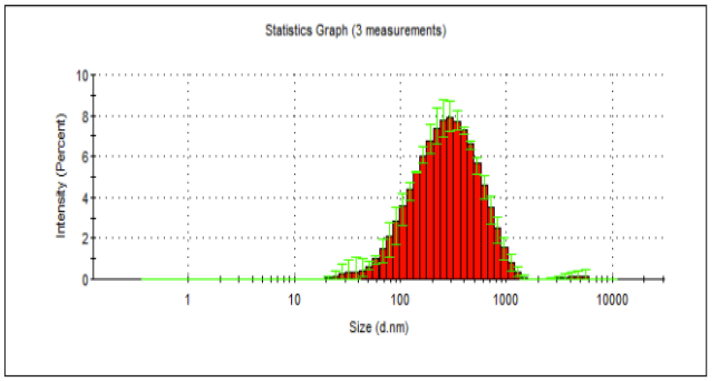

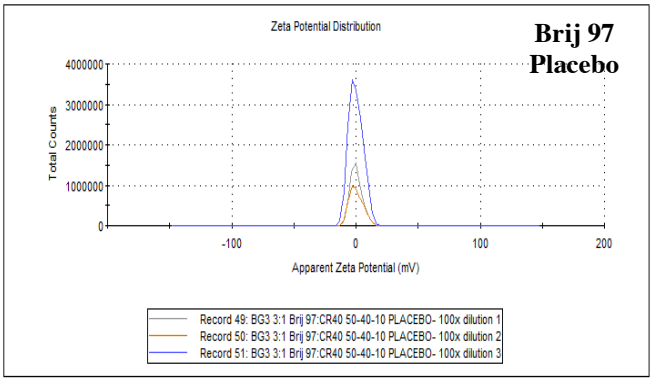

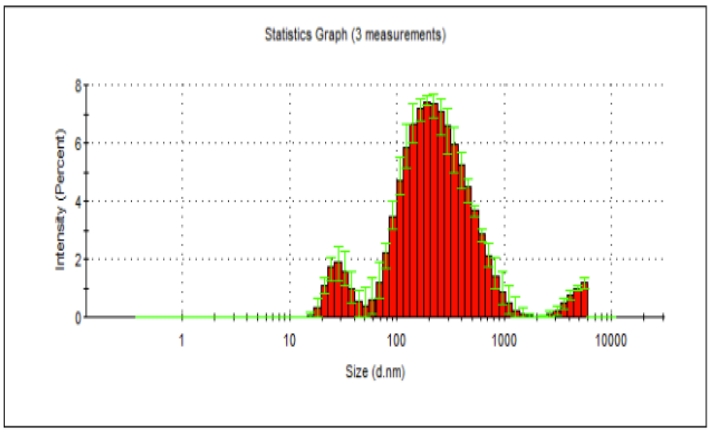

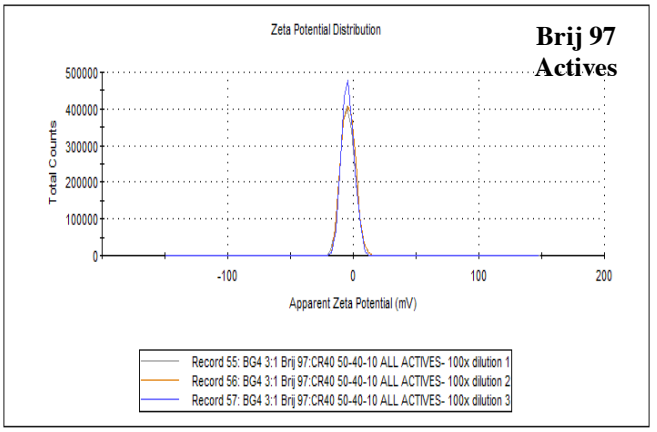

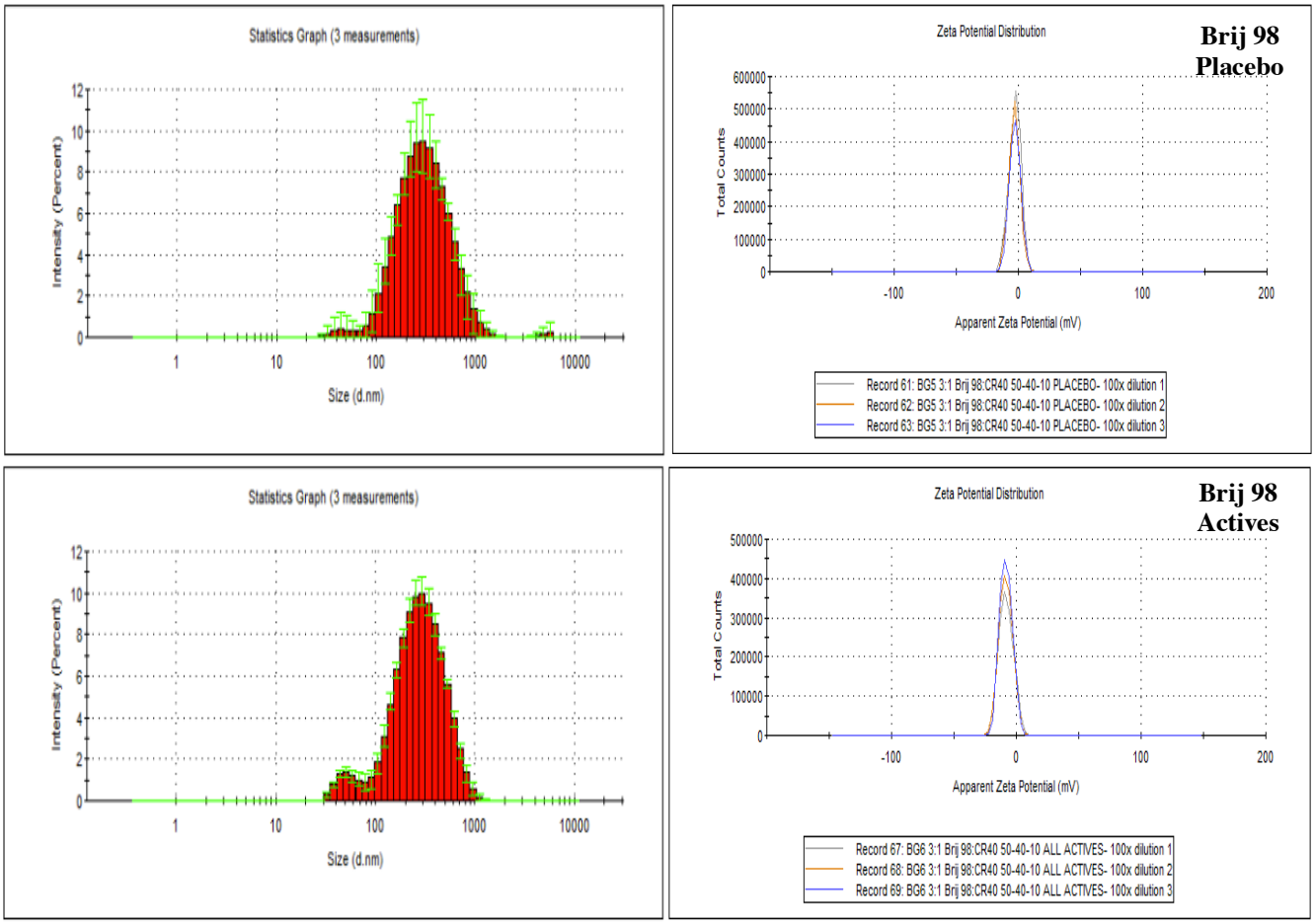

Figure D-2: Size histograms and zeta potential curves of Brij 93, Brij 97 and Brij 98-containing microemulsions before and after API incorporation

Polysorbate 20, Polysorbate 40 and Polysorbate 60

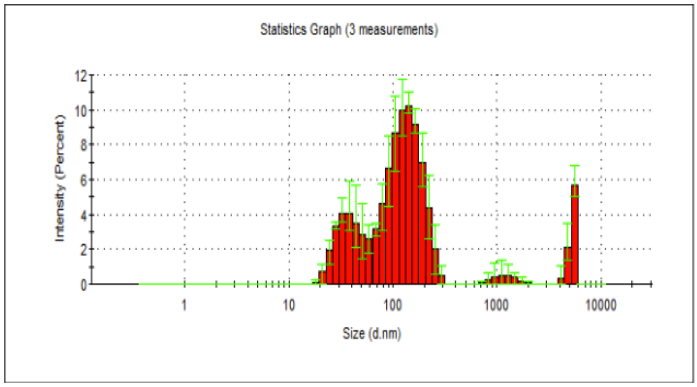

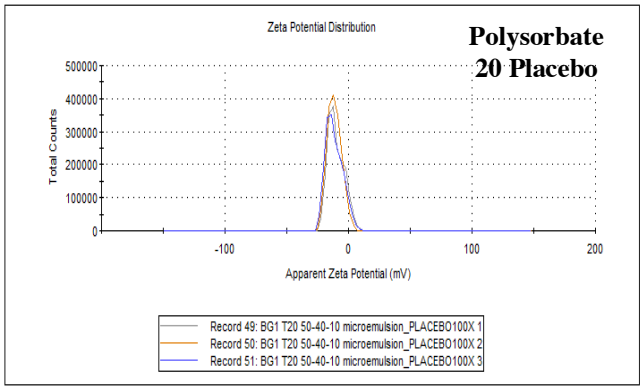

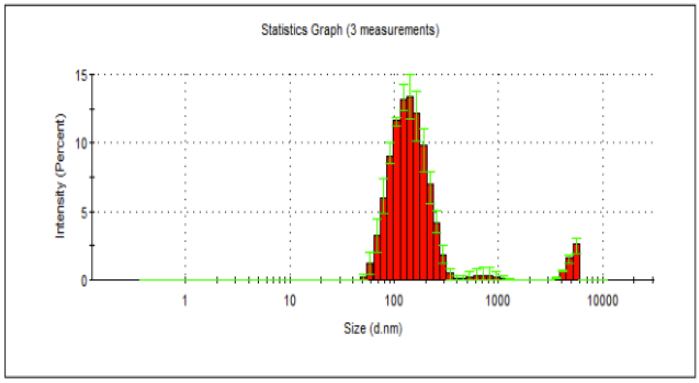

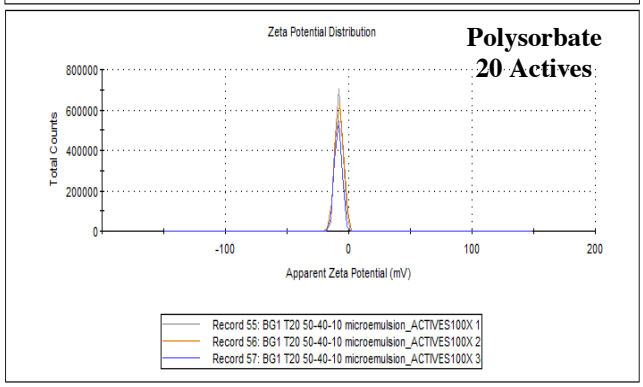

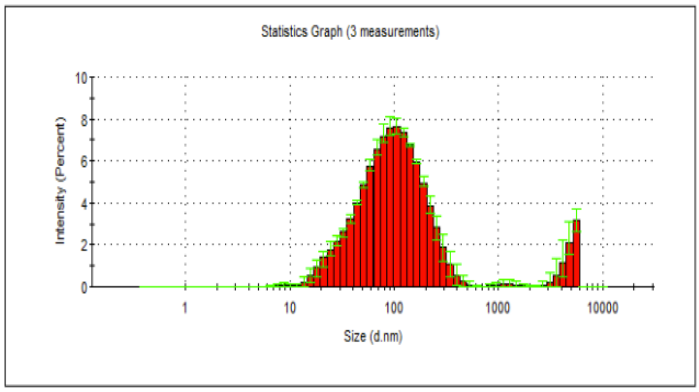

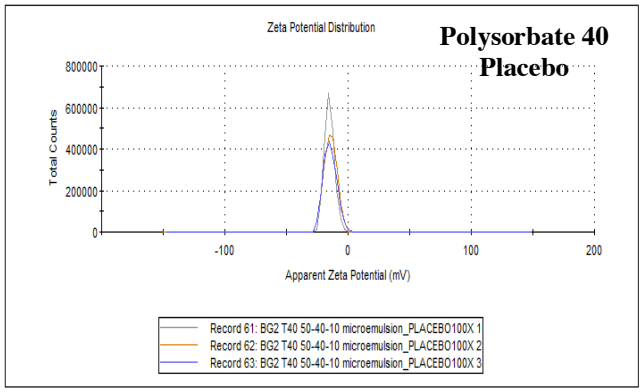

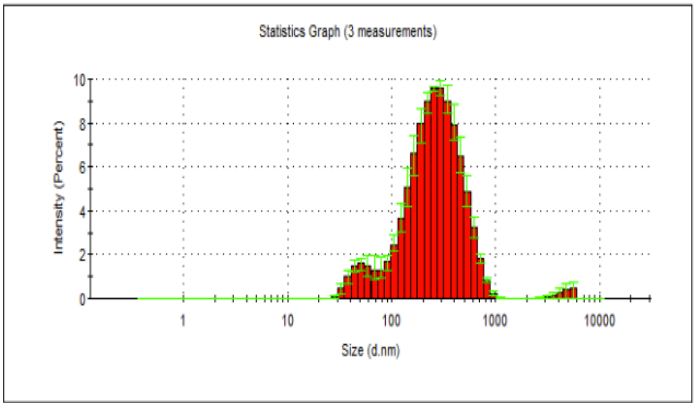

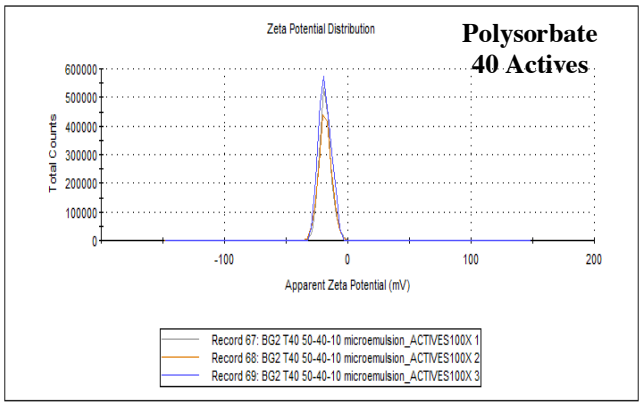

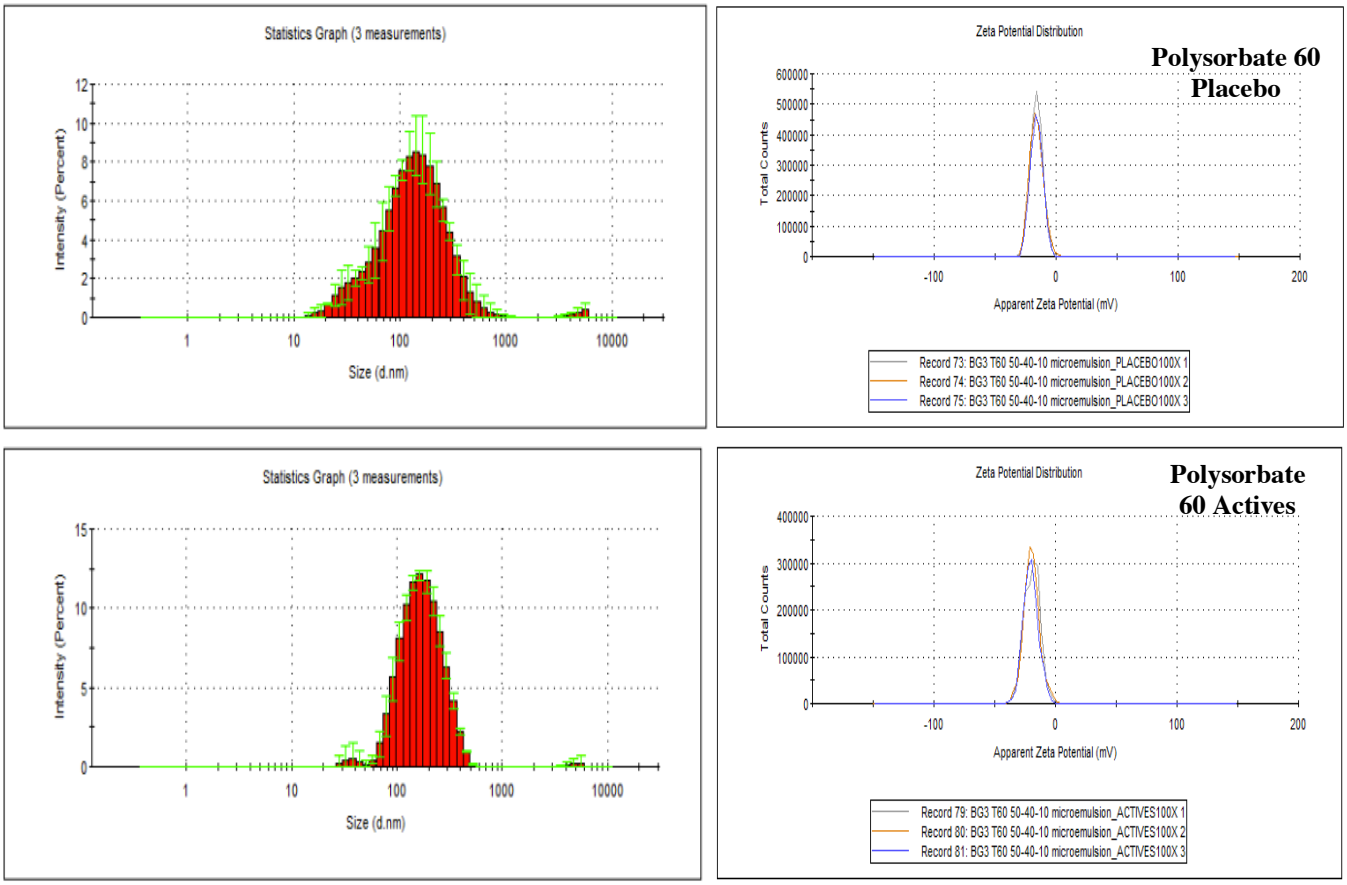

Figure D-3: Size histograms and zeta potential curves of Polysorbate 20, Polysorbate 40 and Polysorbate 60-containing microemulsions before and after API incorporation

Cremophor RH 60-containing Microemulsions

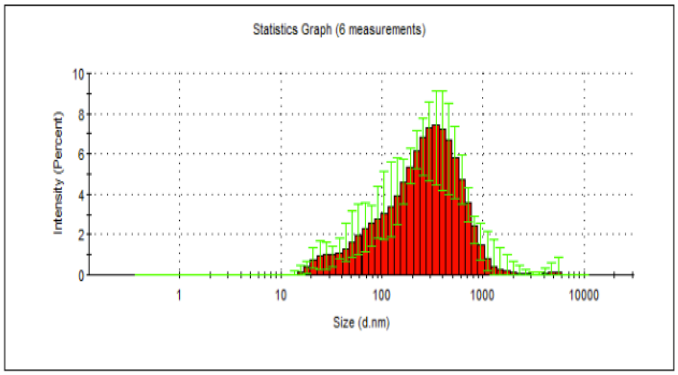

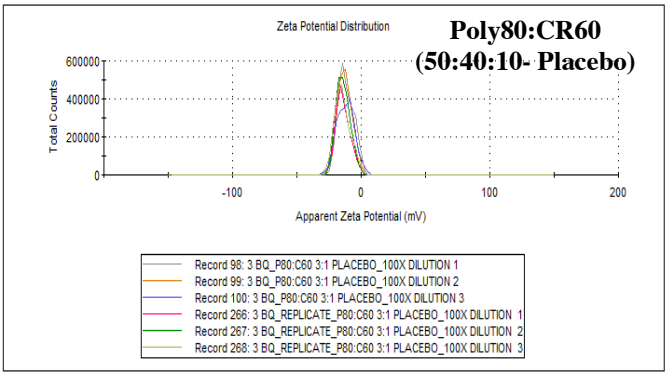

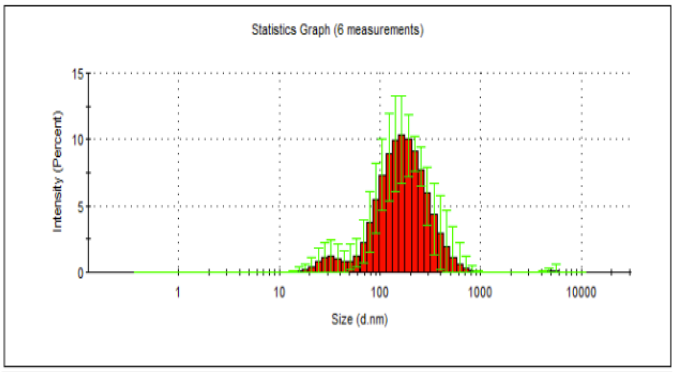

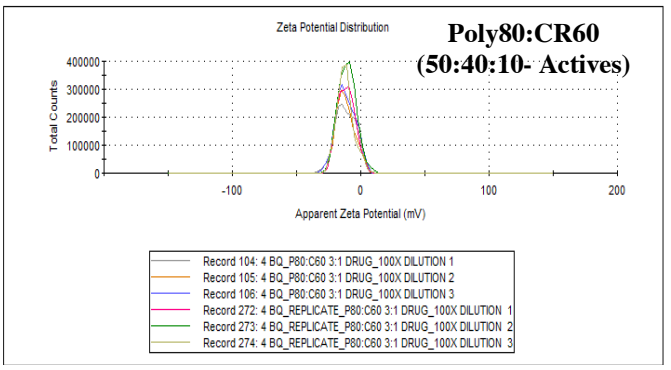

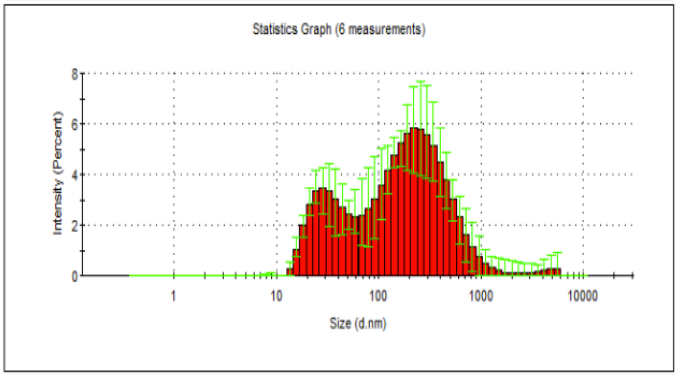

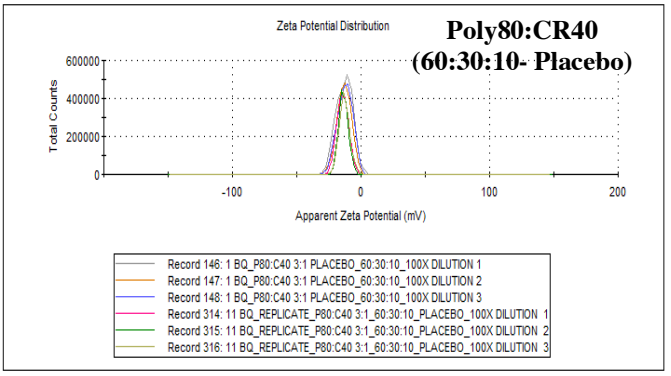

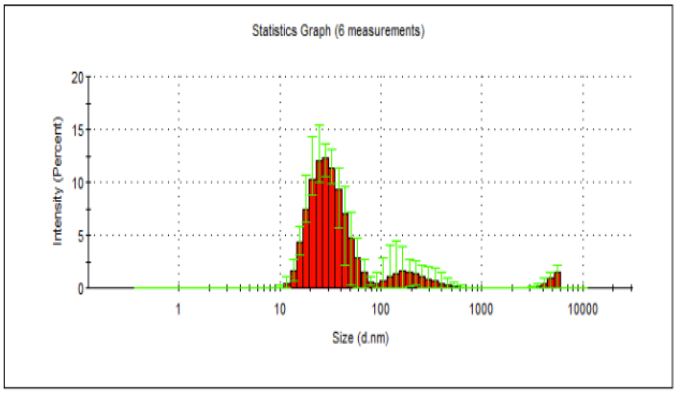

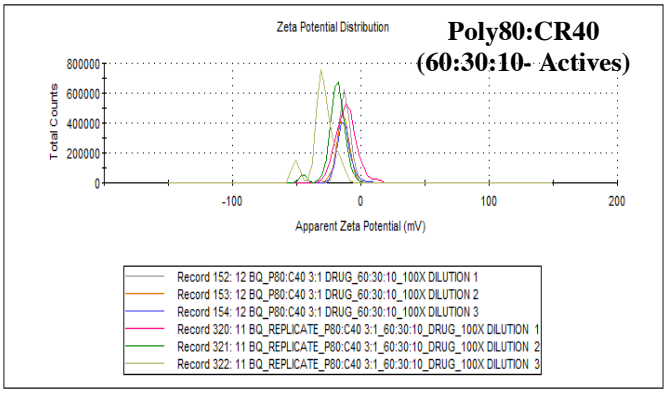

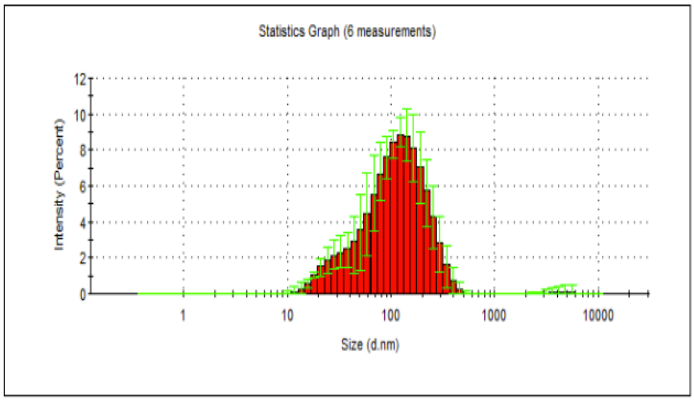
Statistics Graph (6 measurements)
Intensity (Percent)
Size (d.nm)

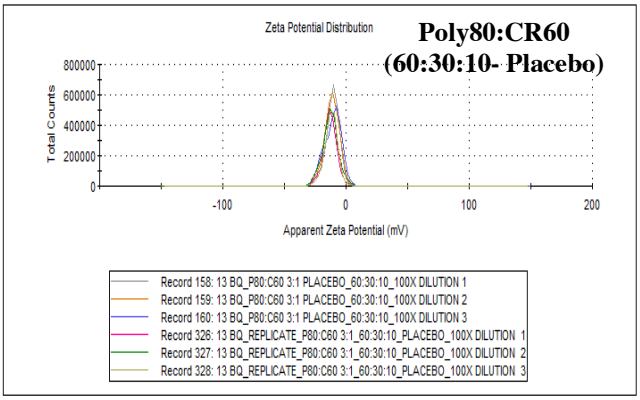
Zeta Potential Distribution
Poly80:CR60
(60:30:10- Placebo)
Total Counts
Apparent Zeta Potential (mV)
Record 158: 13 BQ_P80:C60 3:1 PLACEBO_60:30:10_100X DILUTION 1
Record 159: 13 BQ_P80:C60 3:1 PLACEBO_60:30:10_100X DILUTION 2
Record 160: 13 BQ_P80:C60 3:1 PLACEBO_60:30:10_100X DILUTION 3
Record 326: 13 BQ_REPLICATE_P80:C60 3:1_60:30:10_PLACEBO_100X DILUTION 1
Record 327: 13 BQ_REPLICATE_P80:C60 3:1_60:30:10_PLACEBO_100X DILUTION 2
Record 328: 13 BQ_REPLICATE_P80:C60 3:1_60:30:10_PLACEBO_100X DILUTION 3

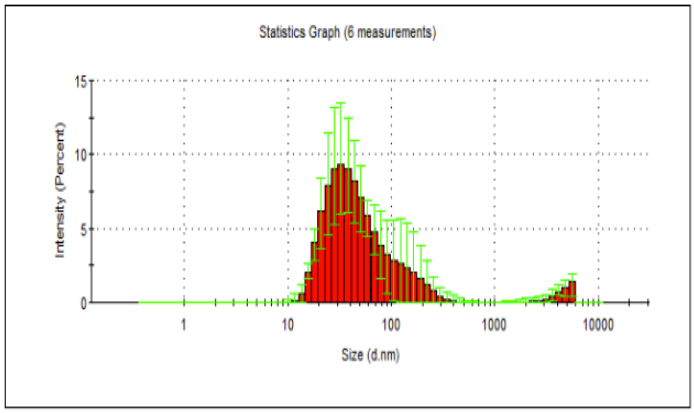
Statistics Graph (6 measurements)
Intensity (Percent)
Size (d.nm)

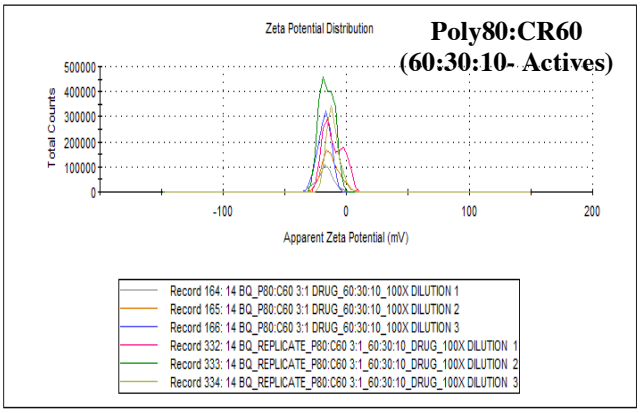
Zeta Potential Distribution
Poly80:CR60
(60:30:10- Actives)
Total Counts
Apparent Zeta Potential (mV)
Record 164: 14 BQ_P80:C60 3:1 DRUG_60:30:10_100X DILUTION 1
Record 165: 14 BQ_P80:C60 3:1 DRUG_60:30:10_100X DILUTION 2
Record 166: 14 BQ_P80:C60 3:1 DRUG_60:30:10_100X DILUTION 3
Record 332: 14 BQ_REPLICATE_P80:C60 3:1_60:30:10_DRUG_100X DILUTION 1
Record 333: 14 BQ_REPLICATE_P80:C60 3:1_60:30:10_DRUG_100X DILUTION 2
Record 334: 14 BQ_REPLICATE_P80:C60 3:1_60:30:10_DRUG_100X DILUTION 3

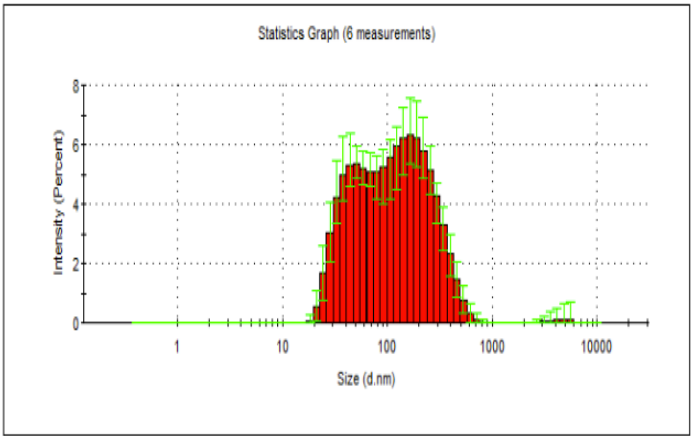
Statistics Graph (6 measurements)
Intensity (Percent)
Size (d.nm)

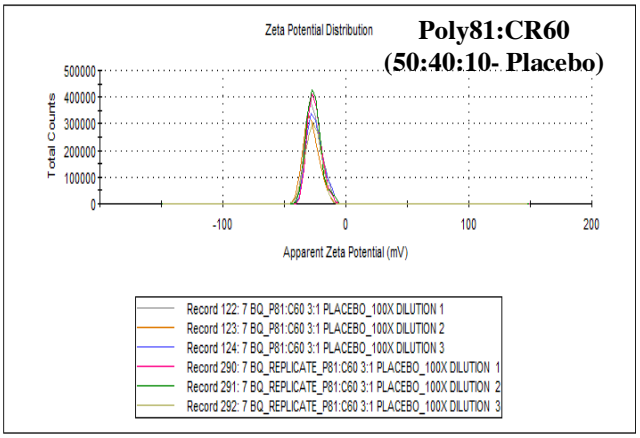
Zeta Potential Distribution
Poly81:CR60
(50:40:10- Placebo)
Total Counts
Apparent Zeta Potential (mV)
Record 122: 7 BQ_P81:C60 3:1 PLACEBO_100X DILUTION 1
Record 123: 7 BQ_P81:C60 3:1 PLACEBO_100X DILUTION 2
Record 124: 7 BQ_P81:C60 3:1 PLACEBO_100X DILUTION 3
Record 290: 7 BQ_REPLICATE_P81:C60 3:1 PLACEBO_100X DILUTION 1
Record 291: 7 BQ_REPLICATE_P81:C60 3:1 PLACEBO_100X DILUTION 2
Record 292: 7 BQ_REPLICATE_P81:C60 3:1 PLACEBO_100X DILUTION 3

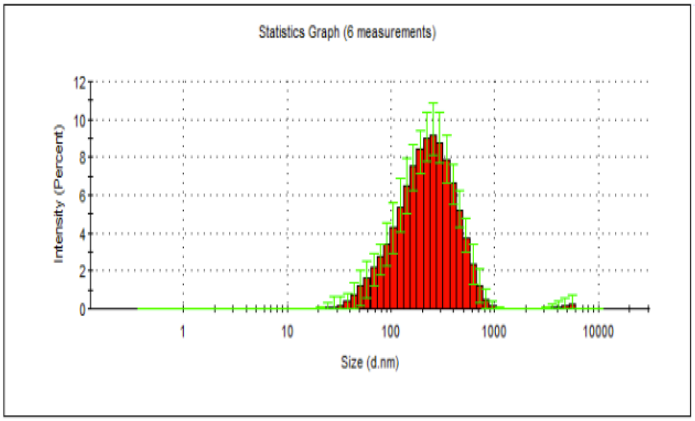
Statistics Graph (6 measurements)
Intensity (Percent)
Size (d.nm)

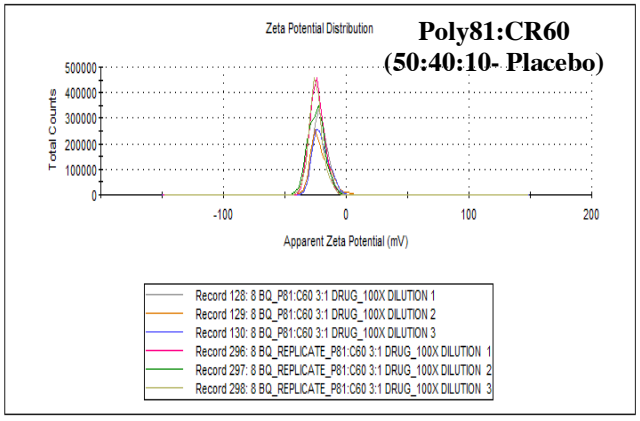
Zeta Potential Distribution
Poly81:CR60
(50:40:10- Placebo)
Total Counts
Apparent Zeta Potential (mV)
Record 128: 8 BQ_P81:C60 3:1 DRUG_100X DILUTION 1
Record 129: 8 BQ_P81:C60 3:1 DRUG_100X DILUTION 2
Record 130: 8 BQ_P81:C60 3:1 DRUG_100X DILUTION 3
Record 296: 8 BQ_REPLICATE_P81:C60 3:1 DRUG_100X DILUTION 1
Record 297: 8 BQ_REPLICATE_P81:C60 3:1 DRUG_100X DILUTION 2
Record 298: 8 BQ_REPLICATE_P81:C60 3:1 DRUG_100X DILUTION 3

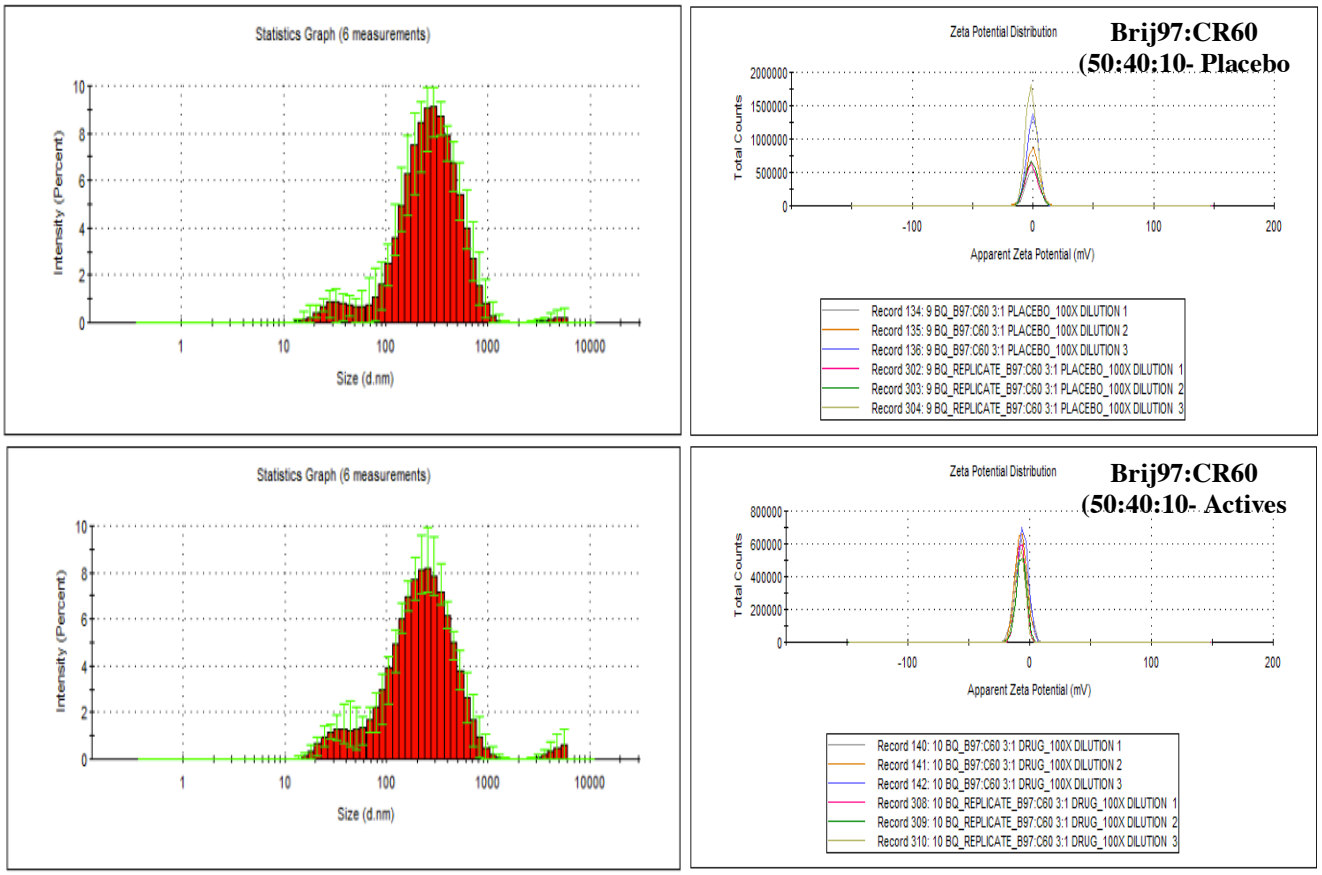

Figure D-4: Size histograms and zeta potential curves of Polysorbate 80, Polysorbate 81 and Brij 97 with various surfactant:oil:water (S:O:W) combinations of Cremophor RH 40 or Cremophor RH 60 before and after API incorporation.

Polysorbate 85

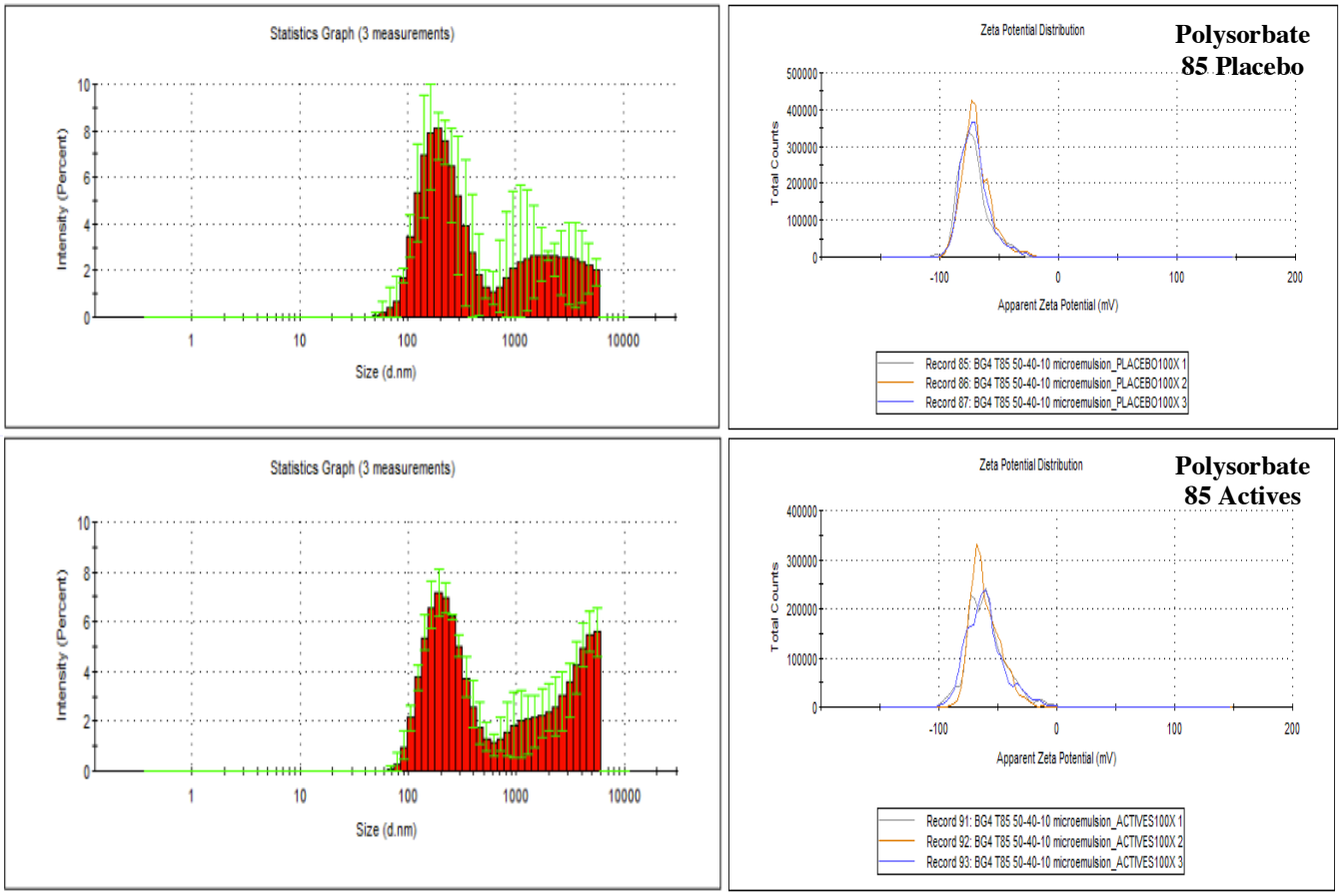

Figure D-5: Size histograms and zeta potential curves of Polysorbate 85-containing microemulsions before and after API incorporation

Polysorbate 81
Replicate 1

Surfactant Concentration (mM)	Log Surfactant Concentration	Average Surface Tension (mN/m)	Standard Deviation
0	-3.7	69.14	0.33
0.0005	-3.301247089	67.82	0.02
0.0010	-3.000434077	66.07	0.04
0.0015	-2.824559695	64.47	0.09
0.0020	-2.699837726	61.57	0.16
0.0025	-2.603144373	58.61	0.12
0.0031	-2.506505032	54.60	0.36
0.0037	-2.427594291	51.15	0.12
0.0050	-2.303196057	47.71	0.02
0.0056	-2.252313535	46.09	0.04
0.0062	**-2.206825876**	**45.04**	**0.01**
0.0074	-2.128183791	44.32	0.03
0.0099	-2.004321374	43.58	0.04
0.0123	-1.908485019	42.60	0.02
0.0160	-1.796147193	41.87	0.02
0.0196	-1.707570176	41.01	0.01
0.0244	-1.612783857	40.16	0.01
0.0315	-1.502006699	39.61	0.03
0.0361	-1.441956838	39.40	0.02
0.1209	-0.917648707	38.64	0.02

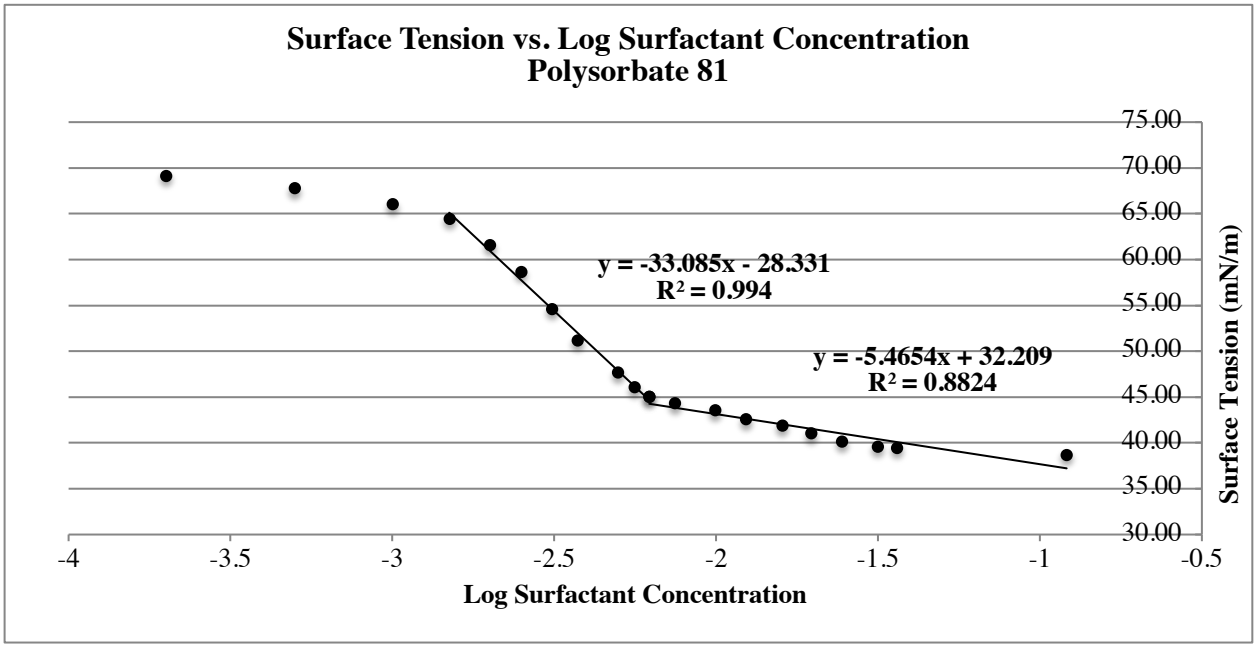

Figure D-6: Surface tension versus log surfactant concentration for Polysorbate 81 was determined experimentally to be 0.0062 mM. CMC values are highlighted in yellow.

Polysorbate 81
Replicate 2

Surfactant Concentration (mM)	Log Surfactant Concentration	Average Surface Tension (mN/m)	Standard Deviation
0	-3.7	69.47	0.22
0.0005	-3.303970684	68.17	0.04
0.0015	-2.827066468	64.11	1.13
0.0030	-2.526361827	54.36	0.41
0.0050	-2.304946506	48.76	0.08
0.0054	-2.26366211	44.74	0.05
0.0059	**-2.225981811**	**44.05**	**0.06**
0.0069	-2.159251465	43.05	0.03
0.0079	-2.101475854	42.72	0.04
0.0089	-2.05053956	42.28	0.04
0.0099	-2.00499819	42.03	0.02
0.0342	-1.466298502	40.59	0.01
0.0810	-1.091489266	39.34	0.01

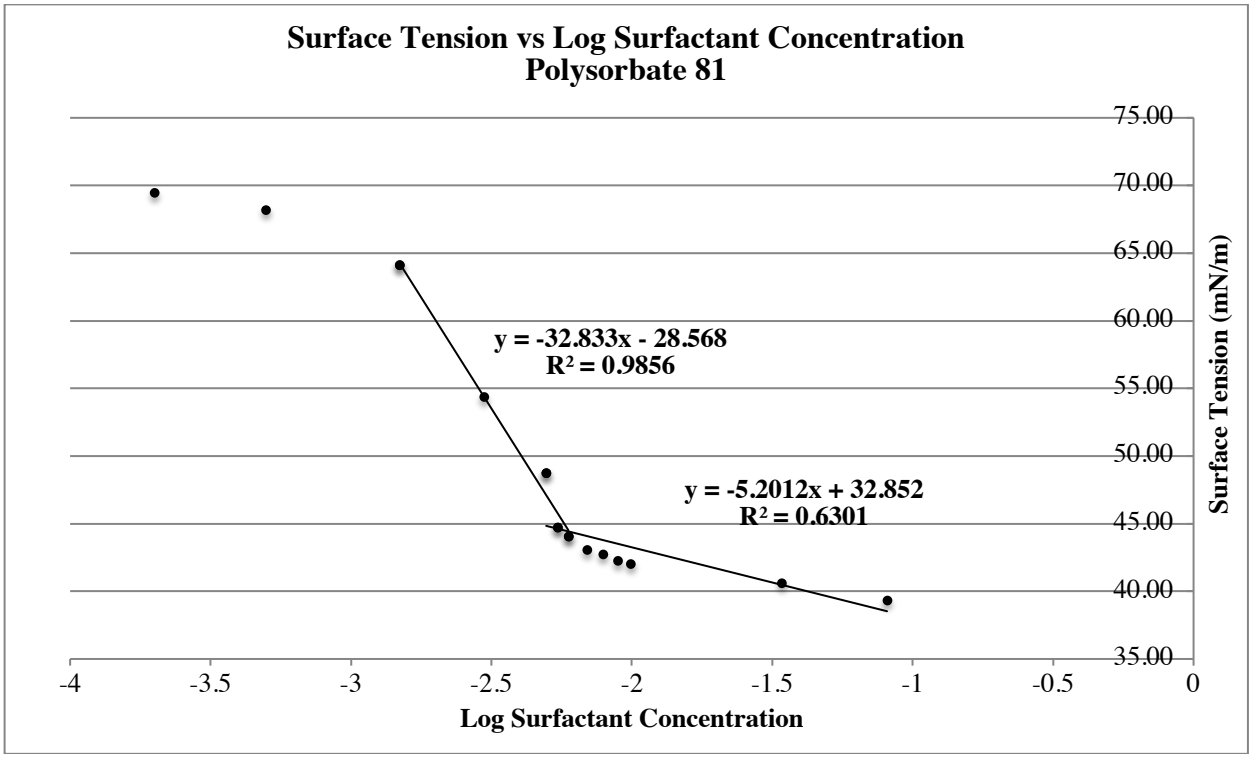

Figure D-7: Surface tension versus log surfactant concentration for Polysorbate 81 (replicate) was determined experimentally to be 0.0059 mM.

3:1 Polysorbate 81:Cremophor RH 40
Replicate 1

Surfactant Concentration (mM)	Log Surfactant Concentration	Average Surface Tension (mN/m)	Standard Deviation
0	0	68.76	0.32
0.0002	0.0002	65.47	0.08
0.0004	0.0004	62.69	0.27
0.0006	0.0006	59.14	0.10
0.0011	0.0011	56.02	0.10
0.0015	0.0015	53.30	0.10
0.0019	0.0019	50.91	0.11
0.0025	0.0025	48.03	0.12
0.0034	0.0034	45.76	0.10
0.0042	0.0042	44.01	0.05
0.0054	**0.0054**	**42.25**	**0.02**
0.0070	0.0070	41.78	0.04
0.0090	0.0090	41.27	0.03
0.0113	0.0113	40.79	0.04
0.0138	0.0138	40.42	0.02
0.0174	0.0174	40.31	0.04
0.0224	0.0224	40.25	0.07
0.0287	0.0287	39.69	0.06
0.0358	0.0358	39.54	0.03
0.0446	0.0446	39.06	0.09
0.0554	0.0554	38.67	0.42

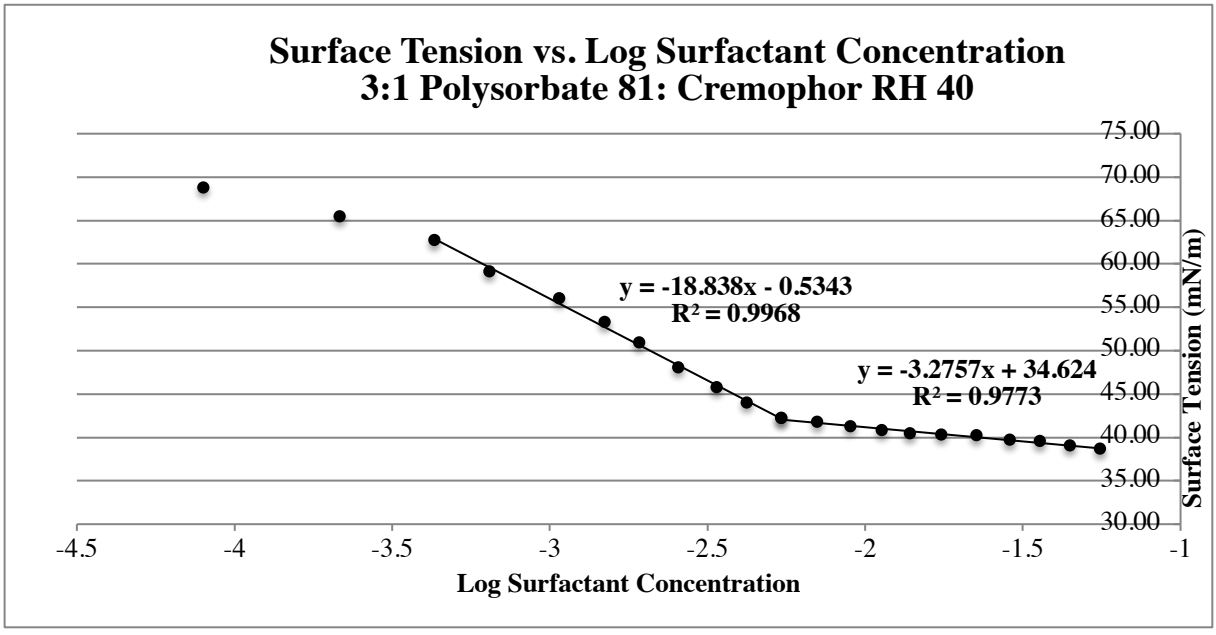

Figure D-8: Surface tension versus log surfactant concentration for 3:1 Polysorbate 81:Cremophor RH 40. The critical micelle concentration of 3:1 Polysorbate 81:Cremophor RH 40 was determined experimentally to be 0.0055 mM.

3:1 Polysorbate 81:Cremophor RH 40
Replicate 2

Surfactant Concentration (mM)	Log Surfactant Concentration	Average Surface Tension (mN/m)	Standard Deviation
0	-4.6	67.76	0.02
0.0001	-4.26757612	67.80	0.02
0.0002	-3.791537894	67.01	0.04
0.0006	-3.231571773	64.51	0.15
0.0010	-2.998473904	60.53	0.45
0.0015	-2.820100136	56.90	0.10
0.0020	-2.696640957	54.35	0.10
0.0025	-2.602655214	52.46	0.10
0.0032	-2.50061385	50.32	0.19
0.0041	-2.390826215	48.07	0.17
0.0049	-2.306794129	46.20	0.23
0.0058	**-2.239240193**	**44.31**	**0.08**
0.0066	-2.183119259	43.61	0.08
0.0081	-2.094046032	43.92	0.26
0.0107	-1.970521119	43.20	0.31
0.0159	-1.799765963	43.17	0.16

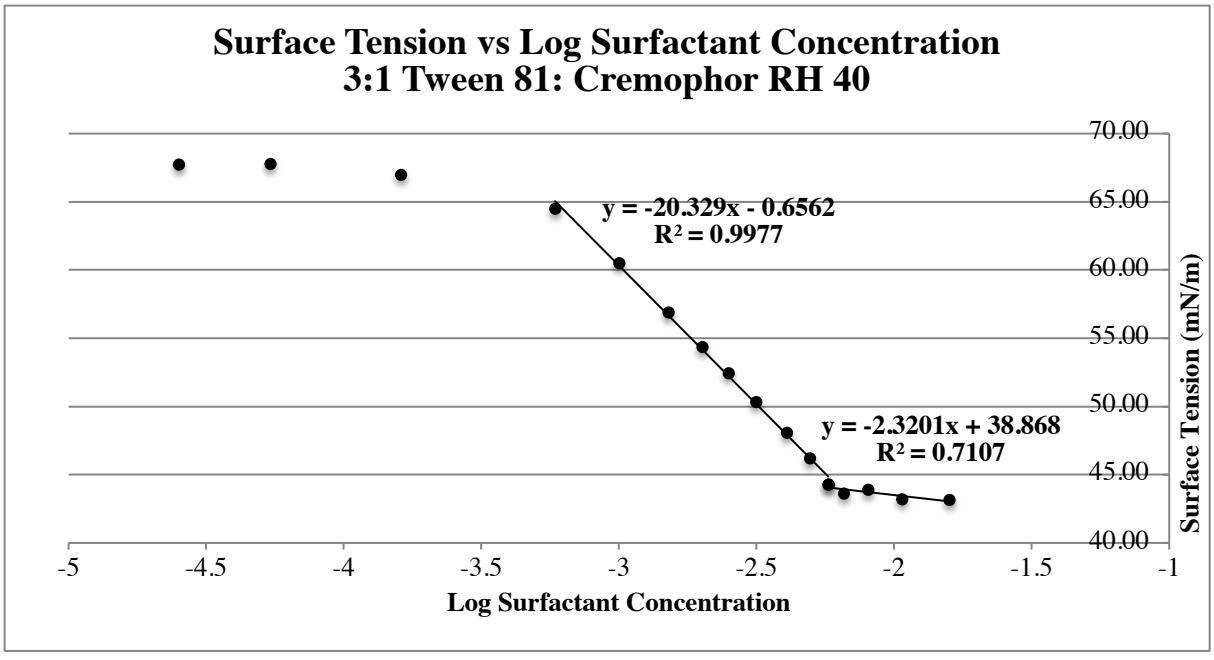

Figure D-9: Surface tension versus log surfactant concentration for 3:1 Polysorbate 81:Cremophor RH 40. The critical micelle concentration of 3:1 Polysorbate 81:Cremophor RH 40 was determined experimentally to be 0.0062 mM.

3:1 Brij 97:Cremophor RH 40

Surfactant Concentration (mM)	Log Surfactant Concentration	Average Surface Tension (mN/m)	Standard Deviation
0	-4	68.71	0.28
0.0002	-3.66362512	59.20	0.09
0.0004	-3.363676805	52.84	0.11
0.0006	-3.188664539	46.92	0.21
0.0009	-3.064802121	40.98	0.09
0.0011	-2.968965766	37.86	0.08
0.0013	-2.890855531	36.66	0.09
0.0015	**-2.824977117**	**35.63**	**0.03**
0.0017	-2.768050923	34.80	0.06
0.0019	-2.717961546	34.29	0.08
0.0021	-2.673264604	33.96	0.02
0.0023	-2.632929884	33.48	0.09
0.0025	-2.596196717	33.09	0.02
0.0027	-2.562487447	32.80	0.02
0.0029	-2.531353053	32.85	0.08
0.0031	-2.502437585	32.77	0.03
0.0033	-2.475454095	32.72	0.09
0.0035	-2.450167881	32.88	0.07
0.0037	-2.426384524	32.96	0.10

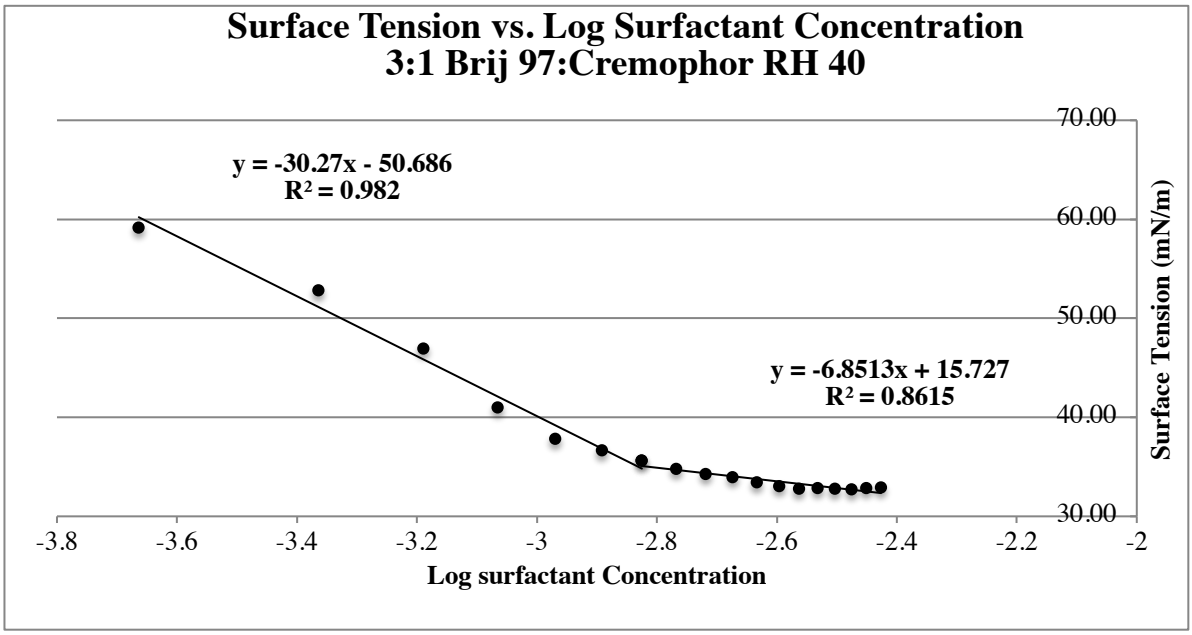

Figure D-10: Surface tension versus log surfactant concentration for 3:1 Brij 97:Cremophor RH 40 where CMC determined experimentally to be 0.0015 mM. The CMC of Brij 97 was reported to be 0.940 mM (Hait 2001) such that the ideal CMC was 0.019 mM.

3:1 Brij 98:Cremophor RH 40

Surfactant Concentration (mM)	Log Surfactant Concentration	Average Surface Tension (mN/m)	Standard Deviation
0	-4.3	69.73	0.30
0.00007	-4.13647665	67.42	0.04
0.00015	-3.835988507	64.01	0.07
0.00022	-3.660438424	59.82	0.07
0.0003	-3.536040191	57.12	0.05
0.00036	-3.43967001	54.94	0.05
0.0004	-3.361027925	52.73	0.06
0.0006	-3.237165508	49.80	0.05
0.0007	-3.141329153	47.76	0.02
0.0009	-3.063218917	46.08	0.01
0.0010	-2.997340503	44.77	0.02
0.0011	-2.94041431	43.90	0.04
0.0013	-2.890324932	43.18	0.04
0.0014	**-2.845627991**	**42.62**	**0.02**
0.0017	-2.768560104	41.81	0.06
0.0020	-2.703716439	41.14	0.02
0.0023	-2.647817482	40.61	0.03
0.0027	-2.576304556	40.16	0.03
0.0030	-2.515733904	39.84	0.08
0.0034	-2.463293055	39.69	0.08
0.0041	-2.389191335	39.50	0.03
0.0053	-2.274236819	39.57	0.03
0.0065	-2.187086643	39.25	0.07
0.0117	-1.931814138	39.38	0.03
0.0195	-1.709965389	38.82	0.05

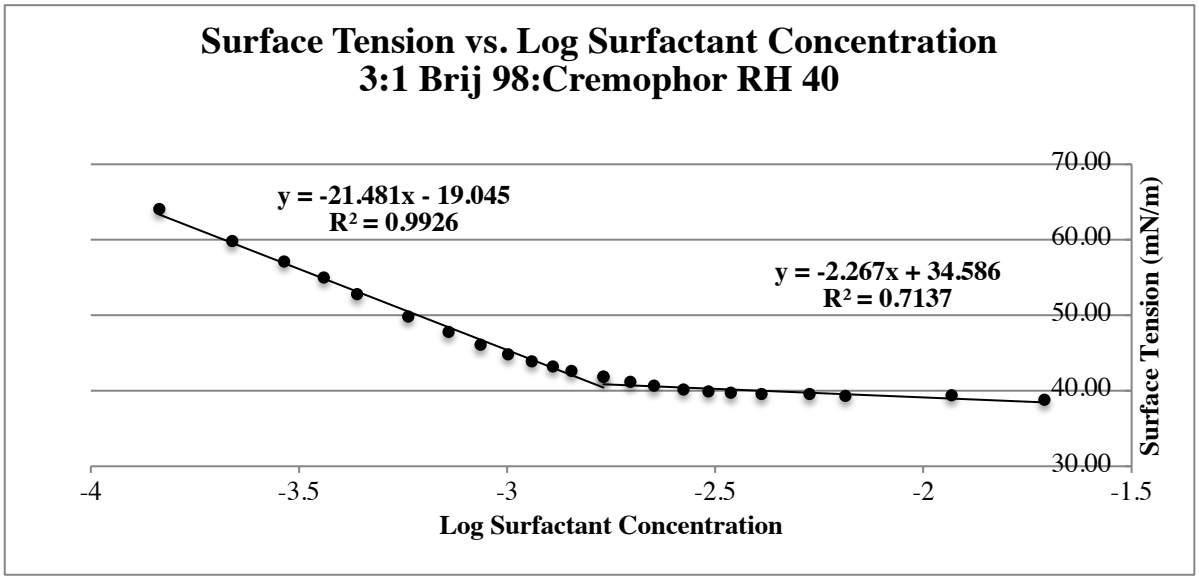

Figure D-11: Surface tension versus log surfactant concentration for 3:1 Brij 98:Cremophor RH 40 where CMC was determined experimentally to be 0.0016 mM. The CMC of Brij 98 was reported to be 0.265 mM (Hait 2001) such that the ideal CMC was 0.019 mM.

3:1 Polysorbate 40:Cremophor RH 40

Surfactant Concentration (mM)	Log Surfactant Concentration	Average Surface Tension (mN/m)	Standard Deviation
0	-4.5	69.39	0.30
0.0001	-4.14775766	67.50	0.02
0.0001	-3.847269517	64.37	0.05
0.0002	-3.671719435	60.99	0.07
0.0003	-3.547321202	58.24	0.05
0.0004	-3.372308936	56.12	0.06
0.0006	-3.248446518	54.13	0.06
0.0007	-3.152610163	52.54	0.03
0.0008	-3.074499928	51.77	0.03
0.0011	-2.95169532	50.84	0.03
0.0014	-2.856909001	50.02	0.03
0.0017	-2.779841114	49.24	0.03
0.0019	-2.71499745	48.48	0.02
0.0022	**-2.659098492**	**47.69**	**0.02**
0.0025	-2.610028921	47.09	0.02
0.0031	-2.508737676	46.06	0.03
0.0037	-2.428410882	45.25	0.02
0.0049	-2.305815658	44.05	0.03
0.0067	-2.175947477	43.43	0.05
0.0117	-1.932855905	42.61	0.06
0.0192	-1.716946419	41.63	0.05

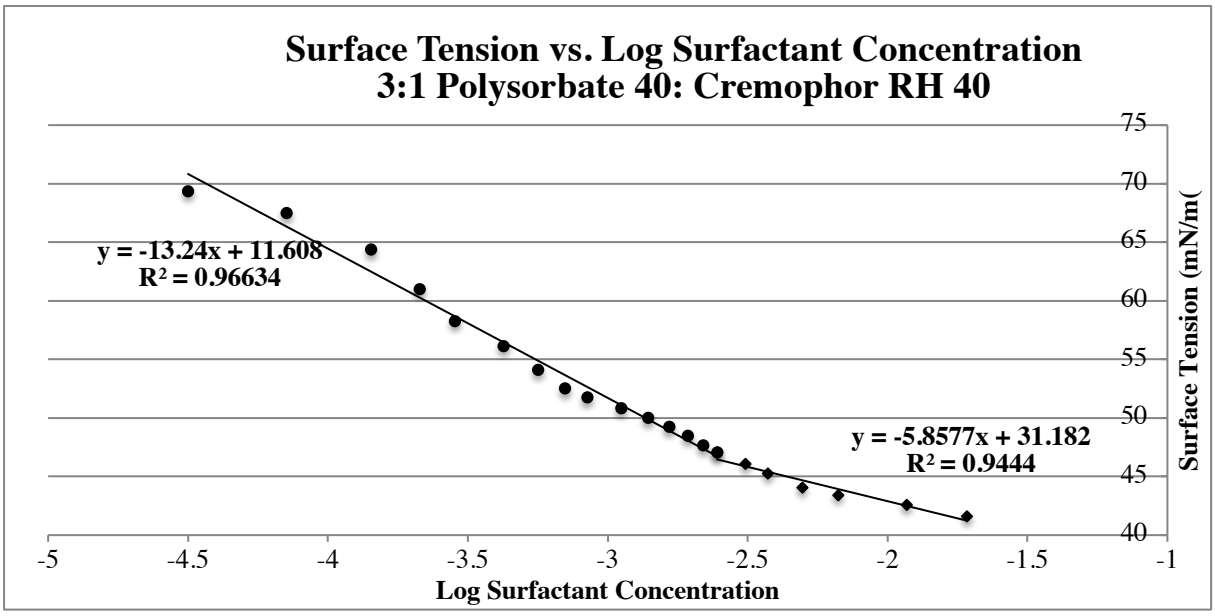

Figure D-12: Surface tension versus log surfactant concentration for 3:1 Polysorbate 40:Cremophor RH 40 where CMC determined experimentally to be 0.0022 mM. The CMC of Polysorbate 40 was reported to be 0.023 mM (Hait, 2001) such that the ideal CMC was 0.012 mM.

3:1 Polysorbate 80:Cremophor RH 60

Surfactant Concentration (mM)	Log Surfactant Concentration	Average Surface Tension (mN/m)	Standard Deviation
0	-4.7	68.90	0.19
0.0001	-4.204782704	54.75	0.09
0.0001	-3.903806985	52.13	0.12
0.0002	-3.602885523	51.76	0.02
0.0004	-3.426902769	51.24	0.02
0.0006	-3.20527095	47.28	0.08
0.0009	-3.059359736	47.13	0.01
0.0012	-2.904782807	46.41	0.02
0.0019	-2.729232725	45.37	0.03
0.0025	-2.604834491	44.40	0.02
0.0037	**-2.429822225**	**43.19**	**0.08**
0.0062	-2.210123453	41.91	0.02
0.0110	-1.959119233	40.80	0.03
0.0204	-1.691325568	40.13	0.01
0.0348	-1.457985635	39.38	0.05

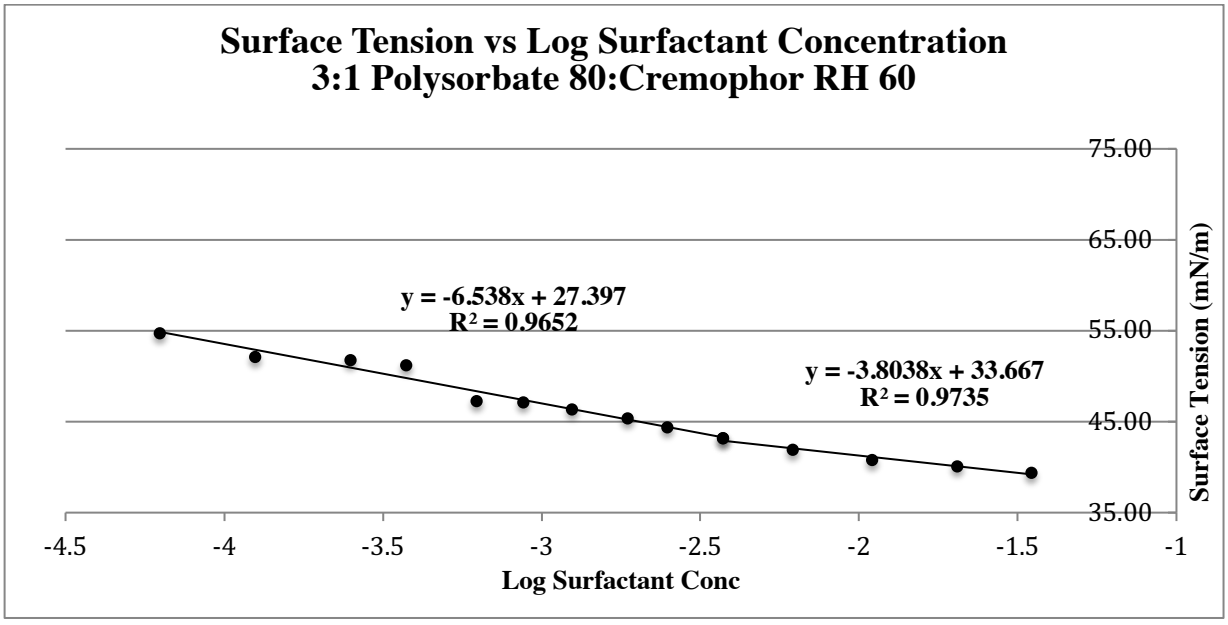

Figure D-13: Surface tension versus log surfactant concentration for 3:1 Polysorbate 80:Cremophor RH 60 where CMC determined experimentally to be 0.0051 mM. The CMC of Polysorbate 80 was experimentally determined to be 0.0047 mM while that of Cremophor RH 60 has been reported as 0.005-0.05 % w/v (Matsaridou, 2012) leading to an ideal CMC of 0.0056-0.0062 mM.

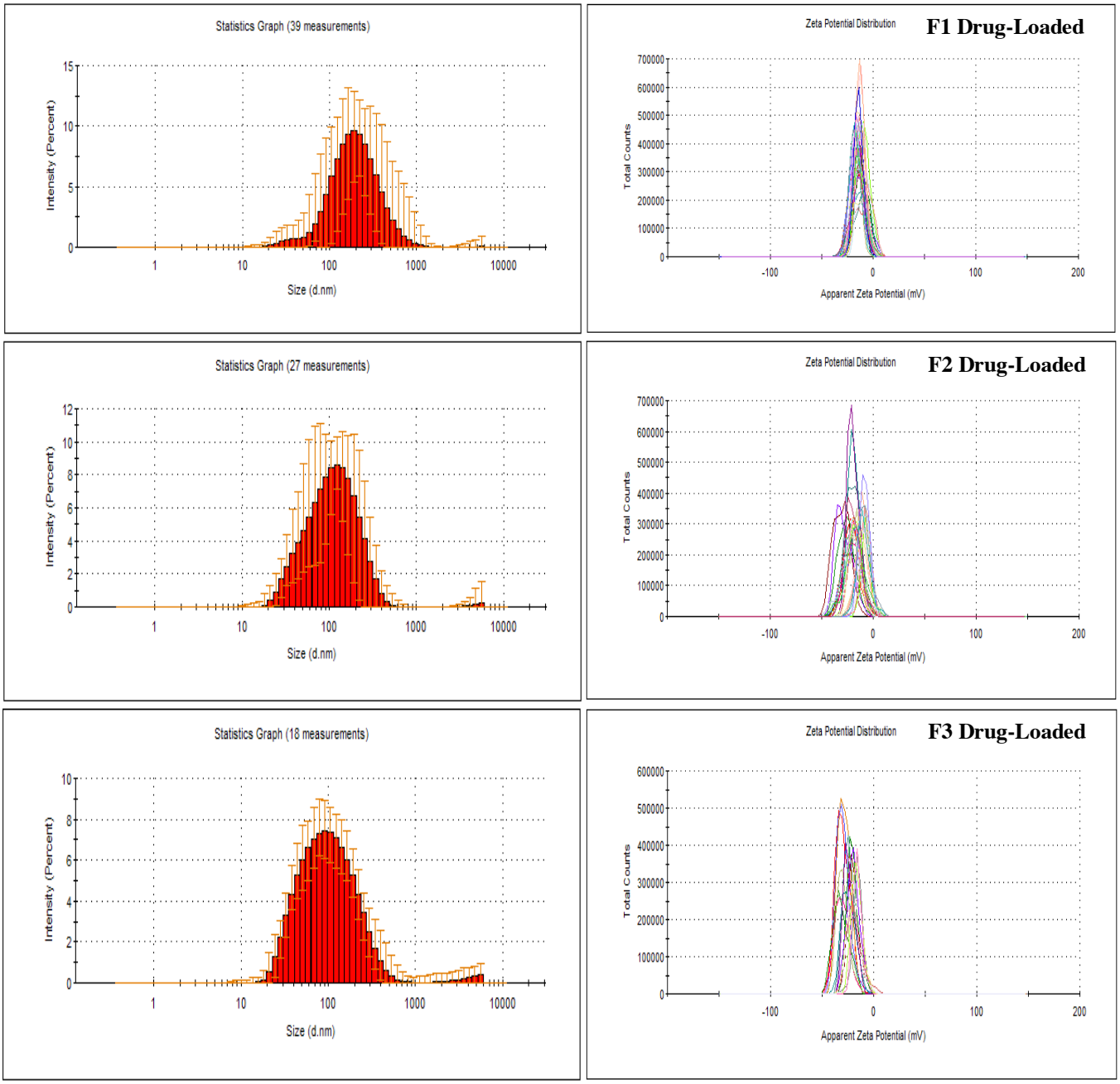

Figure D-14: Size and zeta potential values of drug-loaded formulations, F1, F2 and F3.

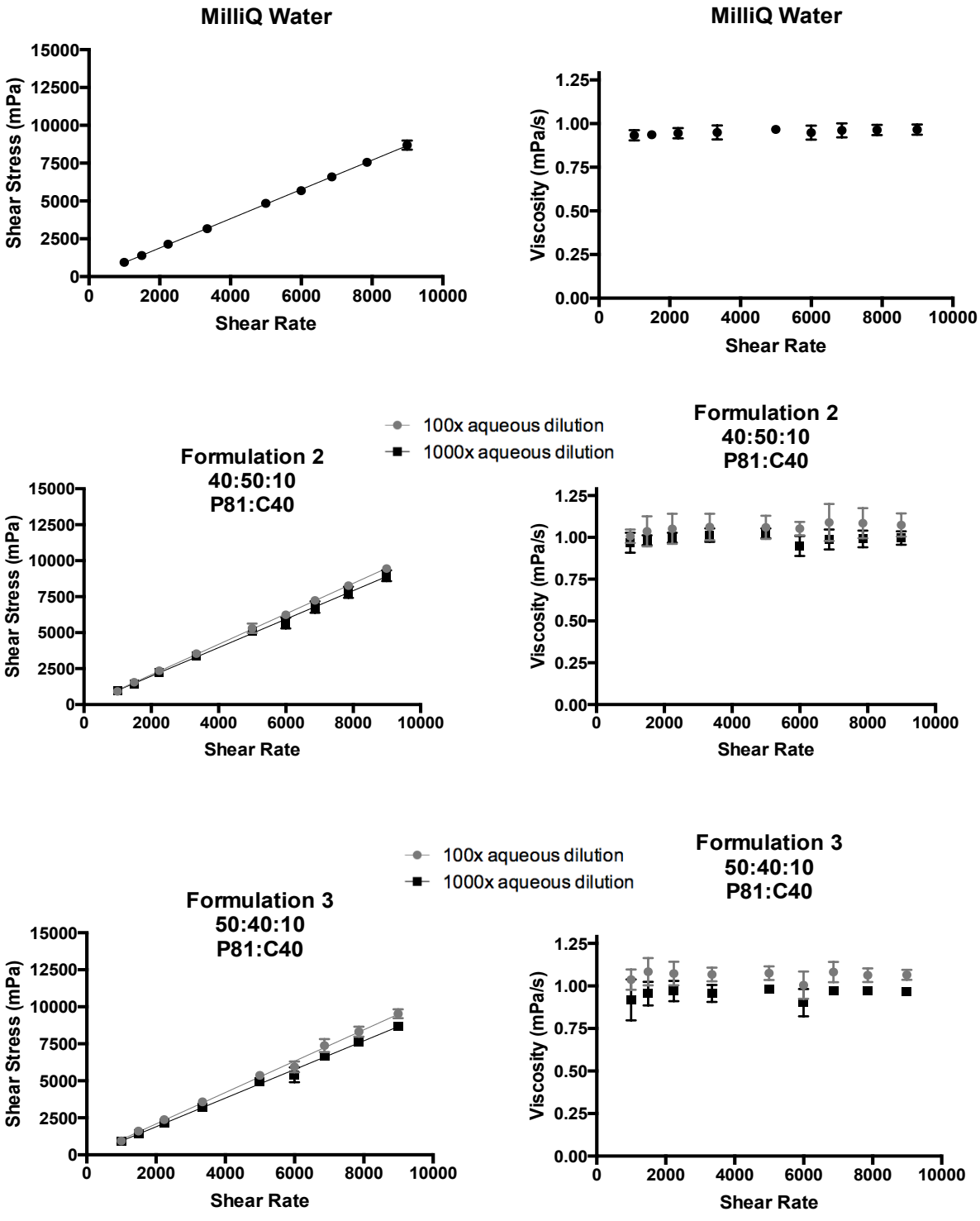

Figure D-15: Rheology measurements of F2 and F3 after 100 and 1000x aqueous dilution. R^2 values (F2: 0.999 at 100x and 0.998 at 1000x || F3: 0.997 at 100x and 0.998 at 1000x) Viscosity in mPa/s (F2: 1.06 ± 0.03 at 100x and 0.999 ± 0.02 at 1000x || F3: 1.06 ± 0.03 at 100x and 0.955 ± 0.03 at 1000x)

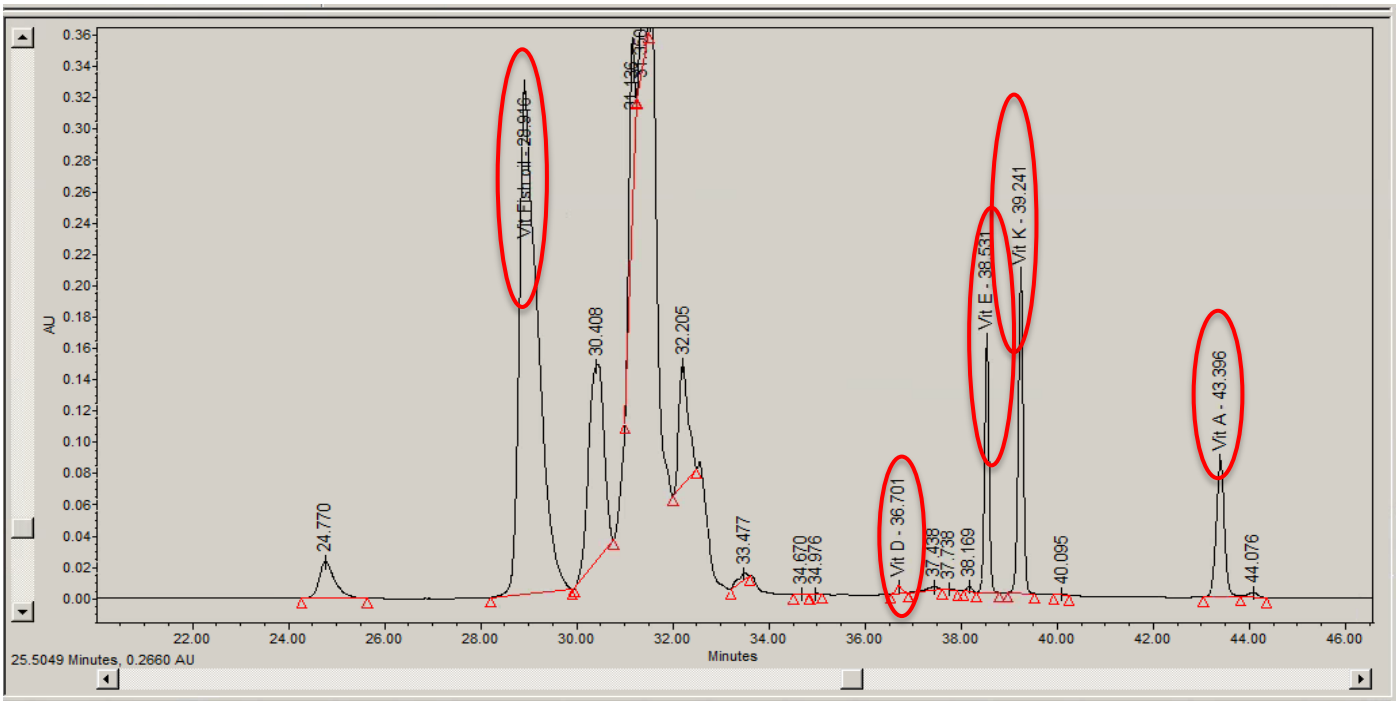

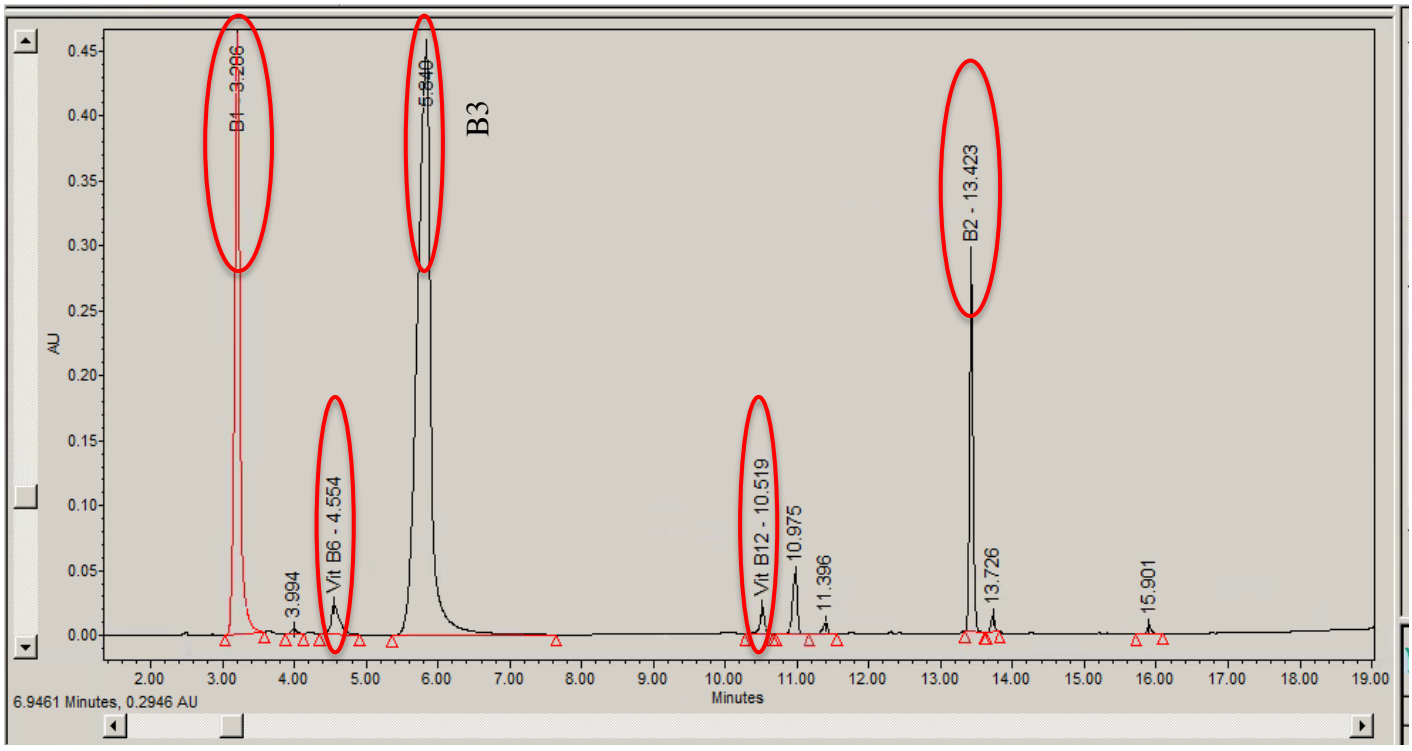

Figure D-16: HPLC Chromatogram of extracted fat soluble vitamins (top) and water-soluble vitamins (bottom) from microemulsion formulation 1. Both chromatograms were obtained with a C18 250 mm x 4.6 mm, 5 uM column. Acceptability linearity of each fat-soluble vitamin using concentrations of 50, 70, 100, 130 and 150% was also obtained (not shown)

Freeze-thaw Cycle

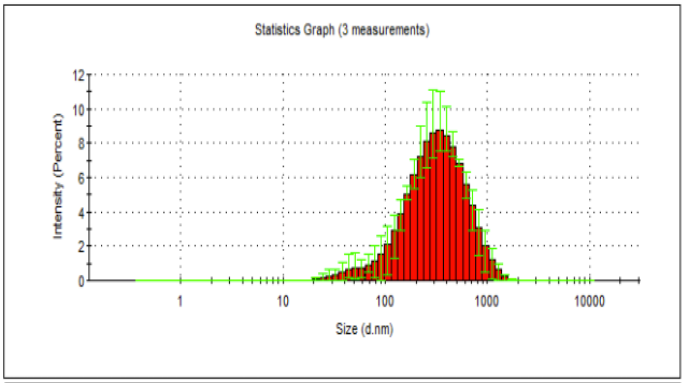

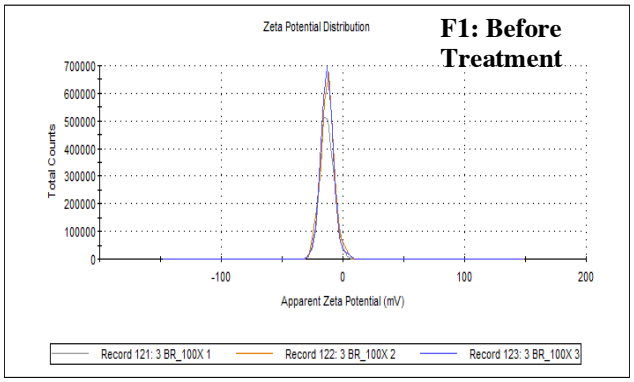

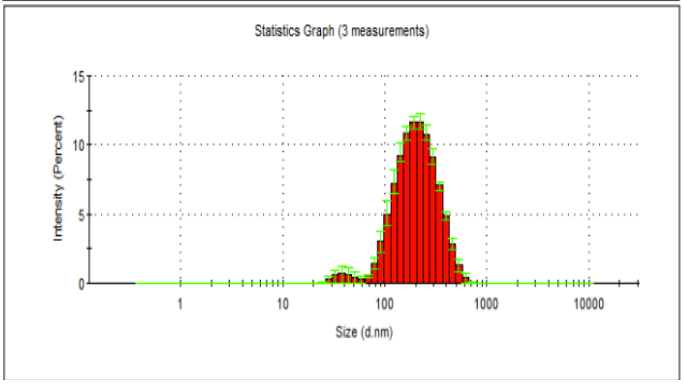

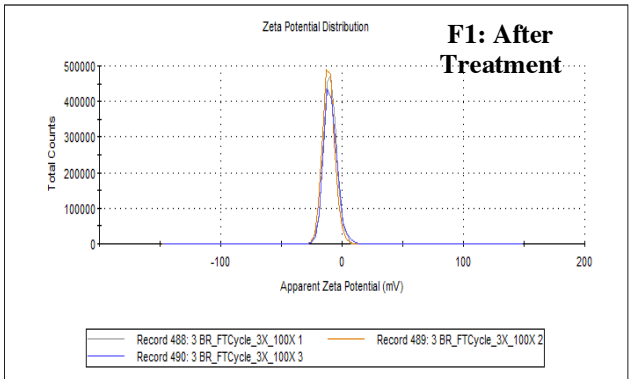

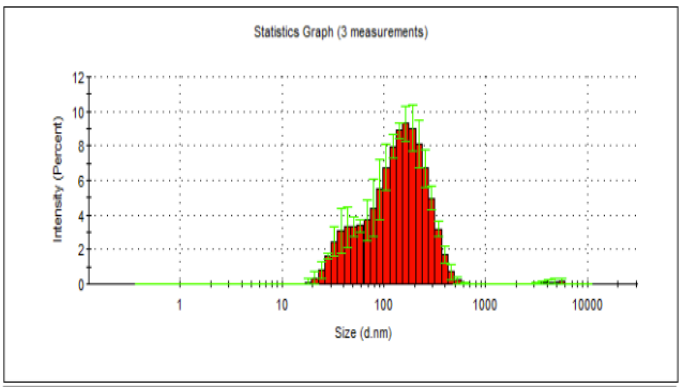

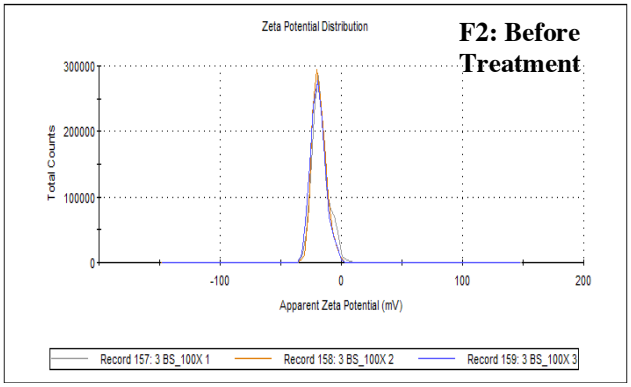

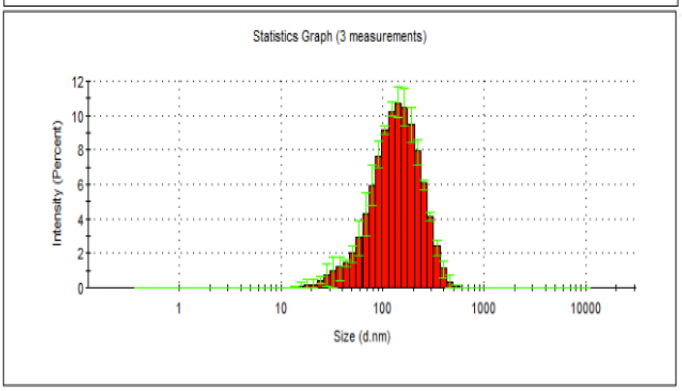

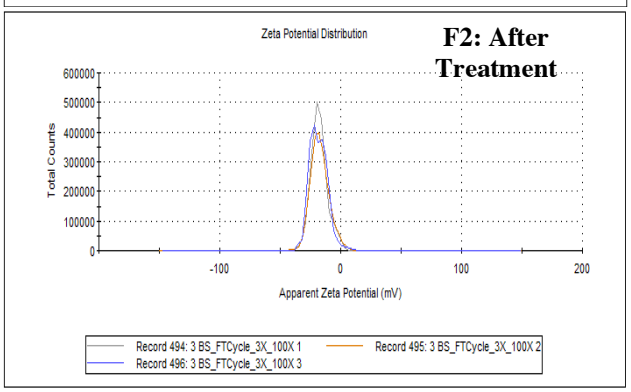

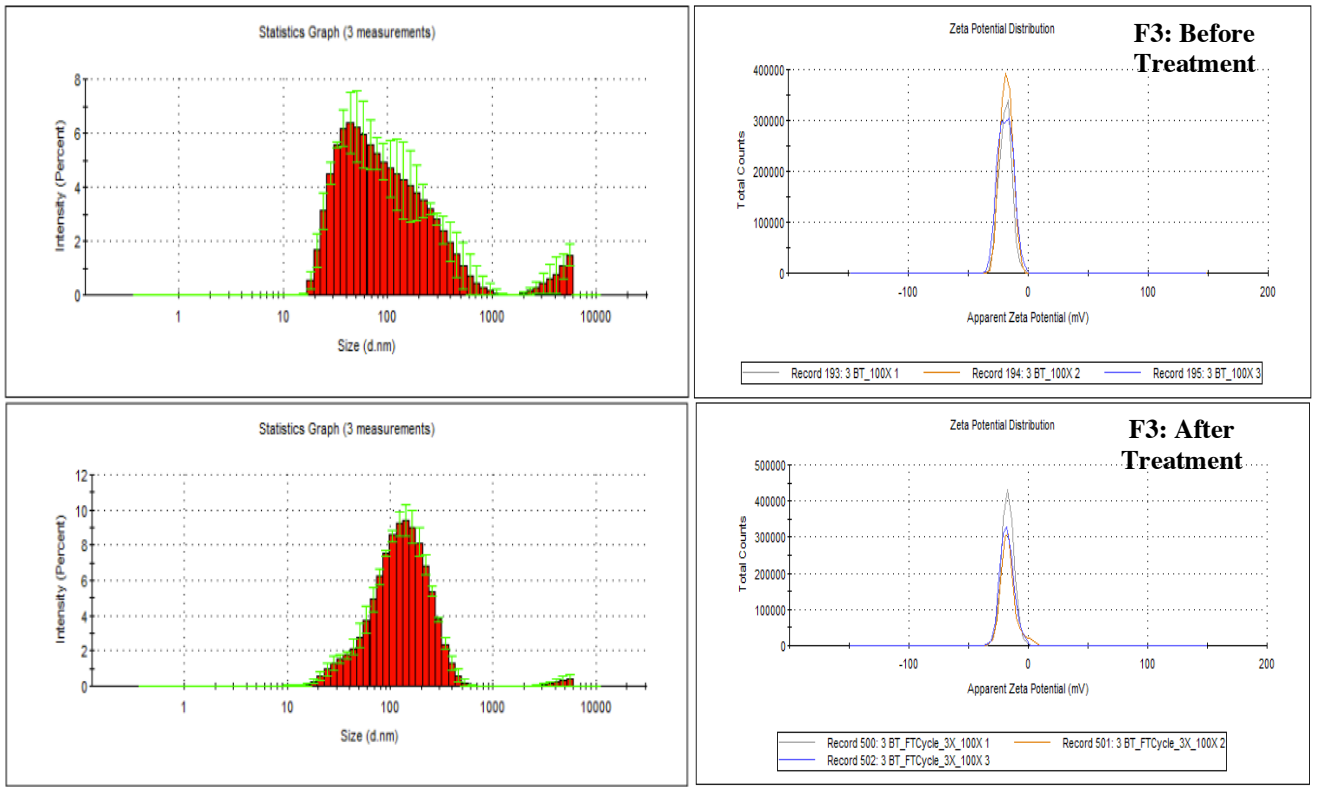

Figure D-17: Size and zeta potential values of F1, F2 and F3 before and after subjection to three freeze-thaw cycles

Heat Cycle

F1

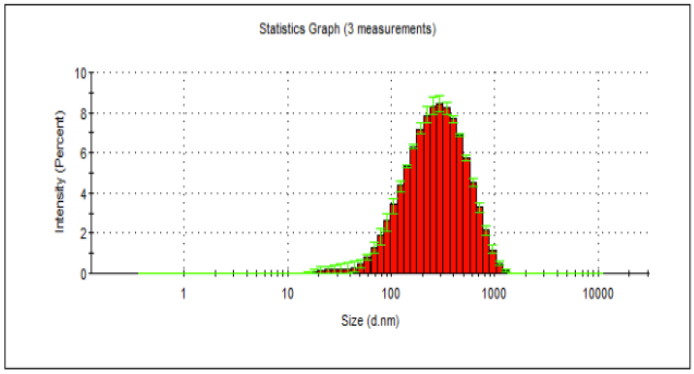

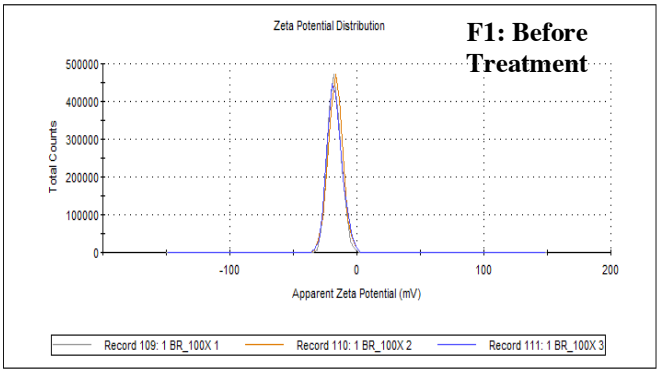

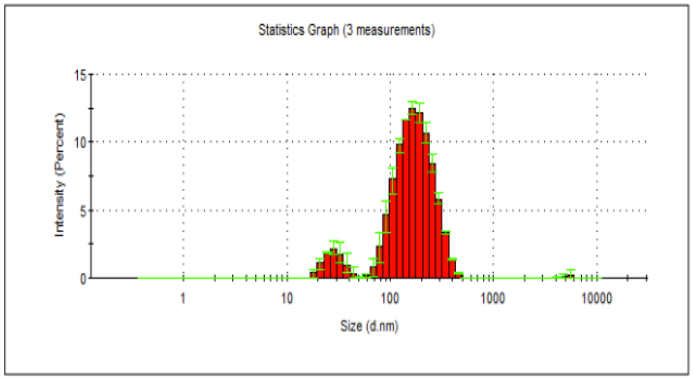

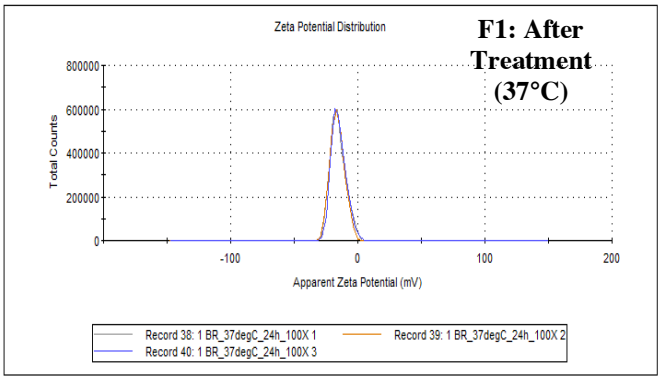

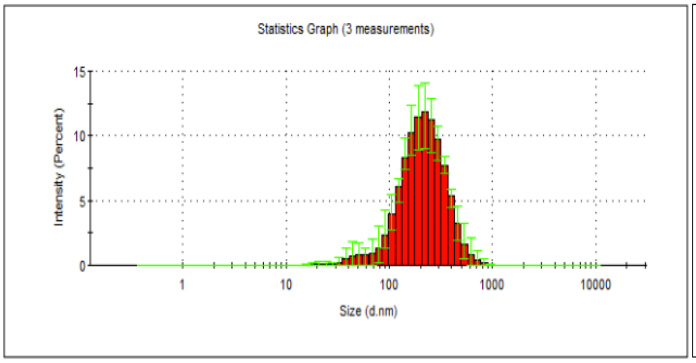

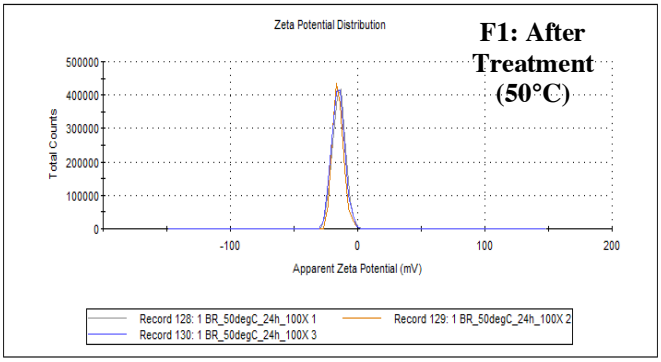

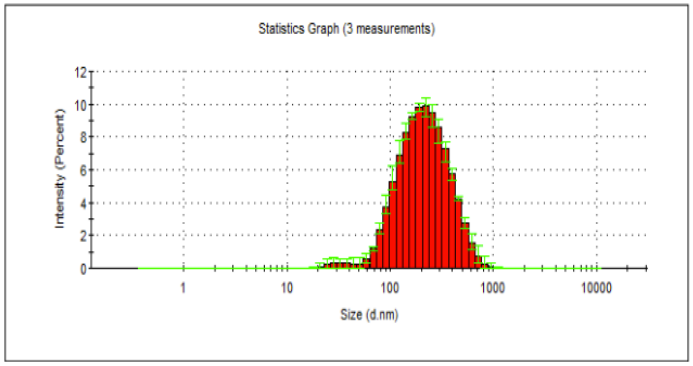

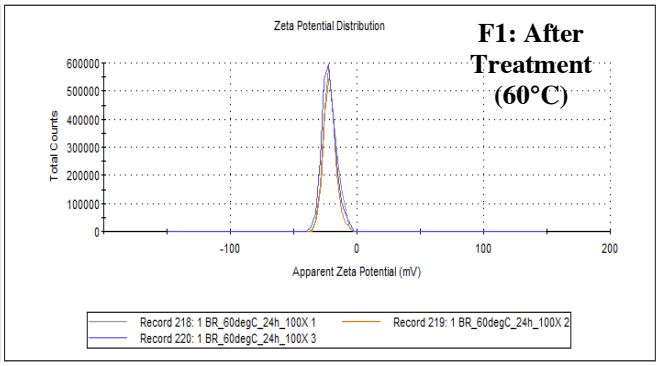

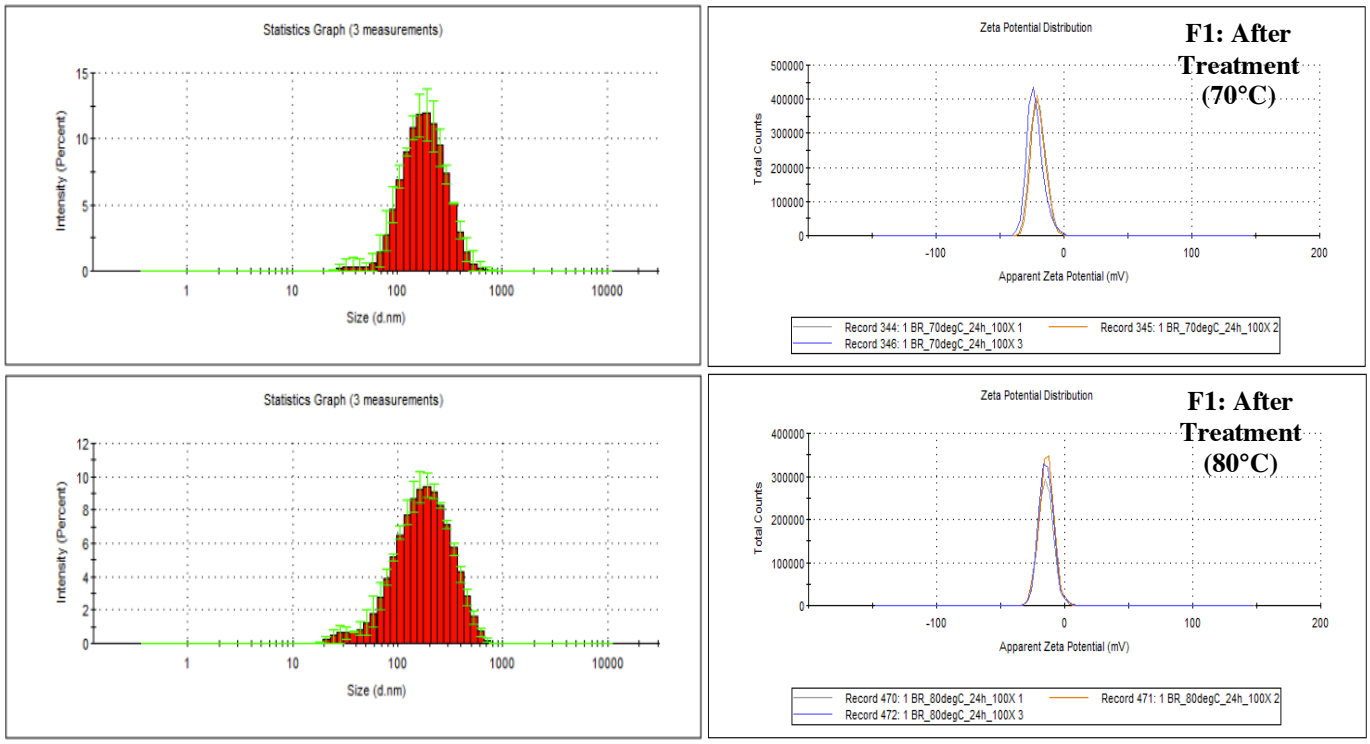

Figure D-18: Size and zeta potential values of F1 before and after subjection to heating cycles

F2

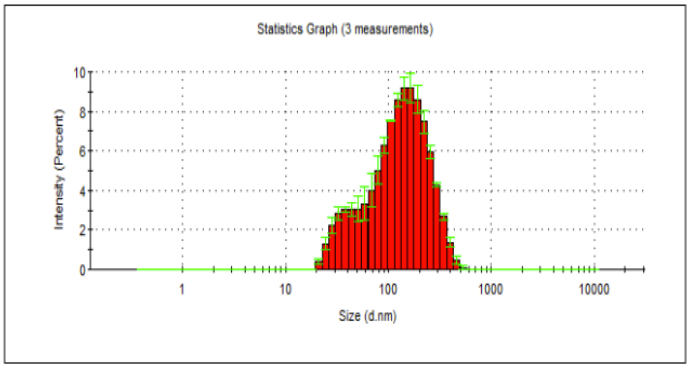
Statistics Graph (3 measurements)
Intensity (Percent)
Size (d.nm)

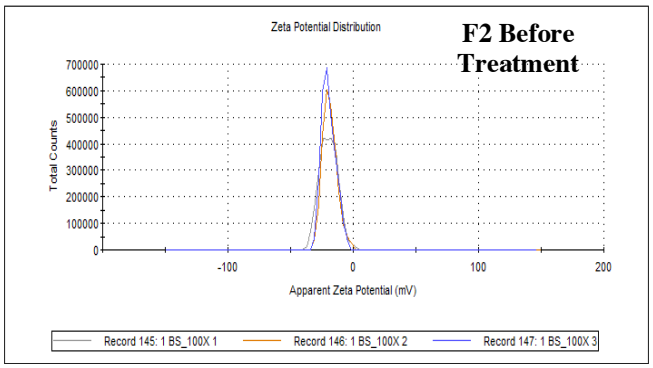
Zeta Potential Distribution
F2 Before Treatment
Total Counts
Apparent Zeta Potential (mV)
Record 145: 1 BS_100X 1
Record 146: 1 BS_100X 2
Record 147: 1 BS_100X 3

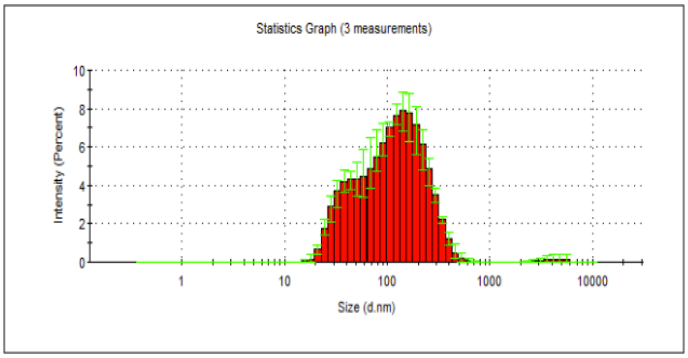
Statistics Graph (3 measurements)
Intensity (Percent)
Size (d.nm)

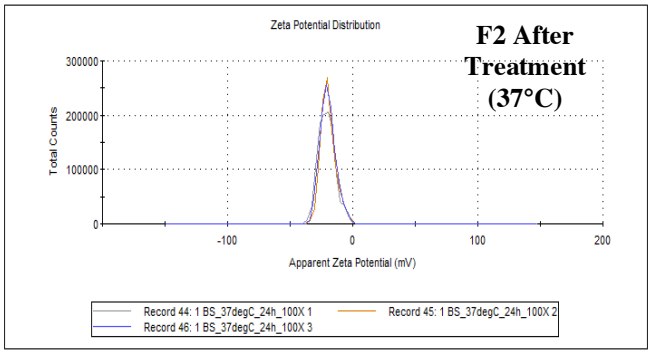
Zeta Potential Distribution
F2 After Treatment (37°C)
Total Counts
Apparent Zeta Potential (mV)
Record 44: 1 BS_37degC_24h_100X 1
Record 45: 1 BS_37degC_24h_100X 2
Record 46: 1 BS_37degC_24h_100X 3

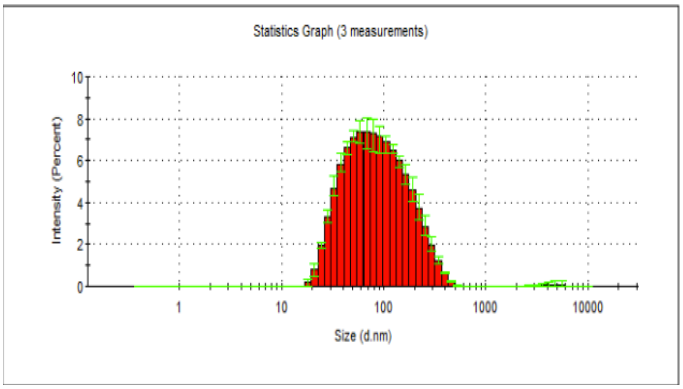
Statistics Graph (3 measurements)
Intensity (Percent)
Size (d.nm)

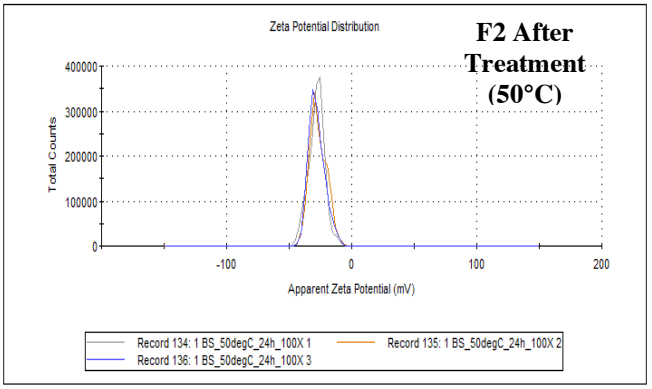
Zeta Potential Distribution
F2 After Treatment (50°C)
Total Counts
Apparent Zeta Potential (mV)
Record 134: 1 BS_50degC_24h_100X 1
Record 135: 1 BS_50degC_24h_100X 2
Record 136: 1 BS_50degC_24h_100X 3

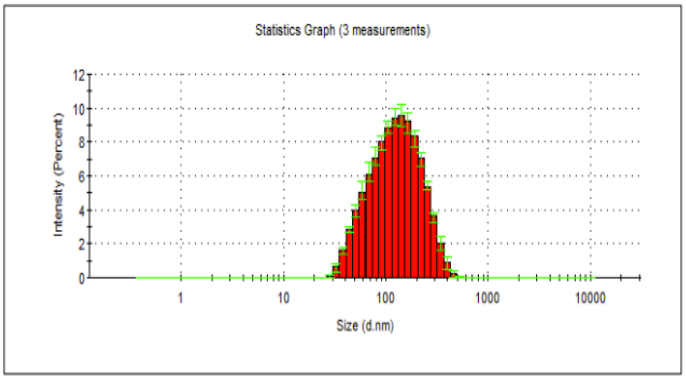
Statistics Graph (3 measurements)
Intensity (Percent)
Size (d.nm)

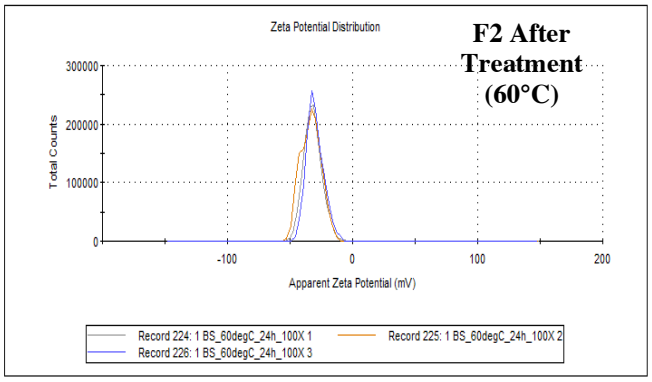
Zeta Potential Distribution
F2 After Treatment (60°C)
Total Counts
Apparent Zeta Potential (mV)
Record 224: 1 BS_60degC_24h_100X 1
Record 225: 1 BS_60degC_24h_100X 2
Record 226: 1 BS_60degC_24h_100X 3

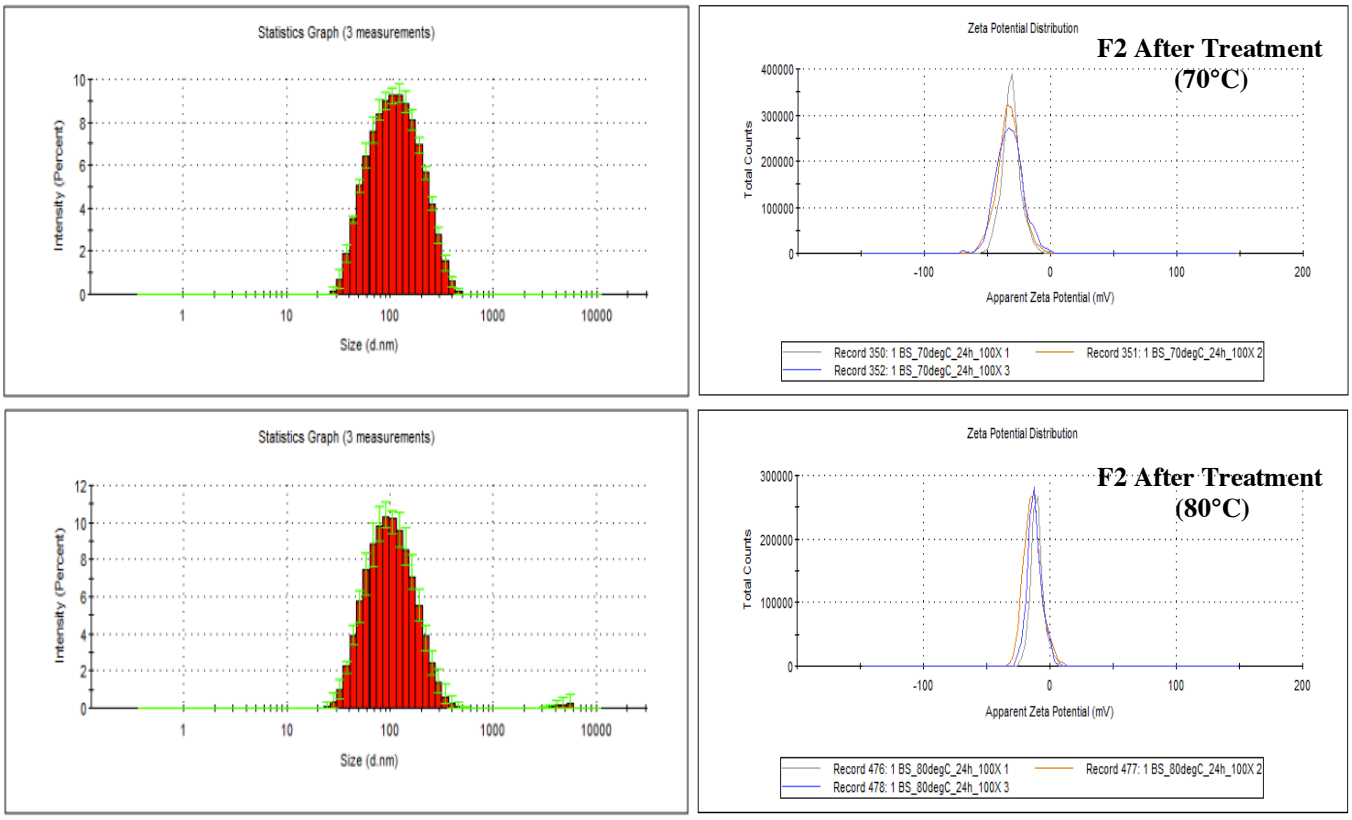

Figure D-19: Size and zeta potential values of F2 before and after subject to heating cycles

F3

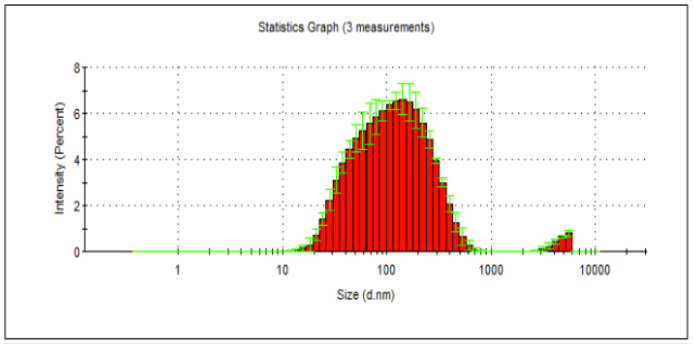
Statistics Graph (3 measurements)
Intensity (Percent)
Size (d.nm)

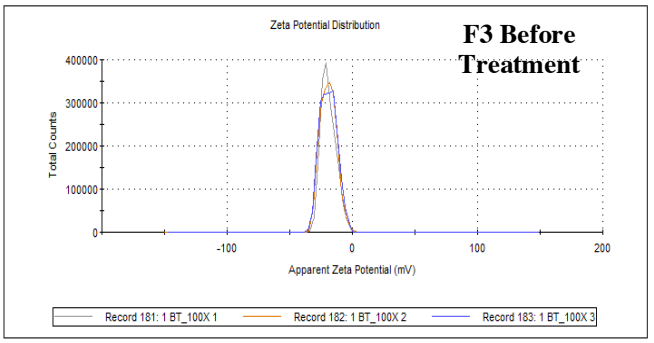
Zeta Potential Distribution
F3 Before Treatment
Total Counts
Apparent Zeta Potential (mV)
Record 181: 1 BT_100X 1
Record 182: 1 BT_100X 2
Record 183: 1 BT_100X 3

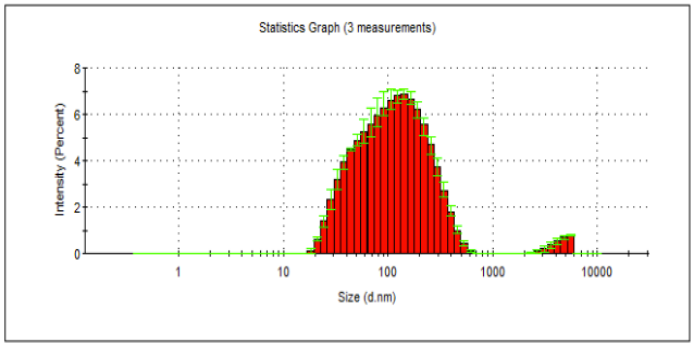
Statistics Graph (3 measurements)
Intensity (Percent)
Size (d.nm)

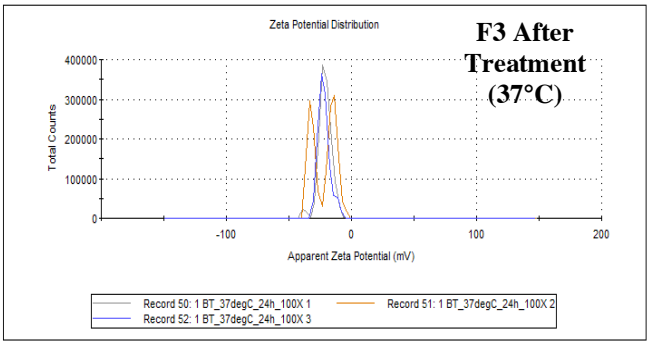
Zeta Potential Distribution
F3 After Treatment (37°C)
Total Counts
Apparent Zeta Potential (mV)
Record 50: 1 BT_37degC_24h_100X 1
Record 51: 1 BT_37degC_24h_100X 2
Record 52: 1 BT_37degC_24h_100X 3

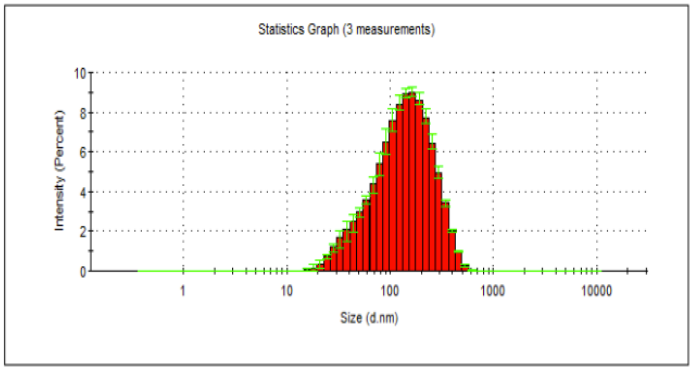
Statistics Graph (3 measurements)
Intensity (Percent)
Size (d.nm)

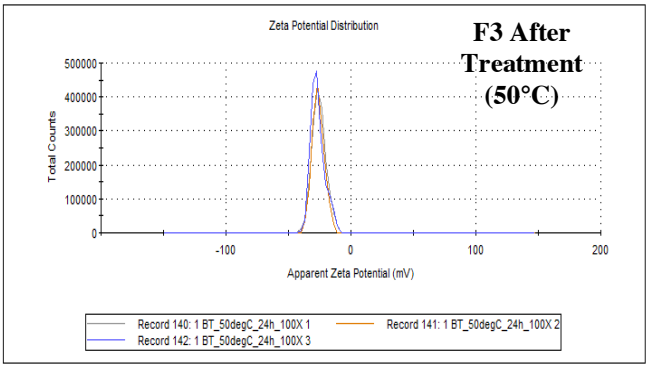
Zeta Potential Distribution
F3 After Treatment (50°C)
Total Counts
Apparent Zeta Potential (mV)
Record 140: 1 BT_50degC_24h_100X 1
Record 141: 1 BT_50degC_24h_100X 2
Record 142: 1 BT_50degC_24h_100X 3

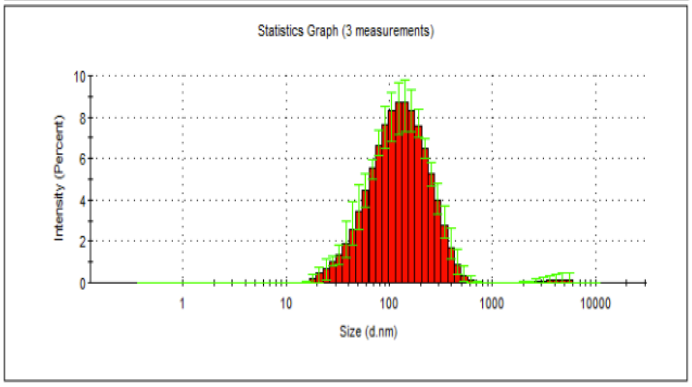
Statistics Graph (3 measurements)
Intensity (Percent)
Size (d.nm)

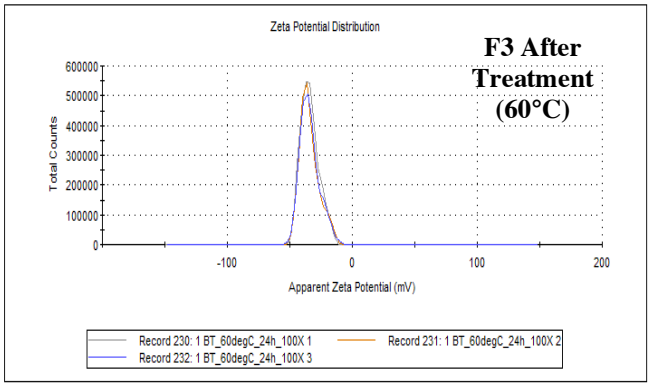
Zeta Potential Distribution
F3 After Treatment (60°C)
Total Counts
Apparent Zeta Potential (mV)
Record 230: 1 BT_60degC_24h_100X 1
Record 231: 1 BT_60degC_24h_100X 2
Record 232: 1 BT_60degC_24h_100X 3

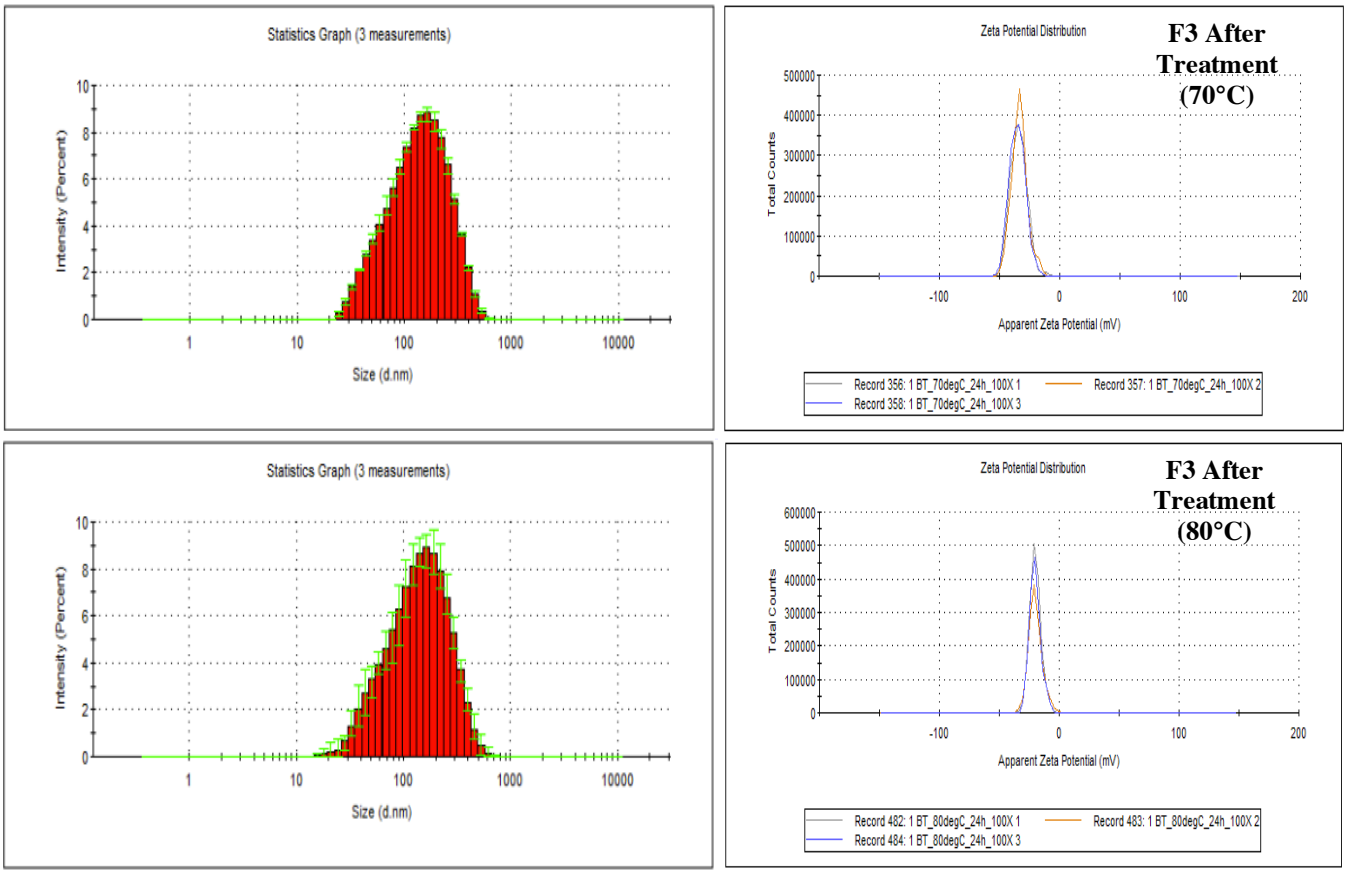

Figure D-20: Size and zeta potential values of F3 before and after subjection to heating cycles

Light Exposure

F1

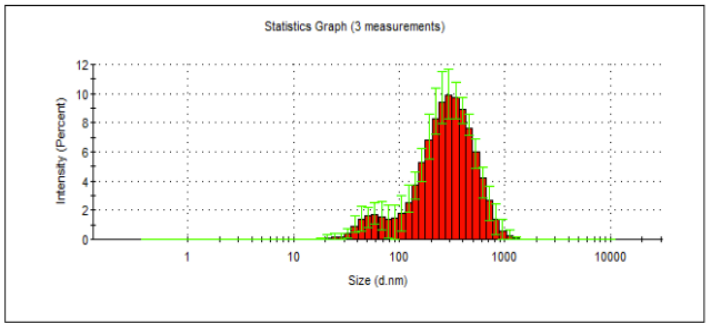

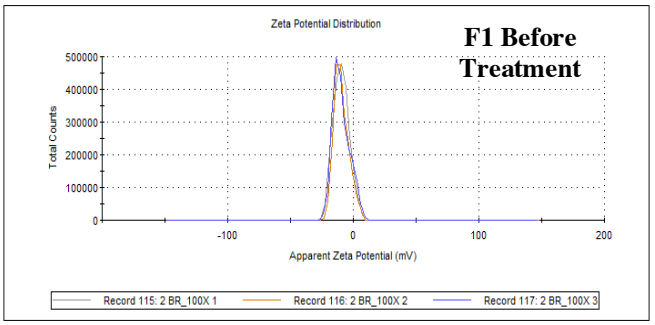

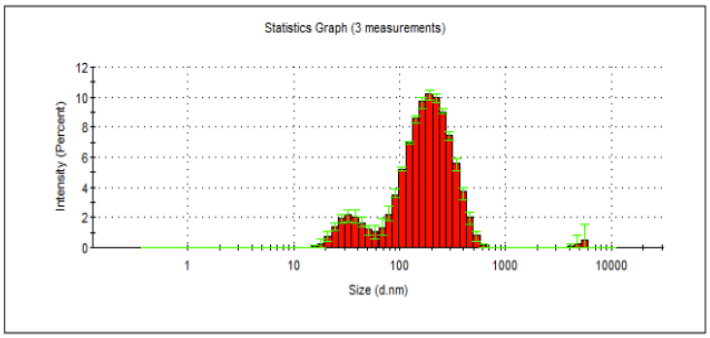

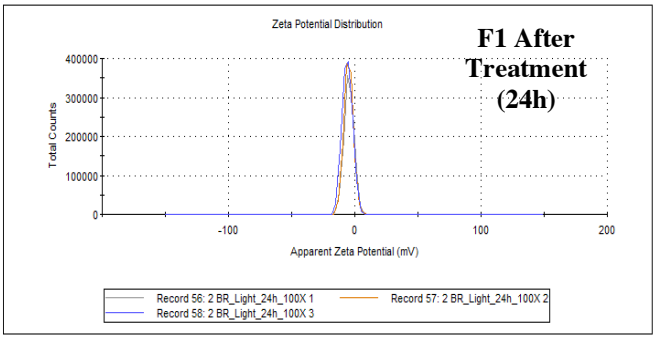

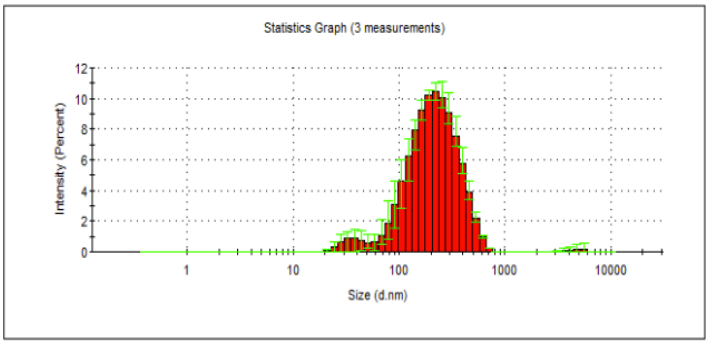

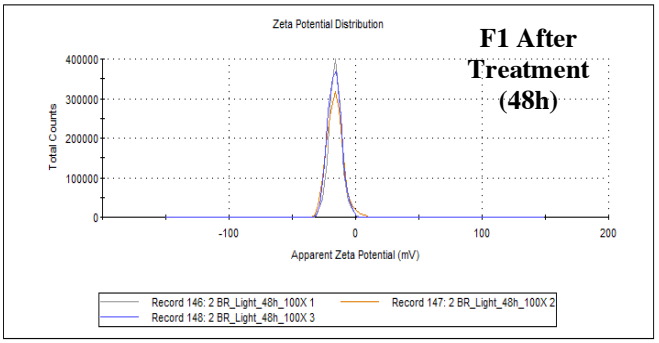

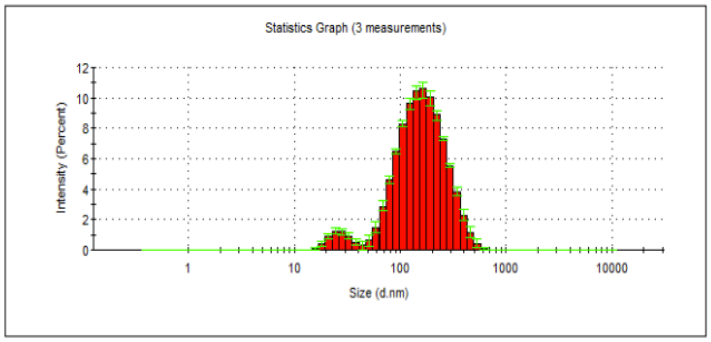

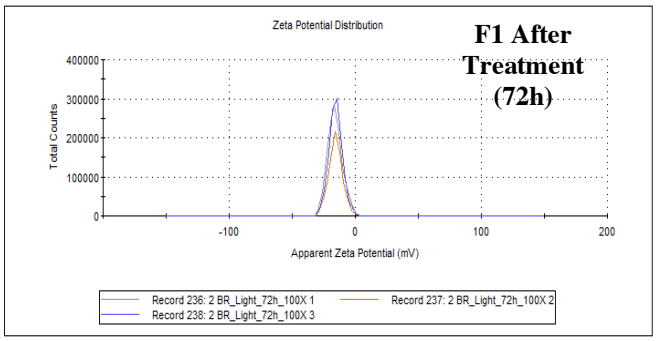

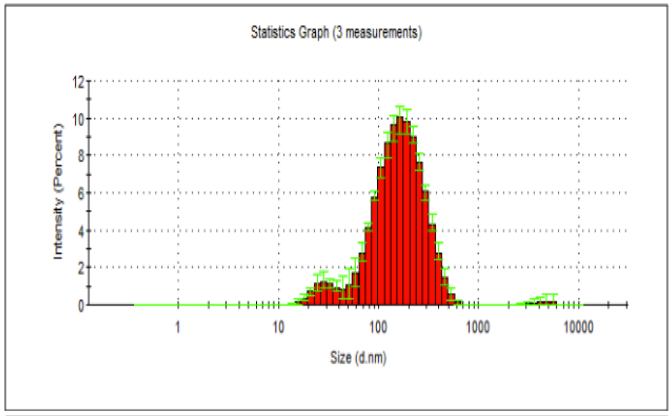
Statistics Graph (3 measurements)
Intensity (Percent)
Size (d.nm)

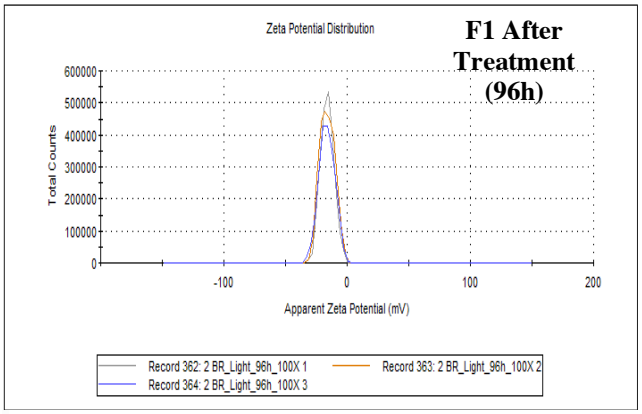
Zeta Potential Distribution
F1 After Treatment (96h)
Total Counts
Apparent Zeta Potential (mV)
Record 362: 2 BR_Light_96h_100X 1
Record 363: 2 BR_Light_96h_100X 2
Record 364: 2 BR_Light_96h_100X 3

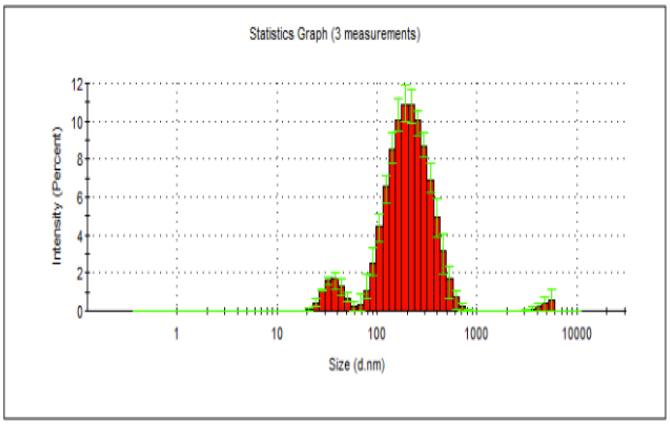
Statistics Graph (3 measurements)
Intensity (Percent)
Size (d.nm)

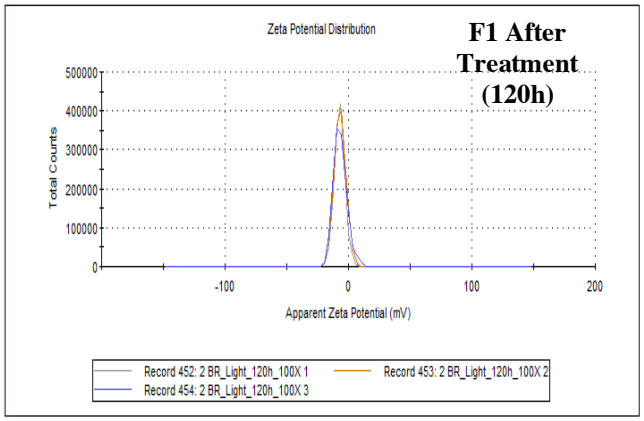
Zeta Potential Distribution
F1 After Treatment (120h)
Total Counts
Apparent Zeta Potential (mV)
Record 452: 2 BR_Light_120h_100X 1
Record 453: 2 BR_Light_120h_100X 2
Record 454: 2 BR_Light_120h_100X 3

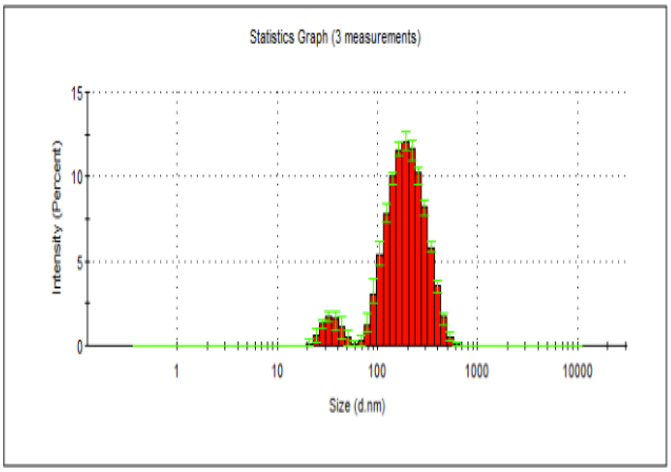
Statistics Graph (3 measurements)
Intensity (Percent)
Size (d.nm)

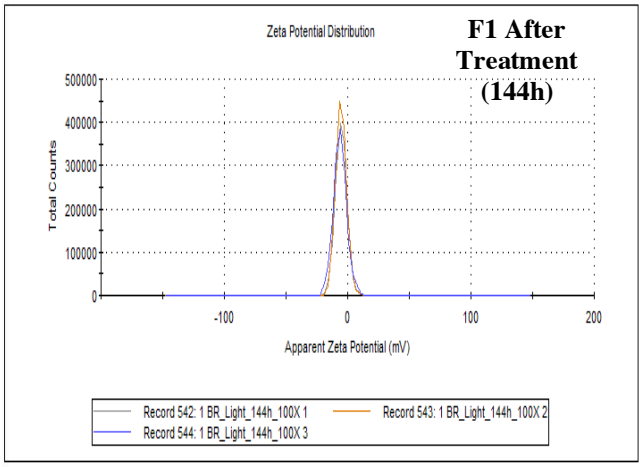
Zeta Potential Distribution
F1 After Treatment (144h)
Total Counts
Apparent Zeta Potential (mV)
Record 542: 1 BR_Light_144h_100X 1
Record 543: 1 BR_Light_144h_100X 2
Record 544: 1 BR_Light_144h_100X 3

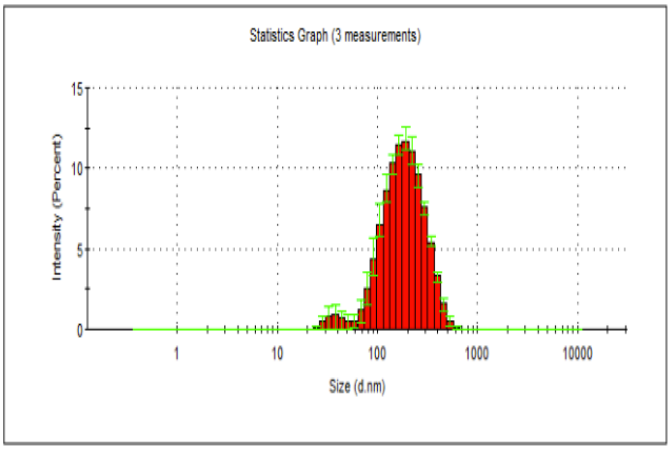
Statistics Graph (3 measurements)
Intensity (Percent)
Size (d.nm)

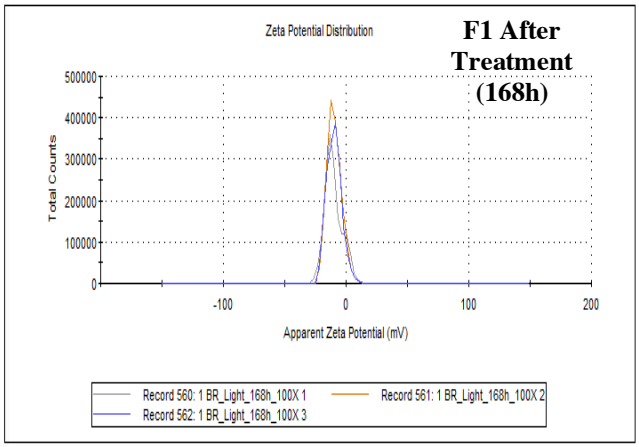
Zeta Potential Distribution
F1 After Treatment (168h)
Total Counts
Apparent Zeta Potential (mV)
Record 560: 1 BR_Light_168h_100X 1
Record 561: 1 BR_Light_168h_100X 2
Record 562: 1 BR_Light_168h_100X 3

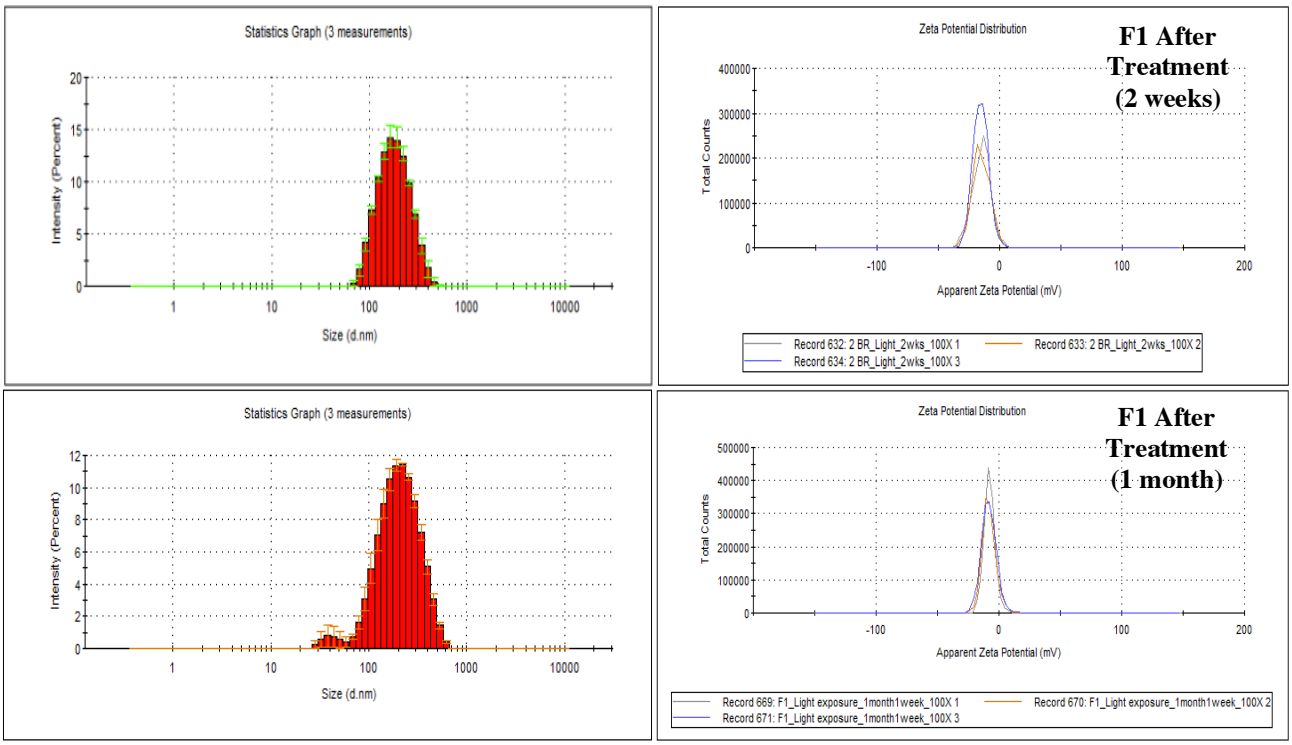

Figure D-21: Size and zeta potential values of F1 before and after exposure to light

F2

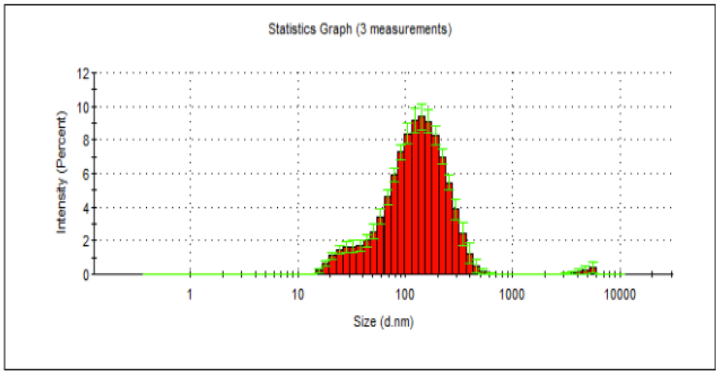
Statistics Graph (3 measurements)
Intensity (Percent)
Size (d.nm)

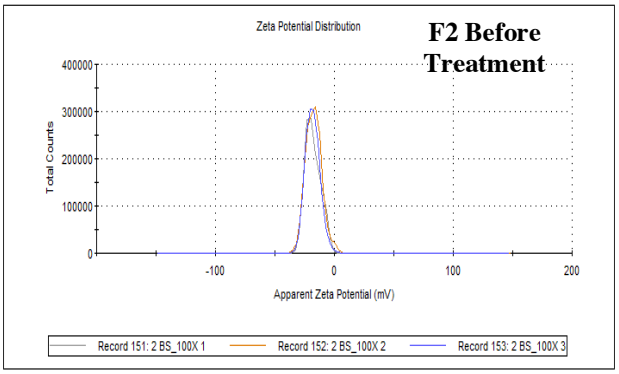
Zeta Potential Distribution
F2 Before Treatment
Total Counts
Apparent Zeta Potential (mV)
Record 151: 2 BS_100X 1
Record 152: 2 BS_100X 2
Record 153: 2 BS_100X 3

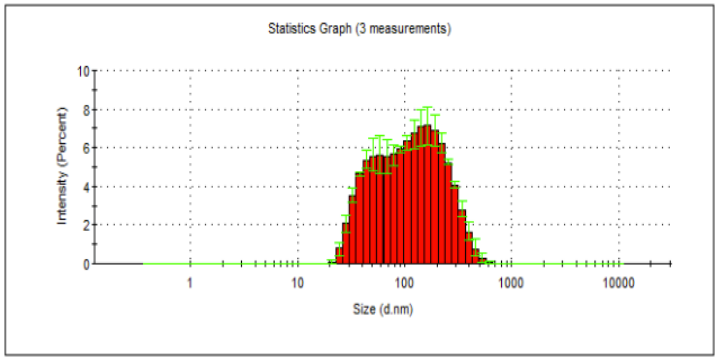
Statistics Graph (3 measurements)
Intensity (Percent)
Size (d.nm)

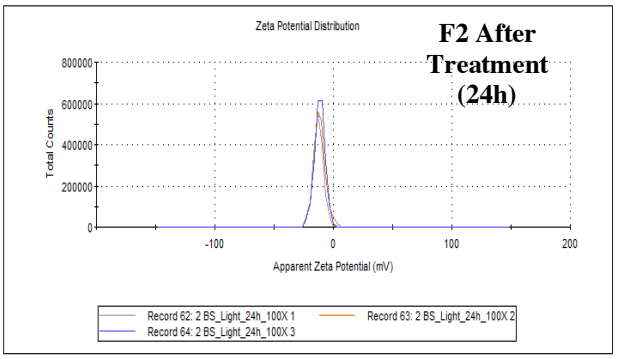
Zeta Potential Distribution
F2 After Treatment (24h)
Total Counts
Apparent Zeta Potential (mV)
Record 62: 2 BS_Light_24h_100X 1
Record 63: 2 BS_Light_24h_100X 2
Record 64: 2 BS_Light_24h_100X 3

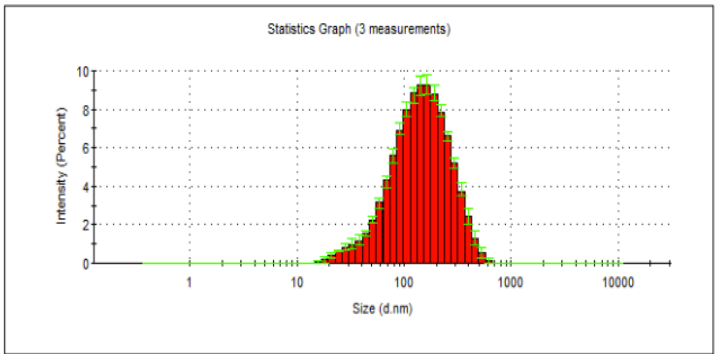
Statistics Graph (3 measurements)
Intensity (Percent)
Size (d.nm)

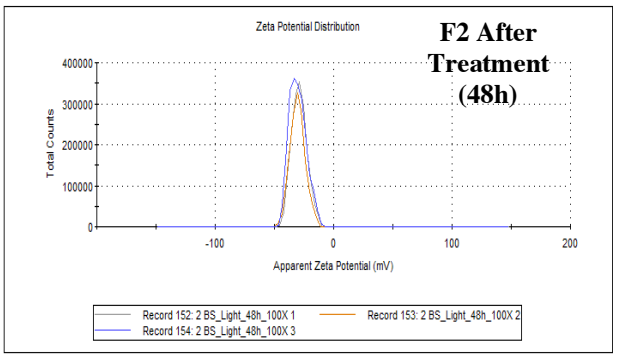
Zeta Potential Distribution
F2 After Treatment (48h)
Total Counts
Apparent Zeta Potential (mV)
Record 152: 2 BS_Light_48h_100X 1
Record 153: 2 BS_Light_48h_100X 2
Record 154: 2 BS_Light_48h_100X 3

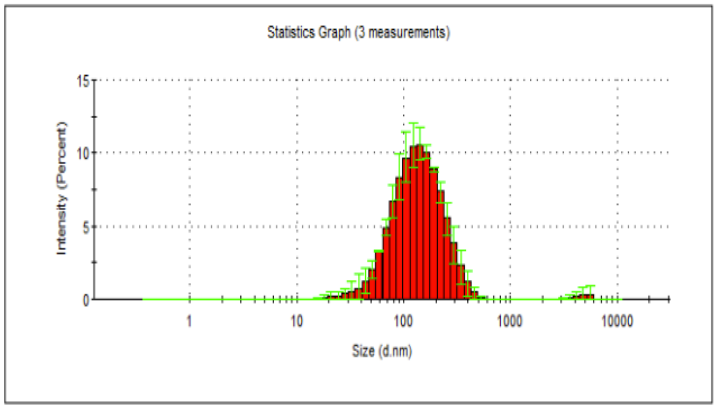
Statistics Graph (3 measurements)
Intensity (Percent)
Size (d.nm)

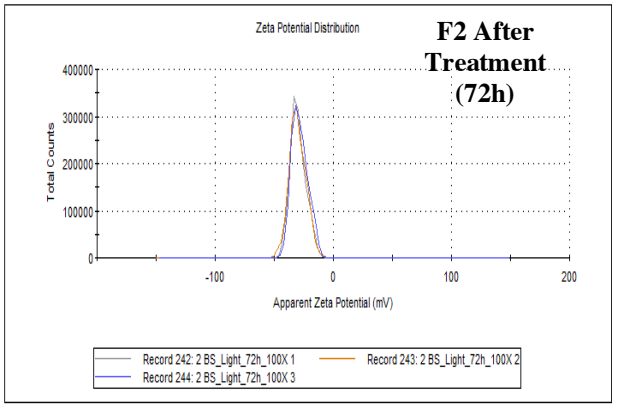
Zeta Potential Distribution
F2 After Treatment (72h)
Total Counts
Apparent Zeta Potential (mV)
Record 242: 2 BS_Light_72h_100X 1
Record 243: 2 BS_Light_72h_100X 2
Record 244: 2 BS_Light_72h_100X 3

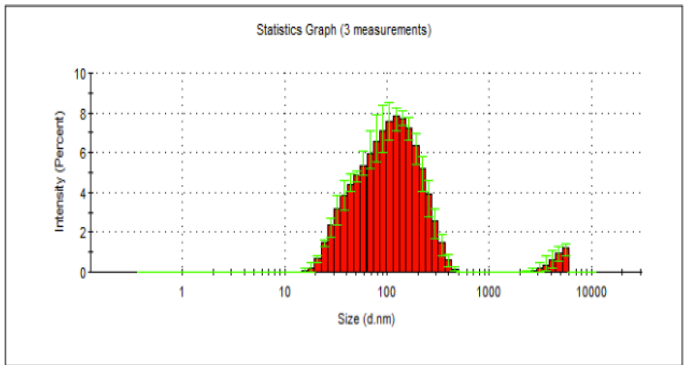
Statistics Graph (3 measurements)
Intensity (Percent)
Size (d.nm)

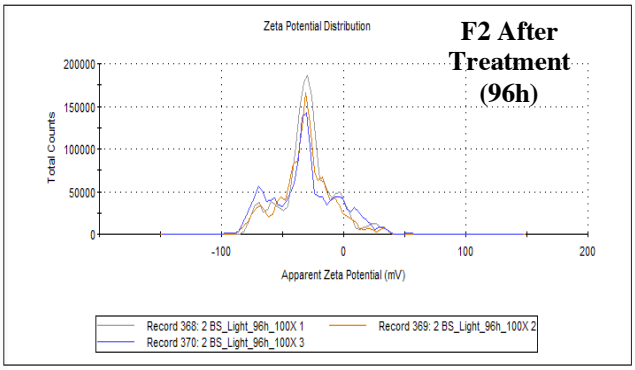
Zeta Potential Distribution
F2 After Treatment (96h)
Total Counts
Apparent Zeta Potential (mV)
Record 368: 2 BS_Light_96h_100X 1
Record 369: 2 BS_Light_96h_100X 2
Record 370: 2 BS_Light_96h_100X 3

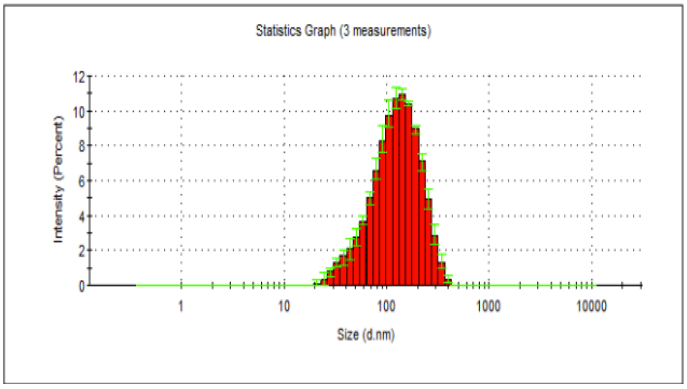
Statistics Graph (3 measurements)
Intensity (Percent)
Size (d.nm)

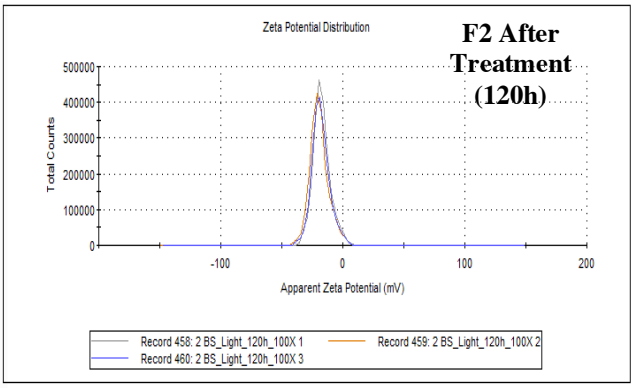
Zeta Potential Distribution
F2 After Treatment (120h)
Total Counts
Apparent Zeta Potential (mV)
Record 458: 2 BS_Light_120h_100X 1
Record 459: 2 BS_Light_120h_100X 2
Record 460: 2 BS_Light_120h_100X 3

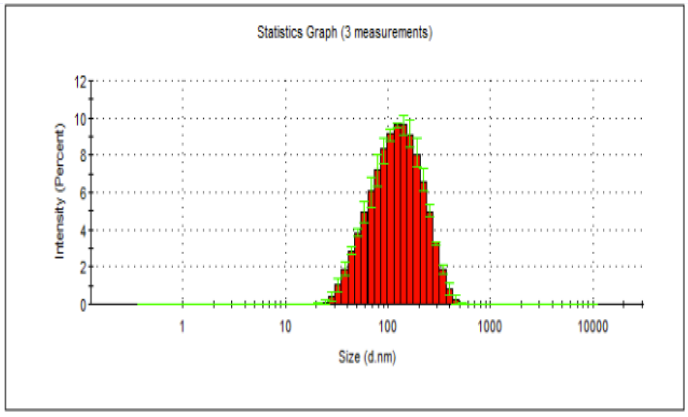
Statistics Graph (3 measurements)
Intensity (Percent)
Size (d.nm)

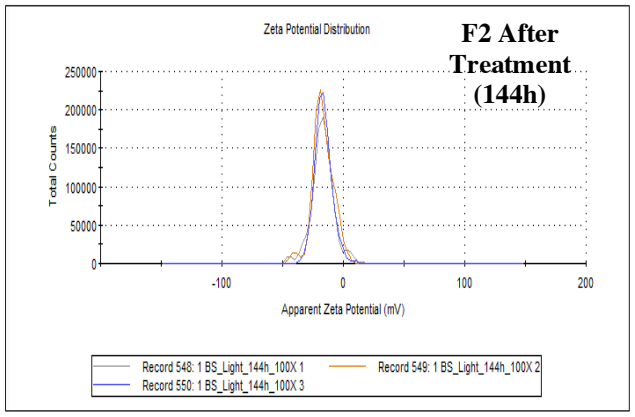
Zeta Potential Distribution
F2 After Treatment (144h)
Total Counts
Apparent Zeta Potential (mV)
Record 548: 1 BS_Light_144h_100X 1
Record 549: 1 BS_Light_144h_100X 2
Record 550: 1 BS_Light_144h_100X 3

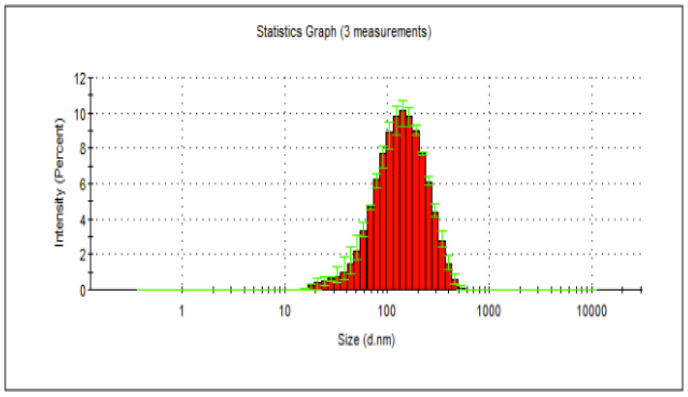
Statistics Graph (3 measurements)
Intensity (Percent)
Size (d.nm)

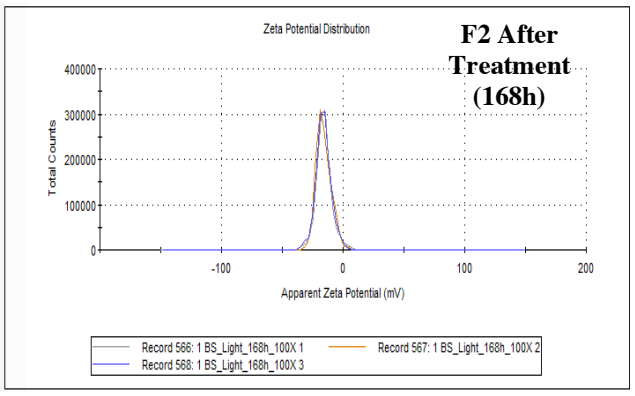
Zeta Potential Distribution
F2 After Treatment (168h)
Total Counts
Apparent Zeta Potential (mV)
Record 566: 1 BS_Light_168h_100X 1
Record 567: 1 BS_Light_168h_100X 2
Record 568: 1 BS_Light_168h_100X 3

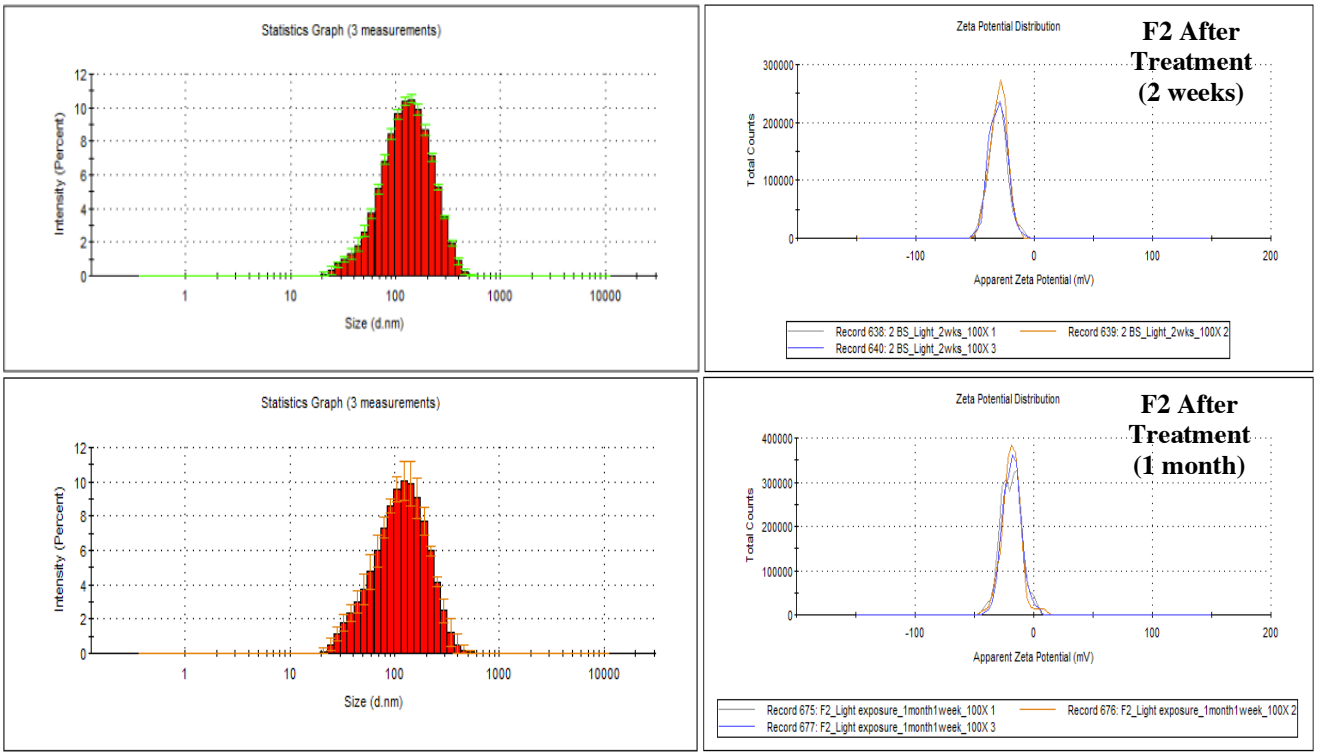

Figure D-22: Size and zeta potential values of F2 before and after exposure to light

F3

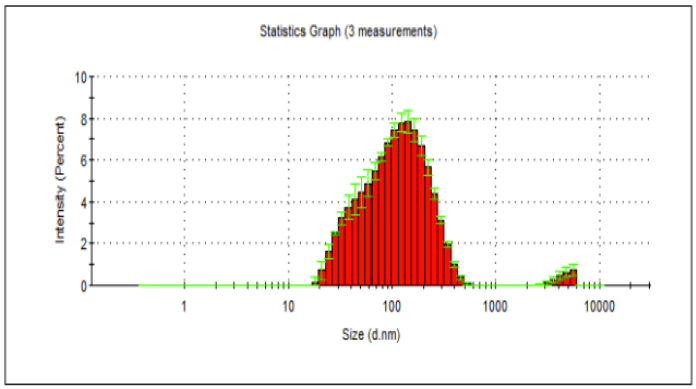
Statistics Graph (3 measurements)
Intensity (Percent)
Size (d.nm)

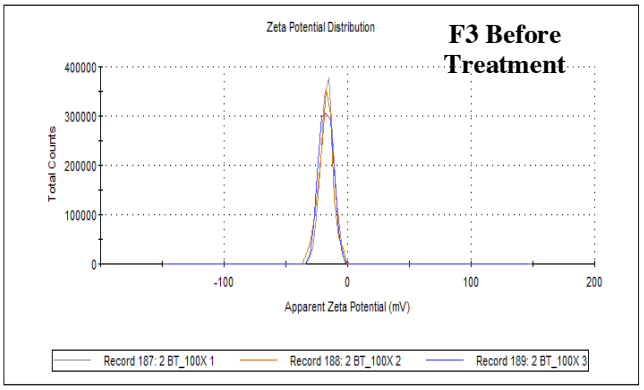
Zeta Potential Distribution
F3 Before Treatment
Total Counts
Apparent Zeta Potential (mV)
Record 187: 2 BT_100X 1
Record 188: 2 BT_100X 2
Record 189: 2 BT_100X 3

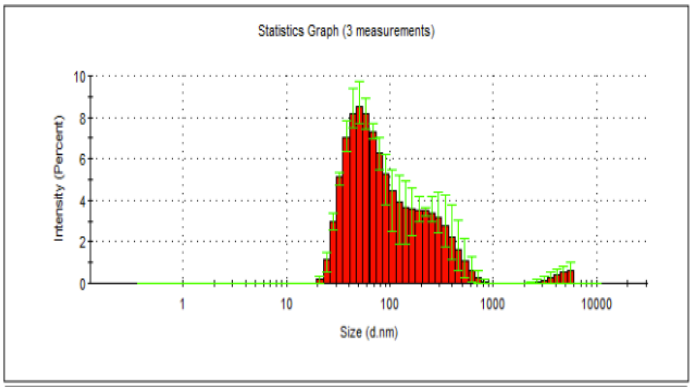
Statistics Graph (3 measurements)
Intensity (Percent)
Size (d.nm)

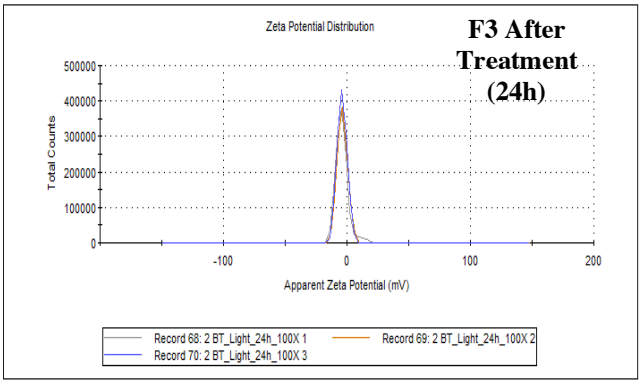
Zeta Potential Distribution
F3 After Treatment (24h)
Total Counts
Apparent Zeta Potential (mV)
Record 68: 2 BT_Light_24h_100X 1
Record 69: 2 BT_Light_24h_100X 2
Record 70: 2 BT_Light_24h_100X 3

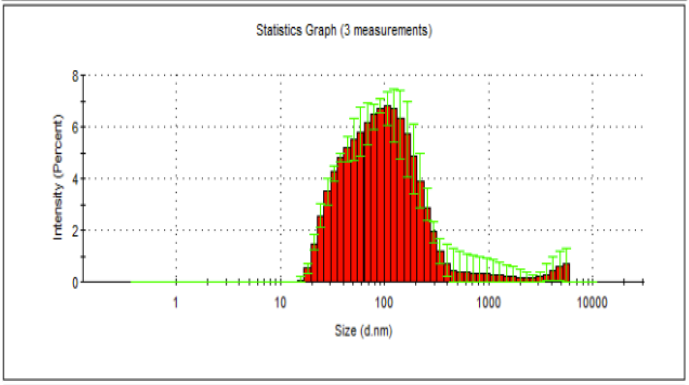
Statistics Graph (3 measurements)
Intensity (Percent)
Size (d.nm)

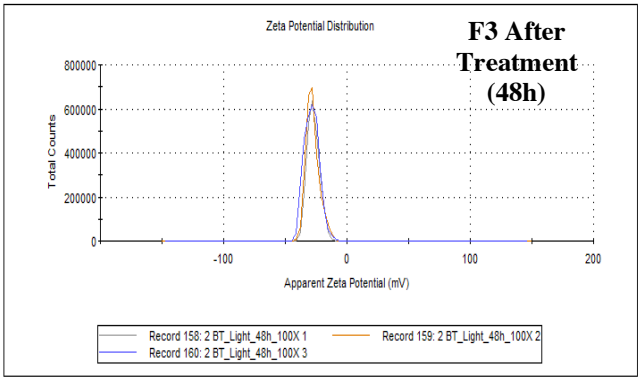
Zeta Potential Distribution
F3 After Treatment (48h)
Total Counts
Apparent Zeta Potential (mV)
Record 158: 2 BT_Light_48h_100X 1
Record 159: 2 BT_Light_48h_100X 2
Record 160: 2 BT_Light_48h_100X 3

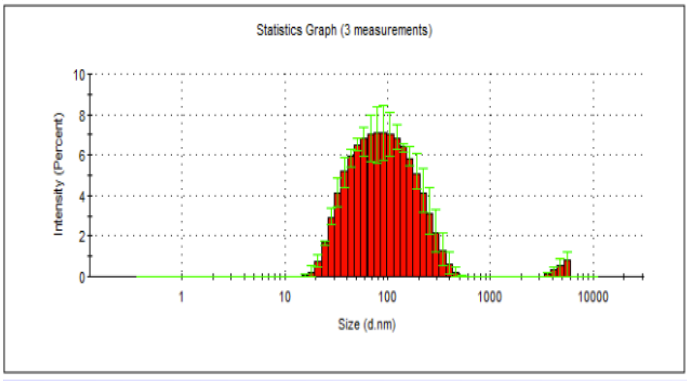
Statistics Graph (3 measurements)
Intensity (Percent)
Size (d.nm)

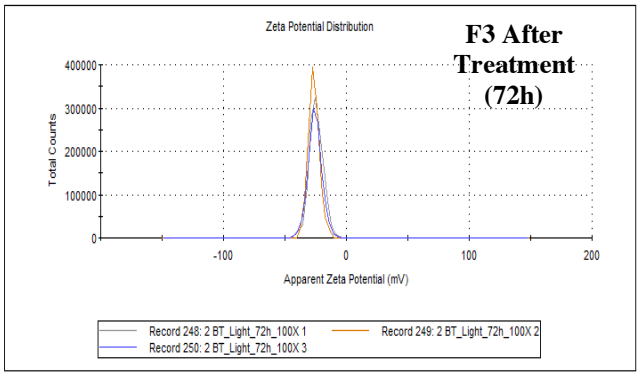
Zeta Potential Distribution
F3 After Treatment (72h)
Total Counts
Apparent Zeta Potential (mV)
Record 248: 2 BT_Light_72h_100X 1
Record 249: 2 BT_Light_72h_100X 2
Record 250: 2 BT_Light_72h_100X 3

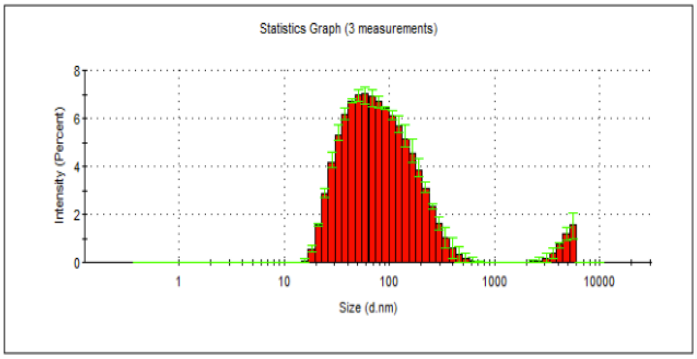
Statistics Graph (3 measurements)
Intensity (Percent)
Size (d.nm)

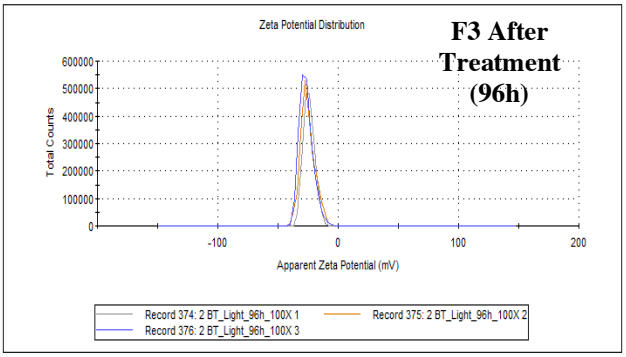
Zeta Potential Distribution
F3 After Treatment (96h)
Total Counts
Apparent Zeta Potential (mV)
Record 374: 2 BT_Light_96h_100X 1
Record 375: 2 BT_Light_96h_100X 2
Record 376: 2 BT_Light_96h_100X 3

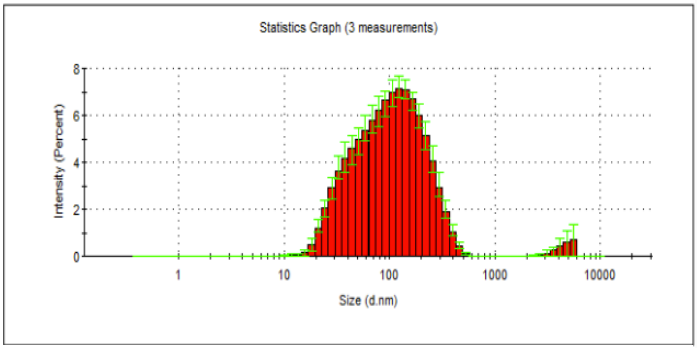
Statistics Graph (3 measurements)
Intensity (Percent)
Size (d.nm)

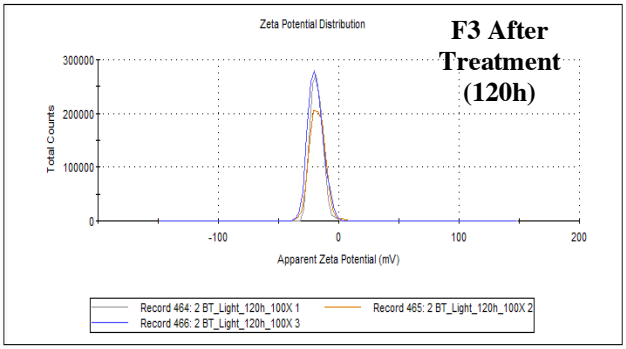
Zeta Potential Distribution
F3 After Treatment (120h)
Total Counts
Apparent Zeta Potential (mV)
Record 464: 2 BT_Light_120h_100X 1
Record 465: 2 BT_Light_120h_100X 2
Record 466: 2 BT_Light_120h_100X 3

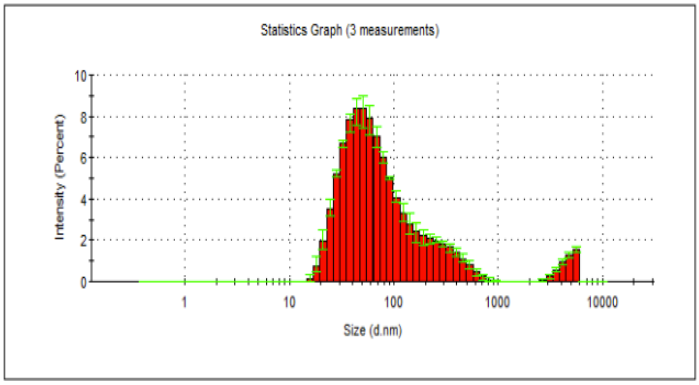
Statistics Graph (3 measurements)
Intensity (Percent)
Size (d.nm)

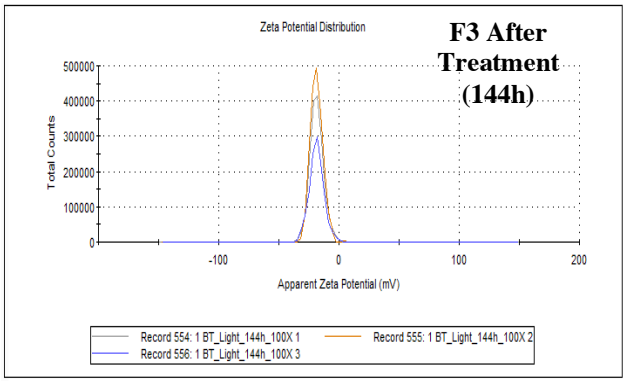
Zeta Potential Distribution
F3 After Treatment (144h)
Total Counts
Apparent Zeta Potential (mV)
Record 554: 1 BT_Light_144h_100X 1
Record 555: 1 BT_Light_144h_100X 2
Record 556: 1 BT_Light_144h_100X 3

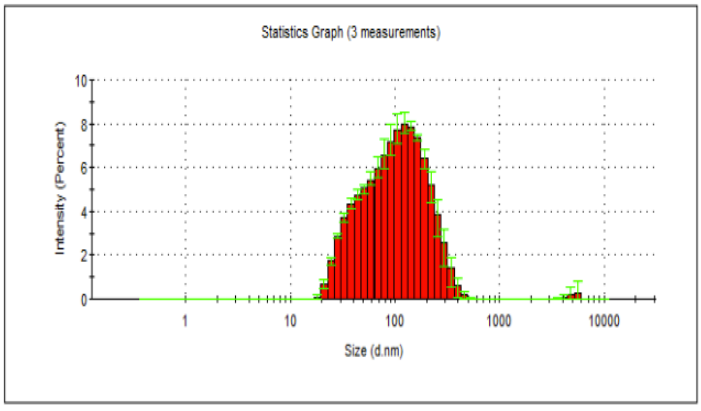
Statistics Graph (3 measurements)
Intensity (Percent)
Size (d.nm)

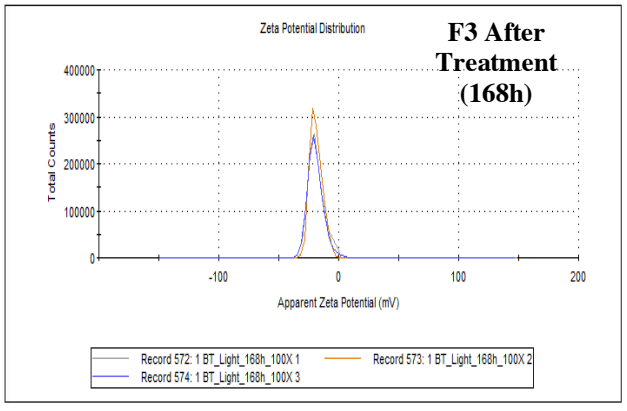
Zeta Potential Distribution
F3 After Treatment (168h)
Total Counts
Apparent Zeta Potential (mV)
Record 572: 1 BT_Light_168h_100X 1
Record 573: 1 BT_Light_168h_100X 2
Record 574: 1 BT_Light_168h_100X 3

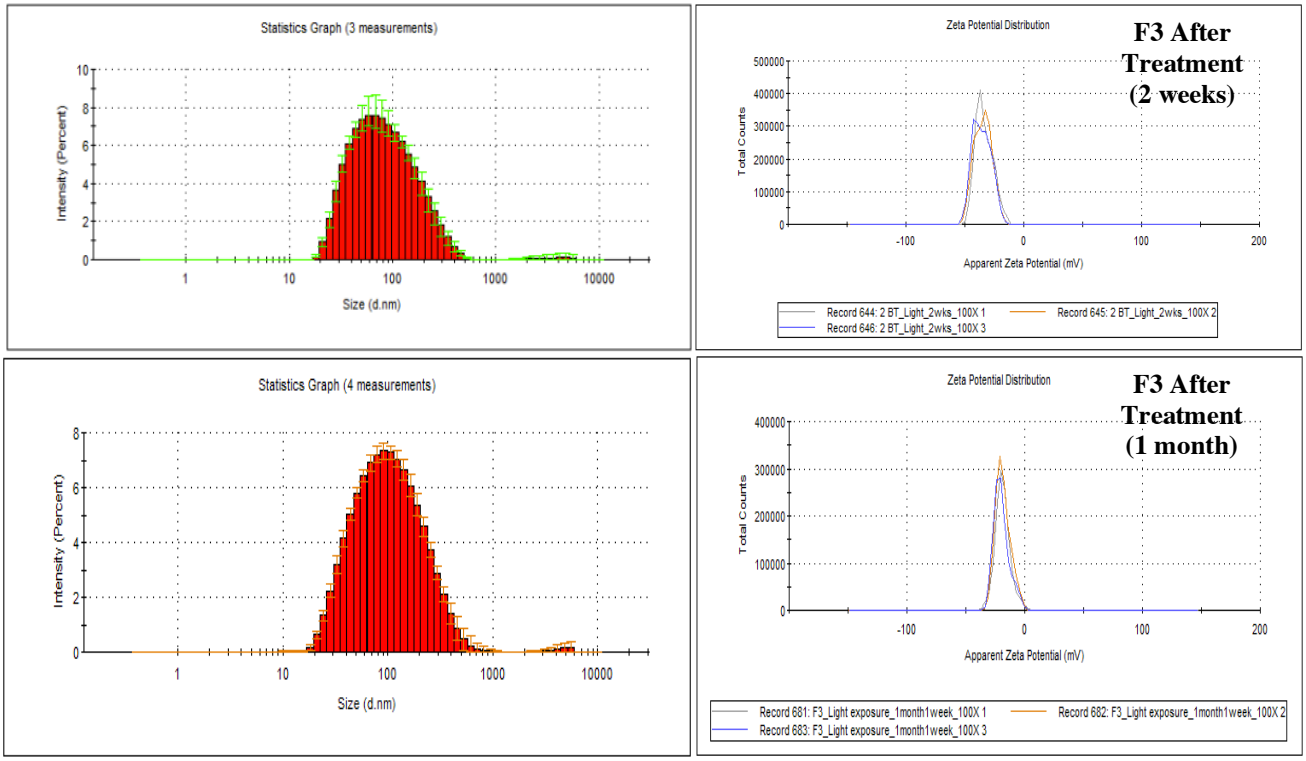

Figure D-23: Size and zeta potential values of F3 before and after exposure to light

Droplet Size & Zeta Potential Vs. Time

F1

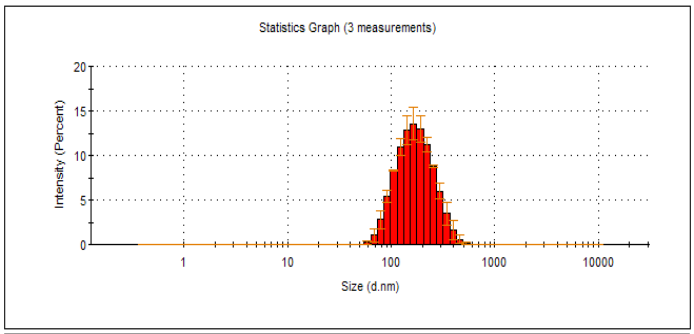

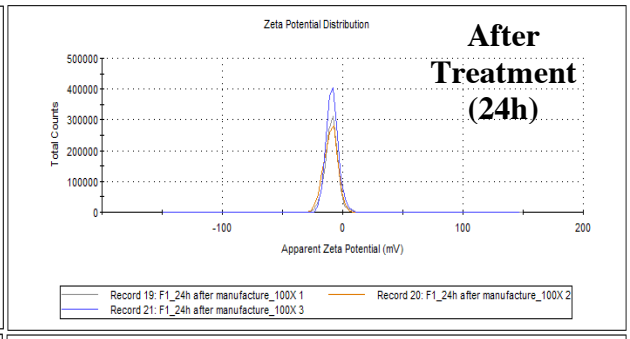

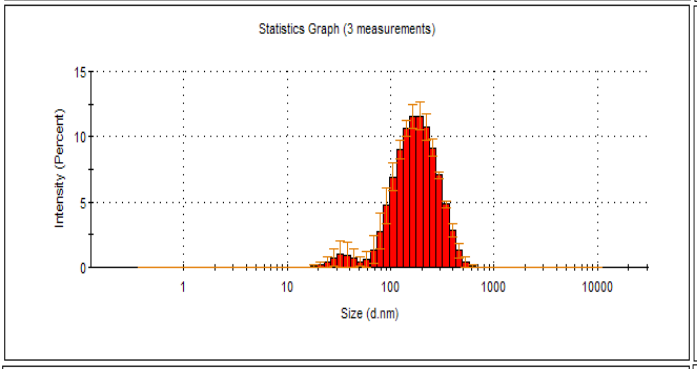

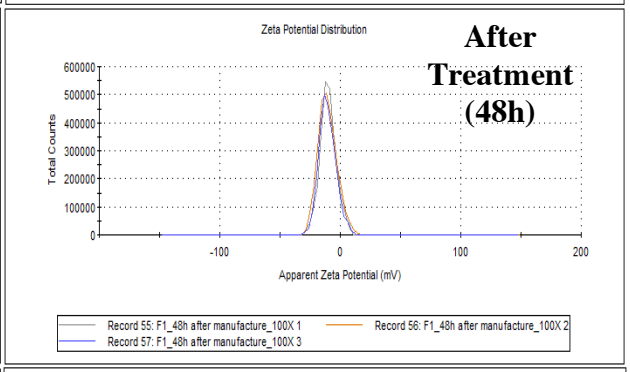

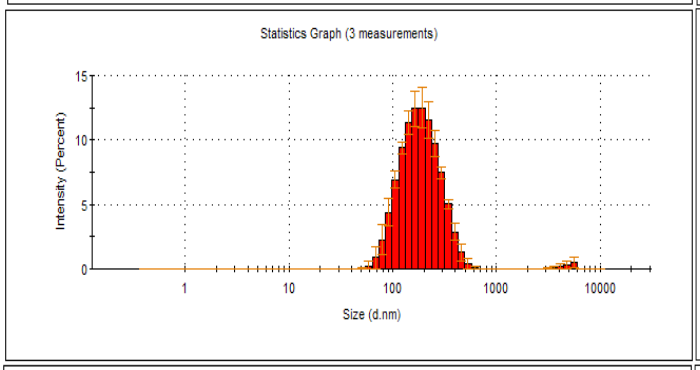

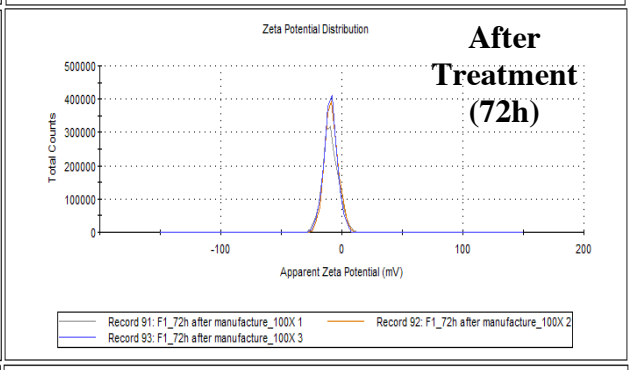

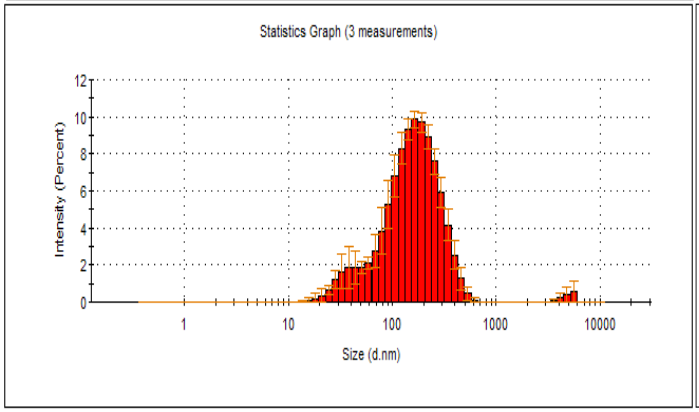

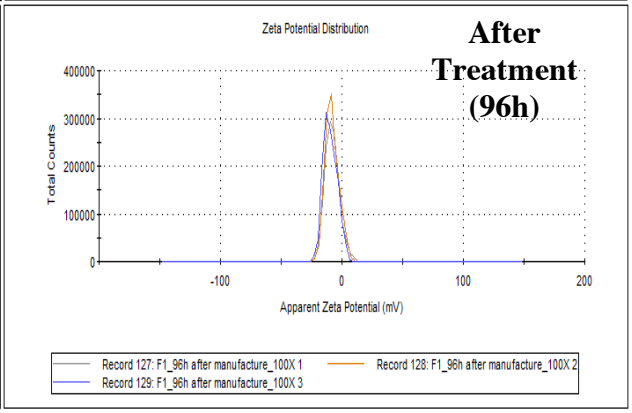

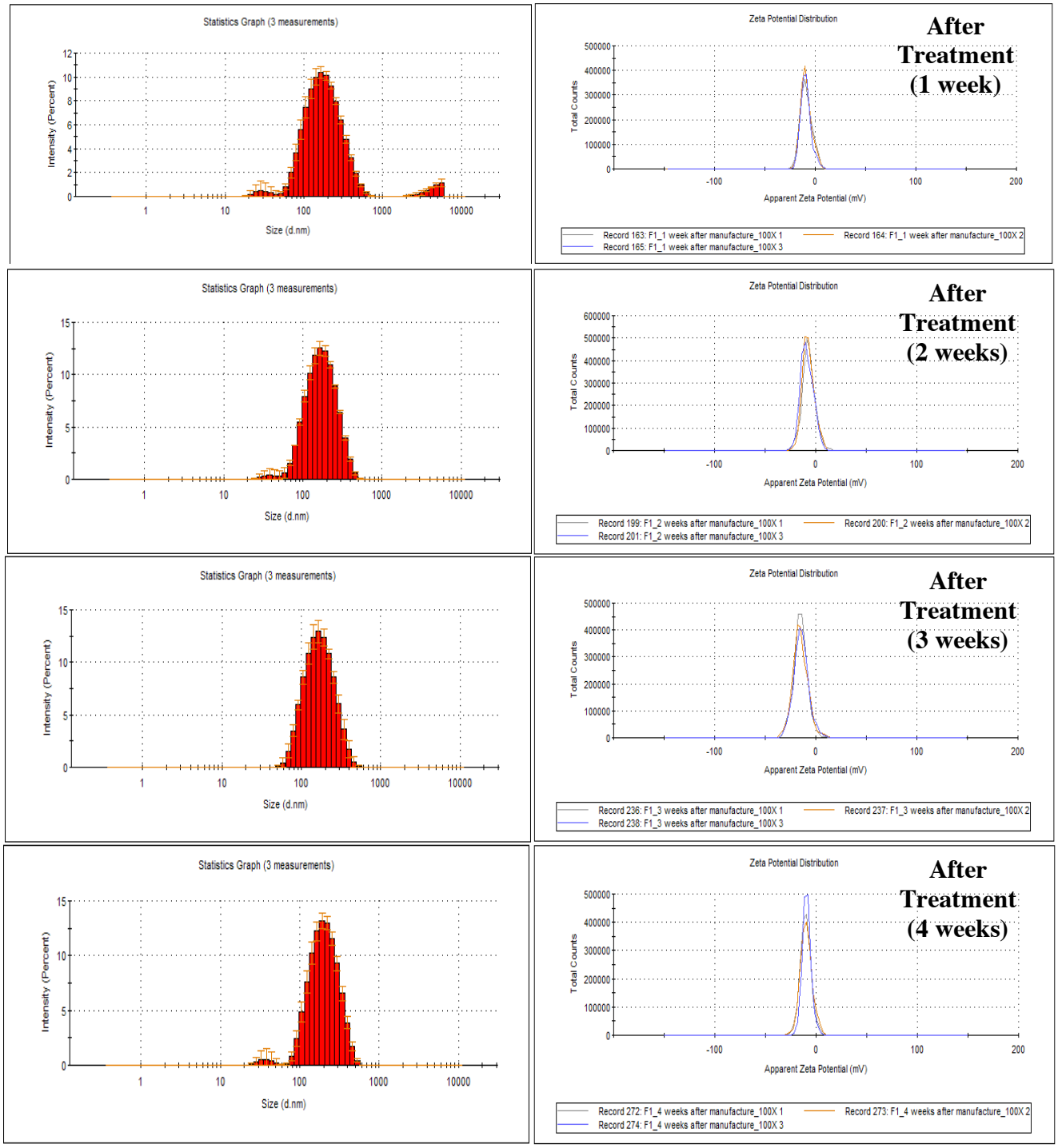

Figure D-24: Size and zeta potential values of F1 across various periods of time

F2

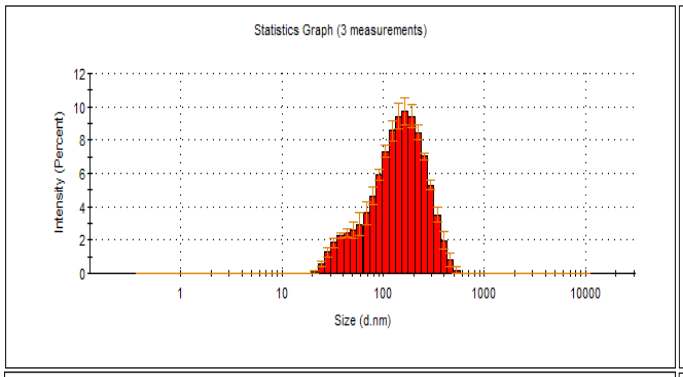
Statistics Graph (3 measurements)
Intensity (Percent)
Size (d.nm)

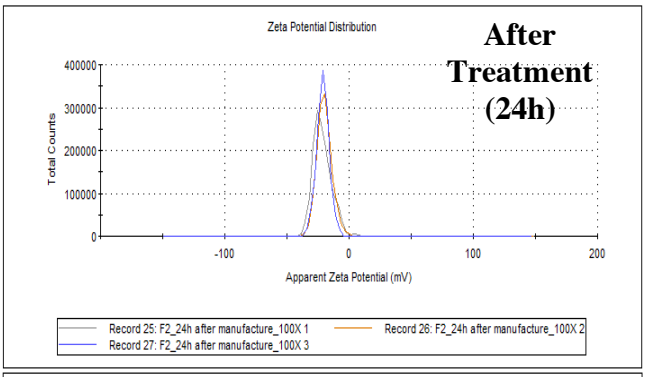
Zeta Potential Distribution
After Treatment (24h)
Total Counts
Apparent Zeta Potential (mV)
Record 25: F2_24h after manufacture_100X 1
Record 26: F2_24h after manufacture_100X 2
Record 27: F2_24h after manufacture_100X 3

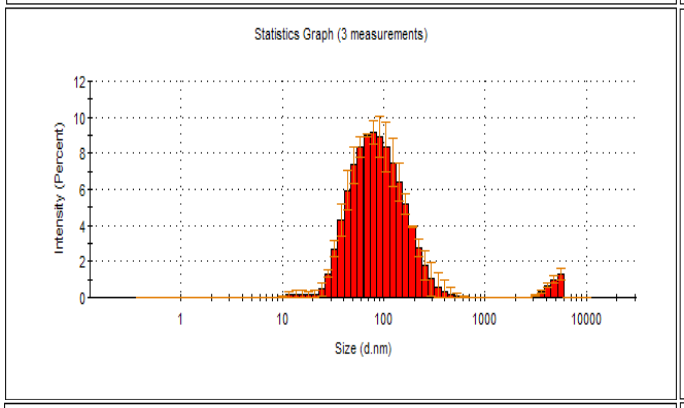
Statistics Graph (3 measurements)
Intensity (Percent)
Size (d.nm)

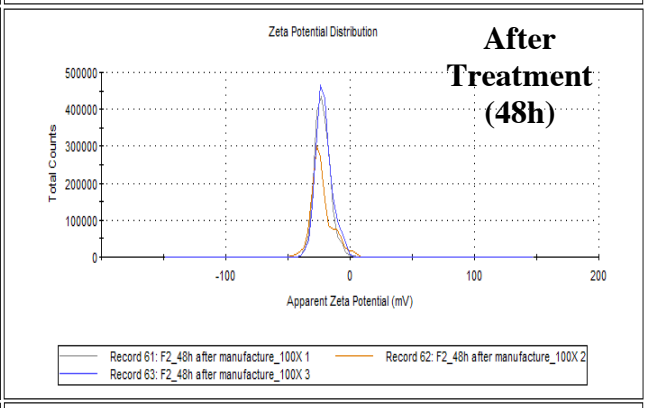
Zeta Potential Distribution
After Treatment (48h)
Total Counts
Apparent Zeta Potential (mV)
Record 61: F2_48h after manufacture_100X 1
Record 62: F2_48h after manufacture_100X 2
Record 63: F2_48h after manufacture_100X 3

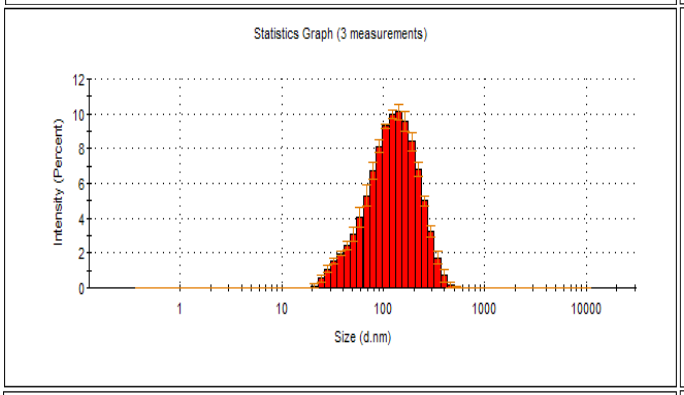
Statistics Graph (3 measurements)
Intensity (Percent)
Size (d.nm)

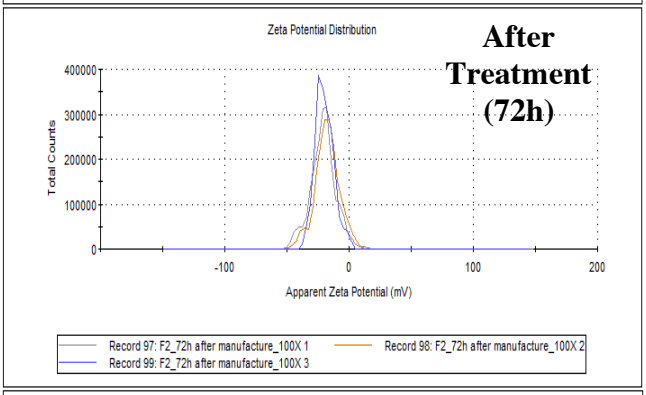
Zeta Potential Distribution
After Treatment (72h)
Total Counts
Apparent Zeta Potential (mV)
Record 97: F2_72h after manufacture_100X 1
Record 98: F2_72h after manufacture_100X 2
Record 99: F2_72h after manufacture_100X 3

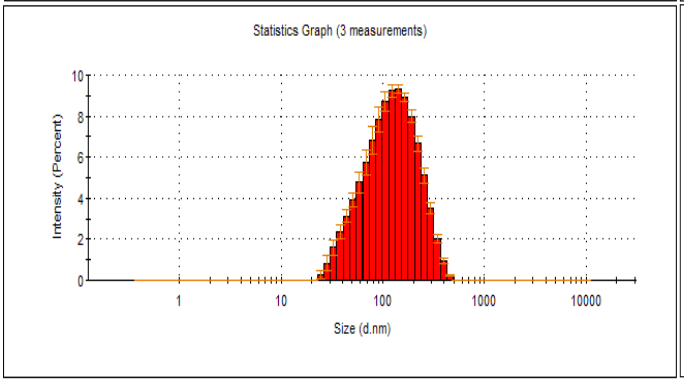
Statistics Graph (3 measurements)
Intensity (Percent)
Size (d.nm)

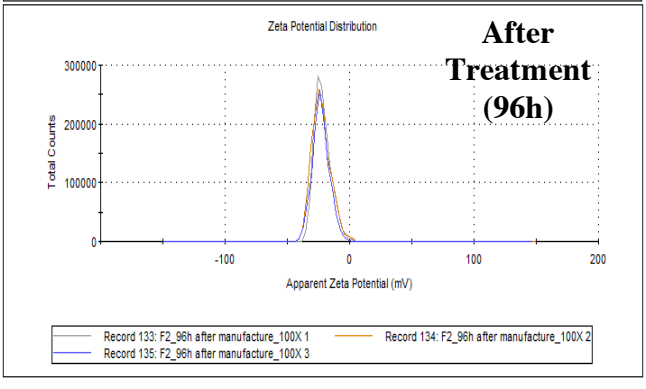
Zeta Potential Distribution
After Treatment (96h)
Total Counts
Apparent Zeta Potential (mV)
Record 133: F2_96h after manufacture_100X 1
Record 134: F2_96h after manufacture_100X 2
Record 135: F2_96h after manufacture_100X 3

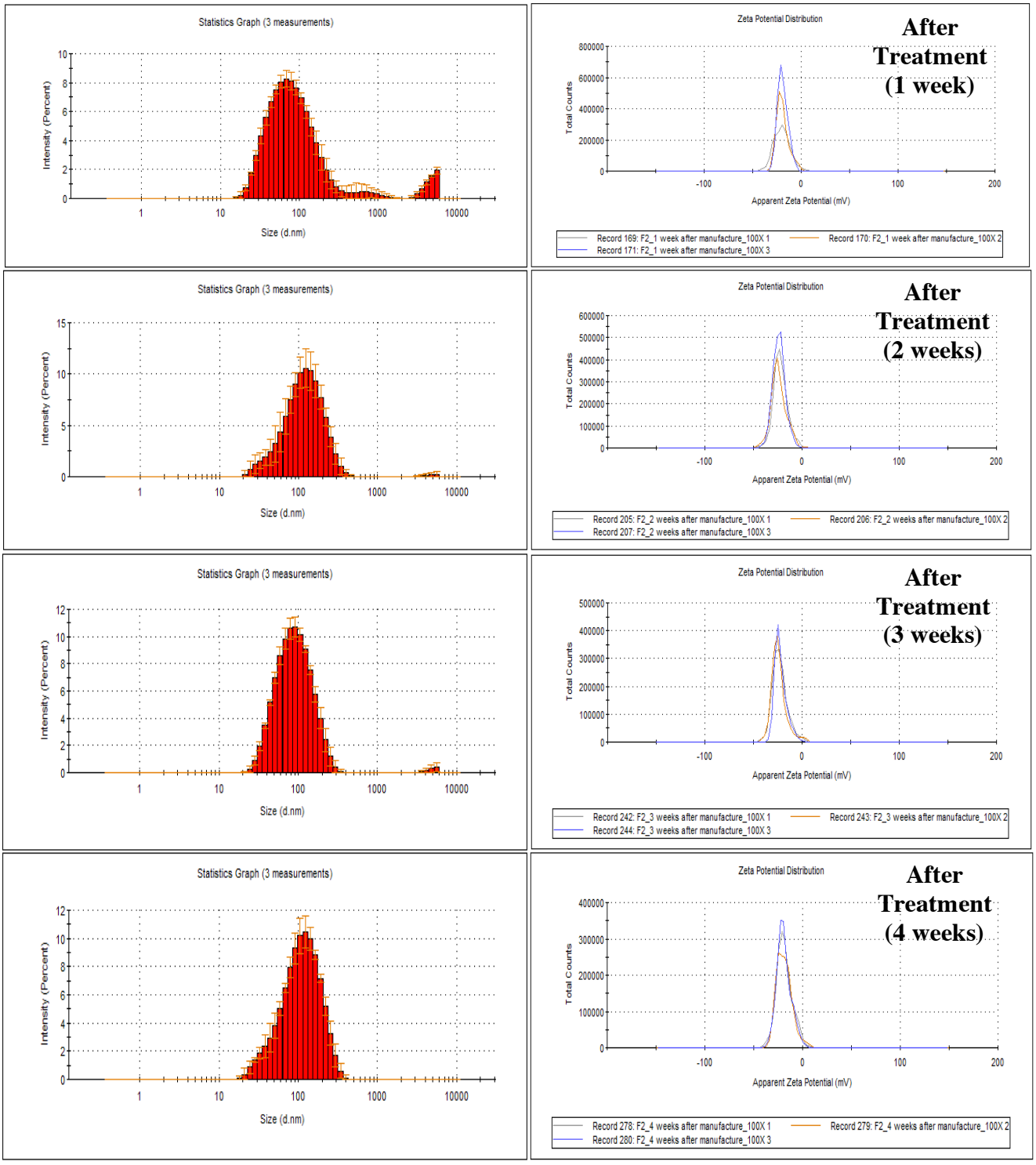

Figure D-25: Size and zeta potential values of F2 across various periods of time

F3

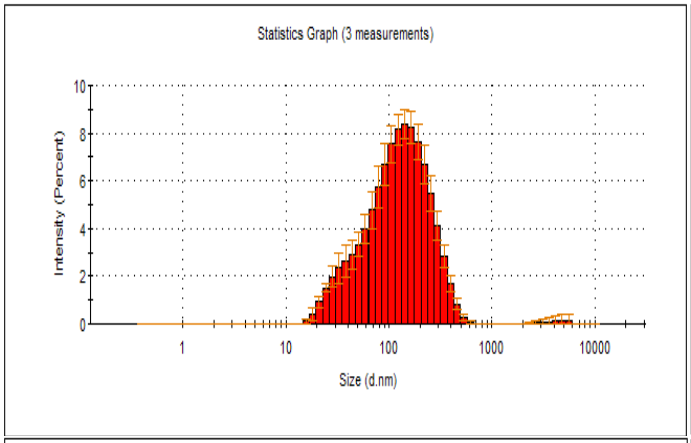
Statistics Graph (3 measurements)
Intensity (Percent)
Size (d.nm)

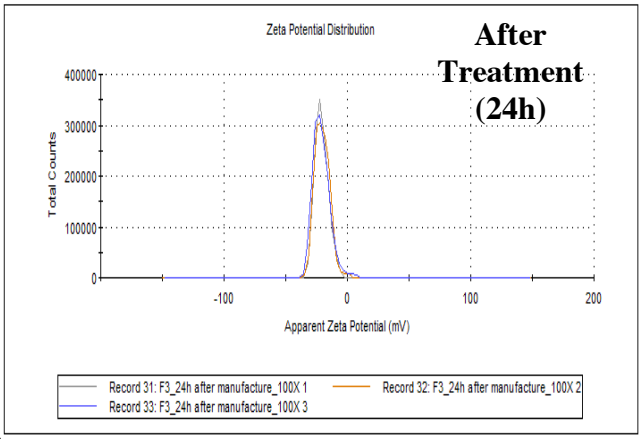
Zeta Potential Distribution
After Treatment (24h)
Total Counts
Apparent Zeta Potential (mV)
Record 31: F3_24h after manufacture_100X 1
Record 32: F3_24h after manufacture_100X 2
Record 33: F3_24h after manufacture_100X 3

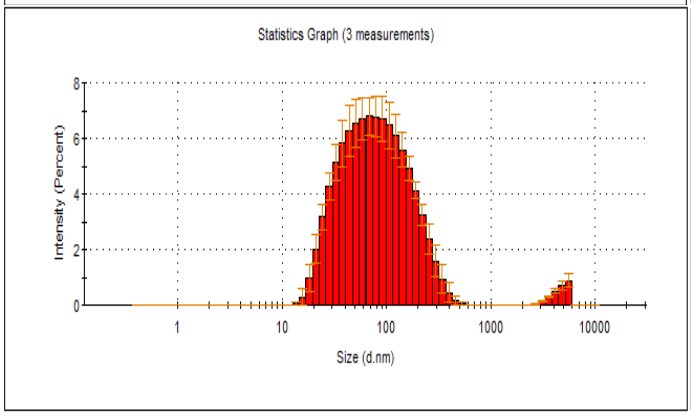
Statistics Graph (3 measurements)
Intensity (Percent)
Size (d.nm)

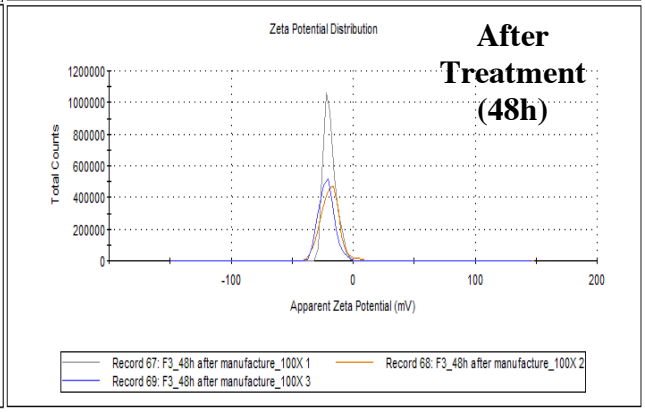
Zeta Potential Distribution
After Treatment (48h)
Total Counts
Apparent Zeta Potential (mV)
Record 67: F3_48h after manufacture_100X 1
Record 68: F3_48h after manufacture_100X 2
Record 69: F3_48h after manufacture_100X 3

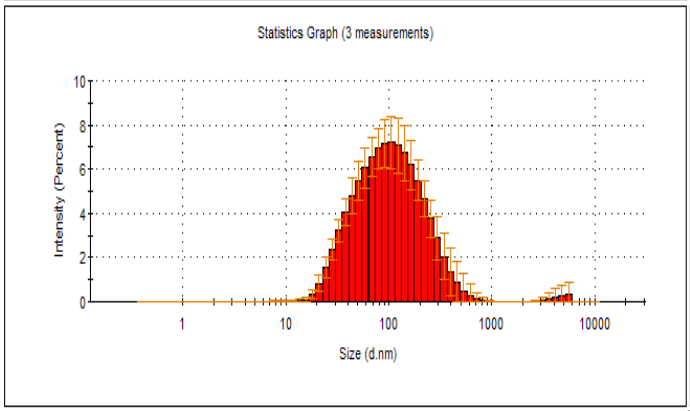
Statistics Graph (3 measurements)
Intensity (Percent)
Size (d.nm)

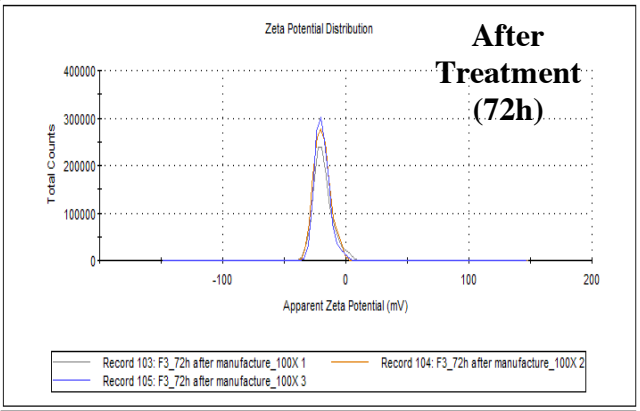
Zeta Potential Distribution
After Treatment (72h)
Total Counts
Apparent Zeta Potential (mV)
Record 103: F3_72h after manufacture_100X 1
Record 104: F3_72h after manufacture_100X 2
Record 105: F3_72h after manufacture_100X 3

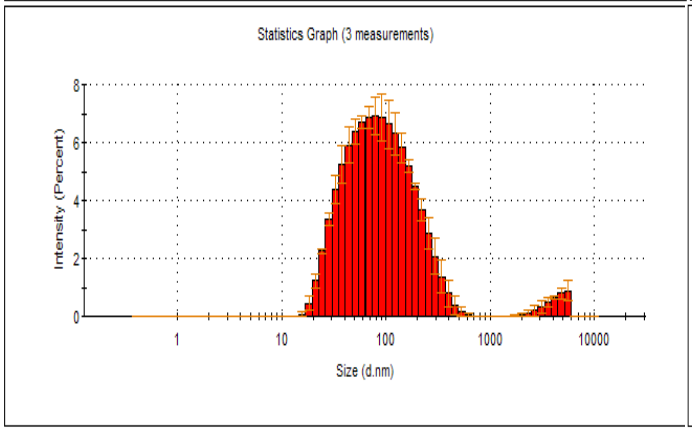
Statistics Graph (3 measurements)
Intensity (Percent)
Size (d.nm)

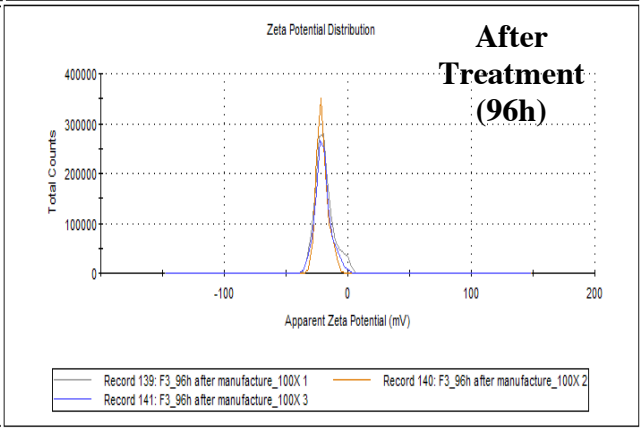
Zeta Potential Distribution
After Treatment (96h)
Total Counts
Apparent Zeta Potential (mV)
Record 139: F3_96h after manufacture_100X 1
Record 140: F3_96h after manufacture_100X 2
Record 141: F3_96h after manufacture_100X 3

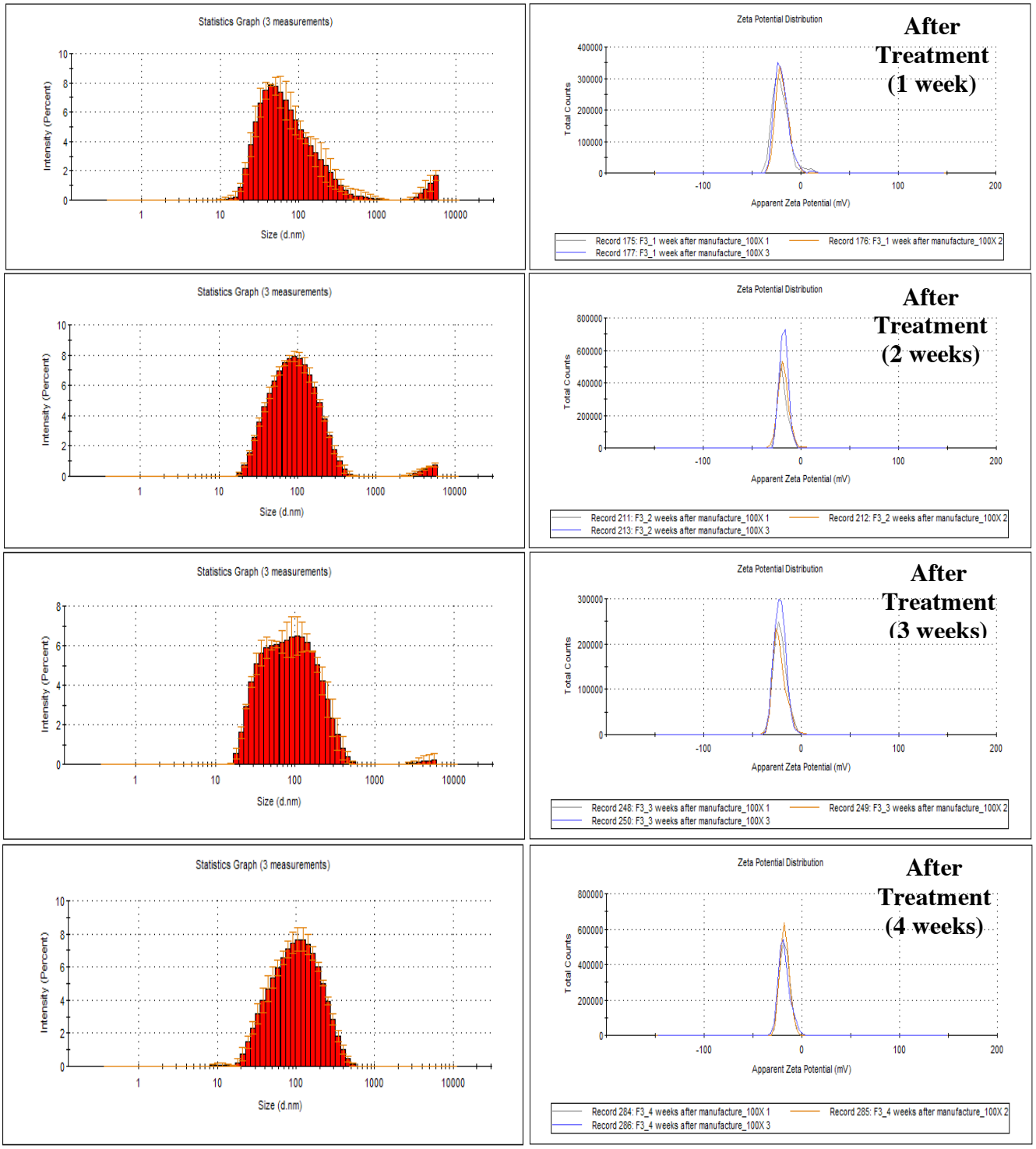

Figure D-26: Size and zeta potential values of F3 across various periods of time

Surfactant Parameter Calculations/Equations

Critical Micelle Concentration (CMC) for Mixed Surfactant Systems:

$$\frac{1}{CMC_{MIXED}} = \frac{a}{cmc_1} + \frac{1-a}{cmc_2}$$

where CMC_{MIXED} is the critical micelle concentration of the mixed system
a is the molar fraction of surfactant 1
cmc_1 is the critical micelle concentration of surfactant 1
1-a is the molar fraction of surfactant 2
cmc_2 is the critical micelle concentration of surfactant 2

3:1 Brij 97:Cremophor RH 40

$$\frac{1}{CMC_{MIXED}} = \frac{0.75}{0.940\ mM} + \frac{0.25}{0.0049\ mM}$$

$$= 0.019\ mM$$

where cmc_1= Brij 97= 0.940 mM[1]
cmc_2= Cremophor RH 40= 0.0049 mM (**Chapter 2)**

- 3:1 Brij 98:Cremophor RH 40

$$\frac{1}{CMC_{MIXED}} = \frac{0.75}{0.265\ mM} + \frac{0.25}{0.0049\ mM}$$

$$= 0.019\ mM$$

where cmc_1= Brij 98= 0.265 mM[1]
cmc_2= Cremophor RH 40= 0.0049 mM (**Chapter 2)**

- 3:1 Polysorbate 40:Cremophor RH 40

$$\frac{1}{CMC_{MIXED}} = \frac{0.75}{0.023\ mM} + \frac{0.25}{0.0049\ mM}$$

$= 0.012\ mM$

where cmc_1= Polysorbate 40= 0.023 mM[1]
cmc_2= Cremophor RH 40= 0.0049 mM (**Chapter 2)**

- 3:1 Polysorbate 80:Cremophor RH 40

$$\frac{1}{CMC_{MIXED}} = \frac{0.75}{0.047\ mM} + \frac{0.25}{0.0049\ mM}$$

$= 0.0048\ mM$

where cmc_1= Polysorbate 80= 0.0047 mM (**Chapter 2)**
cmc_2= Cremophor RH 40= 0.0049 mM (**Chapter 2)**

- 3:1 Polysorbate 80:Cremophor RH 60

$$\frac{1}{CMC_{MIXED}} = \frac{0.75}{0.0047\ mM} + \frac{0.25}{(Range\text{: } 0.0139\ to\ 0.139\ mM)}$$

$= 0.0056\text{-}0.0062\ mM$

where cmc_1= Polysorbate 80= 0.0047 mM (**Chapter 2)**
cmc_2= Cremophor RH 60= 0.005-0.05 % w/v[2]
MW: Cremophor RH 60: 3578 g/mol

- 3:1 Polysorbate 81:Cremophor RH 40

$$\frac{1}{CMC_{MIXED}} = \frac{0.75}{0.0061\ mM} + \frac{0.25}{0.0049\ mM}$$

$= 0.0057\ mM$

where cmc_1= Polysorbate 81= 0.0061 mM (**Figures D-6** and **D-7**, **Appendix D)**
cmc_2= Cremophor RH 40= 0.0049 mM (**Chapter 2)**

Calculation References:
1. Hait et al. *J Surf Det*. 2001;4; 303-311
2. Matsaridou et al. *AAPS PharmSciTech*. 2012;**13**:1319.